Elastomers and Rubber Elasticity

Elastomers and Rubber Elasticity

James E. Mark, EDITOR
The University of Cincinnati

Joginder Lal, EDITOR
The Goodyear Tire & Rubber Company

Based on a symposium

sponsored by the ACS Division

of Polymer Chemistry

at the 182nd Meeting of the

American Chemical Society,

New York, New York,

August 23–28, 1981.

ACS SYMPOSIUM SERIES **193**

ACS Symposium Series

M. Joan Comstock, *Series Editor*

FOREWORD

The ACS SYMPOSIUM SERIES was founded in 1974 to provide a medium for publishing symposia quickly in book form. The format of the SERIES parallels that of the continuing ADVANCES IN CHEMISTRY SERIES except that in order to save time the papers are not typeset but are reproduced as they are submitted by the authors in camera-ready form. As a further means of saving time, the papers are not edited or reviewed except by the symposium chairman, who becomes editor of the book. Papers published in the ACS SYMPOSIUM SERIES are original contributions not published elsewhere in whole or major part and include reports of research as well as reviews since symposia may embrace both types of presentation.

PREFACE

THE LAST FEW YEARS HAVE BROUGHT remarkable progress in research on elastomers and rubberlike elasticity. For example, regarding the synthesis and structural characterization of new elastomers, there are multi-phase block copolymers, the organophosphazenes, and polymers of carefully controlled microstructure and capacity for strain-induced crystallization. In the area of new cross-linking techniques, there are very specific chemical reactions used to form model or ideal networks of known structure; for example, end-linking of chains having reactive groups placed at both ends. Important advances in the molecular theories of rubberlike elasticity, with particular regard to the forms of the elastic equation of state, the importance of junction fluctuations, and the nature or degree of non-affineness of the elastic deformation have been reported. Also, improvements in experimental techniques, including the use of model networks to test newly developed theoretical concepts, and neutron scattering measurements to characterize the structure of elastomeric networks and the nature of the deformation process have developed.

A wide variety of such topics are covered in this book. Most of the chapters are from papers presented at a symposium held in August 1981. This symposium was preceded by a half-day tutorial session, with corresponding introductory review articles on synthesis of elastomers by G. Odian and rubber elasticity by J. E. Mark (published in the November 1981 issue of the *Journal of Chemical Education*). To aid the reader, a brief review of thermoplastic elastomers is included in this book.

It is a pleasure to acknowledge that the symposium from which these chapters derive has received financial support from the following: Division of Polymer Chemistry, Inc., Petroleum Research Fund, American

ix

Hoechst Corporation, Ashland Chemical Company, Cabot Corporation, Dow Chemical U.S.A., Dunlop Research Centre, E. I. du Pont de Nemours & Company, The Firestone Tire & Rubber Company, The General Tire & Rubber Company, The BF Goodrich Company, The Goodyear Tire & Rubber Company, Monsanto Company, Polysar Limited, Shell Development Company, 3M Chemicals Division, and Uniroyal Chemical Division.

JAMES E. MARK
The University of Cincinnati
Cincinnati, OH 45221

JOGINDER LAL
The Goodyear Tire & Rubber Company
Akron, OH 44316

FOREWORD

BY PAUL J. FLORY

RUBBER ELASTICITY IS A PROPERTY THAT is unique to polymers consisting of long, flexible chains. No substance otherwise constituted will sustain, without rupture, the high deformation that is typical of rubberlike materials, while simultaneously retaining the capacity to recover its original dimensions. Moreover, rubber elasticity is a nearly universal property of long chain polymers under suitable conditions, i.e., in the amorphous state above the glass transition. It is not peculiar to a restricted class of such materials; nearly all conventional polymers are rubberlike when neither crystalline nor glassy, provided however that the long chains are so interconnected as to yield a network whose permanency extends beyond the "use life" of the material in a practical application or the duration of an experiment in the laboratory. In addition to common organic polymers, rubber elasticity is manifested also in certain inorganic polymers, notably elastic sulfur and the polyphosphazenes (Singler and Hagnauer). Biopolymers such as the prominent structure proteins, elastin, denatured collagen, and myosin, display rubber elasticity, a characteristic that is requisite to their functions in living organisms.

Covalent cross-linkages usually serve to bind the long chains into a network. The necessary interconnections may, however, be provided by other means, e.g., by small crystalline regions (Morton) or by chelate linkages (Eichinger).

It was recognized a half century ago by K. H. Meyer, by E. Guth and H. Mark, and by W. Kuhn that rubber elasticity originates in the capacity for randomly coiled long-chain molecules to adopt diverse configurations, and that recovery from deformation is a manifestation of the tendency of such chains to assume the most probable distribution of configurations. Early theories of rubber elasticity were developed on the basis of these well-conceived insights. Subsequent experimental investigations, especially the analysis of stress-temperature coefficients and observations on effects of swelling, confirmed that the retractive force originates primarily within the chains of the network, and not to an appreciable degree from forces of attraction between chains and their neighbors in the space they share. The elastic free energy of an elastomeric network is therefore appropriately treated as the sum of contributions of its individual chains, the resultant being sensibly independent of their mutual interactions.

The chains of typical networks are of sufficient length and flexibility to justify representation of the distribution of their end-to-end lengths by the most tractable of all distribution functions, the Gaussian. This facet of the problem being so summarily dealt with, the burden of rubber elasticity theory centers on the connections between the end-to-end lengths of the chains comprising the network and the macroscopic strain.

Early theories of Guth, Kuhn, Wall and others proceeded on the assumption that the "microscopic" distribution of end-to-end vectors of the chains should reflect the macroscopic dimensions of the specimen, i.e., that the chain vectors should be affine in the strain. The pivotal theory of James and Guth (1947), put forward subsequently, addressed a network of Gaussian chains free of all interactions with one another, the integrity of the chains which precludes one from the space occupied by another being deliberately left out of account. Hypothetical networks of this kind came to be known later as phantom networks (Flory, 1964, 1976). James and Guth showed rigorously that the *mean* chain vectors in a Gaussian phantom network are affine in the strain. They showed also that the fluctuations about the mean vectors in such a network would be independent of the strain. Hence, the instantaneous distribution of chain vectors, being the convolution of the distribution of mean vectors and their fluctuations, is not affine in the strain. Nearly twenty years elapsed before his fact and its significance came to be recognized (Flory, 1976, 1977).

In deformed real networks attainment of the molecular state predicted by phantom network theory is generally precluded by non-specific, diffuse entanglements of the chains, which restrict fluctuations of the junctions of the network about their mean positions. The stress consequently is enhanced to a degree that depends on the strain. With proper account of this restriction, the relationship of stress to strain in typical rubbers is well reproduced by recent theory (Flory, 1977) over the full range of uniaxial and biaxial deformations accessible to experiment (Erman and Flory, 1980, 1982). At large strains, including dilation, the effects of restrictions on fluctuations vanish and the relationship of stress to strain converges to that for a phantom network. The primary connectivity of the network may thus be ascertained. Experimental results (J. E. Mark 1977–1981; Rehage and Oppermann; Erman and Flory) show the measured stress in this limit to be in close agreement with that calculated from chemical degrees of cross-linking. Topological entanglements (alias "trapped entanglements") that allegedly intertwine chains with one another, and hence should act like cross-linkages, do not contribute appreciably to the stress.

This deduction from analysis of experiments according to recent theory contradicts entrenched views on the role of chain entanglements.

Two conditions must be met if this conclusion is to be revealed by the analysis. First, appropriate experimental procedures must be adopted to assure establishment of elastic equilibrium. Second, the contribution to the stress from restrictions on fluctuations in real networks must be properly taken into account, with due regard for the variation of this contribution with deformation and with degree of cross-linking. Otherwise, the analysis of experimental data may yield results that are quite misleading.

PAUL J. FLORY
Stanford University
Stanford, CA 94305

Basic Concepts in Elastomer Synthesis

GEORGE ODIAN

College of Staten Island, City University of New York, Staten Island, NY 10301

The synthesis of elastomers by step, chain,
and ring-opening polymerizations is reviewed.
These reactions are characterized as to the
process variables which must be controlled
to achieve the synthesis and crosslinking of
an elastomer of the required structure. Both
radical and ionic chain polymerizations are
discussed as well as the structural varia-
tions possible through copolymerization and
stereoregularity.

Requirements of an Elastomer

An elastomer or rubber is a material which undergoes very
large (up to 400% or more), reversible deformations at relatively
low stresses. These characteristics are met by flexible, cross-
linked polymer molecules (1). Only polymer molecules have the
ability to undergo very large deformations. A long-chain
molecule can respond to stress, without distortions of bond
angles or bond lengths, by conversion from a random coil to a
more extended chain through rotations of the bonds in the polymer
chain. The polymer must be essentially completely amorphous
(non-crystalline) with a low glass transition temperature and low
secondary forces so as to obtain high flexibility of the polymer
chains. Precluded from use as elastomers are polymers such as
nylon-6 (I), polyethylene (II), and polystyrene (III). Highly
polar polymers (e.g., nylon-6) or those with highly regular

$$\text{+(CH}_2)_5\text{CONH+}_n \qquad \text{+CH}_2\text{CH}_2\text{+}_n \qquad \text{+CH}_2\text{CH}\phi\text{+}_n$$
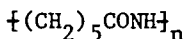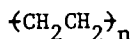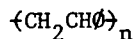
$$\text{I} \qquad\qquad\qquad \text{II} \qquad\qquad\qquad \text{III}$$

structures (e.g., polyethylene) are quite crystalline and, thus,

do not have the necessary chain flexibility. Polymers with large
bulky substituents (e.g., polystyrene), although non-crystalline,
are also too rigid to be elastomers. (These polymers do, however,
find large-scale use -- polyethylene and polystyrene as plastics
and nylon-6 as both a plastic and fiber.) Polymers which find
uses as elastomers are those which have irregular or unsymmetrical
structures [e.g., ethylene-propylene copolymer (IV)], or non-
polar structures, [e.g., polyisobutylene (V)] or flexible units
in the polymer chain [e.g., polysiloxane (VI), polysulfide (VII),
1,4-polyisoprene (VIII)].

$$\{CH_2CH_2CH_2\overset{\overset{\displaystyle CH_3}{|}}{CH}\}_n \qquad \{CH_2C(CH_3)_2\} \qquad \{OSi(CH_3)_2\}_n$$

IV   V   VI

$$\{(CH_2)_6S_m\}_n \qquad \{CH_2\overset{\overset{\displaystyle CH_3}{|}}{C}=CHCH_2\}_n$$
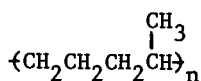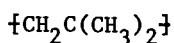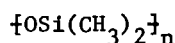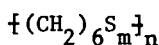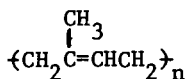
VII   VIII

    The reversible recovery of a deformed elastomer to its
original (undeformed) state is due to an entropic driving force.
The entropy of polymer chains is minimum in the extended con-
formation and maximum in the random coil conformation. Cross-
linking of an elastomer to form a network structure (IX) is
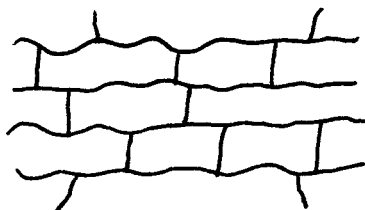
            IX

necessary for the recovery from deformation to be rapid and
complete. The presence of a network structure prevents polymer
chains from irreversibly slipping past one another upon deforma-
tion. Either chemical or physical crosslinking can be used to
obtain the required network structure. The synthetic strategy for
producing an elastomer differs depending on whether chemical or
physical crosslinking is involved. The synthesis of a chemically-
crosslinked elastomer requires the polymerization of an
appropriate low molecular weight reactant or mixture of reactants
(referred to as monomers) such that the polymer molecules

produced contain functional groups capable of subsequent reaction to form crosslinks between polymer chains. An example is 1,4-polyisoprene which is found in nature and also produced by polymerization of isoprene. 1,4-Polyisoprene is crosslinked by heating with sulfur. Sulfur crosslinks are formed between polymer chains through reaction of the double bonds present in 1,4-polyisoprene. Thus, the overall process involves two separate synthetic reactions. First, a polymer is synthesized from a monomer or mixture of monomers. Second, the polymer is fabricated (e.g., by compression molding) into the desired shape (e.g., an automobile tire) and chemically-crosslinked while in that shape. The crosslinking and polymer synthesis reactions are carried out separately.

Certain block copolymers comprise a category of elastomer in which crosslinking occurs by a physical process. The two main types of block copolymers which have been commercialized are the ABA and $(AB)_n$ block copolymers (X and XI) where A and B represent
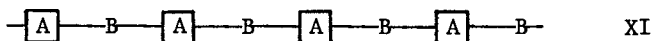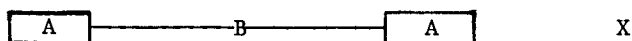
alternating blocks of two different chemical structures, e.g., polystyrene and 1,4-polyisoprene blocks. The ABA and $(AB)_n$ block copolymers, referred to as triblock and multiblock copolymers, respectively, are synthesized such that the A blocks are hard (e.g., polystyrene) and short while the B blocks are flexible (e.g., 1,4-polyisoprene) and long. These block copolymers, referred to as thermoplastic elastomers (TPE), behave as elastomers at ambient temperatures but are thermoplastic at elevated temperatures where they can be processed by molding, extrusion, or other fabrication techniques. The behavior of thermoplastic elastomers is a consequence of their micro-heterogenous, two-phase structure. The hard A blocks from different polymer chains aggregate to form rigid domains at ambient temperatures. The rigidity of the A blocks is a consequence of either their T_m or T_g being above ambient temperatures. The rigid domains constitute a minor, non-continuous phase dispersed (on a microscopic scale) within the major, continuous phase composed of the rubbery B blocks from different polymer chains. The rigid domains act as physical crosslinks to hold the soft, rubbery B blocks in a network structure. However, the physical crosslinking is reversible since heating above the crystalline melting or glass transition temperature of the A blocks softens the rigid domains and the polymer flows. Cooling reestablishes the rigid domains and the material again behaves as a crosslinked elastomer. Thermoplastic elastomers have the advantage over conventional elastomers that no additional chemical

crosslinking reaction is needed and fabrication into products is
accomplished in the same manner as for thermoplastics. However,
the synthesis of thermoplastic elastomers generally involves more
complicated polymerization procedures compared to conventional
elastomers.
      The various reactions for synthesizing elastomers from
monomers are discussed below together with a consideration of the
reactions used to achieve crosslinking (2-15). The most important
consideration in carrying out a polymerization reaction is the
control of polymer molecular weight (MW). For most applications
a polymer must have a minimum molecular weight of 5,000 or so
since it is only then that it has sufficient physical strength to
be useful. Most specific applications require higher molecular
weights to maximize the strength properties. However, some
polymer properties are adversely affected by higher MW, e.g., the
viscosity increases with increasing MW and it becomes more
difficult to form the polymer into the desired shape of the final
product by molding or other processing operations. Thus, the
desired MW is usually some compromise high MW based on obtaining
sufficient strength for the end-use application while retaining
the ability to readily form the polymer into the product shape.
This need to control molecular weight at some high level places
stringent requirements on any reaction to be used for polymer
synthesis. The required polymer molecular weight may vary
considerably for different elastomers since the same strength
will develop at lower molecular weights for the more polar
elastomers such as polyurethanes compared to less polar elastomers
such as polyisobutylene.

Step Polymerization

      Polymerizations are classified as either step (condensation)
or chain (addition) polymerizations. The two differ in the time-
scale of various reaction events, specifically in the length of
time required for the growth of large-sized molecules. The
synthesis of polysulfides (Eq. 1) and polyurethanes (Eq. 2) are

$$nCl-R-Cl + nNa_2S_m \xrightarrow{-NaCl} (R-S_m)_n \qquad (1)$$

$$nHO-R-OH + nOCN-R'-NCO \longrightarrow (O-R-OCO-NH-R'-NH-CO)_n \qquad (2)$$
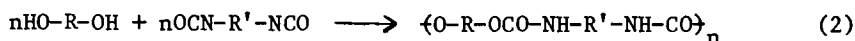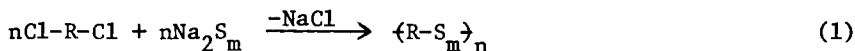
examples of step polymerizations which lead to elastomeric
materials. The reactions can be generalized as

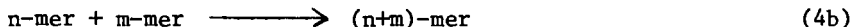$$nX-X + nY-Y \xrightarrow{k} (X-XY-Y)_n \qquad (3)$$

where X and Y are the two different functional groups whose

reaction leads to polymer growth. The structural entity which
repeats itself many times in the polymer (e.g., the structure
within the parenthesis in Eq. 1 or Eq. 2) is referred to as the
repeating unit. The small molecule reactants which supply the
X and Y functional groups are referred to as bifunctional
monomers.

Step polymerization proceeds by the stepwise reaction between
the two different functional groups of the monomers. One proceeds
slowly from monomer to dimer and larger-sized species:

$$
\begin{aligned}
&\text{Monomer + monomer} &&\longrightarrow &&\text{dimer} \\
&\text{Dimer + monomer} &&\longrightarrow &&\text{trimer} \\
&\text{Dimer + dimer} &&\longrightarrow &&\text{tetramer} \\
&\text{Trimer + monomer} &&\longrightarrow &&\text{tetramer} \\
&\text{Trimer + dimer} &&\longrightarrow &&\text{pentamer} \\
&\text{Trimer + trimer} &&\longrightarrow &&\text{hexamer} \\
&\text{Trimer + tetramer} &&\longrightarrow &&\text{heptamer} \\
&\text{Trimer + pentamer} &&\longrightarrow &&\text{octamer} \\
&\text{Tetramer + tetramer} &&\longrightarrow &&\text{octomer} \\
&\text{Tetramer + pentamer} &&\longrightarrow &&\text{nonamer} \\
&\text{etc., etc.}
\end{aligned}
\tag{4a}
$$

or in general

$$
\text{n-mer + m-mer} \longrightarrow \text{(n+m)-mer} \tag{4b}
$$
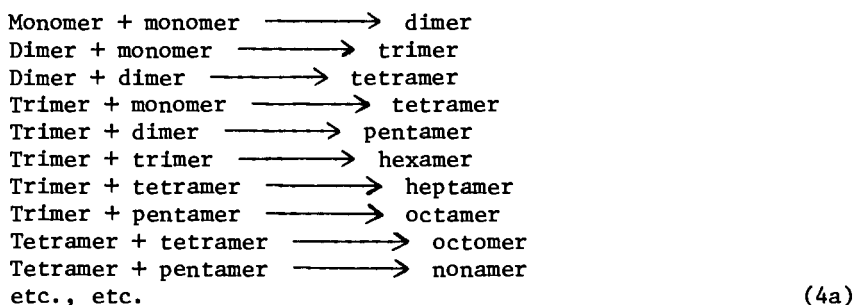
As each larger sized species is formed, it competes simultaneously
with the smaller-sized species for further reaction. There is a
distribution of different sized molecules at any time -- each
species containing one functional group at each of its two chain
ends. The average size of the molecules increases with conversion
until eventually large polymer molecules are obtained.

The rate of a step polymerization is the sum of the rates of
reaction between molecules of various sizes, i.e., the sum of all
reactions described by Eq. 4. Kinetic analysis of this difficult
situation is greatly simplified if one assumes that the
reactivities of both functional groups of a monomer are the same,
the reactivity of one functional group of a monomer is the same
irrespective of whether or not the other functional group has
reacted, and the reactivity of a functional group is independent
of the size of the molecule to which it is attached. These
simplifying assumptions, referred to as the concept of equal
reactivity of functional groups, make the kinetics of step
polymerization identical to those for the analogous small molecule
reaction. Although there are obvious instances where it does not
hold, unsymmetrical monomers and monomers in which the two
functional groups are very close to each other, the equal
reactivity concept holds for most polymerizations. In this
situation, the kinetics take the same general form (Eq. 5) as the
corresponding small molecule reaction where [X] and [Y] represent

$$\text{rate} = k[X][Y] \tag{5}$$

the concentrations of X and Y groups, respectively, and k is the rate constant for reaction between X and Y groups.

Stoichiometric or very nearly stoichiometric amounts of the X and Y functional groups are used in the typical polymerization, $[X] = [Y] = [M]$, and the polymerization rate, defined as the rate of decrease of X or Y groups, is given by

$$- \frac{d[M]}{dt} = k[M]^2 \tag{6}$$

Integration yields

$$\frac{1}{[M]} = \frac{1}{[M]_0} + kt \tag{7}$$

where $[M]_0$ and $[M]$ are the concentrations of X (or Y) groups at time 0 and t, respectively. It is useful to introduce p as the fraction of the original functional groups that has reacted at time t and to define DP, referred to as the average degree of polymerization, as the average number of monomer molecules linked together per molecule in the reaction system at time t.

$$DP = \frac{[M]_0}{[M]} = \frac{[M]_0}{[M]_0(1-p)} = \frac{1}{(1-p)} \tag{8}$$

Combination of Eqs. 7 and 8 yields

$$DP = 1 + [M]_0 kt \tag{9}$$

The polymer molecular weight (more specifically, the number-average molecular weight) is DP multiplied by one-half the molecular weight of the repeating unit.

The size of the polymer molecules increases at a relatively slow rate in step polymerization compared to chain polymerization due to the lower rate constants in the former since k is of the order of $10^{-3}-10^{-2}$ liter/mole-sec. One proceeds slowly from monomer to dimer, trimer, tetramer, pentamer, and so on until eventually large polymer molecules have been formed. Any two molecular species containing respectively the two different functional groups can react with each other throughout the polymerization. The average size of the molecules increases slowly with time and high molecular weight polymer is not obtained until near the very end of the reaction (i.e., above 95% conversion).

The successful synthesis of useful polymers is more difficult than carrying out the corresponding small molecule reaction since

high molecular weights can only be achieved at very high conver-
sion.   Equation 8 shows that DP values of 20, 50, 100, and 200
(corresponding to molecular weights of 2000, 5000, 10000,
and 20000, respectively, for the case where the repeating unit has
a molecular weight of 200) are obtained at conversions of 95, 98,
99, and 99.5%, respectively. A conversion such as 90% which would
be considered excellent for the synthesis of a small molecule
product is a disaster for the synthesis of the corresponding
polymer. The need for very high conversions means that only a
relatively small fraction of all chemical reactions can be used to
synthesize polymers. Several stringent requirements must be met
by any polymerization system in order to produce high molecular
weights:

   1. Side reactions which prevent the required high conver-
sions must be absent. The chemistry of the reaction used for
polymerization must be well understood so as to carry out the
polymerization under conditions where the extent, if any, of side
reactions does not limit the polymer molecular weight.

   2. Reasonable reaction rates are needed to achieve the
required DP in a reasonable time. Equations 8 and 9 indicate
that it takes progressively longer and longer times to achieve
each of the last few percent conversion, e.g., it takes about as
long to go from 95% conversion to 96% conversion as it takes to
reach 95% conversion from zero conversion.

   3. Reversible reactions such as polyesterification must be
driven to high conversion by displacement of the equilibrium
toward the polymer product. For reactions where there is a small
molecule by-product such as water, this can be done by removal of
that by-product by polymerization at temperatures above its
boiling point. Only low molecular weight products are obtained
without displacement of the equilibrium. For example, even for
an equilibrium constant of 16, which would be highly favorable for
a small molecule reaction since the conversion is 80%, the DP is
only 5 for polymerization carried out under equilibrium condi-
tions.

   4. The polymer molecular weight may be greatly diminished if
polymerization takes place under conditions where polymer
precipitates from solution and/or is not well solvated. The
reacting functional groups become inaccessible to each other and
polymerization stops before the desired DP is reached.

   5. High molecular weights can only be achieved by using near
stoichiometric amounts of the two different reacting functional
groups. The dependence of DP on p and r, the molar ratio of X
and Y groups defined so that r is either equal to or less than
one, is given by

$$DP = \frac{(1 + r)}{(1 + r - 2\ rp)} \tag{10}$$

Molecular weight control at the desired level is achieved by

simultaneous control of p and r. For any specific value of p, the
molecular weight increases the more nearly stoichiometric amounts
(r closer to 1) of X and Y functional groups are used. Stoichio-
metric imbalance lowers DP since at some point all molecules in
the reaction system will contain the same type of functional
group, e.g., X groups if X groups are in excess, and subsequent
growth does not occur since X groups do not react with each other.
The greater the stoichiometric imbalance, i.e., the more r is
smaller than 1, the earlier this occurs and the lower the polymer
molecular weight. For example, for p = 0.99, r values of 0.999,
0.990, and 0.980 yield DP values of 95.2, 66.3, and 49.5,
respectively. This shows how critical is the need to control r
since a difference of a few tenths of a percent excess of one
reactant over the other results in significant differences in the
molecular weight of the polymer product. Control of r requires
the use of high purity monomers. Reactant purity and stoichio-
metric balance between reactants is much more critical in step
polymerization relative to small molecule reactions. The
presence of a few tenths percent of an imbalance or impurity is
generally carried along in the latter and ends up as a very minor
impurity in the final product. However, the same level of
imbalance or impurity can be disastrous for polymerization --
resulting in a lowered DP which makes the product unsuitable for
a particular application.

    6. Step polymerizations have reasonably high activation
energies but are not highly exothermic (since the reaction
involves breaking and making single bonds) and the viscosity is
not too high until the very late stages of reaction. Since mixing
and thermal control will be reasonably easy, most step polymeriza-
tions are carried out as bulk (mass) polymerizations without any
added solvent or diluent.

    It should be noted that the product of a step polymerization
is a mixture of polymer molecules of different molecular weights.
The molecular weight distribution is characterized by the number-
average and weight-average degrees of polymerization, $\bar{X}_n$ and $\bar{X}_w$,
respectively, defined by

$$\bar{X}_n = \sum \underline{N}_x M_x \tag{11}$$

$$\bar{X}_w = \sum w_x M_x \tag{12}$$

where $\underline{N}_x$ and w_x are the mole-fraction and weight-fraction,
respectively, of molecules whose weight is M_x and the summations
are over all the different sizes of polymer molecules from x = 1
to x = infinity. $\bar{X}_n$ is exactly the same as DP. The ratio $\bar{X}_w/\bar{X}_n$
is useful as a measure of the polydispersity of a polymer. For
step polymerizations, this ratio is given by

$$\frac{\overline{X}_w}{\overline{X}_n} \approx (1 + p) \tag{13}$$

which indicates that the polydispersity increases with conversion and approaches 2 in the limit of complete conversion.

Step polymerization is used to synthesize multiblock copolymeric elastomers (referred to as segmented elastomers). An example is the polyester-polyurethane system produced by the reaction of a diisocyanate with a mixture of macro diol and small-sized diol (Eq. 14). The macro diol (usually referred to as a

$$nHO(ORO-CO-R'-CO)_b OR-OH + naHO-R-OH + (n+na)OCN-R''-NCO \longrightarrow$$

$$(ORO-CO-R'-CO)_b OR-O(CONH-R''-NHCO-O-R-O)_a CONH-R''-NHCO)_n \tag{14}$$
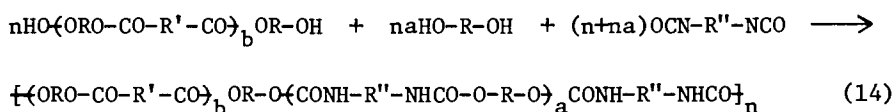
diol prepolymer) is synthesized by polyesterification between HOROH and HOOCR'COOH. An excess of HOROH is used in order to produce the macro diol having hydroxyl groups at both chain ends. The length of the polyester blocks in the multiblock copolymer is determined by the value of r in the prepolymer synthesis. The length of the polyurethane blocks is determined by the relative amounts of diol prepolymer and small-sized diol, i.e., by the value of a. The polyester and polyurethane blocks function as the soft and hard segments, respectively, of the thermoplastic elastomer. A variation of this product is the polyether-polyurethane system in which the diol prepolymer is produced by the ring-opening polymerization of a cyclic ether such as propylene oxide or tetrahydrofuran. A second type of multiblock copolymer which finds practical utility is the polyether-polyester system. Polyether blocks formed by ring-opening polymerization of a cyclic ether serve as the soft segments. Polyester blocks formed from an aromatic acid serve as the hard segments. For most multiblock copolymers, DP is in the range 1-10 for the hard blocks and 15-30 for the soft blocks.

Chain Polymerization

Monomers, such as ethylene, propylene, isobutylene, and isoprene, containing the carbon-carbon double bond undergo chain polymerization. Polymerization is initiated by radical, anionic or cationic catalysts (initiators) depending on the monomer. Polymerization involves addition of the initiating species R*, whether a radical, cation, or anion, to the double bond followed by its propagation by subsequent additions of monomer

$$CH_2=CHY \xrightarrow{R*} RCH_2-\overset{*}{C}HZ \xrightarrow{monomer} \sim\sim\sim CH_2\overset{*}{C}HZ \tag{15}$$
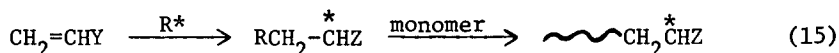
Ionic polymerizations are much more selective than radical
polymerization. All monomers except 1-alkyl and 1,1-dialkyl-
ethylenes undergo polymerization by radical initiation. Cationic
initiation is limited to monomers containing substituents
(Z = ether, 1,1-dialkyl but not monoalkyl ether) which can
stabilize the propagating center (* = + in Eq. 15) by electron-
donation. Anionic initiation requires the presence of electron-
withdrawing substituents (Z = ester, nitrile, aldehyde) to
stabilize the propagating anion. Styrene and conjugated dienes
undergo polymerization by both radical and ionic initiation.
Ethylene and 1-alkylethylenes are polymerized by Ziegler-Natta
initiators, a special class of ionic initiators. 1,2-Disubsti-
tuted ethylenes are not polymerized by any initiators due to
steric hindrance.

   Radical Polymerization. Radical chain polymerization
involves initiation, propagation, and termination. Consider the
polymerization of ethylene. Initiation typically involves thermal
homolysis of an initiator such as benzoyl peroxide

$$(\phi COO)_2 \xrightarrow{\ k_d\ } 2\ \phi COO\cdot \tag{16}$$

$$\phi COO\cdot\ +\ CH_2{=}CH_2 \longrightarrow \phi COOCH_2CH_2\cdot \tag{17}$$
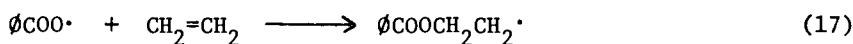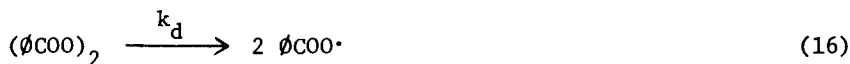
(Other methods of producing the initiating radicals include
photochemical and redox reactions.) Initiation is followed by
propagation of the radical by the successive additions of very
large numbers (usually thousands) of monomer molecules

$$\sim\!\!\sim\!\!CH_2CH_2\cdot\ +\ CH_2{=}CH_2 \xrightarrow{\ k_p\ } \sim\!\!\sim\!\!CH_2CH_2CH_2CH_2\cdot \tag{18}$$
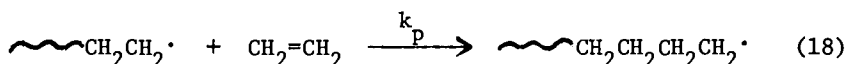
Propagation ceases when two propagating radicals annihilate each
other by combination

$$2\ \sim\!\!\sim\!\!CH_2CH_2\cdot \xrightarrow{\ k_t\ } \sim\!\!\sim\!\!CH_2CH_2CH_2CH_2\!\!\sim\!\!\sim \tag{19}$$
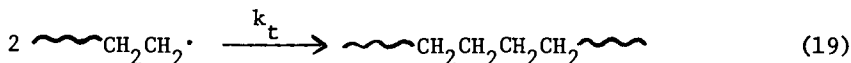
(Disproportionation between propagating radicals also occurs.)
   The characteristic of chain polymerization which distin-
guishes it from step polymerization is the rapid growth of high
molecular weight polymer. Propagation is favored over termination
since large propagation rate constants (10^2-10^4 liter/mole-sec.)
are coupled with high monomer concentrations (1-10 molar) and
very low radical concentrations (10^{-7}-10^{-9} molar). Thousands or
more monomer molecules add to a propagating radical in times of
10^{-1}-10 seconds. High molecular weight polymer is produced from

the very beginning and continuously throughout the polymerization.
At any instant only two types of species exist -- monomer and
polymer. High conversion is not a requirement for high molecular
weight. Molecular weight is essentially independent of conversion
except for variations due to the changes occurring in the con-
centrations of reactants with conversion.

The polymerization rate R_p is given by the rate of propaga-
tion

$$R_p = k_p [M \cdot][M] \tag{20}$$

where [M·] is the concentration of propagating radicals. [M·] is
difficult to accurately determine and Eq. 20 can be put in a more
useful form by introducing the steady-state assumption that the
initiation and termination rates are equal

$$R_i = k_d[I] = R_t = k_t[M \cdot]^2 \tag{21}$$

Combination of Eqs. 20 and 21 yields

$$R_p = \frac{k_p[M](k_d[I])^{1/2}}{k_t^{1/2}} \tag{22}$$

where [M] and [I] are the concentrations of monomer and initiator,
respectively. Noting that the average number of monomer molecules
adding to a propagating radical is given by the propagation rate
divided by the initiation rate, the degree of polymerization is
derived as

$$DP = \frac{k_p[M]}{(k_d k_t[I])^{1/2}} \tag{23}$$

Successful application of radical polymerization requires the
appropriate choice of the specific initiator to achieve the
desired initiation rate at the desired reaction temperature and
the realization that higher polymerization rates achieved by
increasing the initiation rate (either by increasing [I] or k_d)
come at the expense of lowered molecular weights. Higher radical
concentrations result in more propagating chains but each
propagates for a shorter time.

Polymer molecular weight is always found to be lower than the
value described in Eq. 23 due to radical displacement (chain
transfer) reactions of the type

$$\sim\!\!\sim\!\!\sim\!CH_2CH_2\cdot \;\; + \;\; XA \;\; \xrightarrow{\;\;k_{tr}\;\;} \;\; \sim\!\!\sim\!\!\sim\!CH_2CH_2X \;\; + \;\; A\cdot \qquad (24)$$

where XA may be monomer, polymer, initiator, solvent or any other substance. Chain transfer decreases the size of a polymer molecule by prematurely terminating growth of the propagating chain. The polymerization rate is usually not affected by chain transfer since A$\cdot$ is sufficiently reactive to reinitiate polymerization. The DP in the presence of chain transfer reactions is given by

$$\frac{1}{DP} \;\; = \;\; \frac{(k_d k_t [I])^{1/2}}{k_p [M]} + k_{tr,M} + \frac{k_{tr,I} [I]}{k_p [M]} + \frac{k_{tr,S} [S]}{k_p [M]} \qquad (25)$$

where $k_{tr,M}$, $k_{tr,I}$, and $k_{tr,S}$ are the rate constants for chain transfer to monomer, initiator, and solvent (or other added substance S), respectively. Equation 25 describes how polymer molecular weight is controlled at the desired level -- by the appropriate choice of all components of the reaction system (which defines the values of the various rate constants) and their concentrations. In some polymerizations, this may involve the deliberate addition of a highly active transfer agent such as n-butyl mercaptan to decrease the molecular weight to the desired level. A particular transfer reaction -- transfer of a propagating radical with polymer -- is important with certain monomers and has a significant effect on the properties of the final product. Such transfer leads to branch formation which decreases the ability of the polymer to crystallize and increases its viscosity.

   Other considerations important in carrying out radical polymerizations include:

   1. The effect of temperature on the polymerization rate and DP manifests itself by the effects of temperature on initiation, propagation, and termination. The propagation and termination steps have small activation energies (about 5-10 and 2-5 kcal/mole, respectively) while initiation by thermal decomposition of a catalyst has a large activation energy (about 30-35 kcal/mole). The overall result is that the polymerization rate increases rapidly with increasing temperature while DP decreases. The difference is due to DP being inversely dependent on initiation while the polymerization rate is directly dependent. It is important that attempts to increase the polymerization rate by increasing the temperature take into account the decrease in DP. Higher polymerization rates are obtained at the expense of lower molecular weight. Polymerizations initiated by redox reactions or photolysis are less sensitive to temperature because the initiation steps have smaller activation energies.

   2. Although the polymerization rate increases with

temperature, the polymerization of many monomers becomes appreciably reversible at higher temperature. For a particular monomer at a particular concentration, there will be an upper temperature limit -- the ceiling temperature -- at which polymerization does not occur.

   3. Physical control (i.e., thermal control, ease of stirring) of polymerization is more difficult than in step polymerization since the reaction is highly exothermic ($\Delta H \sim -20$ kcal/mole for conversion of π-bonds to σ-bonds), the rate increases rapidly with increasing temperature ($E_a \sim 20$ kcal/mole), and the viscosity of the reaction system increases rapidly throughout the process (since high molecular weight polymer is produced early and continuously). The rates of step polymerizations are less sensitive to temperature (since the reaction is only moderately exothermic) and viscosity does not increase greatly until high conversions are reached.

   4. Most polymerizations proceed with autoacceleration as the increasing viscosity of the reaction system results in an increase in the $k_p/k_t^{1/2}$ ratio. Both k_p and k_t decrease with increasing viscosity but k_t decreases more than does k_p since termination involves reaction between two large-sized species while propagation involves reaction between one large and one small species.

   5. Polymerization is inhibited or retarded by the presence of certain substances, e.g., p-benzoquinone, 4-t-butylcatechol, 1,3,5-trinitrobenzene, and oxygen. These substances react with radicals to yield species which are no longer capable of chain propagation. The deliberate addition of such substances is useful for stabilizing monomers during transportation and storage. The removal of retarders and inhibitors is often required prior to polymerization; the alternate approach is to use extra amounts of initiator.

   6. The molecular weight distributions in chain polymerizations are broader than in step polymerization. The ratio $\bar{X}_w/\bar{X}_n$ can reach as high as 5-10 due to the autoaccelerative effect and as high as 20-50 due to chain transfer to polymer.

   7. Emulsion polymerization, involving the polymerization of monomers that are in the form of emulsions, offers certain advantages relative to polymerizations of bulk monomer or monomer in solution or suspension. Radicals are produced in an aqueous phase and then migrate into the colloidal particles, referred to as micelles, where propagation takes place with an on-off mechanism. Immediate termination occurs whenever a radical enters a micelle containing a propagating radical since the micelle size is such that the presence of two radicals corresponds to an exceptionally high molar radical concentration. Thus, the entry into a micelle of each odd-numbered radical corresponds to initiation and propagation while the entry of each even-numbered radical corresponds to termination. The rate and degree of polymerization are given by
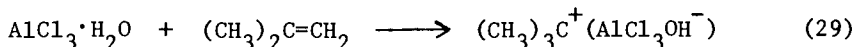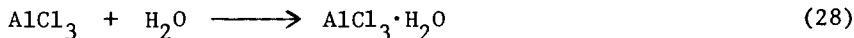
$$R_p = \frac{Nk_p[M]}{2} \tag{26}$$

$$DP = \frac{Nk_p[M]}{R_i} \tag{27}$$

where N is the concentration of micelles. Emulsion polymerization has the unique feature that both R_p and DP can be increased by increasing N. For other radical polymerizations, increasing R_p by altering a parameter (e.g., R_i or temperature) almost always results in a simultaneous decrease in DP. Increased molecular weights are quite compatible with increased polymerization rates in emulsion polymerization. Emulsion polymerization is especially useful for monomers such as 1,3-dienes whose $k_p/k_t^{1/2}$ ratios are small. Polymerization of such monomers in bulk, solution, or suspension yields low rates and low molecular weights. High rates and high molecular weights are achieved in emulsion polymerization by using high concentrations of micelles.
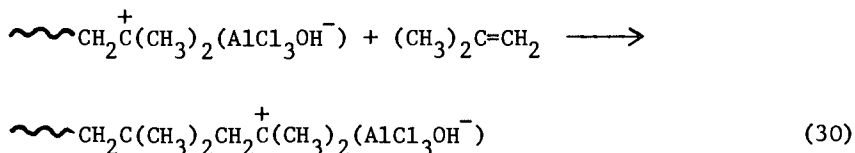
Ionic Polymerization. Ionic polymerizations, especially cationic polymerizations, are not as well understood as radical polymerizations because of experimental difficulties involved in their study. The nature of the reaction media is not always clear since heterogeneous initiators are often involved. Further, it is much more difficult to obtain reproducible data because ionic polymerizations proceed at very fast rates and are highly sensitive to small concentrations of impurities and adventitious materials. Butyl rubber, a polymer of isobutene and isoprene, is produced commercially by cationic polymerization. Anionic polymerization is used for various polymerizations of 1,3-butadiene and isoprene.

A variety of initiators have been used for cationic polymerization. The most useful type of initiation involves the use of a Lewis acid in combination with small concentrations of water or some other proton source. The two components of the initiating system form a catalyst-cocatalyst complex which donates a proton to monomer

$$AlCl_3 + H_2O \longrightarrow AlCl_3 \cdot H_2O \tag{28}$$

$$AlCl_3 \cdot H_2O + (CH_3)_2C=CH_2 \longrightarrow (CH_3)_3C^+(AlCl_3OH^-) \tag{29}$$

Protonic acids are less suitable because the conjugate base is too active a nucleophile. HCl, for example, will not initiate polymerization because chloride ion adds immediately to the carbenium ion before the latter can propagate. Other initiators which have been studied include electroinitiation, photoinitiation and ionizing radiation.

Propagation proceeds by successive additions of monomer molecules to the carbenium ion center

$$\sim\sim CH_2\overset{+}{C}(CH_3)_2(AlCl_3OH^-) + (CH_3)_2C{=}CH_2 \longrightarrow$$

$$\sim\sim CH_2C(CH_3)_2CH_2\overset{+}{C}(CH_3)_2(AlCl_3OH^-) \tag{30}$$

Since the solvents used (e.g., chlorinated hydrocarbons, benzene, THF) are only mildly polar, the negative counter-ion will be held near the propagating carbenium ion center. Highly polar solvents are not generally useful since they either react with and destroy the initiator and propagating centers or deactivate them by strong complexation.

Termination occurs either by expulsion of H^+ and $AlCl_3OH^-$ from the propagating chain end

$$\sim\sim CH_2\overset{+}{C}(CH_3)_2(AlCl_3OH^-) \longrightarrow \sim\sim CH{=}C(CH_3)_2 + H^+(AlCl_3OH^-) \tag{31}$$

or chain transfer of a negative fragment from the counter-ion to the carbenium ion center

$$\sim\sim CH_2\overset{+}{C}(CH_3)_2(AlCl_3OH^-) \longrightarrow \sim\sim CH_2CCl(CH_3)_2 + AlCl_2OH \tag{32}$$

Chain transfer reactions with solvent or some other component of the reaction system also occur (Eq. 33).

$$\sim\sim CH_2\overset{+}{C}(CH_3)_2(AlCl_3OH^-) + XA \longrightarrow$$

$$\sim\sim CH_2C(CH_3)_2A + X^+(AlCl_3OH^-) \tag{33}$$
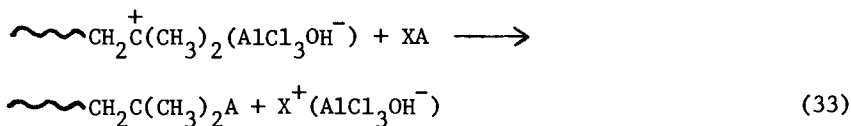
The kinetic expressions which describe the rate and degree of polymerization in cationic polymerizations are derived in a manner analogous to that for radical polymerization. The results are similar with the main difference being that the direct and inverse dependencies of the rate and degree of polymerization, respectively, on the initiator concentration or initiation rate are both first-order, not half-order as in radical polymerization. The difference arises from cationic termination being mono-molecular in the propagating species instead of bimolecular as in radical polymerization.
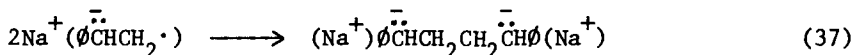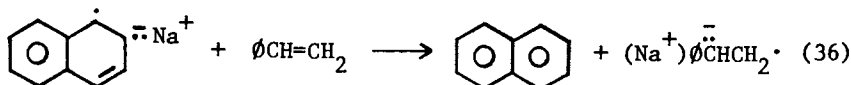
Anionic polymerization can be initiated by a variety of anionic sources such as metal alkoxides, aryls, and alkyls. Alkyllithium initiators are among the most useful, being employed commercially in the polymerization of 1,3-butadiene and isoprene, due to their solubility in hydrocarbon solvents. Initiation involves addition of alkyl anion to monomer

$$R^-(Li^+) + CH_2CH\phi \longrightarrow RCH_2-\ddot{\overset{-}{C}}H\phi \tag{34}$$
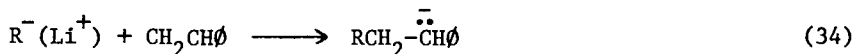
An interesting initiator is the naphthalene radical-anion formed by electron-transfer from sodium to naphthalene

$$\tag{35}$$
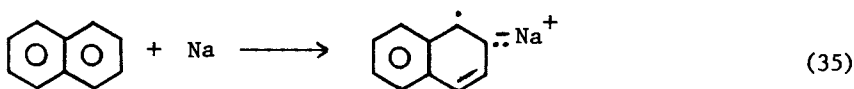
The naphthalene radical-anion transfers an electron to a monomer such as styrene to form the styryl radical-anion which dimerizes to a dianion

$$+ (Na^+)\phi\ddot{\overset{-}{C}}HCH_2\cdot \tag{36}$$

$$2Na^+(\phi\ddot{\overset{-}{C}}HCH_2\cdot) \longrightarrow (Na^+)\phi\ddot{\overset{-}{C}}HCH_2CH_2\ddot{\overset{-}{C}}H\phi(Na^+) \tag{37}$$

Propagation proceeds at both ends of the dianion.

The anionic polymerizations of polar monomers, such as methyl methacrylate, methyl vinyl ketone and acrylonitrile, are complicated since these monomers contain substituents that are reactive toward nucleophiles. This leads to termination and side reactions competitive with both initiation and propagation, resulting in complex polymer structures. For many anionic polymerizations of nonpolar monomers, such as styrene, isoprene, and 1,3-butadiene, there are no effective termination reactions. Termination by combination with a metal counter-ion does not occur. Propagation occurs with complete consumption of monomer and the propagating anionic centers remain intact as long as one employs solvents such as benzene, n-hexane, THF and 1,2-dimethoxyethane, which are inactive in transferring a proton to the propagation anion. These polymerizations, referred to as living polymerizations, are terminated when desired by the deliberate addition of a proton source such as water or alcohol. The degree of polymerization for a living polymerization is given by the ratio of concentrations of monomer and living anionic propagating centers $[M^-]$
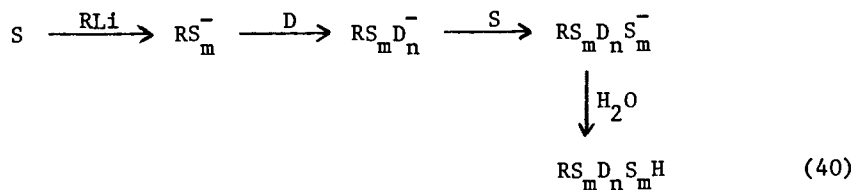
$$DP = \frac{[M]}{[\overline{M}\,]} \tag{38}$$

For the usual situation where all of the initiator I is converted into propagating centers, Eq. 38 becomes

$$DP = \frac{[M]}{[I]} \qquad or \qquad DP = \frac{2[M]}{[I]} \tag{39}$$

depending on whether propagation involves a monoanionic propagating species (Eq. 34) or dianionic species (Eq. 37). A consequence of the absence of termination is that the molecular weight distribution will be quite narrow ($\overline{M}_w/\overline{M}_n$ approaches 1.1) provided that initiation occurs much faster than propagation so that all propagating centers grow for the same length of time.

Sequential addition of different monomer charges to a living anionic polymerization system is useful for producing well-defined block copolymers. Thermoplastic elastomers of the triblock type are the most important commercial application. For example, a styrene-isoprene-styrene triblock copolymer is synthesized by the sequence

$$S \xrightarrow{\text{RLi}} RS_m^- \xrightarrow{\text{D}} RS_mD_n^- \xrightarrow{\text{S}} RS_mD_nS_m^-$$

$$\downarrow H_2O$$

$$RS_mD_nS_mH \tag{40}$$

Styrene(S) is polymerized to polystyryl anions using butyllithium and then the diene (D) added. A second charge of styrene is added after the diene monomer is consumed, followed by the addition of a terminating agent. The length of each of the three blocks is controlled by the ratio of the concentrations of the respective monomer and initiator according to Eq. 39. The optimum combination of the required physical strength and elastic behavior is generally obtained when the DP of the hard, polystyrene blocks is 100-200 and the DP of the soft, polydiene blocks is 1000-2000. Variations of the procedure include the use of a difunctional initiator such as a dilithium compound or sodium-naphthalene. The diene monomer is polymerized via a dianion propagating species and then styrene added. Styrene polymerizes on both sides of the polydienyl dianion to produce the triblock copolymer. Coupling reactions have also been used, e.g., living polystyrene-polydienyl anions can be coupled with a dibromo compound (Eq. 41). The use

$$RS_mD_n^- \xrightarrow{\text{BrR'Br}} RS_mD_nR'D_nS_mR \tag{41}$$

of multifunctional coupling agents such as $SiCl_4$ or dienes produces star (radial) and comb block copolymers.

Both anionic and cationic polymerizations have several features in common:

1. Ionic polymerizations are very sensitive to changes in the solvent due to alterations in the nature of the propagating center. Two types of propagating species coexist -- the free ion and the ion-pair. The ion-pair consists of the propagating center and its tightly held counter-ion. The free ion consists of the propagating center separated from the counter-ion by solvent. Propagations of the ion-pair and free ion occur concurrently in a reaction system. The ion-pair is the more plentiful species in all solvents used in ionic polymerizations although the relative concentration of the free ions increases with solvent polarity. However, since the propagation rate constants for free ions are usually several orders of magnitude higher than those for ion-pairs, even small changes in the free ion concentration result in large changes in the observed polymerization rates. For example, the polymerization rate for styrene by sodium naphthalene at 20°C is increased by three orders of magnitude in 1,2-dimethoxyethane compared to benzene. The identity of the counter-ion also affects polymerization as larger, less tightly held counter-ions leading to higher concentrations of free ions and higher reactivity for the ion-pair. Changes in solvent and counter-ion have correspondingly large effects on polymer molecular weights, activation energies, and overall kinetics.

2. Temperature often has a large effect on polymerization rates and polymer molecular weights. The effect of temperature, which usually manifests itself through changes in the termination mode or in the relative concentrations of free ions and ion-pairs, varies considerably depending on the initiator and solvent. Some cationic polymerizations show the unusual behavior of a decrease in rate with increasing temperature due to the termination rate constant increasing faster with increasing temperature than the initiation and propagation rate constants.

3. Ionic polymerizations are generally much faster than radical polymerizations. Both cationic and anionic polymerizations typically proceed with much higher concentrations of propagating centers (10^{-4}–10^{-2} molar) than in radical polymerizations (10^{-9}–10^{-7} molar) since ionic propagating centers do not annihilate each other as do radicals.
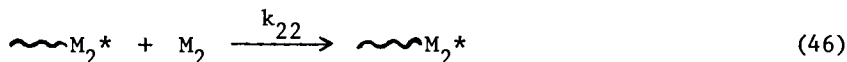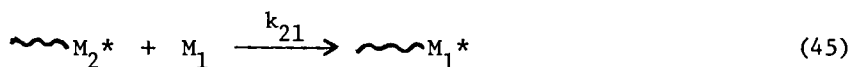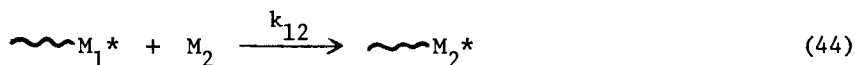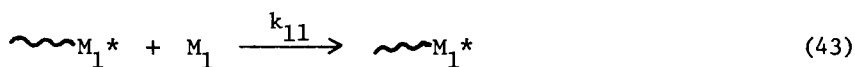
Copolymerization. Chain copolymerization, the polymerization of a mixture of two monomers, yields a copolymer with two different repeating units distributed along the polymer chain

$$M_1 + M_2 \longrightarrow \sim\sim\sim M_1 M_2 M_2 M_2 M_1 M_1 M_2 M_1 M_1 M_1 M_1 \sim\sim\sim \qquad (42)$$
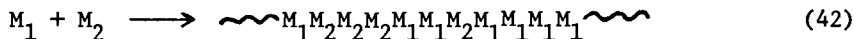
Copolymerization allows one to advantageously alter the properties

of a homopolymer. A number of elastomers are copolymers. Butyl
rubber is a copolymer of isobutylene containing 1-2% isoprene.
The isoprene units in the copolymer impart the ability to cross-
link the product. Polystyrene is far too rigid to be used as an
elastomer but styrene copolymers with 1,3-butadiene (SBR rubber)
are quite flexible and rubbery. Polyethylene is a crystalline
plastic while ethylene-propylene copolymers and terpolymers of
ethylene, propylene and diene (e.g., dicyclopentadiene, hexa-1,4-
diene, 2-ethylidenenorborn-5-ene) are elastomers (EPR and EPDM
rubbers). Nitrile or NBR rubber is a copolymer of acrylonitrile
and 1,3-butadiene. Vinylidene fluoride-chlorotrifluoroethylene
and olefin-acrylic ester copolymers and 1,3-butadiene-styrene-
vinyl pyridine terpolymer are examples of specialty elastomers.
    The properties of a copolymer are dependent on the identity
of the two monomers and their relative proportions within the
copolymer chain. The latter, referred to as the copolymer
composition, is determined by the competition among the four
propagation reactions

$$\sim\sim M_1^* \;+\; M_1 \;\xrightarrow{\;k_{11}\;}\; \sim\sim M_1^* \tag{43}$$

$$\sim\sim M_1^* \;+\; M_2 \;\xrightarrow{\;k_{12}\;}\; \sim\sim M_2^* \tag{44}$$

$$\sim\sim M_2^* \;+\; M_1 \;\xrightarrow{\;k_{21}\;}\; \sim\sim M_1^* \tag{45}$$

$$\sim\sim M_2^* \;+\; M_2 \;\xrightarrow{\;k_{22}\;}\; \sim\sim M_2^* \tag{46}$$

where the * represents a radical, anionic or cationic proprogating
center depending on the initiator used. There are two types of
propagating centers -- those ending in M_1 and those ending in M_2.
Each type of propagating center can react with either of the two
monomers, M_1 or M_2. The mole fraction of monomer 1 incorporated
into the copolymer, F_1, is dependent on the mole fraction of
monomer 1 in the comonomer feed, f_1, and on the four propagation
rate constants according to

$$F_1 \;=\; \frac{r_1 f_1^2 + f_1 f_2}{r_1 f_1^2 + 2 f_1 f_2 + r_2 f_2^2} \tag{47}$$

where $r_1 = k_{11}/k_{12}$ and $r_2 = k_{22}/k_{21}$. r_1 and r_2 are referred to as
the monomer reactivity ratios.
    The copolymer composition is usually different from the

comonomer feed, the difference between F_1 and f_1 depending on the values of r_1 and r_2. The monomer reactivity ratios for any comonomer pair are unique for that particular pair of monomers. For example, r_1 and r_2 for styrene-1,3-butadiene are different from r_1 and r_2 for acrylonitrile-1,3-butadiene. Further, the r_1 and r_2 values for a comonomer pair differ depending on the particular type of propagating center (radical, cationic, anionic). Ionic copolymerizations, like ionic polymerizations, are selective compared to their radical counterparts. Only selected comonomer pairs undergo ionic copolymerization. Thus, a pair such as methyl vinyl ether-acrylonitrile will not undergo either cationic or anionic copolymerization since acrylonitrile is unreactive toward cationic propagating centers while methyl vinyl ether is unreactive toward anionic propagating centers. The opposite behavior is typical of radical copolymerization -- almost any pair of monomers undergoes copolymerization since almost all monomers show some reactivity toward radical propagating centers. The net result is that most commercial applications of copolymerization involve radical copolymerization. The main exceptions are Butyl rubber synthesized by cationic copolymerization, EPR and EPDM rubbers by coordination copolymerization (see below), and some styrene-1,3-butadiene copolymers by anionic or coordination copolymerization.

Stereochemistry; Coordination Polymerization. Stereoisomerism is possible in the polymerization of alkenes and 1,3-dienes. Polymerization of a monosubstituted ethylene, such as propylene, yields polymers in which every other carbon in the polymer chain is a chiral center. The substituent on each chiral center can have either of two configurations. Two ordered polymer structures are possible -- isotactic (XII and syndiotactic (XIII) -- where the substituent R groups on
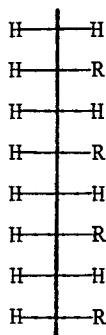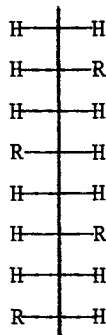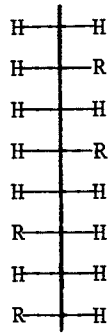
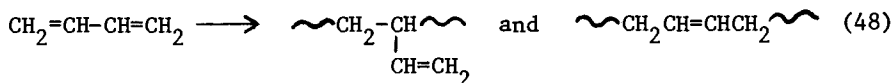XII   XIII   XIV

successive chiral carbons have the same or opposite configurations, respectively. The unordered polymer with random placement

of the substituents along the polymer chain is referred to as the
atactic structure. Polymerization of conjugated dienes such as
1,3-butadiene can proceed by 1,2- and 1,4-polymerization

$$CH_2=CH-CH=CH_2 \longrightarrow \quad \sim\!\!\sim\!CH_2-CH\!\sim\!\!\sim \quad \text{and} \quad \sim\!\!\sim\!CH_2CH=CHCH_2\!\sim\!\!\sim \quad (48)$$
$$\underset{\displaystyle CH=CH_2}{\big|}$$

Isotactic, syndiotactic, and atactic polymers are possible for
1,2-polymerization -- analogous to the situation for a mono-
substituted ethylene. 1,4-Polymerization yields polymers in
which the repeating unit can be either cis (XV) or trans (XVI)
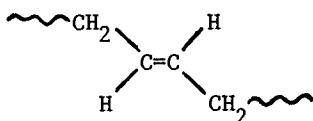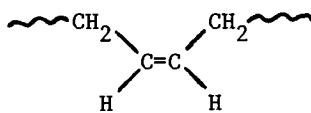
XV   XVI

The polymer structure produced in any polymerization is
highly sensitive to the catalyst, solvent, and temperature.
Radical polymerization of 1,3-dienes proceeds with 1,4-polymer-
ization preferred over 1,2-polymerization and trans-1,4-polymer-
ization over cis-1,4-polymerization. 1,4-Polymerization
predominates since there is less steric hindrance at carbon-4
relative to carbon-2 and the 1,4-polymer is more stable than the
1,2-polymer. The preference for trans-1,4-polymerization is due
to the greater stability of the trans-1,4-polymer compared to the
cis-1,4-polymer. These preferences are greater at lower
polymerization temperatures; higher temperatures lead to more
random placement of successive monomer units in the polymer chain.
The trends for cationic polymerization are similar although
cationic polymerization of 1,3-dienes is not of practical
interest (except for Butyl rubber) as the products are usually
low molecular weight with extensive cyclization. Anionic
polymerizations in polar solvents (where the counter-ion is only
weakly coordinated with the propagating center) favor 1,2-
polymerization over 1,4-polymerization. The anionic propagating
center at carbon-2 is not extensively delocalized onto carbon-4
as in the corresponding radical species since the double bond,
while a strong electron-donor, is a weak electron-acceptor.
Trans-1,4-placement is favored over cis-1,4-placement as in
radical polymerization.
The situation changes dramatically when anionic polymeriza-
tions are carried out under reaction conditions such that there
is strong coordination among the counter-ion, propagating center,
and monomer. Thus, when lithium is the counter-ion and
polymerization takes place in a solvent of low polarity, the

results are in the opposite direction to those with lithium ion
in a polar solvent or with weakly coordinating counter-ions such
as sodium, potassium, and cesium -- 1,4-polymerization is favored
over 1,2-polymerization and cis-1,4- over trans-1,4-polymeriza-
tion. The most remarkable results are observed with the Ziegler-
Natta catalysts, which are obtained by combining a transition
metal derivative (e.g., $TiCl_4$, $TiCl_3$, $Co_2(CO)_8$, $Cr(CN\emptyset)_6$, VCl_3)
with a Group I-III metal derivative (e.g., AlR_3, AlR_2Cl). Very
high degrees of specificity are observed in polymerizations
initiated by these catalysts. One can synthesize either the cis-
1,4-polymer or the trans-1,4-polymer or the 1,2-polymer, each in
high purity (> 95% pure), by the appropriate choice of the
components of the catalyst system. For example, trans-1,4-
polybutadiene is obtained using $TiCl_3/AlR_3$ or VCl_3/AlR_2Cl, cis-
1,4-polybutadiene using TiI_4/AlR_3 or Co chelates/AlR_3 or
$U(OR)_4/AlRCl_2$, and 1,2-polybutadiene using $Ti(OR)_4/AlR_3$ or
V(acetylacetonate)/AlR_3. The detailed mechanism(s) by which
certain catalysts yield the trans-1,4-polymer, others the cis-
1,4-polymer, and still others the 1,2-polymers are not understood.
The identity of the counter-ion is probably decisive in determin-
ing the coordination among counter-ion, propagating center, and
monomer -- which in turn determines the manner in which monomer
is "allowed" to enter the polymer chain. Such polymerizations
are referred to as coordination polymerizations. Although
coordination polymerization is not well understood, the synthetic
polymer chemist has the empirical data available to produce either
the cis-1,4- or trans-1,4- or 1,2-polymer as desired. Coordina-
tion polymerization also achieves high specificity in the
polymerizations of alkenes -- isotactic, syndiotactic or atactic
polymers can be obtained. However, these polymers are not useful
as elastomers with the exception of the ethylene-propylene
copolymer and ethylene-propylene-diene terpolymer rubbers. These
rubbers can only be produced by the Ziegler-Natta catalysts.
(Coordination polymerization is commercially important for the
production of isotactic polypropylene which finds extensive use
as a plastic.)
     Polymer stereochemistry is important because of its effect
on the physical properties of an elastomer. For example, cis-
1,4-polyisoprene has very low crystallinity, low T_m and T_g values,
and is an excellent elastomer over a considerable temperature
range. About two billion pounds per year of cis-1,4-polyisoprene
are used in the United States for tires, coated fabrics, molded
objects, adhesive, rubber bands, and other typical elastomer
applications. Trans-1,4-polyisoprene, since it crystallizes to a
significant extent (due to its higher symmetry compared to the
cis-isomer) and has higher T_m and T_g, is a much harder and much
less rubbery elastomer. Small amounts of trans-1,4-polyisoprene
are used in manufacturing golf balls and for electrical cable
covering. It is interesting to note that both the cis- and
trans-1,4-polyisoprenes are found in nature. Hevea rubber,

containing more than 98% of the double bonds in the cis configura-
tion, is the major naturally occurring 1,4-polyisoprene. Gutta
percha or balata is predominantly the trans isomer. Both cis-
and trans-1,4-polyisoprenes have been synthesized commercially
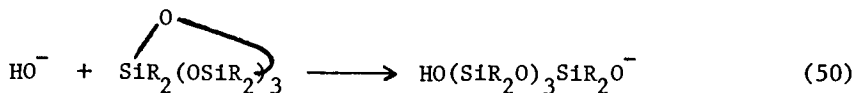using coordination polymerization processes.

1,4-Polybutadienes with high cis-1,4 and mixed cis-1,4/trans-
1,4 contents are produced commercially using Ziegler-Natta or
lithium catalysts. The high cis elastomer crystallizes on
stretching whereas the mixed cis/trans elastomer shows no tendency
to crystallize. The high cis elastomer has higher strength but
poorer low temperature properties compared to the mixed cis/trans
elastomer. SBR, NBR, and Neoprene (polychloroprene) rubbers,
produced by radical emulsion polymerization, are high trans-1,4-
polymers with minor amounts of cis-1,4 and 1,2-units. Some
variations in stereochemistry (as well as molecular weight and
branching) are achieved by varying the polymerization temperature.
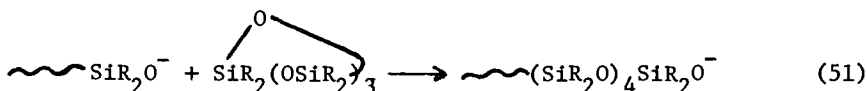
Ring-Opening Polymerization

Ring-opening polymerization of cyclic monomers, usually by
anionic or cationic catalysts, is another route to elastomers.
These include the polymerization of octamethylcyclotetrasiloxane

$$
\text{(49)}
$$
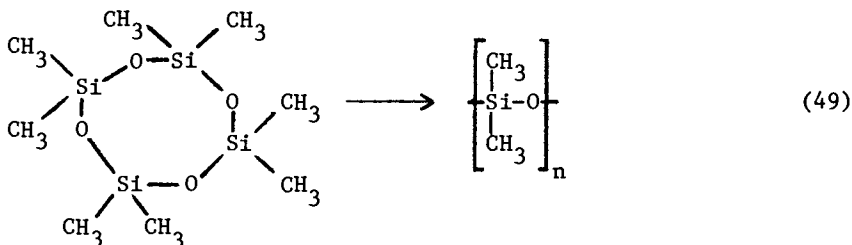
to yield a silicone elastomer. Silicones (also called poly-
siloxanes) can also be synthesized by step polymerization of
chlorosilanes but the molecular weights are lower due to the
difficulty of obtaining sufficiently high purity monomers. Ring-
opening polymerization of the cyclotetrasiloxane is accomplished
commercially using an anionic initiator such as sodium hydroxide.
Both initiation

$$
\text{HO}^- + \text{SiR}_2(\text{OSiR}_2)_3 \longrightarrow \text{HO}(\text{SiR}_2\text{O})_3\text{SiR}_2\text{O}^- \qquad (50)
$$

and propagation

$$\sim\!\!\sim\!\!\text{SiR}_2\text{O}^- + \text{SiR}_2(\text{OSiR}_2)_3 \longrightarrow \sim\!\!\sim\!\!(\text{SiR}_2\text{O})_4\text{SiR}_2\text{O}^- \qquad (51)$$

involve a nucleophilic attack by silanoate anion on monomer. Termination probably occurs by proton transfer from water or other species present. Most ring-opening polymerizations, like the above polymerization, bear a striking resemblance to chain polymerizations in that there is initiation, propagation, and termination. However, they are analogous to step polymerizations in that the polymer molecular weight builds up slowly.

Other polymerizations of commercial interest are the polymerizations of epichlorohydrin with aluminum or zinc alkyls with

$$\text{CH}_2\!\!-\!\!\text{CH-CH}_2\text{Cl} \longrightarrow \{\text{CH}_2\text{-CH-O}\}_n \qquad (52)$$
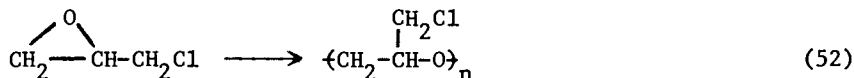
water or alcohol (Eq. 50) as well as copolymerization with ethylene oxide, the polymerization of cyclopentene with $MoCl_5$,

$$\longrightarrow \{\text{CH}_2\text{CH=CHCH}_2\text{CH}_2\}_n \qquad (53)$$
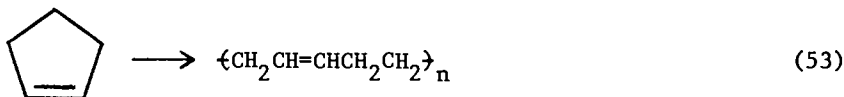
WCl_6, and vanadium-based initiators (Eq. 53), and the thermal polymerization of hexachlorocyclotriphosphazene (Eq. 54). (Ring-opening polymerizations of ethylene and propylene oxides,

$$\longrightarrow \{\text{N=PCl}_2\}_n \qquad (54)$$
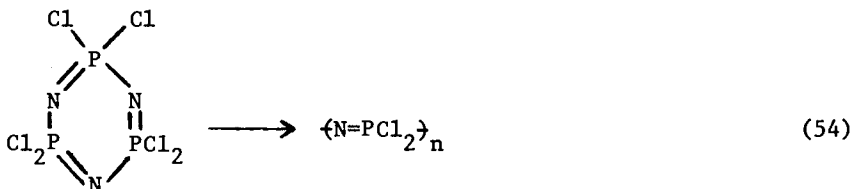
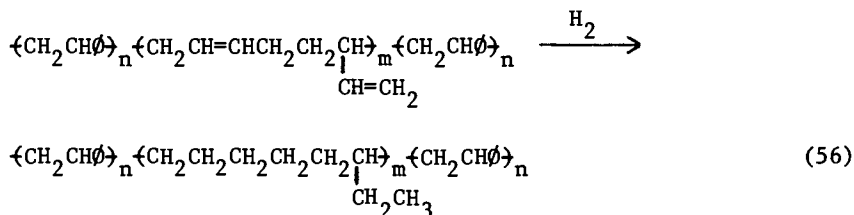ε-caprolactam and ethylenimine yield useful plastics and fibers.)

Modification of Elastomers by Chemical Reaction

Chemical reactions are used to modify existing polymers, often for specialty applications. Although of considerable importance for plastics, very few polymer reactions (aside from crosslinking) are important for elastomers. Chlorination and bromination of Butyl rubber to the extent of about one halogen atom per isoprene unit yields elastomers which are more easily crosslinked than Butyl rubber. Substitution occurs with rearrangement to yield an allylic halide structure

$$\sim\sim\sim CH_2\overset{\overset{\displaystyle CH_3}{|}}{C}=CH-CH_2\sim\sim\sim \quad\xrightarrow{\quad Cl_2\quad}\quad \sim\sim\sim CH=\overset{\overset{\displaystyle CH_3}{|}}{C}-CHCl-CH_2\sim\sim\sim \qquad (55)$$

Chlorination of natural rubber, involving both addition and substitution (with some cyclization), yields a product with improved chemical and corrosion resistance. Chlorination of polyethylene in the presence of sulfur dioxide results in substituting both chloride and sulfonyl chloride groups into the polymer. A commercially useful material is one which contains about 12 chlorides and one sulfonyl chloride per 40-45 repeating units. This extensive substitution converts the polyethylene, a plastic, into an elastomer by destroying crystallinity.

A polystyrene-poly(ethylene,1-butene)-polystyrene triblock copolymer is produced by the selective hydrogenation of the corresponding triblock copolymer in which the center block consists of random placements of 1,2-poly(1,3-butadiene) and 1,4-poly(1,3-butadiene) units.

$$\{CH_2CH\phi\}_n\{CH_2CH=CHCH_2CH_2\overset{\overset{\displaystyle \hspace{0.4em}}{|}}{CH}\}_m\{CH_2CH\phi\}_n\quad\xrightarrow{\quad H_2\quad}$$
$$\hspace{7em}CH=CH_2$$

$$\{CH_2CH\phi\}_n\{CH_2CH_2CH_2CH_2CH_2\overset{\overset{\displaystyle \hspace{0.4em}}{|}}{CH}\}_m\{CH_2CH\phi\}_n\qquad (56)$$
$$\hspace{7em}CH_2CH_3$$

The ethylene-1-butene block cannot be obtained directly since the two monomers do not undergo anionic copolymerization.
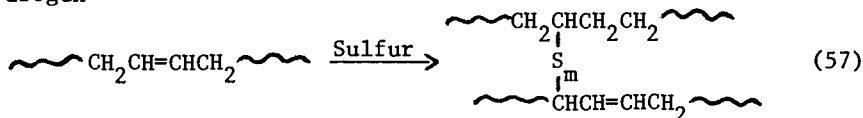
Crosslinking

Approximately 10 billion pounds per year of elastomers are used in the United States. Crosslinking is a requirement if elastomers are to have their essential property of rapidly and completely recovering from deformations. The terms vulcanization and curing are used synonymously with crosslinking. Crosslinking is achieved either by chemical reaction or physical aggregation depending on the elastomer.

Chemical Crosslinking. Only linear polymers are produced from bifunctional monomers. The reaction system must include a polyfunctional monomer, i.e., a monomer containing 3 or more functional groups per molecule, in order to produce a crosslinked polymer. However, the polyfunctional reactant and/or reaction conditions must be chosen such that crosslinking does not occur during polymerization but is delayed until the fabrication step. This objective is met differently depending on whether the synthesis involves a chain or step polymerization. In the typical

chain polymerization one chooses the polyfunctional monomer such
that it is bifunctional under polymerization conditions with the
remaining function(s) becoming reactive only under the conditions
of the fabrication step. The monomer is polymerized to a linear
polymer and the latter mixed with crosslinking agent (e.g.,
sulfur or a peroxide) and fabricated into the shape of the
desired product. Crosslinking takes place during the fabrication.
In the typical step polymerization between bifunctional and poly-
functional monomers, an excess of the bifunctional monomer is
used to produce a low molecular weight (1000–3000) prepolymer by
limiting the extent of reaction. Subsequent polymerization and
crosslinking of the prepolymer is achieved during fabrication by
establishing stoichiometry between X and Y functional groups by
addition of the appropriate monomer.

The 1,4-polymers of isoprene and 1,3-butadiene and some of
their copolymers (Butyl, SBR, NBR) comprise the largest group of
elastomers. Commercial vulcanization is achieved almost
exclusively by heating with sulfur. The reaction mechanism is
probably ionic and involves both sulfur addition to the double
bonds in the polymer chains and substitution at the allylic
hydrogen

$$\sim\sim CH_2 CH=CHCH_2 \sim\sim \xrightarrow{\text{Sulfur}} \begin{array}{c} \sim\sim CH_2 CHCH_2 CH_2 \sim\sim \\ | \\ S_m \\ | \\ \sim\sim CHCH=CHCH_2 \sim\sim \end{array} \qquad (57)$$
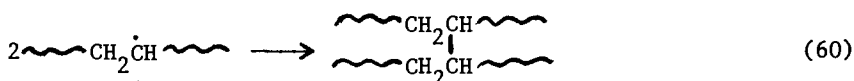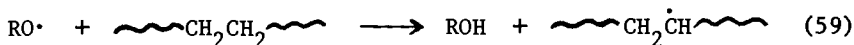
Vulcanization by heating with sulfur alone is a very inefficient
process with approximately 40–50 sulfur atoms incorporated into
the polymer per each crosslink. Sulfur is wasted by the forma-
tion of long polysulfide crosslinks (i.e., high values of m),
vicinal crosslinks which act as single crosslinks from the view-
point of physical properties, and intramolecular cyclic sulfide
structures. The rate and efficiency of vulcanization are greatly
increased by including accelerators (e.g., tetraalkylthiuram
disulfide, zinc dialkyldithiocarbamate) and activators (e.g.,
zinc oxide plus stearic acid). The physical behavior of the final
crosslinked elastomer in terms of strength, extent of elongation
prior to break, and elasticity is dependent on the crosslink
density (the number of crosslinks per repeat unit) and the value
of m. Higher crosslink densities and lower m values yield
stronger elastomers which undergo smaller elongations. Diene
polymers and copolymers are also crosslinked by heating with
p-dinitrosobenzene, phenolic resins, or maleimides for
specialty applications requiring better thermal stability than
available in the sulfur crosslinked elastomers.

Polychloroprene rubbers are not efficiently vulcanized by
sulfur. The chlorine atoms deactivate the double bonds toward
reaction with sulfur. Vulcanization is achieved by heating with
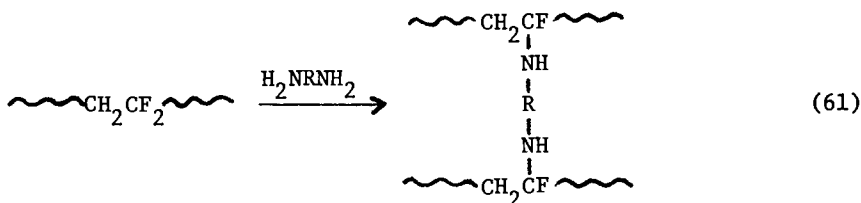zinc and magnesium oxides. Crosslinking involves the loss of

chloride with the formation of ether and/or -OZnO- crosslinks
between polymer chains. Ethylenethiourea or 2-mercaptoimidazoline
are used to accelerate the metal oxide vulcanization. The
accelerated vulcanization probably proceeds with the formation of
sulfide crosslinks between chains.

   Ethylene-propylene and silicone rubbers are crosslinked by
compounding with a peroxide such as dicumyl peroxide or di-t-
butyl peroxide and then heating the mixture. Peroxide cross-
linking involves the formation of polymer radicals via hydrogen
abstraction by the peroxy radicals formed from the decomposition
of the peroxide. Crosslinks are formed by coupling of the
polymer radicals

$$ROOR \longrightarrow 2\ RO\cdot \tag{58}$$

$$RO\cdot\ +\ \sim\sim CH_2CH_2\sim\sim \longrightarrow ROH\ +\ \sim\sim CH_2\overset{\cdot}{C}H\sim\sim \tag{59}$$

$$2\sim\sim CH_2\overset{\cdot}{C}H\sim\sim \longrightarrow \begin{array}{c}\sim\sim CH_2CH\sim\sim\\ |\\ \sim\sim CH_2CH\sim\sim\end{array} \tag{60}$$

Peroxide crosslinking has practical limitations due to its
relative inefficiency and the high cost of peroxides. The cross-
linking efficiency of polysiloxanes is increased by incorporating
a few percent of vinyl groups into the polymer through copolymer-
ization with vinylmethylsilanol. Peroxide crosslinking of the
copolymer is more efficient since crosslinks form by addition of
polymer radicals to the vinyl groups as well as by radical
coupling. Ethylene-propylene elastomers are modified by
synthesizing the EPDM terpolymers containing small amounts of
unsaturation. These can then be advantageously crosslinked by
sulfur.

   Elastomeric copolymers of vinylidene fluoride are cross-
linked by heating with diamine and basic oxide. Crosslinking
involves dehydrofluorination followed by addition of the diamine
with the metal oxide acting as an acid acceptor

$$\sim\sim CH_2CF_2\sim\sim \xrightarrow{H_2NRNH_2} \begin{array}{c}\sim\sim CH_2\overset{|}{C}F\sim\sim\\ NH\\ |\\ R\\ |\\ NH\\ |\\ \sim\sim CH_2\overset{|}{C}F\sim\sim\end{array} \tag{61}$$

   Crosslinking of polyurethanes proceeds in different ways
depending on the stoichiometry and choice of reactants and
reaction conditions. For example, an isocyanate-terminated
trifunctional prepolymer is prepared by reaction of a polyol and

a diisocyanate. (The polyol may be a hydroxyl-terminated poly-
ether or polyester prepolymer synthesized from a triol.)
Subsequent polymerization (chain extension) and crosslinking of
the isocyanate-terminated prepolymer is achieved by the addition
of a diol

$$\tag{62}$$
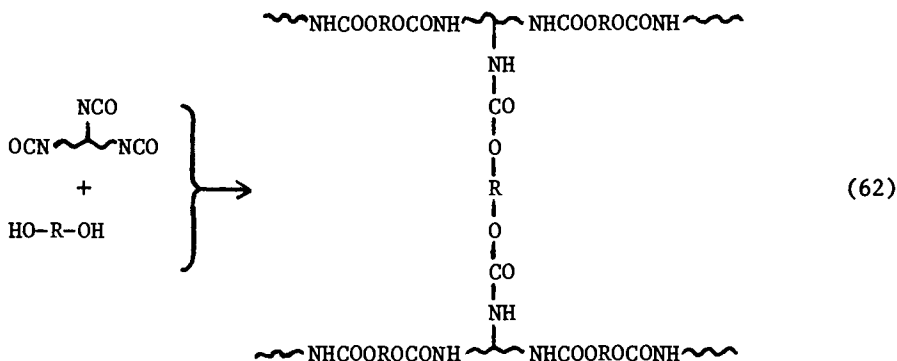
The prepolymer can also be crosslinked by using a dimine instead
of a diol. The reaction between isocyanate and amine groups
proceeds through the formation of urea linkages. A variation of
the above procedure is to directly employ a polyisocyanate
instead of producing it by reaction of a diisocyanate with the
polyol. A number of other crosslinking reactions apparently occur
during polyurethane synthesis depending on temperature, stoichio-
metry, and other reaction conditions. These include the reaction
of isocyanate groups with urethane and urea groups to yield
crosslinks through allophanate and biuret linkages, respectively,
and cyclotrimerization of isocyanate groups.
     The synthesis of polysulfide elastomers involves the use of
a small amount of trichloroalkane in addition to dichloroalkane
and sodium sulfide in order to form a branched polymer. The
prepolymer is treated with a mixture of sodium hydrosulfide and
sodium sulfite followed by acidification to convert all end-groups
to thiol groups. Further polymerization and crosslinking is
achieved by oxidative coupling of the thiol end-groups by treat-
ment with lead dioxide, p-quinone dioxime, or other oxidizing
agent

$$\tag{63}$$
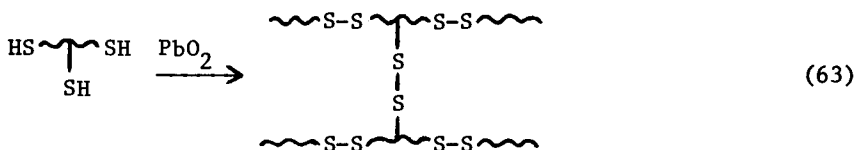
     Physical Crosslinking. A crosslinked network can also be
achieved through physical aggregation of the hard segments of

two-phase block copolymers as described in previous sections. Diblock copolymers are not useful since they do not form network structures. Only one end of the soft block is chemically linked to a domain of hard segments. The formation of a network structure requires two or more hard blocks per polymer molecule. Although this requirement is met by triblock and all higher block copolymers, only the ABA and $(AB)_n$ structures are of importance. Block copolymers in between the triblock and multiblock structures are either too difficult to synthesize with high purity or do not offer sufficient property advantages.

Most approaches to synthesizing block copolymers do not yield well-defined structures due to contamination by homopolymers and/or random copolymers. These include the mechanochemical cleavage of a mixture of two homopolymers to yield polymeric radicals which combine, exchange between functional groups of two homopolymers (e.g., polyester and polyamide), and use of a difunctional initiator (e.g., azoperoxide) in which the two initiator functions can be independently activated. There are only two synthetic approaches which yield block copolymers of predictable and controlled structure with minimum contamination by other polymers -- living anionic polymerization and step polymerization. Both approaches are successful due to certain common features. Contamination by homopolymer and diblock copolymer is minimized in living polymerization by the lack of termination and in step polymerization by stoichiometric control. The identity, location, and concentration of active functional groups for linking together the different blocks are well-defined in both approaches. Living anionic polymerization is used to synthesize triblock copolymers via sequential monomer addition alone (Eq. 40) or in combination with a coupling reaction (Eq. 41). The commercially-available triblock copolymers are those in which polystyrene is the hard block and polyisoprene or poly-butadiene is the soft block. The advantages of living polymerization are control of block length and narrow molecular weight distribution. However, living polymerization is limited to a relatively few monomers -- styrene, isoprene, butadiene. Many monomers, e.g., lactams, lactones, epoxides, methyl acrylate and acrylonitrile, yield less well-defined polymer structures due to side reactions (including terminations) or the inability of their weakly nucleophilic anions to initiate the polymerization of olefin monomers such as styrene. Living polymerization also requires considerable care to perform properly. The presence of reactive impurities which act as terminating agents lead to contamination of the triblock copolymer with homopolymer and diblock copolymer.

Multiblock copolymers are synthesized by step polymerization using prepolymers containing specific end-groups (Eq. 14). Polyester- and polyether-polyurethanes and polyether-polyesters are multiblock copolymers of commercial interest. Step polymerizations has advantages over living polymerization. There is a

wider choice of structures which can be incorporated into the
block structure and the synthesis is less sensitive to reactive
impurities. However, the block lengths show a much wider
distribution due to the usual MW distribution inherent in step
polymerization.

        Thermoplastic elastomeric behavior requires that the block
copolymer develop a microheterogeneous two-phase network
morphology. Theory predicts that microphase separation will
occur at shorter block lengths as the polarity difference between
the A and B blocks increases. This prediction is borne out as the
block lengths required for the polyether-polyurethane, polyester-
polyurethane, and polyether-polyester multiblock copolymers to
exhibit thermoplastic elastomeric behavior are considerably
shorter than for the styrene-diene-styrene triblock copolymers.
DP for the hard blocks is in the range 1-10 and 100-200,
respectively, for multiblock and triblock copolymers; DP for the
soft blocks is in the range 15-30 and 1000-2000, respectively.
The size of the hard domains of the multiblock and triblock
copolymers is in the range 30-100Å and 100-300Å, respectively.

        The nature of the hard domains differs for the various block
copolymers. The amorphous polystyrene blocks in the ABA block
copolymers are hard because the glass transition temperature
(100°C) is considerably above ambient temperature, i.e., the
polystyrene blocks are in the glassy state. However, there is
some controversy about the nature of the hard domains in the
various multiblock copolymers. The polyurethane blocks in the
polyester-polyurethane and polyether-polyurethane copolymers have
a glass transition temperature above ambient temperature but also
derive their hard behavior from hydrogen-bonding and low levels of
crystallinity. The aromatic polyester (usually terephthalate)
blocks in the polyether-polyester multiblock copolymer appear to
derive their hardness entirely from crystallinity.

        Ionomer-type elastomers, containing small amounts (less than
5%) of metal carboxylate or sulfonate groups, have potential as a
new class of thermoplastic elastomers. Carboxylic acid groups
are introduced into polymers such as polybutadiene by copolymeri-
zation with a monomer such as acrylic or methacrylic acid.
Sulfonic acids groups have been introduced into EPDM and other
polymers by sulfonation with sulfur trioxide. The acid groups
are neutralized with a metallic oxide such as zinc oxide. The
resultant polymer is a multiblock copolymer composed of very long
hydrocarbon blocks with randomly-placed, extremely short metal
carboxylate or sulfonate blocks. In fact, the metal carboxylate
or sulfonate block length is typically only one repeating unit
long. The short block length of the polar blocks and the large
difference in polarity between the two blocks results in micro-
phase separation with aggregation of the ionic groups.

        In addition to the triblock and multiblock copolymers
described, certain blends of copolymers and homopolymers behave as
thermoplastic elastomers. A commercial product is obtained by

intensively blending EPDM or EPR rubber with isotactic poly-
propylene. Although EPDM and EPR are random copolymers, one
assumes that physical crosslinking occurs through aggregation of
isotactic polypropylene with short polypropylene blocks present in
the copolymer.

References

1.   Mark, J.E. J. Chem. Ed. 1981, 58, 89.
2.   Allcock, H.R.; Lampe, F.W. "Contemporary Polymer Chemistry";
     Prentice-Hall: Englewood Cliffs, 1981.
3.   Alliger, G.; Sjothun, I.J. "Vulcanization of Elastomers";
     Reinhold: New York, 1964.
4.   Billmeyer, F.W. Jr. "Textbook of Polymer Science"; Wiley-
     Interscience: New York, 1971.
5.   Coran, A.Y. "Science and Technology of Rubber"; Eirich, F.,
     Ed.; Academic: New York, 1978; p. 292.
6.   Eisenberg, A.; King, M. "Ion-Containing Polymers"; Academic:
     New York, 1977.
7.   Elias, H.-G. "Macromolecules"; Plenum: New York, 1977.
8.   Kennedy, J.P.; Tornqvist, E.G.M., Eds.; "Polymer Chemistry
     of Synthetic Elastomers"; Wiley-Interscience: New York,
     1968.
9.   Lenz, R.W. "Organic Chemistry of Synthetic High Polymers";
     Wiley-Interscience: New York, 1967.
10. Manson, J.A.; Sperling, L.H. "Polymer Blends and
     Composites"; Plenum: New York, 1976.
11. Morton, M. "Science and Technology of Rubber"; Eirich, F.,
     Ed.; Academic: New York, 1978, p. 24.
12. Noshay, A.; McGrath, J.E. "Block Copolymers"; Academic:
     New York, 1977.
13. Odian, G. "Principles of Polymerization"; Wiley-Inter-
     science: New York, 1981.
14. Saunders, K.J. "Organic Polymer Chemistry"; Chapman and
     Hall: London, 1973.
15. Schildknecht, C.E., Ed., with Skeist, I. "Polymerization
     Processes"; Wiley-Interscience: New York, 1977.

Synthetic Aspects of Crystallizable Elastomers

MARIO BRUZZONE

ASSORENI-Polymer Research Laboratories, 20097 S. Donato Milanese, Italy

Recent advances in the synthesis of crystalliza-
ble elastomers based on high cistactic and trans-
tactic polybutadiene structures are reviewed.
Extremely high cistactic structures are obtained
by catalysts systems based on 4f and 5f block
elements of Periodic Table (lanthanides and acti-
nides). Some of these catalysts systems are par-
ticularly interesting for saving energy in the
polymerization process.
The synthesis of transtactic structures is based
on catalysts in which the transition metal be-
longs to the 3d block (Ti, Cr, V, Ni). Particu-
lar emphasis is devoted to the synthesis of trans
butadiene/piperylene copolymers and to their
blends with synthetic cis-1,4-polyisoprene, with
the aim of increasing the "green strength" of
the latter.

During the last few years, the tire industry has emphasized
the need of being supplied with improved synthetic elastomers.
The improvement is particularly desirable for two properties,
namely:
(1) "green strength", in relation to the widespread adoption of
     radial tire technology and
(2) low hysteresis.
We shall deal in this lecture with recent improvements in
the elastomers synthesis, that should be able to cope with the
above mentioned requirements, without resorting to important in-
vestments for new plants or to cumbersome feedstocks. The im-
provement of the elastomer synthesis relies upon new catalytic
systems that allow: a control of elastomer tacticity in order to
achieve a strain induced crystallization, and suitable monomer
combinations in order to minimize the hysteresis loss of the
elastomer in a wide range of temperatures and frequencies.

As will be demonstrated later on, the use of some new cata-
lyst systems also affords the possibility of reducing the energy
consumption of the polymerization process, of improving its ecol-
ogy and of broadening the range of products. A necessary, yet
not sufficient, requirement for obtaining a crystallizable elas-
tomer ("crystallizable" means "crystallizable under strain") is a
certain structural order, i.e., a certain tacticity. This means
that constitutional, geometric and steric defects along the chain
should be controlled so as to obtain the adequate placement in a
restricted range of temperatures of isotropic melting point, i.e.,
melting point in an unstretched state. The main routes for obtain-
ing tactic structures suitable for crystallizable synthetic elas-
tomers are:
     low melting point homopolymers (cis-1,4-BR, cis-1,4-IR, TPA,
IIR),
     low melting point copolymers, in which suitable comonomer
units are introduced in a high melting point homopolymer chain
(trans butadiene/piperylene copolymers, trans butadiene/styrene
copolymers) and
     low melting point alternating copolymers (propylene/butadiene
alternating copolymers).
     The third route can be considered a variation of the first
one, in which a monomer couple performs as a new monomer "unit".
Apart from the route chosen, the melting point is so designed as
to fall in a limited range of temperatures (295 ± 20°K). In our
laboratories, we have followed the first two routes for obtaining
crystallizable elastomers and we have found both suitable for the
purpose.

FIRST ROUTE

     As to the first route, we started in 1969 ($\underline{1}$) in investiga-
ting unconventional transition metal complexes of the 5 and 4f
block elements of periodic table, e.g., actinides and lanthanides
as catalysts for the polymerization of dienes (butadiene and
isoprene) with an extremely high cis content. Even a small in-
crease of cistacticity in the vicinity of 100% has an important
effect on crystallization and consequently on elastomer processa-
bility and properties ($\underline{2}$). The f-block elements have unique elec-
tronic and stereochemical characteristics and give the possibility
of a participation of the f-electrons in the metal ligand bond.
A common feature of catalysts based on 4 and 5f block elements is
that of being able to polymerize both butadiene and isoprene to
highly cistactic polymers, independently of the ligands involved.
Butadiene, in particular, can reach a cistacticity as high as 99%
with uranium based catalysts ($\underline{3}$) and cistacticity of > 98% with
neodymium based catalysts ($\underline{4}$). This high tacticity does not
change with the ligand nature (Fig. 1) in contrast to conventional
catalysts based on 3-d block elements. A second feature of f-
block catalysts is that the cis content of polymer is scarcely

affected by temperature (Fig. 2). This fact is important for the
polymerization process because it allows the polymerization rate
to be increased without any loss of polymer tacticity. A third
feature of f-block catalysts is that of being able to perform the
polymerization of dienes in aliphatic solvents. This feature is
important for both the economy and the ecology of the polymeriza-
tion process. The economy is improved by the fact that some
aliphatic solvents require less steam in the stripping section.
A further economic advantage in using aliphatic solvents could
be obtained by increasing the solid content in the aliphatic solu-
tion in relation to its lower viscosity. A fourth important
feature of f-block catalysts is that of being able to copolymerize
dienes such as butadiene, isoprene and others to random polymers
with a high cis configuration of both units. The copolymerization
of dienes allows interesting diversification of the products
range: for example, "all cis" butadiene-isoprene copolymers with
a low isoprene content (e.g. 10%) allow the melting point of the
rubber to be tailored (Fig. 3) in relation to the range of tem-
perature met by the rubber object during its use, whereas "all
cis" butadiene-isoprene copolymers with a high (e.g. 50%) isoprene
content are very interesting as low hysteresis rubber in a wider
range of temperatures in respect to cis-1,4-polybutadiene, to
cis-1,4-polyisoprene, and to their blends (Fig. 4) (33). It is
outside the scope of this paper to discuss this peculiar behaviour
of "all cis" butadiene-isoprene copolymers. The above-mentioned
considerations should be sufficient for realizing that f-block
elements catalysts are not merely one of the many catalyst systems
that joins the already crowded area of catalysts for cis-1,4-
polybutadiene. F-block elements represent indeed a substantial
improvement of diene catalysis. So far, we have dealt with the
general characteristics of 4 and 5 f-block elements as catalysts
for diene polymerization. However, only some of them are effec-
tively suitable for reasons of availability, cost, activity or
others, that we shall discuss now on a case-by-case basis. The
only element of the 5 f-block that has been extensively studied
by us since 1969 is uranium (1,3,5,6,7,8). Earlier studies of
others (9) did not show any peculiar stereo-regulating effect of
this element in the polymerization of dienes and apparently were
soon abandoned. The availability of uranium, and in particular
of depleted uranium, that is a side product of nuclear cycles, is
in principle very high. We have calculated that the stockpiling
of very pure depleted uranium compounds was as high as 23,000
tons per year in 1974 within the western countries (3). Also the
radioactivity of depleted uranium is not a problem in the rubber,
when its content is kept, as in our case, at levels lower than
100 ppm, i.e., less than many igneous rocks and apatites that
are currently used as a source of phosphoric fertilizers (13).
The very problem of using uranium in the chemical industry is the
very strict regulations in several countries that limit the fis-
sile materials trade and, unfortunately, also that of depleted

	TRANSITION METAL	HALOGEN			
		F	Cl	Br	I
3d – BLOCK	Ti	35	75	87	93
	Co	93	98	91	50
	Ni	98	85	80	10
4 and 5f BLOCK	Ce	97	98	98	98
	Nd		98	98	98
	U		98.5	98.5	98.5

Figure 1. *Dependence of polybutadiene cistacticity (%) on the nature of halogen ligand for different catalyst systems. The data of the first four lines are taken from Ref. 18.* cis *content by IR from Ref. 34.*

TEMPERATURE (°C)	20	45	60	70	130 (*)
URANIUM POLYBUTADIENE	99	98.5	98.5	–	
NEODYMIUM POLYBUTADIENE	99	98.5	–	98.5	98

(*) Adiabatic polymerization

Figure 2. *Insensitivity of* cis *content to polymerization temperature for uranium and neodymium catalysts.*
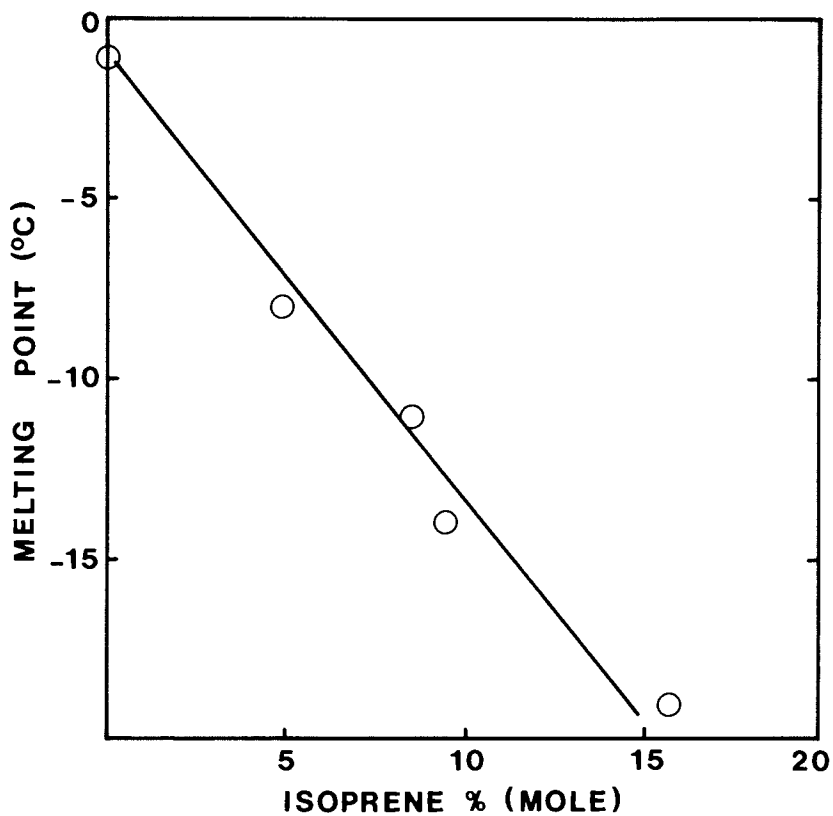
*Figure 3.   Melting points of butadiene–isoprene copolymers. DSC at 20°C/min
on crude polymers.*
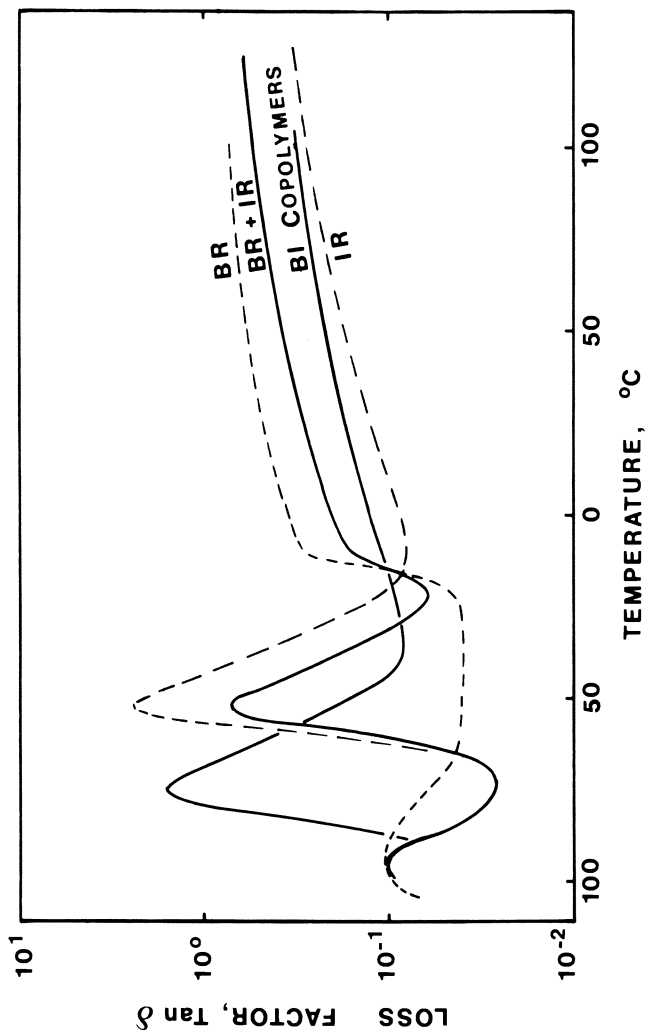
Figure 4. BR + IR is a 50/50 (wt) blend of synthetic cis-1,4-polyisoprene and cis-1,4-polybuta-diene. BI copolymers are random cis-1,4-butadiene–isoprene copolymers with the same composition. Results obtained with Rheovibron on gum vulcanizates at 110 Hz frequency.

uranium. Uranium catalysts are able to polymerize butadiene to
polymers with a cis content as high as 99%. At this level of
tacticity, the crystallization rate is the customary test for
assessing a further improvement of structural purity (3). A list
of uranium based catalyst systems, suitable for both cis-1,4-
polybutadiene and polyisoprene are shown in Fig. 5. π-allyl
complexes of uranium were the first to be developed by us for ob-
taining a 99% cis-polybutadiene in aliphatic solvents, both in
the absence and in the presence of Lewis acids. The polymeriza-
tion is thought to proceed according to the prevalent view that
suggests the growing chain be bonded to the transition metal by
a π-allyl bond and that the incoming monomer be inserted into the
transition metal-allyl bond (Fig. 6). However, we have been un-
able up to now to obtain direct evidence of the active sites
in uranium π-allyl systems by NMR. In fact, mono-metallic cata-
lysts, such as $U(C_3H_5)_3X$ (where X = halogen), although well
characterized in the solid state, show puzzling solution NMR
spectra probably because of a disproportionation into tetraallyl-
uranium and more halogenated species. This disproportionation
apparently takes places even at a very low temperature (-80°C).
Also the synthesis of π-2-butenyl uranium derivatives did not
succeed so far. It was attempted in order to confirm that the
cis structure of the polymer was determined by the "anti" isomer-
ism of the π-allyl complex formed by uranium and growing chain
end (Fig. 7). This lack of evidence has prevented us so far to
reach a conclusion on the most important point, that is, why
f-block catalysts are so selective in orienting the synthesis of
polydienes exclusively to cis polymers and, in particular, what
is the role of f-electrons or of stereochemical characteristics
of the f-block elements in determining the formation of a
π-butenyl complex exclusively in the "anti" form. Going back to
the other uranium-based catalysts, the most suitable catalysts,
from a practical point of view, are based on ternary systems
based on uranium alkoxy derivatives (that are obtained by reaction
of alkaline alcoholates with uranium tetrachloride) with aluminum
alkyls and Lewis acids. Also in this case, a π-allyl uranium
complex is thought to be formed "in situ" as the catalyst site.
The catalyst activity is so high that uranium concentration lower
than 0.1 millimoles per liter allows a complete conversion of
butadiene to be obtained in a few hours, at 20°C. The transfer
reaction of uranium based catalyst is similar to that of conven-
tional 3d-block elements (titanium, cobalt, nickel) so that the
molecular weight of the polymer is affected by polymerization
temperature, polymerization time and monomer concentration in the
customary way. This is in contrast, as we shall see later on,
to some catalysts based on 4 f-block elements. Uranium based
catalysts are able to polymerize isoprene and other dienes to
high cis polymers; the cis content of polyisoprene is 94%, some-
what inferior to titanium based catalysts. In contrast, with
3d-block elements an "all cis", random butadiene-isoprene

Figure 5.   Uranium based catalysts for high cistactic polydienes.

1) $UO_2(acac)_2$ + AlR_2Br + AlR_3	GOODYEAR, 1970 [9]	RATHER LOW CIS WAS OBTAINED
2) π (allyl)$_3$ UX + $AlRCl_2$	OUR LABORATORY, 1971 [10]	99 % CIS
3) $U(OCH_3)_4$ + $AlRCl_2$ + AlR_3	OUR LABORATORY, 1972 [11]	VERY HIGH CIS
4) $U(OOC.C_7H_{15})_4$ + $AlBr_3$ + AlR_3	BAYER, 1976 [12]	VERY HIGH CIS
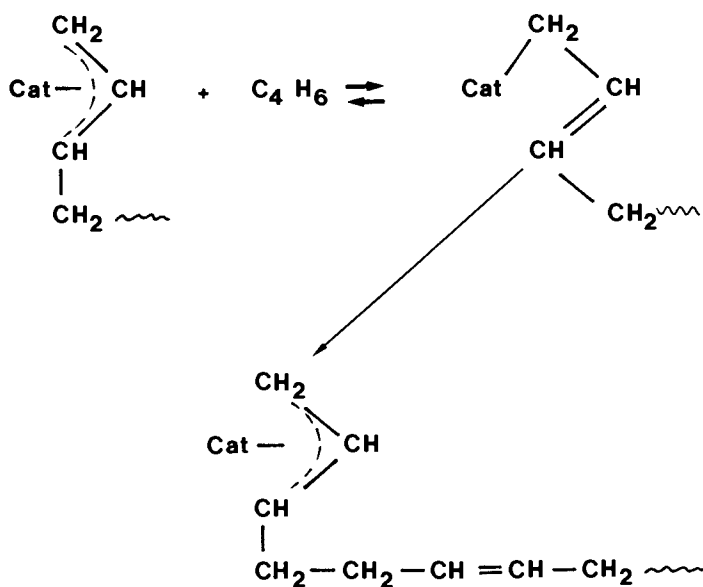
Figure 6. Polymerization scheme for butadiene.

"SYN" FORM ⟶ TRANS 1,4   "ANTI" FORM ⟶ CIS 1,4
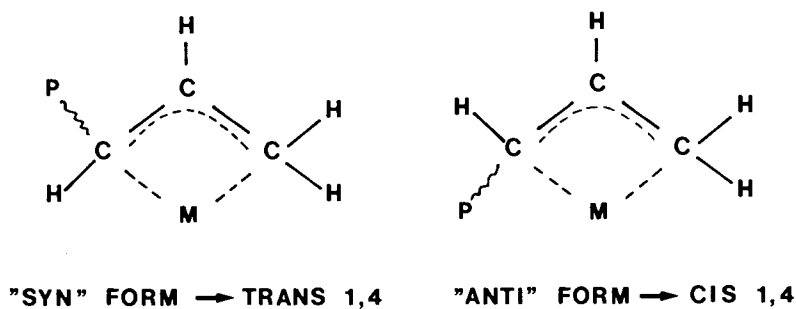
Figure 7. π-Allyl complex formed by uranium and growing chain end.

copolymer can also be obtained. The copolymer randomness has
been assessed by reactivity ratios, by ^{13}C-NMR (4), and by
rubber properties. Let us deal now with catalysts based on 4
f-block elements, i.e., with lanthanides, or rare earths. The
term lanthanides covers 15 elements, with atomic numbers from
57 to 71 inclusive, in which the number of electrons in the 4f
shell varies from 0 (lanthanum) to 14 (ytterbium and lutetium)
(Fig. 8) (14). The term "rare earths" is misleading, because
some of lanthananides are not rare, being more abundant in the
earth's crust than tin, cobalt and molybdenum (15). Neodymium,
one of the more interesting lanthanides as a catalyst for diene
polymerization, is as abundant as cobalt and niobium, more
abundant than lead, molybdenum and much more abundant than ura-
nium, mercury, bismuth and cadmium. Besides the relative abun-
dance of lanthanides in respect to other conventional metals,
some of them, including neodymium, have created a disposal
problem since they are by-products of other more rare lanthan-
ides, that are used in other applications, such as that of color
television phosphors. The price of some lanthanides, including
neodymium, is reasonable today and rather competitive with other
conventional diene catalyst systems. The use of lanthanides as
catalysts for diene polymerization was reported by Von Dohlen
and by Chinese scientists (16,17) as early as in 1963-64. They
were extensively studied by Throckmorton (18) in USA and by
Monakov (20) in USSR for the same purpose. A comprehensive re-
port on the activity of Chinese scientists in this field has
been recently published (22). Independently, when we started
our research on lanthanides in 1975, in the framework of an
extensive research on f-block elements and following that on
uranium catalysts, lanthanides had an undeserved bad reputation
as catalysts for diene polymerization. This bad reputation was
due to the fact that most researchers had limited their atten-
tion to cerium, that ironically enough is the only lanthanide
that is also a powerful oxidation catalyst, and therefore de-
leterious for polymer aging. In fact, in cerium the energy of
the inner 4f level is nearly the same as that of the outer or
valence electrons, and only a small amount of energy is required
to change the relative occupancy of these electronic levels.
This gives rise to dual valency state (+3 and +4) (23). As to
the activity of lanthanide based catalysts we confirm a singular
behavior that has been already reported by Chinese scientists
(22) and that is summarized in Fig. 9. The activity of lantha-
nides in promoting the polymerization of butadiene and isoprene
shows a large maximum centered on neodymium, the only exception
being represented by samarium and europium that are not active,
reasonably because they are reduced to bivalent state by alumi-
num alkyls, as pointed out by Tse-chuan and associates (22).
Some catalyst systems based on lanthanides are shown in Fig. 10.
The ones based on lanthanide alkoxides are based on our work,
whereas the others are taken from the above mentioned work

Element	Atomic No	Electrons in 4 f Shell
La	57	0
Ce	58	2
Pr	59	3
Nd	60	4·
Pm	61	5
Sm	62	6
Eu	63	7
Gd	64	7
Tb	65	9
Dy	66	10
Ho	67	11
Er	68	12
Tm	69	13
Yb	70	14
Lu	71	14

Figure 8. Number of electrons in 4 f shell of lanthanides.
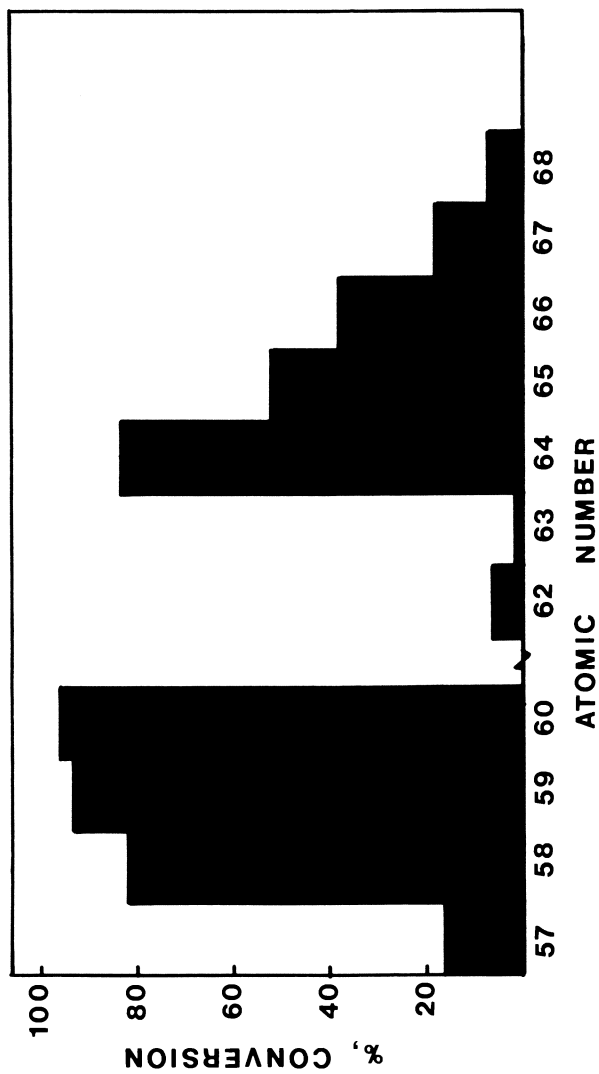
Figure 9. Catalyst activity of lanthanides in diene polymerization. Data from Ref. 22.

Catalyst System	Source	Result
1) $Ln L_3 + AlRX_2 + AlR_3$ were L = bidentate ligand	UNION CARBIDE, 1963 [17]	RATHER LOW CIS WAS OBTAINED
2) $NdX_3 + C_2H_5OH + AlR_3$ $Nd(naph)_3 + AlR_3 + \left\{ \begin{array}{l} AlR_2X \\ Al_2R_3X_3 \end{array} \right.$	CHINESE SCIENTISTS, RESEARCH STARTED IN 1964 [16]	VERY HIGH CIS
3) CATALYST SYSTEM SIMILAR TO 1), AFTER AGING	GOODYEAR, 1969 [18]	VERY HIGH CIS MOST OF WORK DONE ON CERIUM
4) $Nd(O-nC_4H_9)_3 + AlR_2H + AlRX_2$ $Nd(O-nC_4H_9)_3 + AlR_3 + AlRX_2$	OUR LABORATORY, 1977 [19] "	VERY HIGH CIS "
5) $Ln(OOCR)_3 + AlRX_2 + AlR_3$	BAYER, 1978 [21]	VERY HIGH CIS

Figure 10. 4 f block elements catalyst systems for high cistactic polydienes.

of Tse-chuan. The more active catalyst systems are based on
ternary systems in which a lanthanide compound is associated
with aluminum alkyls (or aluminum alkyl hydrides) and a Lewis
acid. As to the higher activity of neodymium in respect to
other lanthanides, the explanation put forward by Chinese sci-
entists is that the energy variation of neodymium (and praseody-
mium) in complexing a diene or other ligands is less than that
of other lanthanides in a trivalent state. The energy variation
in its turn is a function of the number of electrons in the 4-f
orbitals. No hypothesis have been put forward in order to ex-
plain why lanthanides give invariably high cis polydienes, when
used in Ziegler-Natta type catalyst compositions. The activity
of neodymium based catalysts is very high, similar to that shown
by uranium based catalysts. A fraction of a millimole per liter
is sufficient for achieving very fast conversions in a matter of
a few hours. The cis content of polybutadiene is slightly lower
to that obtained with uranium based catalyst: however, a cis
content of 98% in polybutadiene and of 94% in polyisoprene is
easily achieved. The most important and puzzling characteristic
of neodymium as a catalyst for polymerization of dienes is how-
ever the fact that the polymerization is virtually transfer free
and seems to proceed, in certain cases, via a pseudo living
mechanism. Also this fact has been noted independently by us
and by Chinese scientists (22). The increase of molecular
weight concurrently with conversion is shown in Fig. 11 and Fig.
12. In Fig. 11, the polymer Mooney viscosity and conversion
are shown as a function of polymerization time. In Fig. 12,
Mooney viscosity is shown as a function of conversion. Of course
this peculiarity of neodymium based catalyst requires a proper
process design, in order to reach both the right conversion and
the right Mooney at the same time, or the modification of the
catalyst system, in order to induce a certain chain transfer
activity, allowing a regulation of molecular weight to be ob-
tained. The low chain transfer activity of certain neodymium
based catalysts systems allows an increase of monomer concentra-
tion in the polymerization vessel without any adverse effect on
molecular weight. Also the polymerization temperature can be
increased up to 100°C without any dramatic drop of MW and with-
out any gel formation. A polymerization run on a commercial
plant was carried out by us in 1980. Both high cistactic poly-
butadiene and its isoprene copolymers were produced in a quan-
tity of some ten tons. The catalytic activity was confirmed to
be so high as to avoid any washing step to remove catalyst resi-
dues.

SECOND ROUTE

     Let us review now the results obtained in our laboratories
in the synthesis of crystallizable elastomers by following the
second route indicated in the Introduction. As previously
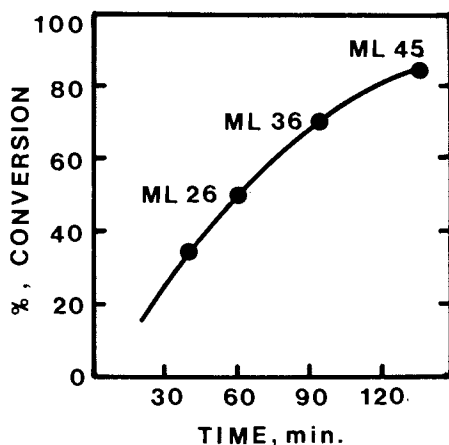
Figure 11. Increase of molecular weight with conversion. Catalyst, Nd(O-n-C_4H_9)$_3$, DIBAH, EADC; Nd, 0.035 $\times$ 10^{-3} m/L; solvent, n-hexane; DIBAH/Nd, 40; Cl/Nd, 3; monomer concentration, 17.5% wt; polymerization temperature, 50°C. Data from Ref. 4.
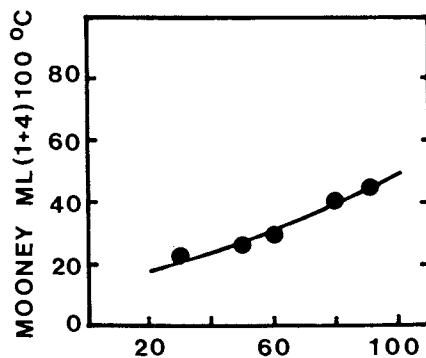
Figure 12. Catalyst, Nd(O-n-C_4H_9)$_3$, DIBAH, EADC; Nd, 0.085 $\times$ 10^{-3} m/L; solvent, n-hexane; DIBAH/Nd, 40; Cl/Nd, 3; monomer concentration, 17.5% wt; polymerization temperature, 50°C. Data from Ref. 4.

mentioned, this route involves the copolymerization of a monomer
that would give rise to high melting point homopolymer, with a
comonomer able to decrease the melting point down to the narrow
range of temperatures suitable for a crystallizable elastomer.
This route is not viable for every high melting point macromol-
ecular structure, for reasons that cannot be dealt with here.
However, we realized that some butadiene-piperylene copolymers,
formerly synthesized at the Polytechnic Institute of Milan (25),
were particularly suitable for the scope of obtaining crystalli-
zable elastomers. These copolymers had the butadiene units in
trans configuration, so that it was possible, by a suitable
non-cocrystallizable monomer unit such as piperylene (a component
of C_5 cut of naphtha cracker), to produce a host of crystalline
polymers with melting points from 145°C (melting point of
trans-1,4-polybutadiene) down to -5°C (Fig. 13). The range of
melting temperatures interesting for a strain crystallizable
rubber was found to range from -5°C to +20°C (DSC), correspond-
ing to a piperylene content from 32% to 22% (mol) (NMR). Besides
the wide possibility of tailoring the melting point and the
strain induced crystallization, these copolymers showed inter-
esting economics in comparison to other crystallizable rubbers
(e.g. trans polypentenamer) since they were based on butadiene
with only moderate quantities of piperylene. Piperylene is
contained in the C_5 fraction of naphtha cracker in amounts close
to that of isoprene. Let us deal now with the synthetic aspects
of this copolymerization. In view of recent publications from
our laboratory on this subject (30, 31, 32). I shall limit my-
self to point out only the main points of this copolymerization:

    (1) the catalyst systems published so far (Fig. 14) are
based on vanadium chelates and mixtures of aluminum alkyl
halides, and on titanium based catalysts. The catalyst activity
is satisfactory.
    (2) the polymerization is performed in aromatic solvents;
however bulk polymerization also is possible.
    (3) piperylene can be used as a pure monomer, but a C_5 cut
enriched in piperylene is also suitable. Cyclopentadiene is
only a moderate poison for this catalyst system, and its content
is tolerable up to 0.2 wt% of the reactive monomer (trans-
piperylene).
    (4) only the trans isomer of piperylene is copolymerized.
The cis isomer acts as a diluent. It could be isomerized to
trans isomer, in order to increase the monomer feed, if nec-
essary.

    The copolymer randomness has been studied by ^{13}C-NMR and
the results will be the subject of a forthcoming publication.
Also the role of the different piperylene units present in the
copolymer (1,2 and 1,4 trans) in depressing the melting point
of trans-1,4-polybutadiene is still under investigation; 1,2
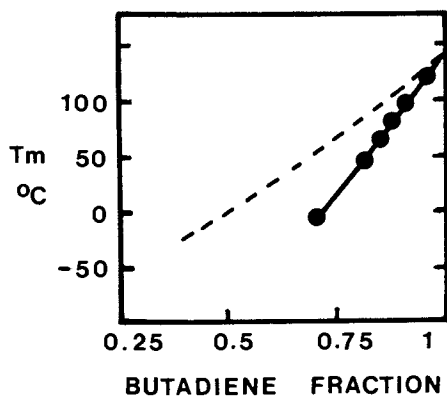
Figure 13. Melting points of trans-*poly(butadiene co-piperylene) as a function of composition. Data from Ref. 30.*

1) $V(acac)_3 + Al R_2 Cl + Al R Cl_2$ MONTEDISON, 1963 [25]

2) CrO_3 on Aluminum Silicate   USSR, 1966 [26]

3) $V(acac)_3 + Al R_2 Cl + C Cl_3 COOH$ SNAMPROGETTI, 1974 [27]

4) $TiCl_4 + Al I_3 + Al R_3 + THT$ EXXON, 1974 [28]

5) $(\pi - C_3 H_5 Ni I)_2$ USSR, 1976 [29]

Figure 14.   Catalyst systems for transtactic butadiene–piperylene copolymers.

units are much more effective in abating the copolymer crystalli-
nity.

    As to the copolymer properties, piperylene/butadiene copoly-
mers outperform natural rubber for green strength, and are useful
for increasing this property of synthetic cis-1,4-polyisoprene,
by merely blending. In Fig. 15, the green strength of this
copolymer is demonstrated by pulling a specimen obtained by cut-
ting an unvulcanized tire carcass ply. The green strength and
the processability of the copolymer can be tailored by acting on
melting point (i.e. on copolymer composition) and on molecular
weight, as shown in Fig. 16. The higher green strength is ob-
tained by polymers with rather high melting point and molecular
weight, whereas a lower molecular weight is preferred for im-
proving the processability when the polymer is not used in blends
with other conventional rubbers.

    In conclusion: f-block element-based catalysts represent
a significant improvement in the synthesis of polydienes, both
from the pont of view of the process and that of the polymer
properties.

    In particular, the increase of tacticity and the possibility
of achieving the synthesis of "all cis" diene copolymers of high
molecular weight allows the possibilities of broadening the range
of products attainable in conventional, solution polybutadiene
plants.

    The copolymerization of butadiene in trans configuration
with suitable comonomers represents a second route for obtaining
a wide range of strain induced crystallizable elastomers, with
melting point tailorable in a wide range of temperatures. These
copolymers can be used, in particular, in blends with other cry-
stallizable rubbers (e.g. synthetic cis-1,4-polyisoprene) in
order to improve their "green strength".
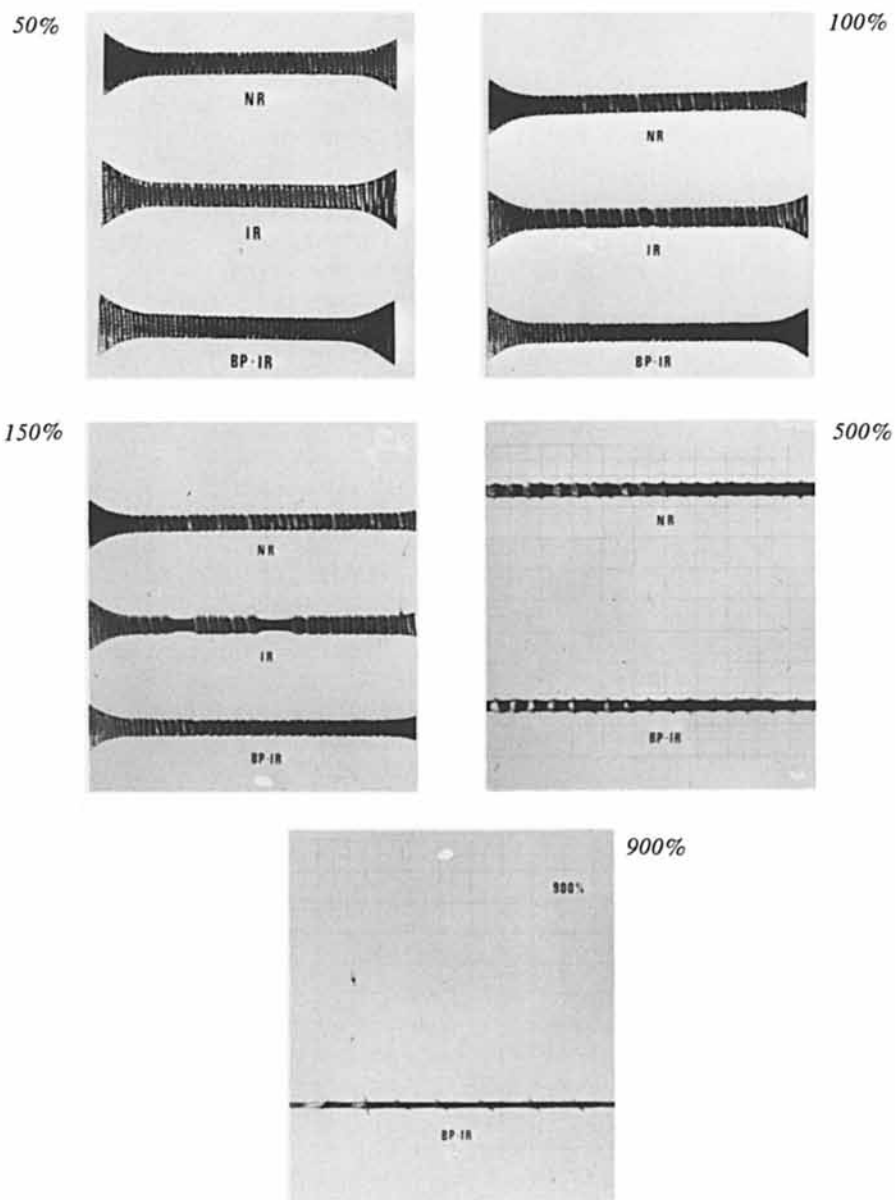
Figure 15.   Behavior under strain of an unvulcanized tire ply (conventional recipe) based on NR (natural rubber 100%), IR (synthetic cis-1,4-polyisoprene 100%), BP/IR (a 50/50 blend of IR and trans-butadiene–piperylene copolymer).
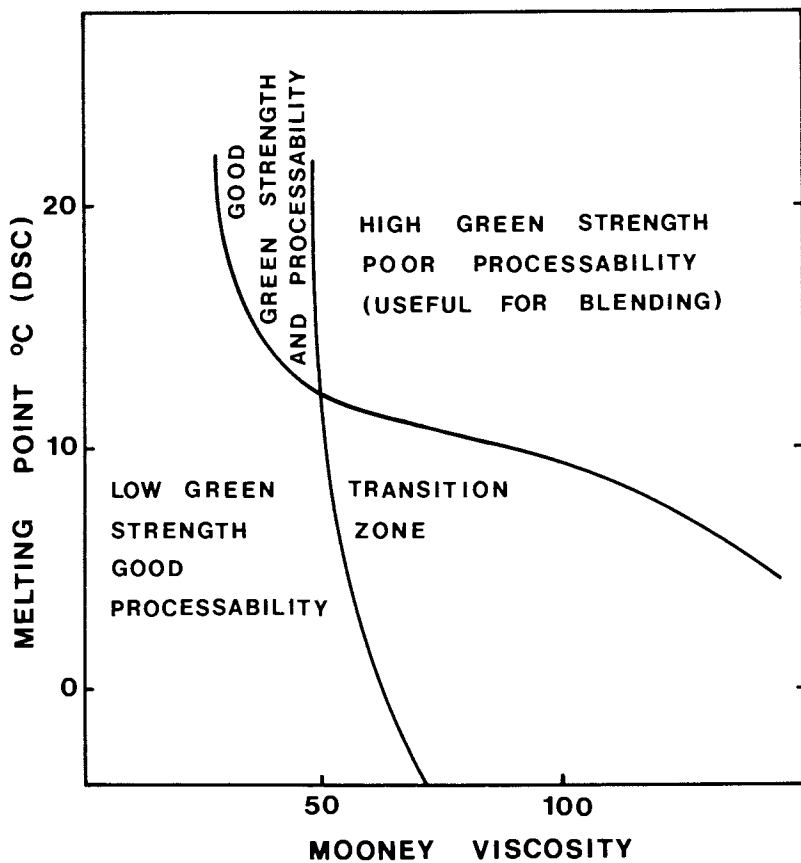
Figure 16.   Processibility and green strength of trans-*butadiene–piperylene copoly-
mers as a function of melting point and Mooney viscosity.*

LITERATURE CITED

1. Lugli, G.; Marconi, W.; Mazzei, A.; Palladino, N. Inorg.
    Chim. Acta 1969, 3, 151.
    Ibid, 1969, 3, 253.
2. Bruzzone, M. Makromol. Chem., 1981, Suppl. 4, 177,
3. Bruzzone, M.; Mazzei, A.; Giuliani, G. Rubber Chem. and
    Technol., 1974, 47, 1175.
4. Mazzei, A. Makromol. Chem., 1981, Suppl. 4, 61.
5. Lugli, G.; Mazzei, A.; Poggio, S. Makromol. Chem. 1974, 175,
    2021.
6. De Chirico, A.; Lanzani, P.; Raggi, E.; Bruzzone, M.
    Makromol. Chem., 1974, 175, 2029.
7. Giuliani, G.; Sorta, E.; Bruzzone, M. Angew Makromol. Chem.,
    1976, 50, 87.
8. Gargani, L.; Giuliani, G.; Mistrali, F.; Bruzzone, M. Angew.
    Makromol. Chem., 1976, 50, 101.
9. U.S.Pat. 3,676,411 (1970) to the Goodyear Tire & Rubber Co.
10. U.S.Pat. 3,937,692 (1971) to Snamprogetti.
11. U.S.Pat. 3,935,175 (1972) to Snamprogetti.
12. DOS 2,625,390 (1976) to Bayer.
13. "Uraniferous phosphate resources and technology"; Earth
    Science Inc.; 1979, Vol. 1, Table I.
14. "Handbook of Chemistry and Physics"; CRC Press 54th Edition;
    1973-74; p. F95.
15. Pings, W.B. Mineral Industries Bulletin, Colorado School of
    Mines, 1969, 12, 1.
16. Tse-Chuan, S.; Chung-Yuan, G.; Chang-chi, C.; Chung, O. Sci.
    Sin., 1964, 13, 1339.
17. Von Dohlen, W.; U.S.Pat. 3,297,667 (1963) to Union Carbide.
18. Throckmorton, M.C.; Mournighan, R.E.; U.S. Pat. 3,794,604
    (1969) to the Goodyear Tire & Rubber Co.
    Throckmorton, M.C. Kautsch. Gummi Kunstst.; 1969 22, 293.
19. Italian Pat. Application 26377 A/77 1977 to ANIC.
20. Monakov, Y. B. Dokl. Acad. Nauk SSSR, 1977, 234, 1125.
21. DOS 2,830,080 (1978) to Bayer.
    U.S.Pat. 4,242,232 (1978) to Bayer.
22. Tse-Chuan, S.; Chun, O.; Fu Sung, W.; Chen Ya, H.; Fu Sheng,
    Y.; Pao Kung, C. J. Polym. Sci. Pol. Chem. Ed., 1980, 18,
    3345.
23. "Handbook of Chemistry and Physics", CRC Press 54th Edition;
    1973-74 p. B10.
24. Engel, E.F. Rubber Plast. Age. 1961, 42, 1215.
25. Porri, L.; Carbonaro, A.; Ciampelli, F. Makromol. Chem.
    1963, 61, 90.
26. Akhmedli, T.; Perel'man, A. Vysokomol. Soyed, 1966, 8, 61.
27. Belg. Pat. 832,059 (1974) to Snamprogetti.
28. U.S.Pat. 3,972,862 (1974) to Exxon.
29. Soboleva, T. et al. Dokl. Akad. Nauk SSSR, 1976, 228, 619.

30. Bruzzone, M.; Ca bonaro, A.; Gargani, L. <u>Rubber Chem. and
     Technol</u>., 1978, <u>51</u>, 907.
31. Carbonaro, A.; Gargani, L.; Sorta, E.; Bruzzone, M.,
     Proceedings Int. Rubber Conf., Venice 1979.
32. Lauretti, E.; Santarelli, G.; Canidio, A.; Gargani, L.,
     Proceedings Int. Rubber Conf., Venice 1979.
33. Ital. Pat. Appl. 23872 A/81 (1982) to ANIC.

Synthesis of Elastomers with Strain-Induced Crystallization

GERD SYLVESTER and WOLFGANG WIEDER[1]

Bayer AG, Research and Development Department, 5090 Leverkusen, Germany

The properties of elastomers are much improved by strain-induced crystallization, which occurs only in polymers with high stereoregularity. The polymerization of butadiene using completely soluble catalysts composed of a) rare earth carboxylates, b) Lewis acids and c) aluminum alkyls leads to polymers with up to 99 % cis-1,4 configuration. These polymers show more strain-induced crystallization than the commercial polybutadienes and consequently their processability is much improved.

Very active catalysts for the preparation of strictly alternating butadiene-propylene copolymers (BPR) consist of $VO(OR)_2Cl/i-Bu_3Al$ (R = neopentyl). The CH_3 side groups in BPR stiffen the polymer chain and were expected to promote the formation of strain-induced structures. The fact that we could not detect strain-induced crystallization is probably due to an atactic configuration of the propylene units.

Alternating isoprene-ethylene copolymers (IER) were prepared with the same catalyst. Due to the strictly alternating sequences of diene and olefin units and the absence of chiral carbon atoms IER shows strain-induced crystallization, but at lower temperatures compared to natural rubber.

[1] Current address: Bayer Elastomeres, BP 41, 76170 Lillebonne, France.

The subject of this paper is the preparation of elastomers with strain-induced crystallization. It is well known that the properties of rubber are significantly improved by strain-induced crystallization. As far as their processability is concerned, the polymers have improved mill behaviour and, in particular, fairly high green strength. The properties of the crosslinked elastomer, e.g. its tensile strength, and, above all, its resistance to tearing and tear propagation, are likewise improved. Strain-induced crystallization occurs only in polymers which have high stereoregularity.

This paper is concerned with some of our experiments in this field. Our purpose was to obtain polymers with extremely high stereoregularity. In the first part we will report on the homopolymerization of butadiene with f-transition metal catalysts. The second part will be devoted to alternating copolymerization of conjugated dienes with olefins.

Homopolymerization of Butadiene. It appeared to us that catalysts based on f-transition metals were the ones most likely to enable us to prepare polybutadiene with an extremely high cis content. We began by investigating catalysts based on uranium compounds. Two such systems were known at the beginning of our work.

The first, consisting of a uranium salt, trialkylaluminum, and a Lewis acid, had been developed at Goodyear (1). The other system, described by Snam Progetti (2), permits the polymerization of butadiene to give polymers with a cis content of up to 99 %.

We found highly active catalysts, which are shown in Table I (3). The main component is a stable carboxylate of uranium in the oxidation state of +4, in combination with a Lewis acid and an aluminum alkyl, e.g. uranium octoate, aluminum tribromide, and triisobutylaluminum in a molar ratio of 1:0.8:25. The catalyst is usually aged for at least 2 hours at room temperature.

At 0.06 millimole of uranium compound per 100 g of butadiene, conversions of more than 90 % were obtained after a reaction time of three hours. The rate of polymerization is of the first order in relation to both the monomer (Figure 1) and the catalyst concentration. The polymers have a cis content of about 98 to 99 % and a broad molecular weight distribution.

Other f-transition metal catalysts have been described by von Dohlen (4) and Throckmorton (5) as well as by Chinese (6,7) and Italian (8-10) scientists. They generally consist of a rare earth compound, an aluminum alkyl, and a halide, the halogens being bound to the rare earth element or aluminum.

When we investigated catalysts based on rare earth carboxylates we found that most of them had extremely low solubility in hydrocarbon solvents, such as cyclohexane and n-hexane.

Table I. Polymerization of butadiene by uranium catalysts.

Catalyst:	g	mmoles
(A) U(octoate)$_4$	1.22	1.5
(B) AlBr$_3$	0.32	1.2
(C) Ali-Bu$_3$	7.44	37.5
Cyclohexane	12	

Catalyst aged 4 hours at 25 ^{o}C

Polymerization Recipe:

Cyclohexane	18000 g
Butadiene	2600 g
Aged catalyst added at	45 ^{o}C
Polym. temp.; time	45 ^{o}C; 3 h
Conversion	95 %
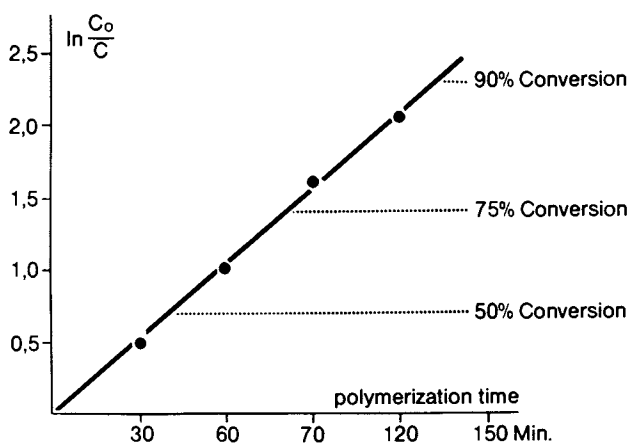
Figure 1. Kinetics of uranium catalyzed polymerization of butadiene. Catalyst system and polymerization conditions are shown in Table 1. Conditions: 45°C; [u], 0.055 mmol/L; and [C$_0$], 1.77 mol/L.

Heterogeneous catalysts have a tendency to cause gel formation in the solution polymerization of dienes. This adversely affects the polymerization and the quality of the end products.

We found that completely soluble compounds can be obtained in two ways. The first method, which is widely applicable, is to react a rare earth carboxylate with a small amount of an aluminum alkyl (11). Neodymium octoate can be converted into a product which is completely soluble in cyclohexane by reacting one mole of it with 1 to 5 moles of triethylaluminum. We also found that the rare earth salts of certain tertiary carboxylic acids are very readily soluble in non-polar solvents (12). In conjunction with a Lewis acid and aluminum alkyls, these compounds form highly active catalysts for the polymerization of butadiene. The neodymium : Lewis acid : aluminum alkyl molar ratio is within the range 1 : (0.4-2.0) : (10-40).

These catalysts are more versatile than the conventional transition metal systems and enable the molecular weight, molecular weight distribution, and cis-1,4 content to be adjusted independently of one another within wide limits.

The polymerization is normally carried out in non-aromatic solvents, such as cyclohexane and n-hexane, at temperatures of 50 to 90 °C. Temperatures within this range influence the stereospecificity of the polymerization to only a small extent. These catalysts, unlike ones based on uranium, do not have to be preformed.

The molecular weight of polybutadiene can be increased by reducing the catalyst concentration, the ratio of AlR_3 to rare earth compound, or the polymerization temperature, but it is independent of the monomer conversion. Figure 2 gives two examples of the ways in which the molecular weight can be controlled. The lower curve shows that one can increase the dilute solution viscosity, DSV, by about four units by reducing the ratio of aluminum trialkyl to neodymium from 60 to 15. But the molecular weight depends also on the polymerization temperature. A reduction of temperature from 60 °C to 0 °C raises the dilute solution viscosity from about four to eleven dl/g.

The stereospecificity of the reaction depends mainly on the choice of the aluminum alkyl. If triisobutylaluminum is used as the only alkyl compound, products with very high cis contents of 98-99 % are obtained independently of the other reaction conditions. Replacement of the triisobutylaluminum by increasing proportions of triethylaluminum makes the cis content fall continuously (Figure 3).

The cis content of the polybutadiene can therefore be controlled without difficulty within a range of less than 90 % to 99 %. The proportion of vinyl double bonds is not affected and is always lower than 1 %.

The molecular weight distribution is an important parameter for controlling the rheological and processing properties of rubber.

DSV [η], dl/g
in toluene, 25°C
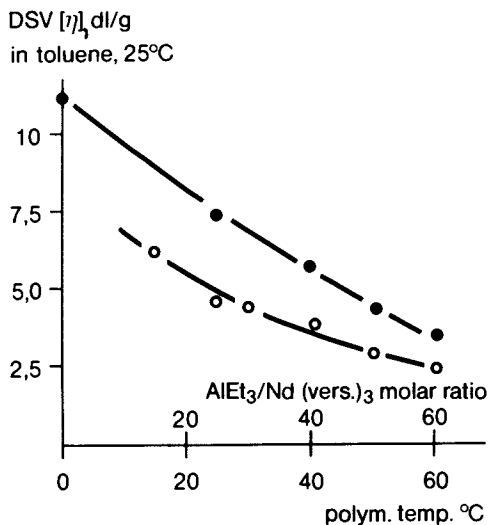
Figure 2. Effect of polymerization temperature (●) and AlR₃:Nd(vers)₃ molar ratio (○) on molecular weight. Et₃Al/ Nd(vers)₃ molar ratio was kept at 40:1 when the temperature was varied, and the temperature was maintained at 60°C when Et₃Al/Nd(vers)₃ molar ratio was varied. Nd(vers)₃ is the neodymium salt of "Versatic 10," which is a mixture of isomeric tertiary carboxylic acids.
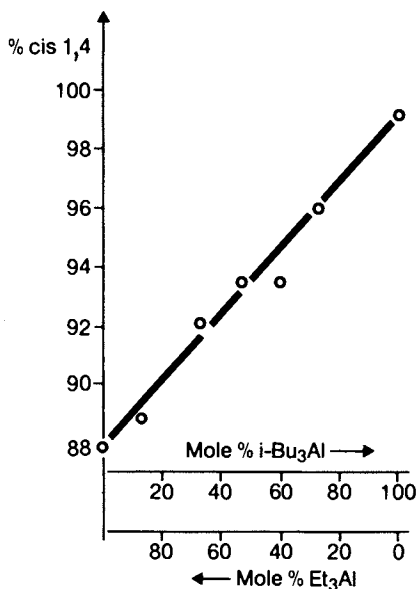
Figure 3. Effect of Et₃Al: i-Bu₃Al molar ratio on microstructure. Polymerization conditions: monomer concentration, 11 wt % in hexane; catalyst concentration, 7.5 × 10⁻⁵ mol/L; molar ratio Nd(vers)₃: Et₃Al₂Cl₃:AlR₃, 1:1:30; polymerization time, 2 h; and 60°C.

In the industrial processes for the production of polybutadiene
with Ti, Co, or Ni catalysts it can be controlled to only a very
small extent. In comparison with the commercially available poly-
butadienes, SE-BR (SE stands for Seltene Erden, which means rare
earths) has a broader molecular weight distribution, which can
be altered, however, by varying the ratio of Lewis acid to neo-
dymium. Table II shows that an increase of this ratio from 0.8 to
2.0 increases the molecular weight distribution from 7 (which is
close to that of Ni-BR) to 27.

The rate of crystallization of polybutadiene depends mainly
on the cis content and therefore on the catalyst system. As far
as commercial catalysts are concerned it increases in the order:
Li < Ti < Co < Ni. High-cis SE-BR, like U-BR, crystallizes more
rapidly than all the other types (Table III). However, SE-BR
with 93 % cis-1,4 content, and even one with only 90 % cis-1,4
content, crystallizes more rapidly than Ti-BR (93 % cis-1,4 con-
tent). In our opinion the reason for this anomaly is a structural
disorder in molecules with different chain length.

In fact, by fractional precipitation we found that the frac-
tions with the highest molecular weights are sterically very uni-
form and contain more than 97 % of cis-1,4 double bonds (Table
IV). Lower molecular weight fractions, on the other hand, have
relatively high trans-1,4 contents. We therefore take the view
that the rate of crystallization is determined mainly by the
high molecular weight fractions.

X-ray diffraction pictures taken with a flat-film camera show
that crosslinked SE-BR samples crystallize on stretching. Sharp
reflections are observed at an extension ratio of 4:1 (Figure 4).
With samples having different degrees of stereoregularity the
order for increasing strain-induced crystallization is the same
as the order for the rate of low temperature crystallization.

SE-BR has several outstanding properties. Above all it has
improved processability. Carbon black-filled compounds based on
commercial BR show the well known bagging and sagging effects on
the batch-off mill (13) unless the BR is blended with NR or SBR.
Figure 5 shows a compound based entirely on Ti-BR and containing
50 parts of carbon black, at various times on the roll mill.
Even after several minutes the sheet is not smooth.

In contrast, as shown in Figure 6, a smooth band on the mill
is obtained almost immediately when the compound is the same ex-
cept that the rubber is SE-BR or U-BR.

As a consequence of the high shear rate to which the rubber
is subjected at the nip of the mill crystallization occurs at
temperatures of up to 80 $^{\circ}$C in compounds based on SE-BR and U-BR,
and this phenomenon is responsible for the improvement in the
processing behaviour.

One of the characteristics of SE-BR and U-BR is the greatly
increased tackiness of uncured carbon black-filled compounds, as
compared with that of corresponding compounds based on the com-
mercially available materials. We determined the tackiness ac-

Table II. Effect of Lewis acid: Nd compound molar ratio on molecular-weight distribution. Polymerization conditions: butadiene concentration, 10 wt % in cyclohexane; catalyst concentration, 7.5×10^{-5} mol/l; molar ratio Nd(vers)$_3$, Et$_3$Al$_2$Cl$_3$, AlEt$_3$ is 1:X:30; polymerization time: 2 h, and 60°C.

$\dfrac{Et_3Al_2\,Cl_3}{Nd\,(vers)_3}$	$\overline{M}_w$ x 10^{-5}	$\overline{M}_n$ x 10^{-5}	Polydispersity $\overline{M}_w/\overline{M}_n$
0.8	9	1.3	7
1.4	8	0.8	10
2.0	16	0.6	27
Ti – BR			3
Co– BR			4
Ni – BR			7
U – BR			8

Table III.   Half-time of crystallization ($t_{1/2}$) at −20°C of uncross-linked *cis*-1,4 BR, *cis* contents were determined by IR spectroscopy.

cis-1,4 BR type	*cis*-content %	t 1/2 (−20°C) min.
Li	35	–
Ti	93	360
Co	96	40
Ni	97	25
U	99	8
SE	90	100
	93	46
	98	7

Table IV.   Structural inhomogeneity of SE-BR.

Fraction No.	Weight, %	Microstructure, % cis	trans	vinyl	$[\eta]$, dl/g toluene, 25°C
1	24.4	97.7	1.8	0.5	11.5
2	19.7	97.5	2.0	0.5	7.7
3	15.5	97.5	2.0	0.5	3.9
4	8.0	96.0	3.4	0.6	1.9
5	12.9	95.4	4.0	0.6	1.2
6	12.8	94.5	5.0	0.5	0.6
Residue	6.7	–	–	–	0.3
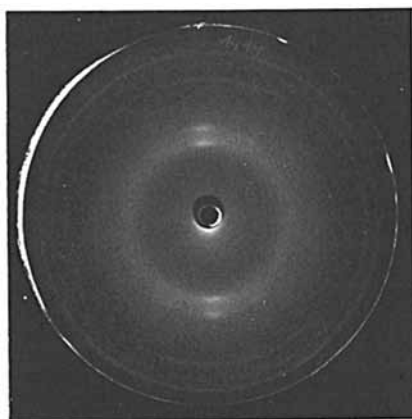
Figure 4.   X-ray diffraction pattern of peroxide-cross-linked SE-BR.   Gum stock, extension ratio 4:1.
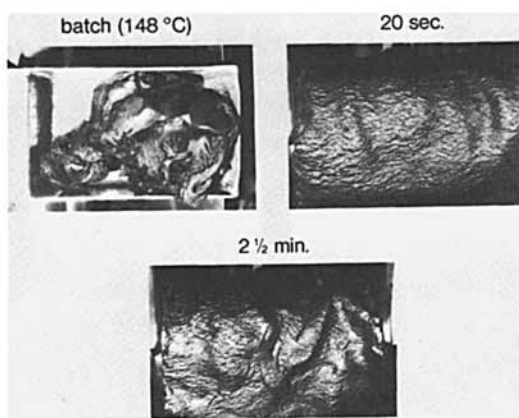
Figure 5.   Mill behavior of Ti-BR.   Mooney viscosity (ML 1 + 4/100°C), 47; compound, 50 parts carbon black N 330/5 parts oil.
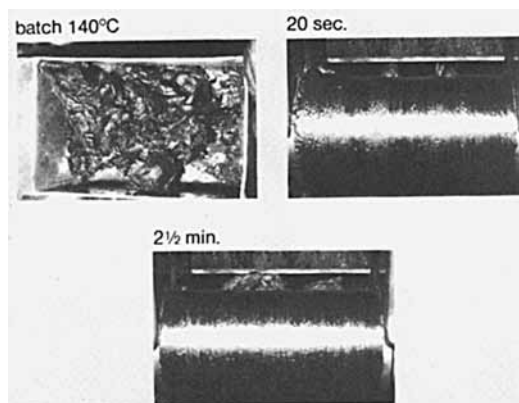
Figure 6.   Mill behavior of SE-BR.   Mooney viscosity (ML 1 + 4/100°C), 45; compound, 50 parts carbon black N 330/5 parts oil.

cording to a method developed by our company (14). The ends of a
small strip of rubber covered on one side with impregnated cot-
ton fabric are pressed together by a constant force for a given
period of time. The resulting loop is pushed onto a fixed roll
and a weight is attached. The time required to separate the bond
is a measure of the tackiness of the rubber compound employed.
Table V shows that the separation times of compounds based on
SE-BR are considerably longer than those of compounds based on
the commercially available BRs under three different weights.

    SE-BR with a broad molecular weight distribution has rela-
tively high green strength. As the stress-strain diagram shows
(Figure 7), the green strength of the uncured carbon black-filled
compound, though not equal to that of a compound based on natural
rubber, considerably exceeds the values of the compounds based
on the other BR types and synthetic cis-1,4 polyisoprene. This
finding is probably attributable to the rapidity with which the
sterically pure high molecular fractions crystallize under ex-
tension.

    Alternating Copolymerization. In the last part of this paper
we would like to refer briefly to our findings in connection with
the alternating copolymerization of dienes with olefins. The al-
ternating copolymerization of butadiene with propylene was first
investigated in 1969 by Furukawa and others (15, 16, 17). They
used catalyst systems based on titanium or vanadium compounds.
The titanium catalysts give copolymers of high molecular weight,
but with relatively low stereoregularity. On the other hand the
vanadium catalysts give the desired high degree of stereoregular-
ity, but they do not readily give polymers of high molecular
weight. About 5 millimoles of the transition metal compound is
needed per 100 g of monomer.

    We prepared a number of dialkoxyvanadium oxychlorides and
investigated their catalytical activity in the alternating co-
polymerization of butadiene and propylene with triisobutylalu-
minum as co-catalyst. The results listed in Table VI show a
marked dependence of the catalyst activity on structural changes
in the alkoxy ligands. We found that the per cent conversion
depends on the bulkiness and position of the substituents in the
alkyl group R. If R is an n-alkyl group, the catalyst is inactive
under our polymerization conditions (numbers 1, 3, 9, and 16).
Although α-branching in the alkyl group increases the activity,
this is still highly unsatisfactory (numbers 2, 4, 6, and 11).
The per cent conversion can be increased considerably by β-sub-
stitution, as shown in examples 5, 7, 12, 14, and 15. The best
results are obtained by introducing two substituents at the β-
carbon atom of R (10), whereas substitution in the γ-position is
ineffective (18, 19).

    Using dineopentoxyvanadium oxychloride we studied the effects
of several organoaluminum compounds as co-catalysts. It was found
that only aluminumtrialkyls are effective co-catalysts and that

Table V.   Tackiness of various types of polybutadienes as determined by the test procedure of Ref. 14.   Compound (phr): rubber 100; carbon black 50; aromatic oil 5.

polybutadiene type	separation time in sec.		
	at 500	1000	2000 9
Ti	85	26	11
Co	260	117	50
Ni	>300	208	65
U	>300	>300	>300
SE	>300	>300	>300
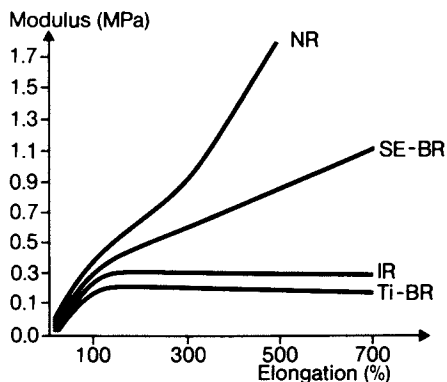
Figure 7.   Green strength of different rubbers.   Elongation rate, 0.3 m/min; compound, 55 parts carbon black N 330; NR, natural rubber; IR, synthetic cis-1,4-polyisoprene.

alkylaluminum hydrides, alkoxides, and halides are not. The activity of aluminum alkyls increases in the order Me < Et < n-Bu < n-Oct << i-Bu (Table VII). The molar ratio of the aluminumtrialkyl to the vanadium compound ranged from 3:1 to 10:1.

In contrast to the catalysts described by Furukawa, our system does not require preforming, which, indeed, brings a loss of activity.

The same catalyst system, consisting of dineopentoxyvanadium oxychloride and triisobutylaluminum, is also suitable for the alternating copolymerization of isoprene with ethylene (20).

The molecular weight of copolymers is controlled by means of the polymerization temperature. As Table VIII shows, butadiene-propylene copolymers with low Mooney viscosity are obtained at temperatures above -40 °C. A decrease of the reaction temperature increases the molecular weight.

The copolymers consist of strictly alternating sequences of diene and olefin. ^{13}C-NMR measurements showed the microstructure of the butadiene units in BPR to be exclusively of the trans-1,4 configuration (Figure 8). The isoprene units in isoprene-ethylene copolymer (IER) contain 84 % trans-1,4, 15 % cis-1,4, and 1 % 3,4 structures (Figure 9). Spontaneous crystallization in unstretched BPR samples was detected by dilatometry and confirmed by X-ray diffraction and DSC measurements. The extrapolated equilibrium melting point is about -10 °C.

X-ray diffraction tests on BPR initially gave no indication of strain-induced orientation. Recently, however, we noticed the formation of dense phases with parallel chain packing, but without three-dimensional periodicity (Figure 10), in crosslinked and highly stretched samples which had been prepared under modified polymerization conditions. The dense phase is retained until the temperature reaches about 60 °C. The imperfect crystallization indicates that the molecules have a considerable proportion of disordered structure. In view of the high stereoregularity of the butadiene units and the strictly alternating structure of the molecules, the imperfect crystallization should be attributed to the lack of ordered configurations of the chiral C atoms in the propylene units.

The absence of asymmetric carbon atoms in IER could explain why the strain-induced crystallization is more pronounced in this case. Numerous strong reflections of the type shown in Figure 11 were obtained by X-ray diffraction of stretched IER samples at 30 °C. It is therefore evident that a well-formed crystal lattice exists.

Figure 12 shows the stress-strain curves of IER at various temperatures. A strain-induced reinforcing effect is not observed at temperatures above -10 °C. This fact may be due to network inhomogeneities caused by imperfect crosslinking.

The different results in X-ray and stress-strain tests are probably attributable to differences in the preparation of the

Table VI.   Effect of R in VO(OR)₂Cl on catalyst activity. Polymerization conditions: molar ratio butadiene, propylene is 1.1, monomer concentration, 31 wt. % in *n*-hexane; reaction, −50°C; catalyst, 0.8 mmol VO(OR)₂Cl phm, 6.0 mmol i-Bu₃Al phm; reaction time, 3 h. Data from Ref. 19.
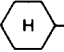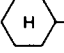
No.	VO(OR)₂Cl R=	conversion %	No.	VO(OR)₂Cl R=	conversion %
1	$CH_3-CH_2-CH_2-$	0	9	$CH_3-CH_2-CH_2-CH_2-CH_2-$	0
2	$(CH_3)_2CH-$	1.2	10	$CH_3-C(CH_3)_2-CH_2-$	80
3	$CH_3-CH_2-CH_2-CH_2-$	0	11	$(CH_3)_2CH-CH_2-CH(CH_3)-$	1.6
4	$CH_3-CH_2-CH(CH_3)-$	8.2	12	$(CH_3-CH_2)_2CH-CH_2-$	14.7
5	$(CH_3)_2CH-CH_2-$	7.7	13	cyclohexyl-H	0
6	$CH_3-CH_2-CH_2-CH(CH_3)-$	1.6	14	cyclohexyl-H-CH_2-	9.8
7	$CH_3-CH_2-CH(CH_3)-CH_2-$	9.8	15	$(CH_3-CH_2-CH_2-CH_2)(CH_3-CH_2)CH-CH_2-$	23
8	$(CH_3)_2CH-CH_2-CH_2-$	0	16	$CH_3-(CH_2)_6-CH_2-$	0

Table VII.   Effect of organoaluminum compounds on catalyst activity. Polymerization conditions: molar ratio butadiene, propylene is 1.1; monomer concentration, 20 wt % in toluene; catalyst, 0.8 mmol VO[OCH₂C(CH₃)₃]₂Cl phm, 5 mmol Al compound phm; reaction time, 4 h; and −45°C. Data from Ref. 19.

Al-compound	conv.%	$[\eta]$ dl/g, toluene, 25°C
Me₃Al	< 5	–
Et₃Al	5.2	0.88
n-Bu₃Al	17	1.05
i-Bu₃Al	66	1.25
Oct₃Al	29	1.20
i-Bu₂Al H	–	
Et₂Al Cl	–	
Et₂Al Br	–	
i-Bu₂Al Cl	–	
Et₂Al OEt	–	
Et₃Al₂ Br₃	–	

Table VIII.   Effect of reaction temperature on molecular weight of butadiene-propylene rubber (BPR). Polymerization conditions as in Table VII, with i–Bu$_3$Al as alkylaluminum compound. Data from Ref. 19.

T °C	$[\eta]$,dl/g toluene, 25°C	ML 1 + 4/100°C	$\bar{M}_w \times 10^{-3}$
–20	0.81	–	55
–30	0.99	10	70
–40	1.25	28	130
–50	1.48	56	175
–55	1.62	63	·200
–60	1.73	70	240
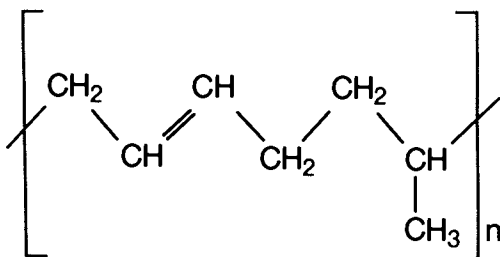
Figure 8.   *Alternating butadiene–propylene copolymer.*
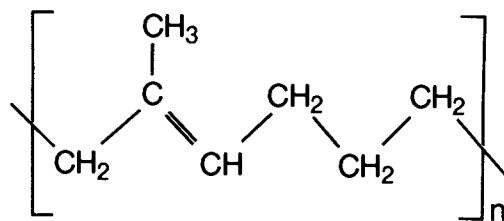
Figure 9.   *Alternating isoprene–ethylene copolymer.*
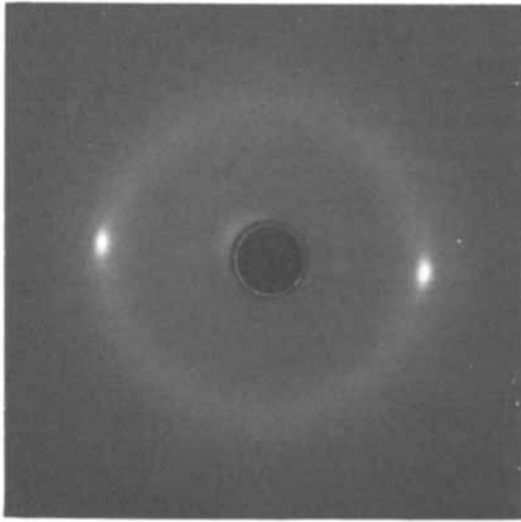
Figure 10.   X-ray diffraction pattern of BPR, gum vulcanizate.   Extension ratio, 8:1; 56°C.
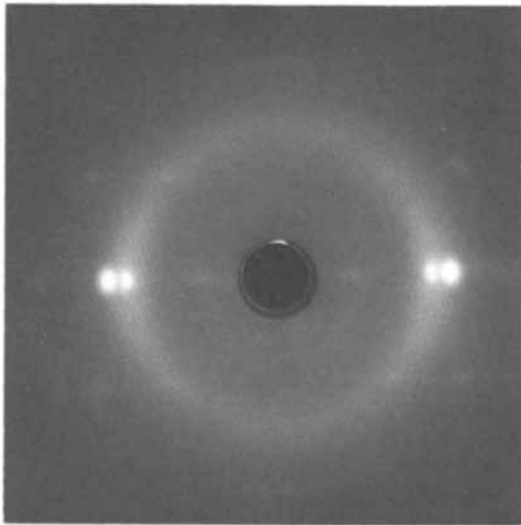
Figure 11.   X-ray diffraction pattern of IER, gum vulcanizate.   Extension ratio, 8:1.

Modulus
(MPa)
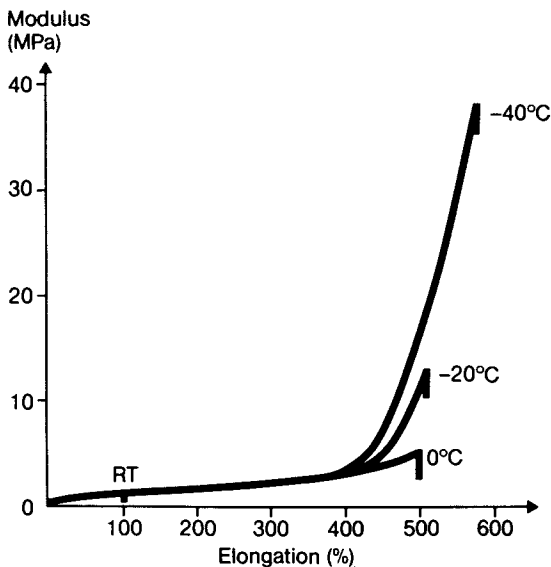
Figure 12.   Stress–strain curves of IER at different temperatures. Gum stock, 0.5 sulfur, 1.5 phr N-cyclohexyl-2-benzothiazyl sulfenamide, and 0.5 phr tetramethylthiuram monosulfide).

crosslinked samples. The samples used for X-ray diffraction were prepared by mixing solutions of rubber and dilauroyl peroxide and subsequent evaporation of the solvent. In this case the curing agent should be well distributed in the rubber. In contrast, samples used for stress-strain tests were prepared by incorporating sulfur and accelerators on a two-roll mill.

LITERATURE CITED

1. Throckmorton, M.C.; Saltman, W.M. (To Goodyear Tire and Rubber Company) U.S. 3,676,411.
2. Lugli, G.; Mazzei, A.; Brandi, G. (To Snam Progetti S.p.A.) U.S. 3,935,175.
3. Sylvester, G.; Witte, J.; Marwede, G. (To Bayer AG) U.S. 4,145,497.
4. Dohlen, von, W.C.; Wison, T.P.; Caflisch, E.G. (To Union Carbide Corp.) U.S. 3,297,667.
5. Throckmorton, M.C. Kautschuk, Gummi, Kunststoffe. 1969, 22, 293.
6. Sheng Tse-chuan; Gung Chung-yuan; Chung Chung-chi; Ouyang-chun. Scientia Sinica. 1964, 8, 1339.

7.   Shen Zhiquan et al. J. Polym. Sci. Polym. Chem. Ed. 1980,
     18, 3345.
8.   Pedretti, U.; Lugli, G.; Poggio, S.; Mazzei, A. (To Anic
     S.p.A.) DE-OS 2,833,721.
9.   Mazzei, A. Makromol. Chem. Suppl. 1981, 4, 61.
10. Bruzzone, M. Makromol. Chem. Suppl. 1981, 4, 177.
11. Sylvester, G.; Witte, J.; Marwede, G. (To Bayer AG)
     U.S. 4,260,707.
12. Sylvester, G.; Witte, J.; Marwede, G. (To Bayer AG)
     DE-OS 2,848,964.
13. Giuliani, G.P.; Sorta, E.; Bruzzone, M. Angew. Makromol.
     Chem. 1976, 50, 87.
14. Esch, E.; Fries, H.; Dahl, H.; Kempermann, Th. Kautschuk,
     Gummi, Kunststoffe. 1979, 30, 524.
15. Furukawa, J. J. Polym. Sci. 1969, 7, 613.
16. Furukawa, J. Makromol. Chem. 1972, 23, 189.
17. Kawasaki, A.; Maruyama, J.; Ichihara, C. (To Maruzen Petro-
     chemical Co.); DE-OS 2,020,168.
18. Witte, J.; Sylvester, G.; Marwede, G. (To Bayer AG)
     U.S. 4,189,558.
19. Wieder, W.; Witte, J. J. Appl. Polym. Sci. 1981, 26, 2503.
20. Wieder, W.; Witte, J. (To Bayer AG) DE-OS 2,943,129.

Synthesis and Properties of Diene Elastomers With Controlled Structure

I. G. HARGIS, R. A. LIVIGNI, and S. L. AGGARWAL

The General Tire & Rubber Company, Research Division, Akron, OH 44305

Using organolithiums or complexes of diorgano-
magnesiums with trialkylaluminums, in combination
with specific barium salts, we are able to control
the trans-1,4/cis-1,4 ratio in butadiene-styrene
copolymers, while still maintaining a low vinyl
content. The important reaction variables for
doing this are the barium/metal alkyl ratio,
polymerization temperature, and initiator con-
centration. For SBR's prepared with Ba-Mg-Al
initiators in comparison to barium modified
alkyllithiums, the trans-1,4 content is higher
(87% vs. 79%) and the vinyl content is lower
(3% vs. 8%). Moreover, the Ba-Mg-Al initiator
system has the characteristics of a "living
polymerization" providing control of average
molecular weight, molecular weight distribu-
tion, and molecular architecture. The crys-
talline melting temperature of these trans-1,4
polybutadienes can be decreased to near room
temperature by adjustment of the trans-1,4
content and/or the incorporation of styrene.
Their crystallization behavior compares with
natural rubber, as follows: (1) their rate of
crystallization is more rapid; and (2) their
amount of crystallinity is temperature dependent,
but considerably less strain dependent. These
experimental rubbers have excellent green strength
and building tack.

During the last two decades, a number of diene homopolymers
and copolymers have been developed to fill the diverse elastomer
needs in the production of tires. The earliest developments
were mainly concerned with the preparation of stereoregular
cis-1,4-polyisoprene, as a substitute for natural rubber, using

Ziegler-Natta catalysts (1) and organolithium compounds (2).
This was soon followed by the synthesis of high cis-1,4 poly-
butadiene using Ziegler-Natta catalysts (3).
    More recently, a number of different copolymer structures
have been prepared from butadiene and styrene, using modified
organolithiums as polymerization initiators (4). Organolithium
initiated polymerizations have gained prominence because stereo-
control is combined with excellent polymerization rates, and
the absence of a chain termination reaction facilitates control
of molecular weights and molecular weight distributions (5).
    This paper will describe the ways in which the present
needs in tire rubbers can be met by preparing butadiene-
styrene solution polymers of controlled structure. This
appears especially realizable today, as a result of two new
classes of organo-alkaline earth polymerization initiators,
Ba-Li and Ba-Mg-Al, which provide unique steric control of the
trans-1,4/cis-1,4 ratio of polybutadiene segments (6). Although
Alfin rubbers (7) contain trans contents at 70-75%, their vinyl
contents are much greater (20-25%) than is characteristic of
the new rubbers reported here.

Experimental

    Materials. Barium t-butoxide-hydroxide was prepared by
reacting barium metal with a mixture of t-butanol and water
(10 mole % water) in liquid monomethylamine, as shown in
Figure 1. n-Butyllithium (Foote Mineral Co., 15 wt.% in n-
hexane) was diluted with dry cyclohexane to the desired con-
centration. MAGALA-7.6E is a trade name for a complex of
n-dibutylmagnesium and triethylaluminum (Mg/Al molar ratio of
7.6) supplied by Texas Alkyls as a 10 wt.% solution in n-
heptane. MAGALA-7.6E was diluted with dry cyclohexane prior
to its use. n-Hexane (Phillips Petroleum Co., 99%) was dried
by passing it through Linde 5A molecular sieves. Butadiene
(Phillips Petroleum Co., 99 mol %) was purified by passing it
through Linde 13X molecular sieves. Styrene (Gulf Oil Chemi-
cal Co.) was vacuum distilled from a small quantity of (n-
butyl)(sec-butyl) magnesium.

    Polymerizations. The polymerizations were carried out in
an argon atmosphere in capped glass bottles fitted with a
neoprene rubber gasket inner liner. In charging the polymer-
izations, the order of addition of materials was solvent first,
then metal alkyls, next the barium salt, and finally the
monomer(s). The amount of metal alkyl charged was sufficient
to titrate the acidic impurities present in the solvent and
polymerization bottle, plus the calculated amount for initia-
tion of polymerizations. The mole ratio of barium to metal
alkyl(s) was based on the moles of total alkalinity of barium
to the moles of carbon-metal assayed. Unless otherwise stated,

the mole ratios of barium salt to BuLi or Bu_2Mg, denoted as Ba^{2+}/Li^+ or Ba^{2+}/Mg^{2+}, were 0.5 or 0.2, respectively. The percent conversion was calculated from a measurement of the total solids after removal of solvent and unreacted monomers by vacuum distillation.

Polymer Characterization. The copolymer composition and polybutadiene microstructure were obtained from infrared analysis and checked for certain copolymers using ^{13}C NMR. The microstructure values determined from IR and ^{13}C NMR were found to be essentially identical. The trans-1,4 and vinyl content were determined using the 967 cm^{-1} and 905 cm^{-1} infrared absorption bands, respectively. Intrinsic viscosities were determined in toluene at 30°C. Gel permeation chromatograms (GPC) were obtained using a Waters Gel Permeation Chromatograph. Solutions at 1 wt.% were injected onto columns at a flow rate of 1 ml/minute. The instrument oven and the differential refractometer were at 50°C. The column set configuration used, as designated by Waters Associates, was $10^6 Å + 10^5 Å + 10^4 Å + 10^3 Å$.

Polymer Crystallinity. Thermal transitions were obtained by Differential Thermal Analysis (DTA) and Differential Scanning Calorimetry (DSC) using a heating rate of 20°C/minute. Crystalline melting temperatures were determined from the position of the endothermic peak(s) present in the curve, obtained after rapidly cooling the sample from room temperature to -150°C. X-ray diffraction patterns were obtained from films cured with 1% dicumyl peroxide in the absence of fillers. All the experiments were carried out at room temperature using CuKα radiation and a nickel filter using flat plate photography. Stress-optical measurements were made with a conventional apparatus. The light source was a mercury lamp. Polymers were cured in the absence of reinforcing fillers with a sulfur based recipe.

Polymer Properties. Green strength data were obtained from stress-strain measurements on unvulcanized polymers with an Instron tester at room temperature. The crosshead speed was 50.8 cm/minute. Sample specimens were prepared by press molding tensile sheets at 121°C for 5 minutes with a ram force of 11360 kg. Tack strength was measured using the Monsanto Tel-Tak machine. The test specimens were compounded polymers pressed between Mylar film at 100°C. Two 0.64 cm x 5.08 cm die-cut sample strips were placed at right angles to each other and retained in special sample clamps. A fixed load, 0.221 MPa, was then applied for specified contact times ranging from 6 seconds to 6 minutes. The samples were pulled apart at a constant separation rate of 2.54 cm/minute. The test was run at room temperature.

There are a number of specific requirements which must be
met for any tire rubber candidate, as shown in Figure 2. In
the production of radial tires, building tack and green strength
are very important, and these performance properties are achieved
by the use of NR. These properties are not readily attainable
from synthetic elastomers prepared from low cost monomers. We
have focused our studies, therefore, on copolymers of butadiene
and styrene prepared with two alkaline earth based catalyst
systems: barium t-butoxide-hydroxide/BuLi (Ba-Li), and barium t-
butoxide-hydroxide/Bu$_2$Mg/Et$_3$Al (Ba-Mg-Al). We have found them
to be extremely useful in controlling stereoregularity of diene
polymerizations and in providing SBR's with high tack and green
strength.

High Trans BR's by Ba-Li Catalyst Systems

Preparation and Properties of Barium Salt. The catalyst
used to prepare this new class of crystallizing polybutadienes
consists of a barium t-butoxide-hydroxide salt in combination
with an organolithium (8, 9, 10). Rather specific preparative
techniques must be used in forming this barium salt, as shown
in Figure 1. The use of an amine solvent provided quantitative
conversion of the metal to barium salts.

The molecular structure of polybutadiene prepared with
BuLi and barium salts is greatly dependent on the presence of
specific amounts of water and t-butanol used in the barium salt
formation. The data in Figure 3 demonstrate that the greatest
effect is obtained as the hydroxide content of the solution
phase of the barium salt increased from 0 to 7.4 mole % Ba(OH)$_2$.
This particular salt results from a H$_2$O-t-butanol mixture con-
taining 2.5 mole % water. The amount of trans-1,4 increased
from 63% to 76%, and accompanying this change the intrinsic
viscosity increased from 1.60 to 5.22. The polymers were gel-
free.

The most important polymerization variables on which the
molecular structure of polybutadienes prepared with Ba-Li
catalysts depends are described as follows.

Mole Ratio of Barium t-Butoxide-Hydroxide to n-BuLi.
Figure 4 shows that the amount of trans-1,4 structure is
increased from 55%, which is the trans-1,4 content of a poly-
butadiene prepared with BuLi alone in nonpolar solvents, to a
maximum of about 80% trans-1,4 content for polybutadienes
prepared at a mole ratio of barium salt to BuLi equal to 0.5.
This barium salt contains about 9 mole % hydroxide ion. It
is important to note that the vinyl content is not affected by
an increase in the mole ratio of Ba/Li from 0 to 0.5. However,
a further increase in the mole ratio above 0.5 results in a
decrease in the trans-1,4 content and a corresponding increase
in the vinyl content.

$Ba + CH_3NH_2 \xrightarrow{-78°C}$ BLUE SOLN. CHARACTERISTIC OF DISSOLVED METAL

t-BUTANOL + H₂O IN BENZENE

GRAY-WHITE PRECIPITATE $\xrightarrow{\text{AGED AT -15°C FOR 16 HRS.}}$ PRECIPITATE SETTLES OUT

CH_3NH_2 EVAPORATED SALT IS VACUUM DRIED

Ba t-BUTOXIDE–HYDROXIDE SALT IS DISSOLVED IN BENZENE AT 50°C
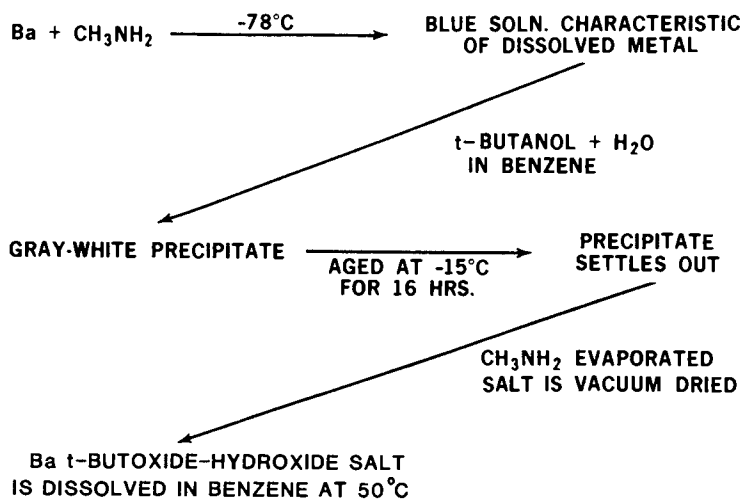
Figure 1. Preparation of Ba t-butoxide–hydroxide salt for polymerization catalyst.

1. PROCESSIBILITY

2. TACK AND GREEN STRENGTH

3. SKID AND ABRASION RESISTANCE

4. THERMAL AND CHEMICAL STABILITY

5. LOW HEAT BUILD-UP

6. LOW CUT GROWTH RATE

7. COST: LOW COST MONOMERS

Figure 2. Requirements for tire rubbers.

BARIUM SALT		% DIENE STRUCTURE		$[\eta]_{25}^{\Phi H}$
MOL % H_2O IN tert-BUTANOL + H_2O	MOL % HYDROXIDE* IN $Ba\left[(t\text{-}BuO)_{2\text{-}X}(OH)_X\right]$	TRANS	VINYL	dl/g
0	0	63	10	1.60
2.5	7.4	76	7	5.22
5.0	8.5	76	7	6.67
7.5	8.9	79	7	5.63
10.0	12.5	76	7	5.51
15.0	——	76	6	8.05
100	0	48	10	2.10

* IN SOL PHASE

Figure 3.   Effect of hydroxide content of Ba t-butoxide–hydroxide on the molecular structure of polybutadiene prepared in toluene at 30°C.
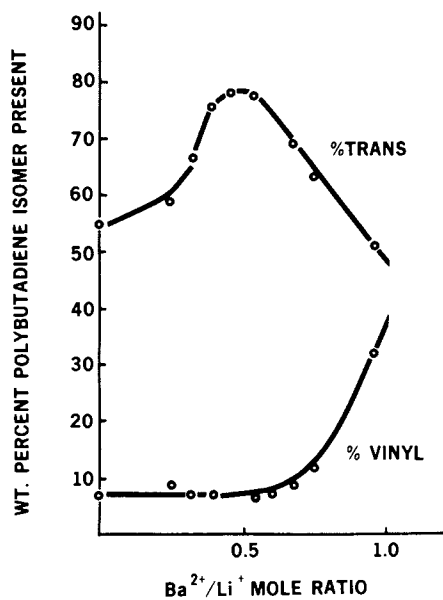
Figure 4.   Polybutadiene microstructure versus the mole ratio of Ba t-butoxide–hydroxide to n-BuLi. Conditions: solvent, toluene; 30°C.

Catalyst Concentration. The concentration of the catalyst
has a marked effect on the trans-1,4 content of polybutadienes
prepared with BuLi and barium t-butoxide-hydroxide in toluene at
30°C, as shown in Figure 5. The trans-1,4 content increases
with a decrease in the molar ratio of the initial butadiene to
BuLi concentration [(M)/(BuLi)]. The trans-1,4 content
approaches a limiting value of about 80% for polybutadienes
prepared with large amounts of this catalyst.

Polymerization Temperature. The stereoregularity of
polybutadienes prepared with the BuLi-barium t-butoxide-hydroxide
catalyst in toluene is exceedingly temperature dependent. Figure
6 compares the trans-1,4 dependence for polybutadiene prepared
with BuLi, alone, and with the BuLi-barium t-butoxide-hydroxide
complex in toluene (the molar ratio of the initial butadiene to
BuLi concentration was 500). The upper curve demonstrates that
the percent trans content increased rapidly from 62% to 80%
trans-1,4 as the temperature decreased from 75°C to 22°C. From
22°C to 5°C, the microstructure does not change. The increase
in trans-1,4 content occurred with a decrease in cis-1,4 con-
tent, the amount of vinyl unsaturation remaining at 5-8%. For
the polybutadienes prepared using BuLi alone, there is only a
very slight increase in the trans-1,4 content as the polymeriza-
tion temperature is decreased.
    The amount of both low and high molecular weight polymer
produced, as a function of polymerization temperature, can be
seen in Figure 7. In this Figure, the MWD's of polybutadienes
prepared with barium t-butoxide-hydroxide and BuLi in toluene
at 30°C and 5°C are compared. Although both polymers show a
broad MWD, the fraction of low molecular weight polymer present
in the polybutadiene prepared at 5°C is greatly decreased.

Variation of Styrene Content with Extent of Conversion.
Figure 8 gives the relationship between copolymer composition
and the extent of conversion for copolymers of butadiene and
styrene (25 wt.% styrene) prepared in toluene, at 30°C, with
n-BuLi and barium salts of t-butanol and water. For comparison
purposes, the copolymer composition curve is shown for the
reaction initiated using n-BuLi alone. Copolymerization using
n-BuLi results in very little incorporation of styrene into the
copolymer chain until about 75% conversion, after which the
styrene content increases very rapidly. In contrast, copolymer-
ization using the barium salts and n-BuLi results in an increased
incorporation of styrene at the same extents of conversion.
Thus, this polymerization catalyst yields more random copolymers
with styrene, while still maintaining a low vinyl content and
high trans-1,4 content.

Chain Termination in Ba-Li Polymerizations. Another
important feature of these butadiene based rubbers, prepared
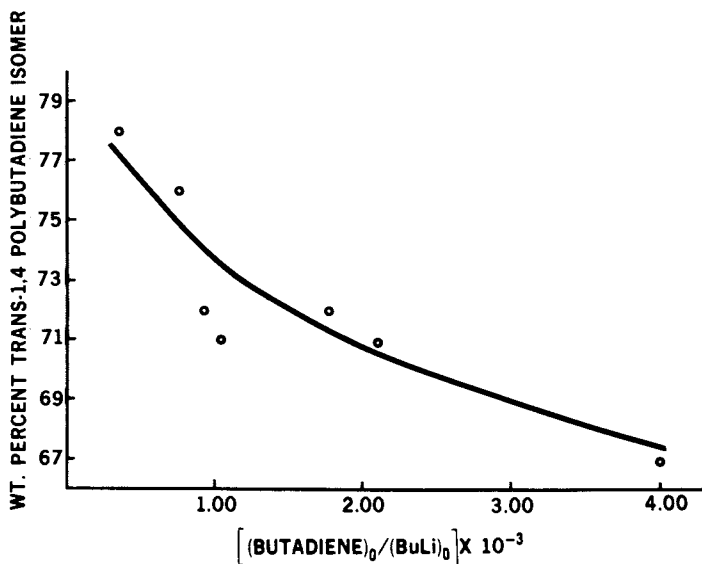
Figure 5.   Variation of trans-1,4 content with the molar ratio of monomer to initiator. Conditions: solvent, toluene; catalyst, $Ba[(t\text{-}BuO)_{2x}(OH)_x]$ and n-BuLi.
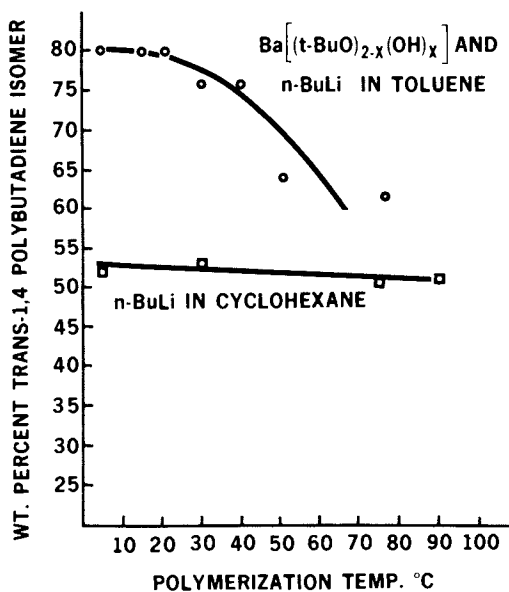
Figure 6.   Variation of percent trans-1,4 content with polymerization temperature.
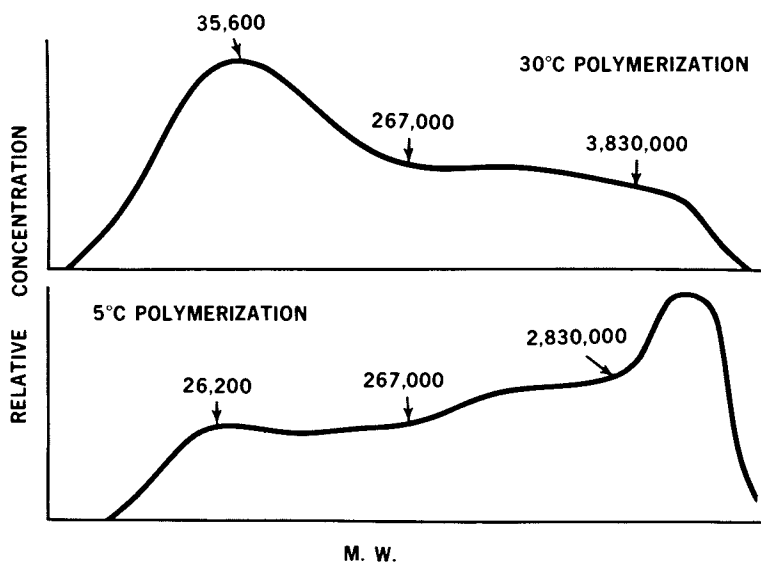
Figure 7.   *Effect of polymerization temperature on molecular weight distribution of polybutadienes.*
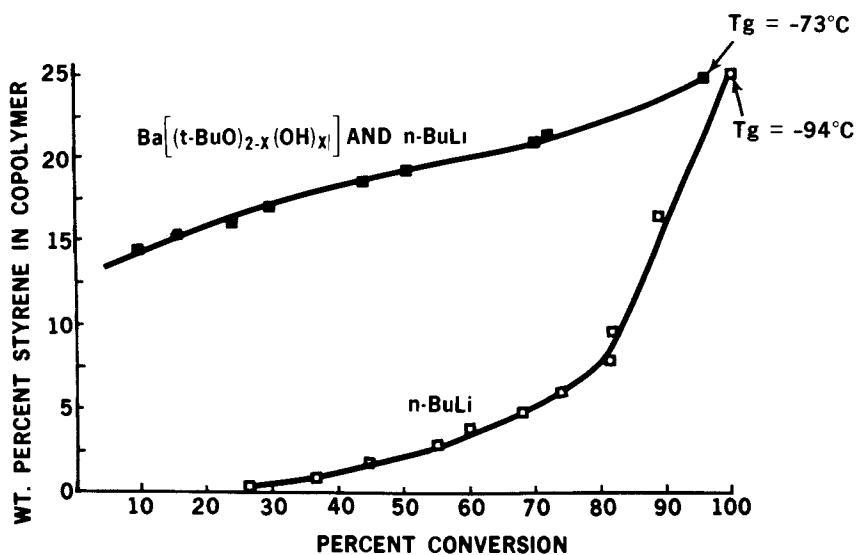
Figure 8.   *Copolymer composition variation with percent conversion. Conditions: butadiene–styrene (75/25) in toluene at 30°C.*

with the barium t-butoxide-hydroxide catalyst, is the variation
in molecular weight with conversion. Extremely high molecular
weight polymer is formed continuously throughout the course of
the polymerization. Intrinsic viscosity is essentially indepen-
dent of conversion, suggesting that the polymer chain growth
reaction is rapid and controlled by a chain termination step.
For polymerizations of butadiene in toluene at 50°C with the
Ba-Li catalyst, we have observed a reduction in molecular weight
and the incorporation of benzyl groups in chains of polybuta-
diene. We conclude from this result that proton abstraction
from toluene occurs to give benzyl carbanions which are capable
of forming new polymer molecules in a chain transfer reaction.
The amount of benzyl incorporation increases with increasing
polymerization temperature and/or Ba/Li mole ratio.

     Differential Thermal Analysis (DTA). One of the character-
istics of a rubber useful in tire rubber compounds is that it is
amorphous at room temperature but readily undergoes strain in-
duced crystallization. For this reason, copolymers were prepared
in order to appropriately adjust the crystalline melt tempera-
ture.
     The polybutadienes prepared with these barium t-butoxide-
hydroxide/BuLi catalysts are sufficiently stereoregular to
undergo crystallization, as measured by DTA (8). Since these
polymers have a low vinyl content (7%), they also have a low
glass transition temperature. At a trans-1,4 content of 79%,
the T_g is -91°C and multiple endothermic transitions occur at
4°, 20°, and 35°C. However, in copolymers of butadiene (equiva-
lent trans content) and styrene (9 wt.% styrene), the endo-
thermic transitions are decreased to -4° and 25°C. Relative
to the polybutadiene, the glass transition temperature for the
copolymer is increased to -82°C. The strain induced crystalli-
zation behavior for a SBR of similar structure will be discussed
after the introduction of the following new and advanced syn-
thetic rubber.

High Trans BR's by Ba-Mg-Al Catalyst System

     Polymer Preparation. A more recent modification in the
molecular structure of styrene-butadiene copolymers has been
obtained with the discovery of a new catalyst system (6). The
catalyst consists of a barium t-alkoxide-hydroxide salt together
with a complex of dialkylmagnesium and trialkylaluminum.
Polymer synthesis is carried out according to the scheme
shown in Figure 9. A major distinction between the Ba-Mg-Al
and Ba-Li catalysts is that no polymerization of butadiene or
copolymerization of butadiene with styrene occurs when only
one of the three catalyst components of Ba-Mg-Al is used alone
at 50°C in nonpolar solvents. This behavior contrasts with the
potential ability of n-BuLi alone to form polymer in the Ba-Li
catalyst system.

STYRENE $\xrightarrow[\text{+ Ba t-ALKOXIDE SALT}]{\text{Bu}_2\text{Mg·AlEt}_3 \text{ COMPLEX}}$ HTSBR (LINEAR CHAINS WITH NARROW MWD)

DIVINYLBENZENE

HTSBR (SLIGHTLY BRANCHED CHAINS WITH BROADENED MWD)
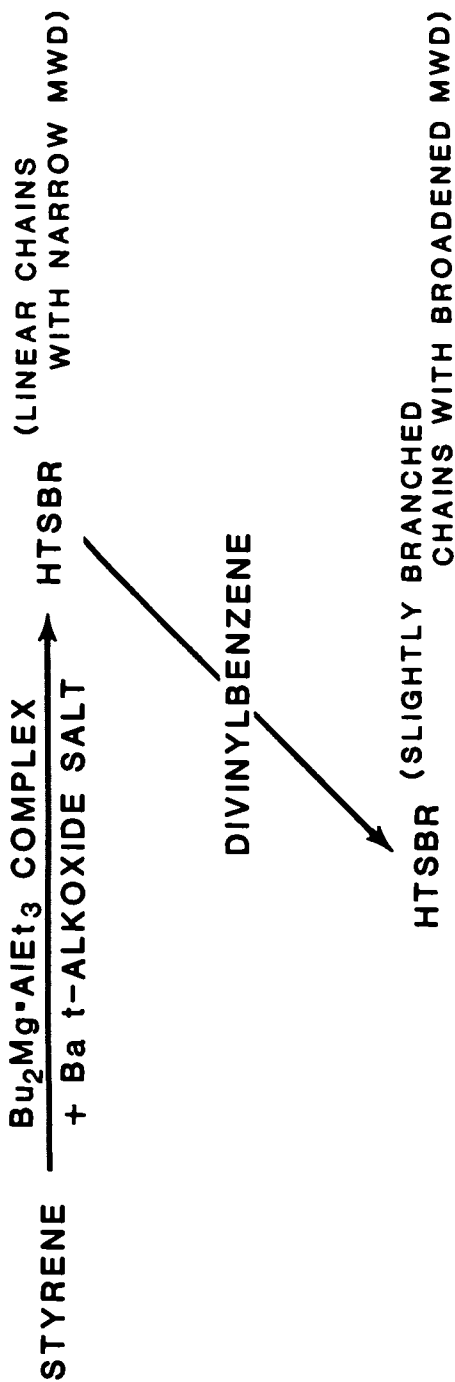
Figure 9. *Process for preparation of high* trans-*SBR.*

The most important polymerization variables on which the
molecular structure of polybutadienes prepared by Ba-Mg-Al
depends are the ratio of barium salt to dibutylmagnesium at
constant Mg/Al, the polymerization temperature, and catalyst
concentration.

Mole Ratio of Ba/Mg at Constant Mg/Al. Figure 10 shows the
dependence of the microstructure of polybutadienes on the mole
ratio of Ba/Mg with a Mg/Al ratio of 6/1 for polymerizations
carried out in cyclohexane at 50°C. The amount of trans-1,4
structure is increased to a maximum of about 90% as the mole
ratio of Ba/Mg is decreased from 1.0 to about 0.20. Con-
currently, the vinyl content decreased from 7% to 2%. At a
mole ratio of 0.05, polymerization was not observed in cyclo-
hexane at 50°C after 3 days.

Polymerization Temperature and Catalyst Concentration.
The stereoregularity of butadiene based polymers prepared in
cyclohexane with Ba-Mg-Al catalysts depends on polymerization
temperature and catalyst concentration. Trans-1,4 content
increases nonlinearly with a decrease in polymerization tem-
perature over the range of 80° to 30°C (Figure 11) and/or a
decrease in the initial molar ratio of butadiene to dialkyl-
magnesium from 3400 to 400 (Figure 12). For polybutadienes
prepared with relatively large amounts of catalyst at 30°C,
the trans-1,4 content approaches a limiting value of about 90%.

Butadiene-Styrene Copolymers from Ba-Mg-Al Catalyst Systems.
Figure 13 shows the relationship between copolymer composition
and extent of conversion for copolymers of butadiene and styrene
(25 wt.% styrene) prepared in cyclohexane with Ba-Mg-Al and with
n-BuLi alone. Copolymerization of butadiene and styrene with
barium salts and Mg alkyl-Al alkyl exhibited a larger initial
incorporation of styrene than the n-BuLi catalyzed copolymeriza-
tion. A major portion of styrene placements in these experi-
mental SBR's are more random; however, a certain fraction of
the styrene sequences are present in small block runs.
        Quantitative polymerizations of butadiene and copolymer-
izations of butadiene with styrene to high molecular weight
polymers have been obtained. Plots of ln (M_0/M_t) versus time
are linear, indicating a first order dependence on monomer.
In the low catalyst concentration range, polymerization rate
is increased with increased amounts of catalyst; however, the
exact rate dependence on catalyst concentration has not been
established. In general, the rate of copolymerization of
butadiene with styrene is increased with increased polymeriza-
tion temperature, increased Ba/Mg mole ratio, increased buta-
diene/styrene comonomer feed ratio, and increased dielectric
constant of the polymerization solvent.
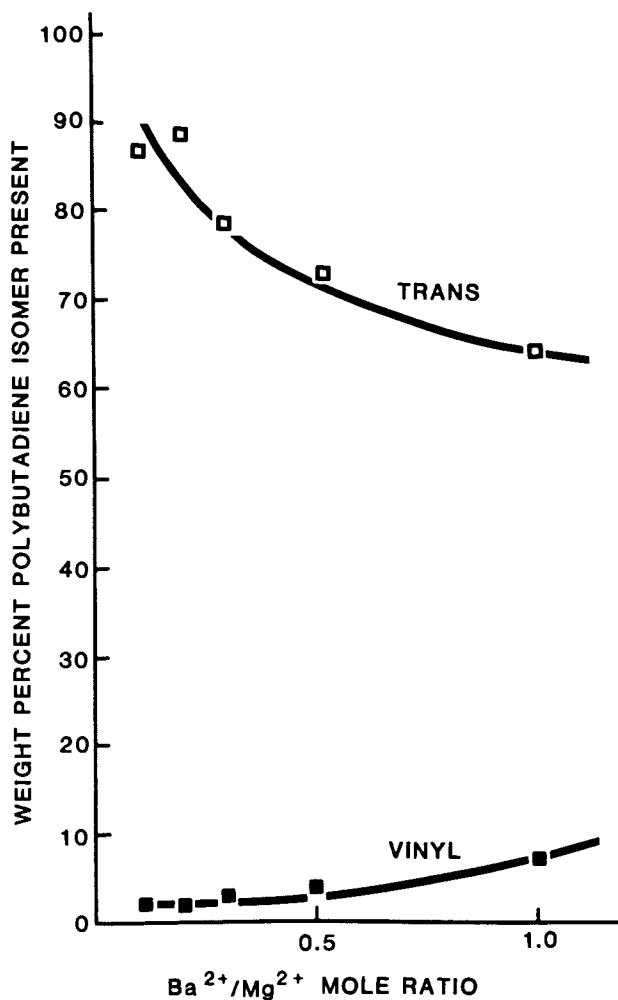
Figure 10. *Polybutadiene microstructure versus the mole ratio of Ba t-alkoxide–hydroxide to Bu₂Mg in Ba-Mg-Al catalyst. Conditions: solvent cyclohexanes; mole ratio Mg/Al (6/1); 50°C.*
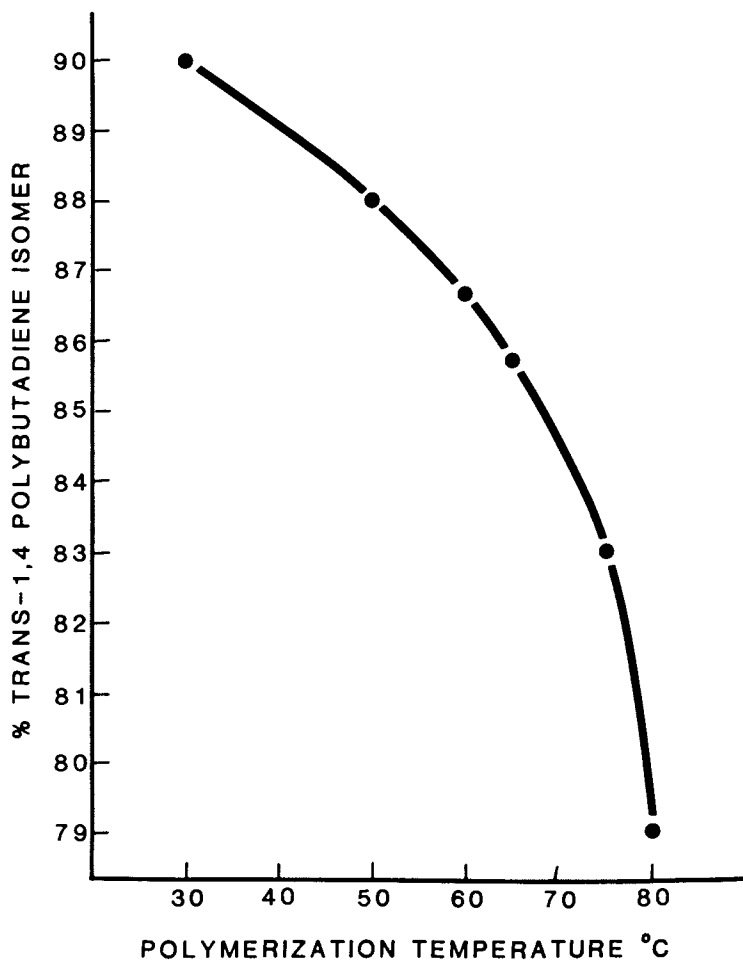
Figure 11. Variation of percent trans-1,4 content with polymerization temperature. Conditions: solvent, cyclohexane; Mg-Al-Ba, 1.0/0.2/0.2; $(Bd)_0/(Mg)_0$, 400–1,000.
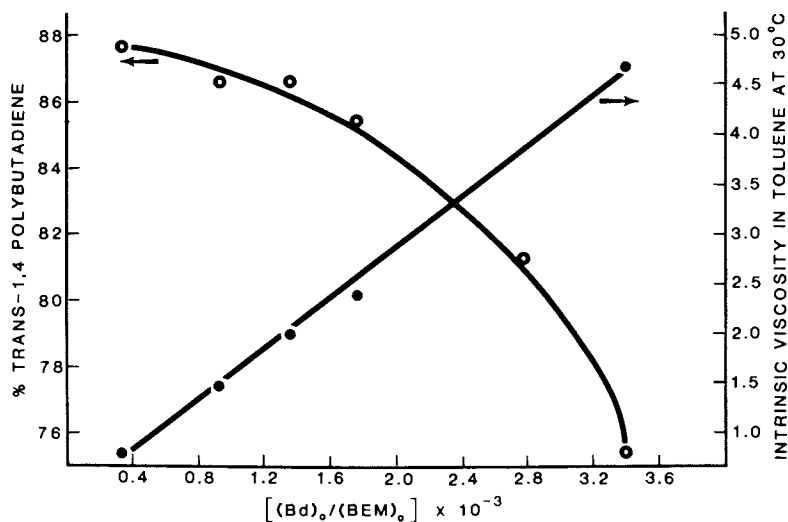
Figure 12. *Variation of* trans-1,4 *content and intrinsic viscosity of polybutadiene with molar ratio of Bd to butylethylmagnesium (BEM). Conditions: solvent, cyclohexane; Mg-Al-Ba, 1.0/0.2/0.2; 60°C.*
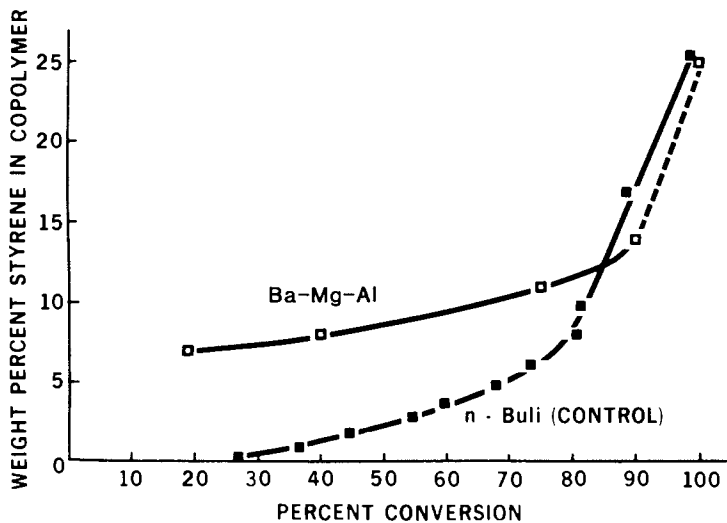
Figure 13. *Copolymer composition variation with percent conversion. Conditions: butadiene–styrene, 75/25; solvent, cyclohexane; 65°C.*

Living Polymerization Features. The lack of an inherent termination step is a well known feature of the organolithium polymerization of the dienes and styrene in hydrocarbon solvent. We have found that, in the absence of adventitious chain transfer agents, the organometallic sites present in polybutadienes prepared with Ba-Mg-Al catalyst are long-lived. The indefinite lifetime of these chain ends has been demonstrated by an increase in molecular weight with both an increase in the extent of conversion as well as with the addition of more monomer to a toluene solution of quantitatively polymerized butadiene. In addition, block copolymers of butadiene and styrene, free of homopolymers, have been prepared by the addition of butadiene to active chains of polystyrene in cyclohexane, as indicated by the relative peak positions and shapes of the MWD curves in Figure 14. Moreover, polybutadienes bearing terminal hydroxyl functionality have been prepared by the addition of ethylene oxide to polybutadiene, followed by hydrolysis of the terminal alkoxide units.

In comparison to Ba-Mg-Al polymerizations, the preparation of block copolymers and functionally terminated polymers has not been successful with Ba-Li initiators. Chain transfer to toluene in Ba-Li systems is considered to be responsible for this behavior.

Before discussing the crystallization results for these elastomers, it is useful to summarize two of the important distinguishing features of the Ba-Mg-Al polymerization system: (1) polybutadienes and styrene-butadiene copolymers have a desirable combination of even higher trans and lower vinyl content as compared to the Ba-Li catalyst system; and (2) polymer chain ends retain their capacity to add monomer.

Crystallinity in Experimental High Trans Butadienes from Ba-Mg-Al Catalyst. The high degree of stereoregularity is demonstrated in Figure 15 by two pronounced crystalline melt temperatures at 50°C and at 88°C in the thermogram, obtained by Differential Scanning Calorimetry (DSC), for a 90% trans-1,4 polybutadiene prepared with Ba-Mg-Al. The crystalline melt temperature can be decreased to near room temperature by adjustment of the trans-1,4 content and/or the incorporation of styrene. A DSC thermogram for a high trans SBR containing 15% styrene and 85% trans-1,4 polybutadiene is shown in Figure 16. The crystallinity in this polymer was characterized by a broad endotherm at 11°C, followed by two smaller endothermic transitions at 33° and 44°C. The glass transition temperature for this copolymer occurred at -83.5°C.
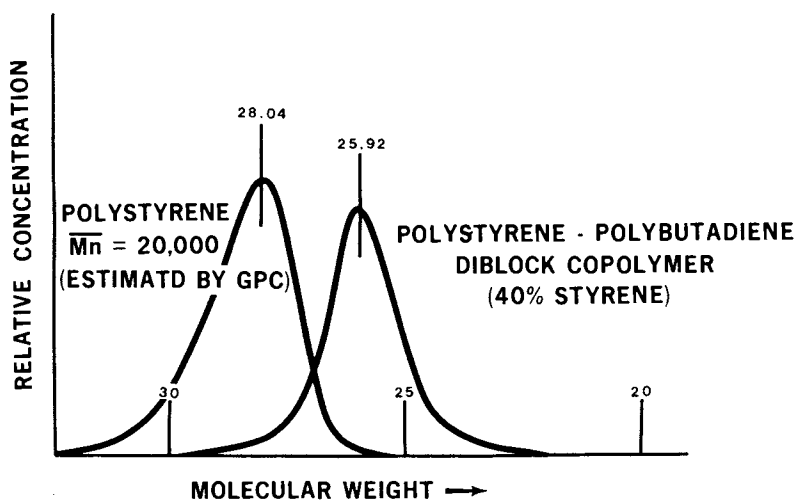
Figure 14. Gel permeation chromatograms of polystyrene and polystyrene–poly-butadiene diblock copolymer prepared with Ba-Mg-Al. Conditions: solvent, cyclo-hexane; 50°C.
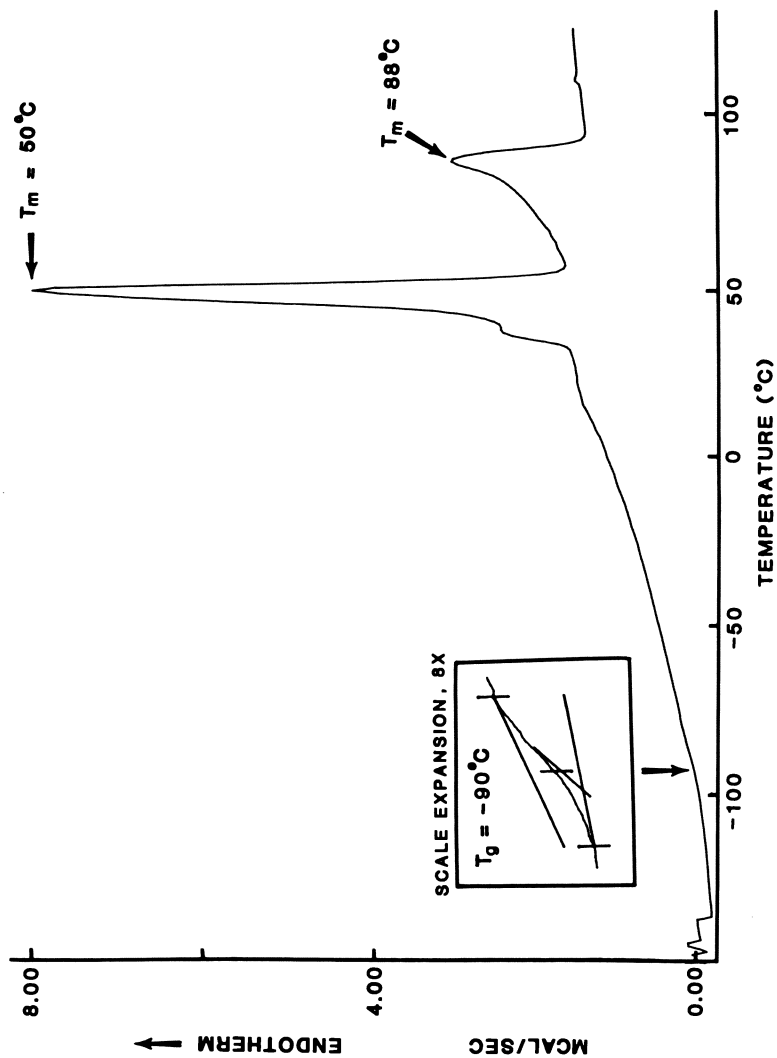
Figure 15.   *Differential Scanning Calorimetry (DSC) curve of 90% trans-1,4-polybutadiene prepared with Ba-Mg-Al.*
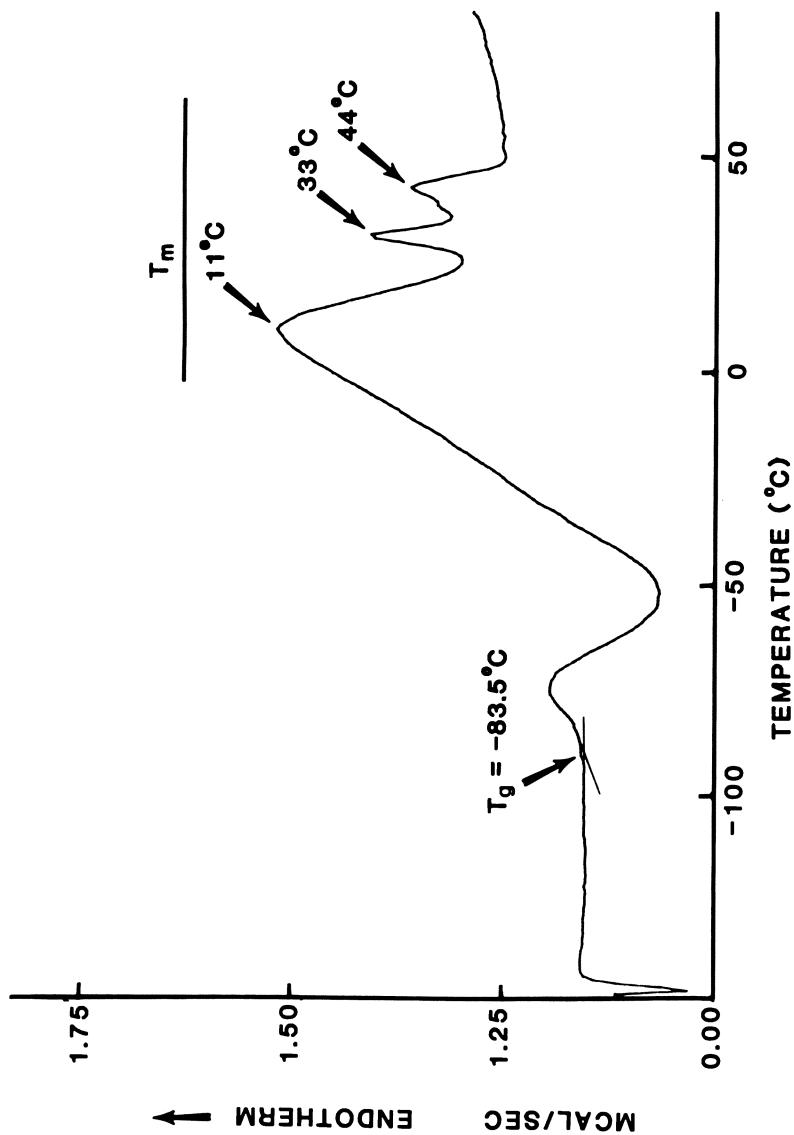
Figure 16. DSC curve of high trans-SBR (15% styrene, 85% trans) prepared with Ba-Mg-Al.

Comparison of Strain Induced Crystallization Behavior of NR with
High Trans SBR's from Ba-Mg-Al and Ba-Li Catalysts

Since the tack and green strength of these rubbers may
depend on their ability to undergo strain induced crystalliza-
tion, this behavior was studied and compared with that shown
by NR. Information on the strain induced crystallization
behavior of these experimental rubbers was obtained from
x-ray diffraction measurements and from rheo-optical studies.

X-ray Diffraction. X-ray diffraction patterns for a
high trans SBR rubber prepared with Ba-Mg-Al catalyst are
shown in Figure 17. The unstrained high trans SBR, containing
15% styrene and 85% trans-1,4 placements, showed only a diffuse
halo. This result suggested the presence of an amorphous
rubber and is supported by the fact that the gum vulcanizate
exhibited only a single crystalline melt temperature of 10°C,
with the melting endotherm extending up to 34°C, in the DSC
thermogram. At 200% strain, a diffraction pattern of oriented
crystalline polymer (equatorial arcs) was observed. Several
off-axial reflections appeared in the x-ray scan in addition
to the equatorial fiber arc as the sample was elongated to
700%. The appearance of discrete spots at strain levels of
700%, and the presence of only a diffuse halo in the pattern
of the unstretched film, demonstrate the ability of this rubber
to undergo strain induced crystallization.

Rheo-optical Studies. One of the most useful techniques
for studying the crystallization behavior of stereoregular
polymers is rheo-optical measurements (11).
Figure 18 shows the percent crystallinity obtained by
birefringence measurements for NR at various elongations as
a function of temperature. The relative shapes of the curves
in this Figure show the pronounced temperature and strain
dependence on the strain induced crystallization of NR. Of
particular importance is the relatively high amounts of crys-
tallinity that develop at room temperature.
Figure 19 shows the temperature dependence of the percent
crystallinity for high trans SBR, prepared with a Ba-Li catalyst
and containing 75% trans-1,4 content with 14 wt.% styrene, at 3
extension ratios. The percent crystallinity that develops is
temperature dependent, there being an increase in the amount
of crystallinity with a decrease in temperature. However, the
amount of crystallinity that develops is essentially indepen-
dent of strain. The amount of crystallinity that develops at
room temperature, regardless of the level of strain, is
extremely small (9).
Figure 20 shows the percent crystallinity as a function
of temperature and extension ratio for high trans SBR (22%
styrene, 87% trans) prepared with a Ba-Mg-Al catalyst. A
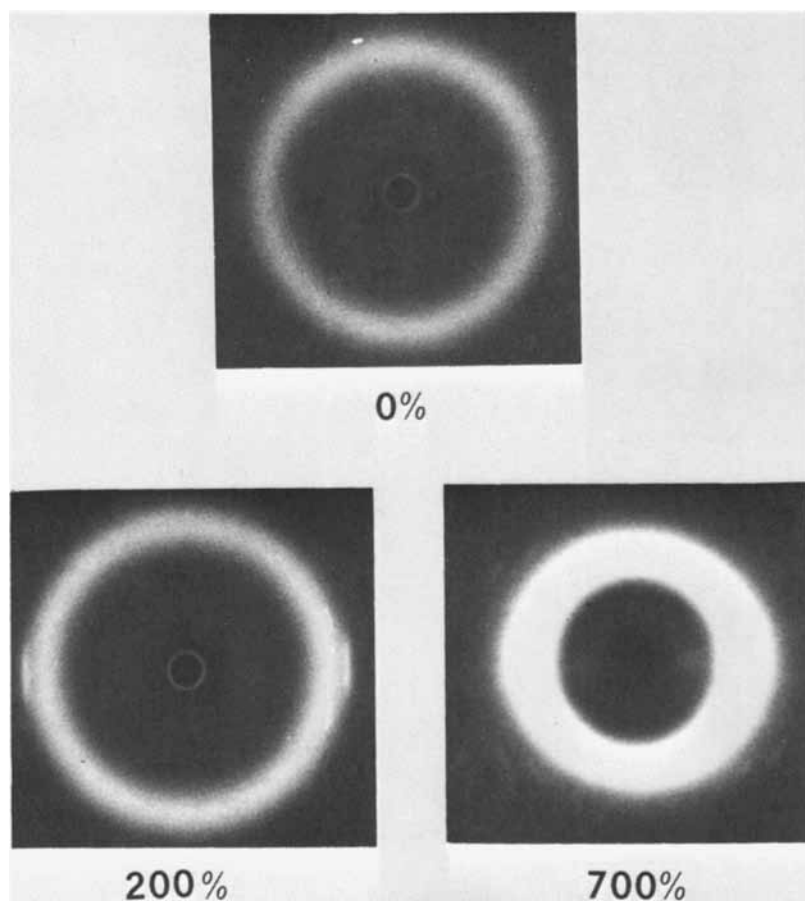
Figure 17. *X-ray diffraction patterns for high* trans-*SBR (15% styrene, 85% trans).*
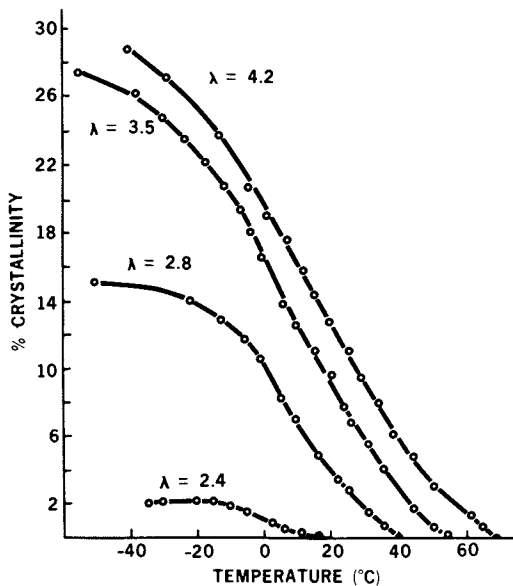
Figure 18.   Percent crystallinity of NR as a function of temperature and extension ratio.
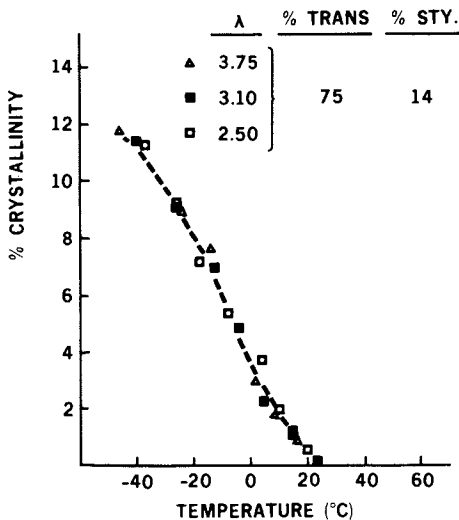
Figure 19.   Percent crystallinity of high trans-SBR prepared with Ba-Li as a function of temperature and extension ratio.
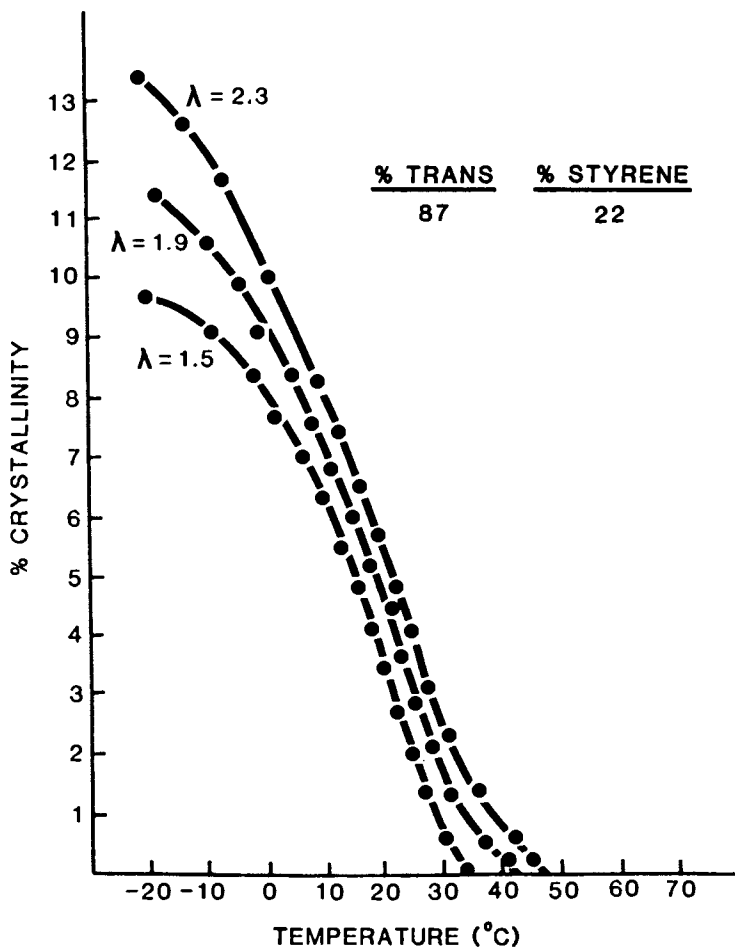
Figure 20.   Percent crystallinity of high trans-SBR prepared with Ba-Mg-Al as a function of temperature and extension ratio.

comparison of Figures 18, 19, and 20 shows that the amount of
crystallinity developed in both Ba-Li and Ba-Mg-Al high trans
SBR's is temperature sensitive, but not as strain sensitive as
that of NR. The most significant difference in the crystalliza-
tion behavior of the two types of SBR's is that the higher
trans-1,4 content (and increased styrene content to adjust the
crystalline melt temperature to near 25°C) leads to an increase
in the dependence of crystallinity on strain and an increase in
the degree of crystallinity at room temperature. That is, the
Ba-Mg-Al catalyzed styrene-butadiene copolymer compared to the
Ba-Li SBR shows a marked improvement in both strain sensitivity
and in the amount of strain induced crystallinity.

In observing the time dependent changes in birefringence
and stress-optical coefficient, for elongated samples at 25°C,
it was found that the rate of crystallization of high trans
SBR's was very much faster, some 10 times more rapid, than that
for NR (8). This is consistent with the reported rates of iso-
thermal crystallization for NR (2.5 hours at -26°C) and for
80% trans-1,4 polybutadiene (0.3 hours at -3°C) in the relaxed
state (12).

The main conclusions of the strain induced crystallization
behavior of high trans polybutadiene based rubber and natural
rubber are: (1) the rate of crystallization is extremely rapid
compared to that of NR; (2) the amount of strain induced crys-
tallization is small compared to that of NR, especially at room
temperature; and (3) for the high trans SBR's relative to NR,
crystallization is more sensitive to temperature at low exten-
sion ratios, and crystallization is less sensitive to strain.

Solution SBR of Controlled Structure for Tire Carcass Compounds

Two additional properties that may depend on the strain
induced crystallization behavior of NR are green strength and
building tack. A comparison of the performance of the experi-
mental high trans SBR's with NR was, therefore, carried out.

Green Strength. Green strength is a measure of the elasto-
meric behavior of an uncured (no chemical cross-links) rubber.
Natural rubber is an outstanding example of a rubber having
good green strength. The criteria that we have used, which are
similar to those of Briggs et al. (13), in evaluating this
property are (1) the value of the slope in the stress-strain
curve for unvulcanized rubber between 100-300% elongation, and
(2) the nominal stress at 300% elongation. Figure 21 shows
the comparison of the stress-strain curves of high trans SBR
prepared with Ba-Mg-Al and containing 15% styrene and 85%
trans-1,4 content versus NR and an emulsion SBR. These rubbers
were compounded with 45 phr HAF carbon black. As evidenced by
a positive slope and a high stress value for 300% elongation,
the high trans SBR has high green strength, as does NR. In

	SBR 1500	HTSBR	NR
SLOPE OF "STRESS" VS ELONGATION (300-100%)	(-)	(+)	(+)
"STRESS" AT 300% ELONGATION	58	125	80
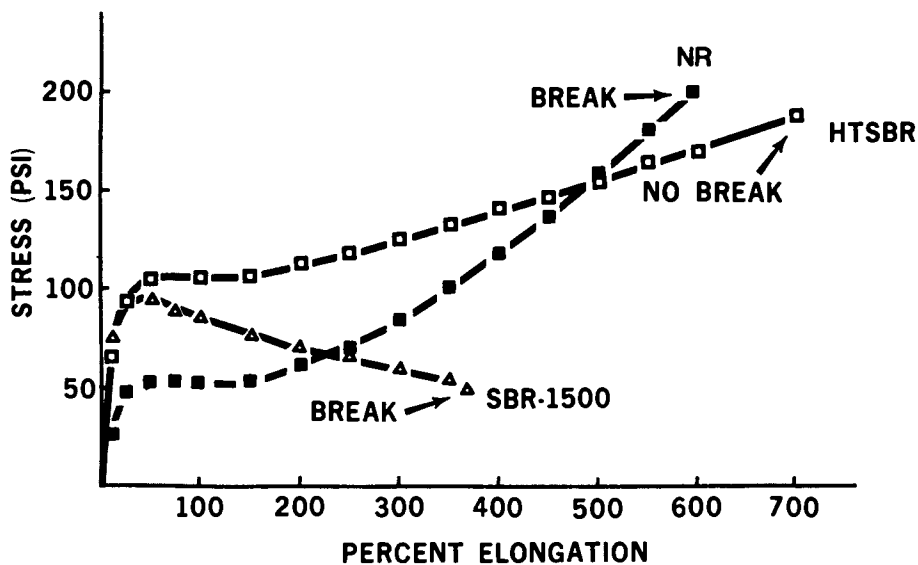
Figure 21. Green strength comparison.

contrast, a typical emulsion SBR has a negative slope and a
very low stress at 300% elongation--a consequence of the
property of unvulcanized SBR to neck down on elongation.

Tack Strength. Tack strength is defined as the force
required to separate two uncured polymer surfaces after they
have been brought into contact. The limiting tack strength
of a rubber is necessarily its green strength, or the force
required for its cohesive failure. Although high green strength
is necessary, it is, by itself, insufficient to insure good tack.
High tack strength is an especially desirable property in the
fabrication of rubber articles, especially those having a com-
plex geometry, prior to vulcanization. This property in tire
rubbers is needed so that the unvulcanized tire, i.e. green
tire, will hold together before curing.
        A comparison of tack values for uncured, black filled (45
phr HAF carbon black) compounds of NR versus high trans SBR
(15% styrene, 85% trans) is shown in Figure 22. These rubbers
are equivalent to those used for the green strength measure-
ments. The tack strength values of high trans SBR and NR are
nearly the same for the various measured contact times. It is
significant that both rubbers have comparable tack strength
for low contact times (six seconds). This behavior is often
referred to as "quick-grab".

Concluding Remarks

        Although the exact nature of the active center in polymer-
izations of butadiene with these Ba-Mg-Al catalysts is not
known, we believe that the preference for trans-1,4 addition
is a direct consequence of two aspects of this polymerization
system, namely: (1) the formation of a specific organobarium
structure in a highly complexed state with Mg and Al species,
and (2) the association of the polybutadiene chain end with a
dipositive barium counterion which is highly electropositive.
        The utility of solution SBR as tread rubbers has become
generally accepted in the tire industry. As we have shown,
high trans-1,4 crystallizing SBR's are excellent candidates
for other parts of the tire as well. The outstanding green
strength and building tack of high trans containing SBR's
certainly justify their consideration as tire rubbers of the
future.

Acknowledgments
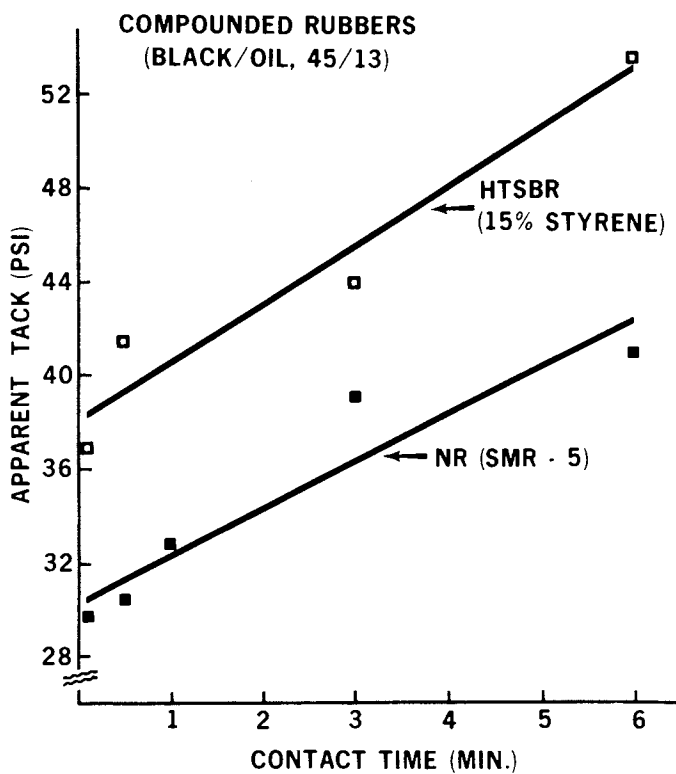
Figure 22. Comparison of tack of high trans-SBR and natural rubber.

Bingham, R. R. Durst, and H. J. Fabris for their contributions in the development of the Ba-Mg-Al polymerization catalyst.

Literature Cited

1. Horne, S. E. Jr. Rubber Chem. & Technology 1980, 53, G71.
2. Stavely, F. W.; and coworkers. Ind. Eng. Chem. 1956, 48, 778.
3. Horne, S. E. Jr. Rubber Chem. & Technology 1980, 53, G74.
4. Hsieh, H. L.; Glaze, W. H. Rubber Chem. & Technology 1970, 43, 52.
5. Morton, M.; Fetters, L. J. Rubber Chem. & Technology 1975, 48, 359.
6. U. S. Patents 3,992,561 (1976); 4,020,115; 4,033,900; 4,048,427 (1977); and 4,297,240 (1981) to The General Tire & Rubber Company.
7. Newberg, R. G.; Greenberg, H. Rubber Chem. & Technology 1970, 43, 333.
8. Livigni, R. A.; Hargis, I. G.; Aggarwal, S. L. "Structure and Properties of Rubbers for Tires and New Developments for Crystallizing Butadiene Rubbers"; Paper presented at Int'l. Rubber Conf., Kiev, U.S.S.R., 1978.
9. Aggarwal, S. L.; Hargis, I. G.; Livigni, R. A. "A New Class of Crystallizing Butadiene Elastomers: Morphology and Properties. II."; Paper presented at Int'l. Symp. on Macromol. Chem., Tashkent, U.S.S.R., 1978.
10. Aggarwal, S. L.; Hargis, I. G.; Livigni, R. A. Polymer Preprints 1981, 22(2), 134.
11. Stein, R. S. "Rheology"; Eirich, F. R., Ed.; Academic Press, New York and London, 1969; Vol. V, p. 279.
12. Mandelkern, L. "Crystallization of Polymers"; McGraw Hill, New York, 1964; p. 264.
13. Briggs, G. J.; Holmes, J. M.; Wei, Y. K. Elastomerics 1979, 111(8), 30.

Elastomeric Polydiene ABA Triblock Copolymers with Crystalline End Blocks

MAURICE MORTON, N.-C. LEE[1], and E. R. TERRILL[2]

The University of Akron, Institute of Polymer Science, Akron, OH 44325

ABA triblock copolymers having crystalline end
blocks and elastic center blocks were prepared by
anionic polymerization of butadiene and isoprene,
followed by hydrogenation. The end blocks con-
sisted of hydrogenated high-1,4 polybutadiene while
the center block was either a high-1,4 polyisoprene
(H_2-BIB) or a hydrogenated 45%-1,2 polybutadiene (H_2-BBB).
The hydrogenation could be carried out to over 99%
with minimal chain scission (~1-2%). At 30% end
block content, both types of polymer exhibited
thermoplastic elastomer behavior, but higher end-
block content led to plastic-type behavior. The
hydrogenated polybutadiene end blocks showed some
degree of spherulitic crystallization, about 50%
crystallinity and a T_m of 107°C., close to that of
high pressure polyethylene. Tensile strengths of
17 to 32 MPa were obtained at 30% end block content,
but this dropped sharply with increasing temperature.
None of the polymers were soluble at room tempera-
ture, showing only mild swelling in benzene.

ABA triblock copolymers of the styrene-diene type are well
known, and owe their unique properties to their heterophase
morphology. This arises from the incompatibility between the
polystyrene A blocks and the polydiene B blocks, leading to the
formation of a dispersion of very small polystyrene domains
within the polydiene matrix. This type of elastic network, held
together by the polystyrene "junctions", results in thermoplastic
elastomer properties.

There has been considerable interest recently in an alterna-
tive type of ABA triblock structure, where the end blocks could
form crystalline domains, by crystallization, rather than
amorphous domains by phase separation. It was felt that, since
such a crystallization process need not depend on the incompati-
bility between the blocks, it should be possible to have a homo-
geneous melt, which should exhibit a much lower viscosity, and
hence much easier processing, than the heterogeneous media of the
conventional triblock copolymers. Furthermore, thermoplastic

Current addresses:
[1] Universal Energy System, Dayton, OH 45432.
[2] E. I. du Pont de Nemours Co., Inc., Wilmington, DE 19898.

elastomers based on crystalline domains should also exhibit an advantageous resistance to solvents.

Since the anionic triblock copolymers are based on monomers susceptible to this mechanism, one recent approach to this synthesis has been to prepare butadiene-isoprene-butadiene triblock copolymers, which are then hydrogenated so that the high-1,4 polybutadiene end blocks become crystallizable, similar to high-pressure polyethylene ($\underline{1}$-$\underline{5}$).

Recent work in this laboratory has been concerned with the preparation and study of two different varieties of this type of triblock copolymer. Both of these triblocks had high-1,4 polybutadiene end blocks, which were then hydrogenated to a "pseudo polyethylene" structure. However, the elastomeric center blocks differed, in that one consisted of a high-1,4 polyisoprene while the other was comprised of a 45%-1,2 polybutadiene. The polyisoprene-containing triblock was hydrogenated selectively, leaving the polyisoprene untouched, while the other polymer was hydrogenated totally, so that the 45%-1,2 polybutadiene was transformed into an ethylene-butene-1 copolymer. These two triblock copolymers were designated (after hydrogenation) as H_2-BIB and H_2-BBB. The molecular "architecture" of these two types of triblocks is listed in Table I.

Table I

Molecular Architecture of Triblock Copolymers

Type	Mol. wt. ($x10^{-3}$)	% End Block	Designation
$H_2$1,4B-I-$H_2$1,4B	46–190–46	34	H_2BIB–34
"	48–140–48	41	H_2BIB–41
"	62–120–62	53	H_2BIB–53
$H_2$1,4B-H_2(45%1,2)B-$H_2$1,4B	19– 25–19	60	H_2BBB–60–19
"	18– 85–18	30	H_2BBB–30–18
"	54– 72–54	60	H_2BBB–60–54
"	55–257–55	30	H_2BBB–30–55

It can be seen from Table I that these polymers varied both in their end block content and molecular weight. In the case of the BIB polymers, all the end blocks were of "high" molecular weight ($\sim$50,000), while the BBB polymers contained both high and low ($\sim$20,000) molecular weight end-blocks. The variation of these two parameters is important, as will be seen later in connection with crystallization and mechanical behavior of these materials.

Experimental

The base polymers were prepared by anionic polymerization using high-vacuum techniques. sec-Butyl lithium was used as initiator. The BIB triblocks were synthesized by sequential addition of the monomers in cyclohexane as solvent, while the BBB triblocks were synthesized by first preparing the first polybutadiene end block, then adding 5% diethyl ether before adding the second charge of butadiene, followed by coupling of the AB diblocks with the correct stoichiometric amount of dimethyldichlorosilane. Both polymers were near-monodisperse in molecular weight, as indicated by the GPC curves in Figures 1 and 2 ($M_W/M_n \sim 1.05$), the BBB type showing a small residual peak of up to 5% unlinked diblock.

Hydrogenation was carried out with the assistance of an n-butyl lithium/cobalt octoate catalyst (6). It was necessary to determine the proper conditions for efficient hydrogenation with minimal degradation (7). For the BIB polymer the Li/Co ratio used was 5/1 to obtain selective hydrogenation of the polybutadiene, while for the total hydrogenation of the BBB polymer, a ratio of 2.2/1 was satisfactory. NMR analysis showed better than 99% hydrogenation.

Since the hydrogenated polymers were insoluble at room temperature, it was not found possible to determine the extent of chain degradation caused by hydrogenation, since this would involve molecular weight measurements. Instead, polyisoprene and a 45% 1,2-polybutadiene were used as controls for this purpose, since they represented the center blocks of the respective polymers, and also retained their solubility after the hydrogenation treatment (the polyisoprene was not expected to, and did not, become hydrogenated). Osmometric molecular weight measurements showed that minimal chain scission had occurred in the case of both polymers during the hydrogenation. Thus Table II shows that the hydrogenation method used led to about 1% degradation of 1,4-polyisoprene. Similar studies on the 45% 1,2-polybutadiene showed that less than 5% of the chains were cleaved. This was considered acceptable, since that amount of free diblocks would not be expected to affect the mechanical properties to any extent.

Samples of the polymers for physical evaluation were prepared by film casting from toluene solution at 90°C. and allowing the crystallization to occur by cooling the melt. It was observed that phase separation occurred in the melt in the case of the H_2-BIB but not for the H_2-BBB. These materials could also be compression molded at 140°C., but optimum results appeared to be obtained with the film-cast samples.
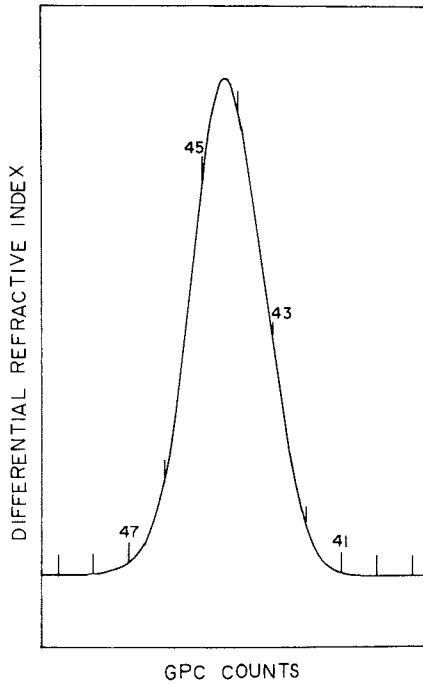
Figure 1.   Gel permeation chromatogram of BIB.
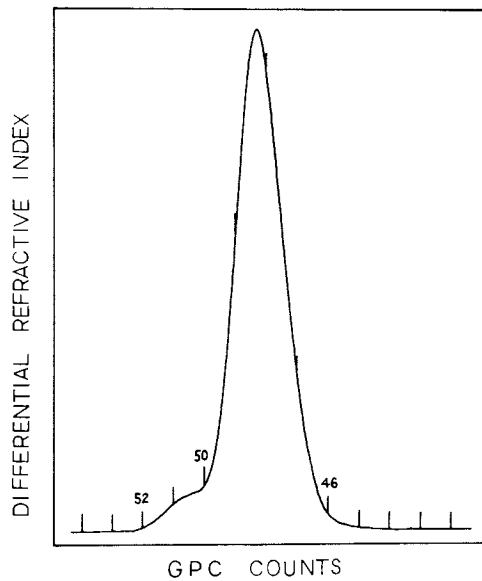
Figure 2.   Gel permeation chromatogram of BBB.

Table II

Degradation of Polyisoprene During Selective
Hydrogenation of Polybutadiene

(Original Mol. Wt. = 209,000)

Hydrogenation Temperature (°)	Reaction Time (hr.)	M_n (Osmometry)	% Chain Scission*
69	10	189,000	11
62	10	197,000	6.1
52	4.5	207,000	1.0

* % of chains cleaved

Results and Discussion

Morphology. Observations with the light microscope, under
polarized light, showed that the end blocks in the case of both
types of polymers crystallized in the form of the usual spheru-
lites, but not as well as the analogous homopolymer, H_2-1,4-
polybutadiene. The formation of the spherulites was improved
with increasing end-block content and/or higher molecular weight
of the end blocks.

The morphology, as revealed by light microscopy, is shown
in Figures 3 to 7. Thus Figures 3 and 4 show photomicrographs of
the hydrogenated 1,4-polybutadiene and a commercial low-density
polyethylene (Dow 991), respectively. The similarity between
the two is obvious. Figures 5 and 6 show the effect of the end-
block content on the crystallization of two H_2-BBB polymers, both
having end-blocks of high molecular weight (∿50,000-60,000). The
more distinct spherulite formation in Figure 5 is clearly seen.
Similarly, the effect of end-block molecular weight on crystalli-
zation is demonstrated in Figure 7 for an H_2-BBB polymer having
end blocks of only 19,000 molecular weight, where spherulite
formation is quite poor even at high end-block content.

As stated previously, phase separation occurred in the melt
in the case of the H_2-BIB polymers, and this is shown in Figure 8,
which represents a photograph taken by transmission electron
microscopy of an ultra-thin film of this type of polymer, stained
by osmium tetroxide. The white domains represent the hydro-
genated 1,4-polybutadiene end blocks, and these have dimensions
similar to those found for polystyrene domains in styrene-diene-
styrene triblock copolymers(8). This type of electron microscopy
could not be used for the H_2-BBB polymers, since OsO_4 staining
was not applicable. However, the compatibility of the two blocks
in the latter was demonstrated by mixing solutions of the
respective hydrogenated homopolymers of similar molecular weight
and casting clear films.
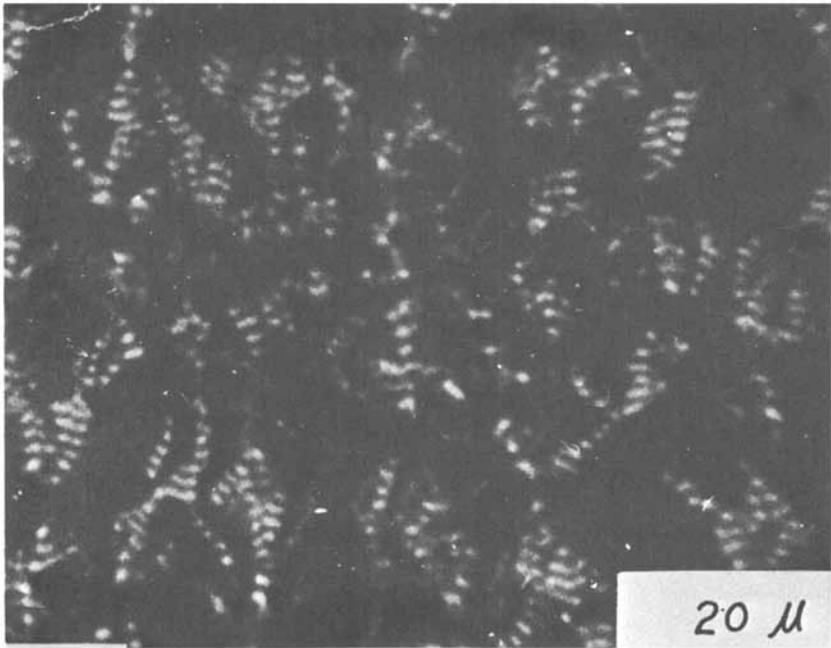
Figure 3.   Photomicrograph of H_2-1,4-polybutadiene.
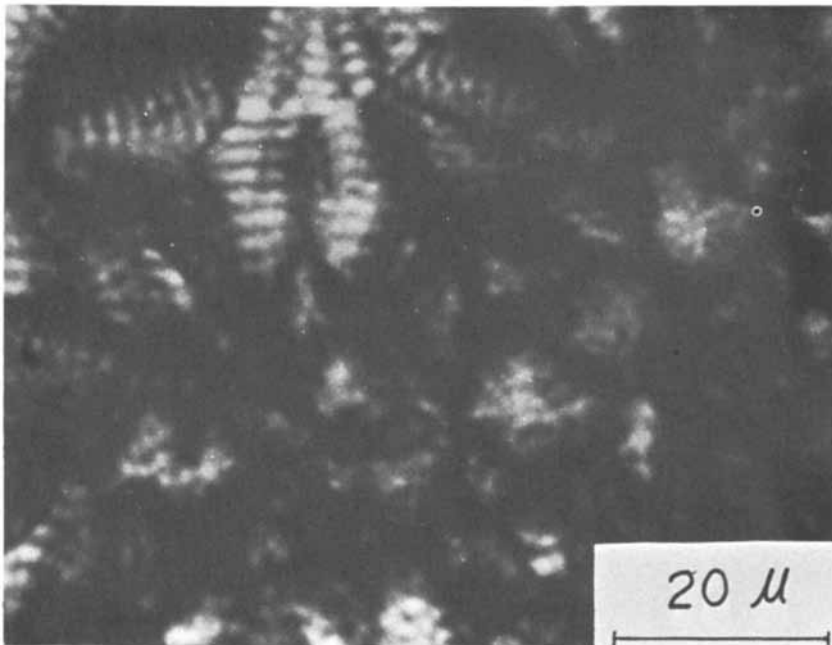
Figure 4.   Photomicrograph of polyethylene (Dow 991).
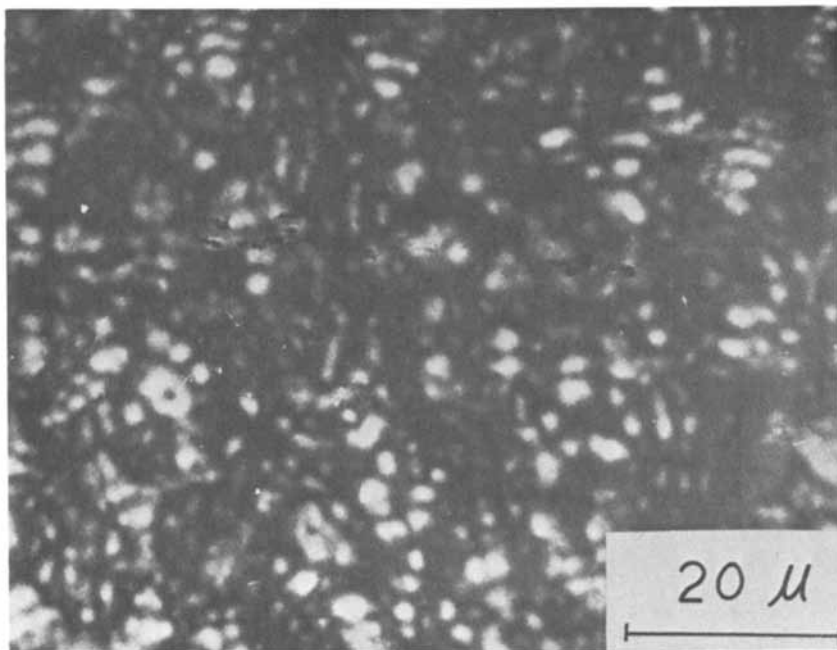
Figure 5. Photomicrograph of H_2–BBB–60-54, (M.W. $\times$ 10^{-3} is 54-72-54).
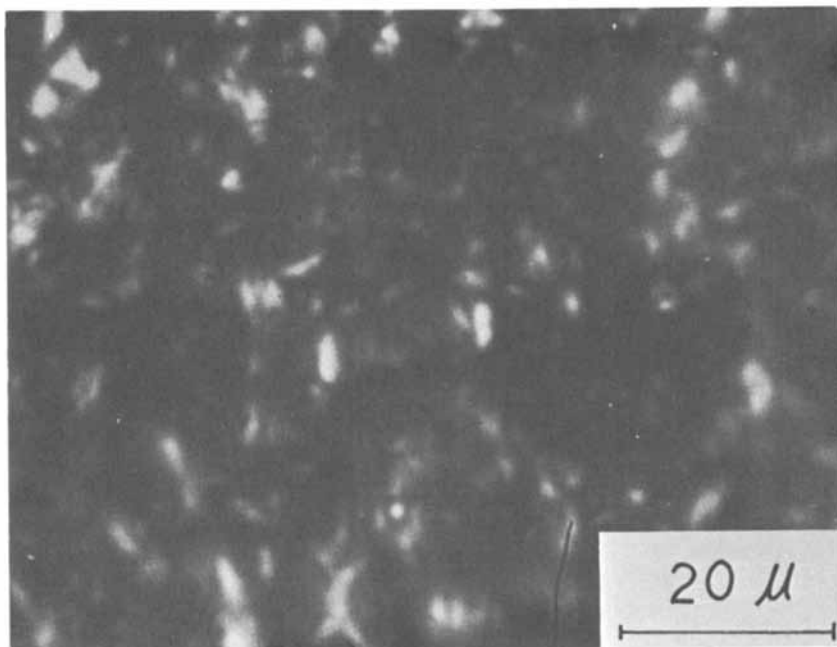
Figure 6. Photomicrograph of H_2–BBB–30-55, (M.W. $\times$ 10^{-3} is 55-257-55).
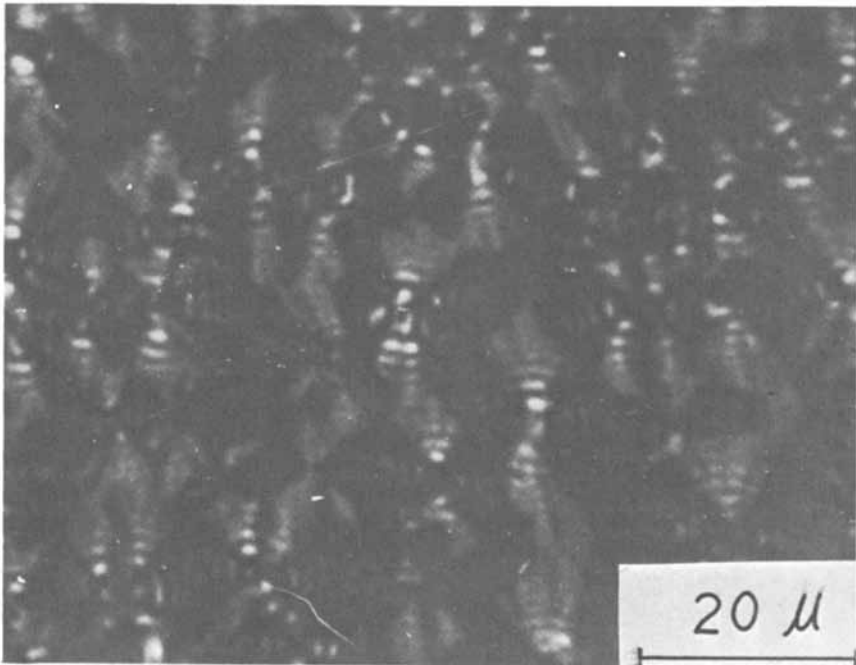
Figure 7.   Photomicrograph of H_2–BBB–60-19, (M.W. $\times$ 10^{-3} is 19-25-19).
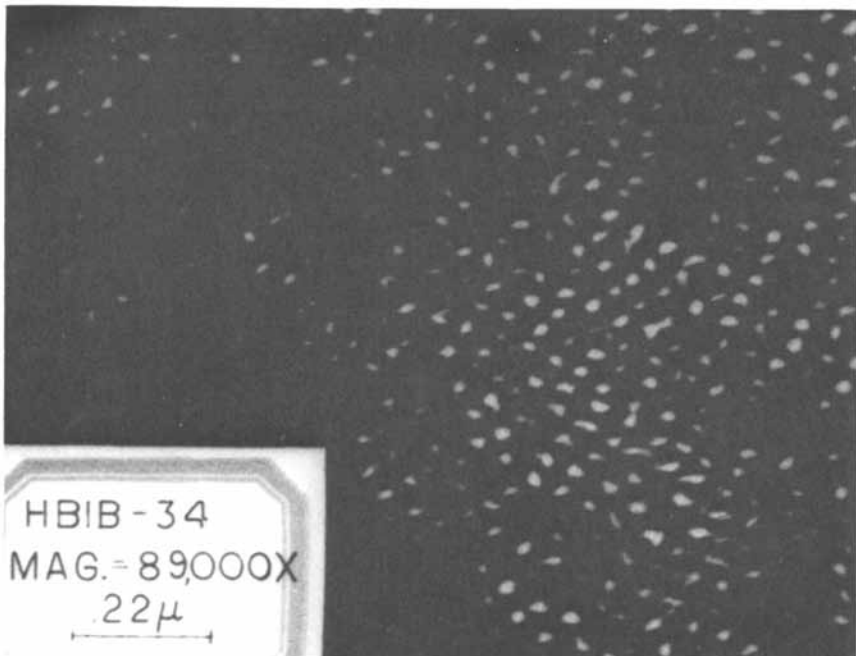
Figure 8.   Transmission electron microphotograph of H_2–BIB–34, (M.W. $\times$ 10^{-3} is 46-190-46).

Thermal Analysis. Differential Scan Calorimetry was carried out with the DuPont 990 Thermal Analyzer at a 5-10°C scan rate. Figures 9 and 10 show the type of DSC Thermograms obtained on samples before and after stretching them to the breaking point. Three points are evident from these figures: a) the endotherm at about 107°C. in both figures indicates a crystal melting point corresponding almost exactly to that found for Dow polyethylene 991; b) the tensile test caused a small increase in both the crystallinity and the melting point; and c) the H_2-BBB polymer exhibits a small broad endotherm peaking at about -10°C, which apparently disappears during stretching. It is suggested that this endotherm is due to some tendency toward crystallization of the hydrogenated 45% 1,2-polybutadiene center block, because of the occurrence of some longer sequences of polyethylene units (9).

Uniaxial Tensile Properties. The stress-strain curves for the H_2-BIB and H_2-BBB polymers are shown in Figures 11 and 12, respectively. As expected, these curves appear to be a function of the end-block content ("hard phase") in both cases. However, in addition, Figure 12 illustrates clearly the deleterious effect of the low molecular weight end blocks on the tensile strength (H_2-BBB-60-19 vs. H_2-BBB-60-54, and H_2-BBB-30-18 vs. H_2-BBB-30-55). This agrees with the morphology shown in Figures 5-7, where crystal formation was shown to depend on the molecular weight of the end block. It also agrees with prior data in the literature (1). Apparently, an end-block molecular weight of about 50,000 is required for high strength in these polymers.

Actually, of all the polymers described here, only the ones with end-block contents of about 30% qualify as thermoplastic elastomers, as defined by reasonably good recovery from strain. Figures 13 and 14 illustrate this point by showing the amount of tensile set obtained after stretching to various degrees of strain. It is obvious that those polymers having more than about 30% end-block content show unusually high unrecovered deformations (i.e., "cold drawing"). Even at 30% end-block, the tensile set reaches a value of 100% for the H_2-BIB polymers at a strain ratio of 9 and for the H_2-BBB polymers at a strain ratio of 6. This value is much higher than those obtained for analogous styrene-butadiene-styrene triblocks(8), and indicates that the crystalline domains apparently suffer greater distortions than the amorphous poly-styrene domains. It should be mentioned, of course, that these dislocations are not "permanent", in that a high degree of recovery can be obtained by annealing the samples at 90°C. or higher.

Strength-Temperature Relations. One of the key properties of thermoplastic elastomers is their resistance to elevated temperatures. Figures 15 and 16 show the effect of temperature on the tensile strength of the two types of block copolymers.
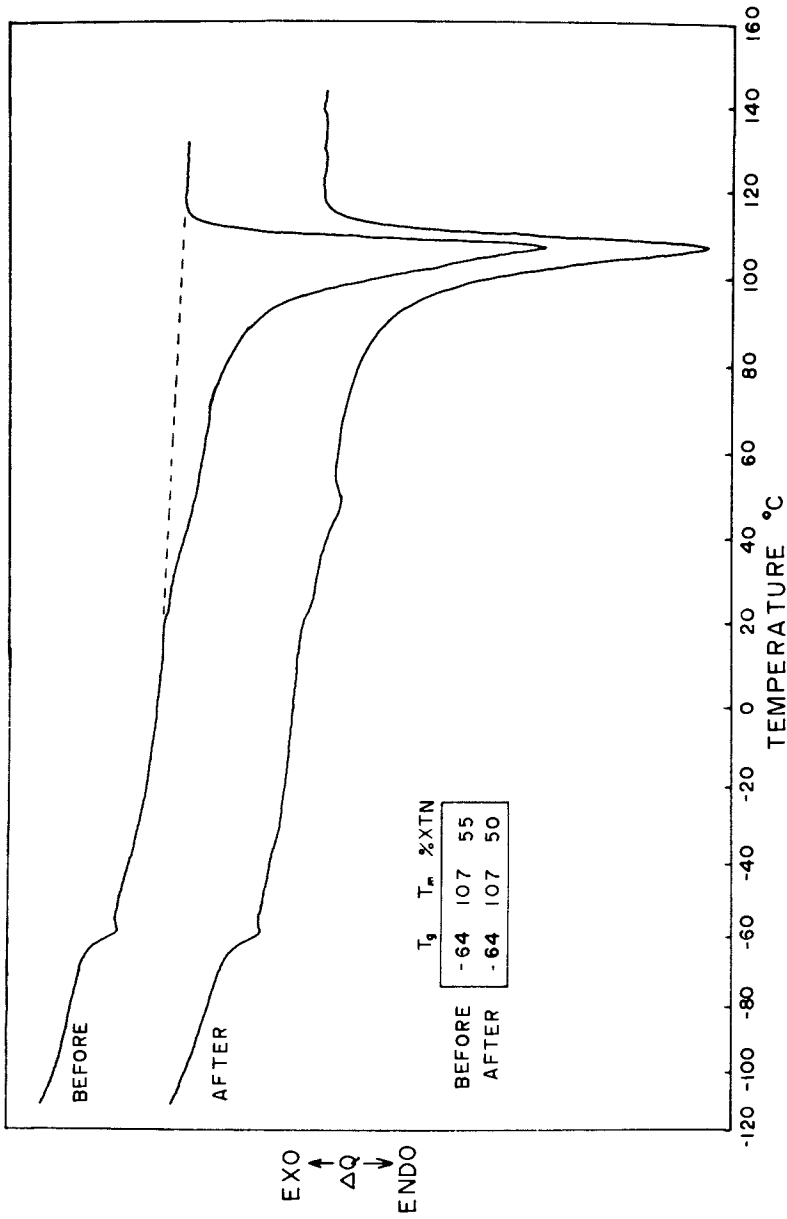
Figure 9. *DSC thermogram of H_2-BIB-34, before and after tensile elongation to break.*
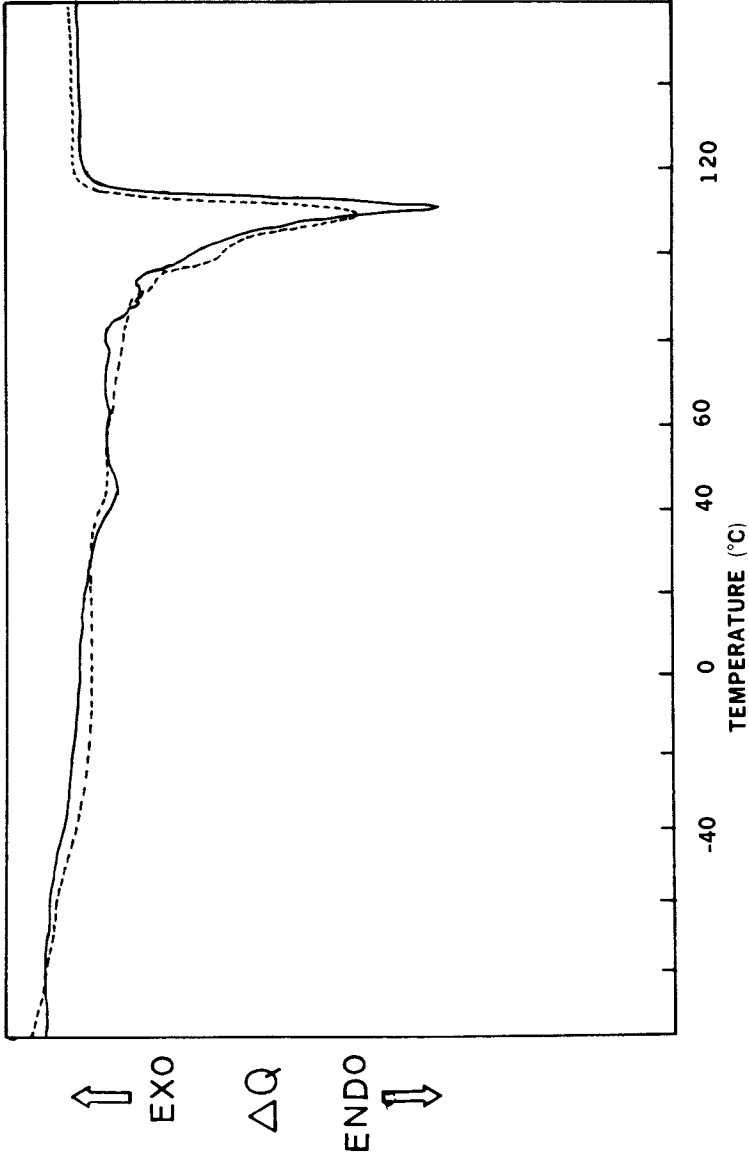
Figure 10. DSC thermogram of H_x–BBB–30-55, before and after tensile elongation to break. Key: – – –, before; ———, after.
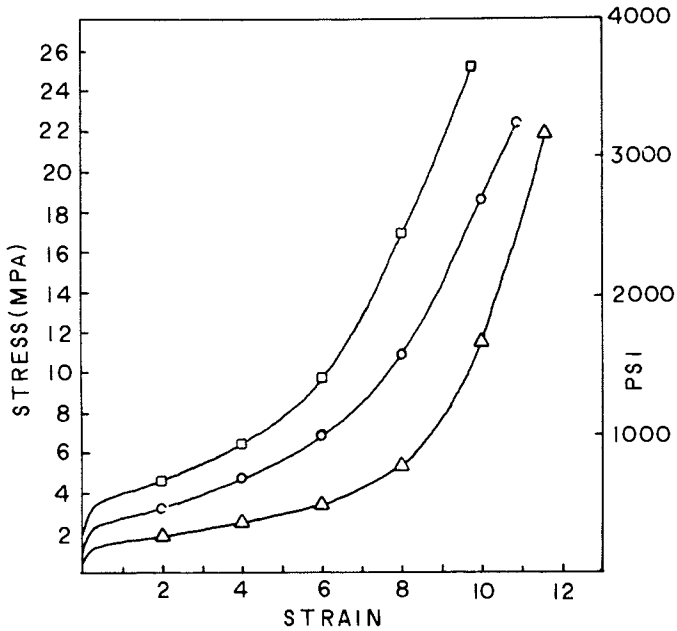
Figure 11.   Stress–strain behavior of H_2–BIB. Key: $\triangle$, H_2–BIB–34; $\bigcirc$, H_2–BIB–41; $\diamond$, H_2–BIB–53.
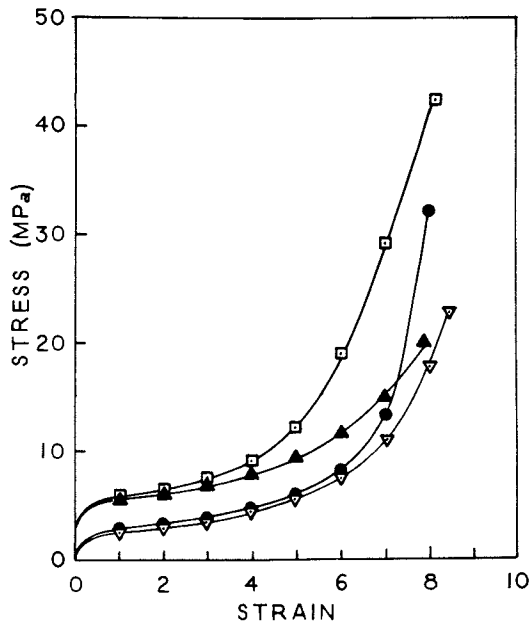
Figure 12.   Stress–strain behavior of H_2–BBB. Key: $\blacktriangle$, H_2–BBB–60-19; $\triangledown$, H_2–BBB–30-18; $\boxdot$, H_2–BBB–60-54; $\bullet$, H_2–BBB–30-55.
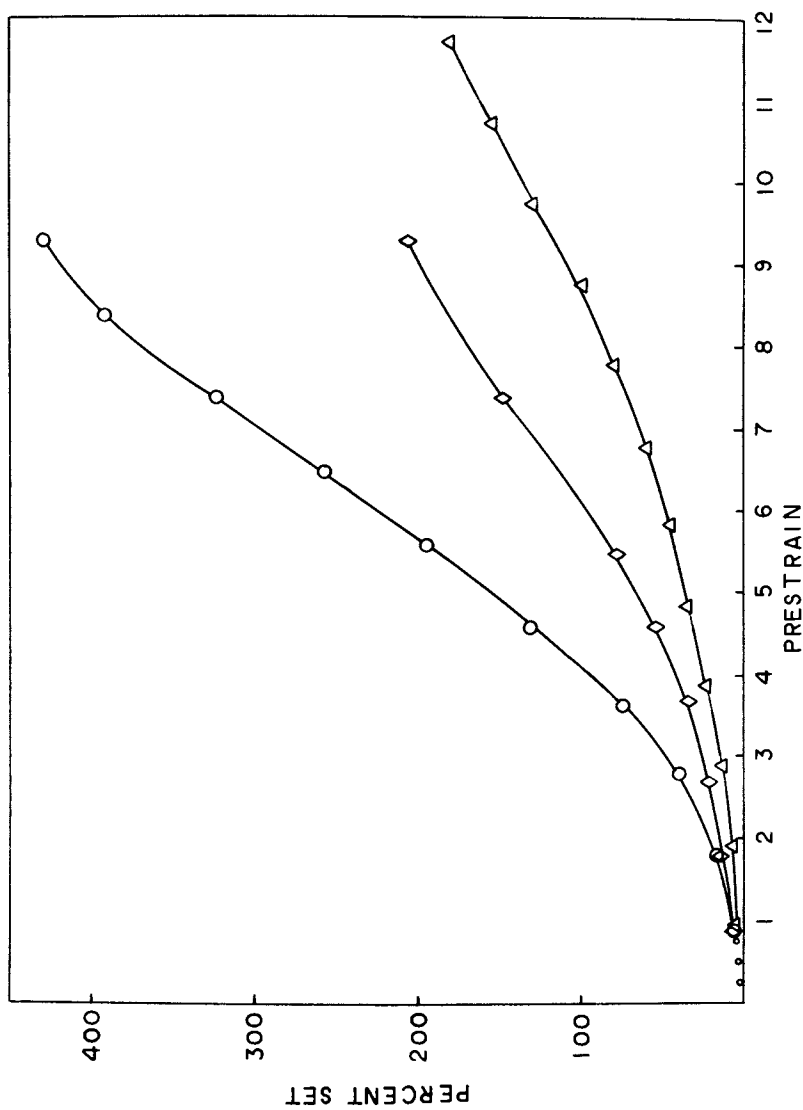
Figure 13. Tensile set of H_s–BIB as a function of strain. Key: $\triangle$, H_s–BIB–34; $\diamondsuit$, H_s–BIB–41; $\bigcirc$, H_s–BIB–53.
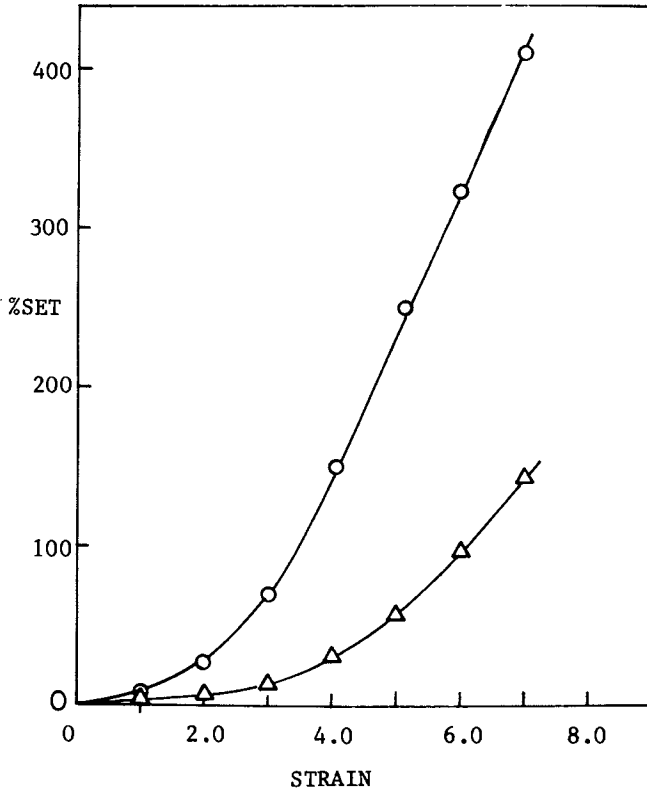
Figure 14. Tensile set of H_2–BBB as a function of strain. Key: △, H_2–BBB–30-55; ○, H_2–BBB–60-54.
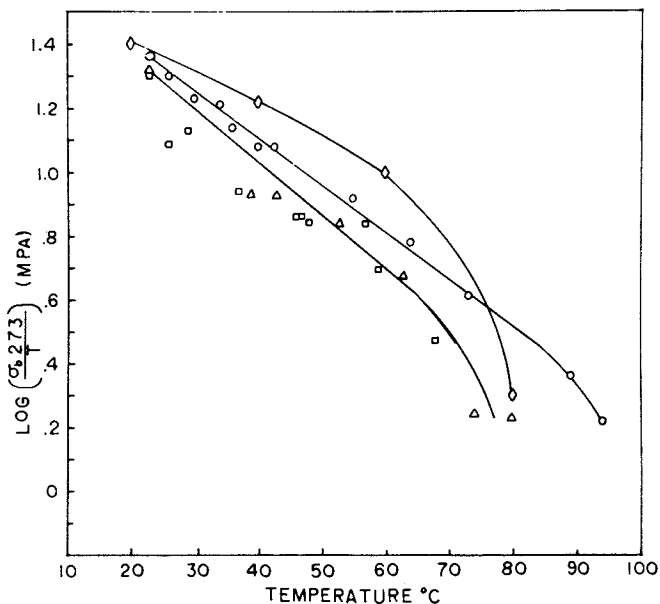
Figure 15. *Effect of temperature on tensile strength. Key:* □, *H_2–BIB–34;* △, *H_2–BIB–41;* ○, *H_2–BIB–53;* ◇, *SIS–20–87–20 (8).*
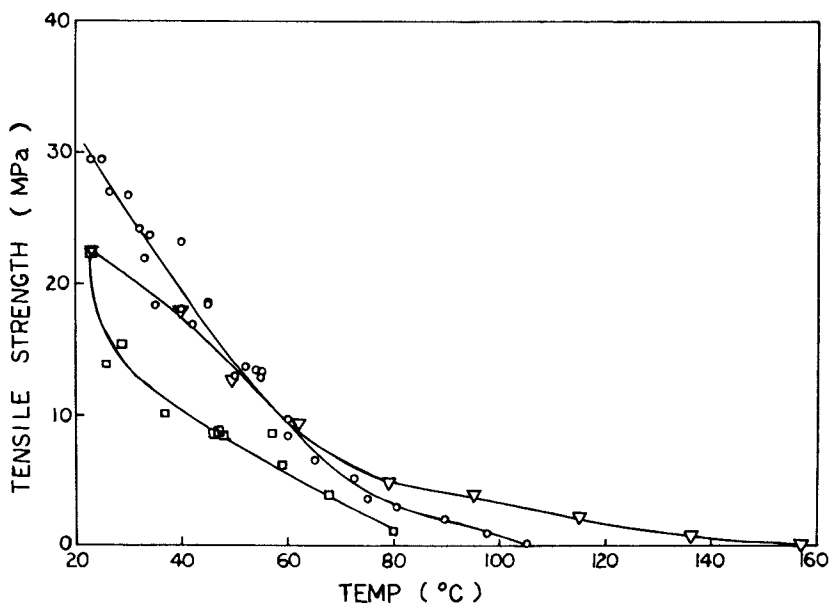
Figure 16. *Effect of temperature on tensile strength. Key:* ○, *H_2–BBB–30–55;* ▽, *Hytrel 4056;* □, *H_2–BIB–34.*

Figure 15 shows that the H_2-BIB polymers suffer a drastic drop
in strength, considerably more than that of an analogous styrene-
isoprene-styrene triblock (8). Thus, at 60°C., the H_2-BIB-34 shows
a strength of only about 5 $\overline{M}$Pa (50 kg. cm^{-2}), which represents a
reasonable strength. The strength-temperature curve of a similar
H_2-BBB triblock is shown in Figure 16, and seems to indicate
better properties (∿10 MPa at 60°C.). In fact it behaves
similarly to the segmented polyester elastomer, Hytrel 4056,
except that its strength drops faster as the temperature
approaches 100°C. This is, of course, not surprising, since the
Hytrel polymer is stated to have a crystal melting point of about
150°C. In general, however, these rapid drops in strength with
increasing temperature correlate with the rapid drop in dynamic
modulus found (10, 11) for other segmented, crystalline block
copolymers.

In this connection, an interesting relation is shown in
Figure 17, where both the tensile strength and the relative
crystallinity (from DSC data) are plotted against temperature,
for the H_2-BBB-30-55 triblock. It can be readily seen that, at
80°C, where the strength has dropped to 10% of its original
value, the crystalline content is still over 80% of its initial
value.

Solvent Resistance. One of the distinct advantages of a
crystalline thermoplastic elastomer over an amorphous one should
be its superior solvent resistance, since the latter types are
generally soluble. Table III shows the swelling behavior of the
H_2-BIB triblocks in toluene at 25°C. It can be seen that the
maximum swelling obtained was in the case of the H_2-BIB-34, which
had the lowest end-block content. Furthermore, the equilibrium
swelling ratio of 3.26 obtained for this polymer is considerably
less than the value of 5 or 6 generally exhibited by a well-
vulcanized natural rubber.

Two other features are notable in Table III. The swelling
values for the compression molded samples (CM) run consistently
less than those for the solvent-cast films. Apparently there is
more "entrapment" of the amorphous portions within the crystal-
lites during and after the molding. Secondly, the degradation
experienced by the polymer hydrogenated at 69°C. (see Table II)
instead of 52°C. is clearly demonstrated by the higher swelling
value.
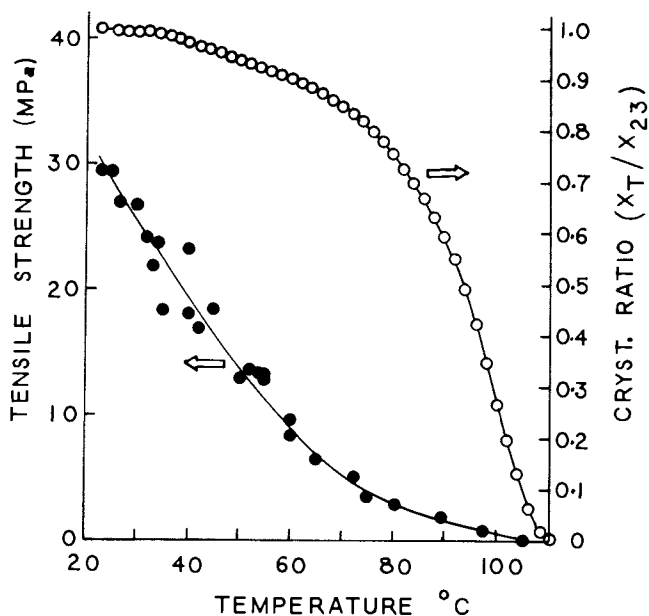
Figure 17. Effect of temperature on crystallinity and tensile strength of H_2–BBB–30-55.

Table III

Swelling of H_2-BIB Polymers
(Toluene -25°C)

Polymer	Swelling Vol. Ratio		M_c **	
	FC *	CM *	FC	CM
H_2-BIB-34	3.26	2.84	6800	4500
H_2-BIB-41	2.13	--	2200	--
H_2-BIB-53	1.82	1.80	1800	1800
H_2-BIB-34 (69)***	4.12	2.75	13,000	3900

 *FC = Film cast from solvent, CM = compression molded
 **M_c = Mol. wt. between "crosslinks", calculated using X_1 =
      $0.43 + 0.05 v_2$ for polyisoprene.
***Polymer hydrogenated at 69°C instead of 52°C.

Literature Cited

1. Hassell, H. L.;   Leandro, S.; Shaw, A. W. U. S. Patent 3,465,063 (Shell Oil Co.), 1969.
2. Falk, J. C.; Schott, R. J. Die Angew. Macromol. Chem. 1972, 21, 17.
3. Mohajer, Y.; Wilkes, G. L.; Wang, I. C.; McGrath, J. E. Polym. Prepr., Div. of Polym. Chem., Am. Chem. Soc. 1980, 21(2), 191.
4. Halasa, A. F. Polym. Prepr., Div. of Polym. Chem., Am. Chem. Soc. 1980, 21(1), 42.
5. Mohajer, Y.; Wilkes, G. L.; Martin, M.; Wang, I. C.; McGrath, J. E. Polymer Prepr., Div. of Polym. Chem., Am. Chem. Soc. 1980, 21(1), 43.
6. Falk, J. C.; Schott, R. J. Macromolecules 1971, 4, 152.
7. Rachpudy, H.; Smith, G. G.; Raju, V. R.; Graessley, W. W. J. Polym. Sci., Polym. Phys. Ed. 1979, 17, 1211.
8. Morton, M. "Encyclopedia of Polymer Science and Technology," Vol. 15, Wiley, New York, 1971, p. 508.
9. Davison, S.; Taylor, G. L. Br. Polym. J. 1972, 4, 65.
10. Huh, D. S.; Cooper, S. L. Polym. Eng. Sci. 1971, 11, 369.
11. Shen, M.; Mehra, U.; Niinomi, M.; Koberstein, J. T.; Cooper, S. L. J. Appl. Phys. 1974, 45, 4182.

Effects of Variation of Composition and Block Sequence on Properties of Copolymers Containing Semicrystalline Block(s)

Hydrogenated Linear Block Copolymers of Butadiene and Isoprene

Y. MOHAJER, G. L. WILKES, I. C. WANG, and J. E. McGRATH

Virginia Polytechnic Institute and State University, Polymer Materials and Interfaces Laboratory, Blacksburg, VA 24061

The effect of variations in molecular architecture and com-
position on bulk properties is reported for a series of well
characterized hydrogenated block copolymers of butadiene (HB) and
isoprene (HI), each with a total molecular weight of ~200,000 and
a narrow distribution (Mw/Mn < 1.1). The polymers were synthe-
sized by sequential anionic polymerization followed by hydrogena-
tion, using p-toluenesulfonylhydrazide. The material properties
of the homopolymeric HI and HB were also investigated. As expect-
ed, HI is rubbery at room temperature and HB is a tough semicrys-
talline plastic with properties simlar to those of a low density
polyethylene (LDPE). The crystallinity, density and ΔH_f for all
of the block copolymers were found to be linearly dependent on HB
content indicating that little mixing exists between the HB and HI
blocks in the solid state. Although the solution cast films of
the block copolymers were spherulitic, the quenched films display-
ed no distinct structure on the supermolecular level indicating
that the aggregation of the crystallites was more random in these
films. The stress-strain properties of triblock copolymers with
different block sequence, HBIB and HIBI, and a diblock copolymer,
HBI, were similar in bulk behavior to each other in the high and
the intermediate butadiene content (50-90%). This was related to
the fact that the mechanical properties were determined predomi-
nantly by the behavior of the more continuous HB phase. For the
lower butadiene compositions (7-29%), there was a major difference
in the behavior of polymers with different block architecture.
HBIB polymers were thermoplastic elastomers, whereas HIBI polymers
behaved like an uncured particulate filled rubber. This differ-
ence was related to the presence of permanent "entanglements" in
HBIB polymers. The permanent entanglements which act as a physi-
cal crosslink are a consequence of the anchorage of the HB end
blocks in the semicrystalline domains. No such arrangment is pos-
sible for either the HIBI or HBI polymers. The hysteresis be-
havior of HBIB polymers were strongly dependent on butadiene con-
tent, decreasing with lowering of the concentration of the semi-
crystalline HB. This dependence was related to the continuity

of the crystalline microdomains. All the members of HIBI (and the
HBI we considered) showed large hysteresis behavior. This large
energy loss during cyclic deformation in these polymers was
related to the absence of the permanent anchor points arising from
end block crystallization. The dynamic mechanical properties of
HB were similar to those of LDPE and showed a strong thermal
history dependence. The block copolymers, in addition to the tan
δ peak similar to that of HB homopolymer, displayed a peak at
around -47 ±2°C at 110 Hz. This transition is believed to be the
Tg of the rubbery block at this frequency. Since the transition
temperature was constant with change in composition of semicrys-
talline blocks (only its magnitude increasing with increase of HI
rubbery block), it is believed that this is an additional indica-
tion of the absence of mixing between the amorphous phases of HI
and HB in the solid state. This is in constrast to the nonhydro-
genated block systems, where molecular homogeneity has been ob-
served in the solid state as denoted by an intermediate Tg.

Introduction

        The need for polymeric materials of outstanding material
properties which can be processed by economic thermoplastic
methods has been a major factor in the development of block
copolymers.(1-5) Although there are some reports on block copoly-
mers containing a semicrystalline block such as poly(ethylene
oxide),(6-7) the main body of the work has been focused on systems
whose blocks are amorphous and are microphase separated.
Establishment of separate microphases or domain texture at the use
conditions of the materials is the prominent reason for the good
properties of these systems.(1) For example, the physical anchor-
age of segments (generally the end blocks) of the macromolecules
in glassy domains is the origin for what has been also called
"physical cross-links" in the thermoplastic elastomers.
        Incompatibility of the blocks, which is a prerequisite for
good properties at the use temperature, often prevents good mixing
of the blocks in the melt, thereby inducing a high melt viscosity
at the processing temperature.(1) If one of the block components
is crystallizable, as pointed out recently,(8) it is possible to
choose a system in which the blocks need not be very incompatible.
For these copolymers, mixing could occur in the melt. Such a
system would have lower viscosity in the melt and could have an
added advantage of being solvent resistance in the solid state due
to the development of crystalline domains.
        In this study, the effects of the variations in block
sequence and composition (and thus relative block length) on the
material properties of two series of triblock copolymers has been
investigated. One of the blocks, the hydrogenated polybutadiene
(HB), is semicrystalline, and the other block, the hydrogenated
polyisoprene (HI) is rubbery at room temperature. Thus in one
series, the HBIB block copolymers, the end blocks are semi-

crystalline, and in the other series, the HIBI block copolymers, only the central block is semicrystalline. In addition and for comparison purposes, one diblock HBI has also been studied.

Hydrogenation of the polyisoprene block results in the formation of the amorphous alternating copolymer of ethylene-propylene. The hydrogenated polyisoprene (HI) block possesses a glass transition temperature below ambient temperature ($T_g \simeq -60°C$ by DSC, heating rate 10°/min) and is rubbery at room temperature. Exhaustive hydrogenation of the polybutadiene block of low 1,2 microstructure will transform this block to a polyethylene-like structure.(9) Hydrogenation of 1,2 microstructure which is present in the parent polymer in around 5-8 mole percent (according to IR analysis and is equivalent to 1.3-2.1 ethyl branches per 100 carbon atoms) would result in formation of pendant ethyl groups. Indeed NMR analysis of the same HB polymer obtained via courtesy of Prof. Mandelkern indicated the presence of ~2 ethyl branch units per 100 carbon atoms. Therefore the resultant HB block is more similar in properties to low density polyethylene (10-11) than to high density polyethylene, but the properties are not exactly the same as LDPE.(12) The HB block is thus semicrystalline but the crystallinity of this block in the quenched samples is lower than 35 percent. The low crystallinity of this exhaustively hydrogenated HB polymer is due to the presence of pendant side chains.

Significant modification in properties of polymers and block copolymers containing isoprene and/or butadiene have been reported following hydrogenation of these macromolecules.(9,13-18) Although the initial motive for this modification of the double bond containing polymers was perhaps directed towards enhancement of the photolytic, oxidative, and thermal stability of these polymers, it was realized subsequently that polymers containing butadiene of low vinyl content produced better mechanical properties.(13-18) This improvement can be attributed to the development of crystallinity in the polyethylene-like segments.(9) Preparation and some structure-property studies on triblock coplymers containing semicrystalline end blocks of hydrogenated polybutadiene have been reported by Falk et al.(14,18) He described the synthesis of triblock copolymers containing polyethylene-like end blocks and a rubbery central block by the catalytic hydrogenation of triblock copolymers of butadiene, where end blocks were low in 1,2 microstructures, but the central block was high in 1,2 microstructure.(14) He also reported that he was able to selectively hydrogenate butadiene blocks in copolymers of 1,4-butadiene-isoprene-1,4, butadiene.(18) The important point is that hydrogenation of a polybutadiene segment which is rich in 1,4 microstructure will yield a semicrystalline polyethylene-like block whereas the block containing moderate to high 1,2 microstructure produces rubbery structure at ambient temperatures.

Recently, hydrogenation of polybutadiene containing high 1,4 microstructure has also been employed for preparation of linear

"polyethylene" of low polydispersity and various studies have been
conducted on this polymer. In a series of papers, Graessley et
al. discussed the preparation and the rheological behavior of
linear and star-branched hydrogenated polybutadiene.(10,11,19)
Cowie et al. used a series of polybutadienes which had been hydro-
genated to different extents in an attempt to determine the glass
transition of amorphous polyethylene.(20) The crystallization
kinetics (21), elastic recovery and the dynamic mechanical proper-
ties (12) of HB have also recently been investigated. The rheolo-
gy, dynamic mechanical behavior and the crystallization kinetics
of HB were very similar to those of LDPE, but the elastic proper-
ties in the solid state were different. In brief, this change was
attributed to the difference in rigidity of the spherulites of HB
from that of LDPE.
      It was the objective of this work to investigate the effect
of variation in block architecture (number and the order of the
blocks) on the crystallinity level, morphology, the stress-strain
and hysteresis behavior of this series of polymers. In addition,
the composition ratio of the two block types is expected to play a
crucial role in determining the bulk material properties of the
block copolymers. This is related to the fact that the mechanical
properties of block copolymer are typically influenced more
substantially by the behavior of the continuous phase, as will be
demonstrated.(1,22)

Experimental

      Polymer Synthesis and Characterization. This topic has been
extensively discussed in preceeding papers.(2,23,24) However, we
will briefly outline the preparative route. The block copolymers
were synthesized via the sequential addition method. "Living"
anionic polymerization of butadiene, followed by isoprene and more
butadiene, was conducted using sec-butyl lithium as the initiator
in hydrocarbon solvents under high vacuum. Under these condi-
tions, the mode of addition of butadiene is predominantly 1,4,
with between 5-8 mole percent of 1,2 structure.(18) Exhaustive
hydrogenation of polymers were carried out in the presence of p-
toluenesulfonylhydrazide (19,25) in refluxing xylene. The rela-
tive block composition of the polymers were determined via NMR.
The relative concentration of the various butadiene microstruc-
tures, (1,4 cis, 1,4 trans, and 1,2 vinyl), were determined from
the infrared spectra of solid films cast on KCl.(26) The 1,2
microstructure content of all the polymers considered in this
paper were between 5-8 mole percent as determined from the IR
spectra. Number average and the weight average molecular weight
of the polymers were obtained via osmotic pressure and HPLC. The
molecular weight of all polymers is around 200,000 g/mole while
the polydispersities were about 1.1; thus, all of these polymers
have a relatively narrow molecular weight distribution. Note,
that both the precursor diene blocks and hydrogenated copolymers

showed narrow monomodal sharp GPC traces at room temperature and
elevated temperatures, respectively. A sample of low density
polymer (LDPE) which was obtained from the Union Carbide
Corporation (Dex 194) was used for comparison with our polymers.
The number and the weight average molecular weight of this poly-
mer, as obtained from GPC, were 13,900 and 77,500 g/mole,
respectively.

The hydrogenated (H) block copolymers will be designated by
giving the butadiene (B) or isoprene (I) block sequence followed
by a number which represents the total weight percentage of
butadiene in the polymer. For example HBIB-27 is a hydrogenated
triblock copolymer of butadiene-isoprene-butadiene which contains
27% butadiene. Since the polymer is symmetric, the relative
composition of each block is therefore 13.5% B –73% I –13.5% B.

Sample Preparation. Samples for mechanical studies were made
by compression molding the polymers at 150°C between Teflon sheets
for 15 minutes followed by rapid quenching to room temperature in
air. These will be referred to as PQ (press-quenched or simply
quenched) samples. The thickness of the PQ samples was around 10
mils (0.25 mm). The thermal history of all of the PQ samples
(HBIB, HIBI, and LDPE) were essentially the same. They were used
within one week after they were pressed. Samples for morphology,
SALS and SEM studies were prepared from toluene solutions. These
films were cast on a Teflon sheet at 80°C from a 1% (by weight)
solution in toluene. These films were about 5 mils in thickness.
When the polymer films had solidified (after 5 hrs), they were
stored in a vacuum oven at 80°C for two days to remove residual
solvent. These samples will be designated by TOL (solution cast
from toluene).

Crystallinity and Morphology. The X-ray diffraction patterns
of the films were taken with a Phillips PW1720 table-top X-ray
unit using a flat plate camera. The SALS H_v patterns were
obtained using a helium neon laser and the photographic technique
developed by Stein.(27) An ISI Super III-A scanning electron
microscope was employed for morphological investigations. Samples
were coated with gold using a SPi sputter T.M., Model 13131. The
density of the polymer samples was measured using a density
gradient column constructed from ethanol and water. Glass beads
with known density were used to calibrate the column. The thermal
properties of the polymers were measured on a Perkin Elmer
differential scanning calorimeter, Model 2. The heating rate was
10°C per minute.

Mechanical Properties. The stress-strain and the hysteresis
behavior of the polymers were measured on a Model 1122 Instron
using dog-bone samples of 0.28 cm width and 1.0 cm effective
length. The strain was measured using the displacement of the
crosshead. In the calculation of the strain it was assumed that

the extension occured mainly in the central 1.0 cm region of the
dogbone sample. The crosshead speed was 10 mm per minute, giving
the initial elongation rate of 100 percent per minute. The
mechanical hysteresis of the samples, which is a measure of energy
loss during cyclic deformation, was obtained from measurement of
the area under loading and unloading curves using a planimeter.
The percentage hysteresis were calculated from the following
relationship:
$$\% \, Hyst = 100 \, (A_\ell - A_u)/A_\ell$$
where A_ℓ and A_u are the area under the respective loading or
unloading stress-strain curve.

Dynamic Mechanical. The dynamic mechanical properties of the
samples were measured on a Rheovibron, Model DDV-II at either 35
or 110 Hz.

Results and Discussion

As already mentioned, the HB block is semicrystalline and its
general behavior is similar to that of LDPE. The HI block on the
other hand is amorphous and rubbery at ambient temperature. The
material behavior of block copolymers containing HB and HI blocks
will now be discussed in the following sections.

Crystallinity and Morphology. The block copolymers of
essentially completely hydrogenated HBIB, HIBI and HBI, in which
the microstructure of butadiene is predominantly 1,4, are
semicrystalline. Our measurements indicate that the extent of
crystallinity is independent of the architecture of the block
copolymer and is linearly dependent on the butadiene content. A
comparison of the X-ray diffraction pattern of a homopolymer of HB
is given in Figure 1 along with that from a triblock copolymer
HBIB-50. The sharp diffraction rings are clearly indicative of
the presence of crystallites in both polymers. Block copolymers
containing as low as 8% butadiene have shown basically the same
type of diffraction patterns, but with a much lower intensity
because of lower concentration of butadiene. This indicates that
aggregation of crystallizable segments and formation of
crystalline domains is not significantly affected by the
surrounding noncrystallizable HI block.
Quantitative measurements of the crystallinity content of the
block copolymers were made from the determination of the heat of
fusion and from the density of the polymer.
The DSC thermograms of several triblock copolymers and
homopolymer HB are compared to that of a low density polyethylene
in Figure 2. The thermograms are those of the first run on
quenched samples. Their behavior is similar except that the
temperature of the maximum in the DSC melting peak, T_m, for LDPE
(110°C) is higher than that of HB (102°C). The depression of the
melting point brought about by the presence of 5 to 8 mole percent
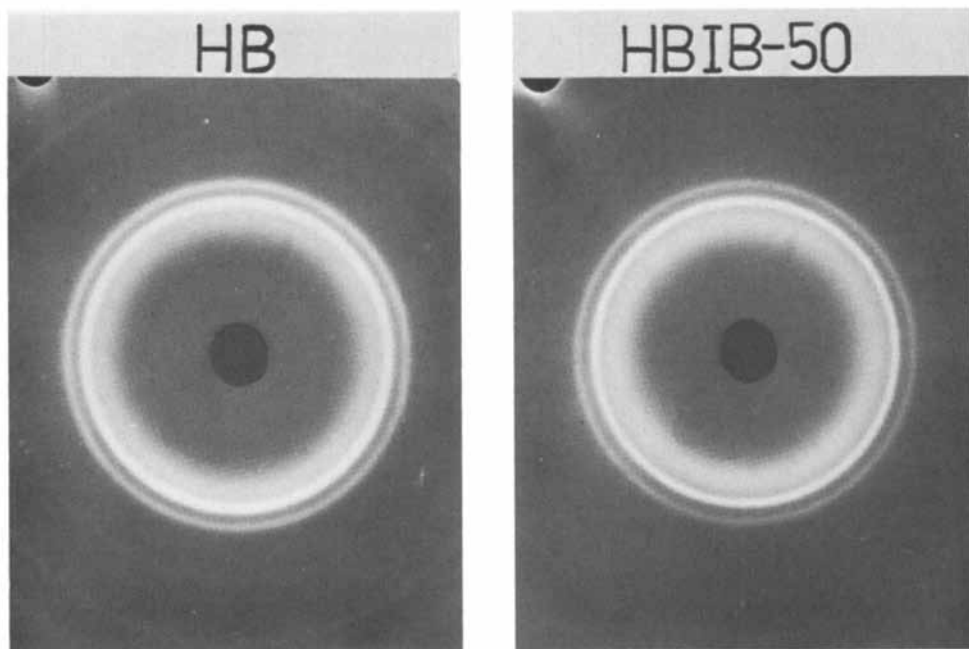
Figure 1. *X-ray diffraction patterns of the semicrystalline homopolymer (HB) and a block copolymer (HBIB–50).*
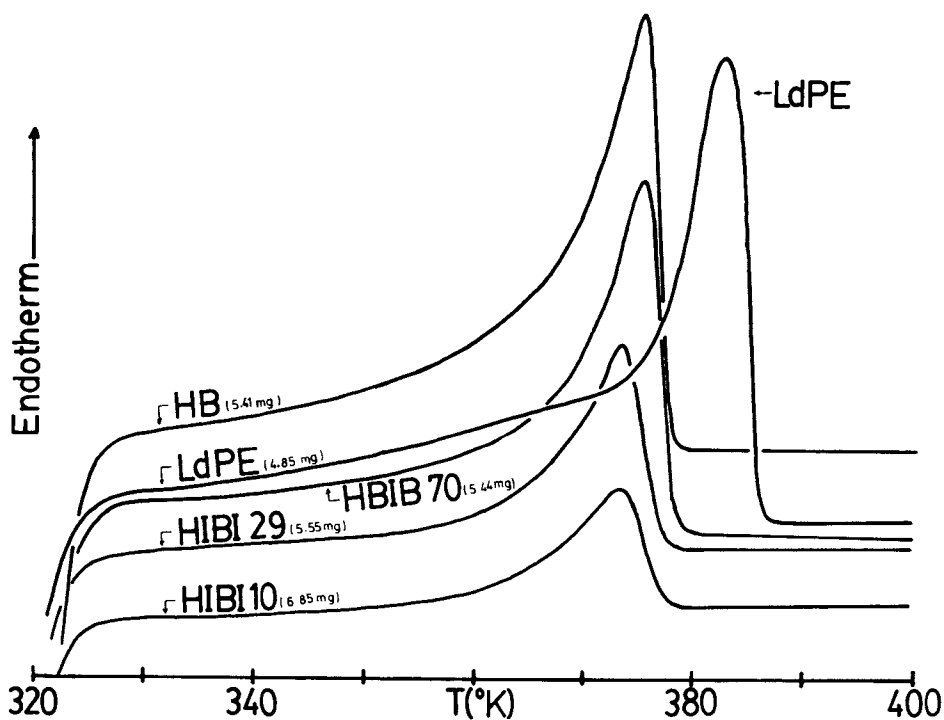
Figure 2. Comparison of the Differential Scanning Calorimetry (DSC) thermograms of the homopolymer HB and various block copolymers to that of the LDPE. Weight of each polymer sample is indicated in the parentheses. The instrument range is 2 mcal/s for all the runs.

of the hydrogenated 1,2 butadiene adduct (equivalent to 1.3 to 2.1 ethyl branches per 100 carbons) far exceeds the theoretical value based on Flory's work.(28) Polyethylene containing methyl, ethyl and n-propyl groups have also shown higher depression of the melting point than the theoretical value and thus the behavior of our system is not unique.(28,29) What is surprising, however, is that the depression of the melting point brought about by the presence of 1.3 to 2.1 ethyl branches per 100 carbons in our system ($\Delta T=36°C$ with respect to T_m of HDPE) is still higher than that produced by the same amount of ethyl or even n-propyl branches ($\Delta T=22°C$ for 2.1 n-propyl branch per 100 carbon atoms as measured by Richardson et al.).(28) At this point we do not have the exact reason for the behavior of our system, but it is possible that the higher depression of the melting point is caused by a very small amount of remaining unsaturation and/or the presence of some p-toluene sulfonyl adduct produced during the hydrogenation of the double bonds. We have recently reported that the addition of a phenolic antioxidant such as Irganox 1010 effectively decreases the minor but the detectable side reaction.(24) Copolymer reprecipitated from hot xylene appear to have only a trace at most of this adduct. Other workers have also reported a lower T_m for HB polymers (12,21) and they also postulated that the depression of the melting temperature, as compared to HDPE, is due to presence of ethyl branches and some remaining unsaturation in the main chain.(12) Lowering of T_m with an increase in the number of ethyl side chains has been observed in copolymers of ethylene-butene.(30) Although the melting temperature of HB has been reported to be inversely related to molecular weight(21) and hence on chain length, our block copolymers do not show such a dependence on HB sequence length. The "peak" melting temperatures of all of the block copolymers, regardless of chain architecture or butadiene composition, are in the vicinity of 102 ±2°C for the quenched samples. The reader may recall that for a given total molecular weight, an increase in butadiene content is followed by an increase of butadiene block chain length. Thus, neither the architecture nor the butadiene block chain length (at least in the ranges that we have studied) affects the melting behavior of the polymer. This is contrary to the findings of O'Malley, et al. who studied the effect of changes in composition of tri-and diblock copolymers of styrene ethylene oxide block copolymers.(31) They attributed the decrease of T_m of the crystalline polyethylene oxide block with the increase of styrene content to the decrease in the perfection of the crystalline lamella. In light of this result, the independence of T_m of composition in our own systems could be rationalized in the following way. The crystallites of HB are generally embedded within the amorphous HB phase and thus are not significantly affected by the rubbery HI block. In fact, there is an indication from our dynamic mechanical studies that there is phase separation between the HI and HB blocks in the amorphous regions. Thus the environment experienced by the HB

crystallites is the same and therefore their perfection (and hence T_m) is not influenced by compositional variation.

The heat of fusion ΔH_f (obtained from the area under the DSC melting curve) and percentage crystallinity calculated from ΔH_f is found to be linearly dependent on butadiene content, and independent of the polymer architecture. This is shown in Figure 3. Also, the density of the block copolymers was found to be linearly dependent on butadiene content (see Figure 4). The linear additivity of density (specific volume) has been observed by other workers for incompatible block copolymers of styrene and butadiene indicating that very little change in density from that of pure components has occurred on forming the block copolymers.(32) While the above statement is somewhat plausible, these workers have utilized the small positive deviation from the linear additivity law to estimate the thickness of the boundary in SB block copolymers.(32)

In Figure 4, the density of a hydrogenated random copolymer of butadiene-isoprene containing 50% butadiene is also given. The X-ray diffraction pattern and the DSC thermogram of this polymer indicates that it is totally amorphous. Extrapolation from the density of HI to the density of this random HBI-50 to the axis corresponding to 100% hydrogenated butadiene would give the density of amorphous HB (or that of amorphous "polyethylene"). The value of the density for amorphous polyethylene obtained in this way is about 0.869 g/cm^3 as compared to the value of 0.855 g/cm^3 obtained from the extrapolation of molten PE.(33) In our calculation of the percentage of crystallinity from density measurements, we have used the following values: 0.869 g/cm^3 for the density of amorphous PE (rather than the literature value of 0.855 g/cm^3), 0.862 g/cm^3 for the density of hydrogenated isoprene (amorphous), and 1.00 g/cm^3 for the density of crystalline PE.(34) While our extrapolated density for PE might be somewhat questionable based on our limited data, the value of crystallinity obtained using the above values is nearly identical to that found from ΔH_f. This value is at least 12% lower than that found using the relationship of Chiang and Flory where the density of the amorphous and crystalline PE are taken at 0.8518 and 0.9995 g/cm^3 respectively at 25°C.(35) The percent crystallinity was also obtained from the areas of the endothermic peaks in DSC graphs using a ΔH_f value of 69 cal/g for completely crystalline polyethylene.(36) A comparison of crystallinity values obtained from density to those from ΔH_f is made in Figure 5. The correspondence of the density from both methods is excellent. It is noteworthy that the behavior of LDPE also falls in this range, even though the crystallinity of this sample is much higher. It is of interest to point out that Hser and Carr have reported percentage crystallinity of a series of HB of different molecular weight using X-ray diffraction methodology.(21) The density of all of their samples were ~0.915 g/cm^3 and for samples in the molecular weight range 60,700 to 340,000 the ΔH_f were 21.7 cal/g
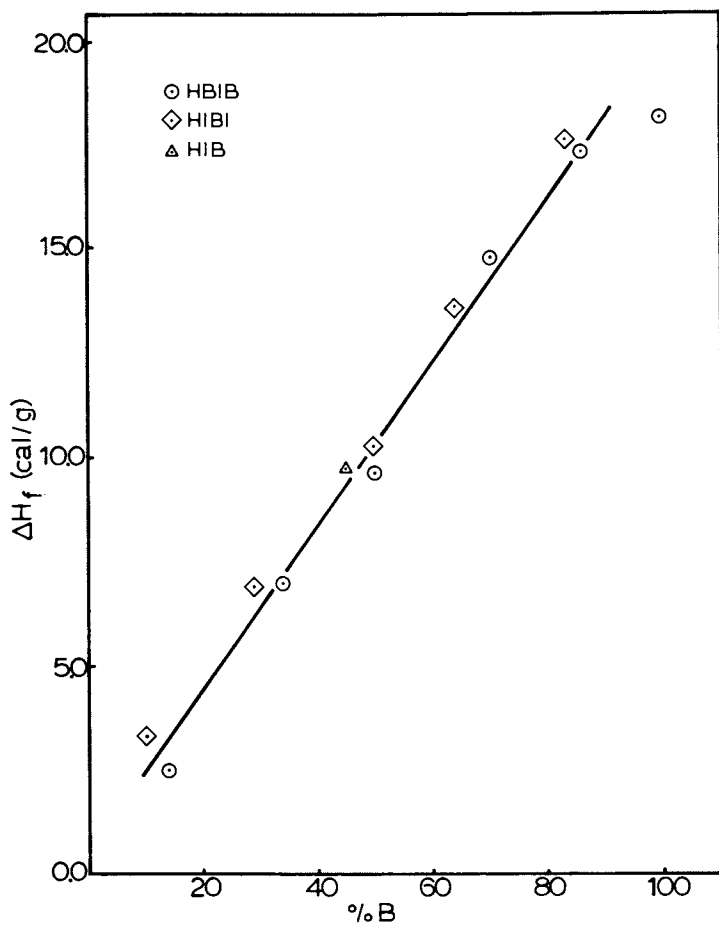
Figure 3.   The linear dependence of ΔH_f on butadiene content in various block copolymers.
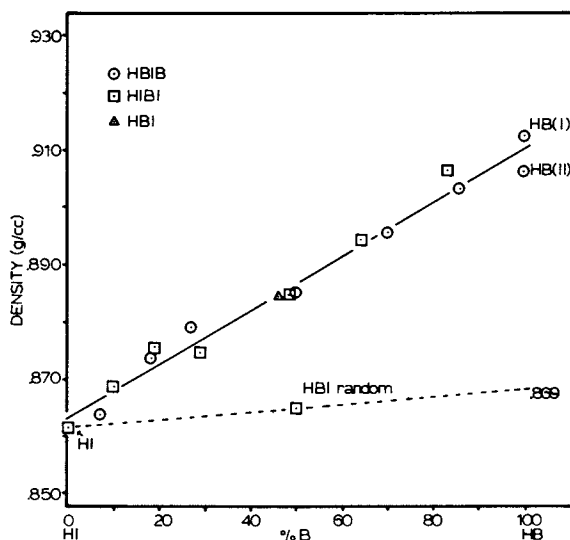
Figure 4.   The linear dependence of density on butadiene content in various block copolymers. Density of amorphous HB (polyethylene) is estimated from the extrapolation of the density of HI through that of the random copolymer HBI–50 to axis where butadiene content is 100%.
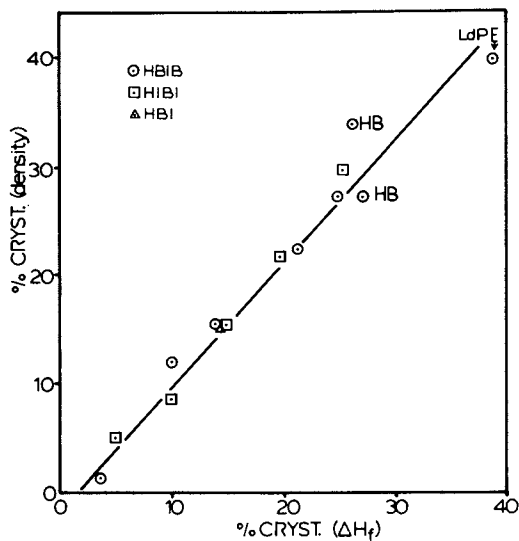
Figure 5.   A comparison of percent crystallinity obtained from density to that obtained from ΔH_f for the various block copolymers.

to 17.4 cal/g respectively. These ΔH_f values correspond to a percent crystallinity varying from 31.4% to 25.3% whereas the respective percent crystallinity values from the X-ray method were 43% and 46%. That is, there is little correlation in their crystallinity values obtained from the ΔH_f and X-ray methods used in their work. While we do not attempt to explain their discrepancy, it stands in contrast to our own data. The important point to be made at this time is that an increase in crystallinity in our series of block polymers is only dependent on the butadiene content and bears no relationship to the block architecture.

The accumulated data from X-ray, ΔH_f and density measurements thus far indicate that there is good separation of the crystallizable HB block from that of the amorphous HI block, regardless of molecular architecture. We as yet have no direct evidence to determine what is the specific morphological nature of the crystalline structure; specifically, as to whether they are composed of fringe micelle or folded chain structures. Dimarzio et al. have carried out calculations of lamella thickness in diblock copolymers where one of the components is crystalline; they have reached the conclusion that chain folding is a stable form in such block copolymers.(37) This is contrary to homopolymers where chain folding is metastable and annealing reduces chainfolding.(38) Our general belief at this time is that the HB block will likely display some degree of lamellar texture in view of workers who have noted such textures in long block copolymer containing one crystallizable component.(31) In order to gain some insight into possible arrangement of the crystalline domains on a higher order level i.e., superstructure, we have applied the SALS technique. The H_v patterns for solution cast films of HB and a series of HBIB polymers are shown in Figure 6. Both the HIBI and HBI polymers produce the same kind of H_v patterns and are not shown here. Polymers with high and intermediate butadiene content clearly display the typical cloverleaf H_v pattern which is associated with the spherulitic structure.(39) In this composition range, the size of the spherulites as calculated from the angle of the maximum intensity in the H_v four-leaf clover scattering patterns, range from 0.5 to 3.0 μm. The SALS patterns suggest that there is a deterioration of the spherulitic perfection with an increase in HI content, and indeed sample HBIB-7 no longer displays a cloverleaf pattern, but rather a more rod-like or sheaf type pattern.

SEM micrographs of two members of these polymers (HB and HBIB-50) are shown in Figure 7 to provide further evidence for superstructure on the micron level within the solution cast films. One can directly observe the surface of the spherulitic structure of the HB homopolymer as well as in that of the copolymer HBIB-50. Clearly, the level of structure (~5 μm) is well above that of the individual domains of either HB or HI and reflects the possible primary nucleation and subsequent growth behavior common to spherulitic semicrystalline polymers. The H_v patterns shown in
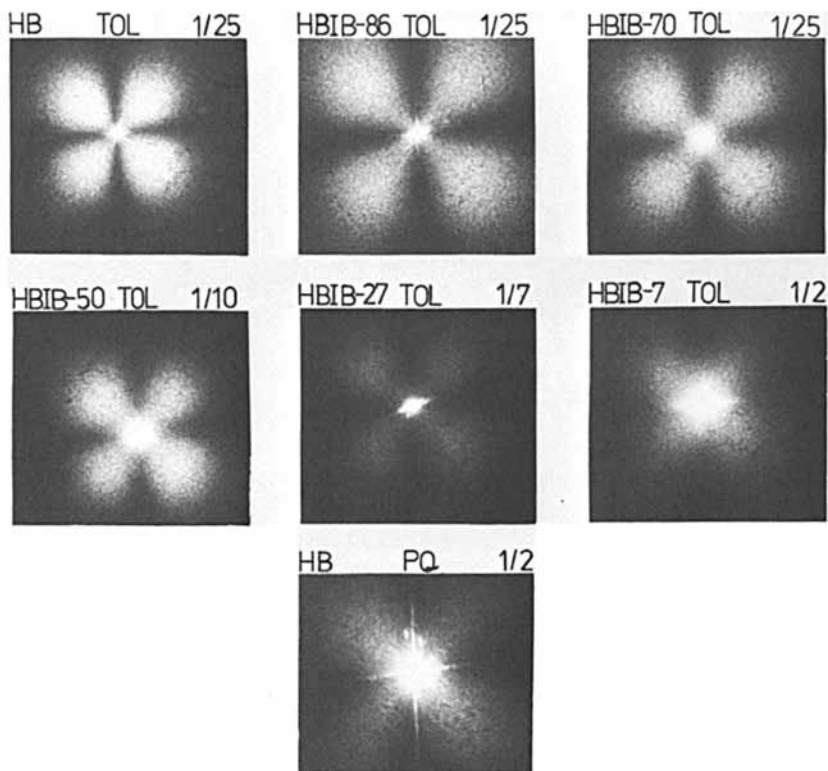
Figure 6.   SALS, H_v light scattering patterns of HB and HBIB of different compositions.   Key: method of film preparation of T.C. is TOL or PQ; exposure time in fractions of a second.
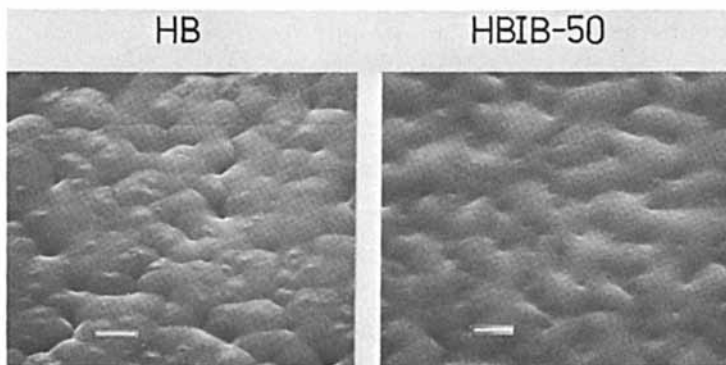
Figure 7.   SEM of the surface of films cast from toluene for HB and HBIB–50. The bars indicate $5\mu m$.

Figure 6 display an important trend. The best formed spherulitic
structure is that of homopolymer HB. When the concentration of
butadiene decreases in the series of the HBIB copolymers the
perfection (anisotropic ordering) of the spherulites is also de-
creased. Indeed, in the polymer HBIB-7, which contains only 7%
butadiene, one can no longer see the H_v scattering pattern as is
observed for well developed spherulites. It is to be noted that
the formation of the spherulitic structure is strongly dependent
on the method of the film preparation. The well developed spheru-
litic structure shown in Figure 6, HB or HBIB-86 for example, were
produced when the films were cast from solution (Tol). By con-
trast, the compression molded samples (PQ) did not show well de-
veloped spherulitic structure. Even the HB homopolymer produced a
very ill defined spherulitic pattern when the film was prepared by
quenching the pressed film (Figure 6). Mandelkern et al. have
studied supermolecular structure of linear polyethylene fractions
and reported that high molecular weight fractions (3 -8 x 10^6) do
not form well developed spherulites if they are crystallized
rapidly.(40) These polymers can, however, produce spherulitic
structure if they are crystallized from the swollen state. (41)
    It should be re-emphasized that although our block copolymers
do not display spherulitic morphology when they are compression
molded, they are nevertheless crystalline. Hence, this indi-
cates that under this mode of film preparation, aggregation into
well developed superstructure is apparently kinetically limited.

    Stress-Strain Properties. A comparison of the stress-stain
properties of the compression molded tri-block HBIB copolymers to
those of the homopolymers HB and HI of the same molecular weight
(~200,000) are made in Figure 8. The stress-stain properties of
the inverted triblock copolymers HIBI are given in Figure 9. As
might be expected, the stress-strain properties of HB are very
similar to that of low density polyethylene. Perhaps linear low
density polyethylene (LLDPE) would be an even better model. The
major difference that we have observed is that the initial modulus
of HB is lower than that of LDPE (75 vs. 170 MPa respectively) and
there is also a lower stress displayed in the region where plastic
deformation begins which is likely associated with yielding
phenomenon involving crystallite reorientation. Both of these
differences are at least partially accountable by the lower crys-
tallinity of the compression molded samples of HB relative to that
of low density polyethylene (the crystallinities are approximately
30% and 40% respectively, (see Figure 5). Tanaka et al., however,
have reported that the material properties of HB are different
from that of LDPE, the most remarkable difference is the higher
elastic recovery of the former.(12) They attribute this differ-
ence to a "looser" structure of spherulites of HB which allows
crystallites to orient in a reversible manner. We have not ob-
served significant differences in the nature of the stress-strain
behavior of HB polymers relative to those of LDPE. Indeed, when a
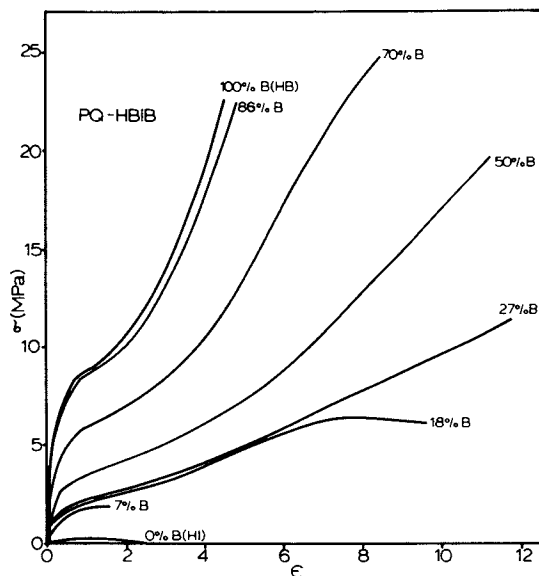
Figure 8.   Comparison of the stress–strain properties of the press–quenched films of HBIB to those from the homopolymers HB and HI.   Composition of each polymer is denoted by the butadiene content next to the graph.
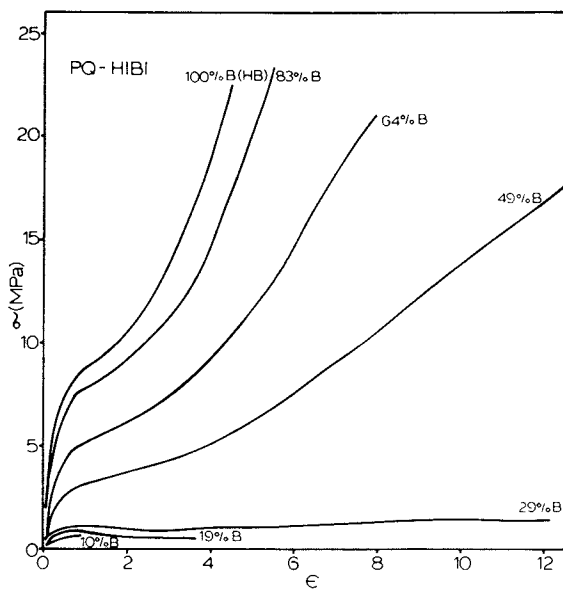
Figure 9.   Comparison of stress–strain properties of the press–quenched films of HIBI block copolymers to those of homopolymer HB.   Butadiene content is next to the graph.

sample of HB was prepared by solution casting from toluene, the
crystallinity of this film was very close to that of a quenched
sample of LDPE. The stress-strain plot of this solution cast film
closely resembled that of quenched LDPE, indicating, as mentioned
before, the earlier difference most likely is <u>principally</u> due to
the difference in the crystallinity level in contrast to molecular
weight distribution discrepancies, etc. One should comment that
the ultimate tensile properties of the HB systems are excellent.

The mechanical properties of HBIB block copolymers are
significantly affected by the increase in the proportion of the
central rubbery HI block. For example, HBIB-86 (14% isoprene)
shows a lower modulus; some yielding behavior is still present but
elongation to break is significantly improved. A further increase
in the rubbery HI content (eg. from 14 to 82%) produces a modulus
which is sharply decreased, but the elongation to break is again
increased. HBIB-70 and HBIB-50 are very tough plastics; the
former has even a higher stress to break than the initial HB. On
the other hand, the behavior of HBIB-27 is typical of a thermo-
plastic elastomer. HBIB-18 also has elastomeric behavior but it
fails earlier than HBIB-27 indicating that the three dimensional
network of physical crosslinks (crystallites) is less well de-
veloped. The behavior of HBIB-7 is somewhat like a particulate
filled and uncrosslinked rubber of low filler content. The last
member of this series, the homopolymer HI (or HBIB-0), is and be-
haves as an uncured rubber. It does not show any strain hardening
indicating that, as expected, at the level of strain experienced
by the sample (~240%) no strain-induced crystallization occurs.

The general stress-strain behavior of our HBIB series has
some similarity to those of the SBS block copolymers.(4) However,
there are two prime differences between these two systems.
Styrene is a brittle glass at room temperature, but HB is a
semicrystalline plastic above its T_g and therefore is rather
ductile. Therefore, a block copolymer of SBS containing as much
as 20% butadiene is still brittle and often breaks at very low
elongation.(1). By contrast, HBIB-86 or even HB itself can be
extended to above 400% elongation before failure occurs. The
other difference is that the block copolymers of SBS may show
considerable amounts of drawing (necking) in the concentration
range of 39% to 65% styrene, whereas none of the members of HBIB
display this behavior.

The stress-strain properties of the inverted triblock copoly-
mers HIBI are shown in Figure 9. Analogous measurement on the di-
block copolymer HBI-50 are not shown but were almost identical to
that of HIBI-49. As expected, an increase in isoprene content
from the homopolymer HB polymer to the HIBI block copolymers and
finally to the homopolymer HI greatly influences the mechanical
properties. An increase in the rubbery HI content is again
followed by a decrease by Young's modulus. In the range of 23% to
49% butadiene, the polymers show higher extension to break than
for the HB. They can be viewed as tough plastics and require a

larger input of energy (higher area under the stress-strain curve)
to break. The next member of the series, HIBI-29, shows a great
deal of extensibility, but it is extremely weak. A further in-
crease in isoprene concentration results in polymers which not
only are weak but also break at low extensions (HIBI-19 and HIBI-
10). Now that the effects of variation of composition on the
mechanical properties of each member of the two series has been
examined, the influence of architecture alone on properties can be
considered. A comparison of some specific properties for the
polymers of various architecture and different compositions are
made in Figures 10A-C and Figure 11. As in the case of Figure
10A, an increase in HB content, i.e., a rise in the concentration
of the semicrystalline blocks, is always followed by a rise in the
modulus of the polymers. This type of behavior of block copolymer
has been expressed in terms of composite theories and the know-
ledge of the modulus of the component blocks (HI and HB). To do
so, however, one has to know the geometry of the microdomains in
the system considered. Calculation of the modulus of block co-
polymers using the modified composite theories developed by
Nielsen (42,43) and Lewis (44) have been reported on SBS triblock
copolymers (3,45) and will not be repeated here.

An interesting observation derived from Figure 10A is that
modulus of the triblock copolymer HBIB is always considerably
higher than that of the inverted block copolymer HIBI. This
difference in modulus is likely due to the presence of more
permanent entanglements in HBIB copolymers since these endblocks
can be partially tied down in the semi-crystalline domains, as
shown schematically in Figure 12. Of course, it is realized that
amorphous regions in HIBI also form entanglements, but since the
end blocks are not mechanically anchored these entanglements can
be lost when the sample begins to undergo deformation.

The ultimate properties, that is the elongation and stress at
break for copolymers with various architectures and compositions,
are given in Figures 10B and 10C respectively. The elongation at
break ε_B goes through a maximum for the block copolymer when the
composition is varied from pure HI to that of HB as shown in
Figure 10B. The maximum is achieved around 30% butadiene content.
Since the ultimate properties are influenced by various parameters
e.g., flaws, hard phase content, etc. (46,47), we have not
attempted to rationalize the details of this behavior at this
time. However, we do wish to point out that while breaking stress
in general rises with HB content, the strain to break passes
through a distinct maximum. Therefore all of these polymers have
high extension in this concentration range. Above this concentra-
tion range ε_B is decreased approximately in the same way for all
chain architectures. Below this value, the ε_B is also decreased,
but now there is a considerable difference in behavior of HBIB
from that of HIBI polymers. In the 10% to 20% butadiene range
HIBI polymers fail at a lower elongation than HBIB polymers and
this behavior is certainly related to the morphological structure
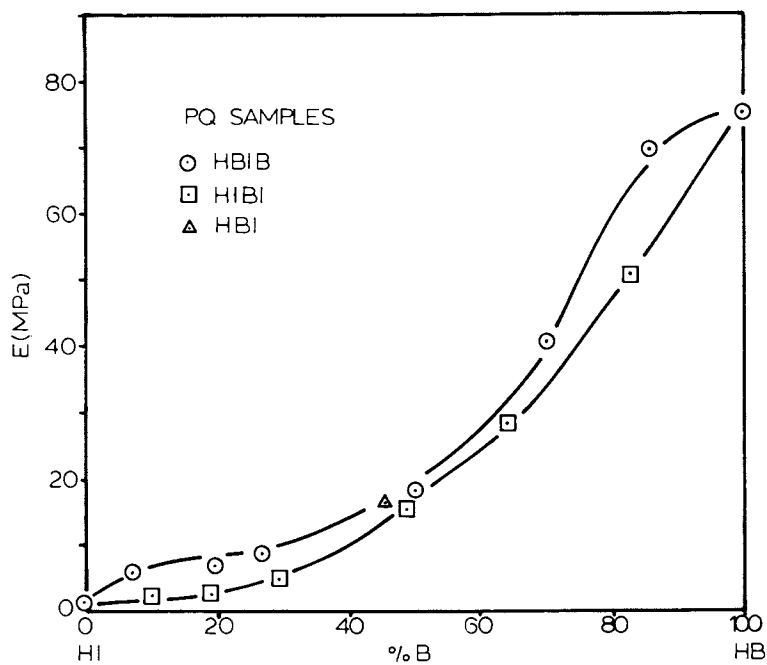
Figure 10A.   Dependence of Young's modulus on butadiene content for various copolymer architectures.
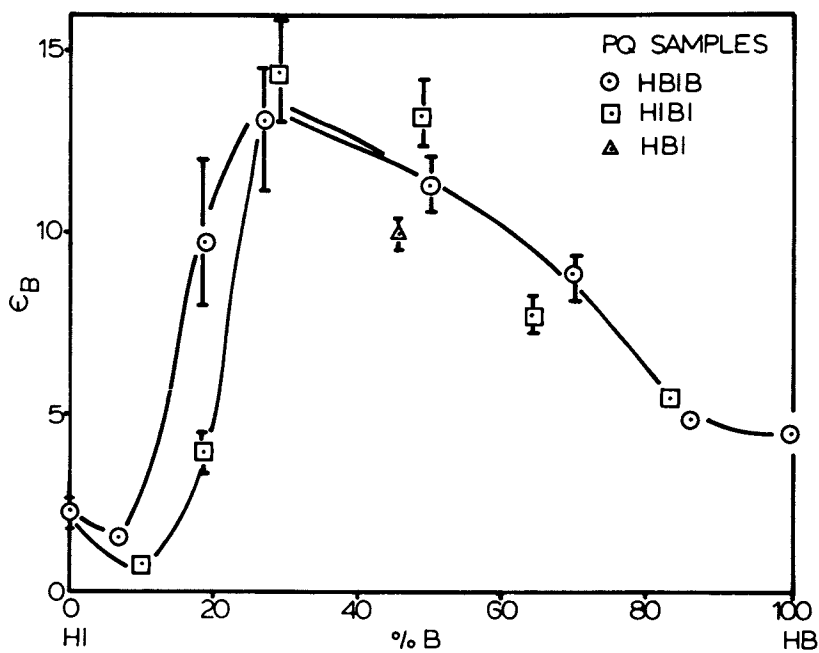
Figure 10B. *Dependence of strain to break on the butadiene content for various copolymer architectures.*
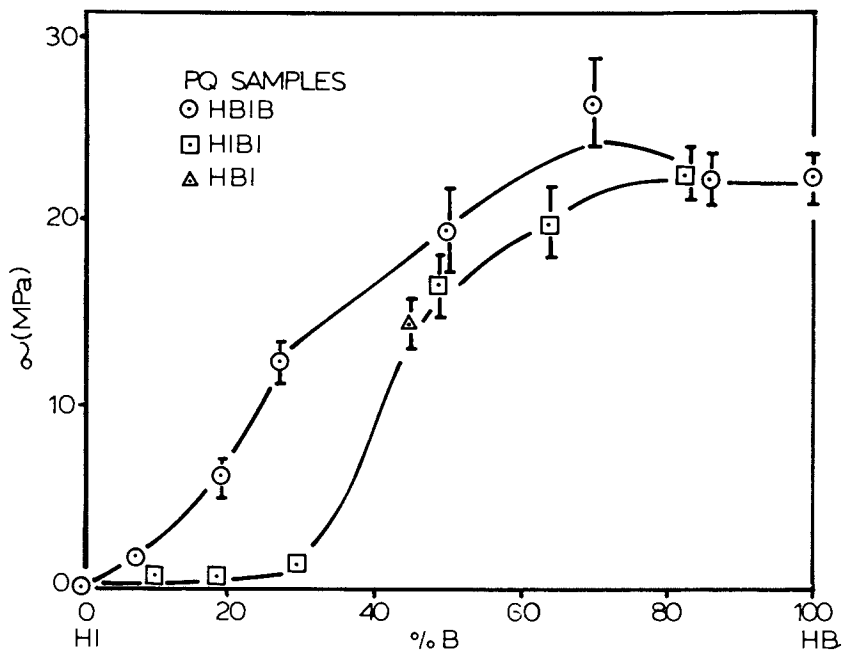
Figure 10C. Dependence of the ultimate stress on the butadiene content for various copolymer architectures.
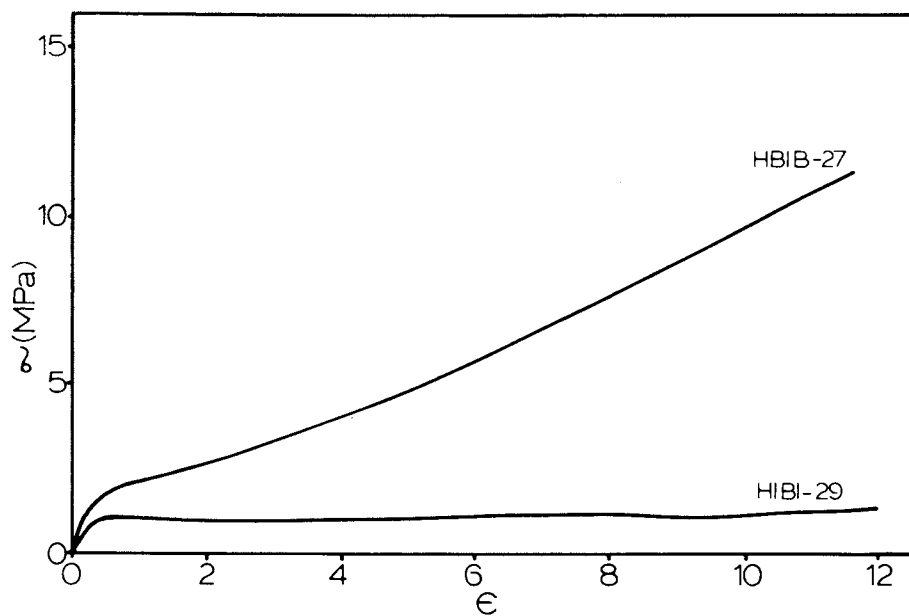
Figure 11.   Comparison of the stress–strain properties of the thermoplastic elasto-
mer HBIB–27 to that of inverted block copolymer HIBI–29.
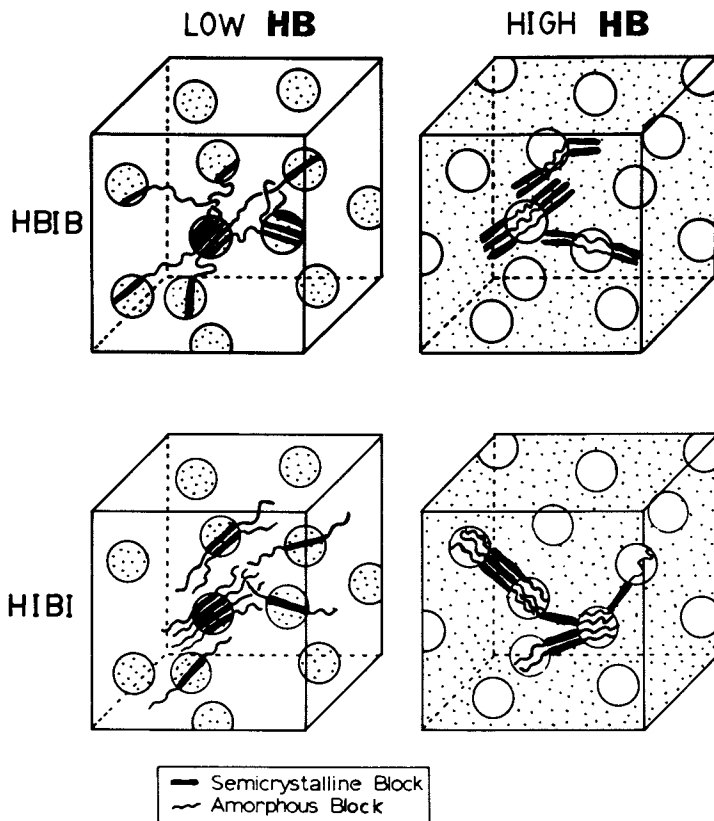
Figure 12. *Oversimplified schematic representation of the morphology of HBIB and HIBI block copolymers in the low and high butadiene concentration ranges.*

Formation of "physical cross-links" by the anchorage of chain ends in semicrystalline domains and production of "permanent" entanglements is shown in the HBIB block copolymers. No such arrangement exists for the inverted polymer HIBI. (No attempt has been made to show possible chain folding, or superstructure development of their absence.)

of the polymers as discussed shortly. The stress to break, σ_β,
does not seem to go through a significant maximum, but rather
there is a considerable increase in σ_β with an increase in
butadiene from the low value of HI. The behavior of the polymers
in regard to ultimate stress falls into two categories. In the
low to intermediate concentration range of butadiene (from 10% to
40% B) the behavior of the HBIB polymers is quite different from
that of the inverted HIBI copolymers and is most pronounced in the
20-29% range. In the high concentration range (40% to 100% B),
the σ_β for HBIB and HIBI is much closer. A comparison of the
stress-strain properties for HBIB and HIBI polymers, in this
concentration range, is made in Figure 11.

The HBIB-27 polymer behaves like a thermoplastic elastomer,
whereas HIBI-29 behaves somewhat like a particulate-filled uncured
elastomer. Both are somewhat rubbery in nature although their
stress-strain behavior deviated from typical crosslinked
elastomers in that the initial stress level is higher, as is
commonly seen for domain forming thermoplastic elastomers. These
differences are clearly related to the morphology and structure of
these systems. In order to discuss the behavior of these polymers
of various architecture containing different levels of semicrys-
talline HB, oversimplified morphological models of these systems
are given in Figure 12. These drawings are not meant to infer
that no superstructure or chain folding may exist but only to
depict the general differences in the continuity of the two com-
ponents as well as the nature of the localized end blocks. Thus,
in polymers where the relative concentration of butadiene is high
(Figure 12), the continuous phase is the semicrystalline HB (or
the polyethylene-like structure). The mechanical properties of
the polymer is controlled primarily by this continuous dominant
phase. The rubber HI domains are dispersed within this semicrys-
talline phase. There is no major difference between HBIB, HIBI or
HBI block copolymers because the properties are determined by the
continuous semicrystalline structure. The behavior of this system
is somewhat similar to that of rubber modified polystyrene.(1)
The main function of the dispersed rubbery phase is to lower the
modulus and to allow higher extensibility by terminating or re-
ducing crack propagation. A schematic drawing for the inter-
mediate concentration of butadiene is not shown but the behavior
is similar since under this condition (of course, depending on the
film processing condition) both phases are continuous. But the
behavior of the polymer is again controlled by the dominant semi-
crystalline phase.

The schematic drawing of morphology of the block copolymers
in the low butadiene range is also given in Figure 12. In this
concentration range, the behavior of the HBIB polymers is very
different from that of HIBI or HBI. The continuous phase in this
case is the rubber HI segments and the semicrystalline domains are
dispersed throughout the sample. The semicrystalline domains in
the case of HBIB not only act as a filler, but also tie down the

end blocks of the polymer producing physical crosslinks. The
entanglements in the HI blocks can no longer be lost by complete
slippage of the chain, and are therefore of a more permanent
nature. The behavior of HBIB polymers under this condition is
that of a thermoplastic elastomer. The HIBI or HBI polymer cannot
form this kind of physical crosslink, the HB block which has
formed the semicrystalline domain can only act as a filler and
therefore these polymers behave like an uncured rubber. This type
of behavior has also been observed for SBS block copolymers.(4)

    <u>Hysteresis Behavior</u>. The hysteresis behavior of the HBIB
triblock copolymers are given in Figure 13A and of that of the
inverted HIBI block copolymer is given in Figure 13B. The
difference in the behavior of these two series of block copolymers
is tremendous. The origin of these differences are again directly
related to the morphology and the architecture of the polymers.
The hysteresis behavior of HBIB is strongly dependent of the
composition of polymer. The first member of this series is the
homopolymer HB which contains the highest (100%) concentration of
the semicrystalline segment and therefore exhibits the highest
hysteresis. That is, during each cyclic loading and unloading, a
considerable amount of energy is lost as heat. Moreover,
irreversible rearrangement of the crystalline domains occurs
during this plastic deformation.
    Introduction of the central rubbery HI block decreases the
continuity of the semicrystalline domains and results in a
successive decrease in hysteresis behavior. Similar behavior has
been observed in segmented polyurethanes when the hard segment
content has been varied.(48) Thus, an increase in HI block con-
tent (or a decrease in the concentration of the semicrystalline
HB) is always followed by a considerable decrease in the hystere-
sis behavior. The lowest hysteresis is observed for HBIB-7 which
contains the lowest butadiene content, but this sample is not very
extensible and fails early because, as mentioned before, there are
not enough crystalline domains to form a three dimensional network
of physical crosslinks. HBIB-18 and HBIB-27 which are both ther-
moplastic elastomers, show considerable extensibility but low hys-
teresis behavior. The hysteresis behavior of the above two elas-
tomers is much lower than that of the conventional segmented poly-
(urea-urethanes).(49) An increase in the butadiene content of the
other members of the HBIB series results in the crystalline HB
domains developing more continuity. This alteration in morphology
leads to a high hysteresis. Further support of the above argument
extends from the recent work of Sequela and Prod'homme who inves-
tigated the properties of SIS and SBS block copolymers.(50) They
have shown, as expected, that the best hysteresis behavior is ob-
tained for samples in which the hard styrene block has formed
microdomains which are well isolated from each other.(50) This
was actually demonstrated much earlier by one of the authors.(51)
The mechanical behavior of such a system is similar to that of un-
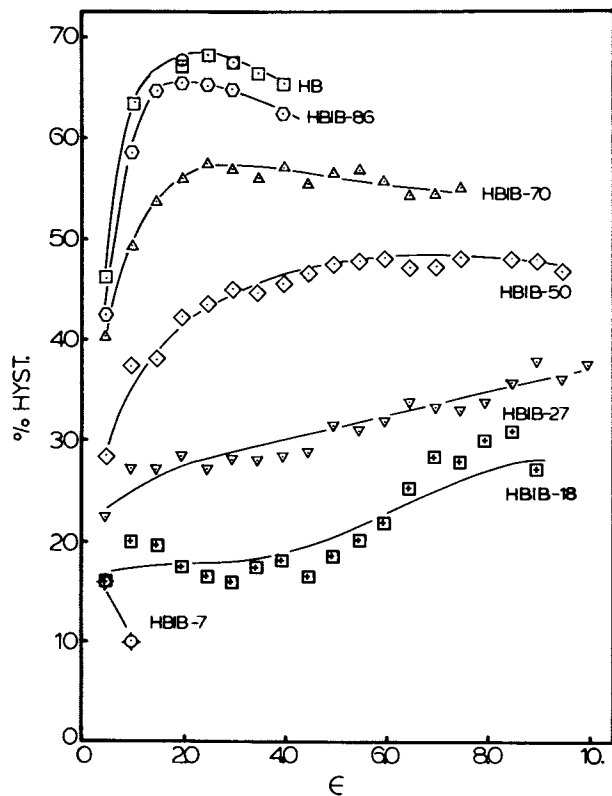
Figure 13A.   The hysteresis behavior of the HBIB polymers.
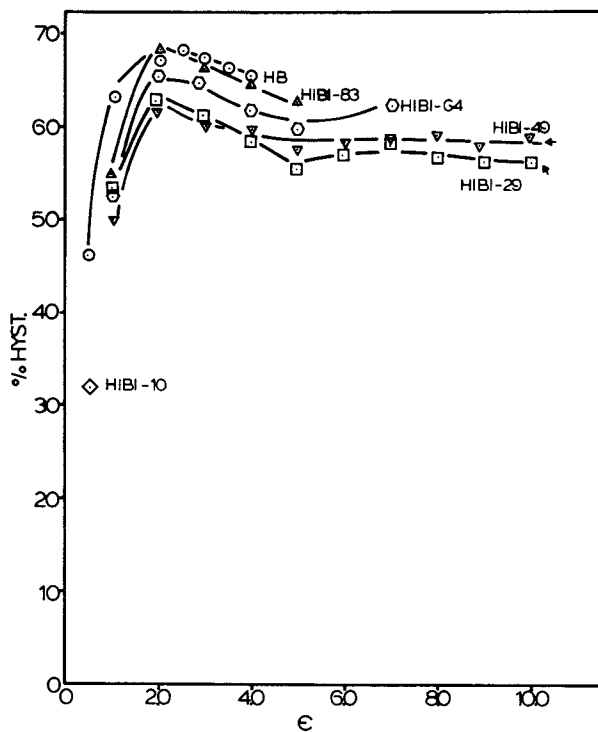
Figure 13B. The hysteresis behavior of the HIBI polymers.

filled crosslinked rubber. If, however, the samples were made
such that there was connectivity between the hard blocks, the
mechanical properties would deviate from that of cross-linked
rubber.
Similar observations have been made with respect to the hysteresis
behavior in segmented urethanes as a function of composition and
domain morphology.
    The hysteresis behavior of the HIBI series is shown in Figure
13B. All of the samples have much higher hysteresis than the
corresponding member (with respect to composition) of the HBIB
series. Although there is a noticeable decrease in the percent
hysteresis with an increase in rubbery HI content, the hysteresis
does not fall below 55% at high extensions.
    The hysteresis behavior of the diblock copolymer HBI-50 is
not shown but is very similar to that of HIBI-49. In summary
then, the difference in hysteresis behavior of the HBIB series to
that of HIBI and HBI is related to the ability of the members of
the first series to form permanent entanglements, by entrapment of
the end blocks in the semicrystalline domains, whereas no such
arrangment is possible for neither HIBI nor HBI series. The
permanent entanglement serves as a physical crosslink which
promotes recovery of the polymer after the deforming stress has
been removed. At the same time, much less energy is lost as
heat.

    Dynamic Mechanical Properties. The dynamic mechanical
properties of branched and linear polyethylene have been studied
in detail and molecular interpretation for various transitions
have already been given, although not necessarily agreed upon in
terms of molecular origin.(52-56) Transitions for conventional
LDPE (prepared by free radical methods) when measured at low
frequencies, are located around +70°C, -20°C and -120°C and are
assigned to α, β, and γ transitions respectively .(53) Recently
Tanaka et al. have reported the dynamic mechanical properties for
a sample of HB which was also prepared by anionic polymerization,
but contrary to our system the hydrogenation of the polybutadiene
was carried out by a coordinate type catalyst.(12) The
transitions reported for such a polymer at 35 Hz are very similar
to those of LDPE.(12)
    A comparison of the dynamic mechanical properties of our HB
at 35 Hz has been made to that of LDPE in Figures 14 A and B. The
thermal and sample preparative history affects the mechanical
properties of HB films to such an extent that in order to make a
meaningful comparison one has to describe the exact history of the
samples. Such a thermal history dependence has been examined for
LDPE(54,57) and recently for HB.(12) Shown in Figures A and B are
the mechanical spectra for HB-PQ, HB-Tol, and LDPE-PQ films. The
compression molded films were prepared 1 to 2 days prior to the
test. The solution cast film (from toluene), HB-Tol, was annealed
at 80°C for 2-3 days and stored at room temperature for 1 week

prior to testing. The tan δ dispersions of LDPE-PQ are located around +70°C, -5°C and -125°C respectively are tentively assigned as the α, β and γ transitions. The behavior of our HB-PQ is different from that of the LDPE-PQ sample and also different from that of HB-PQ reported by Tanaka.(12) In this freshly prepared sample, the high temperature transition is absent, but there is a major peak around -5°C and the usual γ peak is also present at around -120°C. The HB film cast from toluene, on the other hand, behaves very similarly to that of LDPE-PQ. We have already pointed out (in the crystallinity and morphology sections) that PQ samples of HB have a lower crystallinity level and a less developed spherulitic morphology from that of the pressed quenched samples of LDPE. We have also pointed out previously that when HB is cast from toluene, the level of crystallinity, the type of morphology and the general mechanical properties become very similar to that of LDPE-PQ. Thus the variation of the dynamic-mechanical behavior of HB polymer as a function of the sample preparation method is another manifestation of the same character-istics. Indeed annealing of a freshly prepared HB-PQ sample at 80°C, or even at room temperature for long times, shifts the transition from -5°C to higher temperatures and under a suffici-ently longer period of annealing the α transition becomes, dis-tinctively different from that of β transition. We will not address ourselves with this effect in more detail, because the dependence of the α transition on the sample thermal history has already been considered elsewhere.(54,57) It is, however, impor-tant to point out the difference in behavior of our HB-PQ sample to that of a HB material reported by Tanaka et al.(12) From a comparison of their results to our system, the main factor seems to be the level of crystallinity, since the percentage crystal-linity of their pressed quenched sample is around 50% as compared to about 30% for our sample. Factors affecting the crystallinity of the HB polymers include content of the ethyl side chain resulting from hydrogenation of 1,2 adducts of the parent polymers, molecular weight of the polymer, and method and level of hydrogenation. The number of ethyl branches per 100 carbon in Tanaka's HB polymer was reported to be 2.5±.2 as determined from IR spectroscopy and is slightly higher than our value which is 1.3 to 2.1. The molecular weight of their HB material is reported to be 558,000 as compared to 200,000 for ours. Both of the above mentioned factors should favor lower crystallinity of their sample in contrast to the reported higher values. Other factors which might be important but has not been quantitatively dealt with is the level of hydrogenation (in both cases the hydrogenation is essentially complete as determined from NMR & IR spectra). Thus the main cause of this difference in crystallinity level seems to be the method of hydrogenation since, as already mentioned, hydrogenation by p-toluene-sulfonylhydrazide produces some side chain adducts which may lower the relative crystallinity of our polymer. The factors affecting the crystallinity level of HB or

LDPE affect the dynamic mechanical, as well as other material properties of these polymers. The similarity of the temperature dependence of E´ between our toluene cast HB film and the quenched LDPE (both of ~40% crystallinity) in Figure 14A as compared to our quenched HB film (% crystallinity ~30%) is another indication of the importance of the level of crystallinity on properties. (This topic has already been discussed in some length in the section on stress-strain behavior).

The dynamic mechanical behavior of the block copolymers of HB and HI are typified by the results obtained for the HIBI series which are given in Figure 15A and B which display spectra for different composition ratios. The transition behavior of the HBIB series is so similar that it will not be repeated here. The samples used for this study were compression molded and they all had been stored at room temperature between one to two months before use. The experiments were run at 110 Hz. The behavior of HB, represented by HIBI 100, is similar to that given in Figure 14B. Two transition regions are apparent in the tan δ plot: the low temperature γ peak around -120°C and a higher temperature peak centered around +20°C (note that the higher temperature value for this peak as compared to that of HB,PQ in Figure 14B is due to two factors: 1. Longer room temperature annealing for the sample used in Figure 15B. 2. Higher frequency employed in Figure 15B, 110 HZ vs 35 Hz). The peak observed at 20°C is mainly believed to be due to the α transition of HB. The shoulder at -5°C is speculated to be due to the β transition but can not easily be distinguished in this compacted graph. The dynamic mechanical dispersions of the HI homopolymer were not obtained due to the difficulty in handling this tacky material. Although this might be minimized by lightly crosslinking the HI, the reaction could also change this relaxation mechanism.

The behavior of the HI block in the HIBI block copolymer series (as well as in the HBIB series) was easily denoted by a major peak in the tan δ plot at around -47±2°C at the frequency of 110 Hz. There is little doubt that this is the glass transition temperature for the HI block at this frequency. It is denoted that the magnitude of tan δ peak at -47°C increases with a decrease in HB content as expected due to an increase in HI rubber content. For block copolymers containing 10% or less butadiene there is a sharp decrease in modulus at around this temperature as shown in Figure 15A. The sharpness of this transition decreases with an increase in butadiene content and at or above fifty percent butadiene the change of modulus becomes gradual because the property of the bulk polymer is much more controlled by the strength of the tougher continuous semicrystalline matrix.

The independence of the tan δ transition (~ -47°C) on composition for the HI block for these series of block copolymers is another indication of good phase separation existing between the amorphous component of HB and HI blocks. This latter statement seems in order for if there were any appreciable mixing between
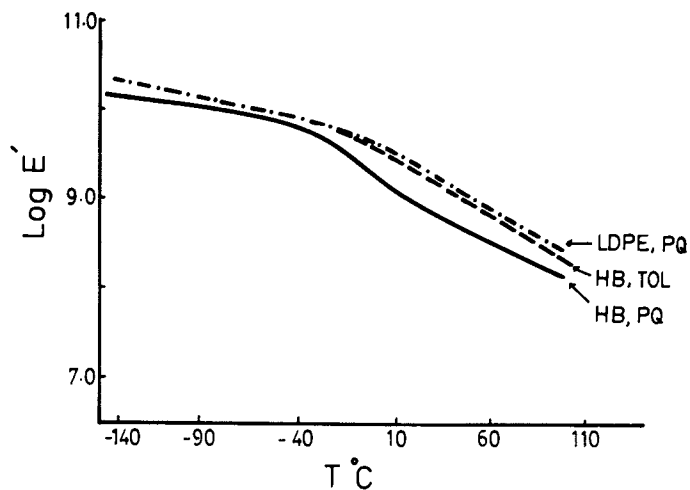
Figure 14A. Temperature dependence of E' at 35 Hz. Data for press–quenched and solution cast HB films.
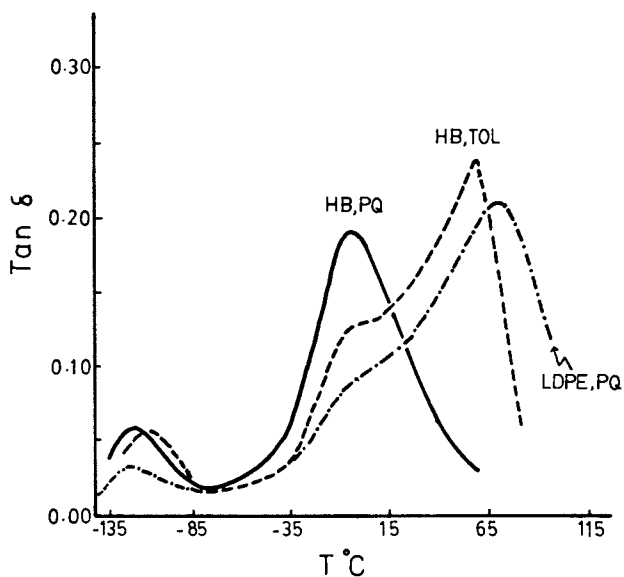
Figure 14B. Temperature dependence of tan δ at 35 Hz for HB-PQ, HB-Tol and LDPE-PQ.
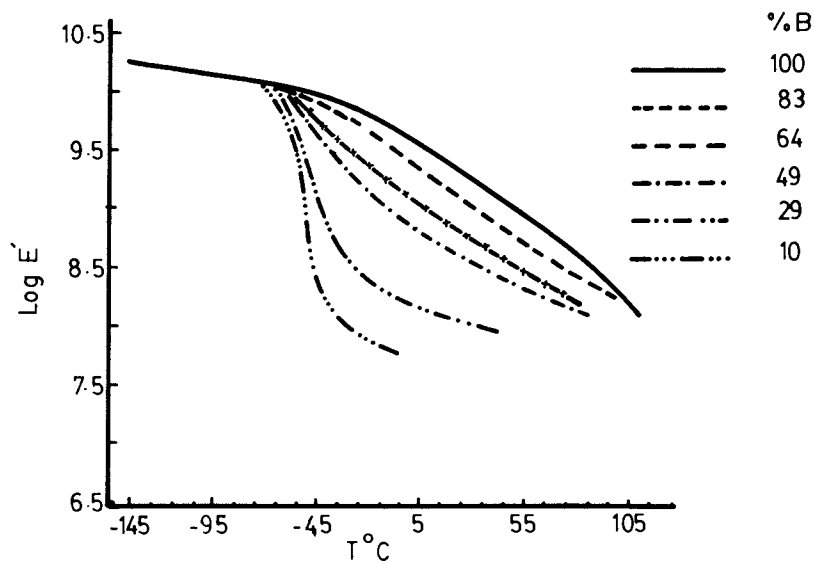
Figure 15A.   Temperature dependence of E' at 110 Hz.   Effect of variation in composition on properties of triblock copolymers on HIBI as compared to those of HB. All films are press–quenched.
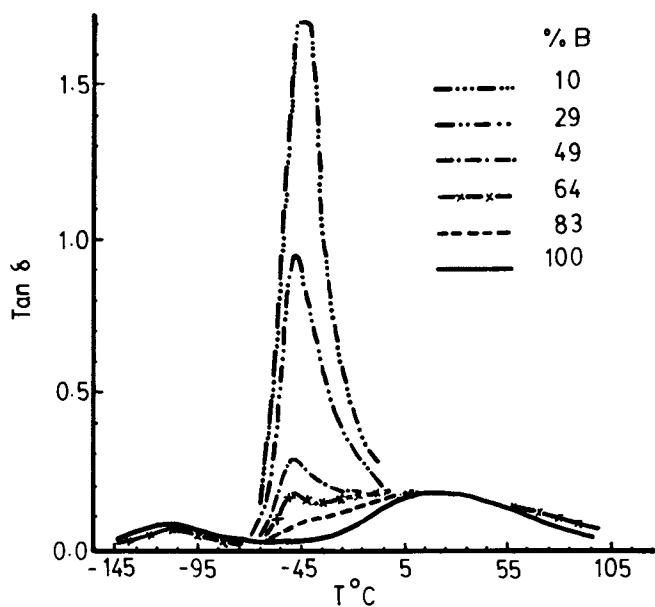
Figure 15B.   Temperature dependence of tan δ at 110 Hz. Effect of variations in composition on properties of triblock copolymers of HIBI as compared to those of HB. All films are press–quenched.

these blocks in the amorphous phases it would have been antici-
pated that the Tg of the HI block would be shifted to a lower tem-
perature as a result of lower Tg of HB (or PE) block.(20)   It
should be mentioned that in some contrast to our hydrogenated sys-
tems, the non-hydrogenated block copolymers of isoprene and buta-
diene, of similar molecular weight, display compatibility in the
solid state as noted by several workers using different methods.
(58,59,60)

Conclusions

    The mechanical properties of block copolymers composed of
rubber HI segments and the semicrystalline HB chains are dependent
both on the composition of the polymers and the architecture of
the blocks. The density, ΔH_f, crystallinity and the morphology of
the block copolymers, on the other hand, are only primarily depen-
dent on butadiene content and show little dependence on architec-
ture. This perhaps indicates that in the solid state there is a
very good phase separation between the HB and HI blocks. Although
the solution cast films show spherulitic morphology, the quenched
films do not show distinct structures indicating that the arrange-
ment of the crystallites in the supermolecular level is not well
organized.
    At high and intermediate concentrations of the HB block,
where the semicrystalline block form the continuous or one of the
continuous phases, the mechanical properties of the samples are
controlled by this phase. At these compositions, the stress-
strain properties are not much different, although there is a
difference in modulus behavior between members of varied architec-
ture. The hysteresis behavior is nevertheless significantly
varied indicating that the permanent end block entanglements pro-
duced in the HBIB series play an important part in retracting the
sample once the extension load is removed. The difference in
mechanical properties between polymers of different architecture
is most apparent when the HB content is low. At this composition,
where the rubbery HI has formed the continuous phase and the semi-
crystalline blocks are dispersed in more discrete or isolated do-
mains, the behavior of HBIB becomes of that of a thermoplastic
elastomer. The HIBI and HBI polymers, on the other hand, cannot
behave as "crosslinked" elastomers because they are not capable of
forming permanent endblock anchorages. The stress-strain proper-
ties of HIBI and HBI are similar to that of modified particulate
filled uncured rubber. These polymers, however, have high exten-
sibility, probably due to crack termination at the interphase.
But contrary to HBIB polymers, they do not show any strain harden-
ing and are very weak materials. The hysteresis behavior of HIBI
and HBI polymers is also very different from that of the HBIB
polymer. The former polymers show tremendously higher energy loss
during cyclic deformations, and these differences are again inter-

preted as being related to the ability to form permanent entangle-
ments.

The dynamic mechanical behavior indicates that the glass
transition of the rubbery block is basically independent of the
butadiene content. Moreover, the melting temperature of the semi-
crystalline HB block does not show any dependence on composition
or architecture of the block copolymer. The above findings com-
bined with the observation of the linear additivity of density and
heat of fusion of the block copolymers as a function of composi-
tion support the fact that there is a good phase separation of the
HI and HB amorphous phases in the solid state of these block co-
polymers. Future investigations will focus attention on charac-
terizing the melt state of these systems to note if homogeneity
exists above Tm.

Acknowledgement

LITERATURE CITED

1. Noshay, A. and McGrath, J. E. "Block Copolymers: Overview
    and Critical Survey," Academic Press, New York, 1977.
2. McGrath, J. E.,editor, "Anionic Polymerization: Kinetics,
    Mechanisms and Synthesis," ACS Symposium Series, No. 166,
    1981.
3. Aggarwal, S. L. Polymer 1976, 17, 938.
4. Holden, G.; Bishop, E. T., and Legge, N. R. J. Polymer Sci.
    (c) 1969, 26, 37.
5. Gallot, B. R. Adv. Polymer Sci. 1978, 29, 85.
6. Gervais, M. and Gallot, B. Makromolek. Chem. 1974, 171, 157;
    ibid 174, 193; ibid 1977, 178, 1577.
7. Lilanitkul, A. and Cooper, S. L. Rubber Chem. Technol. 1977,
    50(1),1.
8. Matzner, M.; Noshay, A.; and McGrath, J. E., Trans.
    Soc. Rheol., 21/22, 273-290 (1977); Morton, M.; Lee, N. C.,
    and Terrill, E. R., Polymer Prep, 1981, 22(2), 136; see also
    their contribution to this book.
9. Duck, E. W.; Hawkins, J. R., and Locke, J. M. J. IRI 1972,
    6(1), 19.
10. Raju, V. R.; Smith, G. G.; Marin, G.; Knox, J. R., and
    Graessley, W. W. J. Polymer Sci., Polymer Phys. Ed. 1979, 17,
    1183.
11. Raju, V. R.; Rachapudy, H., and Graessley, W. W. J. Polymer
    Sci., Polymer Phys. Ed. 1979, 17, 1223.
12. Tanaka, A.; Sahihara, Y., and Onogi, S. Polymer J. 1980,
    12(8), 483.
13. Duck, E. W., and Locke, J. M. J. IRI 1968, 2(5), 1.

14. Falk, J. C., and Schlott, R. J. Macromolecules 1971, 4(2), 152.
15. Pendelton, J. F., and Hoeg, D. F. Polymer Prep. 1972, 13(1), 427.
16. Pendelton, J. F., and Hoeg, D. F. Adv. Chem. Ser. 1973, 129, 27.
17. Zotteri, L., and Giuliani, G. P. Polymer 1978, 19(4), 476.
18. Falk, J. C., and Schlott, R. J. Angew. Makromol. Chem. 1972, 21, 17.
19. Rachapudy, H.; Smith, G. G.; Raju, V. R.,and Graessley, W. W. J. Polymer Sci., Polymer Phys. Ed. 1979, 17, 1211.
20. Cowie, J.M.G., and McEwen, I. J. Macromolecules 1977, 10(6), 1124.
21. Hser, J. C., and Carr, S. H. Polymer Eng. Sci. 1979, 19(6), 436.
22. Fujino, K.; Ogawa, ¨ , and Kawai, H. J. Appl. Polymer Sci. 1964, 8, 2147.
23. Wang, I. C.; Mohajer, Y.; Ward, T. C.; Wilkes, G. L., and McGrath, J. E., in CS Symposium Series, 166, p. 530, 1981.
24. Wang, I. C.; Mohaje , Y.; Wilkes, G. L., and McGrath, J. E. Polymer Bulletin 19 32.
25. Mango, L. A. and Lenz, R. W. Makromol. Chem. 1973, 163, 13.
26. Haslam, J. and Willis, H. A. "Identification and Analysis of Plastics," Iliffe Book LTD, London, 1965, p.190.
27. Stein, R. S., and Rhodes, M. B. J. Appl. Phys. 1960, 31, 1973.
28. Richardson, M. J.; Flory, P. J., and Jackson, J. B. Polymer 1963, 4, 221.
29. Mandelkern, L. "Crystallization of Polymers," McGraw-Hill Book Co., New York, 1963, Ch. 4.
30. Martuscelli, E., and Parcella, M. Polymer 1974, 15, 3 306.
31. O'Malley, J.; Crystal, R. G.,and Erhart, P. F. Polymer Prep. 1969, 10(2), 796.
32. Glass, S. M.,and Dole, M. Macromolecules 1979, 12(5), 965.
33. Allen, G.; Gee, G., and Wilson, G. J. Polymer 1960, 1, 456.
34. Bunn, C. W. Trans. Faraday Soc. 1939, 35, 482.
    Chiang, R. and Flory, P. J. J. Am. Chem. Soc. 1961, 83, 2857.
35. Chiang, R., and Flory, P. J. J. Am. Chem. Soc. 1961, 83, 2857.
36. Wunderlich, B.,and Cormier, C. M. J. Polymer Sci., A-2 1967, 5, 987.
37. DiMarzio, E. A.; Guttman, C. M., and Hoffman, J. D. Macromolecules 1980, 13, 1194.
38. Wunderlich, B. "Macromolecular Physics: Crystal Nucleation, Growth, and Annealing," Vol. 2, Academic Press, New York, 1976.
39. Stein, R. S., and Rhodes, M. B. J. Appl. Phys. 1960, 31, 1873.

40. Maxfield, J., and Mandelkern, L. Macromolecules 1977, 10, 1141.
41. Mandelkern, L.: Go, S.; Peiffer, D., and Stein, R. S., J. Polym. Sci., Polymer Phys. Ed. 1977, 15, 1189.
42. Nielsen, L. E. J. Appl. Phys. 1970, 41, 4626.
43. Nielson, L. E. Rheol. Acta 1974, 13, 86.
44. Lewis, T. B., and Nielson, L. E. J. Appl. Polymer Sci. 1970, 14, 1449.
45. Aggarwal, S. L.; Livigni, R. A.; Marker, L. F., and Dudek, T. J. "Block and Graft Copolymers," Syracuse University Press, New York, 1973, p.157.
46. Noshay, A., and McGrath, J. E. "Block Copolymers: Overview and Critical Survey," Academic Press, New York, 1977, p.227.
47. Andrews, E H., "Fracture in Polymers," American Elsevier Publishing Company, New York, 1968.
48. Abouzahr, S., and Wilkes, G. L., to be submitted to Polymer.
49. Paik Sung C. S.; Smith, T. W., and Sung, N. H. Macromolecules, 1980, 13, 117.
50. Sequela, R., and Prud'homme, J. Macromolecules 1978, 11(5), 1007.
51. McGrath, J. E., Ph.D. Thesis, The University of Akron, June, 1967; Morton, M.; Juliano, P.C.; and McGrath, J. E., ACS Rubber Division Meeting Paper, Montreal, 1967.
52. McCrum, N. G.; Read, B. E., and Williams, G., "Anelastic and Dielectric Effects in Polymeric Solids," John Wiley and Sons, Inc., 1965.
53. Boyer, R. F. Rubber Rev., 1963, 36, 1303.
54. Tanaka, A.; Chang, E. P.; Delf, B.; Kimura, I., and Stein, R. S. J. Polymer Sci., Polymer Phys. Ed., 1973, 11, 1891.
55. McKenna, L. W.; Kajiyama, T., and MacKnight, W. J., Macromolecules, 1969, 2, 58.
56. Stehling, F. C., and Mandelkern, L., Macromolecules, 1970, 3, 242.
57. Sinnott, K. M., J. Appl. Phys., 1966, 37, 3385.
58. Cohen, R. E., and Ramos, A. R., Adv. Chem. Series, 1979, 176, 237.
59. McGrath, J. E.; Wang, I.; Martin, M., and Crane, K., Polymer Prep., 1979, 20, 527; Wang, I. C.; Ph.D. Thesis, Virginia Polytechnic Institute and State University, August, 1981.
60. Abouzahr, S.; Mohajer, Y.; Wilkes, G. L., and McGrath, J. E., Polymer 1981, submitted.

cis/trans Control in Elastomers from Monocyclic Olefins and Diolefins

R. J. MINCHAK and HAROLD TUCKER

B. F. Goodrich Research Center, Brecksville, OH 44141

By using a transition metal chloride catalyst and an iodine modified cocatalyst, ring-opening polymerization of C_5 and C_8 monocyclic olefins is controlled to prepare either cis polymers or trans products that are crystallizable. In copolymerization, the cis/trans units in the copolymers are regulated by adjusting the C_5/C_8 olefin monomer ratio. As the comonomer is increased, the copolymer becomes less crystalline and then completely amorphous at equal amounts of cis/trans units. Polymerization results are reported from WCl_6 and $MoCl_5$ catalysts.

The cis/trans content of elastomers has an important influence on their physical properties. In polymers with both cis and trans units, the lower limit of utility follows the glass transition temperature. Polymers with only cis or trans units are often crystallizable; here the crystalline melting point defines the use temperature. In this paper we will be concerned mainly with the ring opening reaction of the monocyclic olefins at the carbon-carbon double bond. We will consider various catalysts and cocatalysts and compare the resulting cis/trans structure in the polymers against polymer properties such as glass transition temperature and crystalline melting point when it appears.

Introduction

Before discussing the polymerization of monocylic olefins, a brief review of the preparation of polymers from bicycloheptenes will acknowledge their historical contribution with respect to polymerization catalysts, polymer structure and properties. Their monomer reactivity in polymerization is much faster than the reactivity of the less strained monocyclic olefins. Anderson (1) and Truett (2) polymerized norbornene

using a Ziegler-type catalyst and discovered that the polymer contained repeat units of the cis-1,3-cyclopentane ring and a trans olefin bond instead of the typical addition product. Michelotti (3) used ruthenium trichloride trihydrate catalyst in alcohol and also the osmium or iridium catalyst. His products were largely the transpolynorbornene; however, significant levels of cis polymer resulted from the osmium catalysis. Katz (4) synthesized a cispolynorbornene using (diphenylcarbene)pentacarbonyltungsten catalyst (5). Ivin (6) reported that rhenium pentachloride also catalyzes the cis polymer; he used the methylnorbornene monomer.

In Truett's early disclosure (2) he reported that the polymers were highly crystalline. Generally these bicycloheptene polymers are found to be completely amorphous, although there may be molecular alignment when stress is applied. NORSOREX, a polynorbornene that is prepared by CdF Chimie is a commercial example of the trans polymer (7). It has a glass transition temperature near 45°C, and it is noncrystalline or amorphous. Polymer products synthesized from higher homologs of norbornene are reported as having glass transition temperatures above 200°C (8).

Monocyclic Olefins

Monocyclic monomers such as cyclopentene, cyclooctene or 1,5-cyclooctadiene have been the subject of numerous publications on metathesis reactions. These monomers can be ring-opened to unsaturated polymer products that are represented by broad variations in cis/trans structure. Many of their products contain double bonds that are reported to be between 20 to 80% trans units; however, polymers containing only cis or trans units have been synthesized and these are generally crystallizable. The structural variation in the polymers and the presence of crystallinity in certain types emphasizes the broad application potential of these products. Cyclopentene, cyclooctene, and 1,5-cyclooctadiene have received considerable attention as monomers because of their commercial importance. Cyclopentene is readily obtained from the partial hydrogenation of cyclopentadiene, while 1,5-cyclooctadiene may be prepared from the cyclic dimerization of butadiene. Hydrogenation of one double bond in the 1,5-cyclooctadiene gives cyclooctene. Bayer previously had been a leader in the development of a commercial transpolypentenamer but has since dropped this technology. Hüls is making and marketing a transpolyoctenamer (VESTENAMER 8012) as a rubber additive (9).

Cyclopentene. After Eleuterio's early disclosure (10) of cyclopentene polymerization by ring-opening catalysis, Natta and co-workers (11) reported that trans polymer forms using WCl_6 catalyst and the cispolypentenamer forms using $MoCl_5$. The

cocatalyst was trialkylaluminum. There are many published
reviews for cyclopentene polymerization and transpolypentenamer
(12-15). The list of contributors includes Dall'Asta (16),
Calderon (17), Ofstead (18), Natta (19, 20), Marshall (21),
Haas (22), Pampus (23, 24), Oberkirch (25, 26), Nutzel (27) and
Witte (28, 29). An excellent discussion of polyalkenamers,
their preparation and properties was presented by Dall'Asta in
1974 (30). These publications show that the polymerization
catalyst may be derived from a transition metal compound such
as WCl_6 or $MoCl_5$, an oxygen containing activator and an alkyl-
aluminum compound cocatalyst. There are many variations of
procedure and substitutions of catalyst components. The
transition metal compound may be dissolved in or prereacted
with a third component. Recipes use solvent or diluent and
sometimes an acyclic olefin for molecular-weight control of the
polymer.

   Cispolypentenamer has been made to a high degree of
stereoregularity, to about 99%. One preparative method re-
quires using a low R_2AlCl/WF_6 catalyst ratio (24); high ratios
of R_2AlCl/WF_6 produce trans polymer, however. Cis polymers may
be synthesized by polymerizing at low temperature (-20° to
-30°C) using $ReCl_5$ (31) or WCl_6 catalyst in combination with
Et_4Sn (32) or Et_3Al (33). At higher temperature, these cata-
lysts behave differently and become trans directing. Oreshkin
(34) confirmed the effect of the polymerization temperature on
polymer structure using an allylsilane with WCl_6; cis double
bonds formed at -30°C and trans bonds above this temperature.
Ofstead increased the cis polymer content by raising the
monomer/solvent ratio (35). The (diphenylcarbene)pentacar-
bonyltungsten is cis directing for cyclopentene (4).

   Dall'Asta determined the transition temperatures of these
cis and transpolypentenamers (36). See below:

Polymer Type	T_g (°C)	T_m (°C)
Cis	-114	-41
Trans	-97	18

The trans polymer is highly crystallizable. In contrast the
cispolypentenamer is difficult to crystallize; it requires 4 or
5 days at -78°C to develop crystallinity.

   C_8 Cyclic Olefins. Natta (37) found that polyoctenamer
forms readily from cyclooctene using a WCl_6/Et_3Al catalyst.
His product, 85% trans, showed a high degree of crystallinity;
the crystalline melting point varied between 62° and 67°C.
From cycloheptane he reported 85% to 93% trans polymer using
either WCl_6 or $MoCl_5$ catalyst with R_3Al. Strech (38) made
polymers with 54% trans structure from cyclooctene using $WCl_6/$
$EtAlCl_2$ catalyst and 38% trans polymer from 1,5-cyclooctadiene.

Ether compounds and halogenated ethers were included as poly-
merization activators. Calderon ($\underline{39}$) used a $WCl_6/EtAlCl_2$
catalyst at 50°C and obtained 40 to 70% trans polymers from
cyclooctene and 1,5-cyclooctadiene. Grahlert ($\underline{40}$) prepared a
range of 20 to 75% trans polymers from 1,5-cyclooctadiene using
a phenyltungsten trichloride catalyst. He changed the cis/
trans content by adjusting the monomer/solvent ratio. Diluting
the monomer in solvent favored the cis polymer, while bulk
systems gave high trans product. With cyclopentene the bulk
system gave cis polymer ($\underline{37}$).

       Calderon disclosed a shift toward cis polymer from 1,5-
cyclooctadiene using the $WCl_6/EtAlCl_2$ catalyst ($\underline{41}$). He
prepared 75 to 83% cispolybutenamer reaching 44% monomer
conversion; low levels of hindered phenol were included in the
polymerization charge. Lenz ($\underline{42}$) changed the cis/trans isomer
ratio in 1,5-cyclooctadiene polymers by using polar additives
and the WCl_6/R_2AlCl catalyst. With 2,4-dinitrochlorobenzene in
the charge he made 85% cis. With 2,6-ditertbutyl-4-methyl-
phenol he made 80% trans; at low monomer conversion, cis
polymer formed in the presence of the hindered phenol then
changed to trans at high conversion. Castner ($\underline{43}$) added
hindered phenols with the $WCl_6/EtAlCl_2$ catalyst. He reported
98 to 99% cis polymer from 1,5-cyclooctadiene, but the monomer
conversion was only 5 to 7%. By using 2-tertbutylphenol with
cyclooctene monomer, Castner obtained 95% cis polymer at 58 to
87% conversion. By using 2,6-ditertbutylphenol, he found 64%
cis polymer at 100% conversion. In control runs without
phenol, he made 27 to 53% cis polymer. Bell ($\underline{44}$) made cis
polymers by adding organosilicon compounds to the polymeriza-
tion recipe. He used WCl_6 premixed with an alcohol or premixed
with a halogenated alcohol and $EtAlCl_2$ cocatalyst. Bell
synthesized 91 to 96% cispolyoctenamer at 30 to 63% monomer
conversion and 84 to 94% cis polymer at 58 to 87% 1,5-cyclo-
octadiene conversion. With WCl_6 and a halogenated alcohol in
1,5-cyclooctadiene polymerization, Pampus ($\underline{45}$) achieved 15% cis
polymer using R_3Al cocatalyst and 80% cis polymer using $AlBr_3$.
Oreshkin ($\underline{34}$) produced 80 to 90% cis polymer from 1,5-cyclo-
octadiene where the catalyst was an allylsilane/WCl_6 mixture.
Katz ($\underline{4}$) showed that the carbene ($\underline{5}$) catalyst is cis directing
for cyclooctene polymer.

Results and Discussion

       Cyclopentene polymerization is activated by the introduc-
tion of elemental iodine with R_3Al using WCl_6 or $MoCl_5$ catalyst
($\underline{46}$). Besides faster polymerization rates, the final monomer
conversion is higher compared to cocatalyst types without
iodine from Et_3Al, Et_2AlCl, $EtAlCl_2$ or their mixtures (see
Table I). The addition of benzoyl peroxide to the catalyst
also helps polymerization activity. When benzoyl peroxide is

Table I

Polymerization of Cyclopentene

Benzene, ml	30	30	30	30
Cyclopentene, g	9.5	9.5	9.5	9.5
Iodine, mM	0.0	0.05	0.0	0.10
Et_3Al, nM	0.05	0.05	0.05	0.05
WCl_6, mM	0.025	0.025	0.005	0.01
Benzoyl Peroxide, mM	0.0	0.0	0.02	0.02
Time, hr	2	2	2	2
Polymer, g	1.7	4.0	0.0	5.0
Inherent Viscosity, dl/g	3.5	4.6		6.5
% Gel	0	0		0
% Trans	79	77		81

charged with the metal halide catalyst, it increases the catalyst solubility in benzene solvent. Ethyl acetate solution also increases the catalyst solubility; R_2AlI or $RAlI_2$ are effective substitutes for R_3Al/I_2 (47). Importantly, the iodine cocatalyst has utility in copolymerization reactions of cyclopentene with norbornene or 1,5-cyclooctadiene (46).

While good polymerization activity is found from either cyclopentene or 1,5-cyclooctadiene using the iodine containing cocatalyst, cyclooctene polymerization is sluggish resulting in greater than 90% cis polymer at less than 10% conversion. Catalyst levels and polymerization activity are nearly identical from either cyclopentene or 1,5-cyclooctadiene polymerization or from their copolymerization. Table II shows data at 0, 25, 50, 75, and 100% comonomer. The polypentenamer has high trans structure while the polybutenamer is 99% cis, and the mixed compositions are intermediate in cis/trans ratio. Dall'Asta and Motrone (48, 49) and Arlie (50) published earlier studies for cyclopentene and cyclooctene copolymerization. Their polymers contained either trans structure or mixed cis/trans units. Recently, Ivin (51) published copolymerization work for cyclooctene with 1,5-cyclooctadiene and also for cyclopentene with 1,5-cyclooctadiene. He showed no correlation between the composition of the copolymers and the cis double bond content.

The gas chromatographic analysis of the unreacted monomers in the experiments from Table II discloses a constant C_5/C_8 ratio comparing the starting comonomer composition to the final composition. This means that monomer conversion is the same for 1,5-cyclooctadiene and cyclopentene in the copolymerization so that copolymer compositions are equal to the charge ratios. This result is consistent with the product analysis by ^{13}C NMR spectroscopy where the copolymer composition is nearly identical to the starting comonomer composition. ^{13}C NMR is used to determine the composition of the cyclopentene/1,5-cyclooctadiene copolymers as part of a detailed study of their microstructure (52). The areas of peaks at 29-30 ppm (the $\beta\beta$ carbon from cyclopentene units) and at 27.5 ppm (the four $\alpha\beta$ carbons from the 1,5-cyclooctadiene) are used to obtain the mole fractions of the two comonomers (53, 54, 55). ^{13}C NMR studies and copolymer composition determinations are described by Ivin (51, 56, 57) for various systems.

The glass transition temperature varies from -95° to -104°C going from transpolypentenamer to cispolybutenamer by differential scanning calorimetry (58) using a heating rate of 10°C/min. If the homopolymers are brought above their crystalline melting point, they can be quenched to below the glass transition temperature (Tg). Heating these supercooled polymers shows first the Tg and next a crystallization temperature (Tcr). The polymers of higher order crystallize more readily at the lower temperature. The crystallizable polymers then

Table II

Copolymerization of Cyclopentene/1,5-Cyclooctadiene

Benzene, ml	80	80	80	80	80
1,5-cyclooctadiene,g	17.6	13.2	8.7	4.4	0.0
Cyclopentene, g	0.0	3.8	7.6	11.4	15.2
Et_2AlI, mM	0.2	0.17	0.17	0.15	0.2
$MoCl_5$, mM	0.05	0.05	0.05	0.05	0.05
Temperature, °C	25	25	25	25	25
Time, hr	1	1	1	1	1
Polymer, g	9.1	7.5	7.4	7.8	7.8
Inherent Viscosity, dl/g	4.3	4.3	3.8	4.0	4.7
% Gel	3	0	0	1	0
% Trans[a]	0.9	23	50	73	92(85)
% Cis	99.1	77	50	27	8(14)
T_m, °C	-5			-13	8
T_{cr}, °C	-60			-55	-69
T_g, °C	-104	-104	-101	-98	-95
$\bar{M}_w/\bar{M}_n$, GPC	2.3				
Mole Fraction C_5, ^{13}C NMR		0.37	0.63	0.84	
Weight % C_5, ^{13}C NMR		25	51	76	

[a] Data in parentheses are developed from the method of Tosi (60).

show a crystalline melting point (Tm) which occurs at higher
temperature with increasing polymer order.

A more gradual change in polymer properties is followed by
charging comonomer, either cyclopentene or 1,5-cyclooctadiene,
at lower concentration than above (below 25%). The change in
cis/trans structure and the drop off in crystallinity are shown
in Table III at 5, 10 and 15% comonomer for either component.
Looking first at cispolybutenamer, the crystalline melting
point moves from -4°C to -10°C at 5% comonomer (cyclopentene),
to -16°C at 10% comonomer, to -25°C at 15% and is absent at 25%
comonomer from Table II. The temperature at which the amor-
phous cispolybutenamer crystallizes (Tcr) during the heating
cycle begins at -60°C and increases to -55°C at 10% comonomer,
to -50°C at 15% and is not observed at 25% comonomer.

The crystallinity is more persistent for the polypentena-
mer over the same increments of comonomer or 1,5-cyclooctadiene
introduction. The crystalline melting point is 8°C for the
polypentenamer, 2°, -2°, and -8°C at 5, 10 and 15% comonomer
(1,5-cyclooctadiene), respectively, from Table III and -13°C at
25% comonomer from Table II. The position of the crystalliza-
tion temperature during the heating cycle moves upward from
-69°C for polypentenamer, to -65°C at 10% comonomer, to -61°C
at 15% and -55°C at 25% comonomer.

Figure 1 combines the infrared data for the cis/trans
structure in the polymers from Table II and III and shows the
gradual change in microstructure with copolymer composition.
The infrared method is based on the procedure developed for
polybutadienes by Silas (59). The method gives high values for
trans structures with polypentenamer; therefore, a second
procedure is used in the manner of Tosi (60) but calibrated
against ^{13}C NMR (54) - data in parentheses from Table II and
III. The resulting structure in the copolymers depends on the
monomer type as the C_5 monomer directs the microstructure to
the trans type and the C_8 directs the structure to the cis
unsaturation. The configuration of the previous or last double
bond entering the polymer molecule or the previous monomer type
does not influence the entering monomer selection or the
structure of the new double bond (61).

There is an absence of cis-to-trans isomerization with
conversion or time for the C_8 (1,5-cyclooctadiene) polymer.
This is shown from 52 to 58% conversion after 1 to 16 hours
reaction time in Table II and III. The above review (40, 42,
43, 45) shows that the cis structure in polymers from 1,5-
cyclooctadiene using various chloride catalysts fell below 50%
cis even to 20% cis units; this means that the second cis
double bond from the monomer underwent extensive cis-to-trans
isomerization following the ring-opening of the first cis bond.
Where cis-2-butene isomerizes to trans structure using other
catalyst preparations, there is no evidence of this for cis-2-
butene using the iodine system. However, polymer molecular
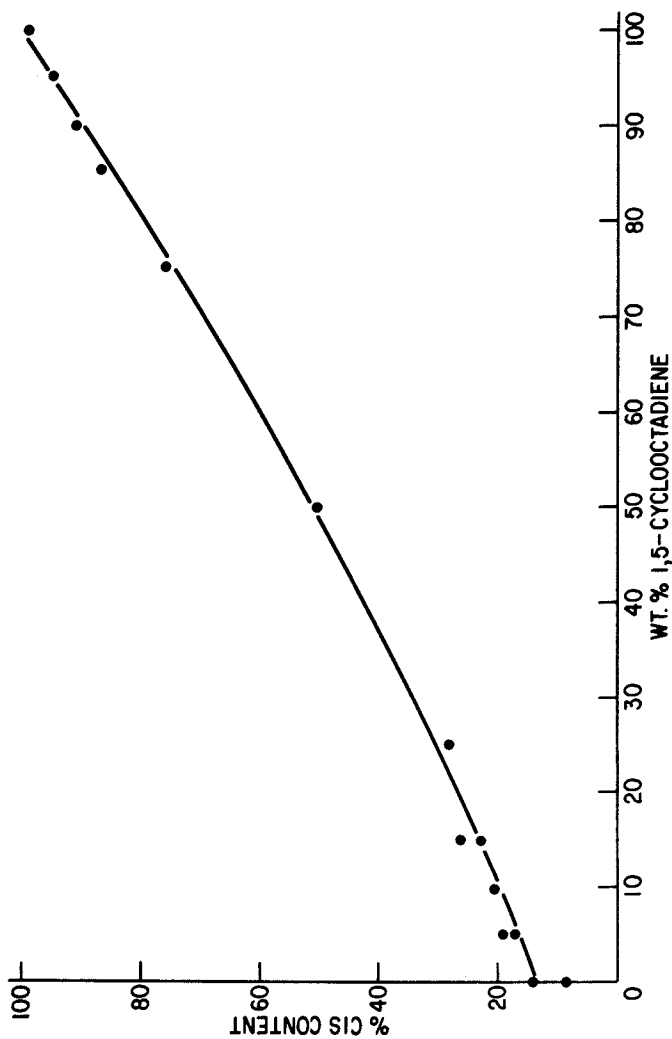
Figure 1.   cis/trans content versus copolymer composition.

Table III

Copolymerization of Cyclopentene/1,5-Cyclooctadiene

Benzene, ml	80	80	80	80	80	80
1,5-Cyclooctadiene,g	16.6	15.6	14.8	2.57	1.70	0.89
Cyclopentene, g	0.79	1.59	2.43	13.2	14.1	14.9
Et_2AlI, mM	0.15	0.15	0.15	0.15	0.15	0.15
$MoCl_5$, mM	0.05	0.05	0.05	·0.05	0.05	0.05
Temperature, °C	25	25	25	25	25	25
Time, hr	16	16	16	16	16	16
Polymer, g	10.1	9.9	9.5	7.7	7.6	7.1
Inherent Viscosity, dl/g	4.8	4.9	4.9	5.2	5.0	5.2
% Gel	0	0	0	0	0	0
% Trans[a]	4.5	8.5	13	73(77)	80(80)	81(83)
% Cis	95.5	91.5	87	27(23)	20(20)	19(17)
T_m, °C	-10	-16	-25	-8	-2	2
T_{cr}, °C	-54	-55	-50	-61	-65	-68
T_g, °C	-104	-103	-103	-97	-96	-95

[a] Data in parentheses are developed from the method of Tosi (60).

weight decreases with the acyclic olefin concentration. The
gel permeation chromatographic data show a relatively narrow
molecular-weight distribution for the copolymers; generally the
$\bar{M}w/\bar{M}n$ ratio is two or slightly greater than two.

The transition temperatures that are combined in Figure 2
show the disappearance of crystallinity in the copolymers as
the Tcr and Tm flow together moving away from either homopoly-
mer. This reflects the random distribution of monomer units in
these copolymers. If the copolymer reactions had given homo-
polymer mixtures, there would be two separate crystalline
melting temperatures. In addition, the ^{13}C NMR indicates that
the copolymer products contain a random distribution of C_5 and
C_8 units and that the resulting double bonds are cis from the
C_8 monomer and largely trans from the C_5 monomer (52).

Using iodine in the catalyst preparation demonstrates a
unique method for preparing copolymers of similar composition,
either two or three methylene groups between double bonds, but
with controlled cis/trans ratio. The monomer ratio, C_5/C_8,
regulates the cis/trans ratio in the copolymer. The products
can be highly crystalline or crystallizable with either high
trans or high cis structure, or the polymer products can be
completely amorphous with outstanding low temperature proper-
ties. The choice depends on the application or the properties
desired.
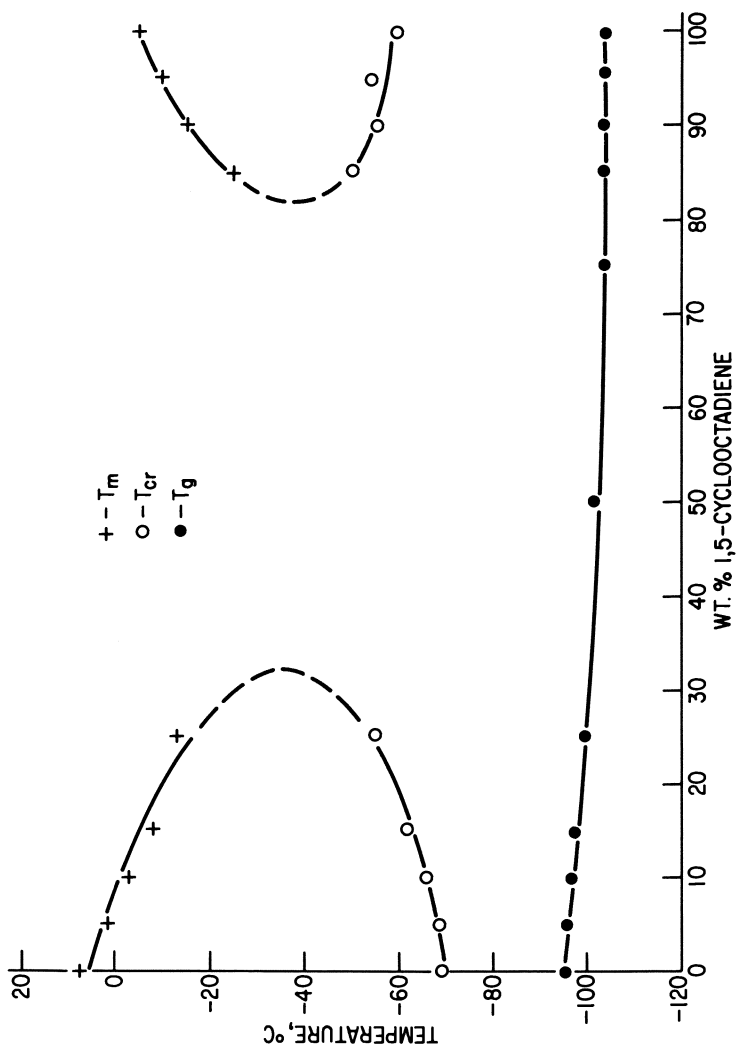
Figure 2. Copolymer transition temperatures.

Literature Cited

1. Anderson, A. W.; Merckling, N. G. (DuPont) U.S. Patent 2,721,189, 1955.
2. Truett, W. L.; Johnson, D. R.; Robinson, U. M.; Montague, B. A. J. Amer. Chem. Soc. 1960, 82, 2337-2340.
3. Michelotti, F. W.; Keaveney, W. P. J. Polym. Sci. A 1965, 3, 895-905.
4. Katz, T. J.; Lee, S. J.; Acton, N. Tetrahedron Lett. 1976, 47, 4247-4250.
5. Casey, C. P.; Burkhardt, T. J. J. Amer. Chem. Soc. 1973, 95, 5833-5834.
6. Ivin, K. J. Pure & Appl. Chem. 1980, 52, 1907-1913.
7. Ohm, R. F.; Vial, T. M. Elast. & Plastics 1978, 10, 150-162.
8. Vergne, J.; Pailloux, C.; Muller, J.; Robinet, J. (Charbonnages de France) U.S. Patent 3,557,072, 1971.
9. Smith, L. P. Elastomerics 1980, 12, 37-39.
10. Eleuterio, H. S. (DuPont) U.S. Patent 3,074,918, 1963.
11. Natta, G.; Dall'Asta, G.; Mazzanti, G. Angew. Chem. 1964, 76, 765-772.
12. Amass, A. J. Br. Polymer J. 1972, 4, 327-341.
13. Calderon, N. J. Macromol. Sci., Revs. Macromol. Chem. 1972, C7, 105-159.
14. Minchak, R. J.; Tucker, H.; Macey, J. H. Polym. Eng. and Sci. 1975 15 (5), 360-366.
15. Ofstead, E. A. Encyl. Polym. Sci. Technol. 1977, Suppl. 2, 610-627.
16. Dall'Asta, G.; Carella, G. (Montedison) U.S. Patent 3,449,310, 1969.
17. Calderon, N.; Judy, W. A. (Goodyear) U.S. Patent 3,492,245, 1970.
18. Ofstead, E. A. (Goodyear) U.S. Patent 3,597,403, 1971.
19. Natta, G.; Dall'Asta, G.; Mazzanti, G. (Montedison), U.S. Patent 3,476,728, 1969.
20. Natta, G.; Dall'Asta, G.; Mazzanti, G. (Montedison), U.S. Patent 3,458,489, 1969.
21. Marshall, P. P.; Ridgwell, B. J. Eur. Polym. J. 1969, 5, 29-33.
22. Haas, F.; Nutzel, K.; Pampus, G.; Theisen, D. Rubber Chem. and Tech. 1970, 43, 1116-1128.
23. Gunther, P.; Haas, F.; Marwede, G.; Nutzel, K.; Oberkirch, W.; Pampus, G.; Schon, N.; Witte, J. Angew. Makromol. Chem. 1970, 14, 87-109.
24. Pampus, G.; Witte, J.; Hoffmann, M. Rev. Gen. Caout. Plast. 1970, 47(11), 1343-1347.
25. Oberkirch, W.; Gunther, P.; Witte, J. (Bayer) U.S. Patent 3,607, 853, 1971.
26. Oberkirch, W.; Gunther, P.; Pampus, G. (Bayer) B. P. 1256650, 1971.

27. Nutzel, K.; Haas, F.; Dinges, K.; Graulich, W. (Bayer) U.S. Patent 3,598,796, 1971.
28. Witte, J.; Pampus, G.; Schon, N.; Marwede, G. (Bayer) U.S. Patent 3,692,796, 1971.
29. Witte, J.; Schon, N.; Pampus, G. (Bayer) U.S. Patent 3,631,010, 1971.
30. Dall'Asta, G. Rubber Chem. Technol. 1974, 47, 511-596.
31. Pampus, G.; Oberkirch, W.; Gunther, G. (Bayer) French Patent 2,025,142, 1968.
32. Pampus, G.; Lehnert, G. Makromol. Chem. 1975, 175, 2605-2616.
33. Minchak, R. J.; Tucker, H. Poly. Prepr. 1972, 13 (2), 885-890.
34. Oreshkin, I. A.; Redkina, L. I.; Kershenbaum, I. L.; Chernenko, G. M.; Makovetsky, K. L.; Tinyakove, E. I.; Dolgoplosk, B. A. Eur. Polm. J. 1977, 13, 447-450.
35. Ofstead, E. A. Rubber Div. ACS, 103rd Meeting, Paper 10, May, 1973.
36. Dall'Asta, G.; Scaglione, P. Rubber Chem. Tech. 1969, 42, 1235-1244.
37. Natta, G.; Dall'Asta, G.; Bassi, I. W.; Carella, G. Makromol. Chem. 1966, 91, 87-106.
38. Streck, R.; Heinrich, Hüls. U.S. Patent 3,974,092, 1976.
39. Calderon, N.; Ofstead, E. A.; Judy, W. A. J. Polym. Sci. A-1 1967, 5, 2209-2217.
40. Grahlert, W.; Milowski, K.; Langbein, U.; Taeger, E. Plaste und Kautschuk 1975, 22, 229-233.
41. Calderon, N. (Goodyear) U.S. Patent 3,932,373, 1976.
42. Lenz, R. W. Makromol. Chem., Suppl. 1981, 4, 47-60.
43. Castner, K. F. (Goodyear) U.S. Patent 4,038,471, 1977.
44. Bell, A. J. (Goodyear) U.S. Patent 3,943,116, 1976.
45. Pampus, G.; Lehnert, G.; Witte, J. (Bayer), U.S. Patent 3,933,778, 1976.
46. Minchak, R. J. (BFGoodrich) U.S. Patent 3,853,830, 1974.
47. Minchak, R. J.; Beauregard, R. E. (BFGoodrich) U.S. Patent 4,025,708, 1977.
48. Dall'Asta, G.; Motroni, G. Europ. Polym. J. 1971, 7, 707-716.
49. Motroni, G.; Dall'Asta, G.; Bassi, I. W. Europ. Polym. J. 1973, 9, 257-261.
50. Arlie, J. P.; Chauvin, Y.; Commereuc, D.; Soufflet, J. P. Makromol. Chem. 1974, 175, 861-872.
51. Ivin, K. J.; Lapienis, G.; Rooney, J. J. Makromol Chem. 1982, 183, 9-28.
52. Komoroski, R. A.; Minchak, R. J. Manuscript in preparation.
53. Chen, H. Y. Poly. Prepr. 1976, 17 (2), 688-692.
54. Carman, C. J.; Wilkes, C. E. Macromolecules 1974, 7, 40-43.
55. Mochel, V. D. J. Polym. Sci. A-1, 1972, 10, 1009-1018.

56. Ivin, K. J.; Laverty, D. T.; Rooney, J. J. Makromol. Chem.
     1977, 178, 1545-1560.
57. Ivin, K. J.;   O'Donnell, J. H.;   Rooney, J. J.;
     Stewart, C. D. Makromol. Chem. 1979, 180, 1975-1988.
58. Wilkes, C. E.; Peklo, M. J.; Minchak, R. J. J. Polym.
     Sci. C, Polym. Symp. 1973, 43, 97-109.
59. Silas, R. S.; Yates, J.; Thornton, V. Anal. Chem. 1959,
     31, 529-532.
60. Tosi, C.; Ciampelli, F.; Dall'Asta, G. J. Polym. Sci.,
     Poly. Phy. Ed. 1973, 11, 529-538.
61. Ivin, K. J.; Laverty, D. T.; Rooney, J. J.   Makromol.
     Chem. 1978, 179, 253-258.

Polymers of 1,4-Hexadienes

JOGINDER LAL, THOMAS L. HANLON[1], HUNG YU CHEN,
and RICHARD N. THUDIUM

The Goodyear Tire & Rubber Company, Elastomer and Chemical Research,
Akron, OH 44316

During the polymerization of trans-1,4-
hexadiene with a $Et_3Al/\delta-TiCl_3$ catalyst (Al/Ti
atomic ratio = 2) at 25°C, concurrent isomerization
reactions account for a major portion of the con-
sumed monomer. The formation of the isomerization
products is kinetically controlled and depends on
polymerization conditions. In marked contrast, 5-
methyl-1,4-hexadiene gives polymer conversions of
80 percent or higher. NMR and IR data show that
poly(5-methyl-1,4-hexadiene) consists of 1,2-polymer-
ization units arranged in a regular head-to-tail
sequence. The structure of this polymer was further
confirmed by characterization of the products
resulting from its ozonolysis and hydrogenation
reactions. Fiber diagrams obtained by X-ray dif-
fraction of stretched samples of the trans-1,4-
hexadiene and 5-methylhexadiene rubbers indicate 3_1
helical conformations typical of isotactic poly-
propylene and poly(5-methyl-1-hexene). These
polymers are the first examples of uncrosslinked,
high unsaturation rubbers containing pendant double
bonds on alternating carbon atoms of an ozone-
resistant saturated carbon-carbon backbone.
    Reactivity ratios for 1-hexene (M_1) with 5-
methyl-1,4-hexadiene (M_2) copolymerization at 30°C
in hexane solvent using a $Et_2AlCl/\delta-TiCl_3$ AA
catalyst system (Al/Ti atomic ratio = 1.5) were
determined. The compositions of copolymers were
measured by 300 MHz ^{1}H-NMR spectroscopy. The re-
activity ratios, calculated by the Tidwell-Mortimer
method, were 1.1 ± 0.2 for each of the two monomers.

[1] Current address: Ethyl Tech Centre, 8000 GSRI Avenue, Baton Rouge, LA 70808.

   The rubber industry needs high unsaturation, ozone-
resistant rubbers which are cure-compatible with conventional
diene rubbers, but which do not adversely affect the
latter's important properties such as flex, stress-strain, and
dynamic mechanical characteristics. EPDM rubbers (copolymers
of ethylene, propylene and a conjugated diene) possess a
saturated carbon-carbon backbone and therefore show excellent
resistance to ozone and aging. However, they have a low degree
of unsaturation and are not entirely satisfactory when blended
with conjugated diene rubbers. There are several reports of
methods for improving the cure-compatibility of EPDM. They
include use of EPDM containing a high level of termonomer (1)
or polydiene unsaturation (2), chemical modification of EPDM
with polar groups (3, 4, 5), and use of accelerators with long
hydrocarbon chains (6). Copolymers of higher α-olefins (C_6-
C_{12}) with 1,4-hexadienes, which also possess a saturated
carbon-carbon backbone and outstanding ozone resistance but
which possess considerably higher levels of unsaturation than
EPDM, have been described (7). One such copolymer, Hexsyn[TM]
rubber (a copolymer of 1-hexene and 5-methyl-1,4-hexadiene) has
exhibited outstanding durability during flexing and is showing
potential for several biomedical applications(8).
   Butyl rubber (a copolymer of isobutylene and 1-3 mole per
cent isoprene) and its halogenated derivatives have unsaturation
in the carbon-carbon backbone and consequently do not have as
good aging properties as EPDM. There are also reports (9-12)
that ozone-resistant butyl rubber with a high degree of un-
saturation can be prepared by copolymerization of isobutylene
with either cyclopentadiene or β-pinene.
   Polymerization of α, ω-dienes containing eight or more
carbon atoms with a triisobutylaluminum – titanium tetrachloride
catalyst system gave substantial amounts of crosslinked (13)
polymers due to the equal reactivity of the terminal double
bonds. The soluble fractions exhibited low values of inherent
viscosities. We have previously reported (14, 15) the synthesis
and characterization of polymers of cis-1,4- and trans-1,4-
hexadienes using δ-TiCl$_3$ based catalysts. These polymers are
the first examples of uncrosslinked, high unsaturation rubbers
containing pendant double bonds on alternate carbon atoms of an
ozone-resistant saturated carbon-carbon backbone (16). Micro-
structural changes resulting from ultraviolet irradiation under
high vacuum of thin films of these two rubbers have been
studied (17). We now present data on the stereochemical con-
figuration of 5-methyl-1,4-hexadiene homopolymer. Reactivity
ratios for the 5-methyl-1,4-hexadiene/1-hexene copolymerization
system are also reported here.

Experimental

Materials. 5-Methyl-1,4-hexadiene was obtained by the co-
dimerization of isoprene and ethylene with a catalyst (18)
consisting of iron octanoate, triethylaluminum and 2,2'-bi-
pyridyl. The product mixture which contained principally
5-methyl-1,4-hexadiene and 4-methyl-1,4-hexadiene was fraction-
ated through a Podbielniack column to yield high purity (>99%)
5-methyl-hexadiene, b.p. 92.8°C, n_D^{25} 1.4250 (Lit. (19) b.p. 88-
89°C, n_D^{20} 1.4249). 1-Hexene (99.9% purity), 1-decene (99.6%
purity), 4-methyl-1-hexene (99.5% purity) and 5-methyl-1-hexene
(99.7% purity) were obtained from Chemical Samples Co. δ-TiCl₃
AA (Stauffer Chemical Co.; contains 0.33 mole AlCl₃ per mole of
TiCl₃). Diethylaluminum chloride was obtained from Texas Alkyls
(1.5 M in hexane).

Polymerization/Isomerization. The polymerization of 5-
methyl-1,4-hexadiene (>99% pure) was carried out in n-pentane
with a δ-TiCl₃/Et₂AlCl catalyst at 0°C according to the pro-
cedure described previously (14). To assess monomer disappear-
ance and identify isomerization products, samples were withdrawn
at specified intervals from the reaction mixture for GLC
analysis (14). The final polymer conversion was determined by
precipitation in excess methanol.

Hydrogenation. Hydrogenation of poly(5-methyl-1,4-hexa-
diene) was carried out with p-toluenesulfonyl hydrazide (20) in
refluxing xylene (2:1 molar ratio of the hydrazide to the polymer
repeat unit).

Ozonolysis. Ozonolysis of the methylhexadiene polymer was
conducted (21) at room temperature on a solution of 1.03 g.
polymer in 20 ml. tetrahydrofuran with the aid of the Wellsbach
ozonizer. The end point for the ozonolysis was observed after
about 15 min. by the reaction of excess ozone with starch-iodide
solution. Triphenylphosphine was added to the reaction mixture
and allowed to react at room temperature for 60 hr. The result-
ing product was analyzed by GLC (Hewlett Packard 5750, Porapak
Q 10 ft. x 1/8 in. column at 110°C, helium pressure 60 psi,
thermal conductivity detector at 190°C, injector 200°C).

Polymer Characterization. Proton NMR spectra at 300 MHz
were obtained from a Varian HR-300 NMR spectrometer. Deutero-
benzene and spectrograde carbon tetrachloride were used as
solvents. The concentration of the polymer solutions was about
1-5%. Carbon-13 NMR spectra were obtained from a Varian CFT-20
NMR spectrometer, using deuterochloroform as the solvent for the
polymers. The concentration of the solutions was about 5%.
Chemical shifts in both proton and carbon-13 spectra were
measured in ppm with respect to reference tetramethylsilane (TMS).
All spectra were recorded at ambient temperature.

The IR spectra were obtained with a Perkin-Elmer PE-467 grating spectrophotometer from about 4000-500 cm^{-1}. Normal slit position and medium scan mode were used. Films of polymer samples were cast from CS_2 solutions on NaCl windows.

Compression molded ($150^{\circ}C$ for 3 minutes; press chilled with cold water immediately thereafter) samples of poly(trans-1,4-hexadiene) (14) and poly(5-methyl-1,4-hexadiene) were examined with a General Electric (XRD-3) X-ray unit. Transmission Laué X-ray photographs were taken using nickel filtered copper X-radiation. Samples were stretched to four times of their original lengths to obtain oriented fibers. The fiber patterns were obtained in a flat plate film holder with the specimen to film distance standardized at 5 centimeters. X-ray diffraction patterns were similarly obtained for the hydrogenated sample of poly(5-methyl-1,4-hexadiene).

Copolymerization. The reactivity ratios of 1-hexene (M_1) with 5-methyl-1,4-hexadiene (M_2) were determined by copolymerization at $30^{\circ}C$ in hexane solvent using a Et_2AlCl_2/δ-TiCl$_3$ AA catalyst system (Al/Ti atomic ratio = 1.5). Copolymerizations were conducted in 4-oz. bottles using concentrations of 10 g. monomer in 40 g. hexane and 5.0 mmoles TiCl$_3$ per 100 g. monomer. All other copolymerizations were conducted under similar conditions. The reactivity ratios were calculated by the Tidwell-Mortimer (22) computer method. The compositions of the copolymers were measured by using 300 MHz ^{1}H-NMR.

Results and Discussion

We have reported earlier (14) that during the polymerization of trans-1,4-hexadiene with a Et_3Al/δ-TiCl$_3$ catalyst (Al/Ti atomic ratio = 2) at $25^{\circ}C$, a major portion of the consumed monomer was converted to isomerized products, thereby accounting for the relatively low conversion to isotactic 1,2-polymer (Figure 1). The relative amounts of the hexadiene isomerization products were in the following order: cis-2-trans-4-hexadiene > trans-2-trans-4-hexadiene > 1,3-hexadiene > 1,5-hexadiene > cis-2-cis-4-hexadiene.

We showed (14) that formation of the isomerization products is kinetically controlled and that it depends on the catalyst system employed, the principal conjugated diene isomer being either the trans-2-trans-4-hexadiene, cis-2-trans-4-hexadiene, or 1,3-hexadiene.

cis-1,4-Hexadiene was considerably more sluggish than the trans isomer during polymerization/isomerization reactions. The predominant isomerization product with the above catalyst system was cis-2-trans-4-hexadiene. In contrast, using reaction conditions similar to those used for trans- and cis-1,4-hexadienes, 5-methyl-1,4-hexadiene gave polymer (methanol-insoluble)
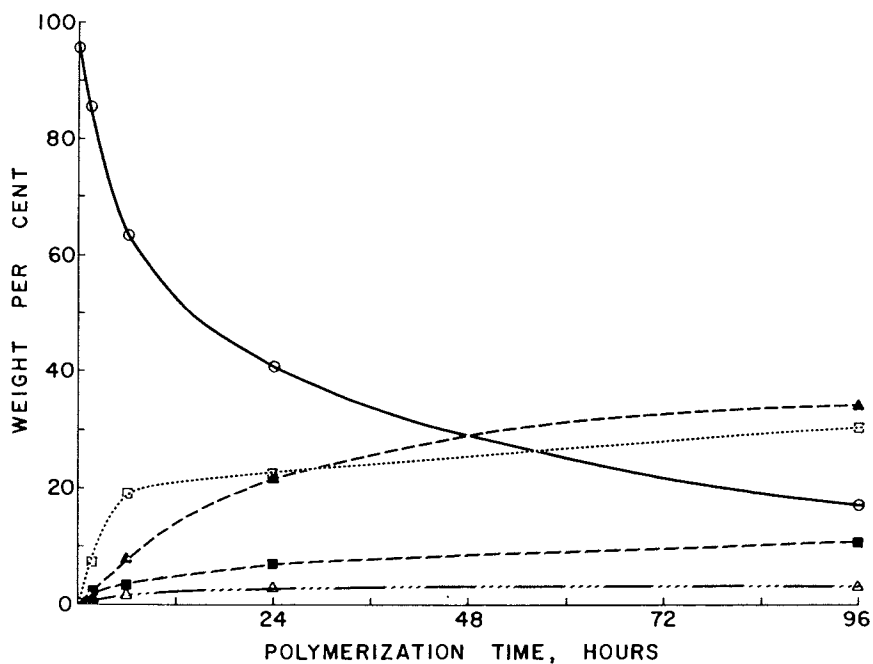
Figure 1. GLC data for the polymerization and isomerization of trans-1,4-hexa-diene at 25°C with a Et₃Al/δ-TiCl₃ catalyst (Al/Ti atomic ratio is 2). n-Hexane *was used as the internal standard. Key:* ○, trans-1,4-hexadiene; □, polymer; ▲, cis-2-trans-4-hexadiene; ■, trans-2-trans-4-hexadiene; △, 1,3-hexadiene. *Repro-duced, with permission, from Ref. 14. Copyright 1980, John Wiley & Sons, Incor-porated*

conversions of 80% with a Et_2AlCl/δ-$TiCl_3$ catalyst and 86% with
a Et_3Al/δ-$TiCl_3$ catalyst. It seems that the methyl group in the
five-position sterically inhibits isomerization reactions, which
is consistent with the isomerization mechanism (15). GLC
analysis of the reaction products showed that only 0.4 - 6.5% of
the monomer was isomerized with these catalyst systems. Here
again, the distribution of the isomerization products was in-
fluenced by the choice of catalyst. Due to the location of the
5-methyl group, only two isomers are possible here. 5-Methyl-
trans-2,4-hexadiene(i.e., 2-methyl-2, trans-4-hexadiene) and 5-
methyl-1,3-hexadiene were obtained as the principal products.
        We have examined poly(5-methyl-1,4-hexadiene) by IR spectro-
scopy and by 300 MHz ^{1}H- and ^{13}C-NMR spectroscopy. The IR
spectrum (Figure 2) of the 5-methylhexadiene polymer is con-
sistent with that of an aliphatic hydrocarbon polymer containing
-CH_2-CH=C(CH_3)$_2$ groups. The spectrum is a close match to that
of a model olefin, 2,5-dimethyl-2-hexene.
        The 300 MHz ^{1}H-NMR spectrum of the 5-methylhexadiene polymer
is shown in Figure 3. The peak intensity in the olefinic region
was found to be 7.7% of the total intensity and is close to the
theoretical value of 8.3. The general features of the spectrum
are also in agreement with the arrangement of 1,2-structural
units in a regular head-to-tail sequence. The measured chemical
shifts and assignments are listed in Table I.
        The ^{13}C-NMR spectrum of the 5-methylhexadiene polymer in
$CDCl_3$ solution is given in Figure 4. The spectrum (six peaks) is
consistent with the structure of a polymer resulting from a
regular head-to-tail 1,2-polymerization. The peak at 33.31 ppm
consists of two overlapped peaks. These are attributed to the
methylene carbons adjacent to the double bond and to the backbone
methine carbon; these two peaks are in the same position by
coincidence.
        In contrast to the spectrum of isotactic trans-1,4-hexadiene
polymer (Figure 5), the 300 MHz ^{1}H-NMR spectra of the 5-methyl-
hexadiene polymer in both CCl_4 and C_6D_6 solutions exhibit only
one peak for its backbone methylene protons. As in the case of
cis-1,4-hexadiene polymer (14), the backbone methylene protons
were not resolvable. The absence of a doublet for the methylene
protons in these polymers does not necessarily preclude the
possibility that they are isotactic.
        The 1,2-polymerization of 5-methyl-1,4-hexadiene was further
confirmed by ozonolysis of the polymer. The resulting solution,
after triphenylphosphine treatment, contained only acetone and
no detectable formaldehyde by GLC. As shown below in Scheme 1,
the volatile products expected by the above chemical treatment
of poly(5-methyl-1,4-hexadiene) are acetone and formaldehyde if
the polymer was formed by 1,2- and 4,5-polymerization,
respectively.
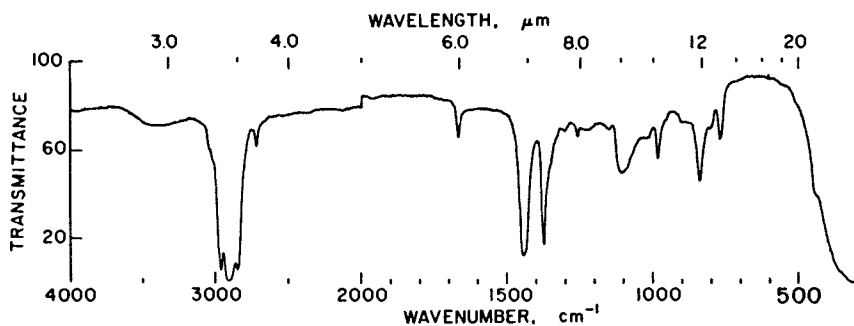
Figure 2. IR spectrum of poly(5-methyl-1,4-hexadiene) prepared with a $Et_2AlCl/$ δ-$TiCl_3$ catalyst at $0\degree C$ in pentane solvent. Reproduced, with permission from Ref. 13. Copyright 1979, American Institute of Physics.
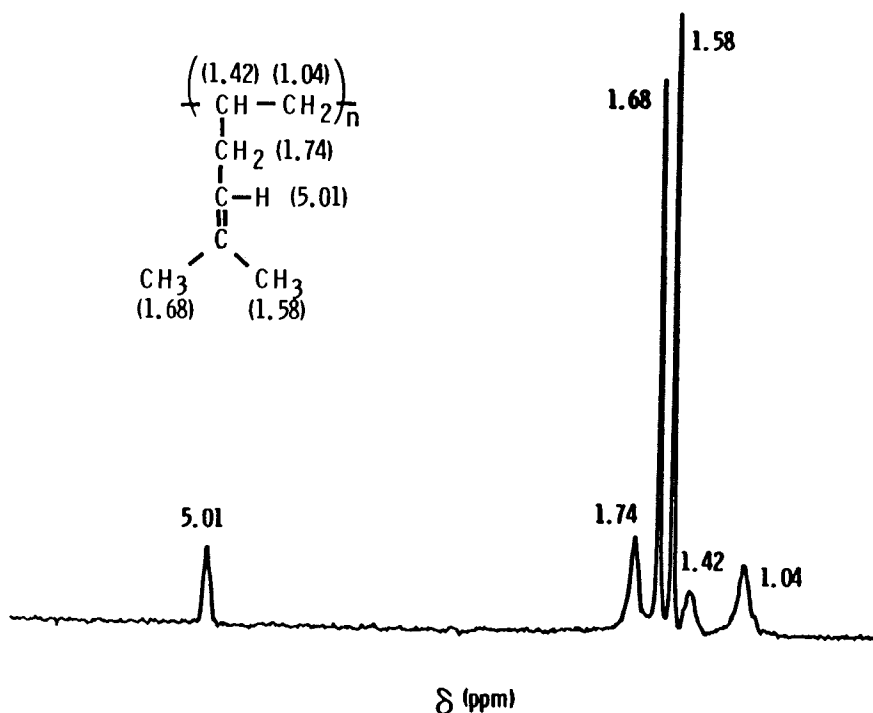
Figure 3. 300 MHz ^1H-NMR spectrum of a CCl_4 solution of poly(5-methyl-1,4-hexadiene) prepared with a Et_2AlCl/δ-$TiCl_3$ catalyst at $0\degree C$ in pentane solvent, ambient temperature. Reproduced, with permission from Ref. 13. Copyright 1979, American Institute of Physics.

<u>TABLE I</u>

300 MHz ^{1}H-NMR SPECTRAL DATA OF 5-METHYL-1,4-HEXADIENE POLYMER
(Et$_2$AlCl/δ-TiCl$_3$ Catalyst, 0°C) in CCl$_4$ and C$_6$D$_6$

Chemical Shift (ppm from TMS)	Relative Intensities	Assignments
5.39 [C$_6$D$_6$] 5.01 [CCl$_4$]	1.03	$- \underline{CH} = C \big\langle {}^{CH_3}_{CH_3}$
2.21 [C$_6$D$_6$] 1.74 [CCl$_4$]	2.01	$- \underline{CH_2} - CH = C \big\langle {}^{CH_3}_{CH_3}$
1.85 [C$_6$D$_6$] 1.42 [CCl$_4$]		$- \underline{CH} - CH_2 -$
1.81 [C$_6$D$_6$] 1.68 [CCl$_4$] 1.72 [C$_6$D$_6$] 1.58 [CCl$_4$]	6.89	$\begin{matrix} H \\ \diagdown \\ \diagup \end{matrix} C = C \big\langle {}^{CH_3}_{\underline{CH_3}}$ $\begin{matrix} \diagdown \\ H \diagup \end{matrix} C = C \big\langle {}^{CH_3}_{\underline{CH_3}}$
1.45 [C$_6$D$_6$] 1.04 [CCl$_4$]	2.07	$- CH - \underline{CH_2} -$

Figure 4. ^{13}C-NMR spectrum of a $CDCl_3$ solution of poly(5-methyl-1,4-hexadiene) prepared with a Et_2AlCl/δ-$TiCl_3$ catalyst at $0°C$ in pentane solvent, ambient temperature. Reproduced, with permission from Ref. 13. Copyright 1979, American Institute of Physics.

Figure 5. 300 MHz ^1H-NMR spectrum of a CCl_4 solution of poly(trans-1,4-hexadiene) prepared with a Et_2Al/δ-$TiCl_3$ catalyst at $25°C$ in pentane solvent (Ref. 14). Reproduced, with permission from Ref. 13. Copyright 1979, American Institute of Physics.

OZONOLYSIS OF POLY(5-METHYL-1,4-HEXADIENE)

$$\text{POLYMER} \quad \xrightarrow{\text{OZONE}} \quad \xrightarrow[\text{THF, 25}^\circ\text{C}]{\phi_3\text{P}} \quad \text{PRODUCT ANALYSIS}$$

```
-(CH2 - CH-)n
         |
         CH2
         |
         CH                    ───────────→     ACETONE
         ‖
         C - CH3
         |
         CH3                                     (Scheme 1)
```

1,2-Polymerization

```
      CH3
       |
-(C - CH-)m
   |    |
   CH3  CH2
        |
        CH                     ───────────→     FORMALDEHYDE
        ‖
        CH2
```
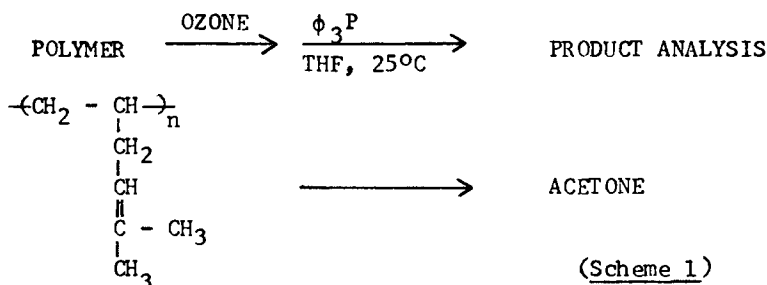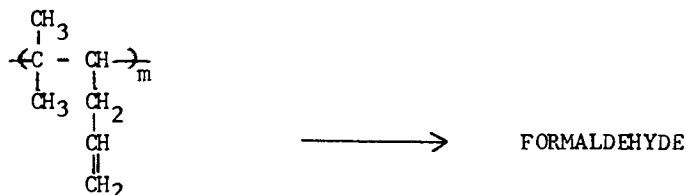
4,5-Polymerization

A chromotrophic acid spot test for formaldehyde (23) was also negative for the polymer ozonolysis solution, while it was positive for a control solution containing formaldehyde equivalent to that expected in the experimental solution if one per cent of the double bonds were vinyl, i.e., polymerization via the internal double bond.

   To clarify the tacticity problem, trans-1,4-hexadiene and 5-methyl-1,4-hexadiene polymers were examined by X-ray diffraction. Fiber diagrams were obtained from samples stretched to four times their original lengths. Eight reflections from the poly(trans-1,4-hexadiene) fiber pattern may be interpreted on the basis of a pseudo-orthorhombic unit cell with a = 20.81 $\pm$ 0.05 Å; b = 12.95 $\pm$ 0.02 Å; c = 6.41 $\pm$ 0.02 Å (fiber axis) and $\alpha = \beta = \gamma = 90^\circ \pm \bar{1}.5^\circ$. An identity period of 6.41 Å indicates a trans-left gauche $(TG)_3$ or trans-right gauche $(T\bar{G})_3$ chain form. This structure is designated as a 3_1 isotactic helix. Other isotactic vinyl polymers show good agreement with this identity period. These values are 6.50 Å for both isotactic polypropylene (24) and poly(1-butene) (25) and 6.33 Å for isotactic poly(5-methyl-1-hexene) (26).

   The crystallographic spacing values and their assigned Miller indicies are listed below in Table II.

TABLE II

MILLER INDICES AND BRAGG DISTANCES

FOR POLY (TRANS-1,4-HEXADIENE)

(hkl)	"d" Spacing	Intensity
(100)	19.8 Å	Strong
(010)	13.5	Weak
(200)	10.5	Strong
(020)	6.4	Weak
(410)	4.84	Very weak
(130)	4.24	Very weak
(301)	4.83	Strong
(221)	4.30	Strong

The poly(5-methyl-1,4-hexadiene) fiber pattern (Figure 6) gave an identity period of 6.3 Å, indicating a 3_1 isotactic helix structure. The X-ray diffraction pattern was not very sharp, which may be due to the difficulty of the side chain with a double bond to fit in a crystalline lattice. The crystallinity was determined to be 15% using the Hermans and Weidinger method (27). A chloroform-soluble fraction free from catalyst residues showed no improvement in the sharpness of the X-ray diffraction pattern. These data show that the configuration of the 1,2-polymerization units in the homopolymer of 5-methyl-1,4-hexadiene is isotactic.

$$
\begin{array}{c}
\overset{*}{\underset{|}{CH}} - CH_2 \Big)_n \\
CH_2 \\
| \\
CH \\
\| \\
C - CH_3 \\
| \\
CH_3
\end{array}
$$
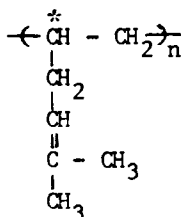
Further confirmation of the structure and tacticity of poly(5-methyl-1,4-hexadiene) was obtained from X-ray diffraction and ^{13}C-NMR data of its hydrogenated polymer (Scheme 2). The hydrogenated polymer sample showed a highly crystalline pattern (Figure 7), with diffraction spots that were well defined. This pattern was identical to that of isotactic poly(5-methyl-1-hexene) as reported in the literature (26) (measured identity period, 6.2 Å; lit., 6.33 Å).
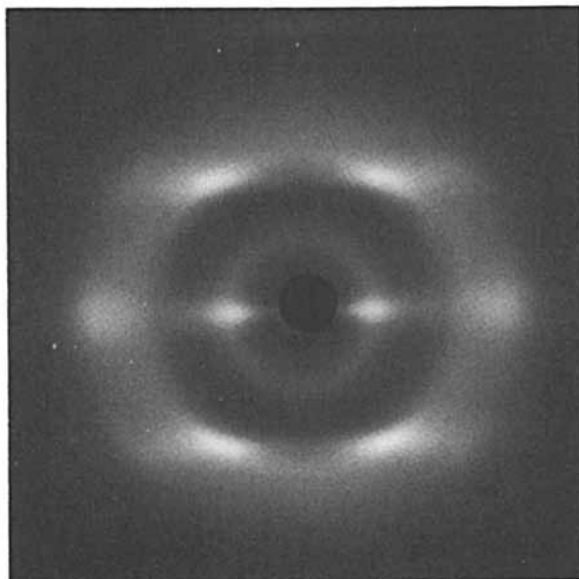
Figure 6. *X-ray fiber diagram of poly(5-methyl-1,4-hexadiene) prepared with a $Et_2AlCl/\delta\text{-}TiCl_3$ catalyst at 0°C in pentane solvent. Compression molded sample cold drawn to four times its original length.*
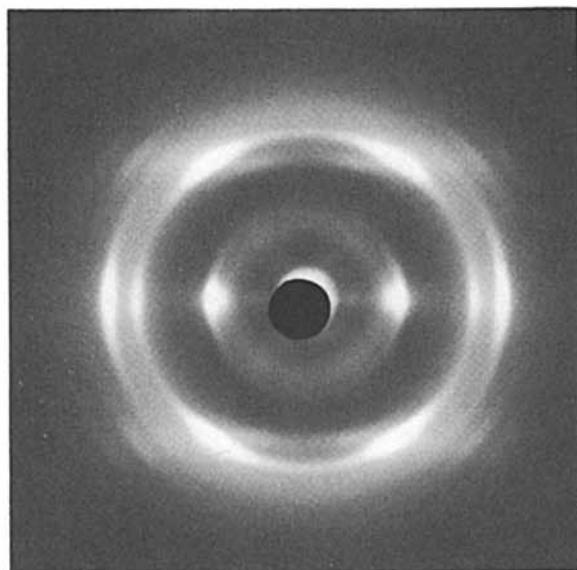
Figure 7. *X-ray fiber diagram of hydrogenated poly(5-methyl-1,4-hexadiene). Solvent cast film strip cold drawn to four times its original length. Reproduced, with permission, from Ref. 19. Copyright 1976, John Wiley & Sons, Inc.*

HYDROGENATION OF POLY(5-METHYL-1,4-HEXADIENE)

POLY(5-METHYL-1,4-HEXADIENE)

POLY(5-METHYL-1-HEXENE)

5-METHYL-1-HEXENE

(Scheme 2)
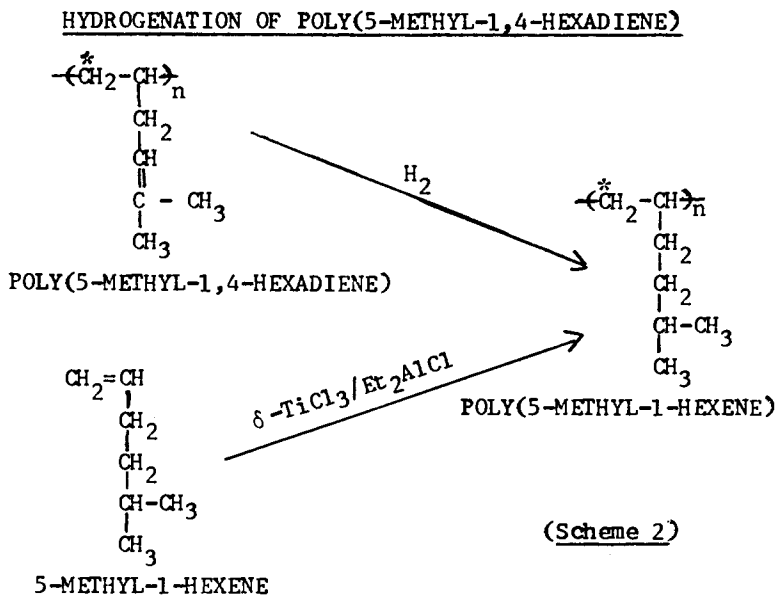
The ^{13}C-NMR spectrum of the hydrogenated polymer sample in CDCl$_3$ solvent (Figure 8) was identical to that of the polymer we obtained by the direct polymerization of 5-methyl-1-hexene with Et$_2$AlCl/δ-TiCl$_3$ AA catalyst (Al/Ti atomic ratio = 1.5, hexane solvent, 30°C). The hydrogenation was essentially complete.

The polymers of 1,4-hexadienes have unusually wide molecular weight distributions. This is illustrated by the gel permeation chromatogram of the methanol-insoluble fraction of poly(5-methyl-1,4-hexadiene) in tetrahydrofuran (Figure 9). The polymer was obtained in 82% conversion and had an inherent viscosity of 2.1 dl./g. in toluene at 25°C.

We showed (7) earlier that copolymers of higher α-olefins, particularly 1-hexene, with 5-methyl-1,4-hexadiene can be sulfur-cured readily and that they contain unsaturation approximating the level of the methylhexadiene charged. In view of this and the excellent durability (8) during flexing exhibited by vulcanizates of such copolymers, we were interested in determining the copolymer structure and the reactivity ratios of 1-hexene and 5-methyl-1,4-hexadiene during copolymerization.

The NMR spectrum of the copolymer prepared from an equimolar mixture of the monomers is shown in Figure 10. In this spectrum, five well separated regions of NMR peaks were observed. The assignments of the peaks (Table III) were made by using the existing spectral information on homopolymers of 1-hexene and 5-methyl-1,4-hexadiene as well as the intensity variations among the copolymers with different monomer charge ratios.
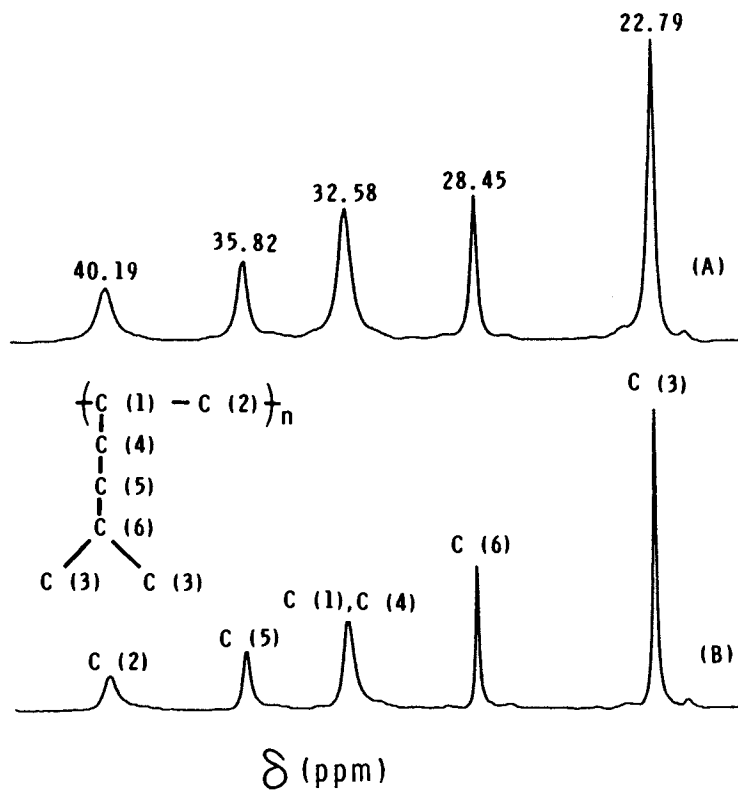
Figure 8. ^{13}C-NMR spectra of (A) hydrogenated poly(5-methyl-1,4-hexadiene) and (B) poly(5-methyl-1-hexene).

$\overline{M}n$ = 48,000

$M w$ = 967,000

$\overline{M}w/\overline{M}n$ = 20
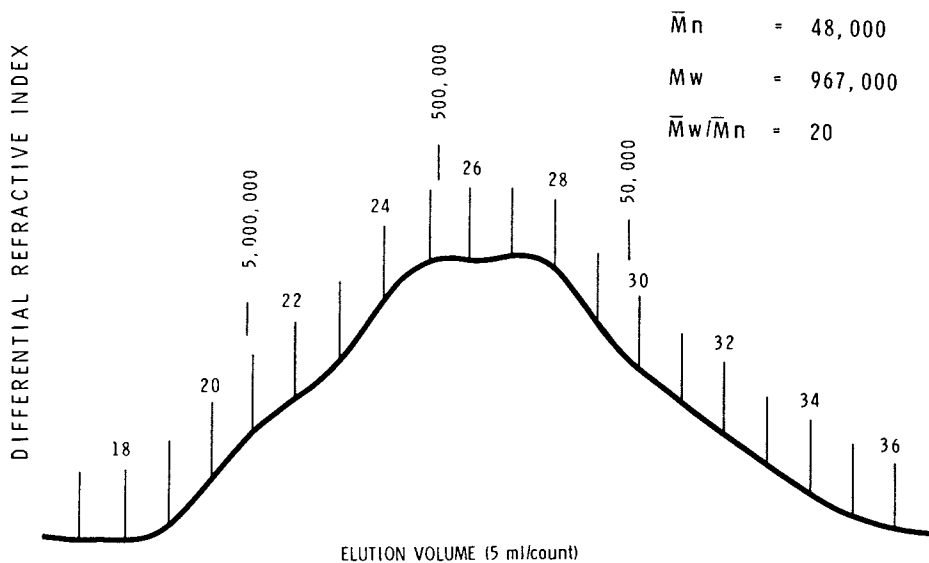
Figure 9. *Gel permeation chromatogram of methanol–isoluble fraction of poly(5-methyl-1,4-hexadiene). THF solvent.*
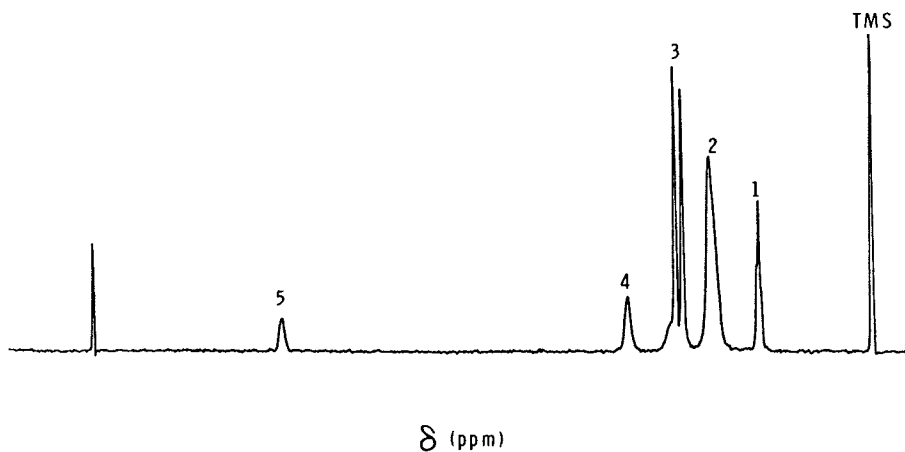
Figure 10. *300 MHz ^{1}H-NMR spectrum of a deuterobenzene solution of an equimolar copolymer of 5-methyl-1,4-hexadiene and 1-hexene prepared with a $Et_2AlCl/$ δ-TiCl$_3$ catalyst at $0°C$ in pentane solvent.*

TABLE III

300 MHz ^{1}H-NMR SPECTRAL DATA OF AN EQUIMOLAR COPOLYMER OF
1-HEXENE AND 5-METHYL-1,4-HEXADIENE

Peaks	Chemical Shift, ppm	Assignments
1	1.04	$\underline{CH}_3$-CH$_2$-CH$_2$-CH$_2$-CH-CH$_2$-
2	1.20-1.60	CH$_3$-$\underline{CH}_2$-$\underline{CH}_2$-$\underline{CH}_2$-CH-$\underline{CH}_2$-
		$\begin{matrix} CH_3 \\ \quad \diagdown \\ \quad\quad C=CH-CH_2-CH-\underline{CH}_2- \\ \quad \diagup \\ CH_3 \end{matrix}$
3	1.65-2.00	$\begin{matrix} \underline{CH}_3 \\ \quad \diagdown \\ \quad\quad C=CH-CH_2-\underline{CH}-CH_2- \\ \quad \diagup \\ \underline{CH}_3 \end{matrix}$
		CH$_3$-CH$_2$-CH$_2$-CH$_2$-$\underline{CH}$-CH$_2$-
4	2.24	$\begin{matrix} CH_3 \\ \quad \diagdown \\ \quad\quad C=CH-\underline{CH}_2-CH-CH_2- \\ \quad \diagup \\ CH_3 \end{matrix}$
5	5.44	$\begin{matrix} CH_3 \\ \quad \diagdown \\ \quad\quad C=\underline{CH}-CH_2-CH-CH_2- \\ \quad \diagup \\ CH_3 \end{matrix}$

The chemical structure of the copolymers was also studied by using 20 MHz ^{13}C-NMR spectroscopy. The spectrum of the above copolymer prepared from an equimolar mixture of monomers is shown in Figure 11. The measured chemical shifts and peak assignments for the various types of carbon atoms in the copolymer structure are based on spectral data of the homopolymers of 5-methyl-1,4-hexadiene and 1-hexene as well as the additivity rules of Grant and Paul (28) and Lindeman and Adams (29). The data are given in Table IV. The spectrum of the copolymer corresponds to merely the superposition of the spectra of those of the individual homopolymers. Neither additional peaks, nor fine structures, were observed under the conditions of the experiment. Only a slight broadening of the peak at 40.03 ppm, which is due to the backbone methylene carbons in the copolymer, was noted. The lack of the additional peaks in the copolymer spectrum may be interpreted as being due to the fact that both monomers are incorporated in a regular head-to-tail manner analogous to the homopolymerizations of both these monomers. The lack of fine structures also precludes the elucidation of monomer sequence distribution.

Only a limited amount of work has been reported in the area of reactivity ratios in higher α-olefin systems. Lipman (30) has reported that the relative reactivities of 1-butene, 1-hexene and 1-decene during copolymerization in the presence of δ-TiCl$_3$/Et$_2$AlCl catalyst system (Al/Ti = 2, 23°C, cyclohexane solvent) are, respectively, 1.00, 0.83, and 0.69, i.e., there is only a slight decrease in reactivity as the length of the R group in RCH=CH$_2$ is increased from C$_2$ to C$_8$. Branching, especially at the 3- and 4-carbon positions of α-olefins drastically reduces their reactivity (31).

As a check on our experimental and calculation procedures, we examined the copolymerization of 1-hexene and 1-decene (Table V) which had been investigated by Lipman (30). The copolymer composition was determined by using 300 MHz ^{1}H-NMR and the reactivity ratios were calculated by the Tidwell-Mortimer method (22). The values of r$_1$ (1-hexene) = 1.1 ± 0.2 and r$_2$ (1-decene) = 0.9 ± 0.2 are in excellent agreement with Lipman's values of 1.3 and 0.9, respectively. It should be noted that in the latter investigation the copolymers were analyzed by IR spectroscopy and the reactivity ratios were calculated according to the method of Mayo and Lewis (32).

Copolymer composition vs. monomer feed data were then obtained for 1-hexene (M$_1$) and 5-methyl-1,4-hexadiene copolymerizations (Table VI). The data show that the copolymer compositions measured by 300 MHz ^{1}H-NMR spectroscopy are essentially identical to the monomer feed. The calculated reactivity ratios were 1.1 ± 0.2 for each of the two monomers.

These results were somewhat unexpected in view of the possible decrease in the reactivity of 5-methyl-1,4-hexadiene due to methyl substitution at the 5-carbon position. To differentiate the effect of the double bond at the 4-carbon position
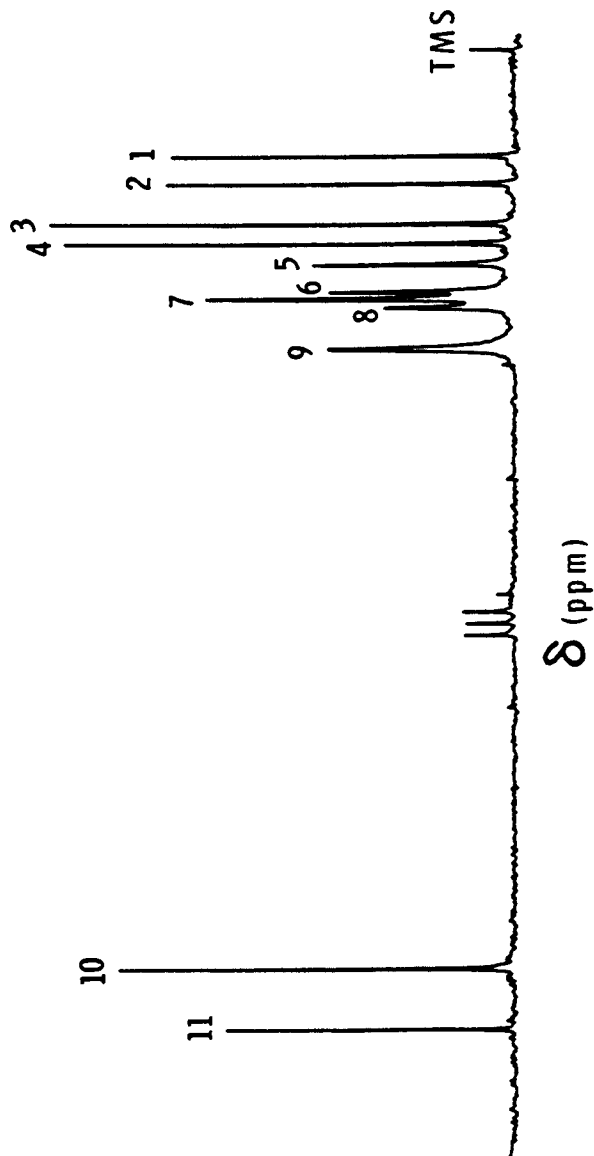
Figure 11. *13C-NMR spectrum of a CDCl3 solution of an equimolar copolymer of 5-methyl-1,4-hexadiene and 1-hexene prepared with a Et2AlCl/δ-TiCl3 catalyst at 0°C in pentane solvent.*

TABLE IV

^{13}C-NMR SPECTRAL DATA OF AN EQUIMOLAR COPOLYMER OF
1-HEXENE AND 5-METHYL-1,4-HEXADIENE

Peaks	Chemical Shift, ppm	Assignments
1	14.19	$\underline{CH_3}$-CH_2-CH_2-CH_2-$\overset{\mid}{CH}$-CH_2-
2	17.94	$\underset{CH_3}{\overset{\underline{CH_3}}{>}}C=\overset{\mid}{C}\text{-}CH_2\text{-}\overset{\mid}{CH}\text{-}CH_2\text{-}$ (with H)
3	23.25	CH_3-$\underline{CH_2}$-CH_2-CH_2-$\overset{\mid}{CH}$-CH_2-
4	25.86	$\underset{\underline{CH_3}}{\overset{CH_3}{>}}C=C\underset{H}{\overset{CH_2\text{-}\overset{\mid}{CH}\text{-}CH_2\text{-}}{<}}$
5	28.72	CH_3-$\underline{CH_2}$-$\underline{CH_2}$-CH_2-$\overset{\mid}{CH}$-CH_2-
6	32.38	CH_3-CH_2-CH_2-CH_2-$\overset{\mid}{\underline{CH}}$-$CH_2$-
7	33.30	$\underset{CH_3}{\overset{CH_3}{>}}C=CH\text{-}\underline{CH_2}\text{-}\overset{\mid}{\underline{CH}}\text{-}CH_2\text{-}$
8	34.55	CH_3-CH_2-CH_2-$\underline{CH_2}$-$\overset{\mid}{CH}$-CH_2-
9	40.03	$\left\{\begin{array}{l} CH_3\text{-}CH_2\text{-}CH_2\text{-}CH_2\text{-}\overset{\mid}{CH}\text{-}\underline{CH_2}\text{-} \\ \underset{CH_3}{\overset{CH_3}{>}}C=CH\text{-}CH_2\text{-}\overset{\mid}{CH}\text{-}\underline{CH_2}\text{-} \end{array}\right.$
10	123.36	$\underset{CH_3}{\overset{CH_3}{>}}C=\underline{CH}\text{-}CH_2\text{-}\overset{\mid}{CH}\text{-}CH_2\text{-}$
11	131.54	$\underset{CH_3}{\overset{CH_3}{>}}\underline{C}=CH\text{-}CH_2\text{-}\overset{\mid}{CH}\text{-}CH_2\text{-}$

TABLE V

COPOLYMER COMPOSITION vs MONOMER FEED COMPOSITION
FOR 1-HEXENE/1-DECENE COPOLYMERIZATIONS

Mole % 1-Hexene		Copolymer Conversion, Wt %
Monomer Feed	Copolymer	
25	25	14
25	22	87
40	45	17
40	45	29
50	46	77
50	51	18
60	66	21
60	63	51
75	76	40
75	74	10

Calculated Reactivity Ratios

r_1(1 - hexene, M_1) = 1.1 $\pm$ 0.2

r_2(1 - decene, M_2) = 0.9 $\pm$ 0.2

TABLE VI

COPOLYMER COMPOSITION vs MONOMER FEED COMPOSITION FOR

1-HEXENE/5-CH$_3$-1,4-HEXADIENE COPOLYMERIZATIONS

Mole % 1-Hexene		Copolymer Conversion, Wt %
Monomer Feed	Copolymer	
75	76	17.0
75	77	45.4
60	60	9.3
60	60	46.0
50	53	29.3
50	50	45.7
40	38	34.4
40	43	23.5
25	27	22.2
25	21	30.4

Calculated Reactivity Ratios:

r_1 (1-hexene, M_1) $= 1.1 \pm 0.2$

r_2 (5-CH$_3$-1,4-hexadiene, M_2) $= 1.1 \pm 0.2$

from that of the methyl substitution at the 5-carbon position on reactivity, we determined reactivity ratios for the 1-hexene (M_1) and 5-methyl-1-hexene (M_2) pair under similar conditions of co-polymerization, using the same analytical and calculation methods. The values of r_1 and r_2 were, respectively, 1.5 ± 0.2 and 0.7 ± 0.2. The reduced reactivity of 5-methyl-1-hexene is consistent with the expected steric effect due to methyl substitution at the 5-carbon position. Apparently, the internal double bond in 5-methyl-1,4-hexadiene assists in its complexation at the active site(s) of the catalyst prior to its polymerization and thereby the "local concentration" of this monomer is higher than the feed concentration during copolymerization with 1-hexene. This view is consistent with the observation that the overall rates of polymerization, under the same conditions, are much lower for the system containing 5-methyl-1,4-hexadiene.

We also investigated the copolymerizations of 1-hexene with 4-methyl-1-hexene and of 4-methyl-1-hexene with 5-methyl-1-hexene by the aforementioned techniques (33). The monomer reactivity ratios for these two pairs are shown in Table VII.

TABLE VII

Monomer Reactivity Ratios at 30°C.

Catalyst System: Et_2AlCl/δ-$TiCl_3$ AA (Al/Ti = 2)

Monomer 1	Monomer 2	r_1	r_2
1-Hexene	4-Methyl-1-hexene	2.6 ± 0.6	0.03 ± 0.2
5-Methyl-1-hexene	4-Methyl-1-hexene	2.9 ± 0.4	0.6 ± 0.1

These data support the expectation that the substitution of a methyl group at the 4-carbon position has a significantly greater effect in reducing the reactivity than does similar sub-stitution at the 5-carbon atom.

Acknowledgment

Literature Cited

1.   Wirth, K. H. U.S. Patent 3,492,370 (January 27, 1970).
2.   Yasui, S.; Hirooka, M.; Oshima, T. U.S. Patent 3,649,573 (March 14, 1972).
3.   Morrissey, R. T. Rubber Chem. Technol. 1971, 44, 1025.
4.   Baranwal, K. C.; Son, P. N. Rubber Chem. Technol. 1974, 47, 88.

5. Hopper, R. J. Rubber Chem. Technol. 1976, 49, 341.
6. Mastromatteo, R. P.; Mitchell, J. M.; Brett, Jr., T. J. Rubber Chem. Technol. 1971, 44, 1065.
7. Lal, J.; Sandstrom, P. H. U.S. Patents 3,933,769 (January 20, 1976) and 3,991,262 (November 9, 1976).
8. Rubber Plastics News 1978 (April 3) 5; Elastomerics 1978, (May), 25.
9. Kennedy, J. P.; Chou, T. M. U.S. Patent 3,923,759 (December 2, 1975); Adv. Polym. Sci. 1976, 21, 1, 31.
10. Thaler, W. A.; Buckley, D. J.; Kennedy, J. P. U.S. Patents 3,808,177 (April 30, 1974) and 3,856,763 (December 24, 1974).
11. Thaler, W. A.; Buckley, Sr., D. J. Rubber Chem. Technol. 1976. 49, 960.
12. Cohen, J.; Rae, J. A.; Buckley, Sr., D. J. Rubber Chem. Technol. 1976, 49, 967.
13. Marvel, C. S.; Garrison, Jr., W. E. J. Am. Chem. Soc. 1959, 81, 4737.
14. Lal, J.; Chen, H. Y.; Sandstrom, P. H. J. Polym. Sci. Polym. Lett. Ed. 1979, 17, 95.
15. Lal, J.; Hanlon, T. L.; Chen, H. Y. J. Polym. Sci. Polym. Chem. Ed. 1980, 18, 2921.
16. Lal, J.; Sandstrom, P. H. U.S. Patents 3,975,336 (August 17, 1976) and 4,064,335 (December 20, 1977).
17. Golub, M. A.; Rosenberg, M. L. J. Polym. Sci. Polym. Chem. Ed. 1980, 18, 2543.
18. Bryson, J. G. U.S. Patent 3,904,704 (September 9, 1975).
19. Hata, G.; Aoki, D. J. Org. Chem. 1967, 32, 3754.
20. Chen, H. Y. J. Polym. Sci. Polym. Lett. Ed. 1977, 15, 271 and references therein.
21. Andrews, A. M.; Personal Communication.
22. Tidwell, P. W.; Mortimer, G. A. J. Polym. Sci. 1965, A3, 369.
23. Feigl, F.; Anger, V. "Spot Tests in Organic Analysis", 7th English Ed.; Elsevior Publishing Co., New York, 1966; p. 434.
24. Natta, G.; Corradini, P.; Cesari, M. Atti Accad. Nazl. Lincei 1956, 21, 365; Natta, G.; Corradini, P. Nuovo Cimento 1960, 15, Suppl. No. 1, 40.
25. Natta, G.; Corradini, P.; Bassi, I. W. Makromol. Chem. 1956, 21, 240; Nuovo Cimento 1960, 15, Suppl. No. 1, 52.
26. Corradini, P.; Martuscelli, E.; Montagnoli, G.; Petraccone, V. Eur. Polym. J. 1970, 6, 1201.
27. Hermans, P. H.; Weidinger, A. Makromol. Chem. 1961, 44, 24; 1961, 50, 98.
28. Grant, D. M.; Paul, E. G. J. Am. Chem. Soc. 1964, 86, 2984.
29. Lindeman, L. P.; Adams, J. Q. Anal. Chem. 1971, 43, 1245.

30. Lipman, R. D. A. <u>Am. Chem. Soc., Div. of Polym. Chem.</u>
    <u>Preprints</u> 1967, <u>8</u>, 396.
31. Boor, Jr., J. R. "Ziegler-Natta Catalysts and Polymeriza-
    tions", Academic Press, New York, 1979, Chapters 19, 20,
    and references therein.
32. Mayo, F. R.; Lewis, F. M. <u>J. Am. Chem. Soc.</u> 1944, <u>66</u>, 1594.
33. Hanlon, T. L.; Lal, J. Unpublished results.

Structural Factors and Tensile Properties of Ethylene–Propylene–Diene Terpolymers Prepared with Various Catalyst Systems

BAO-TONG HUANG (PAO-TUNG HUANG), LI-TONG ZHAO, YU-LIANG LI, MIN YU, and BAO-YUAN HU

Changchun Institute of Applied Chemistry, Academia Sinica, Changchun, Jilin Province, People's Republic of China

Difference in vulcanizate tensile strength of EPDMs prepared with various catalyst systems, especially the high strength of EPDM prepared with vanadium carboxylates (V_{5-9}), is examined against various structural parameters. Effect of $[\eta]$, $[C=C]$ and $C_3\%$ respectively on tensile strength is noted. The catalyst systems are arranged in the decreasing order of tensile strength for samples with comparable $[\eta]$, $[C=C]$ and $C_3\%$ as: $V_{5-9}-Et_3Al_2Cl_3$ $> V(acac)_3-Et_2AlCl > V_{5-9}-Et_3Al_2Cl_3-ETCA$ (activator) $> VOCl_3-Et_3Al_2Cl_3$. Contributions of third monomer distribution and molecular weight distribution, though important as they should be, did not appear to be decisive. Variations in monomer sequence length distribution and long-chain branching, if present, and their influence on vulcanizate tensile strength remain to be examined.

Ethylene-propylene-diene terpolymers (EPDM), with their inherent complexity in structural parameters, owe their tensile properties to specific structures dictated by polymerization conditions, among which the controlling factor is the catalyst used in preparing the polymers. However, no detailed studies on correlation between tensile properties and EPDM structures have been published (1,2). An unusual vulcanization behavior of EPDMs prepared with vanadium carboxylates (typified by V_{5-9}, carboxylate of mixed acids of C_5-C_9) has been recently reported (3). This EPDM attains target tensile properties in 18 and 12 minutes at vulcanization temperatures of 150 and 160°C respectively, while for EPDMs prepared with $VOCl_3-Et_3Al_2Cl_3$ or $V(acac)_3-Et_2AlCl$, about 50 and 40 minutes are usually required at the respective vulcanization temperatures, all with dicyclopentadiene (DCPD) as the third monomer and with the same vulcanization recipe. This observation prompted us to inquire into the inherent structural factors

that caused this marked difference in vulcanization behavior of
EPDMs prepared with different catalyst systems. This paper
reports some of the preliminary observations.

EXPERIMENTAL

Polymerizations were carried out batchwise in 400-ml
polymerization-grade hydrogenated gasoline or hexane. After
saturating the solvent with the monomer mixture (C_2/C_3=2.0 ± 0.1,
dried through consecutive NaOH, silica gel and 4A molecular sieve
columns), DCPD (together with ETCA, ethyl trichloroacetate, an
activator, when used), vanadium catalyst and alkylaluminum
chloride solutions were syringed in succession into the reaction
mixture. Polymerization continued with stirring under the monomer
gas flow. With the exception of $VOCl_3$-$Et_3Al_2Cl_3$ polymerization,
the 30-minute polymerization was repeated for another cycle with
further addition of catalyst components and diene in order to
boost the yield in one batch to get enough terpolymer for tensile
tests. The terpolymer, after being precipitated from ethanol and
washed with fresh portions of ethanol, with N-phenyl-β-naphthyl-
amine added in the third washing, was vacuum dried at 40°C to a
constant weight. $[\eta]$ was determined in toluene at 30°C, degree
of unsaturation, $[C=C]$ (expressed in mmole/gram polymer), by
iodine chloride method (4) and composition C_3 mole% by infrared
spectroscopy (Zeiss UR-10 or Perkin Elmer 577) using bands at 720
and 1150 cm^{-1} with pressed films employing a pre-constructed
calibration curve (5).

Tensile testing samples were of miniature size (ca. 1.5x1.8
mm in cross-section and 5.5 cm in gauge length. Long practice in
this Laboratory has proven that samples of this size give repro-
ducible results and are eligible for comparison purposes.

The vulcanization recipe was: EPDM 100, stearic acid 1.0,
zinc oxide 5.0, accelerator M 0.5, TMTD 1.5, HAF 50, sulfur 1.5
phr. Peroxide-curing of E-P copolymers was carried out with a
modified procedure of (6): EPR 100, dicumyl peroxide 3, zinc oxide
3, TMTD 0.5, HAF 50, sulfur 0.2 phr, the mixture being masticated
for 20 minutes at 40-50°C and cured at 140°C.

Molecular weight distribution (MWD) was determined on a home-
made GPC column (7), with toluene as the eluant and turbidimetry
in methanol as means of detecting polymer concentrations in the
counts.

RESULTS AND DISCUSSION

Among the main molecular structural variables in EPDMs that
are stipulated by catalyst systems and that affect the vulcanizate
tensile properties we may mention: molecular weight (MW) and MWD,
degree of unsaturation ($[C=C]$) and its distribution in the polymer,
composition (C_3%) and monomer sequence length distribution along
molecular chains, and long-chain branching if present. Effect of

carbon black reinforcement and of chemical structure of cross-
linking bonds on tensile properties can be neglected when samples
are processed and vulcanized under same conditions.

Preliminary Observations

It was observed in the early stage of this work that EPDMs
prepared with different catalysts had varying vulcanizate tensile
properties. For example, it was noted that V_{5-9}-EPDMs had higher
vulcanizate tensile strength than $VOCl_3$-EPDMs with comparable $[\eta]$
and $[C=C]$ (Figure 1A) or with even higher $[\eta]$ and $[C=C]$ (Figures
1B and 1C), even though $Et_3Al_2Cl_3$ + Et_2AlCl should have given
lower vulcanizate tensile strength than $Et_3Al_2Cl_3$ alone (3).
Similar tensile difference existed between vulcanizates of
$V(acac)_3$-Et_2AlCl and V_{5-9}-Et_2AlCl EPDMs of comparable $[\eta]$ and
$[C=C]$ (Figure 1D).

Effect of $[\eta]$, $[C=C]$ and $C_3\%$

The effect of MW on tensile properties of other elastomers
that, before a MW limit is reached, tensile strength increases
with MW was well established. Due to complexity in MW~$[\eta]$ rela-
tionship for EPDMs (3), as an expedient measure, $[\eta]$ is used as a
practical scale of MW. Figure 2 shows examples of EPDM samples
having same $[C=C]$ but varying $[\eta]$ prepared with V_{5-9}-$Et_3Al_2Cl_3$ +
Et_2AlCl (1:1). Thus, the effect of $[\eta]$ is nullified by using
samples having comparable $[\eta]$ when comparing samples prepared with
different catalyst systems.

Under comparable $[\eta]$, samples with higher $[C=C]$ showed higher
tensile strength and 300% modulus and lower elongation at break
for EPDMs obtained with all the catalysts studied---$V(acac)_3$-
Et_2AlCl (Figures 3 and 4), V_{5-9}-$Et_3Al_2Cl_3$ (Figure 5) and $VOCl_3$-
Et_3Al2Cl_3 (Figure 6A). The importance of the degree of unsatura-
tion in determining tensile strength is emphasized in the failure
of the contribution of higher $[\eta]$ to overcome the effect of lower
$[C=C]$ (Figure 6B).

Composition of the terpolymers as expressed in C_3 mole%, of
course, must be kept in the range that yields good elastomeric
properties. E-P polymers of higher ethylene content naturally
result in higher tensile strength as a consequnece of formation
of partial crystallinity due to short ethylene blocks (8). $C_3\%$
of EPDMs studied in this work all abide by the usual EPDM require-
ments.

Systematic Comparison

It became apparent that comparison of samples with similar
$[\eta]$, $[C=C]$ and $C_3\%$ would reveal the degree of tensile difference
brought about by other structural factors. The matching samples
with three structural factors comparable simultaneously were
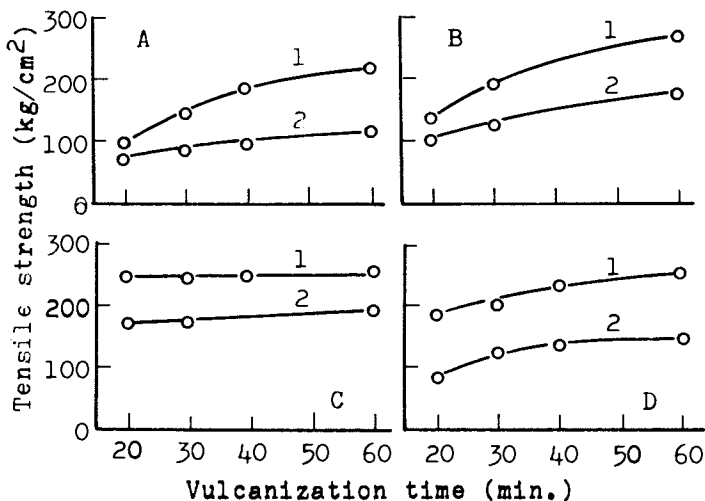
Figure 1.   Tensile differences in EPDMs.
Conditions for A: (1) $V_{5-9}Et_3Al_2Cl_3$; Et_2AlCl, 1:1; (2) $VOCl_3$-$Et_3Al_2Cl_3$; $[\eta]$ (dl/g), 2.05;
$[C=C]$ (mmol/g), 0.49 (1) 0.43 (2); 150°C. Conditions for B: $V_{5-9}Et_3Al_2Cl_3$, Et_2AlCl,
1:1; (2) $VOCl_3Et_3Al_2Cl_3$; $[\eta]$ (dl/g), 1.83 (1) 1.91 (2); $[C=C]$ (mmol/g), 0.42 (1) 0.51
(2); 150°C. Conditions for C: (1) $V_{5-9}Et_3Al_2Cl_3$, (2) $VOCl_3Et_3Al_2Cl_3$; $[\eta]$ (dl/g), 1.85
(1) 2.01 (2); $[C=C]$ (mmol/g), 0.73 (1) 1.01 (2); 150°C. Conditions for D: (1) $V(acac)_3$-
Et_2AlCl; $V_{5-9}Et_2AlCl$ (2); $[\eta]$ (dl/g), 1.18 (1) 1.14 (2); $[C=C]$ (mmol/g), 0.35 (1)
0.37 (2); 160°C.
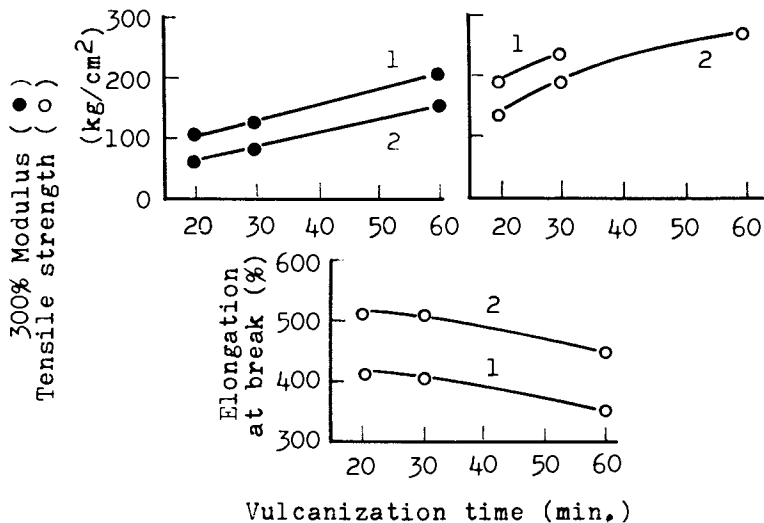
Figure 2.   Effect of $[\eta]$ on vulcanizate tensile properties: V_{5-9}-$Et_3Al_2Cl_3$, Et_2AlCl,
(1:1), 150°C; $[C=C]$ (mmol/g), 1—0.43, 2—0.42; $[\eta]$ (dl/g), 1—2.37, 2—1.83.
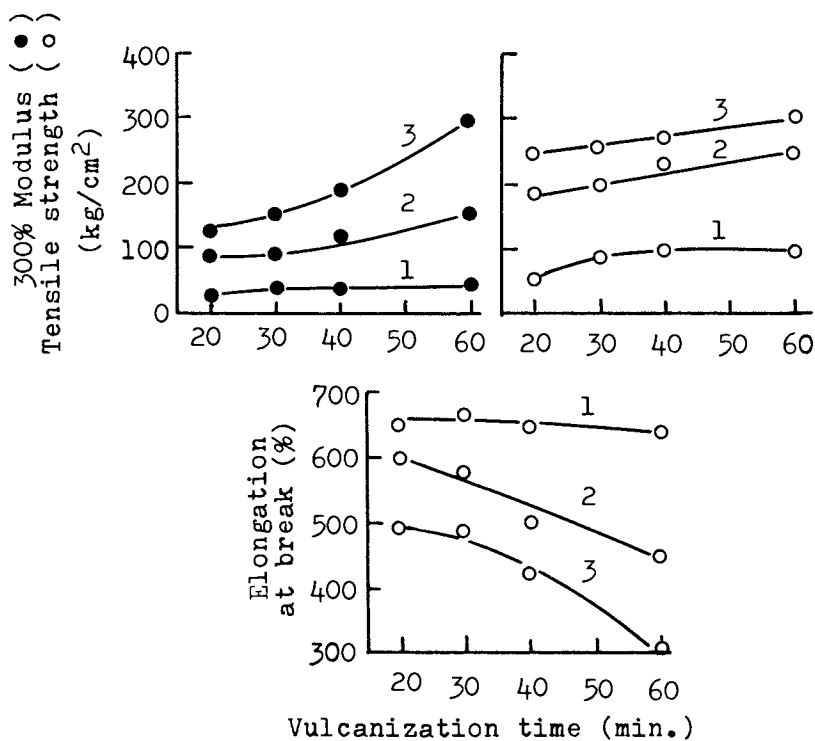
Figure 3. Effect of [C═C] on tensile properties: V(acac)₃-Et₂AlCl, 160°C; [C═C] (mmol/g), 1—0.23, 2—0.35, 3—0.53; [η] (dl/g), 1—1.19, 2—1.18, 3—1.16.
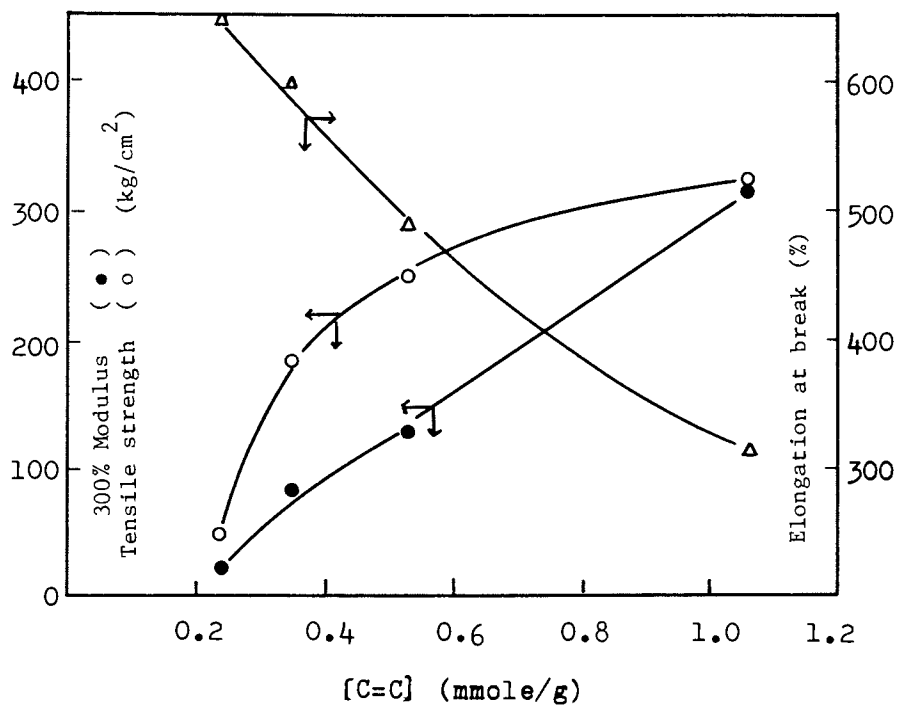
Figure 4.   Effect of [C═C] on tensile properties: V(acac)₃-Et₂AlCl, 160°C; 20 min.
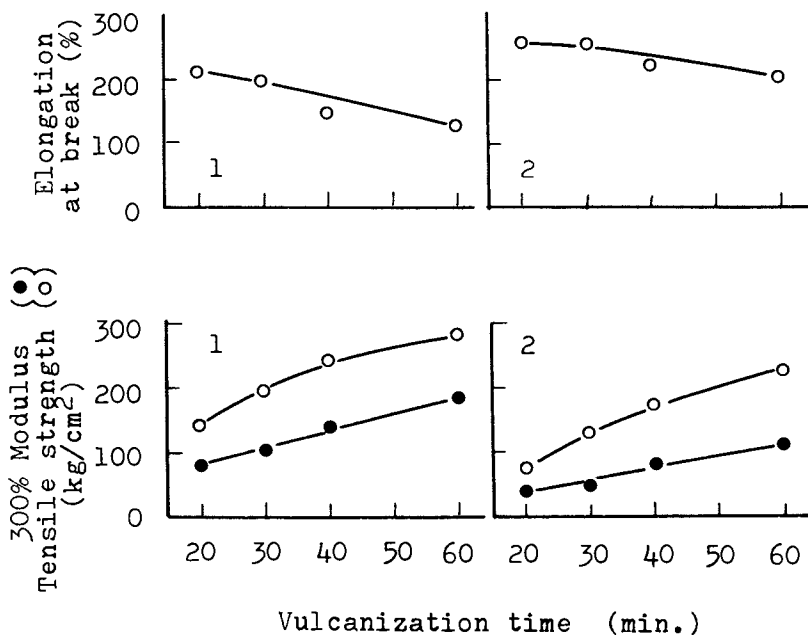
Figure 5. Effect of [C=C] on tensile properties: $V_{5.9}$-$Et_3Al_2Cl_3$, 150°C; [C=C] (mmol/g), 1—0.46, 2—0.32; [η](dl/g), 1—2.54, 2—2.45.
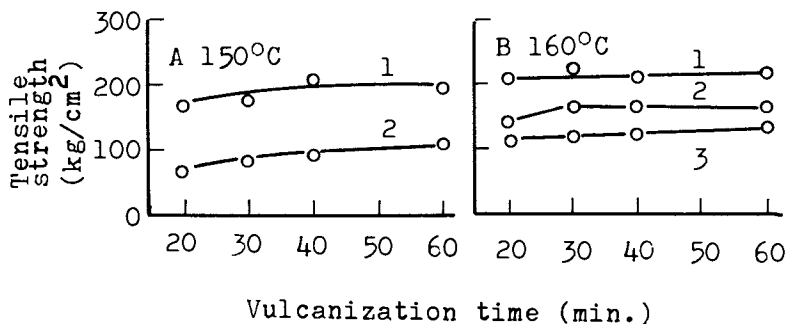
Figure 6. Effect of [C=C] on tensile strength on EPDMs for $VOCl_3EtAl_2Cl_3$. Conditions for A: [η] (dl/g), 2.01 (1) 2.05 (2); [C=C] (mmol/g), 1.01 (1) 0.43 (2); Conditions for B: [η] (dl/g), 1.69 (1) 1.88 (2) 2.30 (3); [C=C] (mmol/g) 0.81 (1) 0.42 (2) 0.24 (3).

assorted from samples from large amount of polymerization work.
Six matched sets of samples, each comparable in $[\eta]$, $[C=C]$ and
$C_3\%$ (Table I), were chosen from terpolymers obtained with V_{5-9}-
$Et_3Al_2Cl_3$, $VOCl_3$-$Et_3Al_2Cl_3$, $V(acac)_3$-Et_2AlCl and the activated
V_{5-9}-$Et_3Al_2Cl_3$-ETCA, respectively.
    Comparison of vulcanizate tensile properties of the six sets
of comparable samples (Figures 7A-F) gave results (Table I, last
column) pointing to the ability of the systems in giving decreas-
ing tensile strength in the following order:

$$V_{5-9}\text{-}Et_3Al_2Cl_3 > V(acac)_3\text{-}Et_2AlCl >$$

$$V_{5-9}\text{-}Et_3Al_2Cl_3\text{-}ETCA > VOCl_3\text{-}Et_3Al_2Cl_3.$$
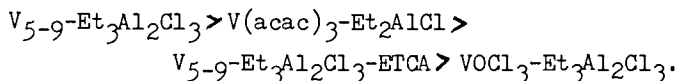
    It is seen that, in some cases, samples having the same
modulus (Figures 7C and F) or even lower modulus (Figures 7D and
E) had even higher tensile strength. Taking 300% modulus as a
measure of cross-linking density, it may mean that, besides $[\eta]$,
degree of unsaturation, composition and cross-linking density as
symbolized by 300% modulus, there are other factors that affect
the tensile strength.
    As supporting evidence, it may also be mentioned that t90
(time needed for 90% vulcanization) and V_e(vulcanization rate)
values on a curometer showed the followed order:

$$V_{5-9}\text{-}Et_3Al_2Cl_3 > VOCl_3\text{-}Et_3Al_2Cl_3;$$

$$V(acac)_3\text{-}Et_2AlCl > V_{5-9}\text{-}Et_3Al_2Cl_3\text{-}ETCA > VOCl_3\text{-}Et_3Al_2Cl_3.$$
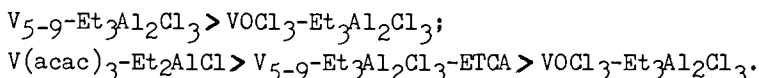
    In the case of V_{5-9}-$Et_3Al_2Cl_3$ system, the vulcanizate tensile
strength is lowered on addition of the activator ETCA, apparently
because of the change in molecular structure of the resulting
polymer as a result of change in the nature of the polymerization-
active centers. But this catalyst still yields vulcanizate
strength higher than that of $VOCl_3$-EPDM.

Effect of Distribution of Double Bonds

    The distribution of the thi: monomer in molecular chains or
in the whole polymer should affect the perfection of the vulcani-
zate network, free chain ends or the uncross-linked parts in the
polymer making no contribution to the tensile strength but acting
as a plasticizer of like structure as the polymer.
    So far it has not been possible to determine the distribution
of the third monomer units in molecular chains. Yet it is
possible to follow the rate of third monomer incorporation in
polymerization so as to estimate the heterogeneity of its distri-
bution in the whole polymer. We have previously reported the
marked difference in incorporation of DCPD in polymerization with
$V(acac)_3$-Et_2AlCl and V_{5-9}-$Et_3Al_2Cl_3$-ETCA ($\underline{3}$). Figure 8 shows that
V_{5-9} in combination with various alkylaluminum halides and $VOCL_3$-
$Et_3Al_2Cl_3$ are not noticeably different in influencing the incor-
poration of DCPD during EPDM polymerization. Thus, difference in

Vulcanization time (min.)
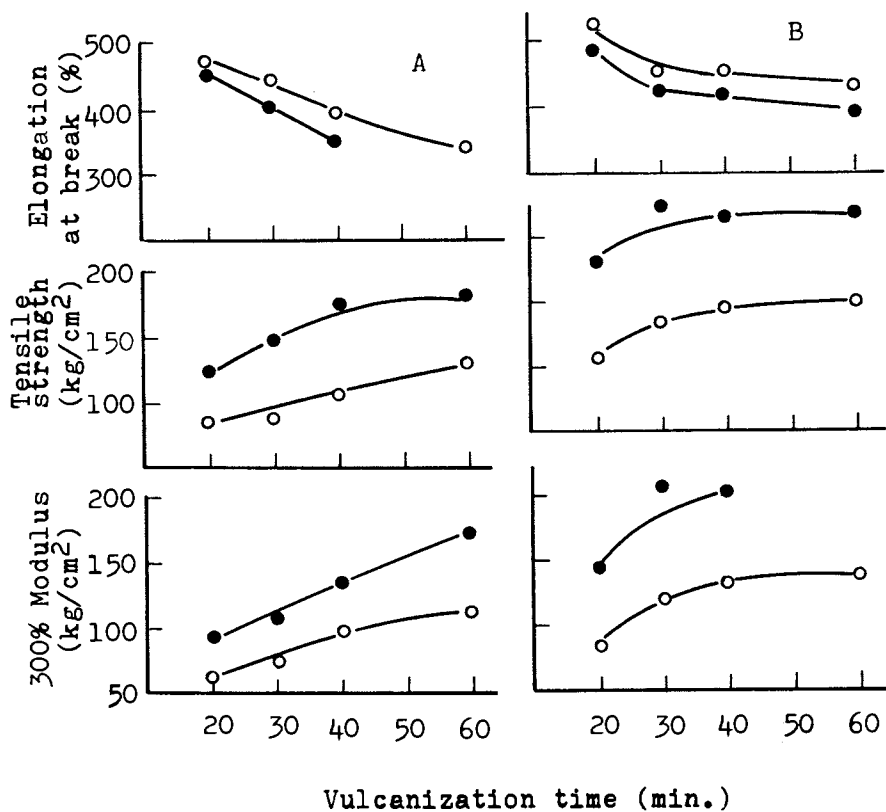
Figure 7. Tensile properties of comparable samples. Key: (A) ●, 78–C33 V$_{5-9}$-Et$_3$Al$_2$Cl$_3$; ○, 78–C29 VOCl$_3$-Et$_3$Al$_2$Cl$_3$; (B) ●, 78–C 1 V$_{5-9}$-Et$_3$Al$_2$Cl$_3$-ETCA; ○, 78–C27 VOCl$_3$Et$_3$Al$_2$Cl$_3$. Sample data in Table I. Continued.
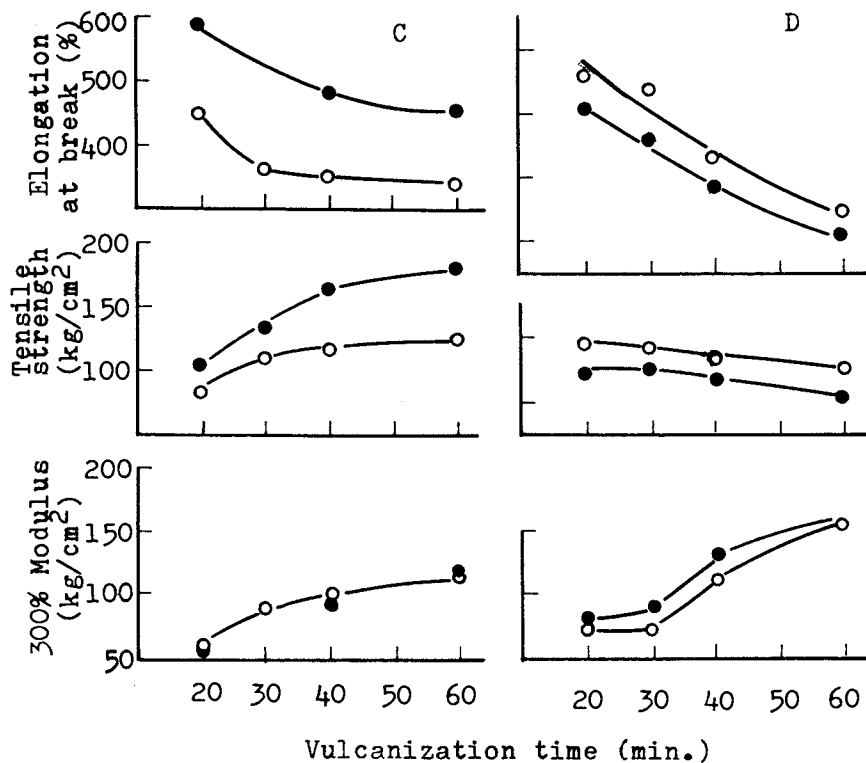
Figure 7. Continued. Tensile properties of comparable samples. Key: (C) ●, 78–C24 V_{5-9}-$Et_3Al_2Cl_3$-ETCA; ○, 78–C11 $VOCl_3$-$Et_3Al_2Cl_3$; (D) ●, 78–C19 V_{5-9}-$Et_3Al_2Cl_3$-ETCA; ○, 78–C5 V_{5-9}-$Et_3Al_2Cl_3$. Sample data in Table I. Continued.
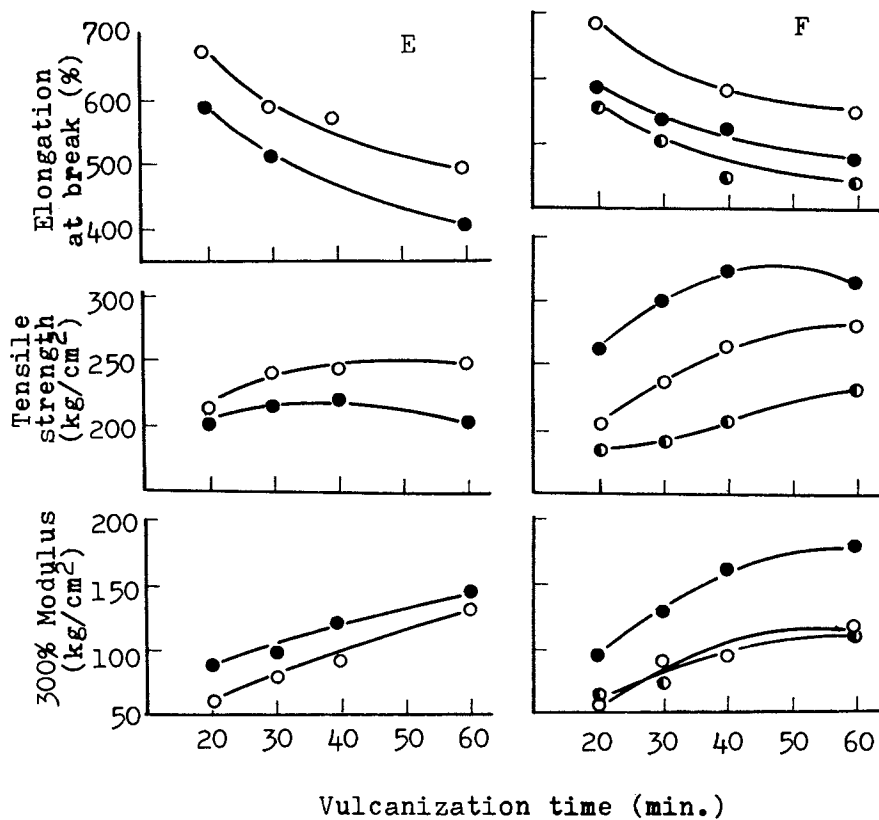
Figure 7. Continued. Tensile properties of comparable samples. Key: (E) ●, 78–C14 V(acac)₃-Et₂AlCl; ○, 78–C6 V₅₋₉-Et₃Al₂Cl₃; (F) ●, 78–C36 V(acac)₃-Et₂AlCl; ○, 78–C24 V₅₋₉-Et₃Al₂Cl₃-ETCA; ○, 78–C29 VOCl₃-Et₃Al₂Cl₃. Sample data in Table I.

Table I   Samples for Vulcanization Comparison of Results[1]

Sample	Catalyst System	[C=C] (mmole/g)	$[\eta]$ (dl/g)	C_3 (mole%)	Comparison Results[1]
78-C33	V_{5-9}-$Et_3Al_2Cl_3$	0.36	1.94	39.9	A modulus and TS higher for V_{5-9}
78-C29	$VOCl_3$-$Et_3Al_2Cl_3$	0.36	1.82	41.9	
78-C 1	V_{5-9}-$Et_3Al_2Cl_3$-ETCA	0.46	2.29	41.2	B modulus and TS higher for V_{5-9}-ETCA
78-C27	$VOCl_3$-$Et_3Al_2Cl_3$	0.44	2.29	41.0	
78-C24	V_{5-9}-$Et_3Al_2Cl_3$-ETCA	0.35	1.72	42.5	C same modulus but higher TS for V_{5-9}-ETCA
78-C11	$VOCl_3$-$Et_3Al_2Cl_3$	0.38	1.65	40.7	
78-C 5	V_{5-9}-$Et_3Al_2Cl_3$	0.62	1.74	39.7	D lower modulus but higher TS for V_{5-9}
78-C19	V_{5-9}-$Et_3Al_2Cl_3$-ETCA	0.55	1.76	40.0	
78-C 6	V_{5-9}-$Et_3Al_2Cl_3$	0.54	1.36	38.3	E lower modulus but higher TS for V_{5-9}
78-C14	$V(acac)_3$-Et_2AlCl	0.59	1.28	38.9	
78-C24	V_{5-9}-$Et_3Al_2Cl_3$-ETCA	0.35	1.72	42.5	F highest modulus and TS for $V(acac)_3$; higher TS for V_{5-9} than $VOCl_3$
78-C29	$VOCl_3$-$Et_3Al_2Cl_3$	0.36	1.82	41.9	
78-C36	$V(acac)_3$-Et_2AlCl	0.38	1.79	40.7	at same modulus

1) Vulcanization data see Figure 7; TS=tensile strength
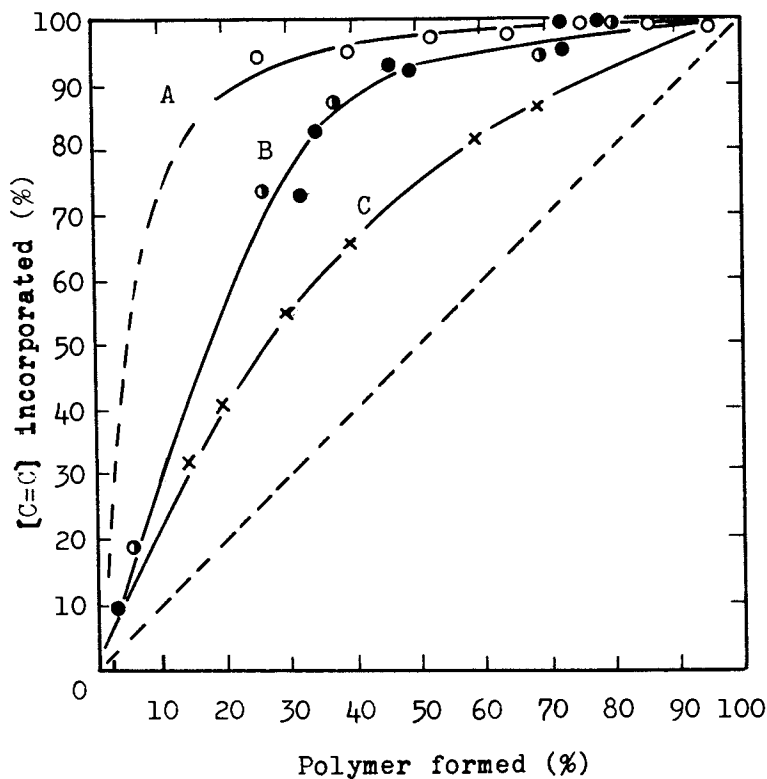
Figure 8.   Incorporation of dicyclopentadiene in EPDMS. Key: A, V$_{5-9}$-Et$_3$Al$_2$Cl$_3$-ETCA; B, V$_{5-9}$-Et$_3$Al$_2$Cl$_3$, Et$_2$AlCl or Et$_3$Al$_2$Cl$_3$/Et$_2$AlCl (1:1); C, V(acac)$_3$-Et$_2$AlCl.

V_{5-9}-EPDM and $VOCl_3$-EPDM vulcanizate tensile strength is not
simply explainable by network quality resulting from differ-
ence in the third monomer distribution in the terpolymers.

In Figure 8 are also reproduced data (curves A and C) of the
other two systems previously given (3). It is clear that although
addition of ETCA to the V_{5-9}-$Et_3Al_2Cl_3$ system makes the DCPD
distribution in the terpolymer much more heterogeneous (curve A,
compared to B) and yields lower vulcanizate tensile strength (see
above), the much more even distribution of DCPD in $V(acac)_3$-EPDM
(curve C, compared to B) did not bring about any improvement in
tensile properties of the latter over those of the V_{5-9}-EPDM.
Thus, the difference in uniformity of third monomer distribution,
though critical as it should be so far as the network perfection
is concerned, is not large enough to compensate for the effects
exerted by some other structural factors that make the V_{5-9}-EPDM
to excel in tensile properties.

Effect of Molecular Weight Distribution

High MW fraction in EPDM ought to contribute favorably to
the vulcanizate tensile properties (9.). The following prelimi-
nary observations were gathered to examine whether difference in
tensile strength of samples prepared with various catalysts
studied was due primarily to the difference in MWD of the ter-
polymers.

The drop in tensile strength of V_{5-9}-EPDM upon addition of
the activator ETCA (see above) was accompanied by a gradual
reduction leading to the disappearance of the high MW hump on the
GPC profiles (Figure 9). Conclusion as to the direct influence
of the high MW fraction on the tensile strength is cautioned by
the fact that addition of ETCA was accompanied by a simultaneous
decrease in $[\eta]$.

The polydispersity index, $\overline{M}_w/\overline{M}_n$, values of comparable samples
78-C24 (V_{5-9}, plus ETCA) and 78-C11 ($VOCL_3$, no ETCA) in Figure
7C were 3.95 and 4.79, respectively. Another set of comparable
samples 78-C19 (V_{5-9}, plus ETCA) and 78-C5 (V_{5-9}, no ETCA) had
$\overline{M}_w/\overline{M}_n$ values of 2.94 and 5.15, respectively. These limited data
show that samples with higher polydispersity do not necessaily
give higher tensile strength.

Furthermore, it has to be noted that both $VOCl_3$- and V_{5-9}-
EPDMs have multimodal GPC profiles signifying the presence of
high MW fractions, yet they have the greatest disparity in
vulcanizate tensile properties, again suggesting MWD to be not
a major determinant in defining the observed tensile differences.

Vulcanizate Tensile Strength of E-P Copolymers (EPM)

To circumvent any effect on tensile properties that might
have concurred in the presence of the third monomer, hydro-
peroxide curing of E-P copolymer samples comparable in $[\eta]$ and
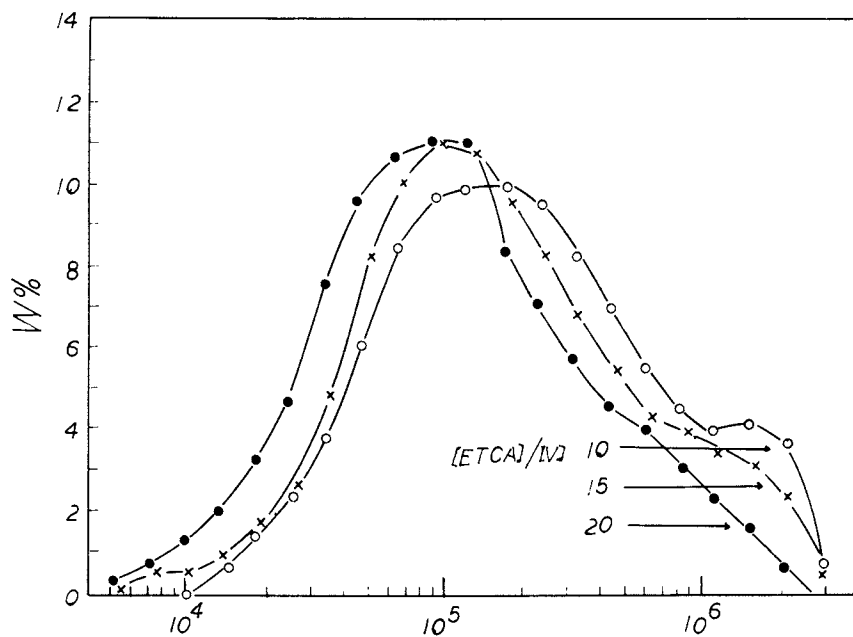
Figure 9. Gel permeation chromatographs of EPDMs. The effect of ETCA addition on MWD of EPDMs prepared with V_{5-9}-$Et_3Al_2Cl_3$ (3). Key: ○, ETCA/V = 10; ✕, ETCA/V = 15; ●, ETCA/V = 20.

$C_3\%$ prepared with different catalyst systems was carried out
(Figure 10). V_{5-9}-EPM still attains the highest strength as
compared to the others, and the tensile strength of $V(acac)_3$-
EPM is higher than that of $VOCl_3$-EPM before "reversion". Thus,
the order of magnitude in the strength of the three terpolymers
is retained in the copolymer series. The lower strength of acti-
vated V_{5-9}-EPM than that of $VOCl_3$-EPM, different from results with
the terpolymers, is probably due to the lower $[\eta]$ of the former.

   Since copolymers contain only ethylene and propylene and $[\eta]$
values of the samples are practically the same, it suggests that
monomer sequence length distribution along molecular chains and
long-chain branching might play a role in determining the strength
of the EPDM vulcanizates.

   A study of the difference in monomer sequence length distri-
bution and hence of the possibility of strain-induced crystalliza-
tion and other structural parameters, including long-chain branch-
ing, of samples prepared with the above-mentioned various catalyst
systems is under way and constitutes the subject of a subsequent
paper.
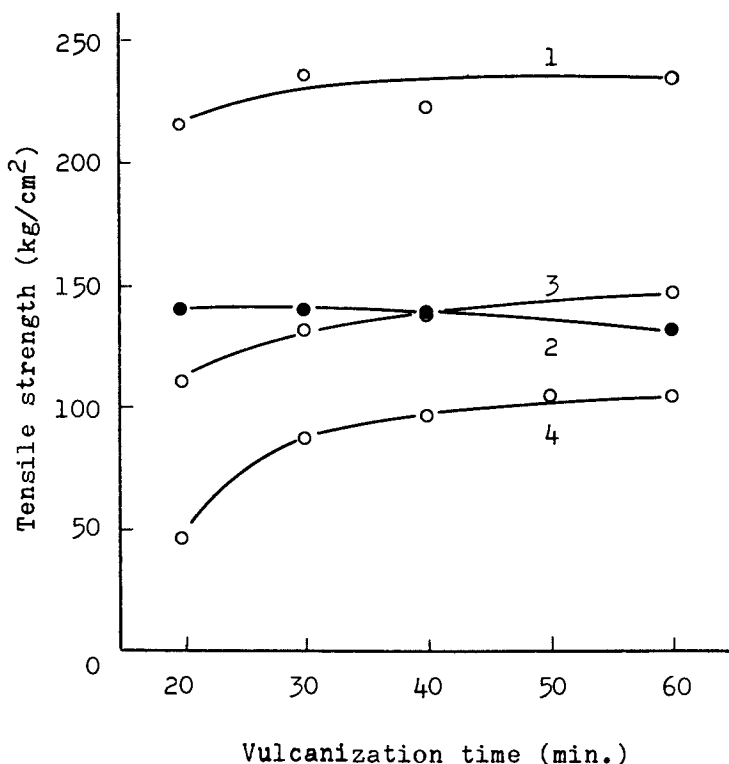
Figure 10.   Vulcanization of E-P copolymers.

EDITOR'S NOTE: (1) The mixing of carbon black was carried out on a two-roll mill. The dispersion of carbon black in the compounded recipes was not evaluated. (2) X-ray studies of the copolymers by the author are in progress. (3) GPC data are relative and may not be comparable to those obtained with commercial instruments.

ACKNOWLEDGMENT

LITERATURE CITED

1. Baldwin, F.P.; Ver Strate, G. Rubber Chem. Technol. 1972, 45, 709.
2. Cesca,S. Macromol. Reviews 1975, 10, 1.
3. Huang, B.T.; Zhang, L. Z.; Zhao, L. T.; Yu, M.; Wu, K. G.; Li, Y. L.; Hu, B. Y. in "Proceedings of China-U.S. Bilateral Symposium on Polymer Chemistry and Physics"; Science Press ; Beijing, and Van Nostrand Company; New York, 1981; p 399.
4. Huang, B. T.; Chen, B. K. Fenxi Huaxue (Analytical Chemistry) 1977, 5, 200.
5. Wei, P. E. Anal. Chem. 1961, 33, 215.
6. Reikh, V. N.; Salnis, K. Yu.; Samoletova, V. V.; Ivanova, L. S.; Milkhailova, S. A. Kauchuk i Rezina 1961 (6), 1.
7. Yu, M. Hecheng Xiangjiao Gongye (Synthetic Rubber Industry) 1980, 169.
8. Emde, H. Angew Makromol. Chem. 1977, 60/61, 1.
9. Natta, G.; Crespi, G. J. Polymer Sci. 1962, 61, 83.

Quasi-living Carbocationic Polymerization of Alkyl Vinyl Ethers and Block Copolymer Synthesis

MITSUO SAWAMOTO[1] and JOSEPH P. KENNEDY

The University of Akron, Institute of Polymer Science, Akron, OH 44325

Quasiliving carbocationic polymerizations of isobutyl vinyl ether (IBVE) and methyl vinyl ether (MVE) were achieved with the bifunctional p-dicumyl chloride (p-DCC)/AgSbF$_6$ initiating system in CH$_2$Cl$_2$ solvent at -70 or -90°C. The quasiliving polymerizations were effected by slow and continuous monomer addition to a premixed initiator solution (quasiliving technique). The number-average molecular weight ($\overline{M}_n$) of polymers increased linearly with the cumulative weight of added monomer (W), and linear $\overline{M}_n$ versus W plots passing through the origin have been obtained. The polymers exhibited narrow molecular weight distributions with $\overline{M}_w/\overline{M}_n$ = 1.4 - 1.7. Polar solvents (CH$_2$Cl$_2$) and lower temperatures (-70 or -90°C) were optimum for these quasiliving polymerizations. Blocking MVE and α-methylstyrene (αMeSt) from quasiliving polymer (IBVE) dications led to novel triblock copolymers: poly(MVE-b-IBVE-b-MVE) and poly(αMeSt-b-IBVE-b-αMeSt), respectively.

"Living" carbocationic polymerizations are most difficult to achieve mainly because of chain transfer to monomer and termination processes both of which frequently occur in carbocationic polymerizations. It has recently been demonstrated (1) that "quasiliving" polymerization of α-methylstyrene (αMeSt) can be achieved by slow and continuous monomer addition and that the number-average molecular weight ($\overline{M}_n$) of PαMeSt increases linearly with the weight of added monomer. A theory for quasiliving polymerizations has been developed (2).

[1] Current address: Kyoto University, Department of Polymer Chemistry, Kyoto 606, Japan.

This paper concerns the quasiliving cationic polymeriza-
tions of isobutyl vinyl ether (IBVE) (3,4) and methyl vinyl ether
(MVE) induced by the bifunctional p-dicumyl chloride (p-DCC)/
silver hexafluoroantimonate (AgSbF$_6$) initiating system. This bi-
functional initiating system was selected because our intention
was to generate two-headed quasiliving growing species that in
turn was expected to lead to triblock polymers. Initiation and
propagation in the p-DCC/AgSbF$_6$/IBVE system, for example, is vis-
ualized to occur as follows:
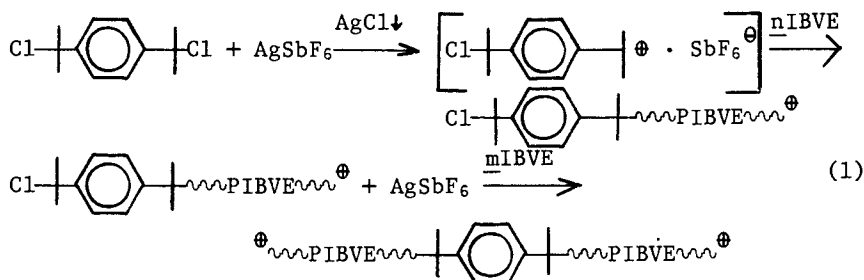
To facilitate ionization of p-DCC, it was premixed with AgSbF$_6$
prior to monomer introduction. The p-dicumyl cation [(CH$_3$)$_2$C$^{\oplus}$-
C$_6$H$_4$-C$^{\oplus}$(CH$_3$)$_2$] may also form during premixing.
     The polymerization behavior of polar alkyl vinyl ethers and
nonpolar olefins (such as αMeSt) are quite different. The pro-
pagating carbocations derived from alkyl vinyl ethers are more
stable than those of hydrocarbon olefins. The high stability of
growing vinyl ether cations is advantageous for quasiliving po-
lymerizations. Although previous studies on IBVE polymerization
suggest the involvement of long-lived growing species (5,6) or
the absence of termination (7,8,9), "living" or "quasiliving" po-
lymerizations of alkyl vinyl ethers have not yet been achieved.
     Applying the slow and continuous monomer-addition (quasi-
living) technique, we polymerized IBVE and MVE with the p-DCC/
AgSbF$_6$ initiating system and defined optimum reaction conditions
for the quasiliving polymerization of these monomers. Subsequent
block polymerization starting poly(IBVE) quasiliving dications led
to novel triblock polymers: poly(αMeSt-b-IBVE-b-αMeSt) and poly-
(MVE-b-IBVE-b-MVE).

Experimental Section

     Materials. Commercial IBVE (GAF Corp.) and αMeSt (Aldrich)
were washed with 10% aqueous sodium hydroxide and water, drived
overnight over sodium sulfate, and freshly distilled twice over
calcium hydride under dry nitrogen. MVE (Matheson, purity >
99.5%) and AgSbF$_6$ (Cationics Inc. and Alfa) were used as received.
The latter was protected from light during storage and handling.
p-DCC was prepared as reported (10,11). n-Heptane (Aldrich),

toluene (Fisher), and methylene chloride (Fisher) were purified
by the usual methods.

Polymerization by Slow and Continuous Monomer Addition.
Polymerizations were carried out under dry nitrogen in a 300-cm^3
three-neck, round-bottom flask equipped with a stirrer, a Teflon
plug for monomer addition, and a serum cap for sampling. First
p-DCC and AgSbF$_6$ solutions (200 cm^3 in total) were mixed and
stirred for one minute at the desired temperature. To this pre-
mixed initiator charge the monomer was added slowly but continu-
ously at a controlled addition rate: IBVE (mostly 25 vol% solu-
tion) was introduced through a precision solvent-metering pump
(Beckman Model 110A) and a glass capillary outlet; MVE was direct-
ly condensed into the reactor from a lecture bottle with a regu-
lating valve through Tygon tubing. At desired times known
amounts of aliquots were withdrawn with a syringe from the reac-
tion mixture and were injected into capped vials containing a few-
cm^3 methanol. After filtration and evaporation of volatiles
yields were determined by gravimetry.

Blocking from Quasiliving Poly(IBVE) Dication. The quasi-
living poly(IBVE) dication was prepared as described above. At a
desired time IBVE addition to the reactor was discontinued, an
aliquot sample was withdrawn with a syringe, and blocking was ef-
fected by introducing the second monomer (αMeSt or MVE) continu-
ously to the reaction mixture. αMeSt (25 vol% solution) was add-
ed through the precision pump; gaseous MVE was directly condensed
into the reactor (see above). The reaction was quenched with pre-
chilled methanol (30 cm^3). After filtering off the silver chlo-
ride, the reaction mixture was concentrated to ca. 30 cm^3 by
evaporation and fractionated with 2-propanol (700 cm^3) for αMeSt-
IBVE blocks or an n-heptane (500 cm^3)/water (200 cm^3) mixture for
MVE-IBVE blocks.

Polymer Characterization. Molecular weight distributions
(MWD) were determined by gel permeation chromatography (GPC) on a
Waters 6000A chromatograph equipped with μStyragel columns. $\overline{M}_n$
and $\overline{M}_w/\overline{M}_n$ were calculated from GPC traces using polystyrene cali-
bration. $\overline{M}_n$'s thus obtained were in good agreement with the cor-
responding absolute values determined by GPC/low-angle laser
light scattering technique (12). The composition of the blocking
products was determined by ^{1}H-NMR spectroscopy on a Varian T-60
spectrometer (ca. 20 wt% polymers in CCl$_4$).

Results and Discussion

Quasiliving Polymerization of IBVE in CH$_2$Cl$_2$ at -70° and
-90°C. IBVE was polymerized by introducing the monomer slowly
and continuously into a premixed p-DCC/AgSbF$_6$ charge in CH$_2$Cl$_2$
at -70 or -90°C. In all experiments polymer yields at any time

were in good agreement with the cumulative weight of added IBVE, W_{IBVE}, W_{IBVE}, indicating consistently quantitative monomer conversions.

Figure 1 shows a typical set of GPC traces for poly(IBVE)'s obtained at -90°C. The MWD's are narrow ($\overline{M}_w/\overline{M}_n$ = 1.4 - 1.7; see Figure 2) and shifting towards higher molecular weights with time; no significant broadening can be observed.

$\overline{M}_n$ and $\overline{M}_w/\overline{M}_n$ values calculated from these data were plotted against W_{IBVE} (e.g., Figure 2). At both -70 and -90°C $\overline{M}_n$ increases with W_{IBVE}. Importantly, $\overline{M}_n$ versus W_{IBVE} plots are linear over a wide range of W_{IBVE}'s and pass through the origin. At higher W_{IBVE}'s, however, the plots tend to deviate from linearity.

Figure 2 also shows $\overline{M}_n$-W_{IBVE} relationships obtained at different monomer-addition rates (0.35 to 1.68 g/min/200 cm^3). The monomer-addition rate does not seem to affect the $\overline{M}_n$-W_{IBVE} relationships, which give a single straight line passing through the origin with W_{IBVE} <10g, provided the monomer is added slowly and continuously.

The effect of the initial initiator concentration ([p-DCC]$_o$) on $\overline{M}_n$ was studied at -90°C (Figure 3). $\overline{M}_n$ increased at all [p-DCC]$_o$'s and the $\overline{M}_n$ versus W_{IBVE} plots passed through the origin. The slopes of the linear portions of these plots were inversely proportional to [p-DCC]$_o$. Similar results were obtained with samples prepared at -70°C.

These results demonstrate that quasiliving polymerization of IBVE can be achieved by the use of CH_2Cl_2 solvent at -70 or -90°C. This novel quasiliving technique leads to poly(IBVE)'s with controlled (and high) molecular weights and narrow MWD.

Number of Polymer Chains. The quasiliving character of IBVE polymerization is further supported by quantitative analysis. Figure 4 illustrates changes in N, the number of poly(IBVE) chains produced per unit initiator (p-DCC), as a function of W_{IBVE}. N is defined by eq. 2:

$$N = \frac{W_{IBVE}}{\overline{M}_n \cdot [p\text{-}DCC]_o} \qquad (2)$$

In ideal living polymerizations N is equal to unity throughout the experiment. At -70 and -90°C the obtained N values are close to unity and remain unchanged during the early stages of the polymerizations, indicating the presence of quasiliving polymerizations. During the later stages of the polymerization, however, N gradually increased with increasing W_{IBVE}, probably because of chain transfer to monomer.

Effect of Temperature. In experiments carried out at -30° using CH_2Cl_2, $\overline{M}_n$'s increased with W_{IBVE} but the absolute values were an order of magnitude smaller than expected and the $\overline{M}_n$
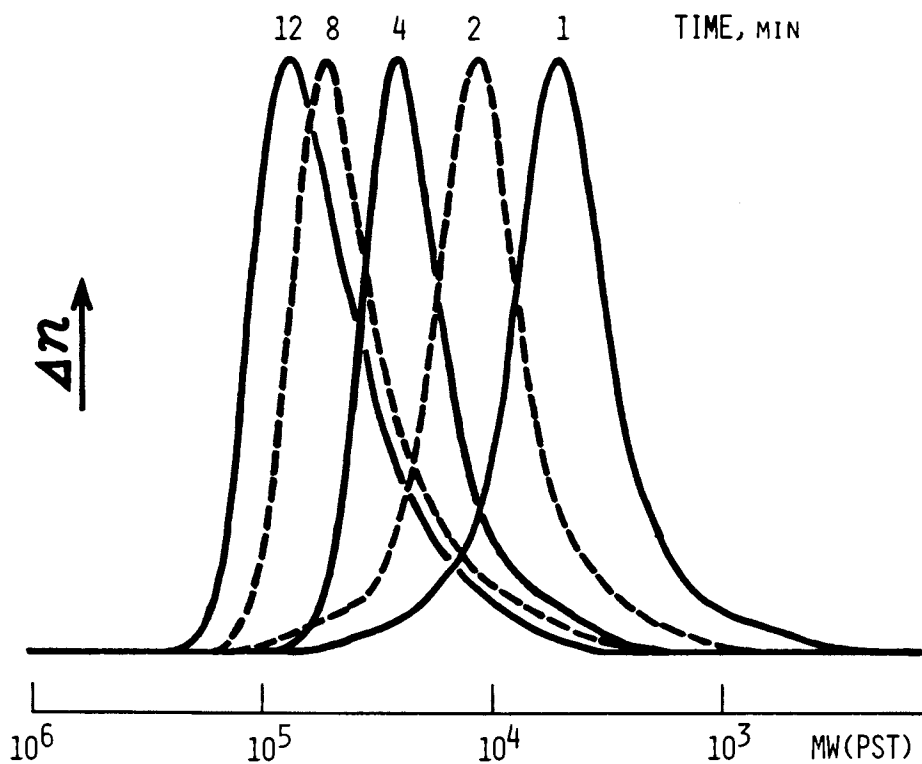
Figure 1. MWD of poly(IBVE) obtained in CH_2Cl_2 at $-90°C$: $[p\text{-}DCC]_o$ is 0.50 mM; $[AgSbF_6]_o$ is 1.1 mM; IBVE addition rate is 0.76 g/min (3).
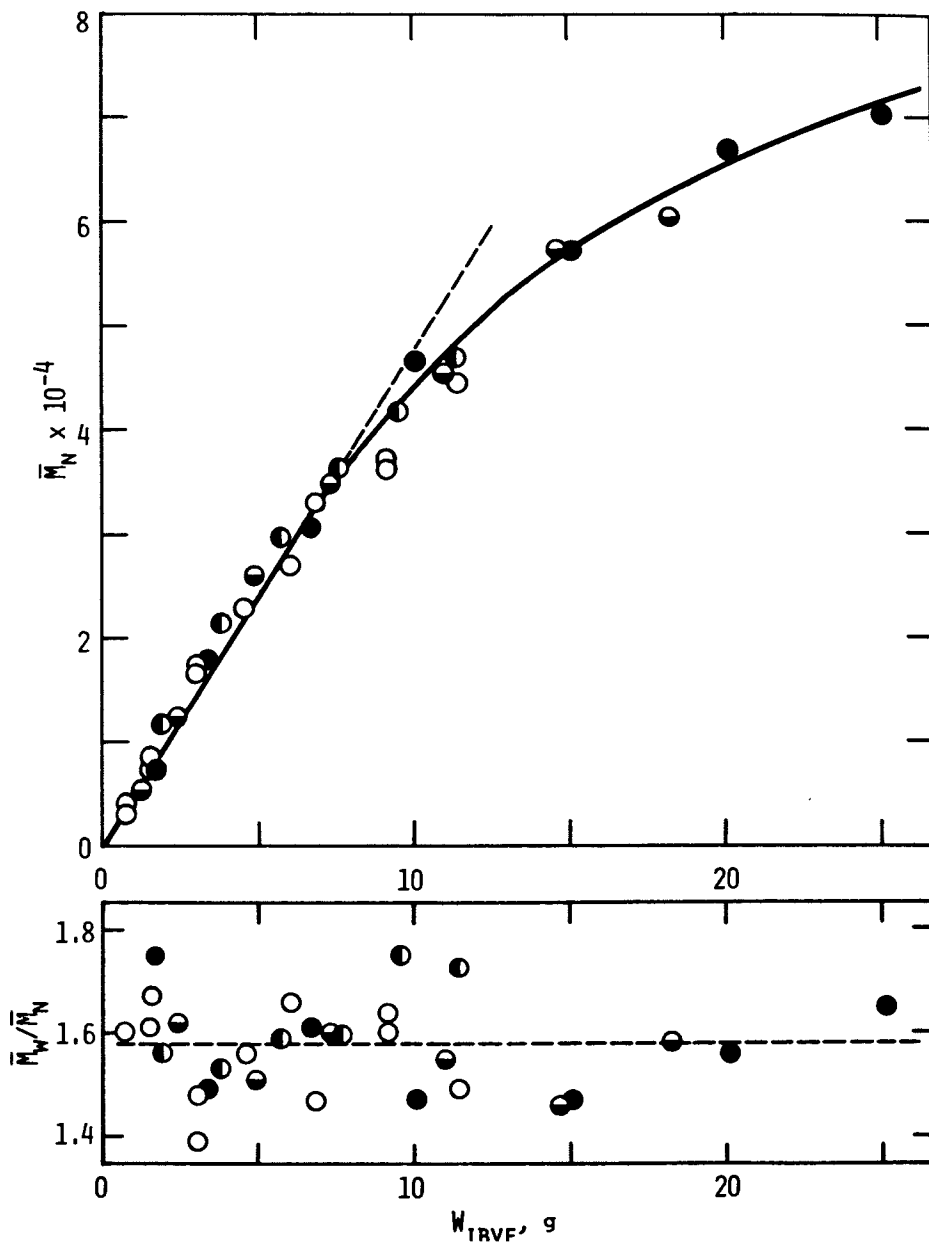
Figure 2. $\overline{M}_n$ and $\overline{M}_w/\overline{M}_n$ as functions of monomer input W_{IBVE} in CH_2Cl_2 at
$-90°C$: $[p\text{-}DCC]_o$ is 0.50 mM; $[AgSbF_6]_o$ is 1.1 mM. IBVE addition rates are
0.38 (◐), 0.76 (○), 1.22 (◑), 1.68 (●).
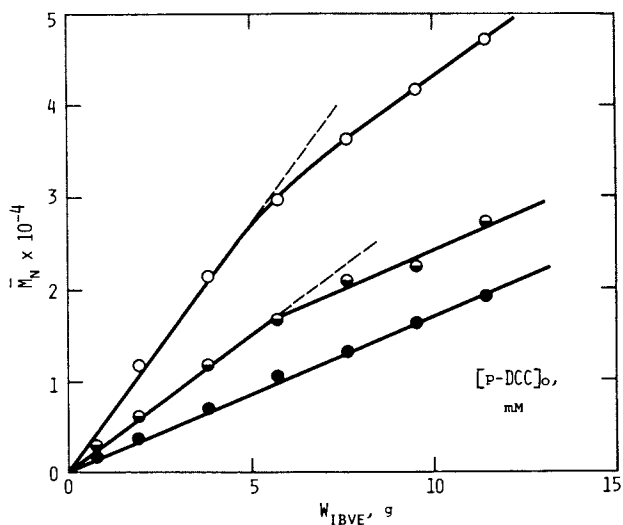
Figure 3. Effect of [p-DCC]$_o$ on M_n — W_{IBVE} relationships in CH_2Cl_2 at $-90°C$.
[p-DCC]$_o$ (mM) and 0.50 (○), 1.0 (◐), 1.8 (●). [AgSbF$_6$]$_o$/[p-DCC]$_o$ is 2.3;
IBVE addition rate is 0.38 g/min (3).
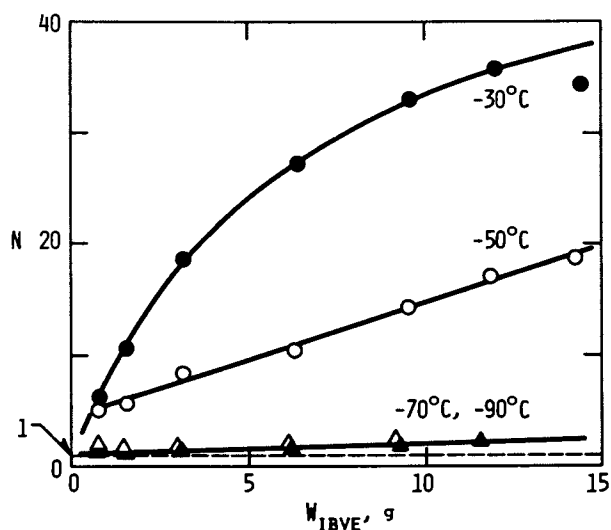
Figure 4. Relationships between monomer input W_{IBVE} and N, the number of
poly(IBVE) chains produced per unit p-DSS molecule, in CH_2Cl_2. [p-DCC]$_o$ is
0.50 mM; [AgSbF$_6$]$_o$ is 1.1 mM; IBVE addition rate is 0.76–0.80 g/min. $-30°C$
(●), $-50°C$ (○), $-70°C$ (▲), $-90°C$ (△), (3).

versus W_{IBVE} plots could no longer be back-extrapolated to the
origin. M_n versus W_{IBVE} plots for -50°C increased continuously
but non-linearly.
        In Figure 4 the number of polymer chains ($\underline{N}$) obtained at
these higher temperatures are compared with those for -70 or
-90°C. In contrast to $\underline{N}$ values obtained at -70 or -90°C which
are close to unity and nearly constant, those for -30 or -50°C
are much higher than unity and increase steeply with W_{IBVE}.
These trends indicate increasing interference of chain transfer
at higher temperatures, i.e., these conditions are not suitable
for quasiliving polymerizations.

        Effect of Solvent Polarity. Quasiliving polymerization of
IBVE was also attempted in a nonpolar solvent, $\underline{n}$-heptane, at -50
and -70°C. Figure 5 gives results obtained at -70°C. The $\overline{M}_n$
versus W_{IBVE} plots obtained at this temperature are strongly
curved. Importantly, the $\underline{N}$ values were less than unity at the
beginning of the reactions and they increased beyond unity with
increasing W_{IBVE}. Evidently initiation is slow in nonpolar media
due to incomplete ionization of the initiator (i.e., $\overline{N}$ >1).
        At -50°C $\overline{M}_n$'s remained unchanged ($\overline{M}_n \sim 3 \times 10^4$, $[\underline{p}\text{-DCC}]_o$ =
0.50 mM) with increasing W_{IBVE} and $\overline{M}_w/\overline{M}_n \sim 2.0$. The polymeriza-
tion is no longer quasiliving but follows a conventional chain-
transfer-dominated course. Nonpolar media are evidently unsuit-
able for quasiliving polymerization of isobutyl vinyl ethers.

        Quasiliving Polymerization of Methyl Vinyl Ether. Similar-
ly to IBVE polymerization, MVE was polymerized with premixed $\underline{p}$-
DCC/AgSbF$_6$ initiating systems in CH_2Cl_2 solvent at -70°C by slow
and continuous monomer addition. Polymer yields were ∿100% at
every reaction time.
        Figure 6 shows plots of $\overline{M}_n$ of poly(MVE) versus the cumula-
tive weight of added MVE, W_{MVE}. $\overline{M}_n$'s increase linearly with in-
creasing W_{MVE} and the lines pass through the origin. $\overline{M}_n$ is higher
at a lower initiator concentration, $[\underline{p}\text{-DCC}]_o$; the slope of the
plots is nearly proportional to the reciprocal of $[p\text{-DCC}]_o$.
        These results show that quasiliving polymerization of MVE
has been achieved by the use of CH_2Cl_2 solvent at -70°C. $\overline{M}_n$'s
obtained at different monomer-addition rates (0.50 to 1.13 g/min/
200 cm^3; Figure 6) lead to a single straight line through the ori-
gin, which indicates that quasiliving conditions can be maintained
independent of the monomer-addition rate in that range.
        The linear $\overline{M}_n$ versus W_{MVE} plots imply that the number of
poly(MVE) chains produced per unit initiator, $\underline{N}$ (cf. eq. 2), is
constant during the polymerization. The absolute values of $\underline{N}$ were
greater than unity (2.50 and 2.79 at $[\underline{p}\text{-DCC}]_o$ = 1.0 and 2.0 $\overline{m}$M,
respectively), suggesting that chain transfer to monomer may have
occurred during the early stages of the polymerization.
        In the polymerization at a higher temperature (-30°C) in
CH_2Cl_2 solvent, $\overline{M}_n$'s were much smaller than expected from $[\underline{p}\text{-DCC}]_o$;
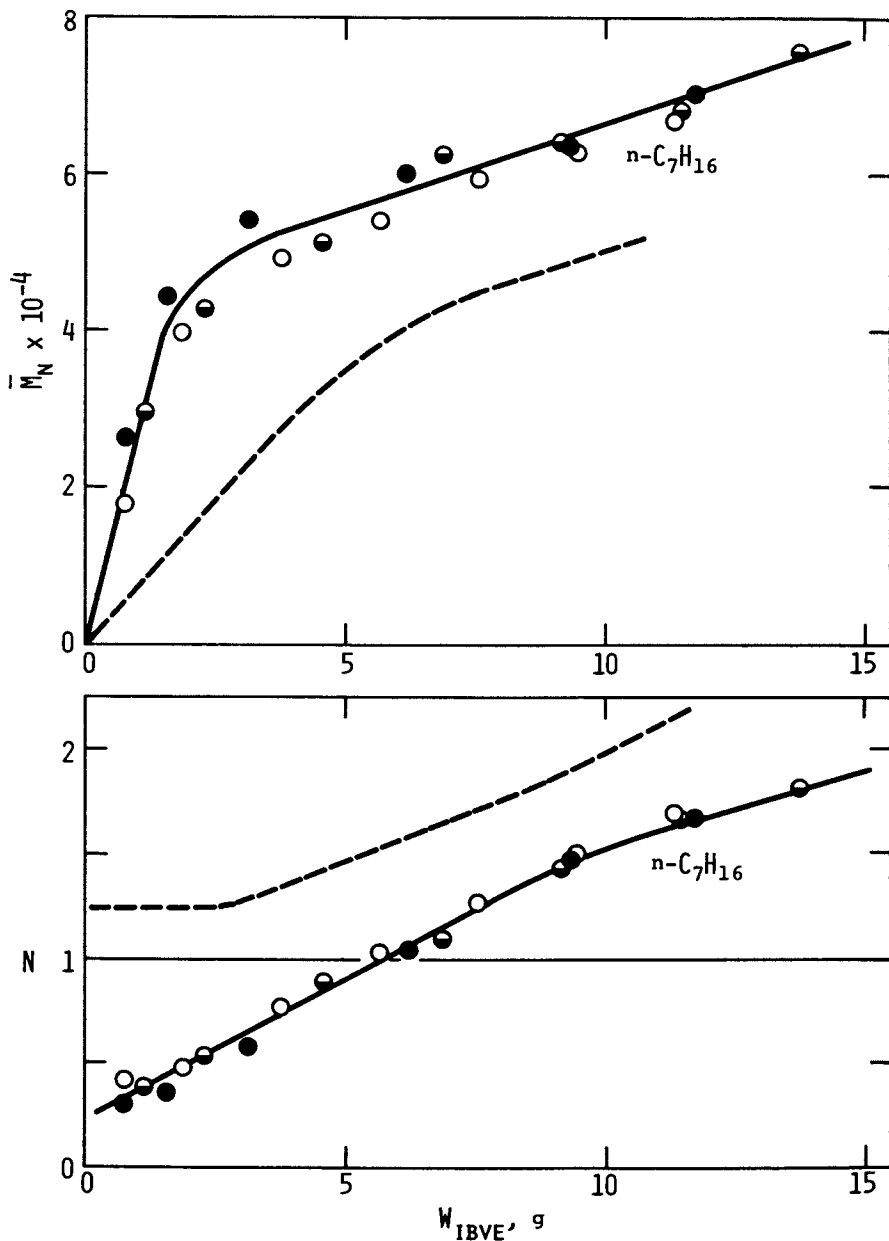
Figure 5. $\overline{M}_n$ *and* N *as functions of monomer input* W_{IBVE} *in n-heptane at* $-70°C$. $[p\text{-}DCC]_o$ *is 0.50 mM;* $[AgSbF_6]_o$ *is 1.1 mM. IBVE addition rates (g/min) are 0.38 (◐), 0.57 (○), 0.78 (●). The dashed lines show the data obtained in* CH_2Cl_2 *under the same conditions.*
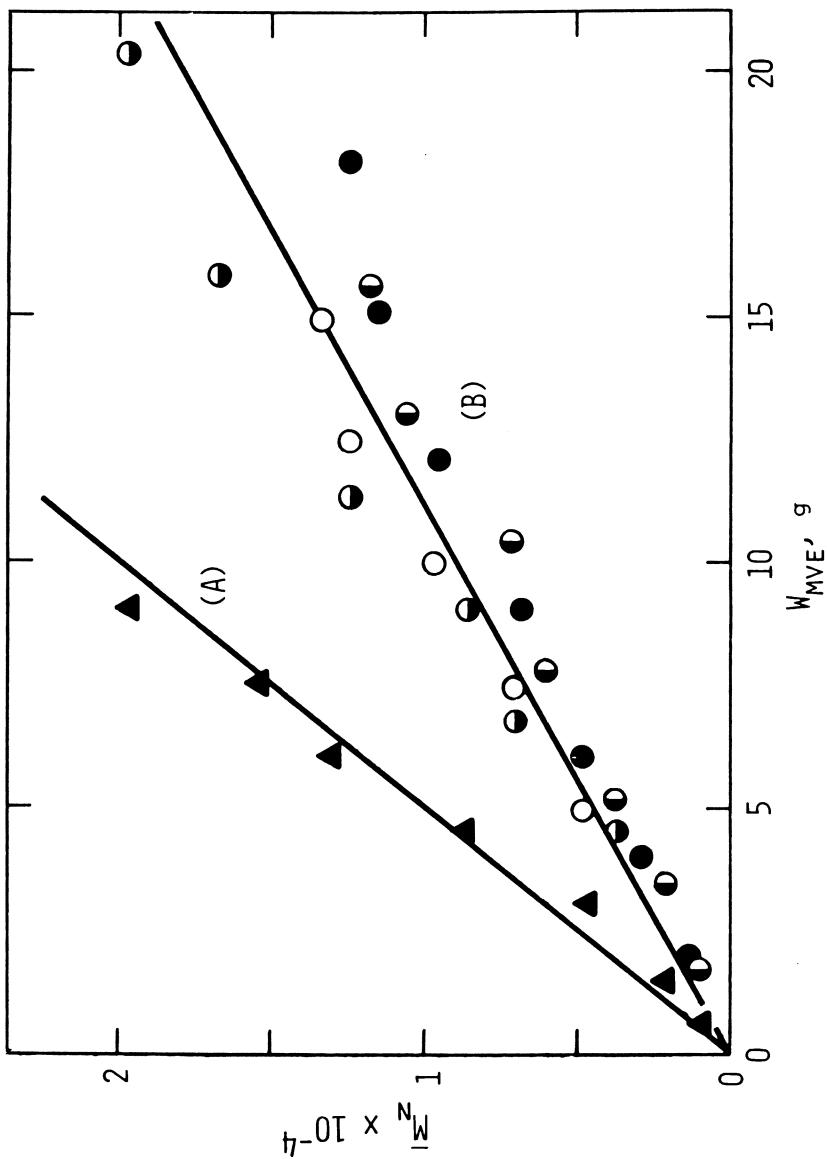
Figure 6. $\overline{M}_n$ as functions of monomer input W_{MVE} in CH_2Cl_2 at $-70°C$. $[p$-$DCC]_0$ (mM): A, 1.0; B, 2.0. $[AgSbF_6]_0/[p$-$DCC]_0$ is 2.3. MVE addition rate (g/min) are 0.30 (▲), 0.50 (○), 0.87 (◑), 1.01 (●), 1.13 (◐).

the $\overline{M}_n$ versus W_{MVE} plots showed an intercept, although $\overline{M}_n$'s increased linearly with W_{MVE}. Polymerizations in a nonpolar solvent (toluene) at $-70°C$ gave strongly curved $\overline{M}_n$ versus W_{MVE} plots; the MWD was broad ($\overline{M}_w/\overline{M}_n$ = 2.4 to 3.9).

Optimum Conditions for Quasiliving Polymerization. Table I summarizes $\overline{M}_n-W_{IBVE}$ relationships obtained under a variety of conditions. The corresponding table for MVE is almost identical. The observed relationships are classified into three categories: 1) (O) Linear $\overline{M}_n$ versus W_{IBVE} plots passing through the origin, indicating quasiliving polymerizations; 2) (X) $\overline{M}_n$ independent of W_{IBVE}, indicating conventional chain-transfer-dominant polymerizations; and 3) (Δ) intermediate cases between (1 and 2), where $\overline{M}_n$ versus W_{IBVE} plots are strongly curved or have an intercept.

TABLE I

$\overline{M}_n-W_{IBVE}$ Relationships under a Variety of Conditions[a]

	Temperature, °C			
Solvent	-90	-70	-50	-30
CH_2Cl_2	O	O	Δ	Δ
$\underline{n}-C_7H_{16}$	—	Δ	X	—

[a] Key:
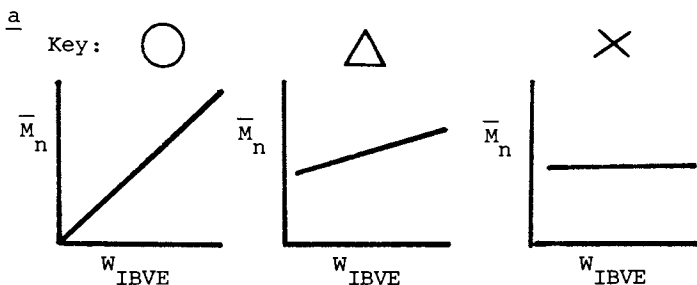
Inspection of Table I shows that optimum conditions for quasiliving polymerization of IBVE (and MVE) prevail in polar

solvents (CH_2Cl_2) and at lower temperatures (-70 or -90°C).
Apparently chain transfer and termination are "frozen out" at low-
er temperatures, and fast initiation and/or re-ionization of dor-
mant growing end are promoted in polar media.

The presence of the ether oxygen in the monomer may or may
not be advantageous for quasiliving polymerizations of alkyl
vinyl ethers in general and IBVE or MVE in particular. Vinyl
ether growing cations are relatively stable and may undergo ter-
minationless polymerization (5-9), however, these monomers are
strongly basic and highly prone to chain transfer to monomer (7,
13, 14). The attainment of quasiliving polymerizations of IBVE
and MVE, as demonstrated in this work, implies that the quasiliv-
ing technique can overcome this drawback by promoting the rever-
sibility of chain transfer to monomer.

Blocking αMeSt or MVE from Quasiliving Poly(IBVE) Dication.
An important application of quasiliving polymerizations may be
for the synthesis of block copolymers. Efforts have been made to
prepare novel block polymers starting from quasiliving poly(IBVE)
dication by the addition of αMeSt and/or MVE as the second mono-
mer. Eq. 3 outlines the principle of the blocking experiments:

$$\text{IBVE} \xrightarrow[\text{CH}_2\text{Cl}_2, \ -70 \text{ or } -90°\text{C}]{\underline{p}\text{-DCC/AgSbF}_6} \overset{\oplus}{\sim\!\sim\!\sim}\text{poly(IBVE)}\overset{\oplus}{\sim\!\sim\!\sim} \xrightarrow{M_2}$$

$$\boxed{\text{poly(M}_2\text{)}} \ \sim\!\sim\!\sim\text{poly(IBVE)}\sim\!\sim\!\sim \boxed{\text{poly(M}_2\text{)}} \qquad (3)$$

$$(M_2 = \alpha\text{MeSt, MVE})$$
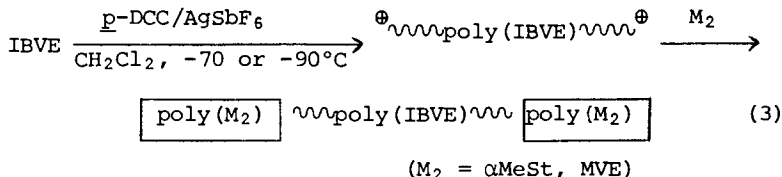
During the second stage of these block polymerizations, αMeSt or
MVE was added slowly and continuously to charges containing qua-
siliving poly(IBVE) dications.

The products obtained in IBVE-αMeSt block copolymerization
were fractionated with 2-propanol, a good solvent for poly(IBVE)
and a nonsolvent for poly(αMeSt). Table II shows molecular
weights and compositions of typical blocking products. Figure 7
illustrates examples of ^{1}H-NMR spectra of the 2-propanol-soluble
and -insoluble fractions.

In expt. C in Table II, for instance, the molecular weight
of the 2-propanol-insoluble fraction was much higher ($\bar{M}_n$ = 30,500)
than that of the starting poly(IBVE) ($\bar{M}_n$ = 7,100). The 2-propanol-
soluble fraction also had an $\bar{M}_n$ (7,700) that was clearly, though
slightly, higher than the starting polymer. The 2-propanol-in-
soluble fractions ranged from 73 to 87 wt% of the products.

^{1}H-NMR spectra of the 2-propanol-insoluble fractions (e.g.,
Figure 7a) exhibited signals due to both αMeSt and IBVE units
(αMeSt, $\delta \sim$ 0.1 and 6.9 ppm; IBVE, $\delta \sim$ 0.9 and 2.8-3.6 ppm), i.e.,
the spectra indicate the presence of both poly(αMeSt) and poly-
(IBVE) segments in these fractions. As 2-propanol-insoluble
fractions cannot contain homopoly(IBVE), the existence of IBVE
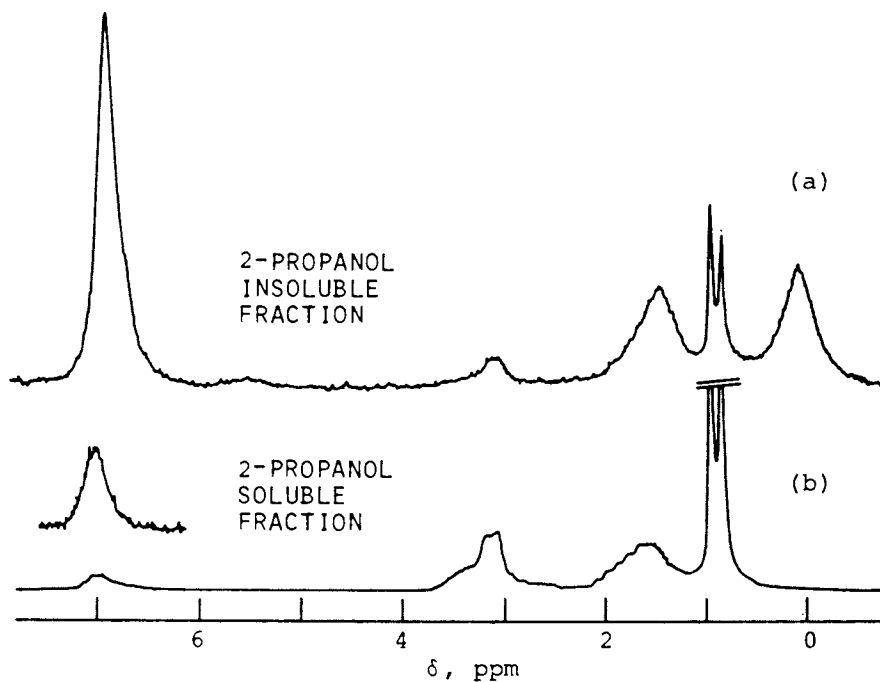
Figure 7. ^{1}H-NMR spectra of the 2-propanol–soluble and –insoluble fractions of IBVE-αMeSt block copolymerization products obtained in experiment A, Table II.

TABLE II

Blocking αMeSt from Quasiliving PIBVE in CH_2Cl_2 at $-90°C$ with
$\underline{p}$-DCC/AgSbF$_6$ Initiator

Expt.	$[\underline{p}\text{-DCC}]_o$,[a]	Feed,[b] wt% IBVE/αMeSt	Fraction(wt%)	Composition,[c] wt% IBVE/αMeSt	$\overline{M}_n$ (GPC)
A	0.50	14/86	Starting PIBVE	100/ 0	10600
			2-PrOH Sol. (13)	89/11	11600
			2-PrOH Insol.(87)	13/87	69100
B	2.0	30/70	Starting PIBVE	100/ 0	6600
			2-PrOH Sol. (22)	90/10	7300
			2-PrOH Insol.(78)	21/79	35700
C	2.0	36/64	Starting PIBVE	100/ 0	7100
			2-PrOH Sol (27)	90/10	7700
			2-PrOH Insol.(73)	29/71	30500

a) $[AgSbF_6]_o$ = 2.3; initial volume of $\underline{p}$-DCC/AgSbF$_6$ charge, 200 cm^3.
b) Expt. A: IBVE, 0.76 g/min, 2 min; αMeSt, 0.91 g/min, 10 min.
   Expt. B: IBVE, 0.37 g/min, 10 min; αMeSt, 0.44 g/min, 20 min.
   Expt. C: IBVE, 0.37 g/min, 10 min; αMeSt, 0.44 g/min, 15 min.
c) Determined by ^{1}H NMR.

units in these fractions is strong evidence for the formation of
IBVE-αMeSt block polymers, which are insoluble in 2-propanol be-
cause of their high αMeSt contents (71 to 87 wt%).
     Although homopoly(αMeSt) should be absent in the 2-propanol-
soluble fractions, ^{1}H NMR spectra of these fractions showed a re-
sonance characteristic of αMeSt units (δ 6.9 ppm) together with
large signals of IBVE units (e.g., Figure 76). Evidently the 2-
propanol-soluble fractions also contain IBVE-αMeSt block polymers
that most likely carry short poly(αMeSt) segments pulled into 2-
propanol by the attached poly(IBVE) segments.
     The formation of IBVE-αMeSt block polymers was further sup-
ported by results of film-casting experiments (12). These data
also show that the starting quasiliving poly(IBVE) dication is
sufficiently reactive to initiate effectively subsequent αMeSt
polymerization.
     Similarly, blocking MVE from quasiliving poly(IBVE) dications
was accomplished. The products were fractionated with a hetero-
geneous mixture of $\underline{n}$-heptane and water (5/2, v/v); the former is a
good solvent for poly(IBVE) only, the latter a good solvent for
poly(MVE) only. The ^{1}H NMR spectra of the $\underline{n}$-heptane-soluble frac-
tions exhibited a sharp resonance at δ 3.3 ppm (-OCH$_3$), character-
istic of MVE units, and a doublet at δ 0.9 ppm (-$\overset{|}{C}$(CH$_3$)$_2$), charac-
teristic of IBVE units. The presence of poly(MVE) segments in
these fractions indicates the formation of IBVE-MVE block polymers.

A full account of the IBVE-MVE block copolymerization will be published separately (12).

Acknowledgment

Literature Cited

1. Faust, R.; Fehérvári, A.; Kennedy, J.P. to be published.
2. Kennedy, J.P.; Kelen, T.; Tüdős, F. to be published.
3. Sawamoto, M.; Kennedy, J.P. Polym. Prepr., Div. Polym. Chem., Am. Chem. Soc. 1981, 22(2), 140.
4. Sawamoto, M.; Kennedy, J.P. Polym. Prepr., Jpn. 1981, 30(6), S2C15.
5. Higashimura, T.; Mitsuhaski, M.; Sawamoto, M. Macromolecules 1979, 12, 178.
6. Ohtori, T.; Hirokawa, Y.; Higashimura, T. Polym. J. 1979, 11, 471.
7. Bawn, C.E.H.; Fitzsimmons, C.; Ledwith, A.; Penfold, J.; Sherrington, D.C.; Weightman, J. A. Polymer 1971, 12, 119.
8. Chung, Y.J.; Rooney, J.M.; Squire, D.R.; Stannett, V.T. Polymer 1975, 16, 527.
9. Rooney, J.M.; Squire, D.R.; Stannett, V.T. J. Polym. Sci., Polym. Chem. Ed. 1976, 14, 1877.
10. Kennedy, J.P.; Smith, R.A. J. Polym. Sci., Polym. Chem. Ed. 1980, 18, 1523.
11. Chang, V.S.C.; Kennedy, J.P.; Iván, B. Polym. Bull. 1980, 3, 339.
12. Sawamoto, M.; Kennedy, J.P. to be published.
13. Imanishi, Y.; Higashimura, T.; Okamura, S. Kobunshi Kagaku 1962, 19, 154.
14. Imanishi, Y.; Nakayama, H.; Higashimura, T.; Okamura, S. Kobunshi Kagaku, 1962, 19, 565.

Polyphosphazene Elastomers:
Synthesis, Properties, and Applications

ROBERT E. SINGLER and GARY L. HAGNAUER

Army Materials and Mechanics Research Center, Polymer Research Division, Watertown, MA 02172

RICHARD W. SICKA

Firestone Tire & Rubber Co., Central Research Laboratories, Akron, OH 44317

   The synthesis of a unique class of polymers
with a phosphorus nitrogen backbone is described,
with an emphasis on poly(dichlorophosphazene)
and poly(organophosphazene) elastomers. Poly
(dichlorophosphazene) can be prepared by high temperature
melt or solution polymerization techniques, with
or without the use of catalysts. High performance
GPC and other dilute solution techniques have been
used to monitor yield and to analyze molecular
weight, molecular weight distribution, and chain
structure. Although poly(dichlorophosphazene) is
an elastomer, it must be modified in order to obtain
long term hydrolytic stability and other useful
properties. From a common poly(dichlorophosphazene)
intermediate, one can introduce a variety of substituents
giving polyorganophosphazenes with a wide range
of physical properties. Some of the useful properties
of phosphazene elastomers and their technological
significance will be shown. This article concludes
with a brief mention of alternate synthetic methods
which may lead to useful polyphosphazene elastomers.

The study of open-chain polyphosphazenes has attracted
increasing attention in recent years, both from the standpoint
of fundamental research and technological development. These
polymers have been the subject of several recent reviews
(1-6). Interest has stemmed from the continuing search for
polymers with improved properties for existing applications
as well as for new polymers with novel properties. The polyphos-
phazenes are highly flexible chains of alternating phosphorus-
nitrogen atoms with two substituents attached to the phosphorus
atom. Although the properties of the polyphosphazenes are
influenced to a degree by the molecular weight and chain
structure, the properties are determined largely by the size
and the nature of the substituent attached to the phosphorus-

nitrogen (P-N) backbone. For the purpose of this paper,
we shall classify polyphosphazenes into two groups, the poly
(halophosphazenes) and the poly(organophosphazenes). Both
groups contain elastomers, and several poly(organophosphazenes)
are currently of interest for commerical development.

Poly(halophosphazenes)

Poly(dichlorophosphazene). Most of the interest in
the poly(halophosphazenes) has centered around poly(dichlorophos-
phazene). The thermal conversion of hexachlorocyclotriphosphazene
(I) to the rubbery poly(dichlorophosphazene) has been known
since the turn of the century (7). This transparent inorganic
polymer exhibits many of the properties of a good elastomer
except that prolonged exposure to a moist atmosphere results
in hydrolysis and degradation with an attendant loss of useful
physical properties. Early attempts to stabilize this "inorganic
rubber" by replacing the chlorine groups with organic substituents
were unsuccessful and interest was rather limited. However,
in 1965, Allcock demonstrated that stable poly(organophosphazenes)
could be prepared from soluble, open-chain poly(dichlorophos-
phazene) (8,9), and work with these inorganic backbone polymers
has increased significantly.

The polymerization of hexachlorocyclotriphosphazene
(I) has been the subject of numerous investigations (9,10).
The polymerization reaction (Figure I) is markedly influenced
by the presence of trace impurities which was one of the
difficulties encountered in earlier investigations. The
conventional route is a melt polymerization of highly purified
trimer $(NPCl_2)_3$ or a mixture of trimer and a small amount
of tetramer $(NPCl_2)_4$, sealed under vacuum in glass ampoules,
at approximately 250°C. Proper selection of time and tempera-
ture is necessary to obtain II and avoid the formation of
cross-linked matrix (III).

More recent studies (4,10) have shown that various acids
and organometallic compounds can serve as catalysts for the
preparation of II. The advantages include lower polymerization
temperatures, higher yields, lower molecular weights, and
the use of conventional large scale equipment. Examples
include bulk polymerizations using H_2O (11), $Et_3Al_2Cl_3$ (12),
$CrCl_3 \cdot 6H_2O$ (13), $(C_6H_5O)_3PO-BCl_3$ (14), polyphosphoric acid
catalyst in trichlorobenzene (15) and sulfur catalyst in
decalin (16).

Recently, gel permeation chromatography (GPC) and other
dilute solution techniques have been directly applied to
the characterization of II (17-20). In our laboratory we
have examined II prepared by the uncatalyzed bulk and solution
polymerization processes. Polymers obtained from the former
process have high molecular weights (MWs) and broad molecular
weight distributions (MWDs, Mw/Mn≈5). The dilute solution

parameters indicate the polymers obtained at low conversions
are randomly coiled in solution. Representative GPCs are
given in Figure 2. Note the bimodal distribution at 100 hr;
this may indicate a change in the polymerization mechanism
at longer times and higher conversions (20).

In contrast to the uncatalyzed bulk polymerization described
in the preceeding paragraph, a catalyzed solution polymerization
using polyphosphoric acid in trichlorobenzene (TCB) gave
a slightly lower MW for poly(dichlorophosphazene) but with
a significantly narrower MWD, Mw/Mn≈1.5 (Figure 3). No gel
formation was observed in this experiment. The solution
polymerization proceeds more rapidly than the uncatalyzed
bulk polymerization, but gel formation (4%) was observed
during the solution polymerization after 16 hrs. at 22% overall
conversion (20).

The elastomeric properties of poly(dichlorophosphazene) have
been the subject of various investigations over the years.
Probably most of these investigators were studying poly(dichloro-
phosphazene) in the partially crosslinked state. Most of
this was summarized by Allcock (9). More recently, highly
purified, uncrosslinked II has been examined in the solid
state (21). The unstressed polymer is amorphous at room
temperature, but crystallization can be induced by cooling
or stretching techniques. The glass transition temperature,
measured by Torsional Braid Analysis, is -66°C (22).

Poly(difluorophosphazene). A brief mention will be made
of poly(difluorophosphazene) $(NPF_2)_n$, which was first reported
by Seel and Langer (23) and has been investigated in greater
detail by Allcock (24). It is prepared by the bulk polymeriza-
tion of hexafluorocyclotriphosphazene $(NPF_2)_3$ at 350°C.
Poly(difluorophosphazene) is an elastomer with a glass transition
temperature of -96°C (for $(NPCl_2)_n$, T_g = -66°C) and a crystalline
melting temperature of -68°C. If care is taken during the
trimer purification and polymerization, $(NPF_2)_n$ can be obtained
as an uncrosslinked white elastomer which can be reacted
with organometallic agents to prepare poly(organophosphazenes)
with phosphorus-carbon bonds (25).

$$[NPF_2]_n \xrightarrow[\text{2) } CF_3CH_2ONa]{\text{1) } C_6H_5Li} [NP(C_6H_5)_x(OCH_2CF_3)_y]_n$$
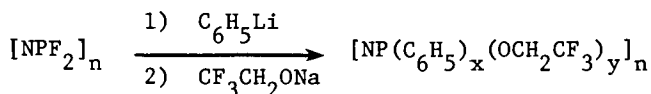
Poly(organophosphazenes)

Synthesis-Structure-Properties. Poly(dichlorophosphazene)
is important as an intermediate for the synthesis of a wide
range of poly(organophosphazenes) (Figure I). The nature
and size of the substituent attached to phosphorus plays
a dominant role in determining the properties of the polyphospha-
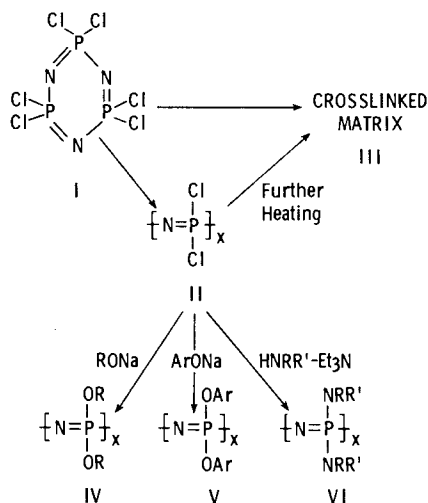
Figure 1.   Synthesis of poly(dichlorophosphazene) and poly(organophosphazenes).
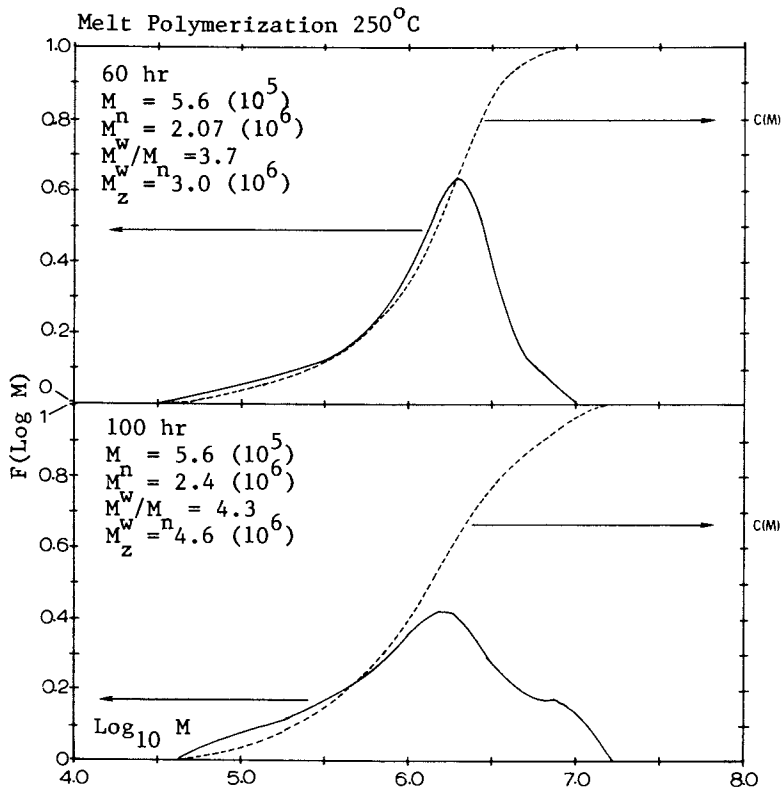
Figure 2.   GPC studies of melt polymerized poly(dichlorophosphazene). Cumulative C(M) and differential F(log M) MWD of II obtained at 60 and 100 h. Ref. 20.
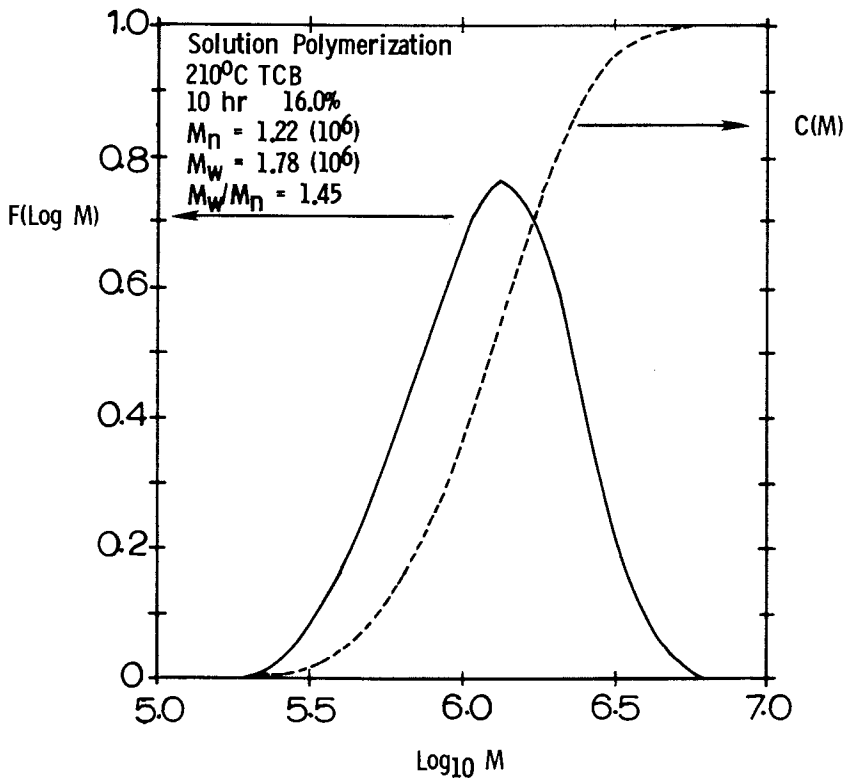
Figure 3. Cumulative C(M) and differential F(log M) MWD of solution polymerized II. Solvent for the polymerization was trichlorobenzene (TCB). Ref. 20.

zenes. If complete replacement of chlorine is not achieved
upon substitution, the resulting polymer may be an elastomer
with properties often quite different from the fully substituted
polymer. The glass transition temperatures (T_g's) vary from
$-84°C$ for $[NP(OCH_2CH_3)_2]_n$ to around $100°C$ for the poly(anilino-
phosphazenes) $[NP(NHAr)_2]_n$. The poly(organophosphazenes) vary
from elastomers to flexible film forming thermoplastics and
glasses at room temperature. Some are highly solvent resistant,
whereas others like certain poly(aminophosphazenes) are water
soluble. This wide range of properties, based on the same
polymer chain, is unique in polymer chemistry.

Poly(alkoxyphosphazenes) (IV) and Poly(aryloxyphosphazenes) (V).
These classes (IV, V) of poly(organophosphazenes) are worthy
of interest since they contain both semicrystalline thermo-
plastics and elastomers (Figure 4). This dramatic change
in properties can arise by employing certain nucleophiles
or combinations of nucleophiles in the substitution process
(Figure 5). Homopolymers prepared from II such as $[NP(OCH_2CF_3)_2]_n$
are flexible film-forming thermoplastics (8). With the intro-
duction of two or more substituents of sufficiently differ-
ent size, elastomeric mixed substituent polymers are obtained
(Figure 5). This principle was first demonstrated by Rose
(26) who used a mixture of fluoroalkoxides during the sub-
stitution step to obtain a fluoroelastomer $[NP(OCH_2CF_3)(OCH_2C_3F_7)]_n$
with excellent chemical resistance and low temperature flexibility
($T_g = -77°C$).   The substitution reaction can be further
modified to allow for the addition of a small amount ($\sim 1\%$)
of a reactive pendant group along with the fluoroalkoxides
providing "terpolymers" with more reactive curing sites to
facilitate crosslinking and rubber processing.

     With the mixed substituent polymers or copolymers, struc-
tures such as $[NP(OR)(OR')]_n$ are only an average representation,
since a random distribution of pendant groups is more likely
(Figure 5). This assumes an equal preference for incoming
groups during the substitution process. If the groups are
not sufficiently different in size or nature, the copolymers
such as $[NP(OC_6H_4-4-Cl)(OC_6H_4-4-C_2H_5)]_n$ or $[NP(OC_6H_5)(OC_6H_4-4-OCH_3)]_n$ can be crystalline (27,28).
     The effect of the substituent on the properties of
the polyphosphazenes is not fully understood. For instance,
$[NP(OCH_3)_2]_n$ and $[NP(OCH_2CH_3)_2]_n$ homopolymers are elastomers
(8,29). Synthesis using lithium, in contrast to sodium,
salts is claimed to produce rubber-like fluoroalkoxyphosphazene
polymers (30). The presence of unreacted chlorine or low mole-
cular weight oligomers can affect the bulk properties (31,32).
Studies with phosphazene copolymers both in solution and
in the bulk state (29,33-38) indicate a rather complex structure,
which points out the need for additional work on the chain
structure and morphology of these polymers.

SEMICRYSTALLINE THERMOPLASTICS

$$\begin{array}{ccc}
\text{OCH}_2\text{CF}_3 & \text{O}-\langle\bigcirc\rangle & \text{O}-\langle\bigcirc\rangle\text{CH}_3 \\
\{\text{P=N}\}_n & \{\text{P=N}\}_n & \{\text{P=N}\}_n \\
\text{OCH}_2\text{CF}_3 & \text{O}-\langle\bigcirc\rangle & \text{O}-\langle\bigcirc\rangle\text{Cl}
\end{array}$$

ELASTOMERS

$$\begin{array}{ccc}
\text{OCH}_2\text{CH}_3 & \text{OCH}_2\text{C}_3\text{F}_6\text{CF}_2\text{H} & \text{O}-\langle\bigcirc\rangle \\
\{\text{P=N}\}_n & \{\text{P=N}\}_n & \{\text{P=N}\}_n \\
\text{OCH}_2\text{CH}_3 & \text{OCH}_2\text{CF}_3 & \text{O}-\langle\bigcirc\rangle\text{C}_2\text{H}_5
\end{array}$$
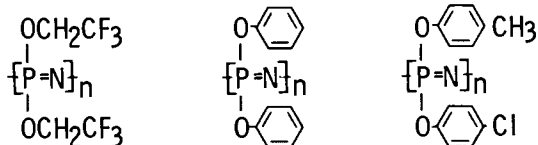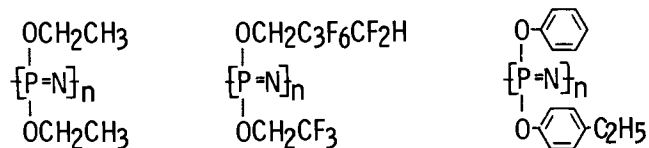
Figure 4. Typical poly(organophosphazene) plastics and elastomers.

$$\{\text{N=P}\}_n \text{ (Cl, Cl)} \xrightarrow{\text{2 NaOR}} \{\text{N=P}\}_n \text{ (OR, OR)}$$

NaOR

NaOR'

$$\{\text{N=P}\}_n \text{ (OR, OR')}$$

$$\left\{ \begin{array}{ccc} \text{OR} & \text{OR'} & \text{OR'} \\ -\text{N=P}- & -\text{N=P}- & -\text{N=P}- \\ \text{OR} & \text{OR} & \text{OR'} \end{array} \right.$$
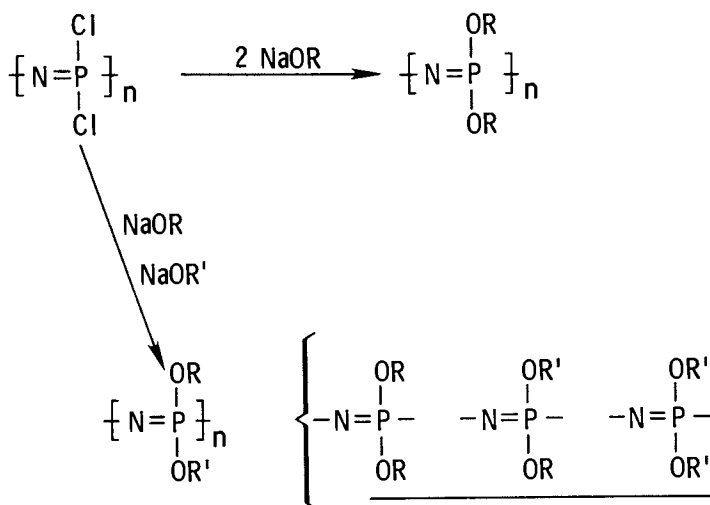
Figure 5. Contrasting synthesis of homopolymers and copolymers with possible copolymer structures.

Poly(aminophosphazenes) (VI). The poly(aminophosphazenes) also
cover a range of properties, but only a few are elastomeric
in nature. The poly(anilinophosphazenes) are glassy materials
(2,3). Many poly(aminophosphazenes) with aliphatic pendant
groups are flexible thermoplastics; some are water soluble.
When diethylamine is used in the substitution process, approxi-
mately 50% substitution occurs. This polymer (VII) is an
elastomer

$$[NPCl_2]_n \quad \underset{NH(C_2H_5)_2}{\xrightarrow{\hspace{2cm}}} \quad [NPClN(C_2H_5)_2]_n \quad \underset{NH_2R}{\xrightarrow{\hspace{1cm}}} \quad [NP(NHR)N(C_2H_5)_2]_n$$

                              VII   VIII
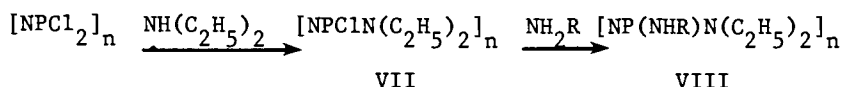
which can be used to prepare flexible thermoplastic mixed
substituent copolymers (VIII) and terpolymers. The copolymer
$[NP(OCH_2CF_3)N(C_2H_5)_2]_n$ was prepared via VII (39). This mixed
alkoxyaminophosphazene was similar in properties to
$[NP(OCH_2CF_3)_2]_n$.

Applications

    Although questions still exist concerning the structure
of polyphosphazene elastomers, several of these polymers
are of technological interest and are undergoing commercial
development (3-5).

Poly(fluoroalkoxyphosphazene) Elastomers. Much of the current
interest in the phosphazene fluoroelastomers is based on
the outstanding combination of properties inherent in these
polymers including petroleum resistance, low temperature
flexibility, thermal and oxidative stability and ozone resistance.
These properties have stimulated work for both military and
commercial applications such as arctic fuel hoses and gaskets
(40,41), seals and O-rings (42,44), coated fabrics (45,46),
channel sealants (47) and biomedical materials (48). The
phosphazene fluoroelastomers can be compounded and processed
using conventional methods to give an excellent balance of
physical properties (Table 1). This polymer was introduced
commercially by Firestone Tire and Rubber Company under the
trademark PNF (49). Typical end items which are undergoing
evaluation or are in use are shown in Figure 6.

Fire Resistant Elastomers. The poly(aryloxyphosphazene)
elastomers offer excellent fire resistance without incorpor-
ating halogen in the polymer or as an additive. These polymers
are self-extinguishing in air and generate only moderate non-
corrosive smoke and a minimum of toxic combustion products upon
combustion (50-53). The poly(aryloxyphosphazene) elastomers
(APN®) have excellent potential for applications such as

Table I

PHOSPHAZENE FLUOROELASTOMER

COMPOUNDING FORMULATIONS		VULCANIZATE PROPERTIES	
POLYMER	100	LOW TEMPERATURE FLEXIBILITY	
SILICA		BRITTLE POINT*	-65°C
CARBON BLACK	30-60	TR - 10†	-55°C
CLAY			
SILICONE GUM	2-10	PETROLEUM RESISTANT	
FLUOROSILICONE		GOOD THERMAL STABILITY (LONG TERM)	175°C
SILANE COUPLING AGENT	2	SHORE A HARDNESS	35-90
MgO	2-10	COMPRESSION SET (%)‡	10-50
$(8-HQ)_2Zn$ (STABILIZER)**	2	70 hr AT 149°C	
PEROXIDE OR SULFUR	1-3	TENSILE STRENGTH, MPa	6.9-17
		psi	1000-2500
PRESS CURE 20-30 min AT	170°C	ELONGATION, %	75-250
POSTCURE (OPTIONAL) 4 hr AT	175°C	100% MODULUS, MPa	2-10
		psi	290-1450

*ASTM D-746 †ASTM D-1329 ‡ASTM D-395 **ZINC 8-QUINOLINOLATE

open and closed-cell foams (Figure 7) and wire coverings.
The feasibility of using these elastomeric foams as fire
retardant thermal insulation has been demonstrated by a Department
of the Navy-National Bureau of Standards Test Program ($\underline{54}$).

Alternate Synthesis - Future Developments

The survey of phosphazene elastomers so far has been
based on the poly(halophosphazene) synthesis. The reason
for this is that while $(NPCl_2)_3$ and $(NPF_2)_3$ react to give
open chain high polymer, fully organo substituted cyclic
derivatives generally do not. There are intermediate examples
such as mono- and diorganosubstituted cyclotriphosphazenes
which yield open chain polymers under certain conditions
($\underline{58}$). One interesting example ($\underline{59}$) is the polymerization
of monoalkylpentachlorocyclotriphosphazene monomers, $N_3P_3Cl_5R$
followed by chlorine replacement to give open chain polymers
$[-(N=P(OR')_2)_2-N=P(OR')R-]_n$. This polymer ($R=CH_3$, $R'=CH_2CF_3$)
is an elastomer with a $T_g = -50°C$. The presence of the methyl
group is sufficient to disrupt the crystallinity as observed
in the related homopolymer $[NP(OCH_2CF_3)_2]_n$.

$\underline{\text{N-Silylphosphinimines}}$. Until recently, no general method
has been available which allows complete incorporation of
the desired substituents before polymerization. The synthesis
of polyphosphazenes with direct phosphorus-carbon bonds has
been possible only in a few cases ($\underline{25,60}$). A new method
which holds promise involves the synthesis of suitably constructed
N-silylphosphinimines which upon heating, eliminate substituted
silanes to give polyphosphazenes ($\underline{61}$). This procedure was

$$Me_3SiN\!\!=\!\!\underset{\underset{R}{|}}{\overset{\overset{R}{|}}{P}}\!\!-\!\!X \longrightarrow Me_3SiX + \left[\!N\!\!=\!\!\underset{\underset{R}{|}}{\overset{\overset{R}{|}}{P}}\!\right]_n$$

used to prepare poly(dimethylphosphazene) ($X=OCH_2CF_3$, $R=R'=CH_3$)
($\underline{61}$). One can easily imagine that with a suitable selection
of substituents, $R \neq R'$, new phosphazene elastomers with novel
properties might be accessible.

$\underline{\text{Other Applications}}$. Thus far the phosphazene fluoroelastomers
(PNF) and aryloxyphosphazene elastomers (APN) have moved
to the commercial stage. In addition to elastomers, phosphazenes
are being investigated as fluids, resins and plastics. Other
areas which hold promise include fire resistant paints ($\underline{55}$),
fiber blends and additives, agrichemicals and herbicides,
drug release agents and electrically conducting polymers ($\underline{6}$).
The large number of different pendant groups with widely
varied chemical functionality which can be attached to the
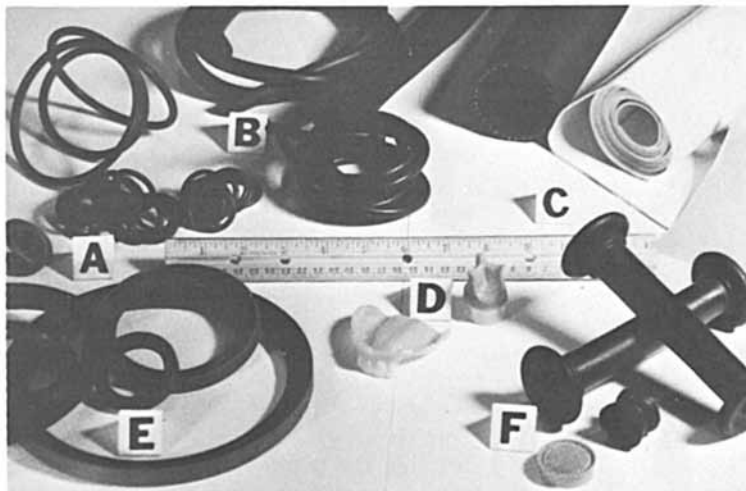
Figure 6. Phosphazene fluoroelastomers (PNF) were used to prepare various rubber end items, some of which are commercially available.

Examples: A, O-rings for rotary and static applications (43); B, extruded items such as hose, tube, and solid splicable stock; C, fuel hose for low temperature service ($-57°C$) and coated fabric for collapsible fuel storage tanks (40, 45); D, biomedical applications such as soft denture liners (48) and blood compatible parts; E, lip seals (42); F, shock absorption and vibration damping mounts. (Photograph courtesy of the Firestone Tire & Rubber Company.)
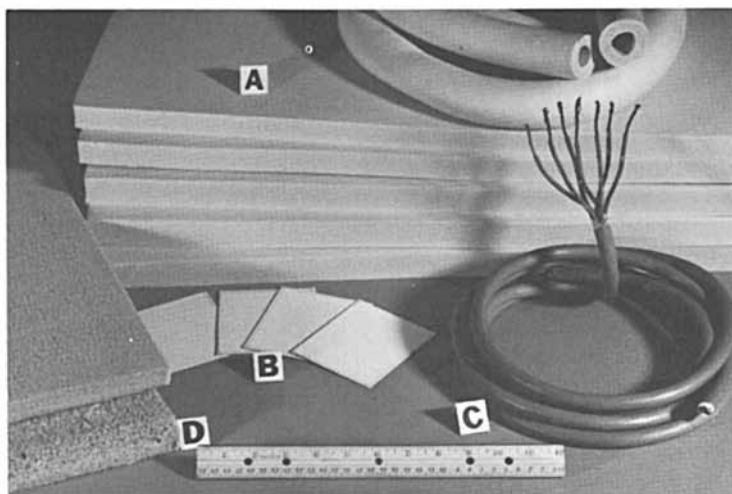
Figure 7. Aryloxyphosphazene elastomers (APN) offer excellent potential.

Examples: A, closed cell thermal insulation with high fire retardency and low smoke generation (52, 54); B, pigmented APN coatings in aluminum substrates with low flammability, low flame spread, and low smoke (55); C, APN insulation and cable jacketing (56); D, open cell APN comfort cushioning (57). (Photograph courtesy of the Firestone Tire & Rubber Company.)

P-N backbone demonstrate the unusual molecular design potential
of this class of polymers. Undoubtedly, some of these will
hold promise for future research and development.

References

1.   Singler, R. E.; Schneider, N. S.; Hagnauer, G. L.
     Polym. Eng. and Sci. 1975, 15, 321.
2.   Allcock, H. R. Angew Chem. Int. Ed. Eng. 1. 1977,
     16, 147.
3.   Singler, R. E.; Hagnauer, G. L.; Schneider, N. S.
     Polym. News. 1978, 5(1), 9.
4.   Gerber, A. H. ACS Div. Org. Coat Plast. Chem. Pap.
     1979, 41, 81; NASA CR 159563, N79-30377.
5.   Tate, D. P. and Antkowiak, F. A. Kirk-Othmer Encycl.
     Chem. Technol. 3rd. Ed. 1980, 10, 936.
6.   Allcock, H. R. Makromol. Chem. Suppl. 1981, 4, 3.
7.   Stokes, H. N. Amer. Chem. J. 1897, 19, 1782.
8.   Allcock, H. R.; Kugel, R. L.; Valan, K. J. Inorg. Chem.
     1966, 5, 1709.
9.   Allcock, H. R. "Phosphorus-Nitrogen Compounds", Academic
     Press, New York, 1972.
10. Hagnauer, G. L. J. Macromol. Sci.-Chem. 1981, A16, 385.
11. Allcock, H. R.; Gardner, J. E.; Smeltz, K. M. Macromole-
     cules 1975, 8, 36.
12. Snyder, D. L.; Stayer, Jr. M. L.; Kang, J. W., U. S.
     Patent 4,123,503, 1978.
13. Pritchard, M. S.; Hilton, A. S.; Stayer, Jr. M. L.;
     Antkowiak, T. A., U.S. Patent 4,137,330, 1979.
14. Fieldhouse, J. W.; Graves, D. F. U.S. Patent 4,226,
     840, 1981.
15. Reynard, K. A.; Gerber, A. H. U.S. Patent 4,257,917, 1981.
16. Halasa, A. F.; Hall, J. E. U.S. Patent 4,225,567, 1981.
17. Hagnauer, G. L. and Singler, R. E. Coat. Plast. Chem. Pap.
     1979, 41, 88.
18. Hagnauer, G. L. ACS Symposium Series 1980, 138, 239.
19. Adams, H. E.; Valaitis, J. K.; Henderson, C. W.; Strauss,
     E. J. ACS Symposium Series 1980, 138, 255.
20. Hagnauer, G. L. and Koulouris, T. N. "Liquid Chromatogr-
     aphy of Polymers and Related Materials - III" Jack
     Cazes, Ed. Marcel Dekker Inc., New York, 1981.
21. Allcock, H. R. and Arcus, R. A. Macromolecules 1979,
     12, 1130.
22. Connolly, Jr., T. M. and Gillham, J. K. J. Appl. Polym.
     Sci. 1975, 19, 2641.
23. Seel, F. and Langer, J. Z. Anor. Allg. Chem. 1958, 295
     (317).
24. Allcock, H. R.; Kugel, R. L.; Stroh, E. G. Inorg. Chem.
     1972, 11, 1120.

25. Allcock, H. R.; Evans, T. L.; Patterson, D. B. <u>Macromole-cules</u>, 1980, <u>13</u>, 201.
26. Rose, S. H. <u>J. Polym. Sci. B</u> 1968, <u>6</u>, 837.
27. Beres. J. J.; Schneider, N. S.; Desper, C. R.; Singler, R. E. <u>Macromolecules</u> 1979, <u>12</u>, 566.
28. Dieck, R. L. and Goldfarb, L. <u>J. Polym. Sci. Poly. Chem. Ed.</u> 1977, <u>15</u>, 361.
29. Mark, J. E.; Yu, C. U. <u>J. Polym. Sci. Polym. Phys. Ed.</u> 1977, <u>15</u>, 371.
30. Sharov, V. N; Ivanova, G. A.; Korol'Ko, V. V.; Mileshkevich, V. P.; Klebanskii, A. L.; Saratovkina, T. I.; Sidorovich, E. A.; Surkova, N. J.; Kurlyand, S. K.; Pchelintsov, V. V. <u>Vysokomol. Soedin. Ser. A.</u> 1981, <u>23(6)</u>, 1389; <u>Chem. Abstr.</u> 1981, <u>95</u>, 44502f.
31. Cheng, T. C.; U.S. Patent 4,152,314, 1979.
32. Cheng, T. C.; Fieldhouse, J. W., U.S. Patent 4,179,555, 1979.
33. Hagnauer, G. L.; Schneider, N. S. <u>J. Polym. Sci. A-2</u> 1972, <u>10</u>, 699.
34. Allen, G; Mortier, R. M. <u>Polymer</u> 1972, <u>13</u>, 253.
35. Andrady, A. L. and Mark, J. E. <u>European Polym. J.</u> 1981, <u>17</u>, 323.
36. Carlson, D. W.; O'Rourke, E.; Valaitis, J. K.; Altenau, A. G. <u>J. Polym. Sci. Polym. Chem. Ed.</u> 1976, <u>14</u>, 1379.
37. Futamura, S; Valaitis, J. K.; Lucas, K. R.; Fieldhouse, J. W.; Cheng, T. C.; Tate, D. P. <u>J. Polym. Sci. Polym. Phys. Ed.</u> 1980, <u>18</u>, 767.
38. Ho, P. K.; Williams, M. C. <u>Polym. Eng. and Sci.</u> 1981, <u>21</u>, 234.
39. Allcock, H. R.; Cook, W. J.; Mack, D. P. <u>Inorg. Chem.</u> 1972, <u>11</u>, 2584.
40. Antkowiak, T. A. "Phosphonitrilic Fluoroelastomer Fuel Hose - Utilization of Extruded Tubes," The Firestone Tire and Rubber Company, Akron, Ohio, 1977; MERADCOM Contract DAAK70-76-0239, AD A047960.
41. Touchet, P. and Gatza, P. E. <u>J. Elast. Plast.</u> 1977, <u>9</u>, 8.
42. Vicic, J. C. and Reynard, K. A. <u>J. Appl. Polym. Sci.</u> 1977, <u>21</u>, 3185.
43. Kyker, G. S. "Development and Evaluation of Phosphonitrilic Fluoroelastomer O-Rings", The Firestone Tire and Rubber Company, Akron, Ohio 1975; AMMRC Contract DAAG46-74-C-0066, AD A012266.
44. Ruby, J. D.; Testroet, F. B.; Williams, J. A.; "Compounding Elastomers for Use In Armament Applications", Rock Island Arsenal III, Feb 1977, AD A039847.
45. Sicka, R. W.; Mitchell, G. B. "Phosphonitrilic Fluoroelastomer Coated Fabrics For Collapsible Fuel Storage Tanks", The Firestone Tire and Rubber Company, Akron, Ohio 1979, AMMRC Contract DAAG46-78-C-0006, AD A074524/4.
46. Wilson, A. <u>J. Coated Fabrics</u> 1978, <u>1</u>, 233.
47. Griffin, W. <u>U.S. Patent 4,185,041.</u>

48. May, P. and Guerra, L.   U.S. Patent 4,251,215.
49. Kyker, G. S. and Antkowiak, T. A. Rubber Chem. Tech. 1974,
    47, 32.
50. Quinn, E. J. and Dieck, R. L. J. Cell. Plast.
    1977, 13, 96.
51. Lawson, D. F. and Cheng, T. C.; Fire Res. 1978, 1, 223.
52. Thompson, J. E. and Reynard, K. A. J. Appl. Polym. Sci.
    1977, 21, 2575.
53. Lien, P. J.; Magill, J. H.; Alarie, Y. C. J. Fire
    Flammability 1980, 11, 167.
54. Widenor, W. M. "Model Fire Tests on Polyphosphazene
    Rubber and Polyvinylchloride (PVC)/Nitrile Rubber Foams"
    David W. Taylor, Naval Ship R&D Center, Annapolis, MD
    1978, NASA TM-78523, N79-12029.
55. Chattopadhyay, A. K.; Hinrichs, R. L.; Rose, S. H.
    J. Coat. Technol. 1979, 51, 87.
56. Peterson, T. C. "Polyphosphazene Wire and Cable Insulation",
    Horizons Research, Inc., Cleveland, Ohio, Dec 1979, DTNSRDC
    Contract N00024-78-C-4644, ADA091410.
57. Gerber, A. H. and Peterson, T. C. "Preparation and Testing
    of Polyaryloxyphosphazene Open Cell Foams", Horizons Research
    Inc., Cleveland, Ohio. July 1979, DTNSRDC Contract
    N0060-78-C-0253.
58. Allcock, H. R., Polymer 1980, 21, 673.
59. Allcock, H. R.; Ritchie, R. J.; Harris, P. J. Macromole-
    cules 1980, 13, 1338.
60. Neilson, R. H. and Wisian-Neilson, P. J. Macromol. Sci.
    -Chem. 1981, A16, 425.
61. Neilson, R. H. and Wisian-Neilson, P. J. Am. Chem. Soc.
    1980, 102, 2848.

The Relation Between Dynamic and Equilibrium Moduli, with Consideration of Entanglements

B. E. EICHINGER

University of Washington, Department of Chemistry, Seattle, WA 98195

The relation between the elastic modulus and the minimum nonzero eigenvalue of the force constant matrix for an elastomer is derived by means of a coarse-graining approximation. The treatment entails identification of the macroscopic fundamental mode with the longest wavelength mode that might be calculated from molecular theory. The coarse-grained view suggests a method by which the problem of entanglements may be approached. The quantitative analysis of some aspects of this problem is developed, and the long range part of the entanglement coupling is shown to be of dipolar strength.

Introduction

Elastomers are solids, even if they are soft. Their atoms have distinct mean positions, which enables one to use the well-established theory of solids to make some statements about their properties in the linear portion of the stress-strain relation. For example, in the theory of solids the Debye or macroscopic theory is made compatible with lattice dynamics by equating the spectral density of states calculated from either theory in the long wavelength limit. The relation between the two macroscopic parameters, Young's modulus and Poisson's ratio, and the microscopic parameters, atomic mass and force constant, is established by this procedure. The only differences between this theory and the one which may be applied to elastomers is that (i) the elastomer does not have crystallographic symmetry, and (ii) dissipation terms must be included in the equations of motion.

The absence of a space group makes the spectral problem a difficult one. Our work in this area[1-3] is far from complete,

but we have been gaining a general idea of what the spectral densities of amorphous materials are like, and it now seems that some statements can be made with sufficient conviction so as to develop theory a little further.

In the first part to follow, the equations of motion of a soft solid are written in the harmonic approximation. The matrices that describe the potential, and hence the structure, of the material are then considered in a general way, and their properties under a normal mode transformation are discussed. The same treatment is given to the dissipation terms. The long wavelength end of the spectral density is of interest, and here it seems that detailed matrix calculations can be replaced by simple scaling arguments. This shows how the inertial term, usually absent in molecular problems, is magnified to become important in the continuum limit.

These observations are equivalent to a coarse-grained view of the system, which is tantamount to a description in terms of continuum mechanics. [It is clear that "points" of the continuum may not refer to such small collections of atoms that thermal fluctuations of the coordinates of their centers of mass become substantial fractions of their strain displacements.] The elastomer is thus considered to consist of a large number of quasi-finite elements, which interact with one another through dividing surfaces.

A dividing surface provides a convenient means to think about the problem of entanglements. A chain from one element may meander across a dividing surface into a neighboring element, and then return. The number of chains from the neighboring element with which it is entangled will certainly be proportional to the square of the number of steps that it has made in the adjoining neighborhood. This approach to the entanglement problem is only given a preliminary treatment here, but what is done has the advantage of being well defined.

Molecular Equation of Motion

The potential energy V of the elastomer is presumed to be given as a function of the atomic coordinates x_i^α ($1 \leq \alpha \leq 3, 1 \leq i \leq n$), where n is the number of atoms in the system. Since an elastomer has a well-defined equilibrium shape, there must be equilibrium positions $\bar{x}_i^\alpha$ for all atoms that are part of the continuous network. Expand the potential in a Taylor series about the equilibrium positions, and set the potential to zero at equilibrium, to obtain

$$V = (1/2) \sum_{\alpha,\beta} \sum_{i,j} k_{ij}^{\alpha\beta} (x_i^\alpha - \bar{x}_i^\alpha)(x_j^\beta - \bar{x}_j^\beta) = (1/2)(x-\bar{x})K(x-\bar{x})' \qquad (1)$$

to first approximation. The coefficient matrix $(k_{ij}^{\alpha\beta})$ = K is the matrix of force constants. For now the potential will be taken to be isotropic in all atom pairs, so that $k_{ij}^{\alpha\beta} = k_{ij}\delta_{\alpha\beta}$. It is then convenient to rearrange the 1x3n matrix into a 3xn matrix X, with transpose X', and write

$$V = (1/2)\text{Tr}[(X-\bar{X})K(X-\bar{X})']\tag{2}$$

where the elements of K are now just the k_{ij}. The trace operation Tr has the effect of computing the scalar product of the displacement vectors.

The Lagrangian L for the system is

$$L = (1/2)\text{Tr}(\dot{X}M\dot{X}') - (1/2)\text{Tr}[(X-\bar{X})K(X-\bar{X})']\tag{3}$$

where M is a diagonal matrix of masses m_i. The equation of motion is simply

$$\ddot{X}M + (X-\bar{X})K = 0\tag{4}$$

We now need to add the dissipation term. A Rayleigh dissipation function will suffice for this purpose, since the hydrodynamic interactions in the elastomer should be well screened. Let F be a matrix such that $\dot{X}F$ has elements of the form

$$f_i[\dot{x}_i^\alpha - z^{-1}\sum_j \dot{x}_j^\alpha]$$

where the sum is over the z neighboring atoms which contact the ith atom. This term represents the average velocity field against which the ith atom moves. The friction depends upon the instantaneous configuration, but we will assume that a pre-averaging approximation has been applied (similar to that used to pre-average the Oseen tensor in single chain dynamics) so that its structure is determined by the mean positions of the atoms. The friction factor f_i is not necessarily the same for all atoms, and since the structure of the matrix F is already complicated, no harm comes from the generalization.

The equation of motion is further generalized by imposition of a 3xn external force matrix σ, so that we finally have

$$\ddot{X}M + \dot{X}F + (X-\bar{X})K = \sigma\tag{5}$$

which requires a solution. This is difficult in general because F and K do not necessarily commute, and they cannot then be simultaneously diagonalized. Nevertheless, there is an argument that one can make for the long wavelength limit that will show what the structure of the solution to eq. (5) must be.

Suppose that a strip of rubber is placed under modest tension, and is then plucked. On performing this experiment, one may observe the fundamental oscillation of the form sin $\pi x/L$, where L is the length of the strip. The oscillation dies away on a time scale of about one second for a typical rubber band, for example. The motion is clearly not overdamped, as are the motions of individual polymer molecules in a solution. How is it that the high frequency modes of eq. (5) have a small effective mass and a large friction constant, while the low frequency modes have large effective mass and small friction. The answer, of course, lies in the structure of the matrix F. For long wavelength modes the corresponding eigenvalues of F are very small, while the same is not true for the short wavelength modes.

Imagine now that the elastomer is repesented by an array of cubes, or more generally by an array of polyhedra that are topologically isomorphic to cubes, and that these are packed together in a simple cubic array. Each polyhedron might be several hundred or more Angstroms on an edge, and hence contain well over 10^6 atoms. The atoms in each cell will be given labels (ℓ) arbitrarily assigned, but the cells will carry indices (i,j,k) corresponding to the usual crystallographic convention. The coordinates of the matrix X might then be written $x_{ijk}^{\ell\alpha}$, and F and K now carry eight indices. The advantage of this supernumeration is that F and K are now blocked into a form such that they will be approximately diagonalized by a transformation whose long wavelength eigenvectors are of the same form as those that diagonalize the K matrix for a simple cubic lattice. Within each cell the coordinates are virtually constant with respect to an eigenvector whose wavelength is very much greater than the average edge length $\underline{a}$ of a single cell.

For these modes, the equation of motion must admit of a scaling argument. On making the transformation X $\longrightarrow$ QT, where Q are the approximate normal mode coordinates, and T is the matrix of approximate eigenvectors (T would diagonalize a regular cubic lattice), TMT' scales relatively as $\underline{a}^3$, TFT' scales as $\underline{a}$, and TKT' scales as $\underline{a}^2$. This follows since we might have ignored the atoms by beginning with a continuum model, then breaking it down into quasi-finite elements. The masses of the elements are proportional to their volumes, they exert a Stokes friction on one another that varies as their effective radii, and the force restoring a displacement between their centers of mass is proportioned to the area of the intervening face. Since the friction term scales with the lowest power of $\underline{a}$, it looses significance most rapidly as the wavelength of the excitation is increased. (Here it is assumed that $\underline{a}$ scales as the wavelength if some fixed percentage accuracy is attached to the representation of eigenvectors being discussed.)

On the basis of this argument, the equation of motion for the longest wavelength mode in the elastomer is

$$m_{eff}\ddot{q}_1 + \kappa_1 q_1 = \sigma t_1 \tag{6}$$

where m_{eff} is an effective mass, κ_1 is the minimum non-trivial eigenvalue of K, and t_1 is the eigenvector corresponding to κ_1. The friction term is omitted since it is small, and because dropping it at this stage does no harm to the relations with continuum equations which will follow. The solution of eq. (6) is

$$q_1 = \sigma t_1/\kappa_1 + q_1^0 \cos\omega_1 t \tag{7}$$

where

$$\omega_1^2 = \kappa_1/m_{eff} \tag{8}$$

and q_1^0 is the extra displacement at time zero away from the equilibrium displacement $\sigma t_1/\kappa_1$. This longest wavelength mode oscillates with a frequency $\omega_1 = (\kappa_1/m_{eff})^{1/2}$, and this we now want to relate to the equilibrium modulus.

Continuum Equation of Motion

The deformation gradient tensor λ is related to the strain tensor η by the equation[4]

$$\eta = (1/2)(\lambda\lambda'-1) \tag{9}$$

and the stress tensor T is given by

$$T = (1/V)\lambda'(\partial A/\partial\eta)\lambda \tag{10}$$

for a homogeneous medium, in which the free energy density A/V is independent of position. The equation of motion in the absence of body forces is

$$\nabla \cdot T - \rho\partial^2\underline{u}/\partial t^2 = 0 \tag{11}$$

where ρ is the density (in the strained state), and $\underline{u}$ is the vector position of an element of volume as measured from its position in the state of equilibrium at zero stress. In the limit of infinitesmal strain $\varepsilon = (\partial u_\alpha/\partial x_\beta)$ the stress is given by

$$T = G(\varepsilon+\varepsilon') \tag{12}$$

where G is the scalar modulus, assumed to be constant for the present discussion. In the infinitesmal limit, the volume

dilation is negligible, which translates into $\nabla \cdot u = 0$ or $Tr(\varepsilon) = 0$. The equation of motion, eq. (11), thus reduces to

$$G\nabla^2\underline{u} - \rho\partial^2\underline{u}/\partial t^2 = 0 \tag{13}$$

For a rectangular solid with clamped surfaces, the solution of eq. (13) is

$$u_\alpha = u_\alpha{}^0 \sin(\underline{k}\cdot\underline{x}) \cos\omega t \tag{14}$$

where

$$-Gk^2 + \rho\omega^2 = 0 \tag{15}$$

The velocity of propagation v of a disturbance is given by v = $(G/\rho)^{1/2}$, and $\omega = v|\underline{k}|$. To satisfy the boundary condition, $\underline{k}$ is a vector of the form

$$\underline{k} = \pi(k_1/L_1, \ k_2/L_2, \ k_3/L_3) \tag{16}$$

if the origin of coordinates is located at one corner of the body, and the rectangular solid has sides of lengths L_1, L_2, and L_3. The lowest frequency mode is the one that is excited in the direction along $L_1 = \max(L_1, L_2, L_3)$, and for this mode $\underline{k} = \pi(1/L_1, 0, 0)$ so that

$$\omega_1 = (G/\rho)^{1/2}\pi /L_1 \tag{17}$$

By combination of eqs. (8) and (17) one finds

$$G = \kappa_1 L_1^2\rho/\pi^2 m_{eff} \tag{18}$$

This establishes the natural relation between the modulus and the minimum nonzero eigenvalue of the force constant matrix. The precise form of this relationship, i.e., the values of the constants, depends upon the geometry of the body, both through the boundary conditions on the continuum and through the structure of the force constant matrix, which indirectly determines m_{eff}.

It can be seen from eq. (18) that κ_1 must be proportional to L_1^{-2} in order for G to be intensive. We thus have a proof of what may now be asserted to be the theorem[3,5] that κ_1 is proportional to $V^{-2/3}$ for an approximately cubical body. It is seen that this statement is not restricted to elastomers, but is valid for all crystalline and amorphous materials. It is also the case that for sufficiently low frequency modes, the spectral density $g(\kappa)d\kappa$

of K must be Debye-like, with $g(\kappa)d \propto \kappa^{1/2}d\kappa$ (this is equivalent to $g(\overline{\omega^2})d\omega \propto \omega^2 d\omega$). To state this more precisely, the limit

$$\lim_{\kappa \to 0} g(\kappa)/\kappa^{1/2} = \text{const.} \tag{19}$$

must be true; it is generally accepted by solid state physicists as obvious. But, it is not at all apparent from the above argument that $g(\kappa)$ departs from the limiting law for quite small values of κ, whereupon profound departures from this law become critical. This is born out in computer calculations on elastomers[1] as well as other amorphous systems[3], the latter of which are described by widely different potential functions. Our current best estimate is that the limiting law cannot be trusted for wavelengths less than several thousand Angstoms, regardless of the precise nature of the amorphous medium. If anything is surprising about this contention it is in the implication that the range of structural fluctuations in amorphous systems is huge. In other words, it seems that network fragments containing more than ca. 10^9 atoms look much alike, but those with fewer units have appreciable fluctuations about the mean.

It is important to note that if the exciting frequency in a viscoelastic measurement is not that of the lowest mode, then the response of the elastomer will have contributions from the larger eigenvalues $\kappa_i > \kappa_1$, and the apparent dynamic modulus will be larger than the equilibrium modulus. The whole question of extrapolation to zero frequency is delicate, and depends critically upon the eigenvalue spectra of both F and K, and upon the relaxation times remaining real. The above discussion requires that this is not the case when the wavelength of the excitation becomes sufficiently long.[6]

Entanglements

The constructions in the above sections, leading to a representation of the elastomer as a coarse-grained collection of cubes each containing perhaps 10^9 atoms, suggests a method whereby the problem of entanglements may be approached. The force exerted by one cube upon a neighbor when the two are displaced is delivered by chains whose ends are bonded to junctions lying in the two different cubes, and perhaps also by chains whose ends lie within one cube, but which cross the interface and become entangled with chains in the neighboring cube. These two types of chains, labeled A and B respectively in Fig. 1, are the only ones which need be considered in the calculation of forces, the short-ranged van der Waals interaction across the interface notwithstanding. The force delivered by chain B will be matched, on the average, by a similar chain related to B by a reflection in the interfacial plane, and in the end a factor of two will
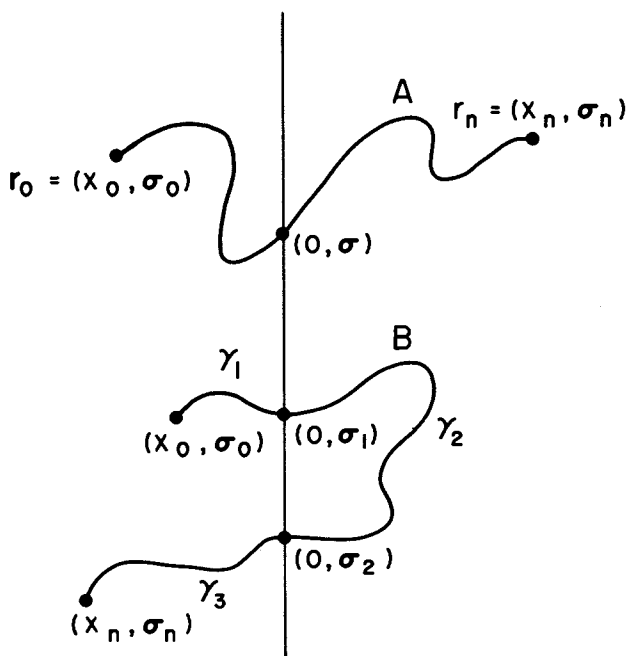
Figure 1.   Representative chains that are capable of delivering a force across an interface.

Chains of class A have their two junctions on opposite sides of the vertical plane defined by $x = 0$. They are capable of delivering a direct force. In class B the chains may be entangled to the right, and thereby deliver an indirect force across the interface.

have to be inserted in the calculation of the force due to entangled chains. The calculation which will be presented here is far short of a complete theory of entanglements, but it does illustrate some interesting features of this difficult problem.

We first require some assumptions. Let the cubes into which the elastomer is decomposed be large relative to the dimensions of a single chain, so that edge and corner effects are negligible. Furthermore, the chains will be represented in the Gaussian approximation, so that for any stretch of a chain containing n segments, the end-to-end separation is described by the probability distribution

$$P(r)dr = (\gamma/\pi)^{3/2} \exp (-\gamma r^2)dr \qquad (20)$$

where $\gamma = 3/2n\ell^2$, and ℓ^2 is the mean square displacement of one segment.

It has been forcefully pointed out[7] that chains tend not to double back upon themselves. In Fig. 1 the depicted configurations are of this type. To be sure, all chains of class A include those which cross the interface an odd number of times, and all those of class B cross an even number of times. However, inspection of the ballot problem[8] convinces one that paths which cross the interface m_2 times are less probable than those which cross m_1 times, if $m_2 \gtrless m_1$. Hence, each of the other configurations in classes A and B contributes less to the probability measure than do the two chains shown in Fig. 1.

The probability that a chain of n segments has ends lying in two adjoining cubes at $\underline{r}_0$ and $\underline{r}_n$ is given by eq. 20, where $\underline{r} = \underline{r}_n - \underline{r}_0$. The probability that the chain crosses the interface only once may be calculated by summing over all two branch paths that begin at $(0,\underline{\sigma})$, one arm extending to the left and the other to the right, neither of which crosses the interface again. If the chain is modeled as a diffusing particle, each arm is equivalent to a particle diffusing into a half space. One may solve the diffusion equation for this case, but in the end there is a difficulty with the appropriate normalization. It is easier to use random walk theory for this problem, since the normalization factors are automatic, and there is some powerful theory to use.

We begin a discussion of chains of class B, which are of most concern, with the

Lemma.[8] The number of paths of class B (that touch or cross the interface x=0), that originate at $\underline{r}_0 = (x_0,\underline{\sigma}_0) = (x_0,y_0,z_0)$ and terminate at $(x_n,\underline{\sigma}_n)$, equals the number of all paths from $(-x_0,\underline{\sigma}_0)$ to $(x_n,\underline{\sigma}_n)$. The probability distribution for the latter paths is just

$$(\gamma/\pi)^{3/2}\exp[-\gamma(x_n+x_0)^2 - (\underline{\sigma}_n-\underline{\sigma}_0)^2],$$

so that we now have a measure of the contribution from all chains which have potential to be entangled. Given P(r) for the probability that a given chain has both ends in one cube with an end-to-end separation r, the probability that the chain touches or crosses the interface is

$$\exp(-4\gamma|x_0 x_n|)\ P(r) \qquad\qquad (21)$$

if its ends are located at distances $|x_0|$ and $|x_n|$ from the interface. Since this distribution falls off rapidly as the ends of the chain move farther from the dividing surface, only those chains with ends very near the surface have the ability to contribute to an entanglement force.

Those chains of class B in Fig. 1, with a loop in the neighboring cube, will embrace a number of segments that is determined by the minimal surface enclosed by the line segment from $\underline{\sigma}_1$ to $\underline{\sigma}_2$, and by the space curve of the portion of the chain in the cube to the right. Given a number n_2 of segments in that portion of the chain, the areas of the minimal surfaces will be described by a probability distribution, the determination of which is a difficult problem. It is clear that the enclosed area will range from zero (when the loop hugs the interface) to $\pi(n_2\ell)^2$ (when $\underline{\sigma}_1=\underline{\sigma}_2$ and the loop is circular). It seems safe to assume that the most probable minimal surface will have an area that is proportional to n_2^2, and that the number of entangled chains is likewise proportional to n_2^2. Not all polymer segments that transect the minimal surface will be entangled. Some of them will originate and terminate in the cube to the left so that they are discounted, others will pass through the minimal surface and quickly return, and still others will be involved with other chains in class B that have smaller loops so that they are entangled with chains other than the one in question. One must expect that only a fraction of the chains that pass through the minimal surface will qualify as entangled.

The average of the square of the number of segments in the cube to the right may be calculated by making further use of adapted theorems on arrangements.

Theorem 1: The probability that a chain of n segments, which originates at the interface at σ_1 and terminates at $(x,\underline{\sigma})$, will stay on one side of the interface is

$$P_1(x,|\underline{\sigma}-\underline{\sigma}_1|)\ =\ \frac{3|x|}{n\ell}\ (\gamma/\pi)^{3/2}\exp[-\gamma(x^2 + (\underline{\sigma}-\underline{\sigma}_1)^2)].$$

This is an obvious adaptation of a theorem given by Feller[8]. The chain takes an average of n/3 steps in the x direction, and the total probability of a walk from $(0,\underline{\sigma}_1)$ to $(x,\underline{\sigma})$ is the usual Gaussian. A similar modification of another theorem,[8] which is valid for $n+1\approx n$, is

Theorem 2: The probability that a chain of n segments, which originates at $\underline{\sigma}_1$ and terminates at $\underline{\sigma}_2$ (both on the interface), will be entirely on one side of the dividing surface is

$$P_2(|\underline{\sigma}_1 - \underline{\sigma}_2|) = \frac{3}{n}(\gamma/\pi)^{3/2}\exp[-\gamma(\underline{\sigma}_1 - \underline{\sigma}_2)^2].$$

The probability that a chain will have the configuration of class B depicted in Fig. 1 is

$$P* = \frac{27|x_0 x_n|(\gamma_1 \gamma_2 \gamma_3 /\pi^3)^{3/2}\exp[-\gamma_1 x_0^2 - \gamma_3 x_n^2}{n_1 n_2 n_3 \ell^2}$$

$$-\gamma_1(\underline{\sigma}_0 - \underline{\sigma}_1)^2 - \gamma_2(\underline{\sigma}_1 - \underline{\sigma}_2)^2 - \gamma_3(\underline{\sigma}_2 - \underline{\sigma}_n)^2] \tag{22}$$

where $\gamma_i = 3/2n_i \ell^2$. The probability that the chain has n_2 segments to the right of the interface is the integral of eq. (22) over all $\underline{\sigma}_1$ and $\underline{\sigma}_2$, which is given by

$$P_2 = (27|x_0 x_n|/n_1 n_2 n_3 \ell^2)(\gamma_1 \gamma_2 \gamma_3 \gamma^2/\pi^5)^{1/2}$$

$$\times \exp[-\gamma_1 x_0^2 - \gamma_3 x_n^2 - \gamma(\underline{\sigma}_0 - \underline{\sigma}_n)^2] \tag{23}$$

where $\gamma^{-1} = \gamma_1^{-1} + \gamma_2^{-1} + \gamma_3^{-1}$. The average $\langle n_2^2 \rangle$ that is sought is

$$\langle n_2^2 \rangle = \frac{\int n_2^2 P_2 \delta(n_1 + n_2 + n_3 - n)dn_1 dn_2 dn_3}{\int P_2 \delta(n_1 + n_2 + n_3 - n)dn_1 dn_2 dn_3}$$

Define

$$I_\alpha(x_0, x_n) = n^{5/2} \iiint n_2^\alpha (n_1 n_2 n_3)^{-3/2}\exp(-\gamma_1 x_0^2 - \gamma_3 x_n^2)$$

$$\times \delta(n_1 + n_2 + n_3 - n)dn_1 dn_2 dn_3 \tag{24}$$

so that $\langle n_2^2 \rangle = I_2/I_0$. The integral simplifies to

$$I_\alpha = n^\alpha \int_{1/n}^{1-1/n}ds \int_{1/n}^{1-s-1/n}(1-s-t)^{\alpha-3/2}s^{-3/2}t^{-3/2}$$

$$\times \exp[-(x_0^2/s + x_n^2/t)]dsdt \tag{25}$$

where the range of integration is determined by the requirement that n_1 and n_3 be no less than unity. The integral may be evaluated by series expansion of the exponential for small $|x_0|$ and $|x_n|$, to give integrals that are tedious to evaluate. If only the highest power of n is retained in the first term one naturally finds

$$\langle n_2^2 \rangle = n^2/2 + O(x_0^2 + x_n^2).$$ (26)

The further development of the power series will be the subject of another communication.

When both $|x_0|$ and $|x_n|$ are large a different approach to eq. (25) is needed. The change of variables $t = (1-s)/u$ gives

$$I_\alpha = n^\alpha \int_{1/n}^{1-1/n} \exp(-\gamma x_0^2/s)(1-s)^{\alpha-2} s^{-3/2} ds$$

$$\times \int_{\frac{1}{1-1/n(1-s)}}^{n(1-s)} (u-1)^{-3/2} u^{1-\alpha} \exp[-\gamma x_n^2 u/(1-s)] du$$ (27)

The inner integral is done by parts, to increase the exponent of the (u-1) term. Then, since the exponential function in the inner integral is small at the upper limit one may take the limit to infinity, and the lower limit will be adequately replaced by unity.

A sequence of approximations, using properties of the confluent hypergeometric function, integration by steepest descents, and judicious discard of all but the dominant terms, gives one the asymptotic form

$$\langle n_2^2 \rangle \sim \pi^{1/2} n^{3/2}/4\gamma^{3/2} (|x_0| + |x_n|)^3.$$ (28)

If the junctions are at large distances from the interface the chain will embrace a small number of chains in the adjoining cube, and thereby will contribute a force which is no stronger than the analogue electrical dipole-dipole coupling. One must also recall expression (21), which shows that the effective force falls much more rapidly, because of the diminishing probability that the chain will meander into the neighboring cube as the junctions move away from the interface.

These considerations, while far from complete, suggest that the role of entanglements in the equilibrium force is fairly small. Chains do not become strongly entangled with one another simply because they tend not to reverse their directions frequently.

Conclusions

The relation between the modulus of elasticity and the smallest nonzero eigenvalue of the connectivity matrix established here lends support to the theory[5] that has been developing in recent years. By utilizing some of the techniques that have been applied to the solid state one gains an important relation between macroscopic theory and statistical mechanics. The method by which this is done might ultimately be used to make a direct molecular theory for the forces on the elementary stress tetrahedron.

The construction of a dividing surface in the discussion of chain entanglements seems to be a generally useful technique for analysis of this problem. It allows for the application of rigorous chain statistics to concrete calculations. Integrals remain to be computed, perhaps numerically, to yield a realistic estimate of the effects of entanglements on the elastic modulus, which can be done by using the minimal surface as the dividing surface to calculate probabilities.

Acknowledgement

Literature Cited

1. Eichinger, B. E. J. *Chem. Phys.*, 1981, 75, 1964.
2. McKay, B. D. in press.
3. Eichinger, B. E.; McKay, B.D. in preparation.
4. Murnaghan, F. D. "Finite Deformation of an Elastic Solid"; Dover Publications, Inc.: New York, 1967.
5. Eichinger, B. E. *Macromolecules* 1981, 14, 1071.
6. Farris, R. J. J. *Polym. Sci.*, *Polym. Symp.* 1978, 63, 185. In this reference the author is mainly concerned with the high frequency domain. The arguments of the present work are somewhat different, but the import of the conclusions are similar to those of Farris.
7. Flory, P. J.; comments at the Symposium on Elastomers and Rubber Elasticity, American Chemical Society New York Meeting, 1981.
8. Feller, W. "An Introduction to Probability Theory and Its Applications"; John Wiley: New York, 1957.

Small Angle Neutron Scattering from Polymer Networks

ROBERT ULLMAN

Ford Motor Company, Engineering and Research Staff, Dearborn, MI 48121

The size and shape of polymer chains joined in
a crosslinked matrix can be measured in a small angle
neutron scattering (SANS) experiment. This is a-
chieved by labelling a small fraction of the pre-
polymer with deuterium to contrast strongly with the
ordinary hydrogenous substance. The deformation of
the polymer chains upon swelling or stretching of the
network can also be determined and the results compared
with predictions from the theory of rubber elasticity.
There are indications which fall short of definite
proof, that a certain amount of chain rearrangement
takes place, thus reducing the real chain expansion
to values less than expected from elementary models.

The theory of rubber elasticity has its origins in the early
work of Guth and Mark (1) who recognized that the reduction in
the number of statistical configurations of an uncoiled polymer
molecule led to the elastic restoring force of rubber. This
idea was pursued by many researchers. A major advance by James
(2) and James and Guth (3) led to a model currently known as the
phantom network. The ideas of James and Guth were strongly con-
tested for many years, but recent analyses of Graessley (4,5),
Ronca and Allegra (6), Flory (7) and Deam and Edwards (8), clar-
ified the problem and established the logical necessity of the
James-Guth contribution.

The phantom network model contains a crucial deficiency,
well known to its originators, but necessary for simplifying the
mathematical analysis. The model takes no direct account of the
impenetrability of polymer chains, not is the impossibility of
two polymer segments occupying a common volume provided for in
this model. Different views have been presented to remedy these
deficiencies, no consensus has been reached on models which are
both physically realistic and mathematically tractable.

When an elastic polymer network is stretched, the polymer
chains are deformed. The verification of the theory has been
largely based on measurements of the elastic restoring forces

and their assumed relation to elongation. Similarly, elastic
forces exerted by the chains in limiting the swelling of the
network in a solvent has been widely used for assessing theoret-
ical results. In the phantom network model, the chain deforma-
tion is in simple one-to-one correspondence with the stresses
induced by elastic deformation. If the phantom network model
were known to be an accurate representation of the behavior of
a real elastomer, an independent method of measuring chain de-
formation would only be of moderate interest.

     It has been clear that trapped entanglements contribute to
the elastic modulus. Recently, Ferry and co-workers (9) in a
highly significant set of investigations on networks crosslinked
under strain have been able to show that the additional forces
arising from entanglements are quite large. It is not at all
evident that the global expansion of polymer chains will follow
the elastic forces in the simple relationship described in a
phantom network model if contributions from entanglements are
major. For this reason, the independent measurement of stress-
strain behavior together with determination of chain deformation
is particularly significant.

     The molecular models of rubber elasticity relate chain
statistics and chain deformation to the deformation of the macro-
scopic material. The thermodynamic changes, including stress are
derived from chain deformation. In this sense, the measurement
of geometric changes is fundamental to the theory, constitutes
a direct check of the model, and is an unambiguous measure of the
mutual consistency of theory and experiment.

     Chain dimensions of polymer molecules in bulk (10,11) or in
a concentrated medium (12) are measurable by small angle neutron
scattering (SANS). The method is based on the idea that molecular
size and shape can be determined by labeling a small fraction of
the chains by deuterium substitution. The scattering lengths of
deuterium and ordinary hydrogen are very different, and a
deuterated chain stands out in strong contrast against a normal
protonated matrix. If the labeled chains are sufficiently
dilute, the scattering method will yield molecular parameters.

     The SANS experiment is applicable to polymeric networks
containing some deuterium labeled chains. The chain geometry
can be probed not only in the unperturbed network, but changes in
chain shape and size can be measured as a function of strain or
swelling. This enhances the applicability of SANS experiments
for elastomeric systems.

Neutron Scattering of Gaussian Chains

     The scattering of neutrons by any molecular system can be
elastic or inelastic, coherent or incoherent. The elastic co-
herent scattering of a labeled polymer in a background matrix can
be extracted from the data in a properly designed experiment.
The excess scattering from an ensemble of isolated chains
(negligible intermolecular interactions in the scattering

function) may be written as

$$I(\underset{\sim}{q}) = A(b_H - b_D)^2 Mc \; S(\underset{\sim}{q}) \qquad\qquad 1$$

$I(q)$ is the intensity at wave vector q, $(b_H-b_D)^2$ is a contrast factor arising from the difference in scattering lengths of deuterated and protonated species, M is molecular weight of the deuterated polymer, c is concentration in gm/ml, S(q) is a particle scattering factor, and A contains machine constants, detector efficiency, and other fixed quantities. For the purpose of the current study, S(q) is the quantity of significance, and it is given by

$$S(\underset{\sim}{q}) = \frac{1}{N^2} \langle \underset{i,j}{\Sigma} \; \exp[i\underset{\sim}{q}\cdot\underset{\sim}{r}_{ij}] \rangle \qquad\qquad 2$$

The number of polymer segments in a chain is N, the sum is taken over all segments i and j, and evidently, S(0)=1. The wave vector q in an elastic experiment is given by $q = (2\pi/\lambda)(k-k_0)$, being the wave length of the neutron, with k_0 and k being unit vectors in the directions of the incident and scattered rays respectively. The magnitude of q, designated as q, is given by $(4\pi/\lambda)\sin(\theta/2)$, where θ is the scattering angle, the angle between k_0 and k. The angle brackets < > refer to an ensemble average taken over all chain configurations.

In an ensemble of flexible polymer chains, the instantaneous separation of two segments i and j varies from one molecule to another. Ensemble averages such as required in Eq. 2 are obtained by specifying $W(r_{ij})$, the probability that segments i and j are separated by r_{ij}. In an elastomeric rubber which is not so highly swollen that excluded volume interactions become important, and which is not too greatly deformed, $W(\underset{\sim}{r}_{ij})$ takes a particularly simple form

$$W(\underset{\sim}{r}_{ij}) = A \; \exp(-ar_{ij}^2) \qquad\qquad 3a$$

Since in the relaxed state the system is isotropic

$$W(\underset{\sim}{r}_{ij}) = w(x_{ij})w(y_{ij})w(z_{ij}) \qquad\qquad 3b$$

where $w(x_{ij})$, the probability that the x coordinates of i and j is x_{ij} is given by

$$w(x_{ij}) = A^{1/3}\exp[-ax_{ij}^2] \qquad\qquad 3c$$

The constants a and A change upon network deformation, but the functional form does not. Simple integration shows that

$$S(\underset{\sim}{q}) = \frac{1}{N^2} \underset{i,j}{\Sigma} \; \exp(-\tfrac{1}{2}(q_x^2 \langle x_{ij}^2 \rangle + q_y^2 \langle y_{ij}^2 \rangle + q_z^2 \langle z_{ij}^2 \rangle)) \qquad\qquad 4a$$

Thus, $S(q)$ is completely determined by the second moments. If swelling is isotropic, $\langle x_{ij}{}^2 \rangle = \langle y_{ij}{}^2 \rangle = \langle z_{ij}{}^2 \rangle = \langle r_{ij}{}^2 \rangle / 3$, and Eq. 4a reduces to

$$S(\underset{\sim}{q}) = \frac{1}{N^2} \sum_{i,j} \exp(-q^2 \langle r_{ij}{}^2 \rangle / 6) \qquad \qquad 4b$$

It is well known that, the centroidal radius of gyration is easily expressed in terms of the mean squared distances between segments

$$R_g{}^2 = \frac{1}{N} \sum_k \langle R_{\sim ok}{}^2 \rangle = \frac{1}{2N^2} \sum_{i,j} \langle r_{ij}{}^2 \rangle \qquad \qquad 5$$

The first of Eq. 5 defines the radius of gyration, $R_{\sim ok}$ being the distance from the center of mass to the kth segment. The second equation is a form useful for the scattering problem. Expansion of Eq. 4b and substitution of Eq. 5 leads to

$$S(\underset{\sim}{q}) = 1 - q^2 R_g{}^2 / 3 + O(q^4) \qquad \qquad 6$$

Eq. 6 is a general result which applies even when Eq. 4b does not; it is directly derivable from Eq. 2 provided that the segment distribution is isotropic.

If the system is anisotropically deformed, uniaxial stretching, for example, the scattering depends on the orientation of the sample with respect to the neutron beam. For convenience, we choose the geometric arrangement shown in Figure 1. The neutron beam propagates in the negative X direction, the unique axis of orientation is along the Z axis, the detector in the scattering system lies in the YZ plane. The scattering angle θ is defined as in the isotropic case, the azimuthal angle ϕ is measured in the YZ plane clockwise from the Z axis. In this framework q_x is of order of θ^2, and since θ is always small, q_x may be set equal to zero. Eq. 4a becomes

$$S(\underset{\sim}{q}) = \frac{1}{N^2} \sum_{i,j} \exp\left[- \frac{q^2}{2} (\langle y_{ij}{}^2 \rangle \sin^2\phi + \langle z_{ij}{}^2 \rangle \cos^2\phi) \right] \qquad 7$$

In analyzing the scattering of the system further, it is necessary to describe the network in greater detail. For simplicity, it will be assumed that all chains are linked in crosslink junctions at their ends, the network is perfect, i.e., there are no dangling chains, and the functionality of the network, f, is a constant. The segments between crosslinks move freely, and obey the Gaussian law subject to constraints imposed by the pinning of the end segments of the junction points. The probability is Gaussian, and since, in general, deformation is anisotropic, it is easiest to focus on a single cartesian component for the purpose of calculation. The probability that the y component of the vector connecting i and j is given by y_{ij}
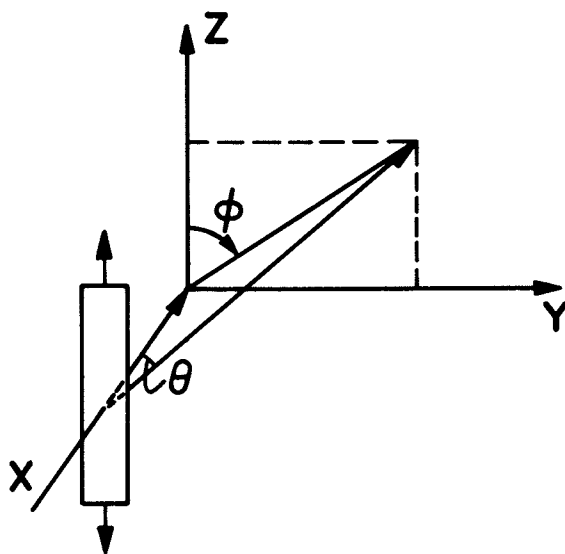
Figure 1.   The physical arrangement of an oriented polymer sample in a neutron scattering experiment showing the scattering angle, θ, and the azimuthal angle, φ.

subject to the fact that the chain ends are separated by Y is (13)

$$W(y_{ij};\ Y)=(\frac{c_{ij}}{\pi})^{\frac{1}{2}} \exp[-c_{ij}(y_{ij}-wY)^2] \qquad 8a$$

$$c_{ij} =\left(\frac{3}{2b^2Nw(1-w)}\right) \qquad 8b$$

$$w = |i-j|/N \qquad 8c$$

b is the length of a single polymer segment.

It is easily shown that, subject to the constraints on the chain ends,

$$<y_{ij}^2>_Y = Nb^2w(1-w)/3 + w^2<Y^2> \qquad 9$$

$< >_Y$ denotes an average over y_{ij} at fixed Y. Substitution of Eq. 7 in Eq. 9 yields

$$S(\underset{\sim}{q})=2\int_0^1(1-w)\exp[-x(w-w^2)- \frac{w^2q^2}{2}(<Y^2>\sin^2\phi+<Z^2>\cos^2\phi)]dw \qquad 10$$

Here $x = q^2Nb^2/6 = q^2R_g^{o2}$ where R_g^{o2} is the radius of an undeformed Gaussian random flight[8] chain. In deriving Eq. 10, the sum in Eq. 7 is replaced by an integral. The effect of the free chain segments, exclusive of the position of the junctions appears in the first two terms in the exponential. The deformations of the chains depend on the constraints on the junctions. Results are immediately derivable from Eq. 10.

A. If the network is undeformed, $<Y^2> = <Z^2>=Nb^2/3$, the terms in w^2 vanish, and S(q), by elementary integration, yields the well known result of Dębye for a random coil (14)

$$S(x) = 2(x - 1+e^{-x})/x^2 \qquad 11$$

B. Eq. 10 also applies for a closed loop in which $<Y^2>= <Z^2>=0$. Upon expansion, integration, and comparison with Eq. 6, we find for a closed loop

$$R_g^2 = Nb^2/12 \qquad 12$$

C. Regardless of the values $<Y^2>$ and $<Z^2>$, Eq. 10 may be written (13,15)

$$S(\underset{\sim}{q})=2 \int_0^1 (1-w)\exp[-aw-bw^2]dw \qquad 13$$

This may be reduced to an elementary function and error functions for b > o and an elementary function and Dawson's Integral for b < o (13,15). Calculations are easily performed since

subroutines for the error function and for Dawson's integral are available on most modern medium and large size computers.

S(q) yields R_g by expansion as seen in Eq. 6. If the system is anisotropically deformed, the scattering in a particular azimuthal direction yields a projection of the radius of gyration. For convenience, this quantity is designated as R_ϕ and is defined by

$$S(\underset{\sim}{q}) = 1 - q^2 R_\phi^2 / 3 \qquad 14a$$

where $\underset{\sim}{q}$ is given by

$$\underset{\sim}{q} = q \ (\underset{\sim y}{e} \sin\phi + \underset{\sim z}{e} \cos\phi) \qquad 14b$$

$\underset{\sim y}{e}$ and $\underset{\sim z}{e}$ being unit vectors along the Y and Z axis.

From Eq. 10 it follows that

$$R_\phi^2 = R_g^{o^2}/2 + [<Y^2>\sin^2\phi + <Z^2>\cos^2\phi]/4 \qquad 15$$

In anisotropic samples, it is convenient to concentrate on the principal directions of deformation. In uniaxial stretch, the parallel and perpendicular radii are given by

$$R_{\parallel}^2 = R_g^{o^2}/2 + <Z^2>/4; \ (\phi = 0) \qquad 16a$$

and

$$R_{\perp}^2 = R_g^{o^2}/2 + <Y^2>/4; \ (\phi = 90°) \qquad 16b$$

In isotropic swelling $R_\phi^2 = R_g^2$ and $<Y^2> = <Z^2> = <R^2>/3$.

Then

$$R_g^2 = R_g^{o^2}/2 + <R^2>/12 \qquad 17$$

$<R^2>$ is the mean square end-to-end distance of the polymer chain. Consider a sample stretched by a factor λ_y in the Y direction and λ_z in the Z direction. A general deformation can be easily treated, but for simplicity only uniaxial stretching or isotropic swelling will be examined. Note that under conditions of uniaxial deformation, the volume of the sample changes very little. This change may be ignored, and it becomes convenient to set $\lambda_z = \lambda$ and $\lambda_x = \lambda_y^{-1/2}$.

We consider four possible relationships between sample deformation and chain deformation.

A. The vector connecting the ends of a chain is deformed affinely. The crosslink junctions are fixed in space.

$$<Z^2> = \lambda_z^2 <Z^{o^2}> \qquad 18$$

$\langle z_o^2 \rangle$, which signifies $\langle z^2 \rangle$ of the mean end-to-end distance of the unperturbed chain, equals $Nb^2/3$.

B. The mean vector connecting the chain ends is deformed affinely. The crosslink junctions fluctuate according to the theory of Brownian motion (2,4,5,7).

$$\langle z^2 \rangle = [(f-2)\ \lambda_z^{\ 2}/f + 2/f]\langle z_o^2 \rangle \qquad\qquad 19$$

Fluctuations are larger in networks of low functionality and they are unaffected by sample deformation. The mean squared chain dimensions in the principal directions are less anisotropic than in the macroscopic sample. This is the phantom network model.

C. Fluctuations are partially damped by chain interferences. This leads to a result intermediate between A. and B. To be specific, a model proposed by Flory (16) is adopted here. In this model, the inhibitory influence on junction fluctuations is assumed to be affine in the strain. One finds

$$\langle z^2 \rangle = \{\lambda_z^2(1 - \frac{2}{f(1+\kappa)}) + \frac{2}{f(1+\kappa\lambda_z^{-2})} \}\langle z_o^2 \rangle \qquad 20$$

The parameter κ is a measure of the constraints on fluctuations of the crosslinks. If κ=o, the phantom network result of Eq. 19 is obtained, for κ=∞, the fixed junction approximation of Eq. 18 results.

D. It cannot be ignored that a network unfolding and rearrangement can take place with crosslink junctions settling in positions in which the vectors connecting chain ends deform less than in the phantom model (17,18). The driving force for this rearrangement is a decrease in free energy relative to that of either A or B. However, the statistical configurations corresponding to such readjustments are partially inaccessible owing to trapped entanglements. The extent to which such rearrangements occur is expressed by an equation in which the deformation of the coordinates connecting chain ends, λ^*, is related to the macroscopic deformation, λ. A suitable expression for the relation is

$$\lambda^{*2} = (1 - \alpha)\lambda^2 + \alpha \qquad\qquad 21$$

Note that $\lambda^*=\lambda$ if α=o, which represents no change from the affine models, and $\lambda^*=1$ where network unfolding takes place upon deformation without chain extension. If α is non-zero, network unfolding can be introduced into the previous equations by substituting λ^* for λ in Eqs. 18, 19 or 20. The most general result of the models discussed above is obtained by replacing λ_z by λ_z^* in Eq. 20. Appropriate choices of κ and α lead to the results of Eq. 18 or 19 as well.

Expressions for $\langle Y^2 \rangle$ are identical in form with those of $\langle Z^2 \rangle$. Using any of the hypotheses A through D leads to the scattering law by means of Eq. 10. Determination of R_ϕ^2 or R_g^2 from these models is obtained by substitution in Eqs. 15, 16a, 16b or 17.

Numerical Results from Scattering Theory

The parameters of neutron scattering theory of polymer networks are λ, the macroscopic stretching of the sample, or linear degree of swelling, f, the network functionality, κ. which accounts for restricted junction fluctuations and α, a measure of the degree to which chain extension parallels the macroscopic sample deformation. The functionality is known from knowledge of the chemistry of network formation, and λ is measured. Both κ and α must be extracted from experiments.

Table I contains calculations of changes in molecular dimensions which would be obtained from a SANS experiment if the models of the network proposed in the previous section apply. Only a few results are shown, others are easily calculated using equations from the previous section. The data in the Table refer to uniaxial stretching only. However, in an isotropically swollen network, the calculated values of $(R^2/R_g^2)^{\frac{1}{2}}$ are identical with the values of $(R_\parallel/R_g^2)^{\frac{1}{2}}$ given in the Table. Of course λ has not the same precise sense in the two experiments.

The following qualitative results are evident from the numbers quoted in the Table. In the phantom network, the macroscopic dimensional change is always greater than increases in R_g or R_ϕ, though chain expansion varies monotonically with sample extension. The higher the functionality, the greater the chain expansion at a given overall deformation. This is a consequence of a reduction in junction fluctuations at junction points of higher functionality.

The chain deformation parallel to the direction of stretch is much greater than that in the perpendicular direction. This is true for all models considered here.

If restricted junction fluctuations are taken into account, the chain deformation is increased, and is more anisotropic. The effect of increasing κ is much more evident in networks of low functionality, since fluctuations of junction points are of minor importance in networks of high functionality.

If network unfolding takes place so that distances between junctions connecting the ends of a polymer chain deform less than that of a phantom network, molecular dimensions change less than by any other of the models considered. This is easily seen from the data presented for α not equal to zero.

TABLE I

CALCULATED DIMENSIONAL CHANGES IN POLYMER
CHAINS IN STRETCHED ELASTOMERS

λ	f	α	κ	$(R_\parallel^2/R^{o^2})^{1/2}$	$(R_\perp^2/R_g^{o^2})^{1/2}$	Description
1.5	3	0	0	1.099	0.972	
1.5	4	0	0	1.146	0.957	
1.5	6	0	0	1.190	0.943	
1.5	10	0	0	1.225	0.931	
2.0	3	0	0	1.225	0.957	
2.0	4	0	0	1.323	0.935	Phantom Network
2.0	6	0	0	1.414	0.913	
2.0	10	0	0	1.483	0.894	
3.0	3	0	0	1.528	0.943	
3.0	4	0	0	1.732	0.913	
3.0	6	0	0	1.915	0.882	
3.0	10	0	0	2.049	0.856	
2	4	0	0.5	1.434	0.890	
2	10	0	0.5	1.524	0.876	
2	4	0	1.0	1.483	0.878	Junction Fluctua-
2	10	0	1.0	1.543	0.871	tion Partially
2	4	0	2.0	1.528	0.871	Restricted
2	10	0	2.0	1.546	0.869	
2	4	0.2	0	1.265	0.941	Network Rearrange-
2	4	0.5	0	1.173	0.953	ment and Diminished
2	4	0.7	0	1.107	0.965	Chain Deformation
1.5	—	0	0	1.274	0.913	Crosslink Junctions
2	—	0	0	1.580	0.866	do not Fluctuate
3	—	0	0	2.234	0.817	

The major emphasis in SANS experiments is often concentrated on R_g^2, $R_\parallel^2$ or $R_\perp^2$, since the results obtained are independent of any molecular model. A great deal of additional information resides in the entire angular scattering pattern, $S(q)$. Calculations of these functions have been presented elsewhere ($\underline{13}$), a few examples are chosen to illustrate how scattering changes with structure and deformation of a network. In the Figures and subsequently in this section, $S(q)$ will be written as $S(x)$ ($x = q^2 R_g^2 = q^2 N b^2/6$) since the scattering depends on q through x only.

Figures 2, 3 and 4 show $S(x)$ versus ϕ for the phantom network model and for the fixed junction case. The largest changes with angle are if the junctions are fixed, the smallest changes are with the phantom network of lowest functionality.

A measurement of $S(x)$ requires that the SANS spectrometer be calibrated by some absolute standard, a process which is often difficult to achieve with precision. An easier measurement in the ratio of scattering intensities of an anisotropic sample in two different directions. Figure 5 shows a graph of $S_\parallel(x)/S_\perp(x)$ versus x for the phantom model and the fixed junction case.

The effect of restricted junction fluctuations on $S(x)$ is to change the scattering function monotonically from that exhibited by a phantom network to that of the fixed junction model. Network unfolding produces the reverse trend, the change of $S(x)$ with x is even less than that exhibited by a phantom network. Figure 6 illustrates how the scattering function is modified by these two opposing influences.

Experimental Results

It is always easy to calculate idealized scattering curves for perfect networks. The experimental systems vary from the ideal to a greater or lesser degree. Accordingly, any estimate of the correctness of a theoretical analysis which is based on an interpretation of experiment must be put forth with caution since defects in the network may play a role in the physical properties being measured. This caveat applies to the SANS measurement of chain dimensions as well as to the more common determinations of stress-strain and swelling behavior.

Figure 7 shows swelling results obtained by Benoit et al. ($\underline{19}$). On each of the curves, the points at lowest λ represent swelling in cyclohexane, the next in tetrahydrofuran and the last in benzene. In all cases, the samples were swollen in the pure solvent. The curves are reproduced from Figure 13 of Reference 19. The networks were made from anionically polymerized polystyrene using a bifunctional initiator crosslinked subsequently by divinyl benzene. The curves correspond to different ratios of divinyl benzene (DVB) per polystyrene living end (LE).
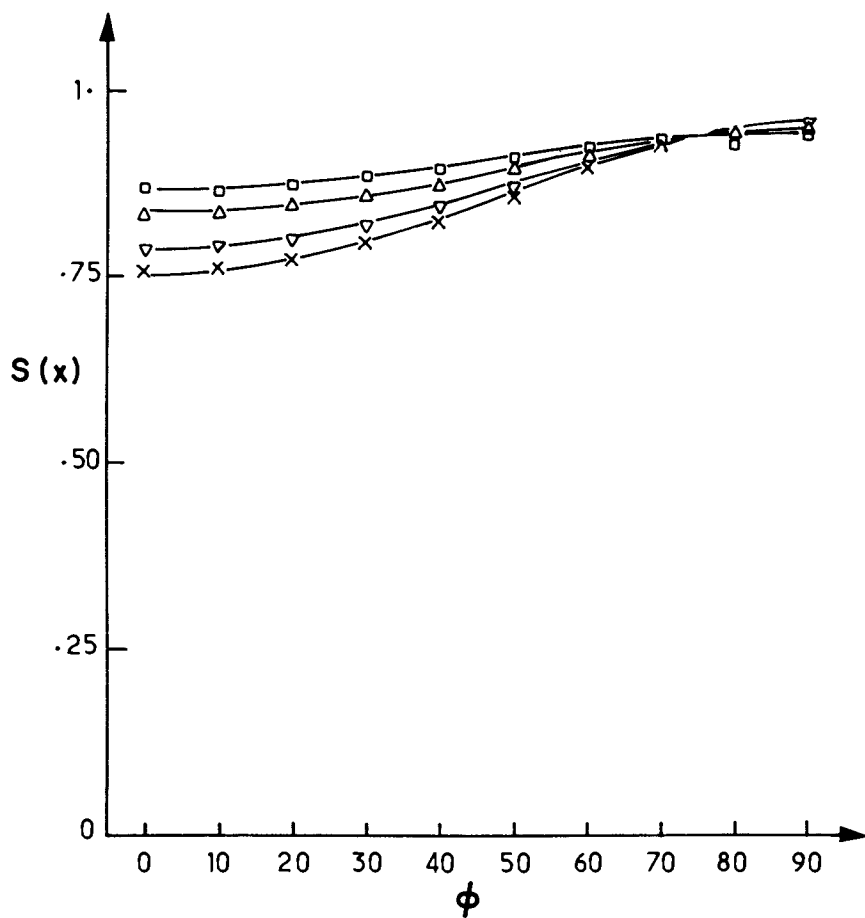
Figure 2.   Scattering intensity versus azimuthal angle for a uniaxially oriented
elastomer , λ is 3, x is 0.2. Phantom network where: □, f is 3; △, f is 4; ▽, f is 10.
Crosslink junctions fixed, X.
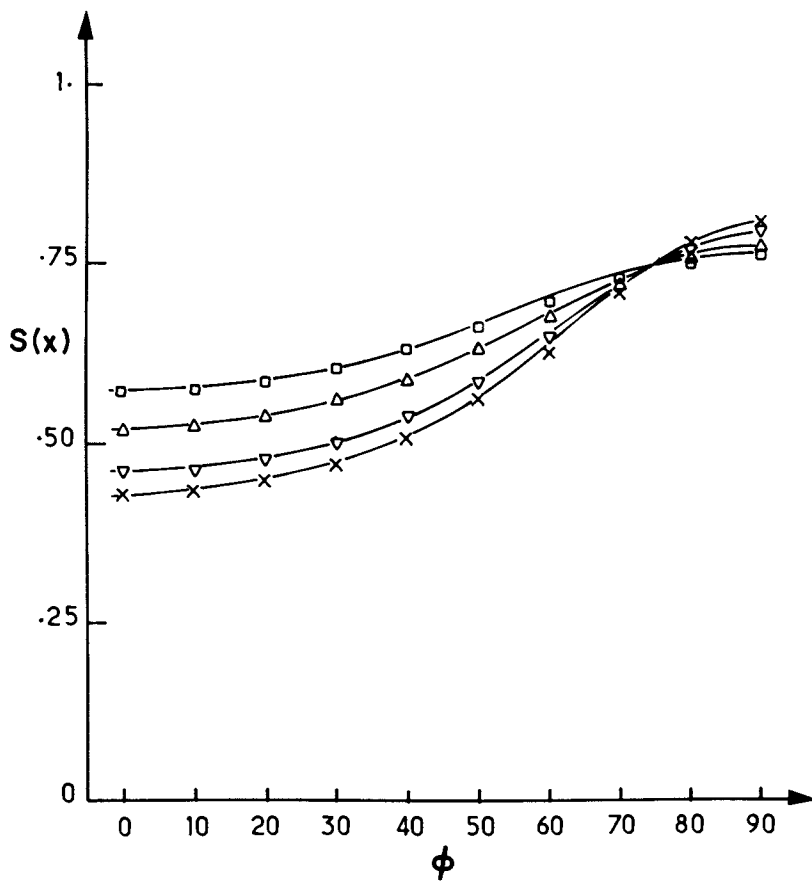
Figure 3.   Scattering intensity versus azimuthal angle for a uniaxially oriented elastomer, λ is 3, x is 1. Phantom network where: □, *f is 3;* △, *f is 4;* ▽, *f is 10. Crosslink junctions fixed,* ✗.
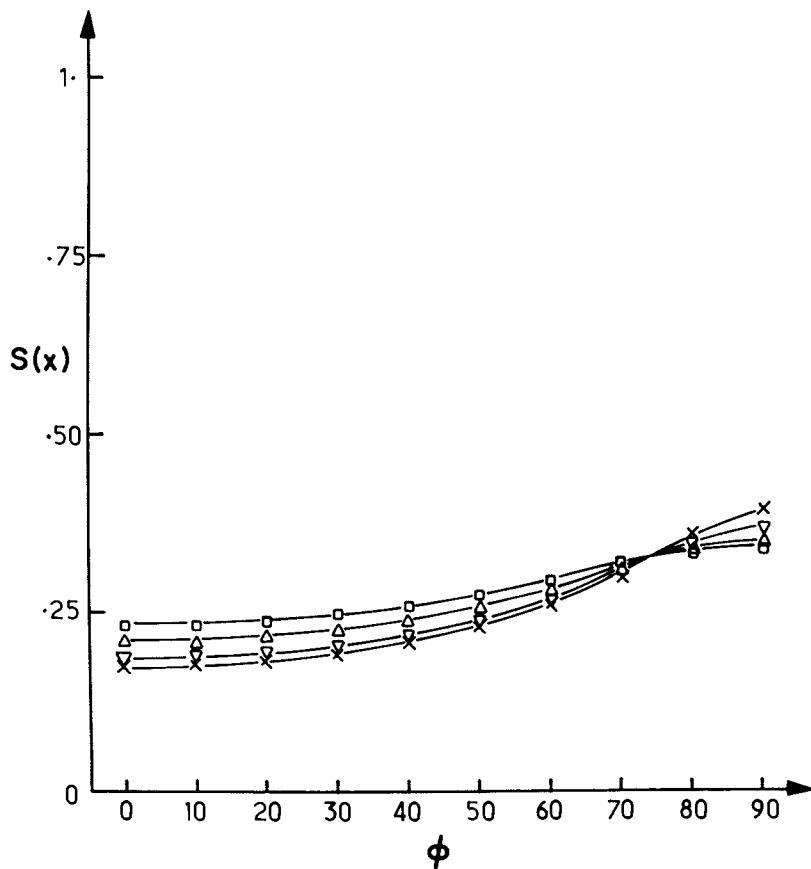
Figure 4. Scattering intensity versus azimuthal angle for a uniaxially oriented elastomer, λ is 3, x is 5. Phantom network where: □, f is 3; △, f is 4; ▽, f is 10.
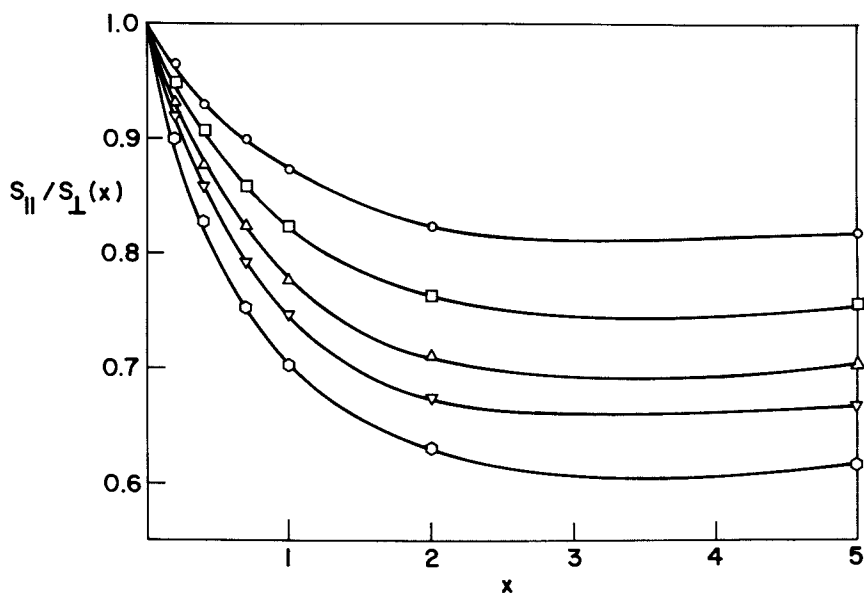
Figure 5. *The ratio $S_{\parallel}(x)/S_{\perp}(x)$ plotted as function of x for the phantom network at different cross-link functionalities, and for a fixed junction network. λ is 2. Key: $\bigcirc$, f is 3; $\square$, f is 4; $\triangle$, f is 6; $\triangledown$, f is 10; $\obar$ is junctions fixed.*
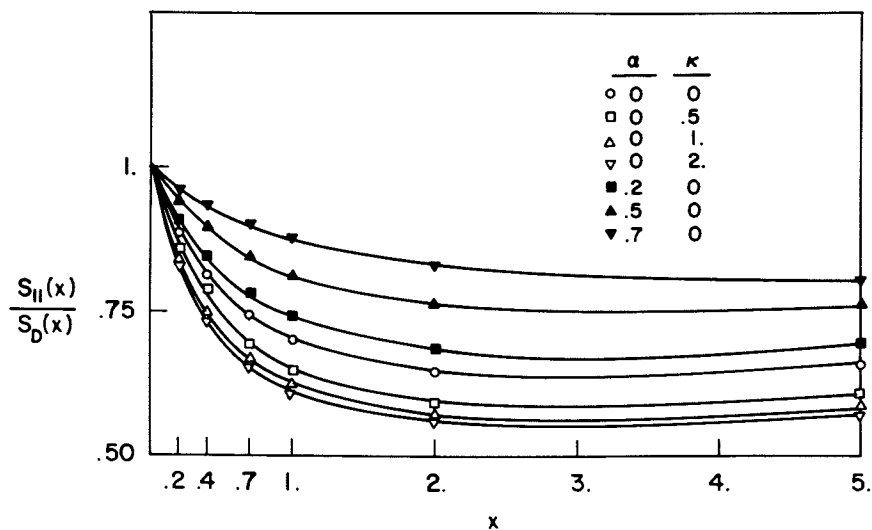
Figure 6. *A plot of $S(x)/S_D(x)$ versus f for a network in which junction fluctuations are partially inhibited ($\kappa \neq 0$) and where molecular deformations are less than affine ($\alpha \neq 0$).*
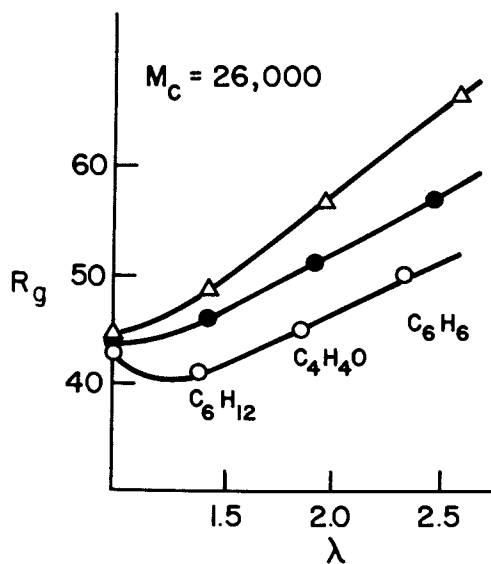
Figure 7.   SANS measurements of R_g versus λ of swollen polystyrene networks. M_c is the molecular weight between cross-links. Key: $\triangle$, DVB/LE = 3; $\bullet$, DVB/ LE = 6; $\bigcirc$, DVB/LE = 10. Data from Ref. 19.

Approximately 5% of the chains were perdeuterated. The chain
dimensions changed slightly or not at all upon crosslinking.
Table II contains measured R_g/R_g^o from the experiment and calcu-
lated R_g/R_g^o from the phantom network model. Since, the function-
ality of these networks is not well known but is probably high,
calculated data at several different functionalities are shown.
In network BI in which chain expansion was the greatest, the
measured results show more chain swelling than a network with f=3
but less than a network with f=4. Chain swelling was less than
that of the phantom network model for the other two networks, and
in one case, the chains coiled to a size slightly less than that
of the unperturbed molecule.

     Beltzung et al. (20) conducted SANS experiments on tetra-
functionally end-linked polydimethylsiloxane chains. The radius
of gyration of the deuterium labeled chains did not change upon
crosslinking. The data presented in Figure 8 are taken from
Figure 2 of Reference 20. The following conclusions can be
drawn. There is little systematic difference between networks
prepared in bulk and networks prepared from solution. The results
cluster around the curve for the phantom network model with
materials of lower molecular weight showing greater chain defor-
mation and those of higher molecular weight exhibiting lesser
chain deformation. This could be accounted for by assuming that
network defects were substantial in the system of higher molecular
weight. If, by contrast it is assumed that invocation of network
defects is not correct, the data can be understood in terms of
restricted junction fluctuations and compensating network un-
folding and chain rearrangement. Network unfolding can only be
important for longer chains. Restricted fluctuations of cross-
link junctions is of comparable importance regardless of molecular
weight in a Gaussian model. Therefore, we suggest that the higher
chain expansion for the lower molecular weights is a measure of
restricted fluctuation of the crosslinks. This influence occurs
at all molecular weights but is compensated by network unfolding
with reduced chain expansion which becomes increasingly important
as molecular weight increases. This is so because the fraction
of neighboring geometric crosslinks in the network which are
topological neighbors as well increases as the molecular weight
between crosslinks decreases.

     The SANS experiments of Clough et al. (21) on radiation
crosslinked polystyrene are presented in Figure 9, and appear to
fit the phantom network model well. However, these networks were
prepared by random crosslinking, and the calculations given are
for end-linked networks, which are not truly applicable.

     The first SANS experiments on end-linked elastomers with a
well-defined functionality were carried out by Hinkley et al. (22).
Hydroxy-terminated polybutadiene was crosslinked by a trifunctional
isocyanate, and the resultant polymer was uniaxially stretched.

TABLE II

COMPARISON OF CALCULATED AND MEASURED SWELLING OF CHAINS

Sample	M_c	R_g^o	Cyclohexane		Tetrahydrofuran		Benzene	
			λ	R_g/R_g^o	λ	R_g/R_g^o	λ	R_g/R_g^o
BI	26,000	45	1.45	1.09	1.96	1.27	2.59	1.49
BII	26,000	44	1.42	1.05	1.93	1.16	2.46	1.30
BIII	26,000	43	1.38	.93	1.84	1.05	2.32	1.16

	R_g/R_g^o			
	Phantom Network			Fixed
λ	f=3	f=4	f=10	Junctions
1.5	1.099	1.146	1.225	1.274
2.	1.225	1.323	1.483	1.580
2.5	1.369	1.521	1.761	1.904
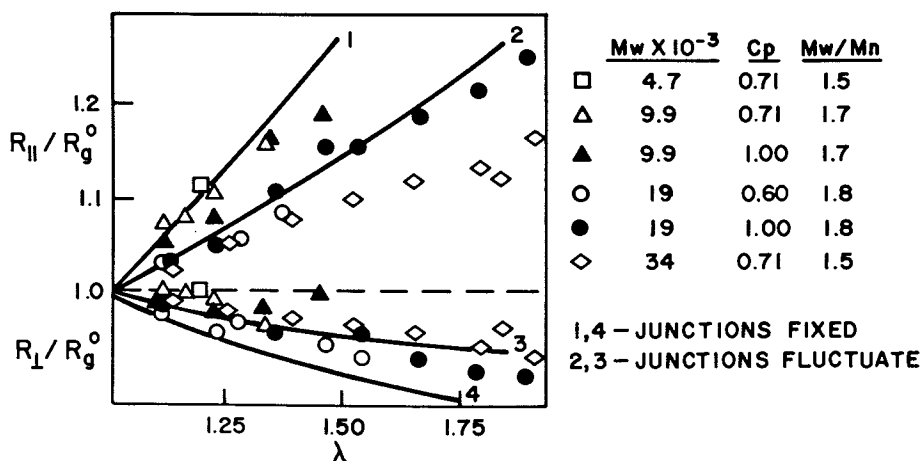
Figure 8. *SANS measurements of $R_{\parallel}/F_g{}^\circ$ and $R_{\perp}/R_g{}^\circ$ versus λ of tetrafunctional polydimethylsiloxane networks. M_w and M_n are weight and number average molecular weights before crosslinking, c_p is the polymer fraction in solution before crosslinking. Data from Ref. 20.*
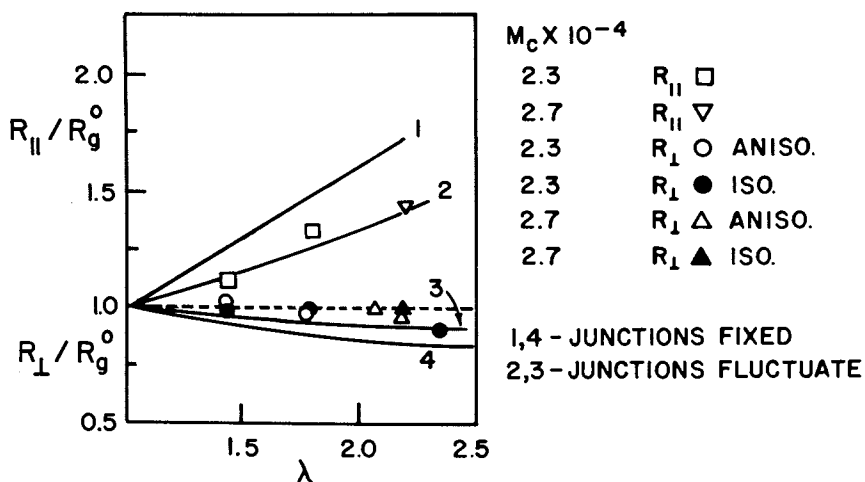
Figure 9. *SANS measurements of $R_{\parallel}/R_g{}^\circ$ and $R_{\perp}/R_g{}^\circ$ for stretched radiation cross-linked polystyrene. $R_{\perp}$ is determined by measurements in which the neutron is parallel (iso) and perpendicular (aniso) to the stretching direction. M_c is molecular weight between crosslinks. Theoretical curves 2 and 3 are drawn for tetrafunctional networks. Data from Ref. 21.*

The experimental error was very large, with the apparent chain
deformation greater than that expected for a phantom network,
and closest to the curve anticipated where crosslink fluctuations
are completely suppressed.

C. C. Han, H. Yu and their colleagues (23) have presented
some new SANS data on end-linked trifunctional isoprene networks.
These are shown in Figure 10. Those materials of low molecular
weight between crosslinks exhibit greater chain deformation
consistent with the thesis that the junction points are fixed.
This is the reverse of that found by Beltzung et al. for siloxane
networks.

Summary

The deformation of polymer chains in stretched and swollen
networks can be investigated by SANS. A few such studies have
been carried out, and some theoretical results based on Gaussian
models of networks have been presented. The possible defects in
network formation may invalidate an otherwise well planned
experiment, and because of this uncertainty, conclusions based
on current experiments must be viewed as tentative. It is also
true that theoretical calculations have been restricted thus far
to only a few simple models of an elastomeric network. An
appropriate method of calculation for trapped entanglements has
not been constructed, nor has any calculation of the SANS pattern
of a network which is constrained according to the reptation
models of de Gennes (24) or Doi-Edwards (25,26) appeared.

In this review, we have given our attention to Gaussian
network theories by which chain deformation and elastic forces
can be related to macroscopic deformation directly. The results
depend on crosslink junction fluctuations. In these models,
chain deformation is greatest when crosslinks do not move and
least in the phantom network model where junction fluctuations
are largest. Much of the experimental data is consistent with
these theories, but in some cases, (19,20) chain deformation is
less than any of the above predictions. The recognition that a
rearrangement of network junctions can take place in which chain
extension is less than calculated from an affine model provides
an explanation for some of these experiments, but leaves many
questions unanswered.

A crucial requirement in future investigations is that
macroscopic measurements of stress and swelling be performed on
the same materials used for small angle neutron scattering. A
sensible program for research is apparent. The work remains
to be done.
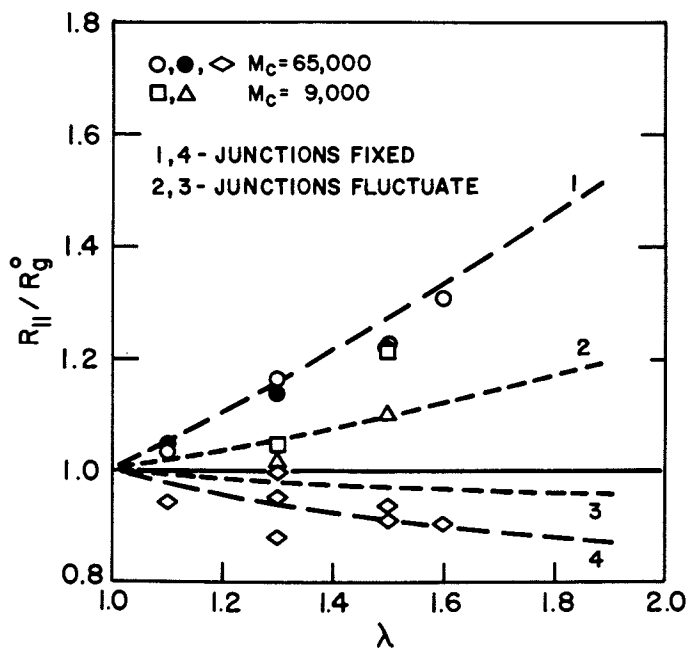
Figure 10.   SANS measurements of $R_\parallel/R_g^\circ$ and $R_\perp/R_g^\circ$ for stretched trifunctional end-linked polyisoprene. Curves 1 through 4 are theoretical. Data from Ref. 22.

Literature Cited

1. Guth, E.; Mark, H. Monatsh. 1934, 68, 93.
2. James, H. M. J. Chem. Phys. 1947, 15, 651.
3. James, H. M.; Guth, E. J. Chem. Phys. 1947, 15, 689.
4. Graessley, W. W., Macromol. 1975, 8, 186.
5. Graessley, W. W., Macromol. 1975, 8, 865.
6. Ronca, G.; Allegra, G., J. Chem. Phys. 1975, 63, 4990.
7. Flory, P. J., Proc. Roy. Soc. 1976, A351, 351.
8. Deam, R. T.; Edwards, S. F., Philos. Trans. Roy. Soc. 1976,
    A280, 1296.
9. See Hvidt, S.; Kramer, O.; Batsberg, W.; Ferry, J. D. Macromol.
    1980, 13, 933 and references contained therein.
10. Cotton, J. P.; Decker, D.; Benoit, H.; Farnoux, B.; Higgins,
    J.; Jannink, G.; Ober, R.; Picot, C.; des Cloizeaux, J.
    Macromol. 1974, 7, 863.
11. Kirste, R. G.; Kruse, W. A.; Ibel, K. Polymer 1975, 16, 120.
12. Daoud, M.; Cotton, J. P.; Farnoux, B.; Jannink, G.; Sarma,
    G.; Benoit, H.; Duplessix, R.; Picot, C.; deGennes, P. G.
    Macromol. 1975, 8, 804.
13. Ullman, R. J. Chem. Phys. 1979, 71, 436.
14. Debye, P. J. Phys. & Coll. Chem. 1947, 51, 18.
15. Pearson, D. S. Macromol. 1977, 10, 696.
16. Flory, P. J. J. Chem. Phys. 1977, 5720 66.
17. Bastide, J.; Picot, C.; Candau, S. J. Macromol. Phys. 1981,
    B19, 13. See Figure 3 and p. 25.
18. Ullman, R. Macromol., In Press.
19. Benoit, H.; Decker, D.; Duplessix, R.; Picot, C.; Rempp,;
    Cotton, J. P.; Farnoux, B.; Jannink, G.; Ober, R. J. Polymer
    Sci. Polym. Phys. 1976, 14, 2119.
20. Beltzung, M.; Herz, J.; Picot, C.; Bastide, J.; Duplessix, R.
    Abstract of Communications, 27th International Symposium on
    Macromolecules, Strasbourg, July 6-9, 1981, p. 728.
21. Clough, S.; Maconnachie, A.; Allen, G. Macromol. 1980, 13, 774.
22. Hinkley, J. A.; Han, C. C.; Mozer, B.; Yu, H., Macromol.
    1978, 11, 836.
23. Han, C. C., personal communication.
24. de Gennes, P. G. J. Chem. Phys. 1971, 55, 572.
25. Doi, M.; Edwards, S. F. J. Chem. Soc. Faraday Trans. 2 1978,
    13, 1789, 1808, 1818.
26. Marucci, G. Macromol. 1980, 14, 434.

Molecular Configurations of Elastomers Via Solid State NMR

Y.-Y. LIN, JAMES E. MARK, and JEROME L. ACKERMAN

University of Cincinnati, Department of Chemistry, Cincinnati, OH 45221

A theoretical investigation of the use of NMR lineshape second moments in determining elastomer chain configurations has been undertaken. Monte Carlo chains have been generated by computer using a modified rotational isomeric state (RIS) theory in which parameters have been included which simulate bulk uniaxial deformation. The behavior of the model for a hypothetical poly(methylene) system and for a real poly(p-fluorostyrene) system has been examined. Excluded volume effects are described. Initial experimental approaches are discussed.

The concept of affine deformation is central to the theory of rubber elasticity. The foundations of the statistical theory of rubber elasticity were laid down by Kuhn (1), by Guth and James (2) and by Flory and Rehner (3), who introduced the notion of affine deformation: namely, that the values of the cartesian components of the end-to-end chain vectors in a network vary according to the same strain tensor which characterizes the macroscopic bulk deformation. To account for apparent deviations from affine deformation, refinements have been proposed by Flory (4) and by Ronca and Allegra (5) which take into account effects such as chain-junction entanglements.

Ullman has summarized three levels of network affine deformation: 1) affine deformation of junction coordinates; 2) of mean (i.e., rms) junction coordinates, with concomitant fluctuations about mean positions; 3) of statistical chain segments; as well as: 4) non-affine behavior at the molecular level. Each of these possibilities engenders different behaviors of the network in response to bulk deformation. Yet it has proved notoriously difficult to obtain a direct experimental categorization of the affineness of macromolecular deformation. This is primarily due to the lack of experimental modalities which can probe molecular configurations, and yet which are sensitive to relative configurations of topologically close (and, potentially, spacially remote) segments, while discriminating against those of topologically remote, spacially close segments.

Small angle neutron scattering (SANS) of "marked" (isotopically labeled) chains in unmarked networks has proven to be of potential value in

determining which affine model is most appropriate for a given system. The theoretical scattering laws for the alternative models have been derived (6). Initial experimental results (7,8) have suggested that the true description of the deformation of a network may involve a combination of the four possibilities, and that the description can depend on the thermal and mechanical history of the sample. In addition, models incorporating entanglements have been evaluated using neutron scattering (9).

Because of the grandiose scale of the apparatus involved, SANS facilities are few in number worldwide; access to them is limited and expensive. We have attempted to devise an experiment which employs solid state nuclear magnetic resonance to examine some aspects of affine deformation.

We have completed a series of computer experiments which indicate that it should be possible to test the validity of segmental affine behavior with our technique.

NMR Second Moments and Segment Configurations

In molecularly rigid systems, the direct (through-space) dipole-dipole interaction between nuclear spins $I = \frac{1}{2}$ is normally the dominant source of broadening of the NMR lineshape. For a pair of similar nuclear spins i and j in a magnetic field H_o the dipolar splitting in their spectrum is given by

$$\omega_D = \gamma_I^2 \hbar \frac{P_2(\cos\theta_{ij})}{r_{ij}^3}$$

$$P_2(x) = \frac{1}{2}(3x^2 - 1)$$

where γ and I are the magnetogyric ratio and spin quantum number respectively. As illustrated in Figure 1, ω_D incorporates geometric information as θ_{ij}, the angle between the internuclear vector and the magnetic field, and as r_{ij}, the length of the internuclear vector.

When a large number of spins interact, the numerous lines of the splitting pattern overlap and merge into a continuous lineshape whose functional form cannot be obtained from theory. Yet this shape contains useful geometrical information. One means of representing this dipolar lineshape $g(\omega)$ is by a moment expansion

$$M_n = \int (\omega - \omega_o)^n g(\omega) d\omega$$

about the nominal resonance frequency ω_o. Because of the properties of the dipolar interaction, the lineshape is symmetric about ω_o, and therefore only even moments are required.

The great utility of moments is that, although the lineshape cannot be calculated analytically for an arbitrary configuration of nuclear spins, any moment may in principle be calculated to arbitrary precision from first principles (10). In practice, only the lowest moments are calculable because of computer time and precision constraints. In particular, the second moment M_2 is the lowest moment containing spacial information

and is given by

$$M_2 = C \sum_{i > j} [P_2(\cos \Theta_{ij}) r_{ij}^{-3}]^2$$

The sum is carried out over all pairs of nuclear spins ij, counting each pair exactly once. C is a collection of fundamental constants and also contains the total number of spins.

If we were to have an isolated polymer chain with a single nuclear spin attached to each segment (the marked chain) crosslinked into an unmarked network, the second moment of the NMR line of that spin species would carry information relating to the separation of chain segments, and to their relative orientation with respect to the field direction. If the network were to be subjected to a bulk deformation, these geometrical parameters would be altered, and hence we would expect a corresponding change in the value of the experimentally measured M_2.

Two limiting geometrical cases illustrate this nicely. For a uniaxial elongation λ, transverse separations decrease by $\lambda^{-\frac{1}{2}}$ at constant mass density. If the magnetic field is collinear with the elongation axis the contribution to M_2 of a spin pair with internuclear vector parallel to the axis changes as λ^{-6}. The contribution of a spin pair oriented transversely would follow λ^3. For other orientations, there will be changes in both separation and angular factor. Clearly, these results are anticipated for spins on segments embedded in an elastic continuum, i.e., for the segmental affine case. Other microscopic segmental changes would be expected to follow different M_2 versus elongation behaviors.

We note here that the use of NMR in determining orientational information is not new; second and fourth moments of the resonance line in bulk materials have been used to obtain second and higher moments (more precisely, Legendre polynomial averages $P_n(\cos\Theta_{ij})$) of segmental orientational distribution functions (11, 12, 13, 14). We are interested more particularly in changes in relative segment orientations (configurations).

These moment studies have been performed on polymer systems such as polyethylene (or on penetrants in polymer systems) in which the interacting spins (protons or fluorines) reside on the same or on adjacent atoms. This allows essentially no freedom of variation in the internuclear vectors upon deformation of the network. The primary informational content therefore relates to independent segmental orientation distributions. By placing single spins on alternate segments, there should be much greater sensitivity to changes in the chain extension upon bulk deformation.

This effect was confirmed in our early computer results. Placing spins on every third segment was also attempted. Because of the strong inverse sixth power dependence on r, the second moment values, although strongly dependent on chain dimensions, were of a magnitude too small to be reliably measured experimentally against a background of other broadening effects (i.e., linewidths of a few hundred Hz).

Rotational Isomeric State Model with Deformation

In order to develop a molecular model of elongation from which M_2's can be calculated, we have chosen the rotational isomeric state (RIS)

model (15). Consider the Monte Carlo generation of a polymethylene chain via the RIS scheme. Each new methylene residue may be appended to the growing chain in one of the three rotational states: trans(t), gauche plus (g^+) or gauche minus (g^-). The statistical weight (SW) of each conformer is given by the corresponding Boltzmann factor. This procedure generates an essentially isotropic chain. If, however, we modify the statistical weights by an angular factor

$$SW \rightarrow (1 + aP_2(\cos\Theta))SW$$

with Θ being the angle between an elongation axis and the potential new bond, we can cause the chain to orient (See Figure 2).

The P_2 function has been chosen as it is the lowest order uniaxial term in the expansion in spherical harmonics of any generalized angular distribution. We note parenthetically that the P_2 function possesses the precise differential behavior corresponding to small ($\lambda \approx 1$) uniaxial deformations at constant bulk density: namely that along z ($P_2(\cos\Theta) \approx 1$) a small deformation $d\lambda$ requires that transverse to z ($P_2(\cos\Theta) \approx -\frac{1}{2}$) the deformation must be $-\frac{1}{2}d\lambda$. The parameter a alters the intensity of the bias, and in fact may be thought of as an order parameter. We can further bias the chain by altering the trans/gauche energy difference. This allows us to manipulate the trans/gauche population ratio, and therefore alters the isotropic elongation of the chain. For each chain generated, we can calculate M_2, and then take averages over many chains.

A problem arises, in that the strong r^{-6} dependence of M_2 requires that close overlap of spins be prevented. Thus, even though excluded volume interactions have no effect on chain dimensions in the bulk amorphous phase, it is important in the present application to build in an excluded volume effect (simulated with appropriate hard sphere potentials), so that occasional close encounters of the RIS phantom segments do not lead to unrealistically large values of M_2.

Computer Method

As a simplified initial approach to the problem, we chose a polymethylene chain with a single spin residing at every other carbon center, to allow sufficient flexibility between spins. The calculational procedure is based on that of Flory and Mark (16), with conformer parameters taken from Abe, et al. (17) and Yoon, et al. (18, 19) The elongation and field directions were collinear.

For each methylene segment to be appended to the chain, the bond directions corresponding to the three possible rotamers are calculated from the transformation matrices in the usual way. The angular weighting factors are then determined and are multiplied with the statistical weights. These weights are normalized to probabilities, and a random number is used to select one rotamer.

The new backbone atom must now be checked for overlap with other atoms on the chain. The distance from every other atom is then calculated. If there is a spin on this atom, terms for the second moment summation are accumulated in this program loop as well.
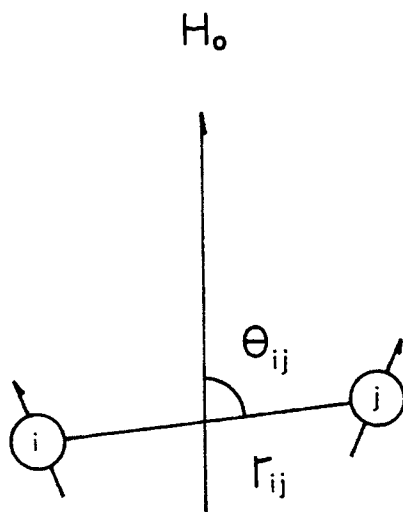
Figure 1.   Spherical coordinates used to calculate the dipolar interaction between two nuclear spins in a strong magnetic field H_o.

These variables, connecting all possible pairs of spins in a multispin system, are used for the evaluation of the second moment M_2.
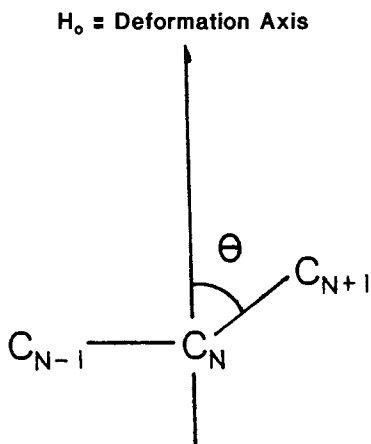
Figure 2.   Angle variable used to bias a polymer chain for orientation.

The Boltzmann statistical weight for each rotamer is multiplied by $(1 + aP_2(\cos \theta))$, with a being an adjustable parameter, before a particular rotamer is selected. Values of a, between zero and unity, will give rise to an order parameter for segment orientations. Average of $P_2(\cos \theta)$ of 0.0 to 0.5.

It is at this point that the bulk of the CPU time is utilized, since the number of distance calculations increases with the square of the number of chain segments. To reduce this time, an abbreviated check is made to determine if a given atomic cartesian coordinate is within a specified distance (e.g., 12 Å) of the newly appended atom. Thus, the vast majority of existing segments are disposed of with one, or at most three, subtraction calculations rather than full calculations of the exact distance. Terms in the second moment from atoms outside this cubic volume are not included in the summation. This is valid because of the rapidity at which the magnitude of a term decreases with increasing separation.

If an overlap is found, the rotamer selection procedure is restarted, but using a new statistical weight matrix in which the disallowed rotamer is totally excluded. If the newly chosen rotamer also overlaps with an existing atom the procedure is attempted again using the remaining possibility. If an overlap is once again found, the chain is denoted as terminated. Further calculations on this chain are abandoned, and the properties of this chain are not included in the averages. In the p-fluorostyrene case, a set of several exclusion distances was required in this vinyl system to attain the experimental characteristic ratios. All of these geometric parameters are summarized in Table I.

The algorithm also incorporates tacticity control for vinyl chains. The random number generator is used to choose between d- and l-versions of the transformation matrix. A single parameter controls the relative probability of d- and l-residues. The poly(p-fluorostyrene) results presented here are for atactic (stereochemically irregular) chains.

Results

All results were obtained from chains of 200 backbone atoms, averaging 100 chains to obtain M_2, axial extensions, end-to-end distances, and segmental and chain order parameters and directors.

For poly(methylene), an exclusion distance (hard sphere diameter) of 2.00 Å was used to prevent overlap of methylene residues. The calculation reproduced the accepted theoretical and experimental characteristic ratios (mean square unperturbed end-to-end distance relative to that for a freely jointed gaussian chain with the same number of segments) of 5.9. This was for zero angular bias and a trans/gauche energy separation of 2.09 kJ mol^{-1}.

Figure 3 shows the variation of chain dimensions expressed as the averaged z component (stretch direction) of the end-to-end distance as a function of the angular bias a and the trans/gauche energy difference ΔE. As expected, for a given angular bias, increasing ΔE causes an isotropic extension of the chains. Fixing ΔE and increasing a causes the chains to orient, producing some net elongations along z, but also a contraction in the transverse direction (the orientational properties are not apparent in the figure). It is interesting to note that except at high elongations ($\gtrsim 100\%$), hard sphere overlaps still occur to the level of 1.0 - 2.5% in the polymethylene chain for the range of averaged segmental order parameters between 0.0 and 0.5 (produced by $0 \leq a \leq 1$), although chain dimensions are unaffected by these encounters. At the high elongations generated by increased ΔE, the volume density of segments becomes small, and therefore the probability of encounters drops off.

Table I. Geometrical Parameters

poly(methylene)

C-C bond length	1.53Å
CCC bond angle	112°
trans/gauche energy (nominal)	2.09 kJ mol^{-1}
pentane interaction energy	8.37 kJ mol^{-1}
CH_2-CH_2 exclusion limit (nonbonded)	2.00Å

poly(p-fluorostyrene)

C-C backbone bond length	1.53Å
CCC backbone bond angle	112°
trans/gauche energy (nominal)	2.09 kJ mol^{-1}
pentane interaction energy	8.37 kJ mol^{-1}
C(backbone)-C(1-phenyl) bond length	1.51Å
CC(backbone)-C(1-phenyl) bond angle	120°
all phenyl bond angles	120°
all phenyl C-C bond lengths	1.39Å
C-F bond length	1.30Å
all C-H bond lengths	1.10Å
backbone C-C exclusion limit (nonbonded)	4.60Å
non-neighboring F-F exclusion limit	2.70Å
neighboring F-F exclusion limit	6.39Å

Figure 4 displays the corresponding M_2 results of the chains whose dimensions were shown in Figure 3. There is a clear correlation of the calculated NMR linewidth (as represented by M_2) with the a and ΔE parameters. At very low angular bias, increasing ΔE causes a decrease in segment volume density (larger r_{ij}), causing M_2 to decrease. At higher angular bias, the chain segments tend to orient along the stretch direction, disposing the nearest neighbor spins with their internuclear vectors nearly parallel with H_o ($\cos\theta_{ij} \approx 1$, a high M_2 situation). This effect is most pronounced for the chains with the largest proportion of trans rotamers, since gauche sequences would tend to divert the chain at least temporarily from the stretch direction. Thus, the apparent crossover region in the M_2 map is expected from qualitative arguments.

The closest physical realization of the system examined above would be a polymer such as poly(vinyl fluoride) doped into poly(ethylene) (observing the ^{19}F resonance) or poly(trifluoroethylene) doped into poly(tetrafluorethylene), observing [1]H. Neither of these systems is likely to be sufficiently miscible, and there is the possibility of significant proportions of head-to-head linkages, which would dominate the experimental M_2 because of the proximity of the spins on adjacent backbone atoms.

A preferable system is poly(p-fluorostyrene) doped into poly(styrene). Since rotations about the 1,4 phenyl axis do not alter the position of the fluorine, the ^{19}F spin may be regarded as being at the end of a long "bond" to the backbone carbon. In standard RIS theory, this polymer would be treated with dyad statistical weights to automatically take into account conformations of the vinyl monomer unit which are excluded on steric grounds. We have found it more convenient to retain the monad statistical weight structure employed for the poly(methylene) calculations. The calculations reproduce the experimental unperturbed dimensions quite well when a reasonable set of hard sphere exclusion distances is employed.

Figure 5 is an ORTEP computer plot of the first 50 backbone carbons in a typical chain. Only the fluorine atoms of the sidechains are shown. The various hard sphere exclusions conspire dramatically to keep the fluorines well separated and the chain highly extended even without introducing any external perturbations. The characteristic ratio from the computer calculations is about 11.6; from data for poly(p-chlorostyrene), CR = 11.1, poly(p-bromostyrene), CR = 12.3, and poly(styrene), CR = 10.3 (all in toluene at $30°C$), we expect the experimental value for the fluoropolymer to be in the range of 10 to 12.

The hard sphere exclusion distances for this system were chosen as follows: nonbonded backbone carbons, 4.60 Å (twice the C-H bond distance plus van der Waals radius for H); non-neighboring fluorines, 2.70 Å (twice van der Waals radius for F); neighboring fluorines, 6.39 Å (distance across phenyl ring using dimensions of Table I and van der Waals radius for H of 1.20 Å).

Figure 6 shows the importance of having separate exclusion distances for neighboring and non-neighboring fluorines. The neighbor fluorine exclusion is the main determinant of overall chain dimensions, serving to keep phenyl groups separated in the same manner as dyad statistics would have done.
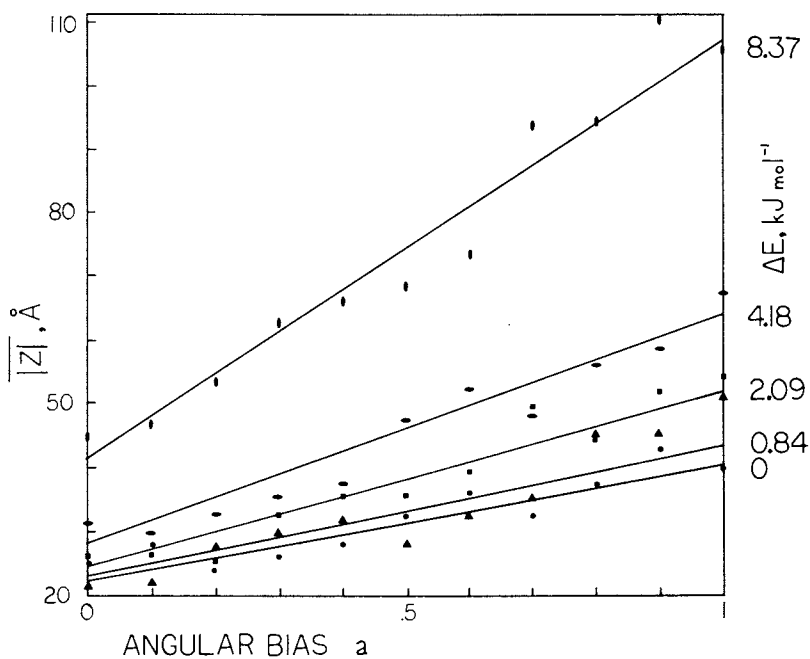
Figure 3.   Average values of the z-component of the end-to-end distance as a function of angular bias, a, and trans/gauche energy separation ΔE.

Each point represents an average of 100 chains of 200 backbone atoms each. In this calculation, ^{19}F spins reside at the coordinates of alternate backbone atoms.
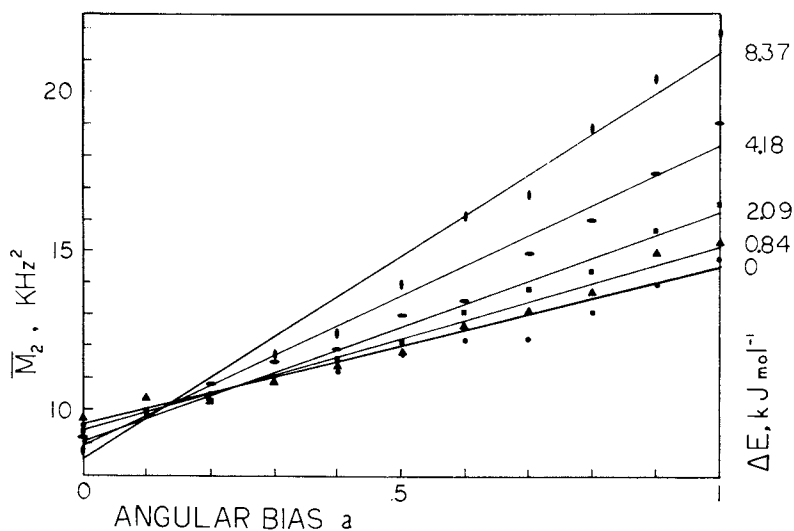
Figure 4.   Average values of M_2 for the same chains represented in Figure 3.
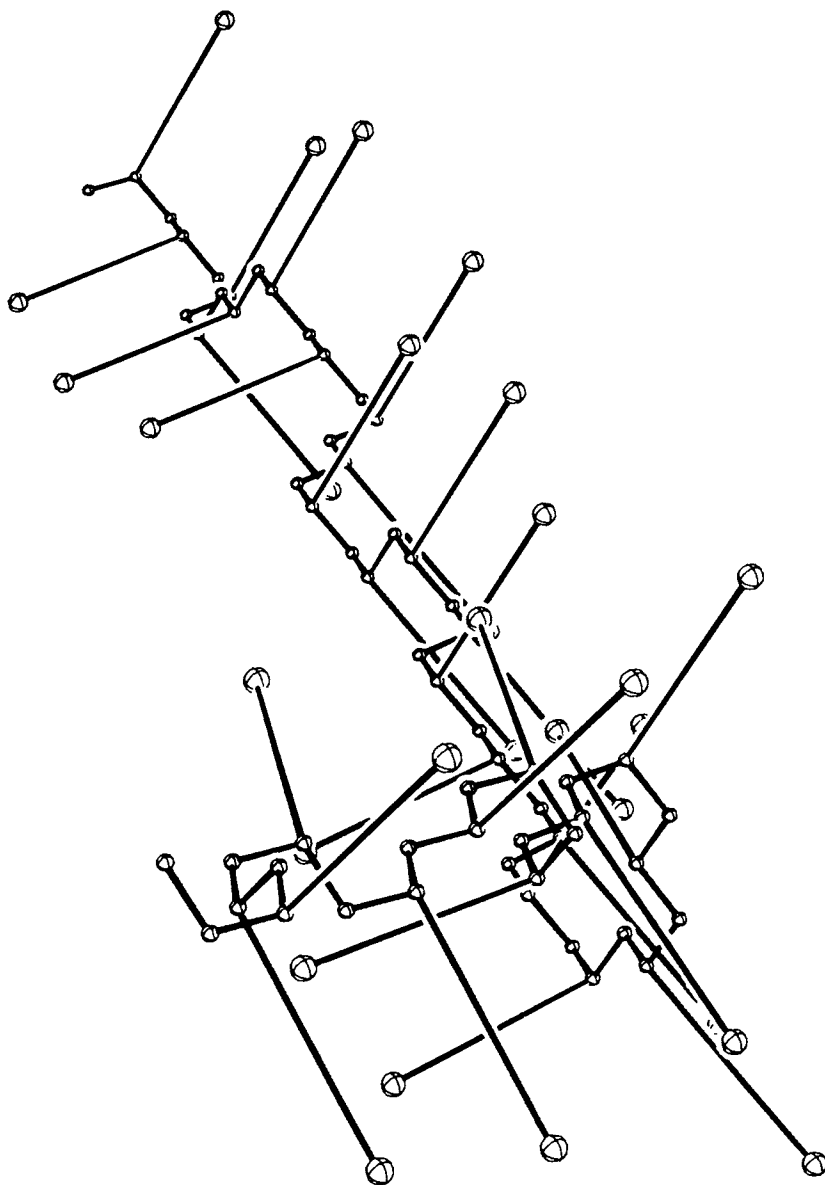
Figure 5. ORTEP computer plot showing the positions of the fluorine atoms of the first 50 backbone carbons of a poly(p-fluorostyrene) chain. The excluded volumes used in the calculation keep the fluorines well separated.
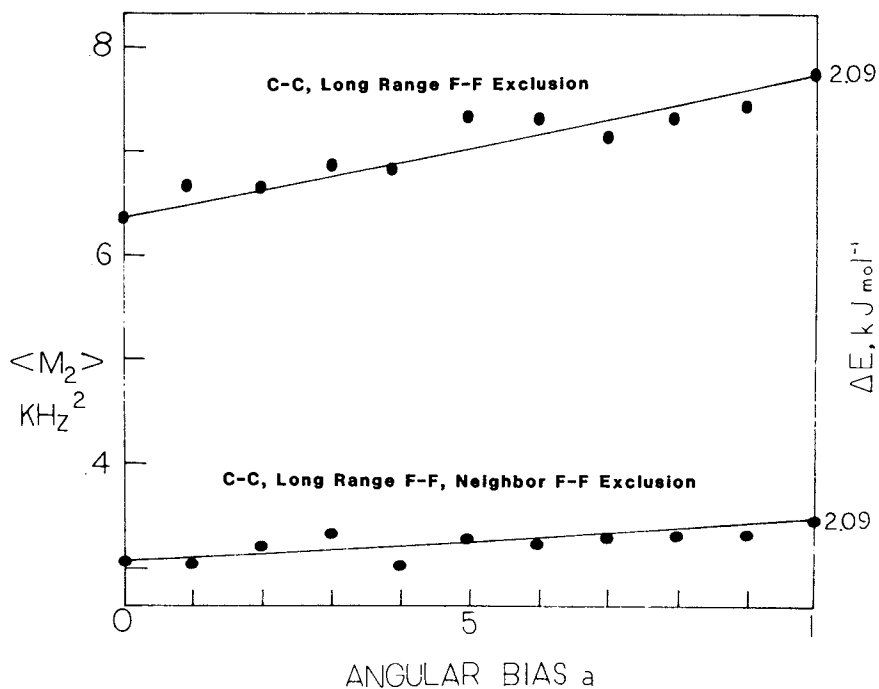
Figure 6. *Effect of using a special near-neighbor fluorine–fluorine excluded volume to account for the steric effects of the phenyl ring. This serves the same purpose as dyad weights which discriminate against certain sterically forbidden conformations.*
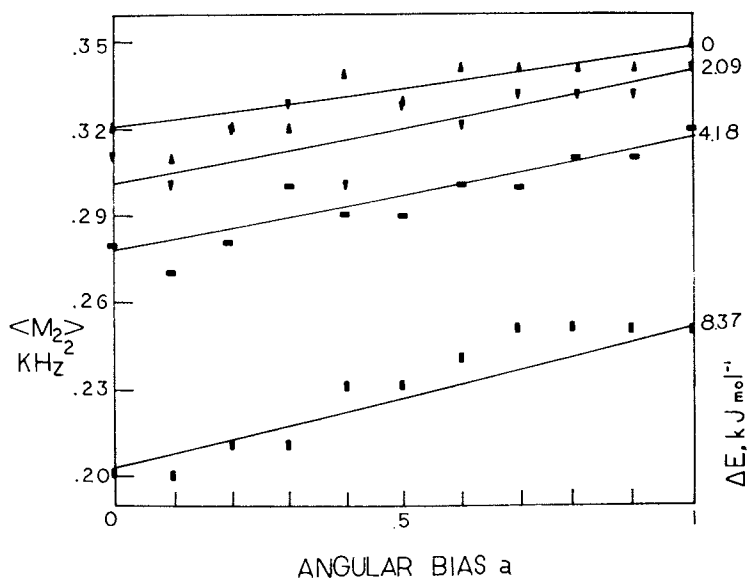
Figure 7.   Average values of M_2 for poly(p-fluorostyrene) chains of 200 backbone atoms, 100 chains per point. In this calculation, the fluorines are at their correct locations on the sidegroups.

The second moments for this system are plotted in Figure 7 for the same range of parameters used in the poly(methylene) case. Because of the large fluorine separation, the overall ^{19}F spin density is much reduced, leading to smaller second moments. These same steric restrictions also reduce the variability in F-F separation, with the result that the range of Figure 7 seems to map into the low-extension range of the poly(methylene) case, Figure 4.

Atomic overlaps become quite significant here, to the extent that in some cases nearly 3000 trials are required to calculate the 200 complete chains needed for each average.

NMR Procedure

The most convenient technique for obtaining dipolar ^{19}F linewidths in the presence of ^{1}H couplings and ^{19}F chemical shift anisotropy is that of transient nutation as suggested by Yannoni ([21], [22]). This allows scaling of heteronuclear couplings and chemical shifts to zero (both of these interactions contribute to M_2, while scaling homonuclear dipolar couplings by $-\frac{1}{2}(M_2$ scaled by $+\frac{1}{4})$. In this procedure, strong ($\omega_1 >> |\ ||\ H_{spin\text{-}spin}\ |\ |$) on-resonance RF is applied to the sample for an interval τ. The spin system evolves under the scaled spin-spin interaction. The corresponding free-induction decay (FID), unobservable during the irradiation, is mapped out by measuring the initial FID amplitude as a function of τ. Certain artifacts may be cancelled with phase alternation of the NMR signal: alternate irradiations are preceded with a π pulse and those signals are subtracted from the computer summation.

Acknowledgements

Literature Cited

1. Kuhn, W. Kolloid Z. 1936, 76, 258.
2. Guth, E.; James, H. M. Ind. Eng. Chem. 1941, 33, 624.
3. Flory, P. J.; Rehner, J., Jr. J. Chem. Phys. 1943, 11, 512.
4. Flory, P. J. J. Chem. Phys. 1977, 66, 5720.
5. Ronca, G.; Allegra, G. J. Chem. Phys. 1975, 63, 4990.
6. Ullman, R. J. Chem. Phys. 1979, 71, 436.
7. Picot, C.; Duplessix, R.; Decker, D.; Benoit, H.; Boue, F.; Cotton, J. P.; Daoud, M.; Farnoux, B.; Jannink, G.; Nierlich, M.; de Vries, A. J.; Pincus, P. Macromolecules 1977, 10, 436.
8. Clough, S. B.; Maconnachie, A.; Allen, G. Macromolecules 1980, 13, 774.
9. Ullman, R., presented at the ACS Symposium on Elastomers and Rubber Elasticity, New York, August, 1981.
10. Abragam, A. "The Principles of Nuclear Magnetism", Oxford University Press: London, 1970.

11. McBrierty, V. J.; Ward, I. M. J. Phys. D 1968, 1, 1529.
12. McBrierty, V. J.; McDonald, I. R.; Ward, I. M. J. Phys. D 1971, 1, 88.
13. Bower, D. I. J. Poly. Sci. Poly. Phys. Ed. 1981, 19, 93.
14. von Meerwall, E.; Ferguson, R. D. J. Poly. Sci. Poly. Phys. Ed. 1981, 19, 77.
15. Flory, P. J. "Statistical Mechanics of Chain Molecules", Interscience: New York (1969).
16. Flory, P. J. Proc. Roy. Soc. Lond. 1976, A.351, 351.
17. Abe, A.; Jernigan, R. L.; Flory, P. J. J. Amer. Chem. Soc. 1966, 88, 631.
18. Yoon, D. Y.; Sundararajan, P. R.; Flory, P. J. Macromolecules 1975, 8, 776.
19. Yoon, D. Y.; Flory, P. J. Macromolecules 1977, 10, 562.
20. Yannoni, C. S., private communication.
21. Yannoni, C. S.; Wind, R. A. J. Magn. Resonan. 1980, 38, 493.

Crystallization of Stretched Networks and Associated Elasticity

K. J. SMITH, JR.

State University of New York, College of Environmental Science and Forestry, Syracuse, NY 13210

A model of lamellae formation in stretched
networks is proposed. Approximately one-half of the
chains do not fold. Formation of such lamellae is
accompanied by declining stress. Highly folded
systems (high crystallinity), however, can cause a
stress increase. In the calculations crosslinks are
assigned to their most probable positions through
the use of a characteristic vector. A contingent of
amorphous chains is also included. The calculations
suggest that the concept of fibrillar-lamellar
transformations may be unnecessary to explain
observed stress-temperature profiles in some cases.

It is thought that crystallization of _stretched_ polymer
networks results in two crystalline morphologies. Upon cooling a
stretched network at either constant length or constant load,
(fibrillar) crystallites appear that seem to transform into
folded-chain lamellae at yet lower temperatures (1, 2). Important
evidence supporting this belief is the observation that retractive
force exerted by a stretched network at constant length decreases
with crystallization in the fibrillar region, then increases when
temperature falls into the lamellar zone (1, 2). Fibrillar
crystallization, in which a chain passes through a crystallite
but once, compresses connecting amorphous chains, thereby de-
creasing the forces they exert (3). But lamellae, in which a
chain may fold back and forth several times, extend the distances
amorphous chains must subtend, consequently increasing their
forces.

This argument was put forth in 1962 by Judge and Stein (1)
to explain the behavior of polyethylene networks under a constant
load. That same year Smith (4) showed that a folded-chain mor-
phology was thermodynamically favored at lower temperatures (high
crystallization) whereas at temperatures near the melting point
(low crystallization) fibrillar morphology was stable; a trans-
formation of one morphology into the other was thermodynamically

possible. Much later Gaylord and Lohse (5) refined Smith's
calculations by incorporating greater morphological detail and
reached the same conclusion. They also attempted an estimation
of the force-temperature profile in the crystallization region.
     At least two major difficulties with this crystallization
picture exist. First, the morphological detail assumed by Gaylord
and Lohse is very speculative. They postulate lamellae composed
of identically regular folded chains that "switch" from one fold
to two, etc., as temperature is changed. How such switching is
possible is unexplained. Indeed, how a lamella forms with all
chains having an identical number of folds is also presented
without comment. A second difficulty is the surprising obser-
vation of Luch and Yeh (6): lamellae formation in stretched
networks of natural rubber is accompanied by stress decline
rather than increase. This observation, if true, cannot be ex-
plained with the existing model of stress-induced crystallization.
     It has recently been shown (7) that a transformation from
fibrillar to lamellar morphology is not required to replicate the
force-temperature profile of stretched networks in the crystal-
lization region. This latest work shows that a close duplication
of the behavior of gutta percha (8) can be predicted with a model
(7) of fibrillar crystallization that incorporates several new
features omitted in earlier theories, specifically:
   1. A network chain may pass through a crystallite in one
       direction or in the exact opposite direction relative to
       the chain displacement vector; the two configurations
       are not equally probable.
   2. Crosslinks are assigned to their most probable positions,
       which change as crystallization changes.
   3. Lateral crystallite growth is permitted by a contingent
       of amorphous chains. All earlier theories allow
       longitudinal (along the chain axis) growth only.
     But that work does not preclude lamellar formation and the
possibility of fibrillar-lamellar transformations. Especially in
need of clarification is the observation (6) that lamellar forma-
tion in stretched networks decreases stress (or force). Force
exerted by an amorphous chain or sub-chain is determined by the
ratio (r/N) of its end-to-end displacement length r to the
number of links (or bonds) N making up its backbone. Whatever
makes this ratio small diminishes force. Yeh's observation, if
it is true, requires a lamellar crystal geometry that does just
that. One capable of this is shown in Figure 1. Two geometrical
arrangements of the chains are incorporated into the lamella :
one has both crosslinks (chain end-points) on the same side of
the lamellar (one fold),and the other has one crosslink on each
side without a fold. An actual lamella may incorporate chains
of two and three folds, or even more. It seems reasonable to
expect that highly crystalline polymers might favor a larger
number of folds, but the density of crosslinks in a network could
have a mitigating effect.

Two questions arise: how many chains fold? and are the folds regular (adjacent re-entry) or irregular (switchboard)? Whether or not a chain folds depends upon where its ends are. If both ends (crosslinks) are located on the same side of the lamella , the chain must fold and pass back through the crystal, assuming that lateral dimensions are large. It may also fold more than once provided it does so an odd number of times. If the two chain ends are located on opposite sides of the lamella , the chain cannot fold unless it does so an even number of times. Since chains in a crosslinked network are relatively short, more than one fold per chain is expected to be rare in low crystalline materials. Unless a selection process operates in favor of one configuration, both should be accreted by a growing lamella with equal frequency; i.e., one-half of the chains fold once and one-half do not fold at all (neglecting a few that might fold more than once). For those that fold, regular folds appear highly improbable. Chains should be incorporated into a growing crystallite as they are encountered in the melt by the crystallite face. This means that end-points of a fold sub-chain are located at their most probable distance apart. Even if some unknown mechanism operates to favor regular folds, it is difficult to expect from it much more than miniscule effeciency in a cross-linked network where topological constraints must surely limit the chain disentanglements necessary for regular folding. Consequently, lamellae in a network, if they form, might be expected to have about one-half of their chains unfolded and one-half folded once in an irregular manner. Lamellae of <u>small</u> lateral dimensions could deviate considerably from this idealized model, as might also highly crystalline materials with multiple folds.

Two additional features of a semi-crystalline network should be considered: one is the presence of some completely amorphous chains, and the other is the displacement of crosslinks by growing crystallites. As a network crystallizes the crystallites upset the balance of forces about the crosslinks, which are then forced to new positions of equilibrium. These problems have recently been attacked ($\underline{7}$) by consigning the chains to their most probable positions.

Such a model for lamellar crystallization is now investigated. Initially the calculations are restricted to the simple lamellar model shown in Figure 1, but multiple fold lamellae are briefly considered even though they present a serious problem stemming from insufficient information about the number of folds.

<u>Theory</u>

Let the network be made of G chains running from crosslink to crosslink. The degree of crystallinity ω is the fraction of repeating units that are crystallized. The free energy of crystallization ΔF_c is usually separated into two terms ($\underline{3}$, $\underline{9}$):
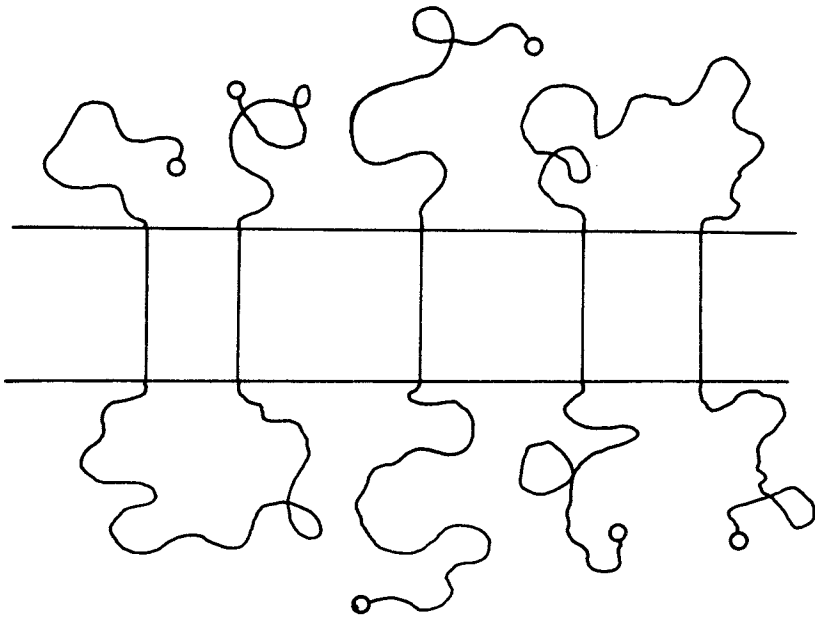
Figure 1. Model of a lamella containing unfolded and irregularly folded chains.

the first is the free energy of crystallization of ωGN repeating units, where N is the average number of links per chain, and the second is the elastic free energy ΔF_e associated with the amorphous portions of the network. Thus (9)

$$\Delta F_c = -\omega GN\Delta H_u \ (1 - T/T_m^{\,o}) + \Delta F_e \qquad (1)$$

ΔH_u is the heat of fusion per repeating unit and $T_m^{\,o}$ is the melting temperature of the crystals in the absence of constraining forces (i.e., $\Delta F_e = 0$).

The elastic free energy ΔF_e causes difficulty because of its sensitivity to the crystallization model assumed. To estimate ΔF_e for lamellar morphology, consider first an important property of a network, amorphous or crystalline. Network crosslinks are considerably restricted in their fluctuations. Fluctuations of crosslinks several chains removed from a particular chain are therefore inconsequential for that chain. A chain in the interior of a path traced through several sequentially connected chains behaves as if the path ends are securely anchored at fixed positions (7). If G_j chain vectors make up the path, then

$$\sum_j \underset{\sim}{r_j} = \underset{\sim}{R_j} = \text{constant}$$

By introducing coefficients C_{ij} the summation can be extended over all network chains, i.e.

$$\sum_i C_{ij}\underset{\sim}{r_i} = \underset{\sim}{R_j} = \text{constant} \qquad (2)$$

For every vector making up R_j the coefficient is unity, and zero otherwise. A similar equation holds for each path required for complete network characterization. Constancy of $\underset{\sim}{R_j}$ is assured by

$$\sum_i C_{ij} \ d\underset{\sim}{r_i} = 0 \qquad (3)$$

If G_c chains crystallize (partially) there will remain $G-G_c$ completely amorphous chains and $G + 3G_c/2$ total elastic elements (amorphous chains and subchains). This is true only for the model described with $1/2 \ G_c$ chains folding once and $1/2 \ G_c$ chains not folding at all. If each elastic element is Gaussian in its behavior, the elastic free energy F_e can be written as

$$F_e = \frac{3kT}{2b^2} \sum_k \frac{r_k^{\,2}}{N_k} + \text{constant} \qquad (4)$$

The sum extends over all amorphous chains and subchains. The

number of statistical links in r_k is N_k, and each statistical link is of length b. The chains are now assigned their most probable positions as determined by the condition. that F_e is a minimum, i.e.

$$\sum_k \frac{r_k \cdot dr_k}{N_k} = 0 \tag{5}$$

Condition (3) still holds, but the relationship between r_k and r_i must be established. Upon crystallization the i<u>th</u> chain may subdivide into two amorphous subchains if it does not fold

$$r_i = r_{i1} + r_{i2} + l_i$$

or three subchains if it folds once

$$r_i = r_{i1} + r_{i2} + r_{i3}$$

These are shown in Figure 2. Substituting these results into equation (2) whenever appropriate gives

$$\sum_i C_{ij} \, r_i = \sum_k C_{kj} \, r_k + \sum_i C_{ij} \, l_i = R_j \tag{6}$$

where the sum over k extends over all amorphous chains and sub-chains in the network. Note that for a completely amorphous chain l_i is zero. At constant l_i the condition expressed by equation (3) is exactly

$$\sum_k C_{kj} \, dr_k = 0$$

Introducing into equation (3) such a condition for each path j gives

$$\left(\frac{r_k}{N_k} - \sum_j \beta_j \quad C_{kj} \right) \cdot dr_k = 0$$

where β_j is the j<u>th</u> Lagrangian vector multiplier. The orthogonal solution can be obviated by imposing the null vector solution in all instances. This requires that F_e be a minimum also with respect to the components of r_k. The null vector solution is

$$r_k = N_k \sum_j \beta_j \quad C_{kj}$$
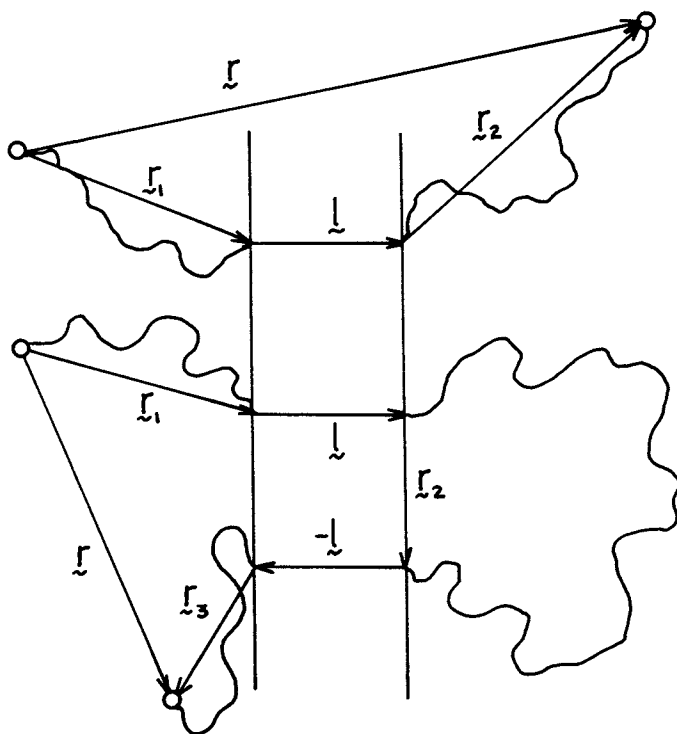
Figure 2.   Diagram of chains making up a lamella of thickness $\underset{\sim}{1}$.

The sum over all j can be denoted as $\beta_k G_k$, where G_k is the number of paths containing $\underset{\sim}{r}_k$, and β_k is a resultant vector analogous to $\underset{\sim}{\beta}_j$. Unfortunately $\underset{\sim}{\beta}_k$ cannot be determined from the information at hand. It is therefore necessary to assume that $\underset{\sim}{\beta}_k$ is the same for all k; i.e., $\underset{\sim}{\beta}_k = \underset{\sim}{\beta}$ and

$$\underset{\sim}{r}_k = \underset{\sim}{\beta}\, G_k\, N_k \tag{7}$$

This corresponds to summing equation (6) over all paths j and holding the resultant constant:

$$\sum_i \sum_j C_{ij}\, \underset{\sim}{r}_i = \sum_j \underset{\sim}{R}_j = \text{constant}$$

Only a single Lagrangian vector β is necessary in this case. Combining equations (6) and (7) gives

$$\sum_i C_{ij}\, \underset{\sim}{r}_i = \underset{\sim}{\beta} \sum_k C_{kj}\, G_k\, N_k + \sum_i C_{ij}\, \underset{\sim}{l}_i$$

This equation reduces to a simpler form if it is summed over j:

$$\sum_i \sum_j C_{ij}\, \underset{\sim}{r}_i = \underset{\sim}{\beta} \sum_k \sum_j C_{kj}\, G_k\, N_k + \sum_i \sum_j C_{ij}\, \underset{\sim}{l}_i$$

or

$$\sum_i G_i\, \underset{\sim}{r}_i = \underset{\sim}{\beta} \sum_k G_k^{\,2}\, N_k + \sum_i G_i\, \underset{\sim}{l}_i$$

where $\sum_j C_{ij} = G_i$, $\sum_j C_{kj} = G_k$. G_i is the number of paths the ith chain participates in. Then

$$\underset{\sim}{\beta} = \frac{\displaystyle\sum_i G_i\, \underset{\sim}{r}_i - \sum_i G_i\, \underset{\sim}{l}_i}{\displaystyle\sum_k G_k^{\,2}\, N_k}$$

We can write equation (4) as

$$F_e = \frac{3kT}{2b^2} \left(\frac{1}{\displaystyle\sum_k G_k^{\,2}\, N_k} \right) \left(\sum_i G_i\, \underset{\sim}{r}_i - \sum_i G_i\, \underset{\sim}{l}_i \right)^2 + \text{constant} \tag{8}$$

The summations are easy to deduce:

$$\sum_i G_i \, \underset{\sim}{r_i} = G <G_i> \underset{\sim}{r}$$

$$\sum_i G_i \, \underset{\sim}{l_i} = \frac{1}{3} G <G_i> Nb\underset{\sim}{\omega}$$

$$\sum_k G_k^2 \, N_k = G <G_i^2> N (1 - \omega)$$

Here the bond vector b is along the same direction as l_{ia}. The symbol $<$ $>$ represents an average. The vector r is an average, characteristic vector of the network that depends only upon the state of deformation. It is independent of crystallization to the extent that density variations accompanying crystallization can be ignored, which is invariably the case. Although actual chains can be perturbed by crystallization, the constancy of $\underset{\sim}{r}$ tends to limit perturbations to those compatible with network size and shape as determined by the state of strain. The constancy of r is exactly equivalent to the constancy of the various path vectors $\underset{\sim}{R_j}$, which is a necessary assumption of our model. Substitution of these sums into equation (8) gives

$$F_e = \frac{3GkT}{2Nb^2} \left[\frac{<G_i>^2}{<G_i^2>} \right] \left(\frac{1}{1-\omega} \right) \left[\underset{\sim}{r} - \frac{1}{3} \omega N\underset{\sim}{b} \right]^2 + \text{constant}$$

The distribution of G_i is unknown, but the information is not required. We can assume a monodisperse distribution and equate $<G_i>^2 = <G_i^2>$ so that

$$F_e = \frac{3GkT}{2Nb^2} \left(\frac{1}{1-\omega} \right) \left[\underset{\sim}{r} - \frac{1}{3} \omega N\underset{\sim}{b} \right]^2 + \text{constant} \qquad (8a)$$

This is possible because the result must conform to the traditional theory of elasticity when crystallinity is zero ($\omega = 0$). This happens if r is interpreted as an average chain vector (made up of N links), the components x, y, z of which deform affinely, so that in simple elongation along z

$$<x^2> = <y^2> = Nb^2/3 \, \alpha$$

$$<z^2> = \alpha^2 Nb^2/3$$

where α is the deformation ratio.

Squaring the bracketed term gives

$$r^2 - \frac{2}{3} \omega N \underset{\sim}{r} \cdot \underset{\sim}{b} + \frac{1}{9} \omega^2 N^2 b^2 \tag{9}$$

The vector product $\underset{\sim}{r} \cdot \underset{\sim}{b}$ is

$$\underset{\sim}{r} \cdot \underset{\sim}{b} = b \left[x \sin \chi \cos \phi + y \sin \chi \sin \phi + z \cos \chi \right]$$

where χ is the orientation angle of b – that is, of the crystal-lite – with respect to the stretch direction (z), and ϕ is the azimuthal crystallite angle. Assuming perfect orientation of the chain axis along the stretch direction (cos χ = 1), the average of equation (9) is

$$<r^2> - \frac{2}{3} \omega N <z> b + \frac{1}{9} \omega^2 N^2 b^2$$

The values of $<x^2>$, $<y^2>$, $<z^2>$ are given above. For $<z>$ we refer to the approximation of Flory (3) that seems satisfactory when stretch is very large

$$<z> = \alpha b (2N/3\pi)^{1/2}$$

Placing these values into equation (8) gives

$$F_e = \frac{GkT}{2} \left(\frac{1}{1-\omega} \right) \left[\alpha^2 + \frac{2}{\alpha} - \frac{2\alpha\omega}{3} \left(\frac{6N}{\pi} \right)^{1/2} \right.$$

$$\left. + \frac{\omega^2 N}{3} \right] + \text{constant}$$

Sub tracting from this F_e ($\omega = 0$, $\alpha = 1$) gives ΔF_e, which when substituted into equation (1) yields ΔF_c

$$\Delta F_c = - \omega G N \Delta H_u \left(1 - \frac{T}{T_m^o} \right) + \frac{GkT}{2} \left(\frac{1}{1-\omega} \right) \left[\alpha^2 + \frac{2}{\alpha} \right.$$

$$\left. - \frac{2\alpha\omega}{3} \left(\frac{6N}{\pi} \right)^{1/2} + \frac{\omega^2 N}{3} \right] - \frac{3GkT}{2} \tag{10}$$

The equilibrium degree of crystallization, ω, can be determined from the condition $\partial \Delta F_c / \partial \omega = 0$, or

$$\frac{2N\Delta H_u}{R} \left(\frac{1}{T} - \frac{1}{T_m^o} \right) = \left(\frac{1}{1-\omega} \right)^2 \left[\alpha^2 + \frac{2}{\alpha} - \frac{2\alpha}{3} \left(\frac{6N}{\pi} \right)^{1/2} + \frac{\omega N}{3} (2-\omega) \right] \tag{11}$$

The melting temperature T_m is obtained from equation (11) when $\omega \to 0$ ($T \to T_m$).

$$\frac{1}{T_m} = \frac{1}{T_m^{\ o}} + \frac{R}{2N\Delta H_u}\left[\alpha^2 + \frac{2}{\alpha} - \frac{2\alpha}{3}\left(\frac{6N}{\pi}\right)^{1/2}\right] \tag{12}$$

T_m is the temperature at which the last vestiges of crystallinity disappear upon heating. The force at <u>equilibrium crystallinity</u> is given by (<u>3</u>,<u>9</u>)

$$f = \frac{1}{L_i}\left(\frac{\partial \Delta F_c}{\partial \alpha}\right)_{T,V,\omega} = \frac{GkT}{L_i}\left(\frac{1}{1-\omega}\right)\left[\alpha - \frac{1}{\alpha^2} - \frac{\omega}{3}\left(\frac{6N}{\pi}\right)^{1/2}\right] \tag{13}$$

where L_i is the initial unstretched length.

Discussion

For a moderately crosslinked network, equation (13) predicts a declining stress with lamellae formation from the amorphous melt. A stress increase can be achieved with this model only by reorientation of the chain axis to the directions perpendicular (or nearly so) to the stress direction. If then this model is suitable for lightly crystalline materials, its behavior is in good accord with the observations of Luch and Yeh (<u>6</u>) on stretched natural rubber networks. They reported simultaneous lamellae formation and declining network stress.

The foregoing theory can be modified to include lamellae containing multiple folds with a fraction γ of chains having crosslinks on opposite sides of the lamellar. In this general case

$$\sum_i C_{ij}\ \underset{\sim}{l_i} = \frac{\gamma}{1+\bar{f}}\ \omega G_j N\underset{\sim}{b} = \zeta\omega G_j N\underset{\sim}{b}$$

where $\zeta = \gamma/(1+\bar{f})$. $\bar{f}$ is the average number of folds per crystalline chain. This gives for ΔF_c

$$\Delta F_c = -\omega GN\Delta H_u\left(1 - \frac{T}{T_m^{\ o}}\right) + \frac{GkT}{2}\left(\frac{1}{1-\omega}\right)\left[\alpha^2 + \frac{2}{\alpha}\right.$$

$$\left. -2\zeta\alpha\omega\left(\frac{6N}{\pi}\right)^{1/2} + 3\zeta^2\omega^2 N\right] - \frac{3GkT}{2} \tag{14}$$

For the model in Figure 1, $\gamma = 1/2$, $\bar{f} = 1/2$, and $\zeta = 1/3$. We can imagine more highly folded models. For example, if half the crystalline chains fold twice and the other half three times, the value of ζ is 1/7. The greater the number of folds, the smaller the value of ζ. Since the force at equilibrium is

$$f = \frac{GkT}{L_1}\left(\frac{1}{1-\omega}\right)\left[\alpha - \frac{1}{\alpha^2} - \zeta\omega\left(\frac{6N}{\pi}\right)^{1/2}\right] \qquad (15)$$

a small value of ζ can reduce the importance of the second term above so that the force will rise as ω increases. It is reasonable to expect that the number of folds increase as ω becomes large. Consequently, incipient crystallization (large ζ) may reduce force, but at high ω (low ζ) force may be regenerated. This may be what happens in polyethylene networks ([1]). A transformation from one morphology to another is therefore not at all required. The observed stress profile may be indicative of nothing more than a normal progression of lamellar growth whereby more and more folds are incorporated by the growing lamellae.

Of course, a morphological transformation cannot be shown to be incompatible with observations on crystallizing networks, but neither has it been theoretically demonstrated to occur. It is easy to propose a transformation between fibrils (with $\zeta = 1$ in the preceding equation, which is the analog of Flory's original model) and lamellae (with $\zeta < 1$), but how does the transformation occur? An abrupt transformation will surely generate an increase in stress. A more gradual transformation, however, may not unless crystallization is quite high. The important question remaining to be answered is therefore does ζ change gradually, or does it change discontinuously at definite intervals to produce distinctive phases?

Some comments on a fibrillar model are in order. If $\zeta = 1$ (no folding), the equations above become identical in form to those given earlier by Flory ([3]). But the theoretical foundations of the two theories differ. Flory's model is that of a single crystal of parallel chains having substantial amorphous end-sections attached to fixed crosslinks. Melting is imagined to occur by a foreshortening of crystal length accompanied by a corresponding increase in the amount of amorphous end-portions. Lateral crystallite dimensions are viewed as unchanging throughout the process. But it is unrealistic to expect a crystallite to spring into existence with a full complement of chains intact, nicely ordered laterally and deficient along the longitudinal, or chain, axis. The model herein, however, includes amorphous chains, which allow for lateral growth. Since crosslinks are assigned to their most probable positions, lateral growth is, in fact, equally favored with longitudinal growth. The practical difference between the two theories is evident only in the definition of ω. Herein ω is the network degree of crystallization. In Flory's theory, ω is the degree of crystallization of a semi-crystalline chain, and all chains are semi-crystalline (which is not true in an actual network). It seems to be nothing more than luck that the two theories agree in form.

Lateral growth occurs in real systems but is not accounted for in the model of Flory. What allows its incorporation into these new calculations is the assignation of the chains to their most probable positions; the chains continuously seek positions of equilibrium as crystallization proceeds. This means that all amorphous links have the same propensity for crystallization, which therefore tends to eliminate a distinction between lateral and longitudinal crystal growth (keep in mind that different levels of crystallinity favor one growth pattern over the other – low crystallinity favors fibrils, high crystallinity favors lamellae).

Most probable positions of the chains are determined by the use of a characteristic vector r. This vector is represent-ative of an average network chain of N links (the average links per chain). It deforms affinely whereas the actual network chains might not, and its value depends only upon network deform-ation. Crystallization leaves r essentially unaltered since the miniscule volume contraction brought about by crystallization can be ignored. But real network chains are severely displaced by crystallization. These displacements, however, must be compatible with the immutability of r. So in a sense, the characteristic vector r limits the configurational variations of the chains to those consistent with a fixed network shape and size at a given deformation.

The chains are assigned to their most probable positions, so too are the sub-chains in the semi-crystalline structure. Consequently, fold sections are also constrained to their most probable positions. Regular hairpin folds do not occur in this model, which means that lateral growth (of the crystallites) occurs by accretion of chains to growing surfaces as they are encountered in the melt. Chains do not unravel from the melt to deposit completely, or nearly so, on the crystallite surface by regular folding before another chain is encountered. Such disentanglements seem prohibited in networks in which topological constraints are permanently secured by crosslinks. The issue is by no means trivial for the geometry of chains in the crystallites is determined by mode of growth. The model adopted here necessitates irregular folding as well as varied folding within the same crystallite. Some chains may not fold at all and others may fold several times.

The average number of folds per chain may be dependent upon the degree of crystallinity, at least in the earlier stages of crystallization when lateral dimensions are relatively small. But as crystallization increases, the folds per chain should level off at a constant value. Even a few folds greatly diminishes the value of ζ, so in the region of high crystallinity we might approximate $\zeta \sim 0$ and obtain from equation (14)

$$\Delta F_c = -\omega GN\Delta H_u \left(1 - \frac{T}{T_m^o}\right) + \frac{GkT}{2}\left(\frac{1}{1-\omega}\right)\left[\alpha^2 + \frac{2}{\alpha}\right] - \frac{3GkT}{2}$$

From this result it follows that

$$\omega = 1 - \left[R\ (\alpha^2 + \frac{2}{\alpha})/2\ N\Delta H_u\ (\frac{1}{T} - \frac{1}{T_m^o}) \right]^{1/2}$$

$$f = \frac{GkT}{L_i}\ (\frac{1}{1-\omega})\ \left(\alpha - \frac{1}{\alpha^2} \right) \tag{16}$$

The retractive force increases as ω increases   in this case
(high ω). This folded chain model is the same as that introduced
twenty years ago (4). Comparing equation (16) with equation (13)
(or with equation (15) where ζ is unspecified) shows clearly
the variation of retractive force that might occur as crystal-
lization proceeds. When crystallization begins the force, at
constant length, might decrease because the crystallites are
small with few folds per chain. The value of ζ may be near
unity initially. As more and more folds are incorporated, ζ falls
to a small value and allows a regeneration of force in accordance
with equation (16). An abrupt transformation from ζ small to ζ
large will produce a qualitatively similar behavior.

At a molecular, rather a chain, level the cause of this be-
havior is clear. Those chains having both crosslinks on the same
side of the lamella always experience an increase in tension upon
crystallization because their amorphous sub-chain are required
to extend in order to meet the constraints of this geometrical
pattern. The effect is greater the greater the number (odd) of
folds. But chains having crosslinks on opposite sides of the
lamella can experience an increase or decrease in tension upon
crystallization depending upon the number of folds per chain. A
chain without a fold is compressed by crystallization; i.e.,
tension decreases – the extended geometry of the crystalline
portion forces the two amorphous subchains into shorter conform-
ations. But an identical chain folded several times (always an
even number of folds) experiences an increase in tension upon
crystallization because its subchains must extend to span the
required distances with the small, reduced number of backbone
links. Behavior of the system is therefore dependent upon the
populations of various geometrical arrangements present at a
given time. These populations are expected to vary with the
state of strain as well as with degree of crystallization.
Highly stretched networks should discourage folding and favor
fibrillar crystallization, or at least favor low folding. High
stretch should also favor an increased fraction of chains having
crosslinks on opposite sides of the lamella. In other words, low
stretch favors large ζ and high stretch favors small ζ.

A final point, subtle but important, ought to be discussed
in some detail. The method adopted herein and in another
publication (7) for assigning chains to their most probable

positions rests squarely on the assertion that

$$\sum_i \sum_j C_{ij} \underset{\sim}{r}_i = \sum_i G_i \underset{\sim}{r}_i = \sum_j R_j = \text{constant} \neq 0$$

The vector directions of r_i (therefore R_j) are therefore not assigned randomly but by some plan compatible with the network structure. This allows us to write

$$\sum_i G_i \underset{\sim}{r}_i = G <G_i> \underset{\sim}{r} \neq 0$$

A calculation of $\underset{\sim}{r}$ (or r^2) is not attempted. In effect, the value of r is specified at this point. The entropy of this specified network is then calculated by assigning the actual chains to their most probable locations consistent with the constant, specified value of r. But many other values of r (or r^2) are possible, so the entropy is computed by averaging the specified network entropy over all values of r; that is, an average entropy is computed. Since r is not in fact calculated, how is such an averaging possible? This is achieved by simply comparing the result with the traditional theory of elasticity. It then turns out that r behaves as an <u>average</u> chain undergoing an affine deformation. It is then described as a <u>characteristic</u> chain because it effectively characterizes the network with respect to deformation. The number of links in the characteristic chain is N, the actual network average. If the distribution of G_i is other than monodisperse some minor adjustments in the identification of the characteristic chain is required. In this case, its displacement vector would be $<G_i>$ r rather than just r, and its links number $<G_i^2>$ N rather than Ñ. But these adjustments are of little importance.

Owing to the ambiguity surrounding the specified structure, the question might be asked: why establish the network constraints in terms of vectors? We might, for example, avoid the issue by choosing for a constraint either

$$\sum_i |\underset{\sim}{r}_i| = G <|\underset{\sim}{r}_i|> = \text{constant}$$

where $|\quad|$ represents absolute value, or

$$\sum_i r_i^2 = G <r_i^2> = \text{constant}$$

Both appear to be acceptable. And indeed they lead to quite acceptable solutions for <u>amorphous</u> networks. But neither of these constraints appear satisfactory for semi-crystalline networks, at least a proper solution has not yet been found. Our choice of vectors then is not a choice at all but rather an imposition.

The equations emerging from the theory are quite reasonable.
If the chains occupy their most probable positions, their end
points must adjust as crystallization proceeds so as to keep
all chains at the same potential. On a thermomechanical basis
no distinction among the chains is possible. A completely
amorphous chain behaves the same elastically as an amorphous sub-
chain of a semi-crystalline chain. The crosslinks adjust to
insure this. What the equations show is that each chain,
amorphous or crystalline, behaves as if it were partially crystal-
line, its effective crystallinity being the network average. In
other words, the total number of crystalline units is divided
among all chains regardless of their actual conditions with
regard to crystallinity. So the network is described by an
average chain of average crystallinity, which is an eminently
sensible conclusion. It then becomes impossible to extract
crystallite dimensions, of any kind, from the degree of crystal-
lization.
        We can assert outright that a semi-crystalline network in a
continuous state of equilibrium might be satisfactorily described
by a representative chain of average contour length and average
crystallization. This is, after all, the same assumption that
is invariably applied to amorphous networks. The results in
this instance are exactly the same as those presented herein.

Literature Cited

1.   Judge, J. T.; Stein, R. S. J. Appl. Phys. 1962, 32, 2357.
2.   Keller, A.; Mackin, M. J. J. Macromol. Sci. (Phys.) 1967,
     81, 41.
3.   Flory, P. J. J. Chem. Phys. 1947, 15, 397.
4.   Smith, K. J., Jr. Ph.D. Dissertation, Duke Univ. 1962.
5.   Gaylord, R. J.; Lohse, D. Polymer Sci. and Eng. 1976,
     16, 1963.
6.   Luch, D.; Yeh, G. S. Y. J. Appl. Phys. 1972, 43, 4326.
     J. Macromol. Sci. (Phys.) 1973, B7, 121. J. Polymer Sci.
     1973, 11, 467.
7.   Smith, K. J. ACS Symposium: Renewable Resource Material for
     Coatings and Plastics, New York 1981. Ed. by L. Sperling
     and C. Carraher. In press. And two papers submitted to
     J. Polymer Sci.
8.   Gent, A. N. J. Polymer Sci. 1966, A2, 4, 447.
9.   Smith, K. J., Jr. Polymer Sci. and Eng. 1976, 16, 168.

Elasticity and Structure of Cross-linked Polymers[1]: Networks with Comblike Cross-links

WILHELM OPPERMANN and GÜNTHER REHAGE

Institute of Physical Chemistry, T.U. Clausthal, Adolf-Römer-Strasse 2a, 3392 Clausthal-Zellerfeld, Federal Republic of Germany

The equilibrium modulus of poly(dimethylsiloxane) (PDMS) networks having comb-like crosslinks changes systematically with the structure of the cross-links, even if the number of chains per volume remains constant. At high branching densities, the experimentally observed moduli are three times greater than those calculated from the theory of phantom networks. As the branching density decreases, this ratio also decreases and tends to approach unity. These observations, though incompatible with either the phantom theory or the affine theory alone, are explained by a transition between the two. The Mooney-Rivlin constant $2C_1$, as determined by stress-strain measurements, considerably exceeds the modulus calculated from phantom network theory. Moreover, $2C_2$ does not vanish at high crosslink functionalities. This indicates that Flory's theory is not applicable to these complicated networks.

During the last five years, new aspects have been introduced into the molecular theory of rubber elasticity (1-4). The older theory sucessfully predicts such properties as thermoelasticity, birefringence, and swelling, but was unable to account for the strain dependence of the modulus. The revised theory claims to overcome with this insufficiency. It originates from the understanding that the two classical approaches, namely the model using affinely transposed crosslinks and the model using fluctuating crosslinks, represent extremes. Real networks should exhibit intermediate behaviour, a transition being induced by strain.

Parallel to the development of the new theoretical approaches considerable experimental work was done on model networks especially synthesized, to show the effects of pendent chains, loops, distribution of chain length, functionality of crosslinks, etc. on properties (5-21). In some instances, the properties turned out

[1] This is Part II of a series. For Part I, cf. Ref. 21.

to depend on the chemical composition of the network, and also on the frequently neglected microstructure in other instances.

We have investigated the static and dynamic mechanical properties of networks of different chemical and topological structures (19,20). In a previous paper, we reported results obtained on networks with crosslink functionality four (21). In the present study, we investigated the effect of the structure of junctions on the mechanical behaviour of PDMS. Rather uncommon networks with comb-like crosslinks were employed, intending that these would be most challenging to theoretical predictions.

Theoretical Considerations

In our first paper, the molecular theory of rubber elasticity was briefly reviewed, especially the basic assumptions and topics still subject to discussion (21). We will now focus on the effects of the structure and the functionality f of the crosslinks and the relevant theory.

In a network where the crosslinks move affinely to the macroscopic strain, the functionality of the crosslinks is insignificant. The modulus of such a network only depends on the number of chains, no matter how they are connected (22-27)

$$G_{aff} = \nu kT \; <r^2>/<r^2>_o \qquad\qquad (1)$$

T is the absolute temperature, k the Boltzmann constant, ν the number of network chains per volume, $<r^2>$ the mean-square end-to-end distance of chains in the undeformed network and $<r^2>_o$ the same quantity for the free, disconnected chains.

If the fluctuations of crosslinks are considered, a functionality-dependent factor, $1 - 2/f$, has to be applied (28-31)

$$G_{ph} = (1-\tfrac{2}{f}) \; \nu kT \; <r^2>/<r^2>_o \qquad\qquad (2)$$

In order to enable these fluctuations to occur, the network chains are assumed to be "phantom" in nature; i.e. their material properties are dismissed and they act only to exert forces on the junctions to which they are attached. With common networks having tetrafunctional junctions, the results of the two approaches differ by a factor of two. Identical results are only obtained from both theories, when the functionality is infinite. From a practical viewpoint, however, a value of about 20 for f can already be equated to infinity because crosslink densities can hardly be obtained with an accuracy better than $\pm$ 10%.

Application of both approaches to describe simple elongation experiments yields that either theory predicts the so-called reduced stress σ_{red} to be equal to the shear modulus G and to be independent of strain.

$$\sigma_{red} = \frac{\sigma^o}{\lambda - \lambda^{-2}} = G \qquad\qquad (3)$$

The reduced stress is defined as the force per cross-sectional area of the undeformed sample, divided by the term $\lambda - \lambda^{-2}$ with λ being the relative elongation L/L_o. With undiluted rubber, this is not found experimentally. In most cases, however, the elastic behaviour in a moderate elongation range is satisfactorily described by the empirical Mooney-Rivlin equation, which predicts a linear dependence of σ_{red} on reciprocal elongation λ^{-1} (32-34)

$$\sigma_{red} = 2C_1 + 2C_2/\lambda \qquad (4)$$

The identity of σ_{red} and G according to Eq. (3) is then only valid in the limiting case $\lambda \Rightarrow 1$. The recent development of molecular theory by Ronca and Allegra and by Flory is in approximate accordance with the observed strain dependence (1-4). It is assumed that the two classical approaches mentioned above represent extremes. A real network should exhibit intermediate behaviour, dependent upon the extent of deformation, state of dilution, and presumably other parameters which can influence the mobility of the junctions. The model using affinely displaced crosslinks gives the upper bound of the reduced stress σ_{red} for undiluted rubber at small strains; the model using fluctuating crosslinks gives the reduced stress at infinite tensile strain. The ratio of the Mooney-Rivlin parameters, C_2/C_1, is predicted by this theory to depend on crosslink functionality according to

$$C_2/C_1 \lesssim \frac{2}{f-2} \qquad (5)$$

Hence the measurement of this ratio for networks with different functionalities can serve to test the theory. Note that C_2/C_1 should be independent of temperature (this is confirmed by measurements) and also independent of crosslink density (however, a decrease of C_2/C_1 with increasing ν is found experimentally (10,34-36)

Experimental

On poly(dimethylsiloxane) (PDMS) networks having comb-like crosslinks, torsional vibration experiments and static stress-strain measurements at small deformations were performed as a function of temperature, torsional vibrations also as a function of frequency.

The networks studied were synthesized by a crosslinking mechanism via end-linking of relatively short chains. The chemical process used, is the highly selective reaction of vinyl groups, which are the terminal groups of a polymer, with active hydrogen atoms on a silane-type crosslinking agent. This reaction goes essentially to completion with no side reactions or isomerization.

In the present study, crosslinking agents are used which are polymers themselves, namely partly hydrogenated PDMS: In a strict nomenclature, this has to be considered a dimethylsiloxane

(DMS,-Si(CH$_3$)$_2$O-)-hydrogenmethylsiloxane (HMS,-SiH(CH$_3$)O-)-copol-
ymer. The structure of the crosslinking molecules was varied
extensively, with respect to chain length and with respect to the
content of HMS units. The characterisation of the crosslinking
agents used to synthesize the samples B1 - B12 is given in
Table I: column 2 gives the fraction of HMS units, column 3 the
molecular weight and column 4 the degree of polymerisation. The
content of active hydrogen varied from one on every monomer unit
(HMS fraction 1) to one on every 40th monomer unit on the aver-
age (HMS fraction 0.025); the degree of polymerisation covers
the range from 35 to 600, corresponding to molecular weights from
2100 to 44200 g·mol^{-1}.

<div align="center">Table I</div>

 Characterisation data for the synthesis of the networks studied

Sample	Characterisation of Crosslinking Molecules			Portions in Reaction Mixture, Weight-% of		Extract. Portion, Weight-%
	Fraction of HMS	Molecular Weight	Degree of Pol.	Crossl. Component	Divinyl Component	
PDMS-B1	1	2100	35	0.91	99.09	0.3
-B2	1	4500	75	0.91	99.09	0.3
-B3	1	7200	120	0.91	99.09	0.3
-B4	1	9000	150	0.91	99.09	0.3
-B5	0.50	6700	100	2.02	97.98	0.3
-B6	0.33	6900	100	3.09	96.91	0.8
-B7	0.25	7000	100	4.13	95.87	0.8
-B8	0.20	7100	100	5.18	94.82	1.0
-B9	0.33	10400	150	3.09	96.91	0.9
-B10	0.33	17300	250	3.09	96.91	0.7
-B11	0.14	11500	160	7.18	92.82	2.3
-B12	0.025	44200	600	31.20	68.80	n.d.

We calculated the molecular weight of the crosslinking molecules
from the ratio of monofunctional (Si(CH$_3$)$_3$Cl) and bifunctional
(Si(CH$_3$)$_2$Cl$_2$ or SiH(CH$_3$)Cl$_2$) units present during the hydrolysis
of chlorosiloxanes, which forms the polymerisation process. It
was checked by viscosity, measured on the undiluted material at
25°C, according to the equation

$$\log \eta = 1 + 0.0123 \quad M \qquad (6)$$

given by Barry (37). Satisfactory agreement between the two meth-
ods was obtained, except for samples with the largest HMS frac-
tion. This was expected because Eq. (6) holds only for PDMS.
     The copolymer-crosslinking agents were made either by acid
equilibration of PHMS and PDMS in suitable proportions (Fig. 1a)
or by cohydrolysis of the corresponding chlorosilanes (Fig. 1b).
Equilibration gave a small amount (<5%) of low molecular weight
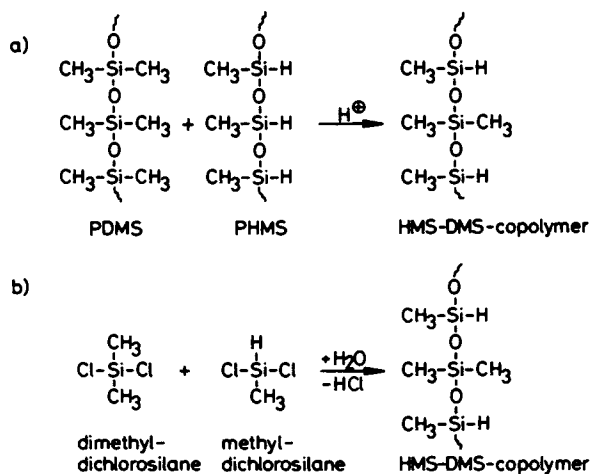
Figure 1. Synthesis of HMS-DMS copolymers. Key: a, acid equilibration of PHMS and PDMS; b, cohydrolysis of chlorosilanes.

cyclics. Their presence was detected by GPC. It could be shown by
IR that their composition was the same as that of the polymers.
The cyclics could be removed by high-vacuum distillation, but this
was not done regularly. Two networks synthesized using a purified
and unpurified crosslinker, had the same modulus within 5%. Hence we
concluded that the cyclics do not affect the crosslinking reaction.

   α,ω-divinyl-poly(dimethylsiloxane) with a number average mo-
lecular weight of 26000 g·mol^{-1} was used to react with the cross-
linking agents in the presence of a platinum complex as catalyst
(Figure 2). After mixing the two components with the catalyst,
they were cast in aluminium forms and heated 5 – 10 hours at 50°C.
To make sure that every vinyl endgroup is linked, the reaction
was conducted with a twofold excess of crosslinking agent. Thus
only half of the active hydrogens react. The weight portions of
the two components employed to obtain this unbalanced stoichio-
metry are tabulated in Table I. The last column in Table I gives
the extractable portions of the networks. It has been determined
by extracting the samples with toluene at 30°C for three weeks.
The samples were weighed before swelling and after deswelling.

   The structure of the resulting networks is shown schematical-
ly in Figure 3. Some molecules, namely the former HMS-DMS-copoly-
mers, form comb-like polyfunctional crosslinks. In Figure 3, these
are drawn as thick lines for reason of clarity. By changing the
hydrogen content of the crosslinking component (that is the HMS-
fraction),we varied the spacing between branch points. For a quan-
titative description of a network, we define the term "branching
density", z, as the number of branch points per monomer unit of
the crosslinking molecule. z is tabulated in Table II. It is half
as big as the HMS fraction in the crosslinking molecules because
of the twofold excess of the crosslinking agent. There are two
ways to look at the system. It can be described as having large,
comb-like crosslinks with very high functionality, f_1, the latter
being equated as $f_1 = z \cdot r$ with r as degree of polymerisation of
the crosslinking agent. Then only the former α,ω-divinyl-PDMS
chains count as network chain in the sense of rubber elasticity
theory. The numbers of chains per unit volume, ν_1, calculated as
a result of this point of view, are given together with the cor-
responding functionalities, f_1, in Table II.

   On the other hand, the parts of each crosslinking molecule
between two adjacent branch points can be taken as short network
chains. In this case the junctions are trifunctional ($f_2 = 3$) and
the chains have a bimodal distribution. The total number of net-
work chains, ν_2, is threefold the number of former α,ω-divinyl
chains, because two short chains and one long chain proceed from
each crosslink. ν_2 is also tabulated in Table II.

   The effect of chain ends, which are elastically ineffective,
has been neglegted in this calculation. But as chain ends are on-
ly formed from crosslinking molecules, whose fraction in the net-
work is rather small, this should cause a negligible correction.

partly hydrogenated
PDMS   α.ω – divinyl–PDMS
(HMS-DMS-copolymer)
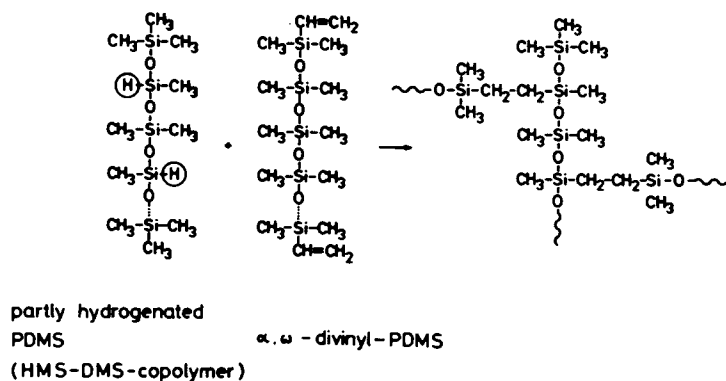
Figure 2.   Cross-linking of α,ω-divinyl-PDMS by HMS-DMS copolymers.
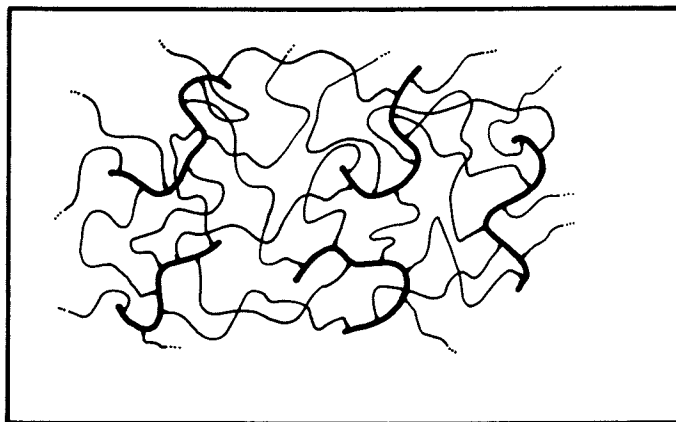
Figure 3.   Sketch of a network with comblike cross-links.

The calculation of the number of chains per volume also did
not take the sol content (Table I) into account. As GPC measure-
ments have shown, the extract consists mainly of small rings
($(Si(CH_3)_2O)_n$;n = 3 - 5), which are not able to react.
They form a kind of a diluent, which is in most cases pres-
ent up to less than 1% by weight. Hence the correction to be
applied to the calculated crosslink densities ν, is also less
than 1%; that means negligible.

In this point we disagree with Macosko, who deduced a rather
large correction from a small sol fraction, assuming that the ex-
tract consists of molecules, which could in principle react, but
did not do so, because the chemical equilibrium was attained, or
because there was steric hindrance etc. (6,7).

<div align="center">

Table II
========
Calculated network densities and
corresponding crosslink functionalities

</div>

sample	branching density z	counting long chains only :		counting long and short chains :	
		f_1	$\nu_1/mol \cdot cm^{-3} \cdot 10^5$	f_2	$\nu_2/mol \cdot cm^{-3} \cdot 10^5$
PDMS-B1	0.5	17.5	3.69	3	11.2
-B2	0.5	37.5	3.69	3	11.2
-B3	0.5	60	3.69	3	11.2
-B4	0.5	75	3.69	3	11.2
-B5	0.25	25	3.66	3	11.0
-B6	0.165	16.5	3.62	3	10.9
-B7	0.125	12.5	3.58	3	10.7
-B8	0.1	10	3.54	3	10.6
-B9	0.165	25	3.62	3	10.9
-B10	0.165	41	3.62	3	10.9
-B11	0.07	11	3.46	3	10.4
-B12	0.0125	7.5	2.57	3	7.7

Results and Discussion

Thermodynamic Analysis. As reported previously, the storage
modulus G' of PDMS networks with tetrafunctional crosslinks is
independent of frequency between 10^{-3} and 1 Hz (21). This behaviour
which is entirely different from that of vulcanized natural rub-
ber or synthetic polyisoprene networks, was attributed to the
lack of entanglements, both trapped and untrapped, in these PDMS
networks. Figure 4 shows that G' of a network with comb-like
crosslinks is also frequency independent within an error of 0.5%.
For comparison, two curves for PDMS having tetrafunctional cross-
links are also shown. The flat curves imply that slower relaxa-
tions are highly unlikely. Hence a thermodynamic analysis of the
G' data below 1 Hz can be made as they equal equilibrium moduli.

Plots of G' at 0.5 Hz and the reduced stress σ_{red} obtained from stress-strain measurements at small strains against temperature, give almost identical straight lines (Figure 5). This similarity was expected because no frequency dependence of G' had been observed. Hence G' equals the equilibrium modulus G; G moreover equals the reduced stress σ_{red}, if the latter is measured in the vicinity of $\lambda = 1$. The measurements were always performed at $\lambda = 1.02 - 1.04$, so that this requirement is fulfilled.

Being a very sensitive quantity, however, the relative energy part of the modulus is different for some of the samples, if calculated from static or dynamic data, respectively. (For the calculation method, compare ref. 20,21.) Table III gives the values for the relative energy part. $\sigma_{red,U}/\sigma_{red}$ is the energy part calculated from stress-strain measurements; G'_U/G' is the corresponding number obtained from dynamic data at 0.5 Hz.

Table III

Relative energy part of the modulus at T = 298K, from stress-strain measurements with $\lambda = 1.02-1.04$ ($\sigma_{red,U}/\sigma_{red}$) and from torsional vibration experiments (G'_U/G')

sample	$\sigma_{red,U}/\sigma_{red}$	G'_U/G'
PDMS-B1	0.122	0.257
-B2	0.096	0.240
-B3	0.100	0.253
-B4	0.181	0.294
-B5	0.215	0.261
-B6	0.183	0.232
-B7	0.216	0.317
-B8	0.199	0.291
-B9	0.118	0.285
-B10	0.283	0.274
-B11	0.278	0.288
-B12	0.264	0.278

In Figure 6, these data are plotted versus the branching density z of crosslinking molecules. G'_U/G' is fairly independent of network microstructure. It covers a range of 0.24 to 0.32 as a result of statistical scattering, averaging to 0.28 as in case of the networks with tetrafunctional crosslinks.

On the contrary, $\sigma_{red,U}/\sigma_{red}$ clearly shows some dependence on the structure of the crosslinks, changing from around 0.27 to 0.10 as the branching density z increases from 0.01 to 0.5. The different time scale of the experiments can not have effected the results, because is was proved that G' is independent of frequency. The deformation ratio λ is 1.00005 in case of torsional vibrations and 1.02-1.04 in case of uniaxial extension. Hence it ap-
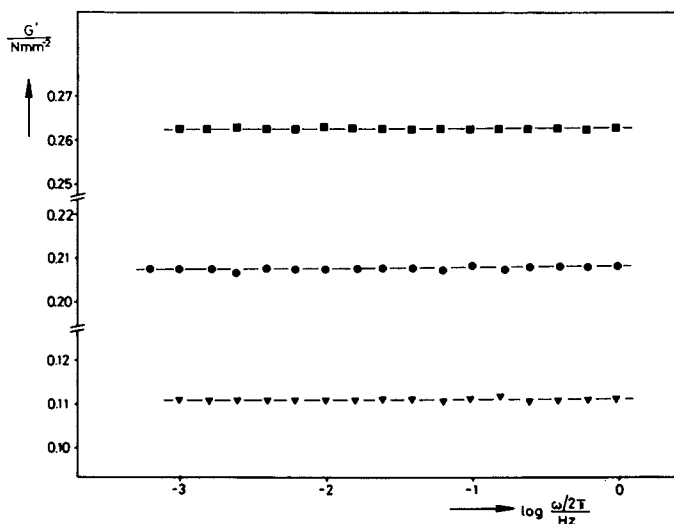
Figure 4. Frequency dependence of the storage modulus G' at 303 K. Key: ■, PDMS-B11, (comblike crosslinks); ●, PDMS-C1, (tetrafunctional cross-links, randomly introduced); ▼, PDMS-A2 (tetrafunctional cross-links, end-linked network).
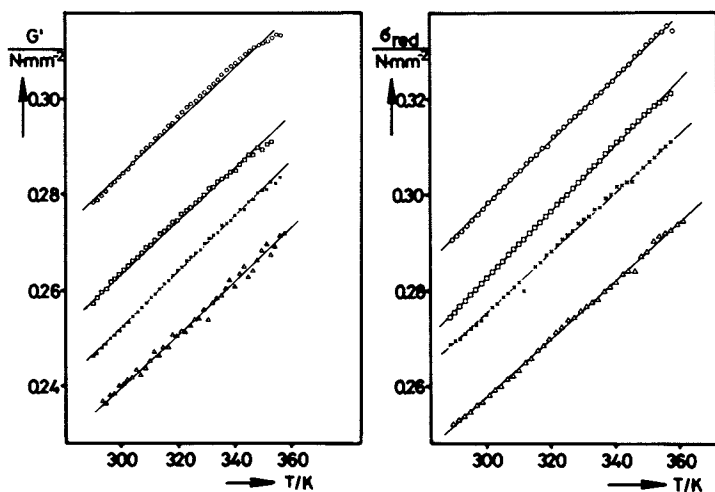
Figure 5. From left to right: temperature dependence of the storage modulus at 0.5 Hz, and of the reduced stress, (λ ≈ 1.03). Key: □, PDMS-B1; ○, PDMS-B2; ×, PDMS-B6; △, PDMS-B7.
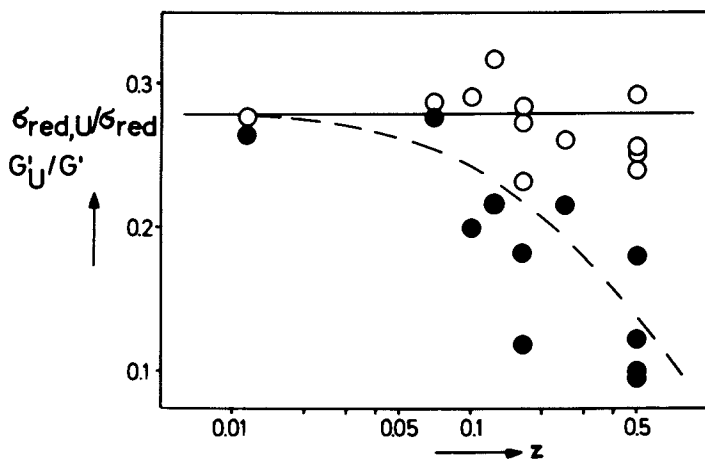
Figure 6. Relative energy part of the modulus at 298 K versus branching density z. Key: ●, $\sigma_{red,v}/\sigma_{red}$; ○, G_{U}'/G'.

pears that at very small deformations the energy part is indepen-
dent of network topology, arising solely from different energy
levels for different conformations of the chains.However, at mod-
erate deformations, an additional effect is found, depending on
the structure of the crosslinks. These findings being quite dis-
tinct at high functionality, are a feature of the exceptional mi-
crostructure of the networks. It should be emphasized that the
results found on these samples can not be generalized with re-
spect to the more common networks with tetrafunctional junctions.
As pointed out in the first part of this work, tetrafunctionally
crosslinked PDMS also shows some dependence of the energy part of
the modulus on network density and on the measuring method, but
the effects observed there, are much smaller than the great varia-
tion of $\sigma_{red,U}/\sigma_{red}$ with branching density in case of networks
with comb-like crosslinks considered here (21).

Literature data for the relative energy part of the modulus
or retractive force show a broad scattering covering the range
from 0.14 to 0.27 (38-44). Some of the authors cited, have found
a distinct dependence on the magnitude of deformation, but sur-
prisingly they do not indicate this finding (43).

Comparison with Statistical Theory, Small-Strain Behaviour.
Calculations of theoretical moduli, using the phantom theory and
the affine theory as limiting cases, were carried out in order to
compare the theoretical predictions with values found experimen-
tally (Table IV).

Table IV
========
Comparison of theoretically calculated moduli
and experimentally observed ones.
(T_c = 323 K, crosslinking temperature)

sample	$\frac{1}{3}\nu_2 \cdot R \cdot T_c$ $N \cdot mm^{-2}$	$(1-\frac{2}{f_1})\nu_1 \cdot R \cdot T_c$ $N \cdot mm^{-2}$	$\nu_2 \cdot R \cdot T_c$ $N \cdot mm^{-2}$	$G'(T_c)$ $N \cdot mm^{-2}$	$\sigma_{red}(T_c)$ $N \cdot mm^{-2}$
PDMS-B1	0.103	0.091	0.309	0.28	0.30
-B2	0.103	0.098	0.309	0.31	0.33
-B3	0.103	0.100	0.309	0.33	0.35
-B4	0.103	0.100	0.309	0.30	0.34
-B5	0.102	0.094	0.306	0.28	0.29
-B6	0.101	0.088	0.303	0.26	0.29
-B7	0.099	0.083	0.297	0.25	0.27
-B8	0.098	0.078	0.294	0.24	0.26
-B9	0.101	0.093	0.303	0.29	0.27
-B10	0.101	0.096	0.303	0.27	0.25
-B11	0.091	0.075	0.273	0.27	0.25
-B12	0.069	0.051	0.207	0.13	0.14

As pointed out in the experimental section, there are two
ways to calculate the network density of networks with comb-like

crosslinks. However, when the modulus is computed from these net-
work densities, ν_1 and ν_2 (comp. Table II), using the theory of
phantom networks, both points of view give approximately the same
results (Table IV, columns 2 and 3). (Identical results would
have been obtained, if the functionalities f_1 were actually in-
finite.) Column 4 gives the calculated modulus, which is obtained
by counting short and long chains and using the affine theory.
(For all calculations, the factor $<r^2>/<r^2>_o$ has been set to uni-
ty, since the crosslinking process occured in bulk.)

The moduli, measured at crosslinking temperature T_c, which
are given in the last two columns of Table IV, are about two to
three fold greater than those computed from phantom theory. Ex-
cept for the samples with the lowest branching densities, the
observed values agree satisfactorily with those for an affine
network.

We reported earlier that PDMS networks with tetrafunctional
crosslinks can be described formally by the theory of phantom
networks even at small strains (20,21). This behaviour which dis-
tinguishes PDMS from various other rubbers, was explained by the
lack of elastically effective entanglements, so that the cross-
links can fluctuate to a great extent. As another possible expla-
nation, we discussed that the term $<r^2>/<r^2>_o$ could be smaller
than unity in PDMS networks. The results of the present study
show a different behaviour, indicating that the microstructure of
the networks is of great importance. To elaborate this influence,
the experimentally observed moduli and reduced stresses, here both
denoted G_{exp}, were divided by the calculated moduli for a phan-
tom network, G_{ph}, and plotted versus branching density z of the
crosslinking molecules in Figure 7.

If the network could be described as a phantom network, a
value of G_{exp}/G_{ph} = 1 would be expected. Furthermore, if the
structure of the crosslinking molecules did not effect the modu-
lus, a horizontal line would be obtained. Neither behaviour is
found. The ratio G_{exp}/G_{ph} covers the range of about 2 - 3, in-
creasing definitely with increasing branching density. Stated
otherwise, G_{exp}/G_{ph} is 3 at highest branching densities and tends
to approach unity as z becomes smaller. Even at the lowest branch-
ing density studied, z = 0.0125, the chain-length distribution
function is strongly bimodal, having maxima at M = 26000 and
M = 6000 $g \cdot mol^{-1}$, corresponding to the former α,ω-divinyl-PDMS
and to the parts of crosslinking molecules between adjacent
branch points. A branching density of z = 0.003 would belong to
a network, where the two maxima fall together. If we extrapolate
the curve in Figure 7 to this value of z, it yields approximate-
ly G_{exp}/G_{ph} = 1. That means that such a network could be descri-
bed by the theory of phantom networks. This extrapolated result
is in agreement with observations on tetrafunctionally crosslinked
PDMS, which obey phantom network theory as well.

The remaining question is, how the deviations from phantom
network theory at high branching densities can be explained.

Our results tend to approach the affine theory with increasing z.
That means, that the fluctuations of crosslinks are more and more
restricted, the reason for this being the change in microstruc-
ture. (This is quite different from the strain dependent restric-
tion of fluctuations as predicted by Flory's recent theory.)
    We now compare a crosslink (1) from which two very short
chains and one long chain proceed, with another, (2), from which
three chains of approximately equal lengths start, so that the
number average molecular weight of the three chains is the same
in the two pictures. The adjacent crosslinks are assumed to be
fixed. The space which is principally available to the crosslink,
determined by the maximum elongation of the chains, is much small-
er for crosslink (1) than for crosslink (2). That means that short
chains, as they occur in these networks with bimodal chain length
distribution, restrict the mobility of the junctions. The restric-
tion is the greater, the shorter the chains are. As the branch-
ing density z is inversely proportional to the length of the
short chains, an increase of the modulus with increasing z is de-
duced by this argument. The experiments clearly show the same
dependence.

    Comparison with Statistical Theory at Moderate Strains. So
far we have shown, that a transition between the two limiting
classical theories, i.e. affine theory and phantom theory, is possi-
ble by a suitable choice of the network microstructure. This ar-
gument goes beyond the revised theory by Ronca and Allegra and
by Flory, which predicts such a transition as a result of
increasing strain, thus explaining the experimentally observed
strain dependence of the reduced stress.
    In order to check this prediction, stress-strain measure-
ments were made up to moderate strains at room temperature. The
obtained data are plotted in the usual manner as σ_{red} versus $1/\lambda$
in Figure 8. Table V gives the Mooney-Rivlin constants $2C_1$ and
$2C_2$ calculated from these plots and also the ratio C_2/C_1.
    According to the theory, the affine limit should apply as an
upper bound at $\lambda = 1$; this seems to be in agreement with our meas-
urements (compare Table IV). At infinite strain, the phantom
limit should apply. Therefore $2C_1$ should equal the theoretical
modulus calculated by phantom theory. This is not confirmed by
our measurements, the data in column 2 of Table V being mostly
twice as large as the predicted ones in column 2 of Table IV. The
reason for this deviation was already explained above: the restric-
tion of junction fluctuation in the samples studied is caused by
the very short chains and not only by the dense interspersion of
chains, as assumed in the derivation of the recent theory. The
influence of these short chains can obviously not vanish with
increasing strain. The theory is therefore not quantitatively ap-
plicable to these networks. However, with decreasing branching
density the predictions of the theory should be approximated bet-
ter. This is actually found. In Figure 9 the ratio $2C_1/G_{ph}$ is
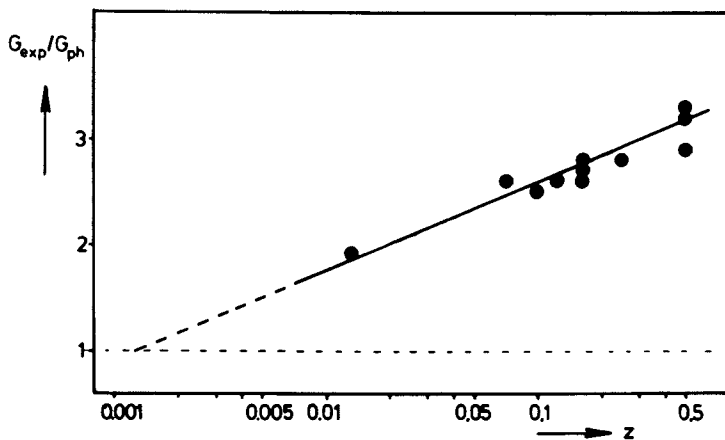
Figure 7.   Ratio of experimentally observed and theoretically calculated modulus, using phantom network theory with f_2 and v_2, versus branching density z.
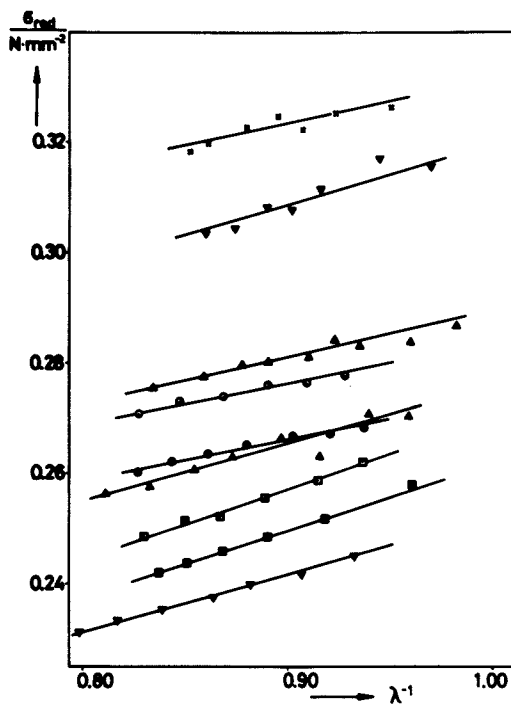
Figure 8.   Mooney–Rivlin plots for strain dependent measurements at 298 K.   Key: ▲, PDMS-B1; ▼, PDMS-B2; ✕, PDMS-B3; ○, PDMS-B5; ●, PDMS-B6; □, PDMS-B7; ▽, PDMS-B8; △, PDMS-B9; ■, PDMS-B10.
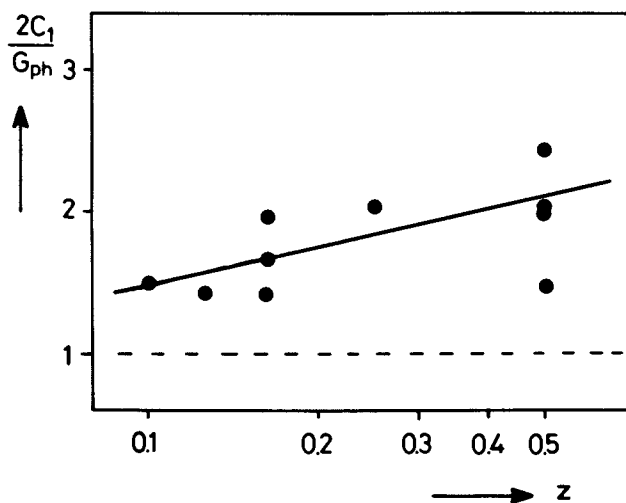
Figure 9. Ratio of $2C_1$ and theoretically calculated modulus, using phantom net-work theory with f_2 and v_2, versus branching density z.

plotted versus branching density. The theory predicts $2C_1/G_{ph}$ to be unity; our data lie above this value, but clearly decrease with decreasing branching density.

<div align="center">

Table V
=======

Mooney-Rivlin constants obtained from
strain dependent measurements at 298 K
</div>

sample	$2C_1$	$2C_2$	C_2/C_1
PDMS-B1	0.205	0.085	0.42
-B2	0.211	0.108	0.51
-B3	0.252	0.080	0.32
-B4	0.152	0.136	0.89
-B5	0.207	0.076	0.37
-B6	0.198	0.076	0.38
-B7	0.142	0.128	0.91
-B8	0.147	0.105	0.72
-B9	0.170	0.106	0.62
-B10	0.144	0.116	0.80

We now take the other point of view and consider the networks to have crosslinks of very high functionality (instead of taking f = 3 as above). This supposition is justified only at high branching densities; it has not lead to an agreement between calculated and observed small-strain moduli (Table IV). According to the theory, the $2C_2$-term should vanish for networks with very high functionality, because 1-2/f then equals unity. Contrary to this hypothesis, even the samples with the highest branching density, B1-B4, which can be treated as having functionalities rangeing from 17 to 75, do show $2C_2$-terms almost half as large as $2C_1$. Thus, there is a disagreement between theory and experiment concerning this point.

Figure 10 shows the dependence of C_2/C_1 on junction functionality, f_1. There is a broad scattering in the data, preventing an exact analysis. A slight decrease of C_2/C_1 seems to occur, falling far behind the predicted drop. Figure 11 shows that C_2/C_1 decreases also with branching density z. This indicates that the branching density is of great importance to describe the behaviour of these networks. However, the theory is still far from having these structural details incorporated.

Concluding, we can state that the absolute values of the small-strain moduli, which are greater for networks having comblike crosslinks, than for those with tetrafunctional junctions, are understandable, if we assume that the fluctuations of junctions are restricted by the very short chains. The strain dependent measurements do not agree quantitatively with the recent theory, although the trends are in accordance. An exact correspondence
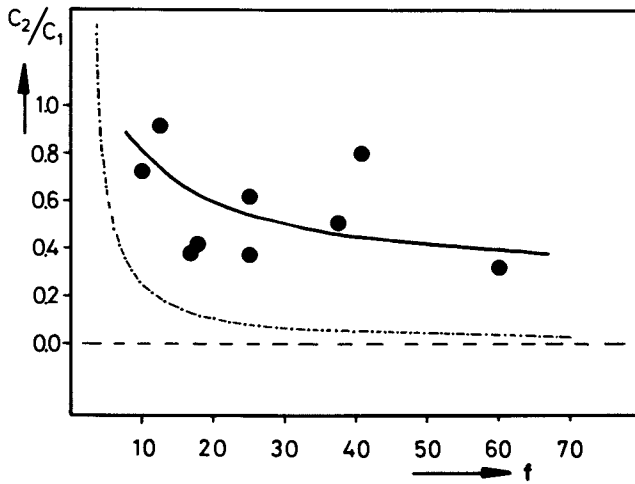
Figure 10.   Ratio C_2/C_1 vs. crosslink functionality $f = f_1$. The dash-dotted line represents the upper bound of theory.
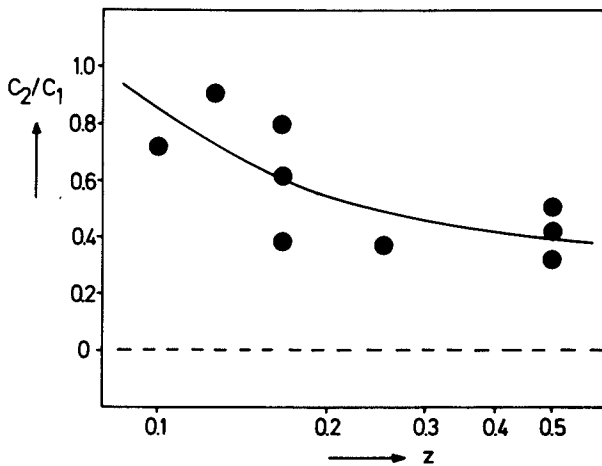
Figure 11.   Ratio C_2/C_1 vs. branching density z.

can not be expected at the present state of the theory because it does not account for the complicated microstructure of the net-works used.

Acknowledgement

Literature Cited

1. Ronca, G.; Allegra, G. J. Chem. Phys. 1975, 63, 4990.
2. Flory, P. J. Proc. Roy. Soc. London. 1976, A351, 351.
3. Flory, P. J. J. Chem. Phys. 1977, 66, 5720.
4. Flory, P. J. Polymer 1979, 20, 1317.
5. Allen, G.; Holmes, P. A.; Walsh, D. A. Discuss. Farad. Soc. 1974, 57, 19.
6. Valles, E. M.; Macosko, C. W. "Networks: Structure and Prop-erties"; Labana, S. S., Ed.; Academic Press, New York 1977.
7. Valles, E. M.; Macosko, C. W. Macromolecules 1979, 12, 673.
8. Belkebir-Mrani, A.; Herz, J.; Rempp, P. Macromol. Chem. 1977, 178, 485.
9. Belkebir-Mrani, A.; Beinert, G.; Herz, J. Europ. Pol. J. 1977 13, 277.
10. Mark, J. E.; Sullivan, J. L. J. Chem. Phys. 1977, 66, 1006.
11. Mark, J. E.; Rahalkar, R. R.; Sullivan, J. L. J. Chem. Phys. 1979, 70, 1794.
12. Falender, J. R.; Yeh, G. S. Y.; Mark, J. E. J. Chem. Phys. 1979, 70, 5324.
13. Llorente, M. A.; Mark, J. E. Macromolecules 1980, 13, 681.
14. Llorente, M. A.; Andrady, A. L.; Mark, J. E. J. Pol.Sci.-Phys. 1981, 19, 621.
15. Pak, H.; Flory, P. J. J. Pol. Sci.-Phys. 1979, 17, 1845.
16. Erman, B.; Wagner, W.; Flory, P. J. Macromolecules 1980, 13, 1554
17. Dossin, L. M.; Graessley, W. W. Macromolecules 1979, 12, 123.
18. Meyers, K. D.; Bye, M. L.; Merrill, E. W. Macromolecules 1980, 13, 1045.
19. Oppermann, W.; Rehage, G.; Preprints 26th Int. Symp. on Macro-molecules, Mainz 1979, Vol. III, 1360.
20. Oppermann, W.; Ph.D. Thesis, T. U. Clausthal 1979.
21. Oppermann, W.; Rehage, G. Coll. Pol. Sci. 1981, 259 (12)
22. Kuhn, W. Kolloid-Z. u. Z. Polymere 1934, 68, 2 ; 1936, 87,258.
23. Wall, F. T. J. Chem. Phys. 1942, 10, 132; 1943, 11, 527.
24. Treloar, L. R. G. Trans, Farad. Soc. 1943, 39, 241; 1946, 42, 77.
25. Hermans, H. J. Trans Farad. Soc. 1947, 43, 591.
26. Flory, P. J. J. Chem. Phys. 1950, 18, 108.
27. Wall, F. T.; Flory, P. J. J. Chem. Phys. 1951, 19, 1435.

28. Duiser, J. A.; Staverman, A. J. "Physics of Non-Crystalline
     Solids"; Prins, J. A., Ed.; North-Holland Publ. Corp.,
     Amsterdam 1965.
29. Graessley, W. W. Macromolecules 1975, 8, 186 and 865.
30. Edwards, S. F. "Polymer Networks, Structural and Mechanical
     Properties"; Chompff, A. J.; Newman S.; Eds.; Plenum Press
     New York 1971.
31. Edwards, S. F. Brit. Pol. J. 1977, 9, 140.
32. Dusek, K.; Prins, W, Adv. Pol. Sci. 1969, 6, 1.
33. Treloar, L. R. G. Rep. Progr. Phys. 1973, 36, 755.
34. Mark. J. E. Rubber Chem. Techn. 1975, 48 495.
35. Gleim, W.; Ph. D. Thesis, T. U. Clausthal 1982.
36. Gebhard, G.; Ph. D. Thesis, T. U. Clausthal 1978.
37. Barry, A. J. J. Appl. Phys. 1946, 17, 1020.
38. Ciferri, A. J. Pol. Sci. 1960, 45, 528.
39. Ciferri, A. Trans. Farad. Soc. 1961, 57, 848.
40. Mark J. E.; Flory, P. J. J. Amer. Chem. Soc. 1964, 86, 138.
41. Barrie, J. A.; Standen, J. Polymer 1967, 8, 97.
42. Price, C.; Padget, J. C.; Kirkham, M. C.; Allen, G. Polymer
     1969, 10, 573.
43. Chen, R. Y. S.; Yu, C. U.; Mark, J. E. Macromolecules 1973,
     6, 746.
44. Flory, P. J.; Hoeve, C. A. J.; Ciferri, A. J. Pol. Sci.
     1959, 34, 337.

Equilibrium Tensile Behavior of Model Silicone Networks of High Junction Functionality

KEVIN O. MEYERS

ARCO Oil and Gas Company, Recovery Processes Research, Dallas, TX 75221

EDWARD W. MERRILL

Massachusetts Institute of Technology, Department of Chemical Engineering, Cambridge, MA 02139

Elastomeric networks with junction functionalities ranging from 4 to 70 were prepared by endlinking α,ω-divinyl poly(dimethylsiloxane) chains having number average molecular weights ranging from 8,800 to 55,300 with polyfunctional junctions provided by linear and branched poly(methylhydrogensiloxanes). The equilibrium stress-strain isotherms in elongation, and the swelling ratios in benzene, were measured at 25°C for these networks. Network chain densities calculated from these measurements exceeded the values predicted from stoichiometry. These excesses diminished for those networks with diluent present during network formation or with low extents of the network formation reaction. Molecular theories presuming a contribution from trapped entanglements in small strain gave good agreement with the data and offered reasonable explanation of the trends observed.

The phenomena of rubber elasticity have been under investigation for over a century. Yet there still remains much controversy as to the correct molecular theory to explain elastomeric behavior. These theories relate an elastomer's network structure to its equilibrium mechanical properties. Verification of such relationships requires knowledge of the network structure acquired independently of the theory under review. Therefore, there has been much interest in the synthesis and investigation of "model" elastomeric networks, i.e. networks whose structure is known from and may be controlled through the network synthesis reaction. Such model networks may be prepared by the endlinking reaction of difunctional polymer chains with plurifunctional crosslinking reagents. This endlinking permits control of M_c (the average molecular weight between chemical crosslinks) and its dispersity via the number average molecular weight, M_n, and

dispersity of the telechelic polymer. The functionality of the
crosslinker, ϕ_o, dictates the final network functionality.
    Until recently (1-5) investigations utilizing model net-
works had been limited to functionalities of four or less. Net-
works with higher functionality are predicted by the various
theories of rubber elasticity to display unique equilibrium ten-
sile behavior. As such, these multifunctional networks provide
insight into the controversy surrounding these theories. The
present study addresses the synthesis and equilibrium tensile
behavior of endlinked model multifunctional poly(dimethylsilox-
ane) (PDMS) networks.

Theory

    The results of uniaxial stress-strain experiments are often
analyzed in terms of the reduced stress defined by

$$[f] = f/[A(\alpha - \alpha^{-2})] \tag{1}$$

where f is the elastic force, A is the undeformed cross-
sectional area, and α is the relative elongation. For moderate
values of α the empirical Mooney-Rivlin (6) relation:

$$[f] = 2C_1 + 2C_2\alpha^{-1} \tag{2}$$

is found to hold quite satisfactorily. $2C_1$ and $2C_2$ are con-
stants independent of strain.
    Classical molecular theories of rubber elasticity (7,8)
lead to an elastic equation of state which predicts the reduced
stress to be constant over the entire range of uniaxial deforma-
tion. To explain this deviation between the classical theories
and reality. Flory (9) and Ronca and Allegra (10) have sepa-
rately proposed a new model based on the hypothesis that in a
real network, the fluctuations of a junction about its mean
position may may be significantly impeded by interactions with
chains emanating from spatially, but not topologically, neigh-
boring junctions. Thus, the junctions in a real network are
more constrained than those in a phantom network. The elastic
force is taken to be the sum of two contributions (9):

$$f = f_{Ph} + f_c \tag{3}$$

f_c is the additional force arising from the aforementioned
constraints on junction fluctuations and f_{Ph} is the force
predicted by the phantom network theory (9):

$$[f_{PH}] = \nu kT(V/V_o)^{2/3} (1-2/\phi)/V \tag{4}$$

where T is the absolute temperature, k is the Boltzmann con-
stant, V_o is the volume in the undeformed state such that the
mean-squared end-to-end length $\langle r^2 \rangle$ of a chain assumes the

value $\langle r^2 \rangle_o$ for unperturbed, free chains, ν is the number of chains, V is the volume of the network, and ϕ is the network functionality.

The theory ($\underline{9}$) predicts that in simple elongation, the ratio f_c/f_{Ph} decreases with increasing strain and eventually goes to zero (phantom network). Furthermore, at $\alpha = 1$, the theory holds that

$$f_c/f_{Ph} < 2/(\phi-2) \tag{5}$$

Therefore, Flory's theory concludes that as the function-ality of a network increases, the constraint contribution, f_c, should decrease and eventually vanish. Furthermore, in the ex-treme limit in which junction fluctuations are totally sup-pressed, the Flory theory reduces to the affine network model:

$$[f] = \nu kT(V/V_o)^{2/3}/V \tag{6}$$

The Flory theory considers topological interactions among junctions and chains only in that they restrict junction fluc-tuations, Ferry ($\underline{11}$), Langley ($\underline{12}$) and Dossin and Graessley ($\underline{13}$) have argued that in the limit of small strain these interactions are also present along the chain contour and contribute directly to the modulus. Their conclusions are based on the rubbery pla-teau modulus, G_N^o, which is observed for high molecular weight linear polymers in dynamic mechanical testing. This plateau modulus is believed to be a measure of topological interactions or entanglements between chains. During network formation, a portion of these entanglements are permanently trapped, result-ing in a small-strain modulus greater than that due to chemical crosslinking alone.

Dossin and Graessley ($\underline{13}$) suggest that

$$G = \nu kT(1 - 2h/\phi)(V/V_o)^{2/3}/V + T_e G_e^{max} \tag{7}$$

where G is the small-strain modulus ($\alpha \to 1$), T_e is the fraction of the maximum concentration of topological interactions, G_e^{max}, which are permanently trapped by the network, and h is an em-pirical constant between one and zero, depending on the extent to which the junction fluctuations are impeded in the network (h = 0 for affine behavior, h = 1 for phantom behavior). Thus equation (7) predicts a small-strain modulus greater than that predicted by the Flory theory due to the $T_e G_e^{max}$ term.

Experimental

Multifunctional poly(dimethylsiloxane) (PDMS) networks were prepared via the addition of a silane hydrogen on poly(methyl-hydrogensiloxanes) (PMHS) to vinyl terminated linear PDMS

polymers in the presence of <u>cis</u>-dichlorobis(diethyl sulfide) platinum (II) catalyst:

$$\phi_0/2 \; CH_2{=}CH{-}\underset{\underset{CH_3}{|}}{\overset{\overset{CH_3}{|}}{Si}}[O{-}\underset{\underset{CH_3}{|}}{\overset{\overset{CH_3}{|}}{Si}}]_n CH{=}CH_2 \; + \; (CH_3)_3Si[O\underset{\underset{\underset{CH_3}{|}}{\phi_0}}{\overset{\overset{H}{|}}{Si}}]OSi(CH_3)_3 \; \xrightarrow{\;Pt\;}$$

Network Functionality ϕ_0
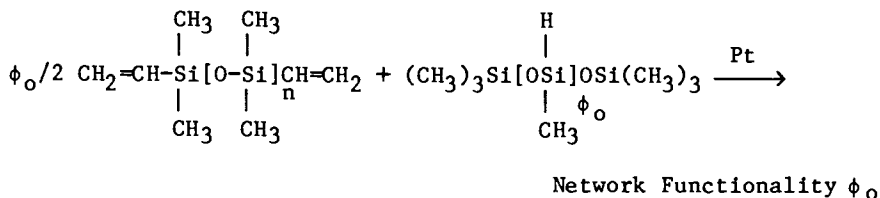
Six linear and three branched PMHS ranging in ϕ_0 from 6 to 84 were used as junction sites. For tetrafunctional networks, $[HSi(CH_3)_2O]_4Si$ was the crosslinking agent.
   Two sets of α,ω-divinyl PDMS were used in this study. The first set consisted of commercially available polymers which were supplied by the General Electric Corporation and the Dow Corning Corporation. Six different number average molecular weight α,ω-divinyl PDMS were provided, with M_n ranging from 8,800 to 28,600 g·mol^{-1}. The second set of α,ω-divinyl PDMS was synthesized by the anionic ring opening polymerization of hexamethylcyclotrisiloxane by the difunctional initiator, dilithium stilbene. This living polymer was capped with vinyldimethyl-chlorosilane $[CH_2{=}CHSi(CH_3)_2Cl]$ to give the desired product. α,ω-divinyl PDMS with 14 different values of M_n ranging from 12,200 to 52,800 were synthesized. The anionic polymerization resulted in α,ω-divinyl PDMS with relatively narrow molecular weight distributions (M_w/M_n = 1.08 – 1.30). The procedures utilized in the synthesis and characterization of the network precursors are given in greater detail elsewhere ($\underline{1},\underline{4}$).
   Networks were prepared both in bulk and in an oligomeric PDMS (no vinyl groups; M_n = 1170) which served as a "solvent". The two network precursors and solvent (if present) were combined with 20 ppm catalyst and reacted under argon at 75°C to produce the desired networks. The sol fractions, w_s, and equilibrium swelling ratio in benzene, v_{2m}, of these networks were determined according to established procedures ($\underline{1},\underline{4}$). Equilibrium tensile stress-strain isotherms were obtained at 25°C on dumbbell shaped specimens according to procedures described elsewhere ($\underline{1},\underline{4}$). The data were well correlated by linear regression to the empirical Mooney-Rivlin ($\underline{6}$) relationship. The tensile behavior of the networks formed in solution was measured both on networks with the solvent present and on networks from which the oligomeric PDMS had been extracted.
   The interested reader will find detailed tabulations of the experimental data ($2C_1, 2C_2, w_s, v_{2m}$) and calculations ($\varepsilon, T_e, v_s/V$) for the networks examined in this study given in references ($\underline{1}$) through ($\underline{4}$).

Results and Discussion

To compare the predictions of the various molecular theories
of rubber elasticity, three sets of high functionality networks
were prepared and tested in this investigation. The first set
of networks tested were formed in bulk and attained a high
extent of the endlinking reaction, i.e., $\varepsilon > 0.9$ where ε is the
extent of reaction of the terminal vinyl groups. The second set
of networks studied were formed in the presence of diluent and
also achieved a high extent of reaction ($\varepsilon > 0.9$). The final group
of experiments were performed on networks formed in bulk at low
extents of reaction ($0.4 < \varepsilon < 0.95$).

Networks Formed in Bulk, $\varepsilon > 0.9$. In Figure 1, $2C_1$, $2C_2$, $2C_1$
+ $2C_2$, and $2C_2/2C_1$ are plotted against the functionality of the
PMHS junction precursor, ϕ_0, divided by the molar ratio of
silane hydrogen to vinyl used in forming the networks, R. This
quotient was used instead of ϕ_0 to correct the functionality
of the PMHS junction precursor for the fact that an excess of
silane hydrogen (R > 1) had been used in forming the networks
to ensure complete reaction of the vinyl groups ($\phi \sim \phi_0/R$). All
the networks represented in Figure 1 were made with the $M_n =$
21,600 α,ω-divinyl PDMS. $2C_1$ and $2C_1 + 2C_2$ are found to increase
with increasing network functionality in the low-functionality
region (4-10); however, further increases in functionality be-
yond 20 result in little change in these moduli. A prediction
of the Flory theory is that in the limit of large strain ($\alpha^{-1} \to 0$),
the network will exhibit phantom behavior. Thus, the infinite-
strain modulus would increase as $1-2/\phi$ with functionality from
$0.5\nu kT/V$ at $\phi = 4$ to $0.9 \nu kT/V$ at $\phi = 20$. Increasing ϕ to
infinity would result in only a 10% further increase in the phan-
tom modulus. $2C_1$ being an extrapolation from finite to infinite
strain, overestimates the phantom modulus but the trend should
remain the same. Therefore, the increase in $2C_1$ qualitatively
follows the Flory predictions.
    The ratio $2C_2/2C_1$ is observed in Figure 1 to decrease as-
ymptotically with increasing ϕ_0/R. Once again the majority of
the decrease occurs between four and ten. $2C_2$, being a measure
of the magnitude of the transition from phantom to affine behav-
ior, is predicted by the Flory theory to decrease asymptotical-
ly with increasing functionality as is $2C_2/2C_1$. However, the
theoretical asymptote for both is zero [see equation (5)]. The
experimentally determined limit for $2C_2$ was found to be 0.11 MPa
for the $M_n = 21,600$ networks. For $2C_2/2C_1$, an asymptote of 0.56
was observed. Both of these values are significantly greater
than the zero prediction.
    Further disagreement with the Flory theory is found in the
magnitude of $2C_1$ and $2C_1 + 2C_2$ in Figure 1. These results are
quantified in terms of the structure factors A_1 and A_2. A_1 and
A_2 relate the small and large-strain moduli to the number of
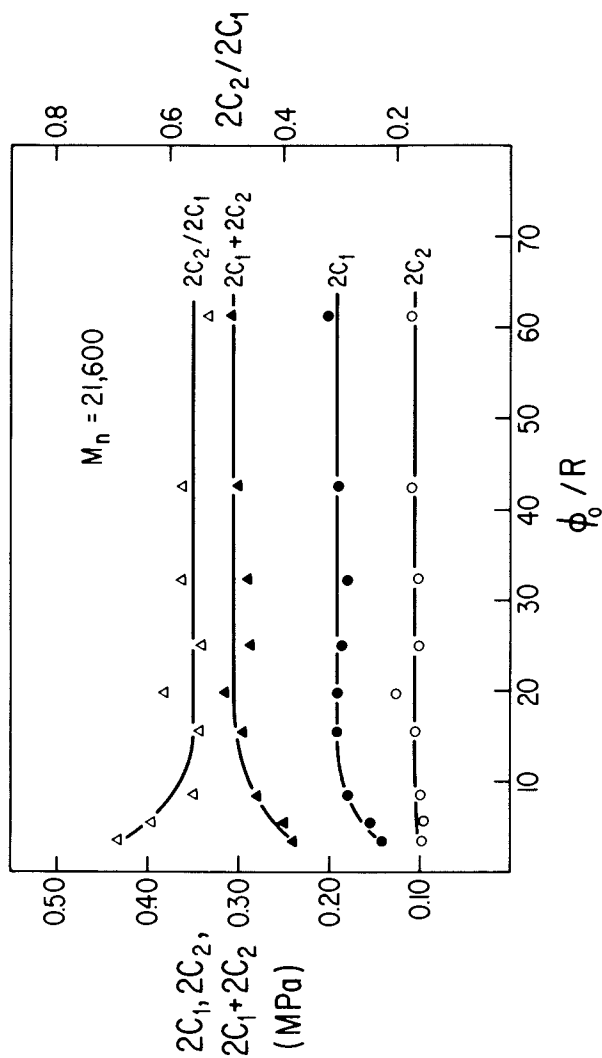
Figure 1.   Dependence of $2C_1$, $2C_2$, $2C_1 + 2C_2$, and $2C_2/2C_1$ on network functionality where M_n is 21,600 PDMS networks (1).

network chains per unit volume as calculated from stoichiome-
try, ν_s/V, and are defined as follows:

$$A_1 = (2C_1 + 2C_2) \left[\frac{\nu_s kT}{V} (V/V_o)^{2/3} \right]^{-1} \tag{8}$$

$$A_2 = 2C_1 \left[\frac{\nu_s kT}{V} (V/V_o)^{2/3} \right]^{-1} \tag{9}$$

According to the Flory theory (9), the predicted range on A_1
and A_2 lies between one and $(1-2/\phi)$. The upper limit, unity,
corresponds to affine behavior and the lower limit occurs in
phantom behavior. Therefore both A_1 and A_2 have predicted
asymptotes of one at high functionalities and should be inde-
pendent of ν_s/V.

In Figure 2, A_1 and A_2 are plotted against ϕ_o/R for the
M_n = 21,600 networks represented in Figure 1. In the calculation
of A_1 and A_2, it was assumed $V_o = V_f$, the volume at network for-
mation. ν_s/V was determined from ϵ, w_s, and M_n according to
relations derived by Miller and Macosko (14) as illustrated
elsewhere (1,4). Although the observed trends in A_1 and A_2 with
functionality are in qualitative agreement with the Flory
theory, their absolute magnitudes are two-to-threefold greater
than the Flory theoretical prediction. Similar results were
observed for a series of networks prepared using, M_n = 11,100
and M_n = 15,200 α,ω-divinyl PDMS (1,4).

A third structure factor, A_3, is also plotted in Figure 2.
A_3 is the ratio of network chain density calculated from the
affine network equililbrium swelling theory (inside the [ ]) to
that obtained from stoichiometry:

$$A_3 = \left[\frac{- (\ln(1 - v_{2m}) + v_{2m} + \chi_1 v_{2m}^2) \, v_{2r}}{V_1 (v_{2m}^{1/3} v_{2r}^{2/3} - 2Rv_{2m}/\phi_o)} \right] (V_o/\nu_s) \tag{10}$$

where $v_{2r} = (V_d/V_o)$, V_d is the volume of the dried extracted
network, V_1 is the molar volume of the solvent and χ_1 is the
polymer-solvent interaction parameter (7). The equilibrium
swelling in benzene was used in the calculation of A_3. χ_1 was
obtained as a function of volume fraction polymer from published
results (15). Good agreement is observed between A_2 and A_3 in
Figure 2.

The ν_s/V dependency of A_1, A_2, and A_3 is explored in
Figure 3 which plots A_1, A_2 and A_3 against ν_s/V for all of the
networks prepared in bulk in this study with $\phi_o/R \gtrless 10$ and $\epsilon > 0.9$.
The open symbols refer to networks prepared using the narrow
molecular weight distribution α,ω-divinyl PDMS. At these high
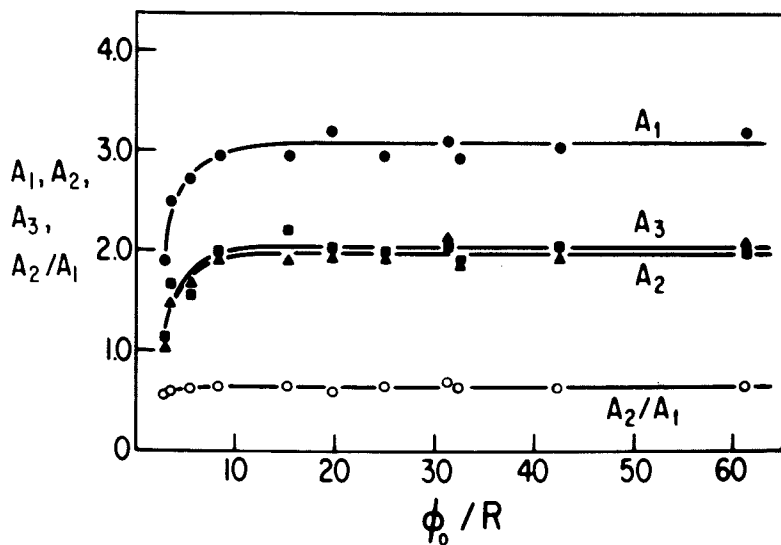
Figure 2. Dependence of the structure factors, A_1, A_2, and A_3. The ratio A_2/A_1 on network functionality for M_n is 21,600 networks (1).
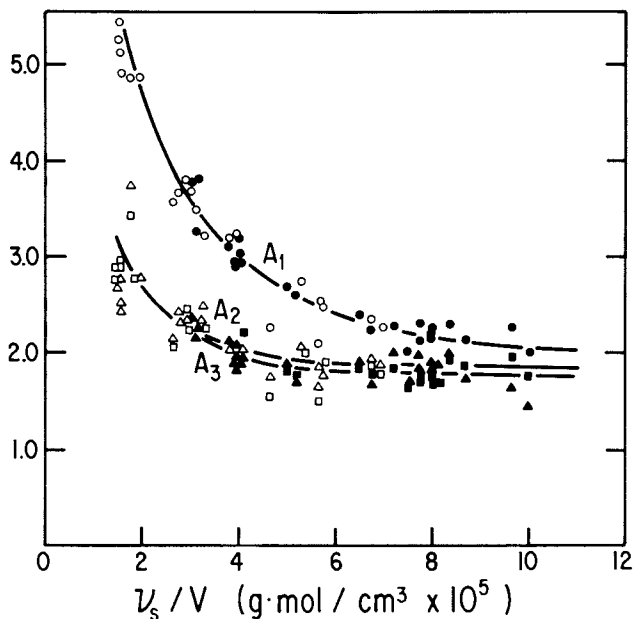
Figure 3. Dependence of the structure factors A_1, A_2, and A_3 on the stoichiometric network chain concentrations.

Key: ●, ▲, ■, networks formed using the commercial α,ω-divinyl PDMS; ○, △, □, networks formed using the narrow molecular weight distribution α,ω-divinyl PDMS; ε > 0.9 (1).

functionalities, the Flory theory would predict all three struc-
ture factors to have the asymptotic value of one and to be inde-
pendent of ν_s/V. The data in Figure 3 do not support these
predictions.

Excellent agreement between the value of ν_s/V calculated
from affine swelling theory (A_3) and ν_s/V calculated from $2C_1$
(A_2) is observed in Figure 3 for all of the high functionality
networks prepared in this study. Furthermore, good agreement is
observed in Figure 3 between the values of the structure factors
for networks formed using commercial α,ω-divinyl PDMS and
the values of the structure factors for networks formed using
the narrow molecular weight distribution α,ω-divinyl PDMS.
This suggests that network chain length distribution had negli-
gible effect on the equilibrium tensile behavior for the range
of M_w/M_n investigated in this study ($M_w/M_n = 1.1-2.5$).

The observed ν_s/V dependency of A_1 is predicted by the
Langley (12) - Graessley (13,16) small-strain theory. According
to equations (7) and (8) for $\phi_o/R > 10$:

$$A_1 = \frac{(2C_1 + 2C_2)V(V_o/V)^{2/3}}{\nu_s kT} \cong \frac{GV(V_o/V)^{2/3}}{\nu_s kT}$$

$$= 1 + \frac{T_e G_e^{max} V(V_o/V)^{2/3}}{\nu_s kT} \qquad (11)$$

Thus, the value of A_1 would be predicted to be everywhere great-
er than unity approaching it asymptotically as ν_s/V increases.
Furthermore, the value of A_1 should increase without limit as
ν_s/V is decreased. A better test of the Langley-Graessley
small-strain theory is to plot equation (7) as G/T_e vs $\nu_s kT/T_e V$
(Langley-Graessley plot). T_e of the high functionality networks
was taken to be ε^4(1-4). The small-strain data of all the
networks prepared and tested in bulk in this study, using PMHS
with $\phi_o > 10$ and $\varepsilon > 0.9$, are plotted in Figure 4. $2C_1 + 2C_2$ was
used to approximate the small-strain modulus. This approxima-
tion can lead to slightly higher G values due to curvature in
the Mooney-Rivlin plots at small extensions. However, from the
data this error appears to be less than 5%. The data were fit
by linear regression to a single line having a slope of 1.27 and
an intercept of 0.215 MPa.

The value of the intercept is in good agreement both with
the values of G^o_N reported in the literature for PDMS [0.24,
0.20, 0.299 MPa (2, 18, 19)] and the literature values of G_e^{max}
for tri- and tetrafunctional networks [0.21, 0.22 MPa (2)].
Since the networks were formed and tested in bulk, $V = \overline{V}_f \approx V_o$,
and a slope of one would be expected. Thus, both the slope and
the intercept are in good agreement with the predictions of equa-
tion (7). Moreover, the excellent fit of the eight different

network functionalities ($\phi > 10$) to a single line offers further
verification of the theory. Furthermore, both networks prepared
with the linear and the branched PMHS were well fit by the same
line.

Networks Formed in the Presence of Diluent, $\varepsilon > 0.9$. A series
of six networks were prepared both in bulk and in the presence
of oligomeric PDMS (M_n = 1170, no vinyl groups) using as junc-
tions a ϕ_0 = 43.9 linear PMHS and as chains α,ω-divinyl
PDMS ranging in M_n from 9,320 to 28,600 g·mol^{-1}. The volume
fraction of solvent present during network formation, v_{1s}, was
0.30 for all six networks and was calculated assuming simple
additivity of volumes. The tensile behavior of the networks
formed in bulk was measured in bulk, v_t = V_f/V = 1. The ten-
sile behavior of the networks formed in solution was measured
both on networks with solvent present (v_t = 1) and on networks
from which the oligomeric PDMS had been extracted (v_t = 1.47).

In Figure 5, the values of A_1 for the three sets of tensile
experiments are plotted against v_s/V_d (V_d = the volume of the
dried, extracted network). A_1 and A_2 were calculated under the
assumption V_0 = V_f (V_f = volume of the network at formation).
The values of A_1 for the three sets of experiments all display a
dependency on v_s/V_d and are well in excess of the limit of
unity predicted by the Flory theory (9). The presence of sol-
vent during network formation significantly decreases the
values of A_1. Removal of the solvent results in an increase
in the values of A_1. Yet, the values of A_1 for these deswollen
networks are still significantly less than those of the networks
prepared and tested in bulk.

In Figure 6, the small-strain data for the three sets of
tensile experiments are plotted as $(2C_1 + 2C_2)/T_e$ vs $v_s kT(V_d/V)$
$(V/V_f)^{2/3}/T_e V_d$ as suggested by the Langley-Graessley theory
[equation (7) with V_0 = V_f]. The small-strain data for the six
networks in each of the three sets of tensile experiments showed
a good fit to a straight line. The slopes and intercepts of the
three lines were determined by linear regression. The data for
the networks formed and tested in bulk have a slope of 1.10
and an intercept of 0.256 MPa. The data for the networks pre-
pared and tested in the presence of diluent have slope of 1.11
and an intercept of 0.119 MPa. The value of the intercept is ex-
tremely close to $(0.256)(0.68)^2$ = 0.118 MPa, calculated from
the value of G_e^{max} for the networks formed in bulk by assuming
a quadratic dependence of G_e^{max} on v_{2f} (= V_d/V_f = 0.68). Dossin
and Graessley (13) have observed a similar quadratic dependence
for polybutadiene networks. Furthermore, G_N^0 of linear polymers
in solution is known to have a quadratic dependence on the vol-
ume fraction of polymer in solution (11,20). The data for the
networks formed in solution but tested in the extracted de-
swollen state have a slope of 1.14 and an intercept of 0.166
MPa. This intercept is close to $(0.119)(1.47)$ = 0.175 MPa,
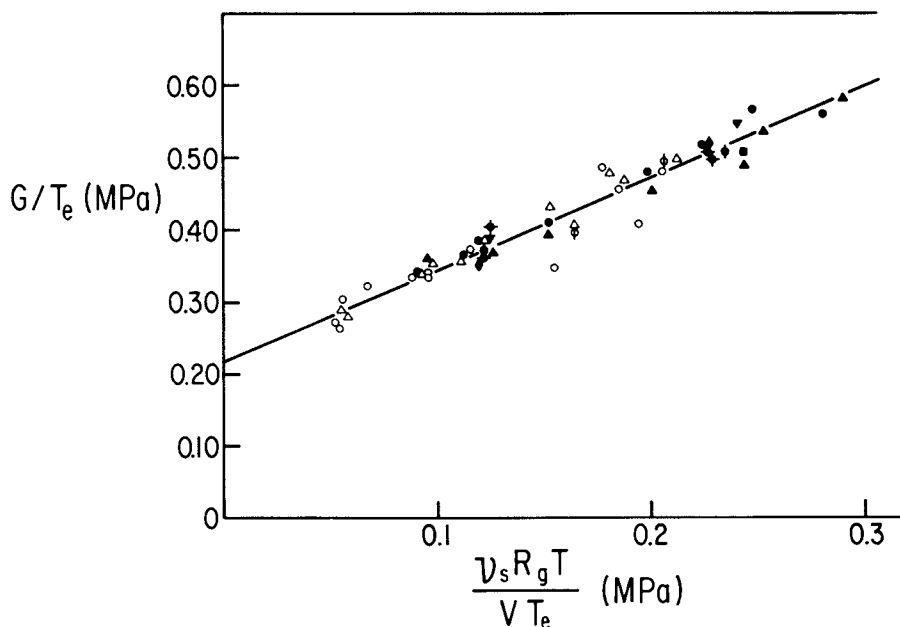
Figure 4.   Langley–Graessley plot for networks with $\phi_o > 10$.

Key: ●, ▲, ■, *commercial* α,ω-*divinyl PDMS networks;* ○, △, □, *narrow molecular weight distribution* α,ω-*divinyl PDMS networks. Functionality* (ϕ_o); ■, *10.58;* ♦, *21.5 L;* ●, *23.8 B;* —●—, *33.0 L;* ▼, *38.1 B;* ▲, *43.9 L;* ◆, *58.4 L;* —●—, *83.6 L;* R_g is gas constant, $\varepsilon > 0.9$ (1).
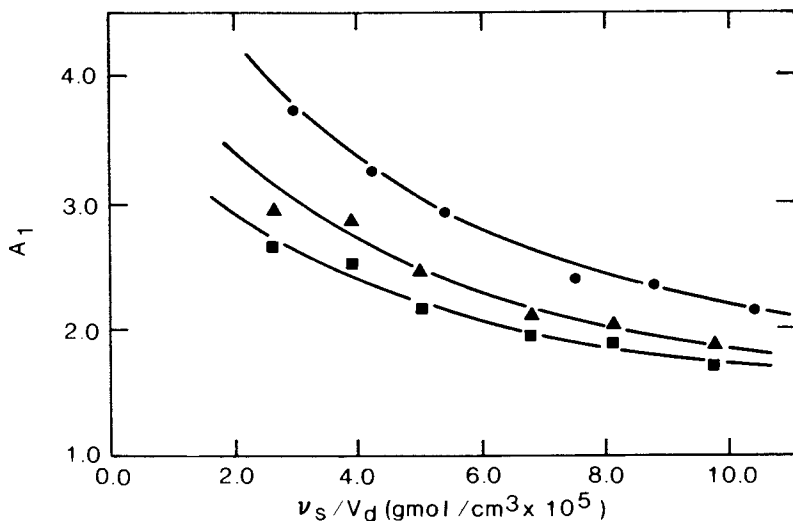
Figure 5.   Dependence of A_1 on v_s/V_d for networks formed and tested in bulk. Conditions: ●, *formed and tested in solution;* ■, *formed in solution but tested in extracted deswollen state;* ▲, $\phi_o = 43.9L$.

calculated from G_e^{max} for the networks formed in solvent by assuming a linear dependence on v_t (= V_f/V = 1.47). Furthermore, the intercept is almost identical to (0.119) $(1.47)^{5/6}$ = 0.164 MPa obtained assuming a 5/6 power dependence on v_t.

The behavior of the small-strain data in the three sets of experiments suggests a more universal format for the small-strain theory of Langley (12) and Graessley (13,16):

$$G = v_s kT(V/V_o)^{2/3}/V + T_e v_{2f}^2 v_t^{5/6}(G_e^{max})^o \qquad (12)$$

wherein a 5/6 power dependence on v_t has been assumed and $(G_e^{max})^o$ is the absolute maximum entanglement contribution to the small-strain modulus. This maximum would be obtained for a network formed and tested in bulk and in which all entanglements had been trapped ($v_{2f} = v_t = T_e = 1$). Equation (12) considers the effects of solvent present during network formation and testing, as well as, the effect the removal of this solvent has on the small-strain modulus.

In Figure 7, the small-strain data plotted in Figure 6 are replotted as suggested by equation (12): $(2C_1 + 2C_2)$ $(V_f/V_d)^2$ $(V/V_f)^{5/6}/T_e$ vs $v_s kT(V_f/V_d)(V/V_f)^{1/2}/T_e V_d$. The data for the three series of tensile experiments displays an excellent fit to a single line. The slope of this line was determined by linear regression to be 1.05 and the intercept, $(G_e^{max})^o$, was determined to be 0.272 MPa.

The large-strain structure factor A_2 is plotted for these networks vs v_s/V_d in Figure 8. The values of A_2 for the three series of tensile experiments all display a dependency on v_s/V_d and are well in excess of unity. The presence of solvent during network formation significantly decreases the value of A_2. Deswelling of these networks results in a further decrease in A_2. The values of A_2 in Figure 8 are considerably less than the corresponding values of A_1 in Figure 5. If the magnitudes of these structure factors in excess of unity are attributed to trapped entanglements, then it would appear that the entanglement contribution to the stress is strain-dependent and decreases with increasing elongation.

Networks Formed in Bulk, $0.4 < \varepsilon < 0.95$. A series of high functionality networks were prepared in bulk using ϕ_o = 43.9 linear PMHS and five different α,ω-divinyl PDMS ranging in M_n from 9,320 to 28,100 g/mol. The extent of reaction of the terminal vinyl groups, ε, was varied in these networks from 0.4 to 0.95 by varying the ratio of Si-H/Si-Vinyl utilized during network formation. Figure 9 is a plot of the Mooney-Rivlin constants, $2C_1$ and $2C_2$, as functions of ε for networks formed from a M_n = 21,600 α,ω-divinyl PDMS. This plot is typical for each molecular weight used (3). As can be seen, both $2C_1$ and $2C_2$ decrease with decreasing ε. For networks of $\phi > 20$, the Flory theory (9) would predict $2C_1 = v_s kT(V/V_o)^{2/3}/V$. Since
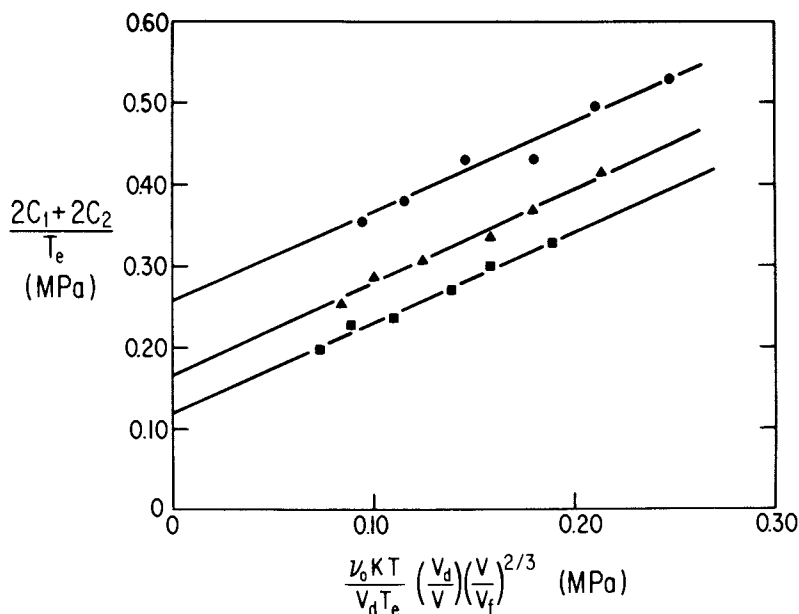
Figure 6.   Langley–Graessley plots for networks formed and tested in bulk. Conditions: ●, *formed and tested in solution, 1.10 slope;* ■, *formed in solution, tested in extracted, deswollen state, 1.14 slope;* ▲, *[φₒ = 43.9L] 1.11 slope.*
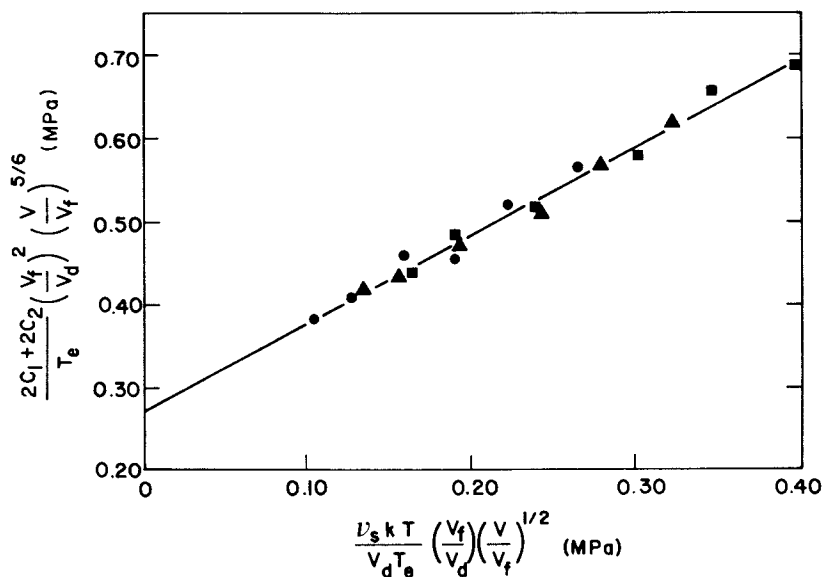
Figure 7.   Modified Langley–Graessley plot for networks formed and tested in bulk. Conditions: ●, *formed and tested in solution;* ■, *formed in solution, tested in extracted, deswollen state;* ▲, *[φₒ = 43.9L].*
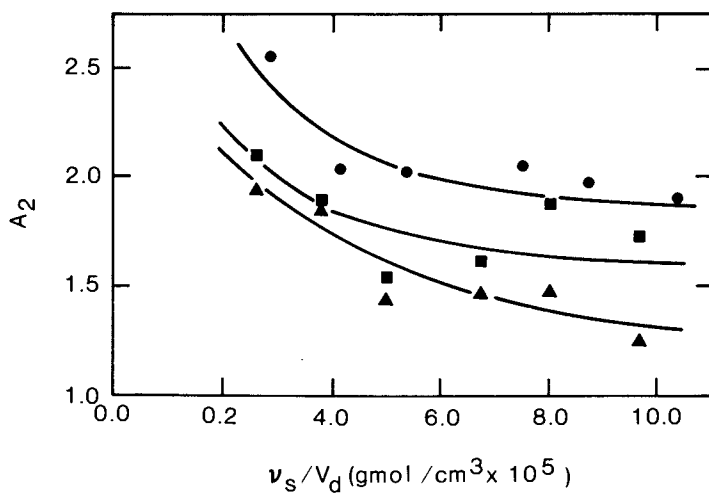
Figure 8.   Dependence of A_2 on v_s/V_d for networks formed and tested in bulk. Conditions: ●, formed and tested in solution; ■, formed in solution, tested in extracted, deswollen state; ▲, [$\phi_0 = 43.9L$].
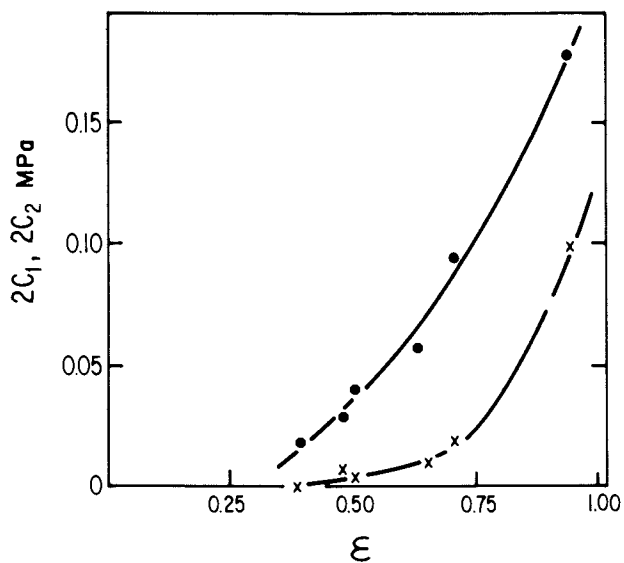
Figure 9.   Dependence of the Mooney–Rivlin constant on extent of cross-linking. M_n is 21,600 PDMS. Key: ●, $2C_1$; ✕, $2C_2$ (3).

ν_s/V is proportional to ε^2 for these high functionality net-works, the observed behavior in $2C_1$ is in qualitative agreement with the Flory theory.

The magnitudes of $2C_1$ and $2C_2$ in Figure 9, however, are in discord with the Flory theory. The theory predicts that for the high functionality networks represented in Figure 9, $2C_2$ should be immeasurably different from zero. The magnitude of the small and large-strain moduli are evaluated in terms of the structure factors A_1 and A_2 in Figure 10. Both A_1 and A_2 are everywhere greater than the Flory theory's predicted value of unity, ap-proaching it asymptotically only as $\varepsilon \to 0$. The ratio $A_2/A_1 = 2C_1/(2C_1 + 2C_2)$ and the equilibrium swelling structure factor, A_3, are also plotted in Figure 10. As before, good agreement is observed between A_2 and A_3.

In Figures 3, 5, and 8, the three structure factors for net-works with $\varepsilon > 0.9$ displayed a regular decreasing tendency with ν_s/V. This phenomenon is extended in Figure 11 in which the dependence of A_1 on chain density is indicated for five differ-ent levels of crosslinking. In each case, A_1 decreases asymp-totically as ν_s/V increases (M_n decreases), approaching unity only for small conversions or for large values of ν_s/V. Further-more, the rate of convergence to the asymptote increases dramat-ically as ε decreases. The observed trends in A_1 with ν_s/V and ε are in excellent qualitative agreement with the Langley-Graessley small-strain theory [equation (11)]. According to this theory for $\phi > 10$, A_1 should be everywhere greater than unity approaching it as an asymptote as ε decreases or ν_s/V increases (M_n decreases)[Note that in equation (11) $T_e \sim \varepsilon^4$ and $\nu_s/V \sim \rho \varepsilon^2/M_n$]. Furthermore, A_1 is predicted by this theory to increase without limit as ν_s/V goes to zero.

The small-strain data of Figure 11 are replotted as a Langley-Graessley plot in Figure 12 according to equation (12). G is approximated by $2C_1 + 2C_2$; T_e for these high func-tionality networks is taken to be $\varepsilon^4 (\underline{1,3,4})$. The data were fit by linear regression to a single line of slope 1.17 and intercept 0.236 MPa. For $\phi > 10$, the predicted slope is unity. The intercept of Figure 12 is predicted by the small-strain theory to be equal to $(G_e^{max})^o$. The experimental value of 0.236 MPa is in good agreement with the previously reported values of G_e^{max} for tri-, tetra- and multifunctional PDMS net-works as well as the literature values of G_N^o for linear PDMS. The degree of agreement between the predictions of the Langley-Graessley entanglement theory and the data reported here and the excellence of the fit of the networks with such a wide range of ε to a single line offer significant evidence favoring a con-tribution in small strain by trapped entanglements.

Data Interpretation. Often the same stress-strain data is utilized by two different research groups as evidence to both support and deny the existence of a trapped entanglement contri-
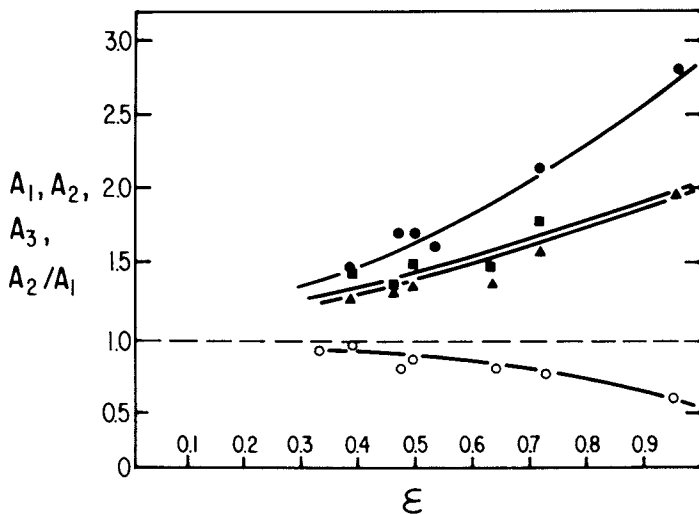
Figure 10.   Dependence of A_1, A_2, A_3, and A_2/A_1 on extent of cross-linking. M_n is 21,600 PDMS. Key: ●, A_1; ■, A_2; ▲, A_3; ○, A_2/A_1 (3).
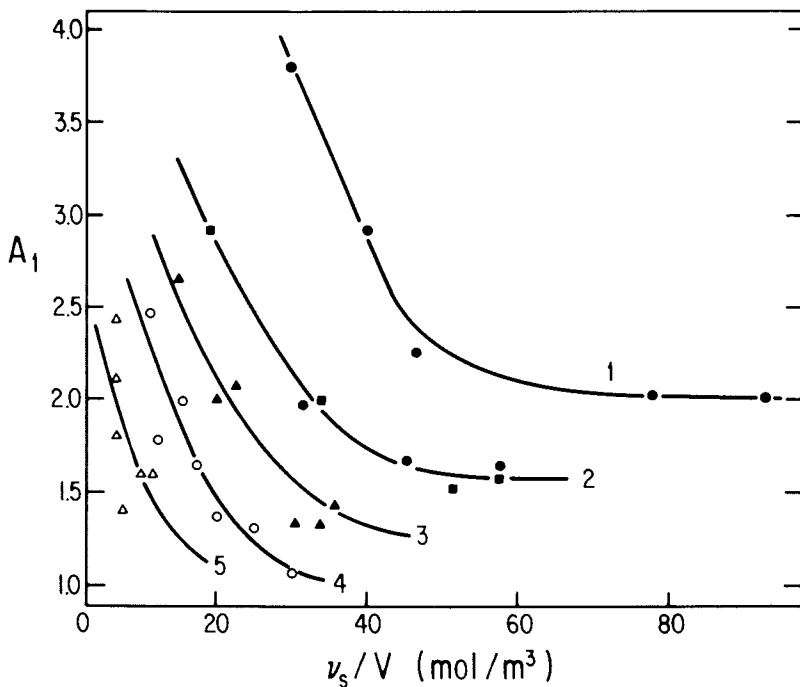
Figure 11.   Dependence of A_1 on network chain density of end-linked elastomers, $0.4 < \epsilon < 0.95$ (3). Key: 1, $\epsilon > 0.9$; 2, $0.7 < \epsilon < 0.8$; 3, $0.6 < \epsilon < 0.7$; 4, $0.5 < \epsilon < 0.6$; 5, $\epsilon > 0.5$.
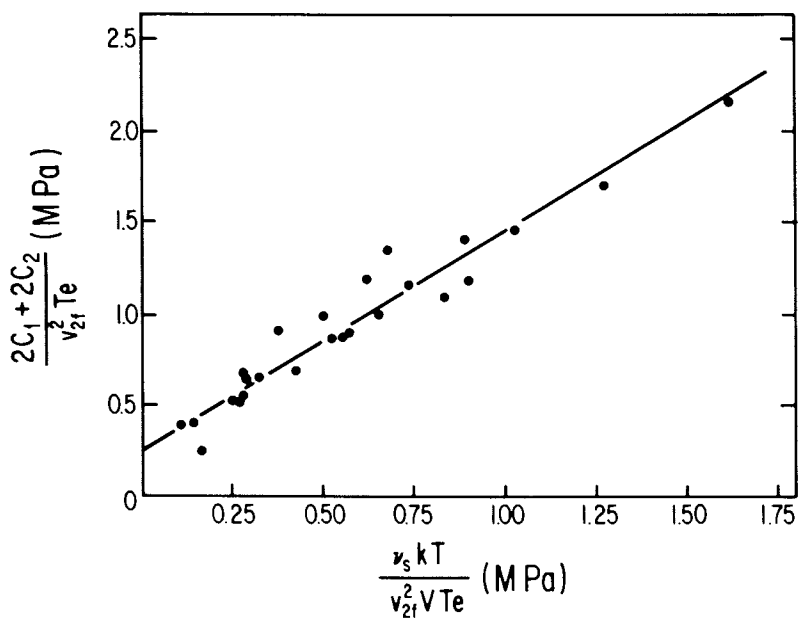
Figure 12.   Langley–Graessley plot for end-linked elastomers, 0.4 < ε < 0.95 (3).

bution to the modulus. The source of these contradictory con-
clusions is often found in the method of data interpretation.
For example, the Langley—Graessley theory applies only in the
limits of small strain, yet, the large-strain modulus, $2C_1$ is
often utilized to evaluate the entanglement contribution to the
modulus. As indicated earlier there is considerable experimental
evidence (1-4, 13, 16, 17) indicating that the entanglement con-
tribution to the stress is strain-dependent, decreases with in-
creasing elongation, and may disappear entirely at large elon-
gations. Therefore, the use of experimental moduli extrapolated
to the limit $\alpha^{-1} \to 0$ (phantom behavior) could lead to the
erroneous conclusion that entanglements do not contribute to the
modulus at small to moderate strains.

       An additional error often made in the evaluation of the en-
tanglement contribution to the modulus is the tacit assumption
that the endlinking reaction goes to completion. As indicated in
equation (12), the entanglement contribution to the small-strain
modulus, G_e, is dependent on $\varepsilon^4(T_e)$ and the chemical contribu-
tion, G_c, is dependent on $\varepsilon^2(\nu_s/V)$. Even for networks with
$\varepsilon = 0.95$, G_e will be decreased by 20% and G_c by 10% below the
corresponding values for a completely reacted network. Thus the
use of this $\varepsilon = 0.95$ network to evaluate equation (12) under the
assumption of complete reaction, will lead to a serious under-
estimation of G_e^{max}. Indeed for networks with ε much below 0.90,
analysis of the small-strain data using equation (12) and the
assumption of complete endlinking reaction, would lead to the
erroneous conclusion that $G_e^{max} \approx 0$ for PDMS networks. Further-
more, the assumption of complete reaction for networks in which
ε is actually less than one will result in the calculation of
structure factors which are significantly less than those that
would be obtained if the endlinking reaction had indeed gone to
completion.

       Verification of an entanglement contribution to the modulus
is also complicated by the relatively low values of G_N^o observed
for many linear "rubbery" polymers. Thus, except for networks
with relatively high M_c, the ratio of G_e/G is small. For an $\varepsilon =
0.95$ PDMS high functionality network with $\nu_s/V = 2 \times 10^{-4}$ gmol
cm^{-3} ($M_c = 5000$), from equation (12), $G_e/G = 0.28$. Decreasing M_c
or ε, will decrease this ratio. The presence of diluent, either
during network formation or tensile testing, will also decrease
the ratio G_e/G. For example, if the above network was formed in
the presence of diluent with $\nu_{2f} = 0.75$, then according to equa-
tion (12) $G_e/G = 0.18$. Therefore, in general, it would appear
entanglements do make a strain-dependent contribution to the
modulus, however, under many experimental conditions ($\varepsilon, \nu_t, \nu_{2f} < 1$)
this contribution may be minimal.

Conclusions

       The stress-strain behavior of the high functionality net-

works prepared in this study differ from the predictions of the
Flory theory of rubber elasticity. However, the small-strain
theory of Langley and Graessley gave good agreement with the
data over a wide range in $\epsilon, \phi, \nu_s/V, \nu_t$, and ν_{2f}. The
magnitude of A_2 and its dependence on ν_t and ν_{2f} strongly
suggest a strain-dependent entanglement contribution to the
large strain modulus as well. Therefore, a reconsideration of
the Flory theory accounting for the direct strain-dependent con-
tribution of trapped entanglements to the stress over the entire
range of strain is recommended.

Acknowledgment

References

1.   Meyers, K. O.; Bye, M.; Merrill, E. W. <u>Macromolecules</u>,
      1980 <u>13</u>, 1045 .
2.   Gottlieb, M.; Macosko, C. W.; Benjamin, G. S.; Meyers,
      K. O.; Merrill, E. W. <u>Macromolecules</u>, 1981, <u>14</u>, 1039.
3.   Kirk, K. A.; Bidstrup, S. A.; Merrill, E. W.; Meyers,
      K. O. <u>Macromolecules</u> 1982, <u>15</u>, 000.
4.   Meyers, K. O. Ph.D.,Thesis, Massachusetts Institute of
      Technology, Cambridge, Massachusetts, 1980.
5.   Oppermann, W. Ph.D.,Thesis, Technical University of
      Clausthal, FRG. 1979.
6.   Mooney, M. <u>J. Appl. Phys.</u> 1948 <u>19</u>, 434; Rivlin, R. S.
      <u>Philos. Trans. R. Soc. London, Ser.</u> A 1948, <u>241</u>, 379.
7.   Flory, P. J. "Principles of Polymer Chemistry,";
      Cornell University Press: Ithaca, N. Y., 1953.
8.   James, H. M.; Guth, E. <u>J. Polym. Sci.</u> 1948, <u>4</u>, 153.
9.   Flory, P. J. <u>J. Chem. Phys.</u>, 1977, <u>66</u>, 5720.
10. Ronca, G.; Allegra, G. <u>J. Chem. Phys.</u> 1977, <u>63</u>, 4490.
11. Ferry, J. D. "Viscoelastic Properties of Polymers";
      Wiley: New York, 1979.
12. Langley, N. R. <u>Macromolecules</u>. 1968, <u>1</u>, 348.
13. Dossin, L. M.; Graessley, W. W. <u>Macromolecules</u> 1979,
      <u>12</u>, 123.
14. Miller, D. R.; Macosko, C. W. <u>Macromolecules</u> 1976, <u>9</u>,
      206.
15. Flory, P. J.,; Tatara, Y. <u>J. Polym. Sci.</u> 1975, <u>13</u>,
      683.
16. Pearson, D. S.; Graessley, W. W. <u>Macromolecules</u>,
      1980, <u>13</u>, 1001
17. Ferry, J. D.; Kan, H. <u>Rubber Chem. Technol.</u> 1978, <u>51</u>,
      731.

18. Plazek, D. J.; Dannhauser, W.; Ferry, J. D. J. Colloid
     Sci. 1961, 16, 101.
19. Langley, N. R.; Ferry, J. D. Macromolecules, 1968,
     1, 353.
20. Graessley, W. W. Adv. Polym. Sci. 1974, 16, 1.

RECEIVED November 16, 1981.

Bimodal Elastomeric Networks

J. E. MARK

The University of Cincinnati, Department of Chemistry and Polymer Research Center, Cincinnati, OH 45221

Elastomeric networks may be prepared by end-
linking mixtures of very short and relatively long
polymer chains, for example, hydroxyl-terminated
polydimethylsiloxane chains. Such networks (in the
unfilled state) frequently show marked increases in
modulus at very high elongations. Experimental
results are cited to show how this unusual behavior
depends on composition, chain length, spatial het-
erogeneity, junction functionality, temperature,
and swelling. It is concluded that the observed
increases in modulus are due to the limited exten-
sibility of the network chains. These elastomers
may therefore be used to study limited chain
extensibility and to evaluate non-Gaussian theories
of rubberlike elasticity. Another, more practical
application is the achievement of ultimate prop-
erties significantly better than those of networks
having the usual unimodal distribution of chain
lengths.

There are now a number of techniques which may be used to
prepare elastomeric networks of known structure (1-8). Two par-
ticularly useful and convenient ones involve the multi-functional
end-linking of hydroxyl-terminated (4-16) or vinyl-terminated
polydimethylsiloxane (PDMS) chains (3,17-21), and the cross-
linking of PDMS chains through vinyl side groups present in known
amounts and in known locations along the chains (4,18,22-25). A
typical reaction of this type is
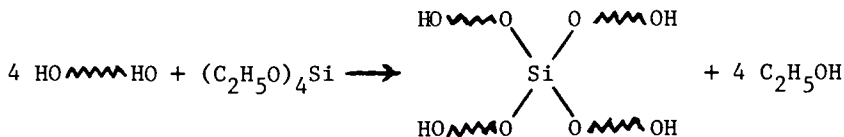
$$4 \ HO\text{\textasciitilde}\text{\textasciitilde}\text{\textasciitilde}HO + (C_2H_5O)_4Si \longrightarrow \begin{array}{c} HO\text{\textasciitilde}\text{\textasciitilde}O \quad O\text{\textasciitilde}\text{\textasciitilde}OH \\ \backslash \quad / \\ Si \\ / \quad \backslash \\ HO\text{\textasciitilde}\text{\textasciitilde}O \quad O\text{\textasciitilde}\text{\textasciitilde}OH \end{array} + 4 \ C_2H_5OH$$

in which HO〰OH represents a hydroxyl-terminated PDMS chain.
Characterizing the uncross-linked chains with respect to molec-
ular weight and molecular weight distribution and then running
the specified reaction to completion gives networks having
known values of the cross-link functionality ϕ and average chain
length, and detailed information on the chain length distribution
as well. Similar reactions have been carried out using hydroxyl-
terminated chains of poly(ethylene oxide)(26), poly(tetramethy-
lene oxide)(26), poly(caprolactone)(27), and poly(propylene
oxide)(28), and a triisocyanate end-linking agent. A related
reaction involving the end-linking of vinyl-terminated PDMS
chains with a multifunctional silane is somewhat more versatile
in that a wider range of values of cross-link functionality may
be achieved. Because of their known structures, such "model"
networks have been extremely useful for the elucidation of mol-
ecular aspects of rubberlike elasticity.
     In several of these studies (12-16,20), bimodal PDMS net-
works were prepared by end-linking mixtures of very short and
relatively long chains, as is illustrated in Figure 1. These
networks, in the unfilled state, were found to be unusually tough
elastomers. Of particular interest is the fact that they have
values of the modulus [f*] which increase very substantially at
high elongations, thus giving unusually large values of the ul-
timate strength. This is rather surprising since usually an
elastomer will have good ultimate properties only when rein-
forced with some mineral filler (or hard, glassy domains in the
case of a multi-phase polymer), or when it can generate its own
reinforcement through strain-induced crystallization (29-32).
Part of these increases in modulus and ultimate strength are due
to the low incidence of dangling-chain irregularities in such
model networks in general (19). Another contribution could be
non-Gaussian effects arising from limited chain extensibility
(12-16,20). It is not known, however, whether these are the
only effects occurring at very low temperatures. Such networks
could also, for example, undergo strain-induced crystallization,
with consequent improvements in ultimate properties from cry-
stallite reinforcement (29-32). PDMS has a very low melting
point (-40°C) (33) and, although elongation significantly raises
it (34,35), unfilled networks of this polymer are thought to re-
main amorphous well below room temperature (35,36,37). Unusually
low temperatures must therefore be employed in any search for
strain-induced crystallization. There are very few relevant data
in the literature and, of course, no relevant results whatever
are available for the new types of networks with the very pecul-
iar distributions of interest here. This question of possible
strain-induced crystallization and the associated network rein-
forcement assumes particular importance because of the very
unusual and attractive properties of these materials.
     A definitive answer to these questions is obtained in this
review by analysis of how the relevant elastomeric properties
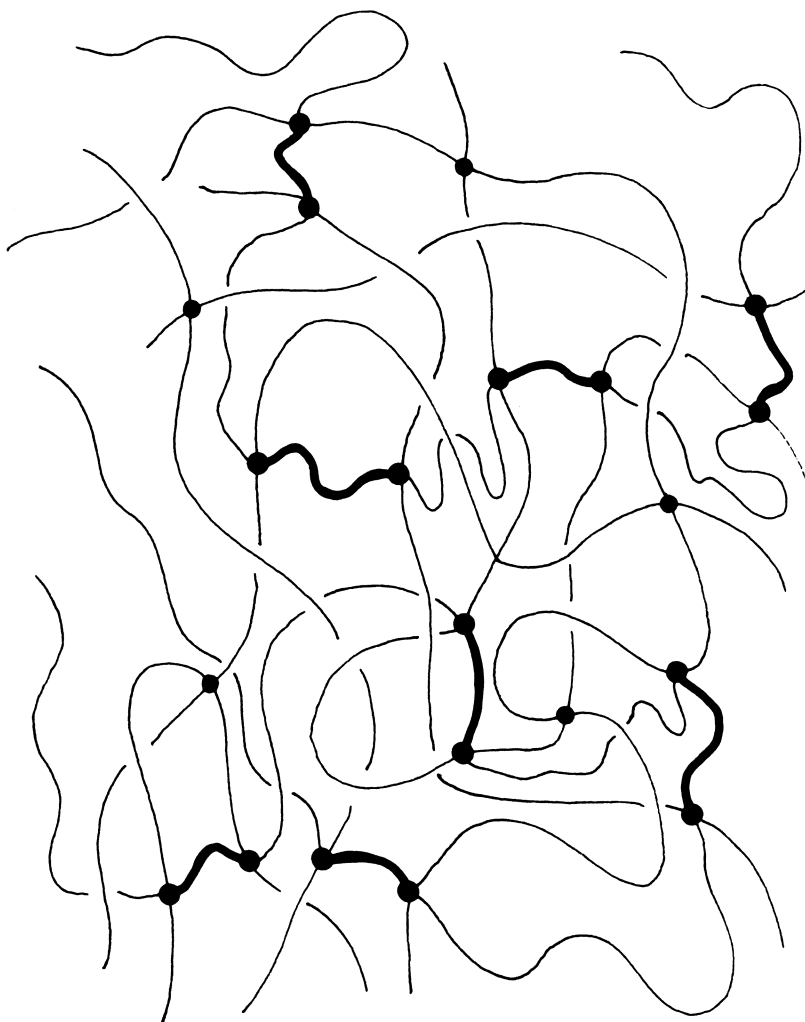
Figure 1. Sketch of a portion of a bimodal network. The very short polymer chains are represented by heavy lines and the relatively long chains by thinner lines.

depend on composition, chain length, spatial heterogeneity,
junction functionality, temperature, and swelling. The result-
ing molecular interpretation of these unusual properties of bi-
modal networks permits the utilization of these elastomers in a
variety of applications, a number of which are discussed in
some detail.

Representations of the Network Moduli in Elongation

The most convenient measure of the stress exhibited by an
elongated elastomeric network is the nominal or engineering
stress $f^* = f/A^*$, where f is the equilibrium value of the force
and A^* is the cross-sectional area of the undeformed sample.
The strain is given by the relative length or elongation
$\alpha = L/L_i$ where L and L_i are the lengths of the sample in the
deformed and undeformed states, respectively. Dividing the
stress f/A^* by the strain function $(\alpha - \alpha^{-2})$ indicated in the
simplest molecular theories of rubberlike elasticity (38,39) then
gives the elastic modulus or reduced stress (38-42)

$$[f^*] \equiv f/[A^*(\alpha - \alpha^{-2})] \tag{1}$$

For rubberlike materials, the modulus thus defined generally
shows an additional dependence on elongation (39,40,42), appar-
ently because of increase in the non-affineness of the deforma-
tion as the elongation increases (43,44). This dependence is
frequently represented (approximately) by the semiempirical
equation of Mooney and Rivlin

$$[f^*] = 2C_1 + 2C_2\alpha^{-1} \tag{2}$$

in which $2C_1$ and $2C_2$ are constants independent of α (39,40,42,
45,46). Thus, the value of the modulus is $2C_1$ in the limit at
large deformation ($\alpha^{-1} \to 0$), and $2C_1 + 2C_2$ in the limit at small
deformation ($\alpha^{-1} \to 1$).

Dependence of Properties on Network Structure and Experimental

Variables

Composition. Some representative isotherms for (unfilled)
bimodal networks prepared from very short and relatively long
hydroxyl-terminated PDMS chains mixed in various proportions are
shown in Figure 2(15). In this and in some of the subsequent
Figures, the modulus is plotted against reciprocal elongation,
as suggested by Equation (2). The bimodal networks are seen to
have very good (maximum) extensibility for these relatively high
values of the modulus $[f^*]$. Furthermore, the networks contain-
ing a large mol % of the short chains show a marked increase in
[f*] at high elongations, which corresponds to a significant

increase in ultimate strength. It is the nature of this increase
and its molecular origin which are the main subjects of the
investigations described in this review. The results presented
in Figure 2 portray the dependence of this effect on network
composition. Specifically, increase in the number of short
chains in the networks gives a more pronounced increase in $[f^*]$,
thus underscoring the importance of the short-chain component in
this regard.

Chain Length. If it is the short chains which give the
improvements in ultimate properties, decrease in their average
length should give even more pronounced upturns in $[f^*]$ at high
elongations. This is indeed found to be the case, as is illus-
trated in Figure 3(15). These stress-strain isotherms are for
PDMS networks similar to those described in Figure 2 but with
short chains having M_n = 220 rather than 660 g mol^{-1}.

Spatial Heterogeneity. Some insight into the mechanism
through which the short chains operate may be obtained using
bimodal networks which are made spatially as well as composition-
ally heterogeneous in a two-state reaction in which some of the
very short chains are prereacted so as to form clusters or do-
mains of high cross-link density. If the increases in $[f^*]$ were
due to some intermolecular organization such as a "filler" effect
(47-50) or strain-induced crystallization (29-32,37), then seg-
regating the short chains should enhance the modulus. Such
networks have been prepared using short chains having values of
M_n of either 1,100 (14) or 220 g mol^{-1} (51), and have been
studied with regard to their values of the high elongation mod-
ulus $2C_1$ and the modulus $[f^*]$ at rupture. The values of $2C_1$
and $[f^*]_r$ for the 1,100-18,500 PDMS networks are shown as a func-
tion of the extent of prereaction X_p in Figure 4(14). In both
cases, increase in X_p appears to give a small initial increase
in these two quantities; unfortunately, the increases are very
small and in fact are within the usual error limits in these
types of measurements. Thus, there does not appear to be any
significant reinforcing effect brought about by the clustering
of the very short chains in the spatially inhomogeneous cross-
linking process. This suggests that the increases in $[f^*]$ are
primarily intramolecular rather than intermolecular.

Junction Functionality. Some results bearing on the possi-
ble effect of cross-link functionality on the upturn in modulus
are shown in Figure 5(20). The magnitude of the increase in
$[f^*]$ does not show any obvious correlation with ϕ, which again
suggests the predominant importance of the intramolecular char-
acteristics of the short chains. At least from the evidence at
hand (20), the functionality of the junction points seems rela-
tively unimportant in this regard.

Temperature. The effect of temperature on the stress-strain
isotherms is of particular importance with regard to the
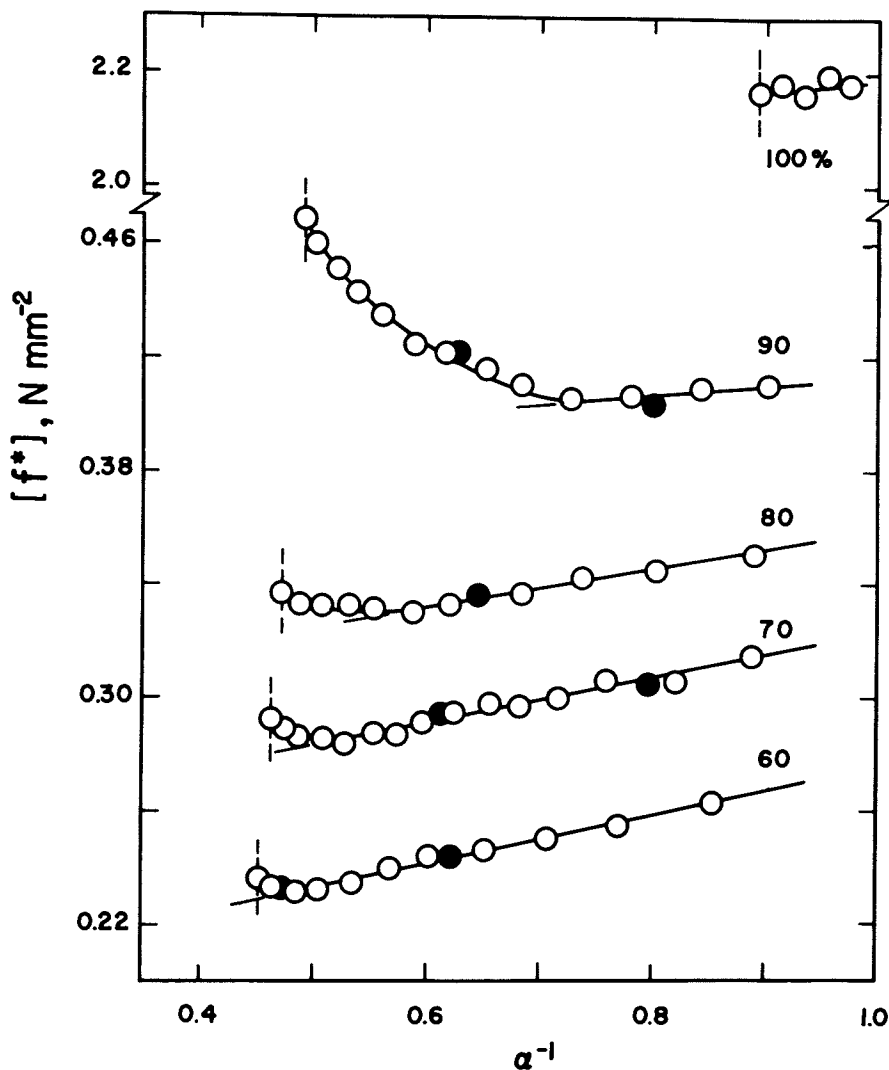
Figure 2.   Typical stress–strain isotherms for PDMS networks prepared by tetra-functionally end-linking very short and relatively long chains.

Number-average molecular weights are $M_n = 660$ and $18,500$ g/mol, respectively (15). Measurements were carried out on the unswollen networks, in elongation at $25°C$. Data plotted as suggested by Mooney–Rivlin representation of reduced stress or modulus (Eq. 2). Short extensions of the linear portions of the isotherms locate the values of α at which upturn in $[f^*]$ first becomes discernible. Linear portions of the isotherms were located by least-squares analysis. Each curve is labelled with mol percent of short chains in network structure. Vertical dotted lines indicate rupture points. Key: $\bigcirc$, results obtained using a series of increasing values of elongation; $\bullet$, results obtained out of sequence to test for reversibility.
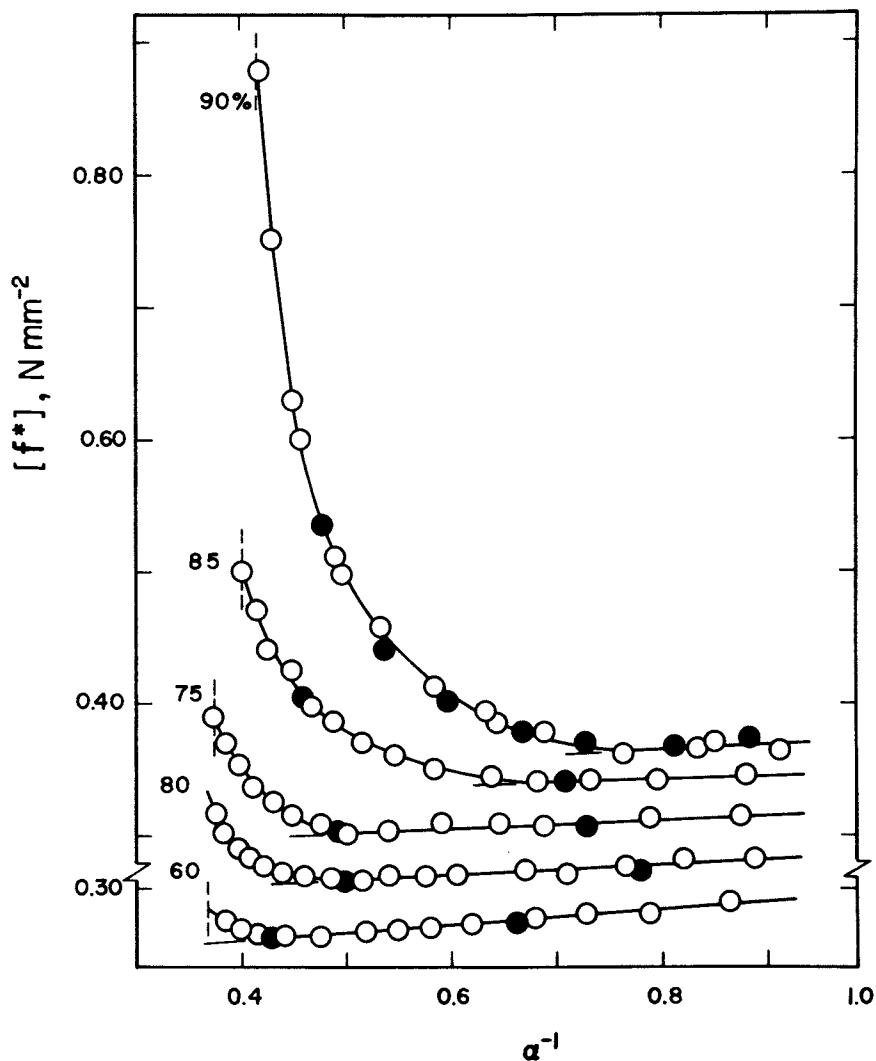
Figure 3.   Results for PDMS networks similar to those described in Figure 2, but with the short chains having $M_n = 220$ *g/mol (15). Lower part of the ordinate refers only to lowest isotherm in the series. See key to Fig. 2.*
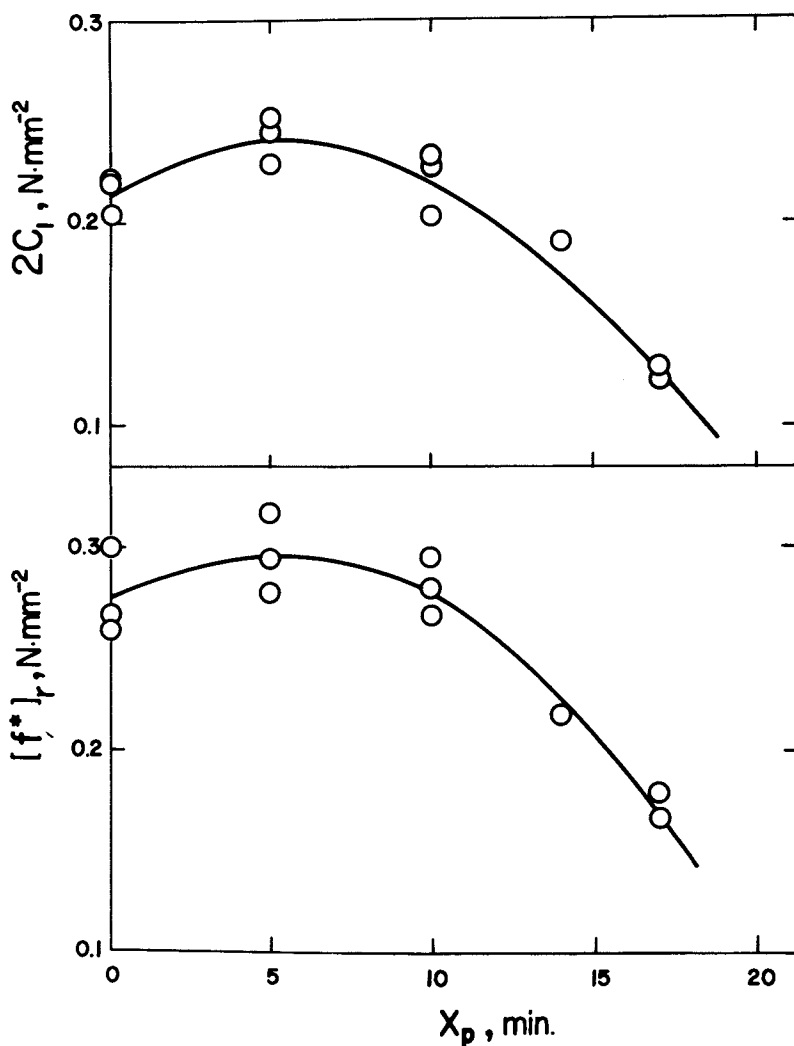
Figure 4.   The elastic properties of some bimodal PDMS networks.   Short chains were segregated by pre-reacting them with a limited amount of (tetrafunctional) end-linking agent (14).

Short and long chains had M_n = 1,100 and 18,500 g/mol, respectively.   Composition was 82 mol % short chains.   High deformation modulus $2C_1$, and ultimate strength as measured by the modulus $[f*]_r$ at rupture, are shown as a function of the extent of pre-reaction.
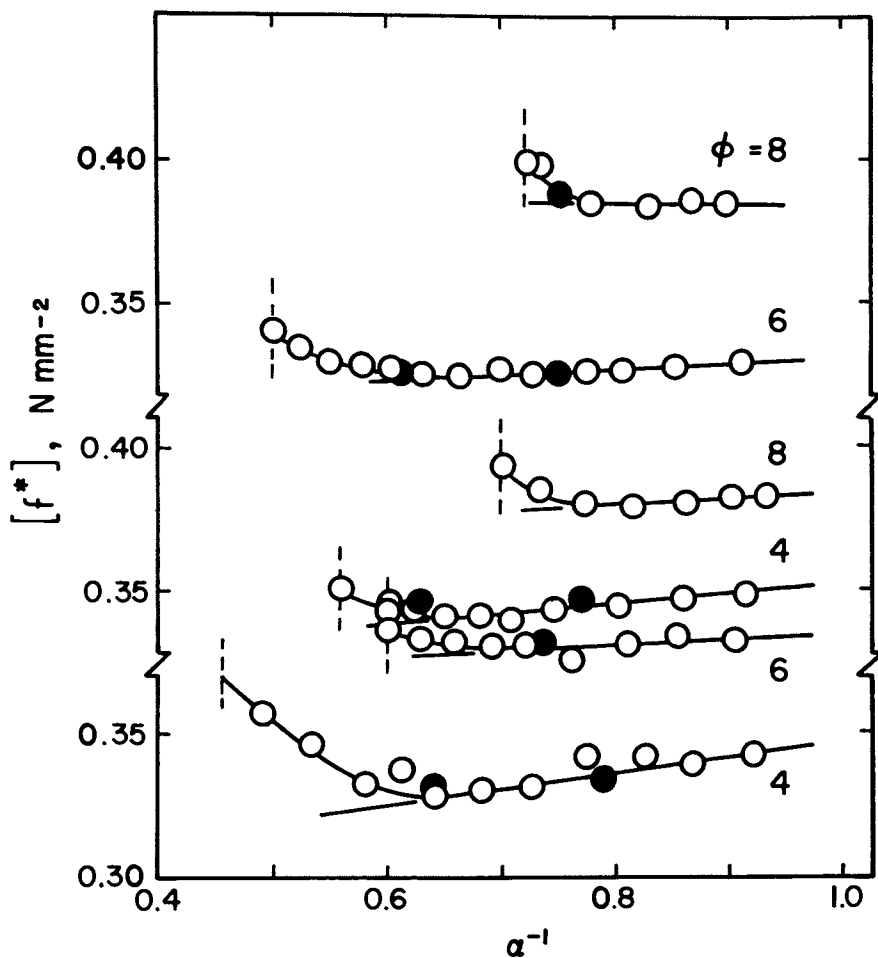
Figure 5. Stress–strain isotherms obtained for bimodal (600–11,300), PDMS networks containing 75.2 mol % short chains (20).

Chains were vinyl-terminated, and end-linked using a silane having values of the functionality φ.

possibility of strain-induced crystallization in the networks.
Typical results of this type are shown in Figure 6(16). Of
particular interest here are the temperature dependence of the
elongation α_u at which the upturn in $[f^*]$ becomes discernible,
of the elongation α_r at which rupture occurs, and of the total
increase $\Delta[f^*]_r$ in modulus up to the rupture point. If the in-
crease in $[f^*]$ had been due to strain-induced crystallization,
α_u would have decreased with decrease in temperature, and α_r and
$\Delta[f^*]_r$ would have increased. These qualities are seen to be
relatively insensitive to temperature, which confirms the con-
clusion that the anomalous behaviour is not due to strain-
induced crystallization.

Also relevant here are some force-temperature ("thermoelas-
tic") results obtained at elongations sufficiently large to give
large increases in $[f^*]$ in the stress-strain isotherm (16).
Such curves, illustrated in Figure 7, show no deviations from
linearity which could be attributed to strain-induced crystal-
lization. Similarly, birefringence-temperature measurements
also carried out at $\alpha > \alpha_u$ show no deviations from linearity
that could be attributed to crystallization, or to other inter-
molecular orderings of the network chains. Typical results of
this type are shown in Figure 8 (16).

Swelling. Work in progress (52) indicates that the upturns
in $[f^*]$ for PDMS bimodal networks are not decreased by swelling,
which would have diminished any strain-induced crystallization
(36,37).

All of the above evidence indicates that the increase in
modulus and improvements in ultimate properties are due to
intramolecular effects, specifically to non-Gaussian effects
arising from limited chain extensibility. A network chain near
its maximum extensibility can no longer increase its end-to-end
separation by configurational changes, i.e., by simple rotations
about its skeletal bonds. Deformations of bond angles (and
possibly even bond lengths) would be required, and the energies
for these processes are much greater than those for configura-
tional changes. This is presumably the origin of the very
marked increases in the modulus at high elongations and the much
improved ultimate properties.

Some Applications

Characterization of Limited Chain Extensibility. The mol-
ecular origin of the unusual properties of bimodal PDMS networks
having been elucidated at least to some extent, it is now possi-
ble to utilize these materials in a variety of applications. The
first involves the interpretation of limited chain extensibility
in terms of the configurational characteristics of the PDMS
chains making up the network structure (5,12,13).
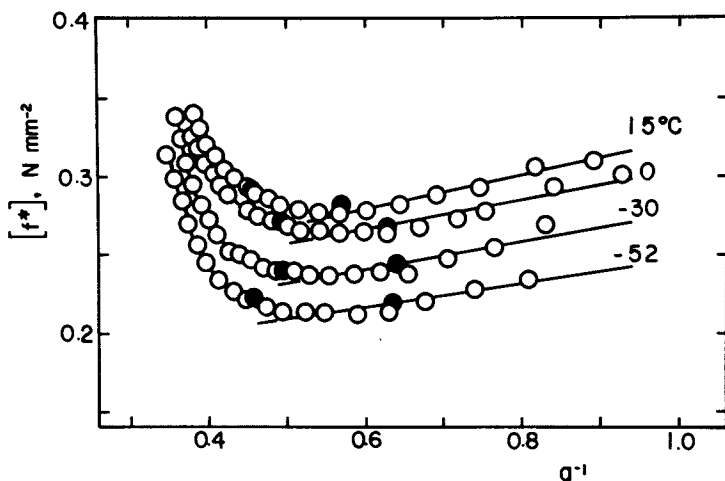
Figure 6. Effect of temperature on the stress–strain isotherms exhibited by a tetrafunctional bimodal (220–18,500) PDMS network containing 75 mol % short chains (16).
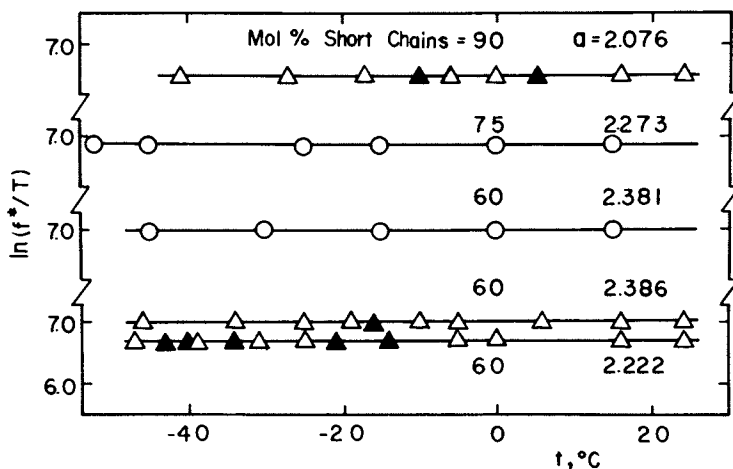
Figure 7. Typical thermoelastic data on 220–18,500 PDMS networks. Key: O, measurements at constant elongation; △, measurements at constant length (16); ●, data obtained to check for reversibility.

The first important characteristic of limited chain extensibility is the elongation α_u at which the increase in $[f^*]$ first becomes discernible. Values of this minimum elongation are readily obtainable from stress-strain isotherms such is those shown in Figures 2, 3, 5, and 6. Although the deformation is non-affine in the vicinity of the upturn, it is possible to provide at least a semi-quantitative interpretation of such results in terms of the network chain dimensions (5,12,13). At the beginning of the upturn, the average extension r of a network chain having its end-to-end vector along the direction of stretching is simply the product of the unperturbed dimension $<r^2>^{1/2}$ and α_u (12). Similarly, the maximum extensibility r_m is the product of the number n of skeletal bonds and the factor 1.34 Å which gives the axial component of a skeletal bond in the most extended helical form of PDMS, as obtained from the geometric analysis summarized in Figure 9(12). The ratio r/r_m at α_u thus represents the fraction of the maximum extensibility occurring at this point in the deformation. The values obtained indicate that the upturn in modulus generally begins at approximately 60-70% of maximum chain extensibility (5,12,13). This is approximately twice the value which had been estimated previously (39), in a misinterpretation of stress-strain isotherms of elastomers undergoing strain-induced crystallization.

It is also of interest to compare the values of r/r_m at the beginning of the upturn with some theoretical results by Flory and Chang (53) on distribution functions for PDMS chains of finite length. Of relevance here are the calculated values of r/r_m at which the Gaussian distribution function starts to overestimate the probability of extended configurations, as judged by comparisons with the results of Monte Carlo simulations. The theoretical results most relevant to the experimental results on the bimodal PDMS networks are shown in Figure 10(53). They suggest, for example, that a network of PDMS chains having n = 53 skeletal bonds should show an upturn at a value of r/r_m a little less than 0.80. The observed value was 0.77 (12), which is thus in excellent agreement with theory.

A second important characteristic is the value α_r of the elongation at which rupture occurs. The corresponding values of r/r_m show that rupture generally occurred at approximately 80-90% of maximum chain extensibility (12). These quantitative results on chain dimensions are very important but may not apply directly to other networks, in which the chains could have very different configurational characteristics and in which the chain length distribution would presumably be quite different from the very unusual bimodal distribution intentionally produced in the present networks.

Evaluation of Non-Gaussian Elasticity Theories. There are now numerous theories of rubberlike elasticity which use non-Gaussian distribution functions to take into account limited
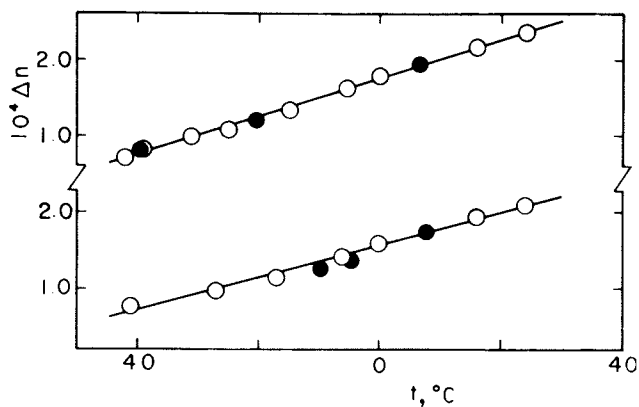
Figure 8.   Representative birefringence–temperature relations for the 220–18,500 PDMS networks. Filled circles locate results obtained to check for reversibility (16).
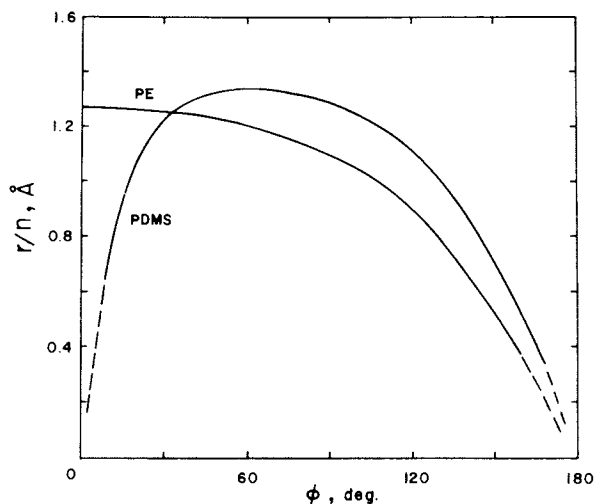
Figure 9.   The end-to-end distance per skeletal bond n *for regular conformations of polydimethylsiloxane and polyethylene network chains (12). Maximum extensibility* r_m *of this chain molecule occurs at* $r_m/n = 1.34$ Å.
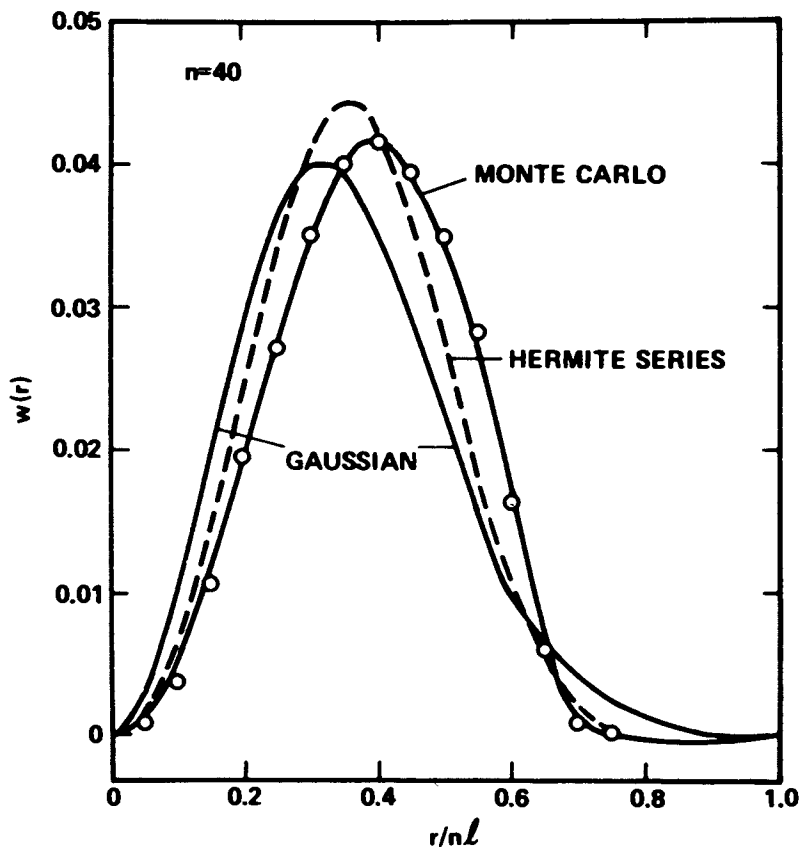
Figure 10.   Radial distributions (in Å⁻¹) for PDMS chains having n = 40 skeletal bonds (each of length l = 1.64 Å) (53).

chain extensibility (39).   Unfortunately, the various theories
have generally been uncritically applied to elasticity results
in which the increases in modulus were due largely if not entire-
ly to strain induced crystallization, as was pointed out prev-
iously (12,36,37).   The results on the bimodal PDMS networks do
not suffer from this complication, and are apparently the only
reliable experimental results available at the present time for
the evaluation of the non-Gaussian theories.   Such evaluations
are in progress (54).

   Improvements in Ultimate Properties.   In this application,
it is most illuminating simply to plot the nominal stress
f/A^* against elongation.   Typical results are shown in Figure 11
(15).   This type of representation has the advantage of having
the area under each curve correspond to the network rupture
energy (per unit undeformed cross-sectional area and per unit
initial length).   This energy E_r (in joules per mm^3 of network
sample) required for rupture was taken as a measure of "tough-
ness" of the PDMS elastomers.   In the case of the unimodal net-
works, E_r is relatively small.   As can be seen from the Figure,
this is due to the small maximum extensibility in the case of
small M_n, and to the small maximum values of the nominal stress
in the case of large M_n.   Thus, unfilled elastomers are generally
very weak materials (31,32).   The bimodal networks have improved
ultimate properties in that they can be prepared so as to have
relatively large values of the nominal stress without the usual
corresponding decrease in maximum extensibility.   This short-
chain reinforcing effect is very striking in that E_r can be
increased by a factor of nearly 5 (15) in going from 0 to 90
mol% of the 220 chains, and this corresponds to an increase of
only 9.7 wt%!
   Strain-induced crystallization would presumably further
improve the ultimate properties of a bimodal network.   It would
therefore obviously be of considerable importance to study the
effect of chain length distribution on the ultimate properties
of bimodal networks prepared from chains having melting points
well above the very low value characteristic of PDMS.   Studies
of this type are being carried out on bimodal networks of poly-
(ethylene oxide) (55), poly(caprolactone) (55), and polyiso-
butylene (56).

Acknowledgements
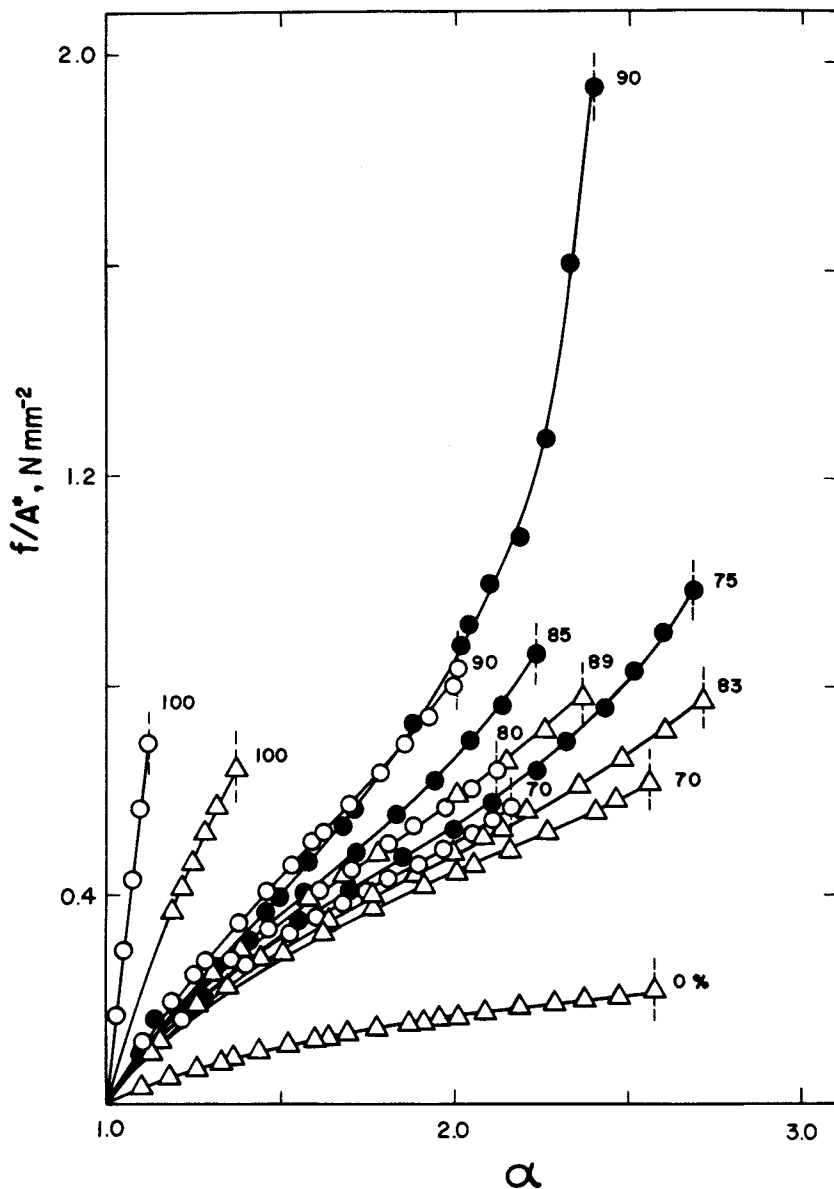
Figure 11.   *Typical plots of nominal stress against elongation, for tetrafunctional PDMS networks at 25°C (15).   All but three networks are bimodal.*

Number-average molecular weight of relatively long chains is $M_n = 18,500$ g/mol.   Key for the networks where short chains had M_n (g/mol): △, 1,100; ○, 660; ●, 220.   Curves are labelled with the mol percent of short chains in the network.   Area below curves represents the rupture energy per unit initial cross sectional area and per unit initial length.

Literature Cited

1. Kraus, G.; Moczvgemba, G. A. J. Polym. Sci. Part A 1964, 2, 277.
2. Rempp, P.; Herz, J. E. Angew. Makromol. Chemie 1979, 76/77, 373 and pertinent references cited therein.
3. Valles, E. M.; Macosko, C. W. Macromolecules 1979, 12, 673 and pertinent references cited therein.
4. Mark, J. E. Makromol. Chem., 1979, Suppl. 2, 87 and pertinent references cited therein.
5. Mark, J. E. Pure Appl. Chem. 1981, 53, 1495.
6. Mark, J. E. Rubber Chem. Technol. 1981, 54, 809.
7. Mark, J. E. J. Chem. Educ. 1981, 58, 898.
8. Mark, J. E. Adv.Polym. Sci. 1982, 00, 000.
9. Llorente, M. A.; Mark, J. E. J. Chem. Phys. 1979, 71, 682.
10. Mark, J. E.; Llorente, M. A. J. Am. Chem. Soc. 1980, 102, 632.
11. Llorente, M. A.; Mark, J. E. J. Polym. Sci., Polym. Phys. Ed. 1980, 18, 181.
12. Andrady, A. L.; Llorente, M. A.; Mark, J. E. J. Chem. Phys. 1980 , 72, 2282.
13. Andrady, A. L.; Llorente, M. A.; Mark, J. E. J. Chem. Phys. 1980, 73, 1439.
14. Mark, J. E.; Andrady, A. L. Rubber Chem. Technol. 1981, 54, 366.
15. Llorente, M. A.; Andrady, A. L.; Mark, J. E. J. Polym. Sci., Polym. Phys. Ed. 1981, 19, 621.
16. Zhang, Z.-M.; Mark, J. E. J. Polym. Sci., Polym. Phys. Ed. 1981, 19, 000.
17. Llorente, M. A.; Mark, J. E. Macromolecules 1980, 13, 681.
18. Llorente, M. A.; Andrady, A. L.; Mark, J. E. J. Polym. Sci., Polym. Phys. Ed. 1980, 18, 2263.
19. Andrady, A. L.; Llorente, M. A.; Sharaf, M. A.; Rahalkar, R. R.; Mark, J. E.; Sullivan, J. L.; Yu, C. U.; Falender, J. R. J. Appl. Polym. Sci. 1981, 26, 1829.
20. Llorente, M. A.; Andrady, A. L.; Mark, J. E. Colloid Polym. Sci. 1981, 259, 000.
21. Meyers, K. O.; Bye, M. L.; Merrill, E. W. Macromolecules 1980, 13, 1045.
22. Falender, J. R.; Yeh, G. S. Y.; Mark, J. E. J. Chem. Phys. 1979, 70, 5324.
23. Falender, J. R.; Yeh, G. S. Y.; Mark, J. E. J. Am. Chem. Soc. 1979, 101, 7353.
24. Falender, J. R.; Yeh, G. S. Y.; Mark, J. E. Macromolecules 1979, 12, 1207.
25. Llorente, M. A.; Mark, J. E. Rubber Chem. Technol. 1980, 53, 988.
26. Mark, J. E.; Sung, P.-H. Eur. Polym. J. 1980, 16, 1223.
27. Sung, P.-H.; Mark, J. E. Polym. J. 1980, 12, 835.

28. Sung, P.-H.; Mark, J. E. J. Polym. Sci., Polym. Phys. Ed.
     1981, 19, 507.
29. Flory, P. J. "Principles of Polymer Chemistry", Cornell
     University Press: Ithaca, N.Y., 1953, ch. XI.
30. F. Beuche, "Physical Properties of Polymers", Interscience:
     New York, 1962, ch. 10.
31. Smith, T. L. Polym. Eng. Sci. 1977, 17, 129.
32. Gent, A. N. in "Science and Technology of Rubber"; by
     Eirich, F. R., Ed.; Academic Press: New York 1978; ch. 10.
33. Brandrup, J.; Immergut, E. H. "Polymer Handbook"; 2nd Ed.,
     Wiley-Interscience: New York, 1975.
34. Flory, P. J. J. Am. Chem. Soc. 1956, 78, 5222.
35. Levin, V. Yu; Slonimskii, G. L.; Andrianov, K. A.; Zhdanov,
     A. A.; Godovskii, Yu. K.; Papkov, V. S.; Lyubavskaya, Ye. A.
     Polymer Sci. U.S.S.R. 1973, 15, 256.
36. Mark, J. E. Polym. Eng. Sci. 1979, 19, 254.
37. Mark, J. E. Polym. Eng. Sci. 1979, 19, 409.
38. Erman, B.; Wagner, W.; Flory, P. J. Macromolecules 1980,
     13, 1554.
39. Treloar, L. R. G. "The Physics of Rubber Elasticity   3rd
     Ed., Clarendon: Oxford, 1975.
40. Mark, J. E.; Flory, P. J. J. Appl. Phys. 1966, 37, 4635.
41. Mark, J. E. J. Am. Chem. Soc. 1970, 92, 7252.
42. Mark, J. E. Rubber Chem. Technol. 1975, 48, 495.
43. Ronca, G.; Allegra, G. J. Chem. Phys. 1975, 63, 4990.
44. Flory, P. J. Proc. R. Soc. London, Ser. A. 1976, 351, 351.
45. Mooney, M. J. Appl. Phys. 1948, 19 434.
46. Rivlin, R. S. Phil. Trans. R. Soc. London, Ser. A. 1948,
     241, 379.
47. Kraus, G. Rubber Chem. Technol. 1978, 51, 297.
48. Boonstra, B. B. Polymer 1979, 20, 691.
49. Rigbi, Z. Adv. Polym. Sci. 1980, 36, 21.
50. Polmanteer, K. E.; Lentz, C. W. Rubber Chem. Technol. 1975,
     48, 795.
51. Pan, S.-J.; Mark, J. E., unpublished results.
52. Thiele, J. L.; Mark, J. E., unpublished results.
53. Flory, P. J.; Chang, V. W. C. Macromolecules 1976, 9, 33.
54. Andrady, A. L.; Llorente, M. A.; Mark, J. E., unpublished
     results.
55. Sung, P.-H.; Mark, J. E., unpublished results.
56. Kennedy, J. P.; Mark, J. E., work in progress.

Threshold Tear Strength of Some Molecular Networks

A. N. GENT and R. H. TOBIAS

The University of Akron, Institute of Polymer Science, Akron, OH 44325

The tear strength of polydimethylsiloxane (PDMS)
networks was found to be only one-third as large as
that of polybutadiene (PB) or polyisoprene (PI) net-
works of similar M_c when the tear strength was
measured under threshold conditions, i.e., at high
temperatures, low rates of tearing, and with swollen
samples. This striking difference in strength is
attributed to the smaller length and extensibility
of PDMS molecules in comparison with PB or PI mole-
cules of the same molecular weight. Networks formed
by trifunctional or tetrafunctional endlinking reac-
tions with difunctional PDMS polymers were found to
be only slightly stronger under threshold conditions,
by up to 30 per cent, than PDMS networks formed by
random crosslinking to the same M_c. Endlinked PB
networks were found to have substantially the same
threshold strength as randomly-linked PB networks of
the same M_c. Thus, the threshold tear strength does
not appear to depend strongly upon the uniformity of
network strand lengths.

When dissipative processes are minimized, the tear strength
of elastomeric materials is found to reach a lower limit, termed
here the threshold strength (1, 2). Experimentally, the thres-
hold strength is reached at high temperatures, at low rates of
tearing and when the material is highly swollen with a low-
viscosity liquid. Its magnitude has been predicted theoretically
from the length of the molecular strands comprising the network
and the dissociation energy of the chemical bonds comprising the
strand (3). Expressed as the energy T_0 required to tear through a
unit area of the material, the theoretical result takes the form

$$T_0 = KM_c^{\frac{1}{2}} \tag{1}$$

where M_c is the mean molecular weight of the network strands and K

is a constant involving the mass, length and effective flexi-
bility of a monomeric unit, the density of the polymer and the
dissociation energy of the relevant bonds. For C-C molecular
strands K is predicted to be about 0.3 J/m^2/(molecular weight
unit)$^{\frac{1}{2}}$. Experimental values of T_0 for randomly-crosslinked net-
works of polybutadiene were found to be consistent with equation
1, when K was given a somewhat higher value, about 1.0 J/m^2/
(molecular weight unit)$^{\frac{1}{2}}$. Thus, apart from this numerical dis-
crepancy, the threshold strength of polybutadiene networks is
reasonably well accounted for. We now address two further aspects
of threshold strength. Does the tear strength of other elasto-
mers, of different chemical type, conform to equation 1? And are
randomly-crosslinked materials weaker than more regular networks,
prepared, for example, by linking strands of uniform molecular
weight into a network by endgroup coupling reactions? A higher
tensile strength has been reported for endlinked networks of poly-
isoprene in comparison with randomly-crosslinked networks of
similar average strand length (4). However, those measurements
were not made under threshold conditions and did not examine a
wide range of strand lengths, so that direct comparison with
molecular theory is not possible.

    Measurements have now been carried out on endlinked and
randomly-linked samples of polybutadiene, polydimethylsiloxane,
and randomly-linked samples of cis-polyisoprene. The results are
presented here.

Experimental Details

    Endlinked PDMS. Linear polydimethylsiloxanes with vinyl
endgroups were supplied by Dow Corning Corporation. Three dif-
ferent molecular weight ranges were employed. Membrane osmometry
yielded values for $\overline{M}_n$ of 16,000, 24,000, and 37,000 g/g-mole.
Endgroup analysis using mercuric acetate (5) gave vinyl contents
of 0.47 ± 0.03, 0.24 ± 0.02, and 0.15 ± 0.02 per cent, corres-
ponding to values for $\overline{M}_n$ of 11,500, 22,500 and 36,000 g/g-mole.
GPC data gave $\overline{M}_w/\overline{M}_n$ ratios of approximately 2.0, as reported by
Valles and Macosko (6, 7) for their similar polymers.
    Trifunctional and tetrafunctional silane linking agents were
supplied to us by Prof. Macosko. They consisted of trikis-dime-
thylsiloxyphenylsilane and tetrakis-dimethylsiloxysilane and are
denoted here A3 and A4, respectively. Gas chromatography,
carried out by Prof. Macosko, revealed that they were approximate-
ly 95 and 89 per cent pure. Si-H group analysis (5) gave average
functionalities of 3.15 and 3.50, somewhat different from the ex-
pected values of 3 and 4, indicating that other constituents are
present.
    The linking agent, A3 or A4, was mixed in various concentra-
tions with the divinyl-PDMS, together with 5 ppm of a Pt catalyst
(8). The mixture was then degassed and cast as a thin sheet on a
Teflon surface. Complete reaction was found to occur on heating

for about 3 days at 70°C, as judged by equilibrium swelling mea-
surements in benzene; thereafter, a period of 4 days at 70°C was
used to ensure complete reaction.

As shown in Figure 1, values of M_c calculated from equili-
brium swelling ratios in benzene (9), were found to depend
strongly upon the concentration of endgroups in the linking agent
relative to those in the polymer. The highest effective degree
of crosslinking, i.e., the lowest degree of swelling and the low-
est value for M_c, was obtained at a characteristic endgroup ratio
lying between about 1.1 and 1.6 instead of the expected ratio of
1.0. Thus, even when allowance is made for the true functional-
ity of the linking agent, it is still necessary to employ a
greater amount than expected to produce a minimum value for M_c.
Presumably, a significant fraction of polymer endgroups do not
become linked into the network until an excess of linking agent
is present. This implies that the junction points are not ex-
clusively trifunctional or tetrafunctional in nature.

Networks were prepared in all cases using the amount of end-
linking agent necessary to give a minimum M_c. Values of M_c were
calculated from the Mooney-Rivlin elasticity coefficient C_1,
determined from tensile stress-strain measurements (10),

$$M_c = \rho RT/2C_1, \tag{2}$$

where ρ is the density, 0.97 g/ml, R is the gas constant and T is
absolute temperature, for comparison with earlier work (2). Ex-
perimentally-determined values of the elastic coefficients C_1 and
C_2 and values of M_c calculated from C_1 are given in Table I.

Randomly - Crosslinked PDMS. The polydimethylsiloxane
(PDMS) used to make random networks was obtained from General
Electric. Membrane osmometry showed $\overline{M}_n$ to be 430,000 g/g-mole.
The polymer was mixed with various amounts of a free-radical
crosslinking agent, dicumylperoxide (Di-Cup R, Hercules Chemical
Co.). Samples were then pressed into sheets and crosslinking was
effected by heating for 2 h at 150°C in a heated press. M_c
values were calculated using equation 2, and are included in
Table I.

Endlinked PB. Endlinked polybutadiene samples were pro-
vided by Prof. F. N. Kelley and Mr. Long-Ji Su of these labora-
tories. They were made by reacting toluene -2,4- diisocyanate
with the hydroxy endgroups of hydroxy- terminated polybutadiene
(Arco R45-HT, $\overline{M}_n$ = 2,800 g/g-mole) and then employing trimethyl-
olpropane as a trifunctional linking agent. The prepolymer was
also chain-extended with 1,4 - butanediol to give a higher M_c
value on subsequent endlinking. M_c values, calculated by means
of equation 2, were 3,100 g/g-mole for the sample made with the
initial polymer and 7,100 g/g-mole when the chain-extended
material was used.
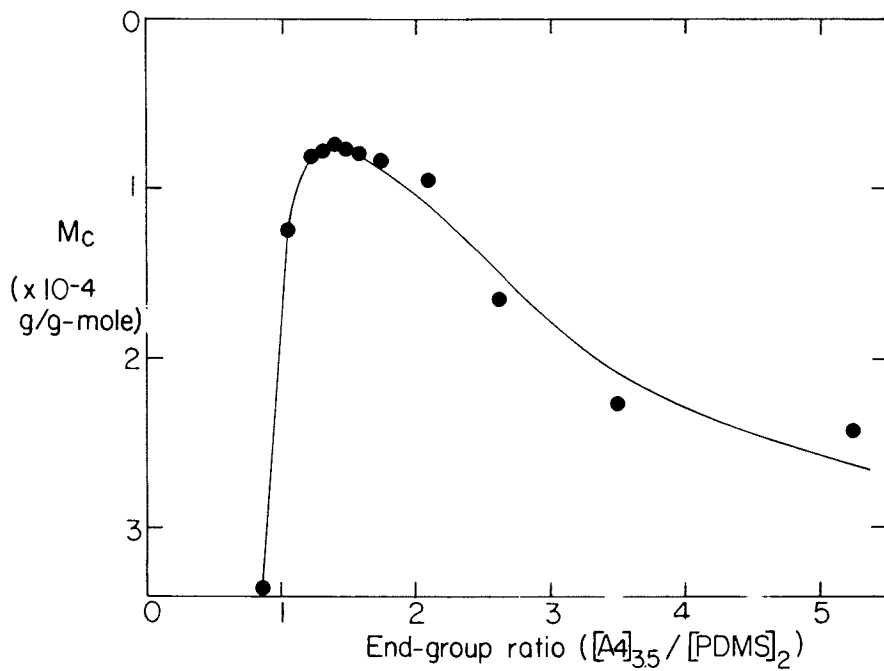
Figure 1. M_c from equilibrium swelling in benzene vs. concentration of A_4 end-linking agent in divinyl–PDMS, $M_n = 11,500$.

Table I. Threshold Tear Strength T_0 of Randomly-linked and Endlinked Elastomers of Varying M_c

$\overline{M}_n \times 10^{-4}$ [a] (g/g-mole)	C_1 (kPa)	C_2 (kPa)	$M_c \times 10^{-4}$ [b] (g/g-mole)	T_0 (J/m^2)
	PDMS endlinked with A3			
3.6	54	45	1.23	39 ± 2
2.25	65	43	1.10	33 ± 2
1.15	110	48	0.75	27 ± 2
	PDMS endlinked with A4			
3.6	46	45	1.32	48 ± 2
2.25	61	47	1.11	42 ± 2
1.15	97	46	0.84	35 ± 2
	Endlinked PB			
ca 0.84	168	165	0.71	62 ± 4
ca 0.28	389	165	0.31	47 ± 3

Dicumyl peroxide (%)	C_1 (kPa)	C_2 (kPa)	$M_c \times 10^{-4}$ [b] (g/g-mole)	T_0 (J/m^2)
	PDMS randomly linked with dicumyl peroxide			
1.0	9	20	13.6	78 ± 6
1.2	14	23	9.0	74 ± 3
1.5	19	29	6.3	62 ± 3
1.75	21	30	5.9	56 ± 3
2.0	26	31	4.6	48 ± 3
2.5	31	31	3.9	46 ± 2
2.75	32	35	3.7	44 ± 3
3.0	36	33	3.4	42 ± 3
4.0	45	25	2.6	39 ± 2
	PI randomly linked with dicumyl peroxide			
1.0	121	71	1.01	108 ± 9
2.0	197	78	0.62	63 ± 4
4.0	387	48	0.31	51 ± 5

[a] Molecular weight of polymer before endlinking.
[b] Calculated from C_1 by means of equation 2.

Randomly – Crosslinked PB and PI. Polybutadiene (Diene 35 NFA, Firestone Tire and Rubber Co.) and cis-polyisoprene (Natsyn 2200, Goodyear Tire and Rubber Co.) were crosslinked with dicumyl-peroxide, as for PDMS. M_c values were also calculated by means of equation 2. They are given for PI in Table I and are listed for PB in reference 2.

Measurements of Threshold Tear Strength. Rectangular strips, about 50 mm long, 10 mm wide and 1.4 mm thick were scored along a central line to a depth of about 0.7 mm, leaving about one-half of the original thickness to be torn through. The tear energy T was calculated from the measured tear force F,

$$T = 2 \ F/t, \qquad\qquad\qquad (3)$$

where t is the width of the tear path (Figure 2). Tearing was found to take place at an angle of approximately 45° to the sheet thickness (11).

Measurements were carried out on both swollen and unswollen samples, using m-xylene or silicone oil as swelling liquids with PDMS networks and m-xylene or paraffin oil with PB and PI networks. Samples were torn at temperatures between 70°C and 140°C. Values of the tear energy T for swollen samples were multiplied by λ_s^2, where λ_s is the linear swelling ratio, to take into account the reduced number of network strands crossing the tear path (1-3). Typical results for samples of endlinked PDMS, both unswollen and swollen with m-xylene, are given in Table II. Close agreement was obtained with the results obtained for unswollen samples at the high temperatures and low rates of tearing (about 4μm/s) used in the present experiments, when the values for swollen samples were multiplied by λ_s^2. The mean values have therefore been taken as measures of the threshold tear strength T_0 in all cases. They are given in Table I.

Experimental Results and Discussion

Experimentally-determined values of T_0 for PDMS networks are plotted in Figure 3 against values of M_c calculated from the elastic coefficient C_1 by means of equation 2. T_0 was found to be accurately proportional to $M_c^{\frac{1}{2}}$, in accordance with equation 1, with the coefficient of proportionality K being about 0.30, 0.25, and 0.23 J/m^2/(molecular weight unit)$^{\frac{1}{2}}$ for the A4, A3, and random-ly-linked materials, respectively. These differences are small, barely significant, but in the expected direction. Values of T_0 are also shown in Figure 3 for the other materials examined. Again, a proportionality to $M_c^{\frac{1}{2}}$ was found, in accordance with theory. Moreover, the present values for endlinked PB and randomly-linked PI are in good agreement with previously-reported data on randomly-linked PB, with K = 0.85 J/m^2. This is much larger than for the PDMS materials, however. Thus, at the same
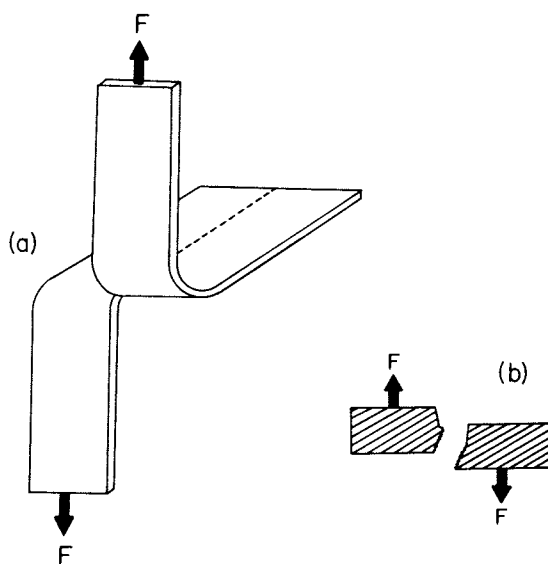
Figure 2. Tear test (a). Sketch of torn cross-section (b).

Table II.   Effect of Swelling with m-Xylene on
the Threshold Tear Strength of PDMS

$\overline{M}_n \times 10^{-4}$ (g/g-mole)	T_o (Unswollen) (J/m^2)	λ_s	T_o (Swollen) (J/m^2)	$\lambda_s^2 T_o$ (Swollen)
	PDMS endlinked with A3			
3.6	38 ± 3	1.62	15 ± 1.5	39 ± 3
2.25	32 ± 3	1.57	13 ± 2	33 ± 4
1.15	26 ± 3	1.48	13 ± 1.5	28 ± 3
	PDMS endlinked with A4			
3.6	49 ± 1	1.65	17 ± 1.5	47 ± 4
2.25	41 ± 5	1.57	18.5 ± 1.5	46 ± 4
1.15	35 ± 2	1.52	15 ± 1	35 ± 2
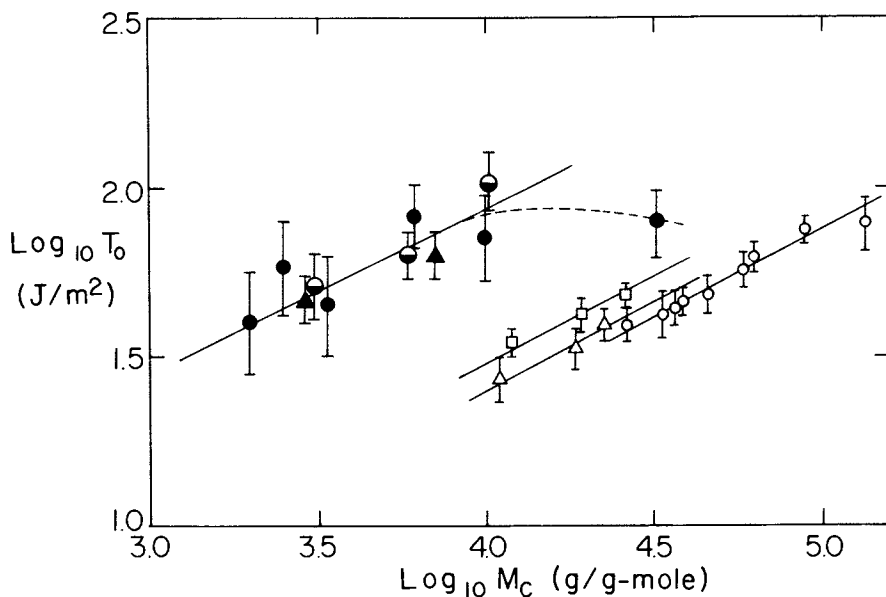
Figure 3.   Threshold tear energy T_o. Key: ○, △, □, PDMS networks; ●, ▲, PB networks; ◐, PI networks; versus molecular weight M_c between cross-links calculated from C_1. ○, ◐, ●, random cross-linking; △, ▲, trifunctional end-linking; □, tetrafunctional end-linking.

value of M_c, elastomeric networks based on C-C molecular chains have a threshold strength about three times that of Si-O networks.

Values of M_c calculated from the small-strain tensile modulus, i.e., using $C_1 + C_2$ in equation 2 in place of C_1, were, of course, smaller than those obtained from C_1 values. However, the general form of the dependence of threshold tear strength upon M_c and the relative values obtained for different polymers at the same M_c were not significantly affected by this alternate procedure for calculating the mean molecular weight of network strands.

Although the bond dissociation energies for C-C and Si-O bonds are quite similar, 89 and 80 kcal/g-mole respectively, the molecular weight per main-chain atom is considerably higher for PDMS (37 molecular weight units) than for PI (17) and PB (13.5). The extended length of a network strand is therefore much smaller for PDMS at the same value of M_c. There are also steric restrictions on straightening the Si-O chain due to unequal main-chain bond angles. Thus, the threshold strength of PDMS networks would be expected to be less than one-half as large as for C-C networks, in accordance with observation.

Conclusions

The threshold tear strength of elastomeric molecular networks does not appear to depend strongly, if at all, upon the uniformity of network strand lengths. It is found to be proportional to $M_c^{1/2}$ where M_c is the mean molecular weight of the strands, in accordance with the theory of Lake and Thomas (3). However, it is considerably smaller for Si-O networks than for C-C networks at equal M_c values. This is attributed to differences in strand length and extensibility.

Acknowledgements

Literature Cited

1. Mueller, H. K.; Knauss, W. G. Trans. Soc. Rheol. 1971, 15, 217.
2. Ahagon, A.; Gent, A. N. J. Polym. Sci: Polym. Phys. Ed. 1975, 13, 1903.
3. Lake, G. J.; Thomas, A. G. Proc. Royal Soc. (London) 1967, A300, 108.

4. Morton, M.; Rubio, D. C. Plastics and Rubber: Mat. Appl. 1978,
     3, 139.
5. Smith, R. C.; Angelotti, N. C.; Hanson, C. L. "Analysis of
     Silicones", Smith, A. L. ed., John Wiley & Sons, New York,
     1974, p. 150.
6. Valles, E. M.; Macosko, C. W. Rubber Chem. Technol. 1976, 49,
     1232.
7. Valles, E. M.; Macosko, C. W. Macromolecules 1979, 13, 521.
8. Kauffman, C. B.; Cowan, D. O. "Inorganic Synthesis", Vol. 6,
     Rochow, E. G., ed., McGraw-Hill, New York, 1969, p. 214.
9. Shih, H.; Flory, P. J. Macromolecules 1972, 5, 759.
10. Treloar, L. R. G. "Physics of Rubber Elasticity", 2nd Ed.,
     Clarendon Press, Oxford, 1958.
11. Ahagon, A.; Gent, A. N.; Kim, H. J.; Kumagai, Y. Rubber Chem.
     Technol. 1975, 48, 896.

Experimental Studies of the Formation and Properties of Polymer Networks

J. L. STANFORD and R. F. T. STEPTO

The University of Manchester Institute of Science and Technology, Department of Polymer and Fiber Science, Manchester, M60 1QD, England

The paper first considers the factors affecting
intramolecular reaction, the importance of intra-
molecular reaction in non-linear random polymer-
isations, and the effects of intramolecular re-
action on the gel point. The correlation of gel
points through approximate theories of gelation
is discussed, and reference is made to the deter-
mination of effective functionalities from gel-
point data. Results are then presented showing
that a close correlation exists between the amount
of pre-gel intramolecular reaction that has occurred and
the shear modulus of the network formed at complete
reaction. Similarly, the Tg of a network is shown
to be related to amount of pre-gel intramolecular
reaction. In addition, materials formed from bulk
reaction systems are compared to illustrate the
inherent influences of molar masses, functionalities
and chain structures of reactants on network
properties. Finally, the non-Gaussian behaviour of
networks in compression is discussed.

The properties of a polymer network depend not only on the
molar masses, functionalities, chain structures, and proportions
of reactants used to prepare the network but also on the condi-
tions (concentration and temperature) of preparation. In the
Gaussian sense, the perfect network can never be obtained in
practice, but, through random or condensation polymerisations(1)
of polyfunctional monomers and prepolymers, networks with imper-
fections which are to some extent quantifiable can be prepared,
and the importance of such imperfections on network properties can
be ascertained. In this context, the use of well-characterised
random polymerisations for network preparation may be contrasted
with the more traditional method of cross-linking polymer chains.
With the latter, uncertainties can exist with regard to the

distribution of primary chain lengths, chains between junction
points, loose ends and entanglements.

The present paper presents a survey of published and more
recent work on correlations between network properties and re-
actant structures and reaction conditions. The reaction systems
used have been generally polyoxypropylene(POP) triols or tetrols
of various molar masses reacting irreversibly with diisocyanates
(to give polyurethanes) or diacid chlorides (to give polyesters),
the like functional groups having equal reactivities. Reactions
have been carried out in bulk and at various dilutions in inert
solvents. Reaction systems with equimolar amounts of reactive
groups have been used, and emphasis has been placed on the extent
to which pre-gel intramolecular reaction defines the physical
properties of the networks formed at complete reaction. Pre-gel
intramolecular reaction can introduce elastically ineffective
loops into a rubbery network. In general, loops produce the
opposite effects on physical properties to those expected from
entanglements.

Pre-gel Intramolecular Reaction

Previous studies(2) have shown how ring structures formed
during irreversible linear random polymerisations leading to
polyurethanes may be measured. The work has been extended(3,4)
to non-linear polyurethane formation using hexamethylene diiso-
cyanate(HDI) and POP triols. For non-linear polymerisations, it
is found that the number of ring structures per molecule at
extent of reaction p is always significant, even in bulk reactions.
For example, Figure 1 shows the number of ring structures per
molecule (N_r) versus extent of reaction for bulk, linear and non-
linear polyurethane-forming reactions with approximately equi-
molar concentrations of reactive groups(2,3). The much larger
number of ring structures per molecule in the non-linear compared
with the linear polymerisation is due to the larger number of
opportunities per molecule for intramolecular reaction in the
former type of polymerisation. The other factors influencing
intramolecular reaction in the two reaction systems in fact
predict more intramolecular reaction in the linear system, as is
now discussed.

An illustration(5) of the competition between intermolecular
and intramolecular reaction, for the $RA_2 + RB_2$ and $RA_2 + RB_3$ type
random polymerisations of Figure 1, is shown in Figure 2. The
probability that a given A group reacts intramolecularly rather
than intermolecularly depends on the concentration of nearby B
groups from the same molecule compared with the concentration of
B groups from other molecules. In random polymerisations only
ring structures of certain sizes can form as defined by the number
of bonds in repeating units of the chain structures. The situation
is illustrated in Figure 3 with respect to the smallest rings in
$RA_2 + RB_2$ and $RA_2 + RB_3$ polymerisations, where the reacting groups
[A] and [B] are separated by ν bonds(5).
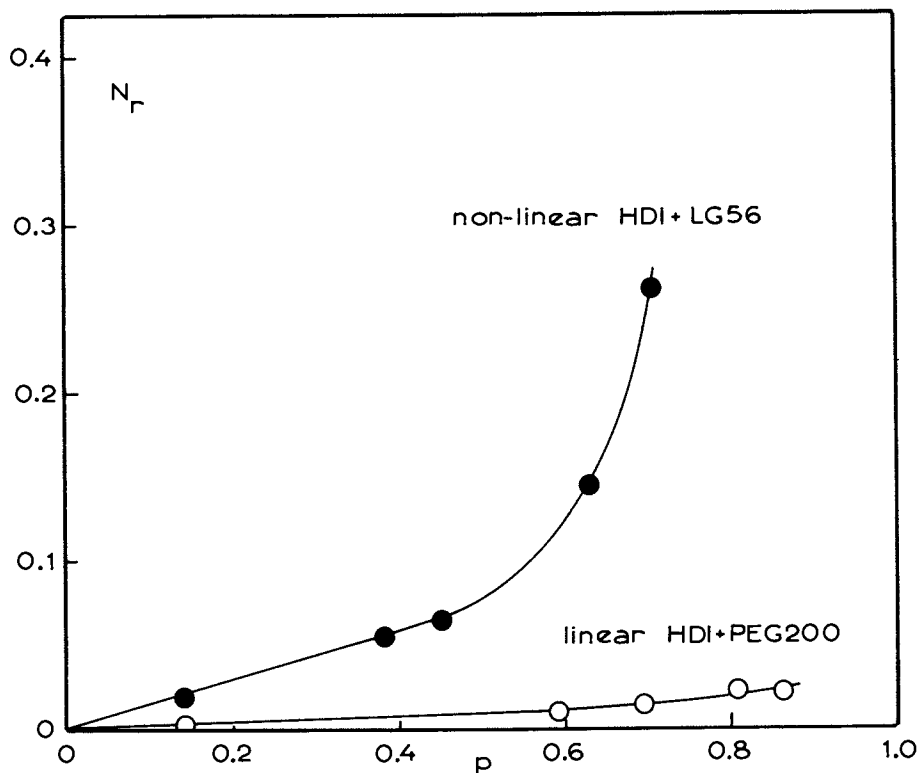
Figure 1. Number fraction of ring structures per molecule (N_r) as a function of extent of reaction (p) for bulk, linear, and nonlinear polyurethane-forming reactions with approximately equimolar concentrations of reactive groups ($r = [NCO]_o/[OH]_o \cong 1$) (2, 3). Conditions: O-linear polymerization, HDI + poly(ethyleneglycol) at 70°, $[NCO]_o = 5.111$ mol/kg, $[OH]_o = 5.188$ mol/kg; number-average number of bonds in chain forming smallest ring structure (v) = 25.2, and nonlinear polymerization, HDI and POP triol at 70°C, $[NCO]_o = 0.9073$ mol/kg, $[OH]_o = 0.9173$ mol/kg; v = 115. Reproduced with permission from Ref. 5.
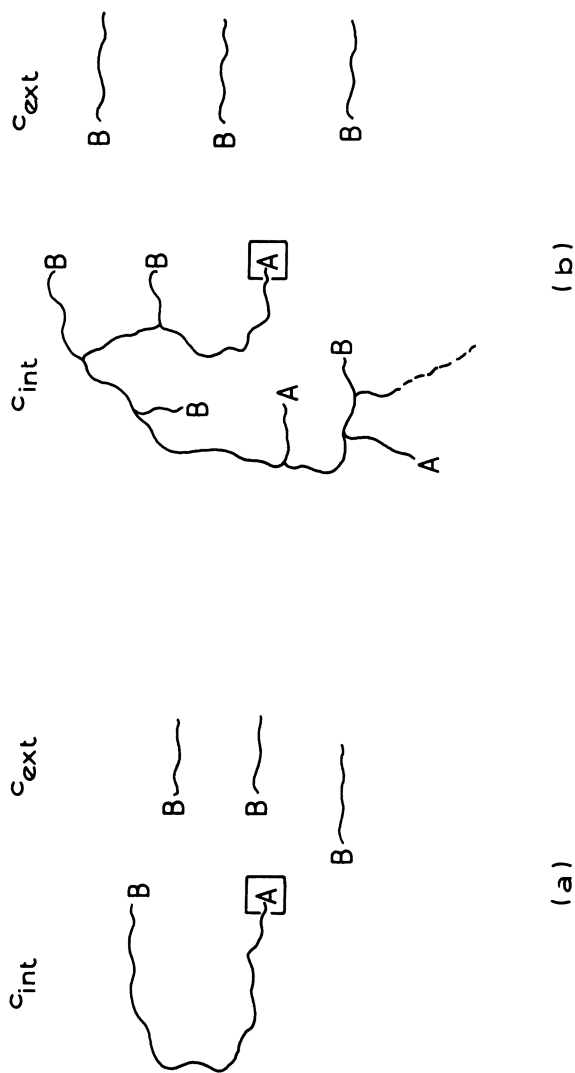
Figure 2.   Concentrations of B groups around a reference $\boxed{A}$ group. From left to right: RA_2 and RB_2 polymerization; RA_2 and RB_3 polymerization. c_{int} is the concentration of B groups from the same molecule. c_{ext} is that from groups on other molecules (5).   Reproduced, with permission, from Ref. 5.

Overall, ring structures can be formed from chains of ν, 2ν, 3ν,.
... bonds.
     Considering for a moment linear polymerisations, the proba-
bility of intramolecular reaction for equimolar reaction mixtures
will be characterised by the ring-forming parameter(5,6,7)

$$\lambda = Pab/c_{ao}, \qquad (1)$$

where

$$Pab = (3/2\pi\nu b^2)^{3/2}/N \text{ (moles functional groups per unit volume)} \qquad (2)$$

In equation(1), c_{ao} is the initial concentration of reactive
groups of one of the reactants, and defines a scale for c_{ext} of
Figure 2, with c_{ext} itself decreasing as a reaction proceeds.
Pab is the mutual concentration of reactive groups separated by
a chain of ν bonds, assuming the chain obeys Gaussian statistics.
N is the Avogadro constant, and b is the effective bond length of
bonds of the chain, such that $<r^2> = \nu b^2$, where $<r^2>$ is the mean-
square end-to-end distance of the chain.
     Thus, returning to Figure 1, one would expect on the basis
of equations(1) and (2) that more ring structures would be formed
in the linear polymerisation compared with the non-linear poly-
merisation. ν for the linear system was 25.2 and for the non-
linear system was 115, and, for the same of value of b, λ varies
as $(c_{ao} \nu^{3/2})^{-1}$, giving a value of λ for the linear system 1.7
times the value for the non-linear system. In addition, the value
of b of the more flexible HDI/polyoxyethylene chain is predicted
to be less than that of the HDI/POP chain(8,9), resulting in an
even larger relative value of λ for the linear system. The
fact that Figure 1 shows that many more ring structures have
formed in the non-linear polymerisation is indeed due to the
larger number of opportunities per molecule for intramolecular
reaction in that system, and Figure 1 demonstrates the. import-
ance of giving due considertation to intramolecular reaction in
non-linear polymerisations. The gel point of the non-linear
system shown in Figure 1 was at p = 0.765 (compared with the
value of 0.707 expected(10) in the absence of intramolecular
reaction) when $N_r \simeq 0.3$, showing that at gel about one molecule
in three contained a ring structure.
     The curves in Figure 1 describe intramolecular reaction in
irreversible, linear and non-linear random polymerisations. For
linear polymerisations, theories have been developed(7,11,12)
which account for the decrease in c_{ext} as a reaction proceeds and
allow N_r to be calculated satisfactorily as a function of p for
a given value of Pab. For non-linear polymerisations, the larger
numbers of ring structures result in less adequate descriptions
of N_r versus p curves using similar theories(12-17). Such theories
require more development before N_r as a function of p and the gel

point can be defined in a consistent manner[16,17,18], that is
with a common value of λ or Pab.

Intramolecular Reaction and Gelation

Several approximate theories of gelation in RA_2 + RBf type
polyemrisations have been developed[6,19,20,21] which assume
that the ring-forming parameter (cf. λ of equation(1)) remains
constant throughout the reaction, and, hence, enable analytical
expressions for the extents of reaction at gelation to be derived
[6,21]. By comparison, the more complete theories[12-17], effect-
ively allow λ to vary as the reaction proceeds. However, the
correlation of gel points through approximate theories can be used
for present purposes, as they enable the effects of reactant
molar mass, functionality, chain structure, and dilution to be
distinguished.

Recently, Ahmad and Stepto[21] compared existing gel-point
expressions[6,19,20] and illustrated shortcomings in them and
in the way they were applied to gelation data. A new expression
for the gel-point in RA_2 + RBf random polymerisations was derived,
namely,

$$\alpha_c (f-1)(1-\lambda_{ab})^2 = 1. \tag{3}$$

Here, α_c = papb, where p_a and p_b are the extents of reaction at
gelation of A and B groups, respectively, and λ_{ab} is the ring-
forming parameter defined by the equation

$$\lambda_{ab} = c_{int}/(c_{int}+c_{ext}), \tag{4}$$

with

$$c_{int} = (f-2)Pab.\phi(1,3/2). \tag{5}$$

Equation(3) was derived from a generalisation of Kilb's
linear sequence[20] for the gelation condition in an RA_2 + RB_3
polymerisations, as depicted in Figure 4. In equation(5), (f-2)
represents the number of opportunities for intramolecular
reaction at each branch unit along the linear sequence i = 1, 2,
3,...... . The sequence grows from B^1 through A^1 to B^2 and

$$\phi(1,3/2) = \sum_{i=1}^{\infty} 1^i i^{-3/2} = 2.612 \tag{6}$$

sums over the relative probabilities for intramolecular reaction
at various branch points. With λ_{ab} taken as constant for a given
polymerisation reaction, c_{ext} has to be chosen arbitrarily[6],
and c_{ext} = c_{ao} + c_{bo} and c_{ext} = c_{ac} + c_{bc}, respectively the
initial and gel-point concentrations of reactive groups, are used
as extreme values.

To analyse gel-point data equations(4) and (5) are combined
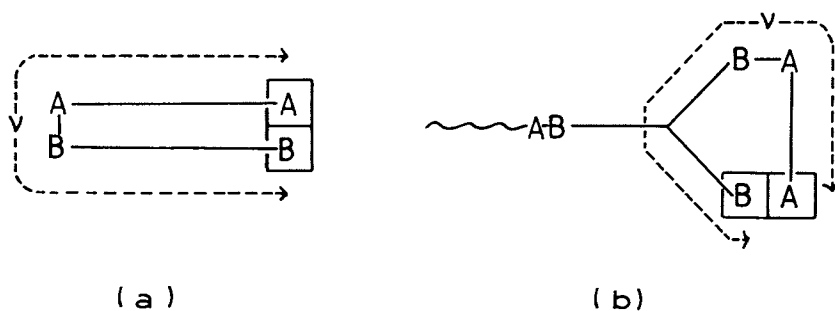
Figure 3.   *Repeating units of the chain structures. From left to right: RA$_2$ and RB$_2$ polymerization; RA$_2$ and RB$_3$ polymerization. The repeating units have v bonds separating the reacting groups* A *and* B *(5). Reproduced, with permission, from Ref. 5.*
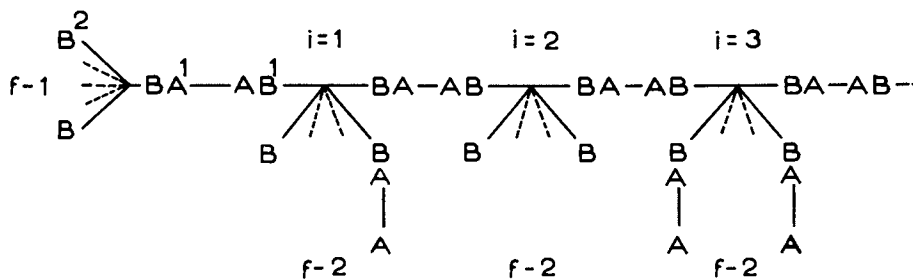
Figure 4.   *Development of Kilb's linear sequence to define the conditions for gelation in RA$_2$ and RB$_f$ polymerization (21). Reproduced with permission, from Ref. 5.*

to give(21)

$$\lambda_{ab}/(1-\lambda_{ab}) = \lambda'_{ab} = c_{int}/c_{ext} = (f-2)Pab.\phi(1,3/2)/c_{ext}, \qquad (7)$$

with λ'_{ab} evaluated from equation(3) using experimental values of
α_c. Thus, λ'_{ab} can be plotted versus c^{-1}_{ext} and the slopes of the
straight lines obtained interpreted in terms of Pab (see equation
(2)). Figure 5 shows gelation data for trifunctional polyester-
forming systems(22) analysed(21)according to equations(7), with
$c_{ext} = c_{ao} + c_{bo}$. c_{ext} was varied by carrying out reactions in
various amounts of inert solvent. As indicated in the caption,
the six systems were chosen to have different values of ν, and,
at a given initial dilution, the value of λ'_{ab} is seen to increase
as ν decreases, as predicted by equation(2). Plots of λ'_{ab} versus
$(c_{ac} + c_{bc})^{-1}$ show slight curvature with slopes decreasing as
dilution at gel increases. However, the initial slopes of such
plots and the slopes of the plots in Figure 5 can be analysed
in terms of equation(2) to give values of b characteristic of the
chains forming the smallest ring structures. The values so obt-
ained are reproduced in Table 1, where the systems are listed in
decreasing order of ν_{AC}/ν.

Table I. Values of b for polyester-forming systems derived(21)
from Figure 5 and plots of λ'_{ab} versus $(c_{ac} + c_{bc})^{-1}$ according to
equations(7). ν_{AC}/ν-fractional length of acid chloride residue
in the chain of ν bonds. (i) $c_{ext} = c_{ao} + c_{bo}$. (ii) $c_{ext} = c_{ac} + c_{bc}$. For explanation of reactants see Figure 5.

System	ν	ν_{AC}/ν	b/nm(i)	b/nm(ii)
2. sebacoyl chloride + LHT240	41	0.268	0.318	0.508
1. adipoyl chloride + LHT240	37	0.189	0.313	0.480
4. sebacoyl chloride + LHT112	70	0.157	0.293	0.433
3. adipoyl chloride + LHT112	66	0.106	0.270	0.399
6. sebacoyl chloride + LG56	136	0.081	0.267	0.390
5. adipoyl chloride + LG56	132	0.053	0.280	0.371

The values of b in Table I and the results in Figure 5
indicate that for chemically similar systems of a given function-
ality the amount of pre-gel intramolecular reaction depends
primarily on the size (ν) of the smallest ring structure with a
secondary dependence on chain stiffness (b). The dependence on
ν is clear from Figure 5, whilst the dependence on b is indicated
by the different values of b for the various systems. With
regard to thelatter, the acid chloride residues of the chains of
ν bonds are reckoned to be stiffer than the oxypropylene resi-
dues(8,9). Accordingly, b is found to decrease as ν_{AC}/ν decreases,
with ν_{AC} being the number of bonds in the acid chloride residue.
It should be noted that, because b varies from system to system,
the slopes of the lines in Figure 5 are not directly proportional
to $\nu^{-3/2}$, although they do decrease as ν increases. Finally, the
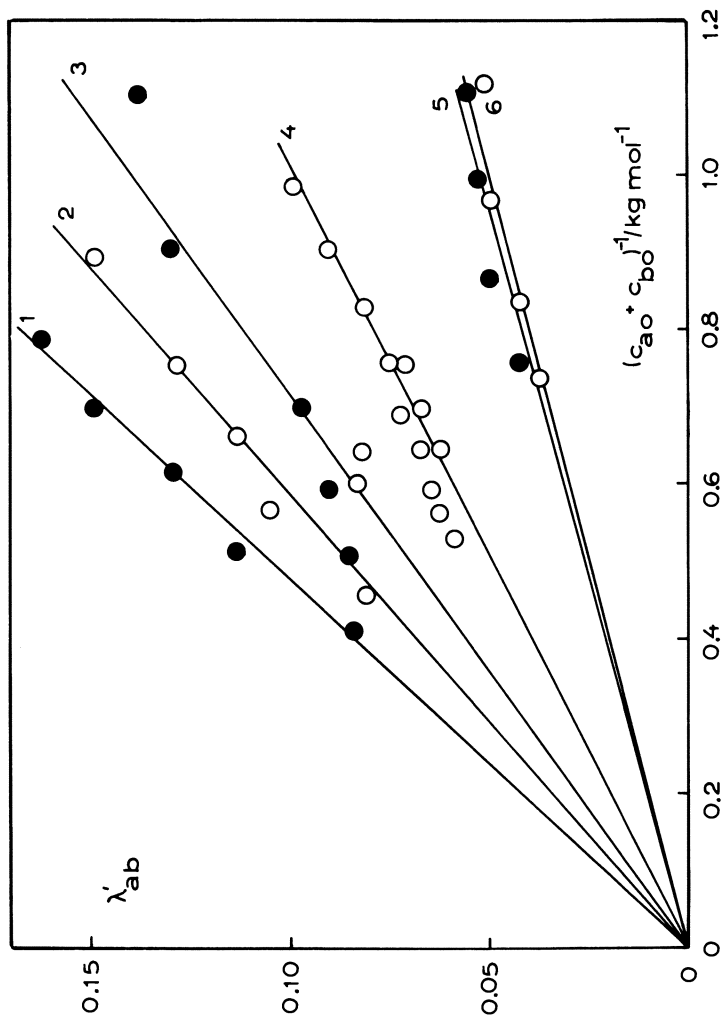
Figure 5. Analysis (21) according to Eq. 7 of gel-point data (22) from reactions of diacid chlorides (adipoyl and sebacoyl chlorides) and POP triols (LHT240, LHT112 (oxypropylated 1,2,6-hexane triols), and LG56 (oxypropylated glycerol)) in bulk and in diglyme solution at 60°C, with $c_{ext} = c_{ao}$

Key: 1, adipoyl chloride and LHT240, v is 37; 2, sebacoyl chloride and LHT240, v is 41; 3, adipoyl chloride and LHT112, v is 66; 4, sebacoyl chloride and LHT112, v is 70; 5, adipoyl chloride and LG56, v is 132; 6, sebacoyl chloride and LG56, v is 136.

pair of values of b given for each system in Table I encompasses the value expected from solution properties(8,9). Hence, the true average value of c_{ext} lies somewhere between $c_{ao} + c_{bo}$ and $c_{ac} + c_{bc}$, as it should.

Behaviour similar to that shown by the polyester-forming systems is shown by the several polyurethane-forming systems which have been studied(3,4,6,15,23-28), and Figure 6 and Table II give the results(29) for polyurethane-forming systems from which network materials have been formed at complete reaction. In general, compared with the polyester-forming systems, curved

Table II. Values of b for polyurethane-forming systems derived(29) from Figure 6 and plots of λ'_{ab} versus $(c_{ac} + c_{bc})^{-1}$ according to equations(7). ν_{DI}/ν - fractional length of diisocyanate residue in the chain of ν bonds (i) $c_{ext} = c_{ao} + c_{bo}$. (ii) $c_{ext} = c_{ac} + c_{bc}$. For explanation of reactants see text and Figures 5 and 6.

System	f	ν	ν_{DI}/ν	b/nm(i)	b/nm(ii)
1. HDI/LHT240	3	33	0.303	0.247	0.400
2. HDI/LHT112	3	61	0.164	0.222	0.363
3. MDI/LHT240	3	30	0.233	0.307	0.488
4. HDI/OPPE-NHI	4	29	0.345	0.240	0.356
5. HDI/OPPE-NH2	4	33	0.303	0.237	0.347

plots of λ'_{ab} versus c_{ext}^{-1} are always obtained, and the values of b, from the initial slopes of such plots are smaller, at least for systems based on aliphatic diisocyanates and POP triols (3,4,6,23,28).

In Figure 6, the larger values of λ'_{ab} for systems 4 and 5 compared with the other systems illustrate the increased opportunities for intramolecular reaction in tetrafunctional compared with trifunctional systems. Further, the smaller values of b for system 5 compared with those for system 1, with the same value of ν, probably indicated that equation(3) relatively undercounts the opportunities for intramolecular reaction for tetrafunctional as compared with trifunctional reactants, so that smaller values of b are required in compensation. System 3, based on aromatic diisocyanate, gives the largest values of b, characteristic of its stiffer chain structure.

Determination of Effective Functionalities from Gelation Data.
Gelation data from reactions at various dilutions are sometimes used to determine chemical functionalities of reactants(30,31). Such a procedure should be viewed with caution as it assumes that the functional form of the dependence of ring-forming parameter upon dilution which is predicted by theory is that obtained in practice, and, as Figure 6 indicates, this assumption is not always justified.
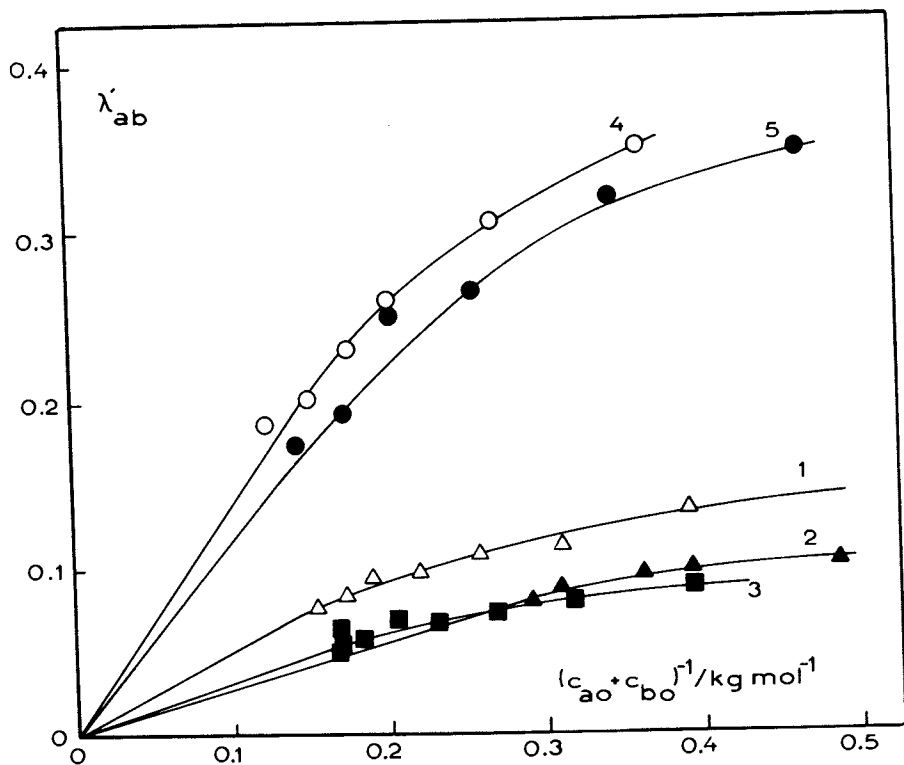
Figure 6. Analysis (29) according to Eq. 7 of gel-point data (25, 26, 28) from reactions of HDI and diphenylmethane diisocyanate (MDI) with POP trilos (LHT-240, LHT112) and tetrols (OPPE-NHI, OPPE-NH2–oxypropylated pentaerythritols) in bulk and in nitrobenzene solution at 80°C, with $c_{ext} = c_{ao} + c_{bo}$.

Systems 1 and 2, HDI and POP triols; 3, MDI and POP triol; 4 and 5, HDI and POP tetrols. Key: 1, HDI and LHT240, v is 33; 2, HDI and LHT112, v is 61; 3, MDI and LHT240, v is 30; 4, HDI and OPPE–NHI, v is 29; 5, HDI and OPPE–NH2, v is 33.

One system studied by the authors[3] used LG56 triol which had been characterised by molar-mass as well as end-group determinations. The data for the samples used are given in Table III, indicating a true number-average functionality (f_n) of between 2.95 and 2.99. The triol was reacted with HDI in bulk (see Figure 1) and at various dilutions in benzene, and values of N_r and α_c determined. To estimate functionality from α_c, equations

Table III.   Characterisation of LG56 triol samples[3]

Sample	EW* ($M_n/g(molOH)^{-1}$)	M_n/g mol^{-1} (M_n/g mol^{-1})	fn (= M_n/EW)
1	1007	3016	2.99
2	1011	2985	2.95

*Equivalent Weight.

(3 - 5) may be recast to give

$$\alpha_c^{\frac{1}{2}} = \frac{1}{(f-1)^{\frac{1}{2}}} + \frac{(f-2)}{(f-1)^{\frac{1}{2}}} \cdot \frac{P_{ab}.\phi(1,3/2)}{c_{ext}} , \qquad (8)$$

according to which a plot of $\alpha_c^{\frac{1}{2}}$ versus c_{ext}^{-1} should be linear with intercept equal to $(f-1)^{-\frac{1}{2}}$, or more strictly $(f_w-1)^{-\frac{1}{2}}$. Figure 7 shows the gelation data obtained[3] plotted according to equation (8) with $c_{ext} = (c_{ao} + c_{bo})$. The dashed line shows a linear plot that could be made, consistent with the data, which leads to $f_w = 2.90$. This value is inconsistent with the known functionality of the triol, according to which the range of possible values of f_w will lie above 2.95 - 2.99. The solid curve is drawn consistent with the known functionality and shows that the data have less scatter than might be expected on the basis of the dashed line. The curved plot in Figure 7, is in fact just an alternative manifestation of the curved λ'_{ab} versus $(c_{ao} + c_{bo})^{-1}$ plot for this system. Note also, that the length of extrapolation from the point at the lowest dilution cannot be reduced as this dilution corresponds to the bulk reaction mixture.

Gel Point and Network Properties

The preceding sections have shown that pre-gel intramolecular reaction always occurs in random polymerisations, and that the amount of such reaction depends on the dilution (c_{ext}^{-1}), molar masses (ν), chain structures (b) and functionalities (f) of the reactants. Intramolecular reaction leads to loops of finite size in the network material finally formed by a reaction mixture. Such loops may be elastically ineffective and have marked effects on the properties of the material. The present section investigates the magnitudes of such effects with regard to shear modulus and Tg.
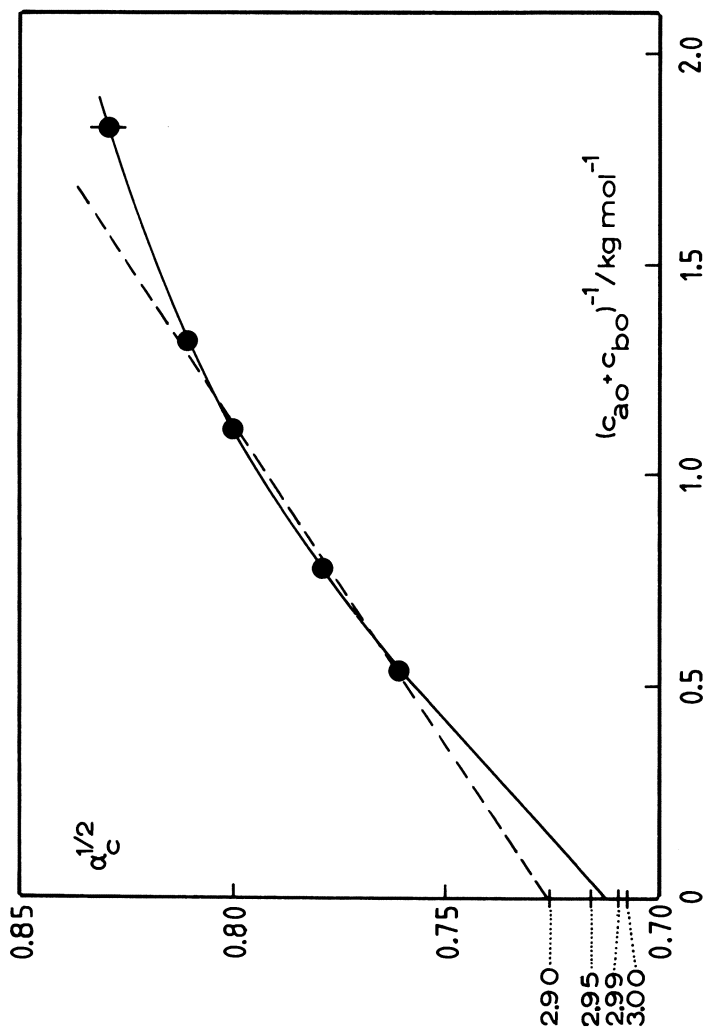
Figure 7. Gelation data (3) plotted according to Eq. 8 to determine an effective functionality. Conditions: reactions at r = 1; HDI and LG56 at 70°C in bulk and in benzene solution; values of f_w correspond to indicated intercepts on the $\alpha_c^{1/2}$ axis. Reproduced, with permission, from Ref. 21. Copyright 1980, Steinkopf.

Gel Point and Shear Modulus.   Trifunctional and tetrafunc-
tional polyurethane(25,26,28) and trifunctional polyester net-
works(32) have been studied. The gelation data for the reaction
systems forming the polyurethane networks were those discussed
with reference to Figure 6 and Table II.

Figure 8 illustrates(29) the close relationship between the
chain defining the molar mass between junction points of the
perfect network (M_c^o) and the chain of ν bonds of the preceding
sections. The illustrations in (b) and (c) are for the RA_2 +
RB_4 random polymerisations relevant to systems 4 and 5 of Figure
6 and Table II. Apart from possible, small end-group effects M_c^o
is in general the molar mass of the chain of ν bonds.

The networks studied were prepared from reactions carried
out at different initial dilutions. Aliquots of reaction mixtures
were transferred to moulds, which were maintained at the reaction
temperature under anhydrous conditions, and were allowed to pro-
ceed to complete reaction(32). Sol fractions were removed and
shear moduli were determined in the dry and equilibrium-swollen
states at known temperatures using uniaxial compression or a
torsion pendulum at 1Hz. The procedures used have been described
in detail elsewhere(26,32). The shear moduli(G) obtained were
interpreted according to Gaussian theory(33,34,35) to give values
of M_c, the effective molar mass between junction points, consis-
tent with the affine behaviour expected at the small strains
used(34,35).

Results for the polyurethane systems of Figure 6 and Table II
are shown in Figure 9, where M_c/M_c^o is plotted versus $p_{r,c}$, the
extent of intramolecular reaction at gelation(29). Here

$$p_{r,c} = \alpha_c^{\frac{1}{2}} - (f-1)^{-\frac{1}{2}}. \tag{9}$$

$p_{r,c} = 0$ corresponds to the ideal (Flory-Stockmayer) gel point,
and $M_c/M_c^o = 1$ to the perfect network. In all cases in Figure 9,
$M_c/M_c^o > 1$ and tends to 1 as $p_{r,c} \rightarrow 0$. Thus, only in the limit of
a perfect gelling system is a perfect network achieved. The
pre-gel intramolecular reaction, which causes α_c to exceed $1/(f-1)$
in value, also produces elastically ineffective loops which have
marked effects on the moduli of the dry networks. The different
slopes of the pairs of lines for similar systems, namely, 1 and
2, and 4 and 5, show that larger proportions of the loops formed
pre-gel are elastically ineffective, the lower is the value of
M_c^o(or ν) for the reactants. That is, system 1 shows higher values
of M_c/M_c^o than system 2 for a given value of $p_{r,c}$ and system 4
shows higher values than system 5. The same relative behaviour
has also been found for POP triol-based polyester networks(32).

The broken curves in Figure 9 are the expected values of
M_c/M_c^o for trifunctional and tetrafunctional networks, assuming
that all the ring structures formed are of the smallest size
(ν bonds), and that only the ring structures formed pre-gel give
elastically ineffective loops(29,32). They show that intramolecular

(a)

(b)

(c)
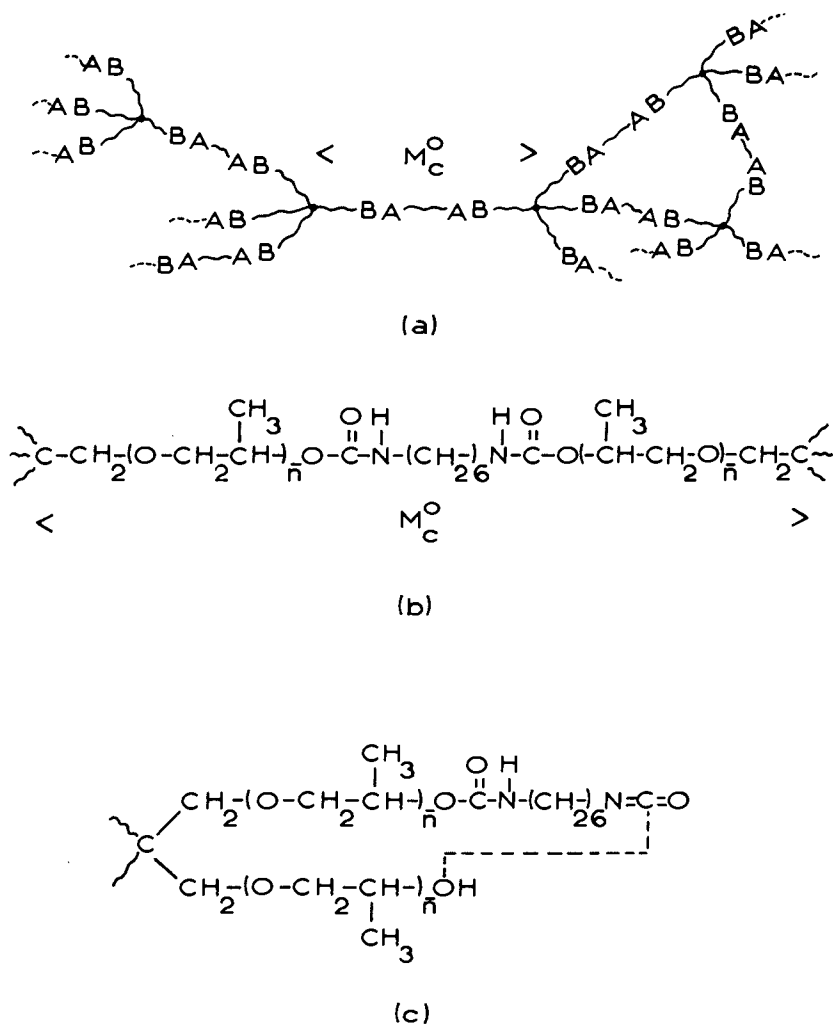
Figure 8. Part of a tetrafunctional network formed from an RA₂ and RB₄ polymerization corresponding to $M_C°$, the molar mass between junction points of the perfect network (a). Detail of the chain structure defining $M_c°$ for HDI reacting with an OPPE, n is the number-average degree of polymerization of each arm with respect to oxypropylene units, (b). Part of the chain structure defining ν, the number of bonds in the chain forming the smallest ring structure (C), for the reaction system in (b) (29). Reproduced, with permission, from Ref. 21. Copyright 1980, Steinkopf.
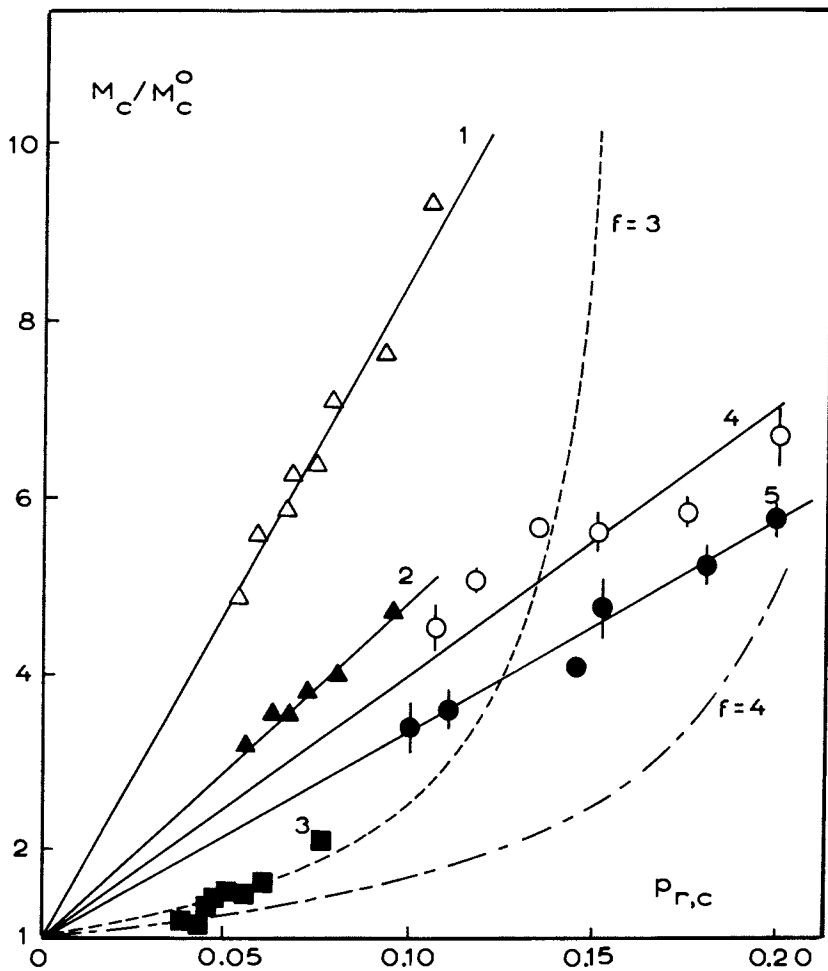
Figure 9.   Molar mass between elastically effective junction points (M_c) relative to that for the perfect network ($M_c°$) versus extent of intramolecular reaction at gelatin ($p_{r,c}$) for polyurethane networks (29).

Reaction systems defined in Figure 6. Key: ——, experimental points for systems 1, 2, 4 and 5; − − −, calculated curves for trifunctional networks; − · − ·, tetrafunctional networks. Assume that network defects are introduced by pre-gel intramolecular reaction leading to only the smallest loops (those of v bonds).

reaction should have a more marked effect on the modulus of tri-
functional compared with tetrafunctional networks. Such relative
behaviour is shown by systems 1 and 2 compared with 4 and 5.
However, the results for these systems do not follow the calculated
curves, indicating that more complicated ring structures, which
remove relatively more junction points, are contributing to the
elastically ineffective loops. However, the results for system 3
do follow the appropriate calculated curve. The simplest inter-
pretation would be that the stiffer MDI/POP chain in this system
yields a different distribution of sizes of ring structures, in
which rings are predominantly of the smallest size and that all
network defects are produced by pre-gel intramolecular reaction.
This interpretation is obviously over-simplified as there is no
reason a priori why the distribution of ring sizes should be
different for system 3, and some elastically ineffective loops
must be introduced post-gel. The similar values of M_C/M_C^o (or
higher relative moduli) for system 3 could result in part from
the stiffer, aromatic chains giving stronger inter-chain inter-
actions.

   Gel Point and Tg. The variation of Tg with α_c was investi-
gated(18,26,29) for dry networks formed from system 3 of Figure
9 at different initial dilutions of reaction mixtures. Measure-
ments were carried out at 1Hz using a torsion pendulum(26). The
results were shown in Figure 10. The two limiting values of Tg
for this system correspond to networks with $M_C = \infty$ and $M_C = M_C^o$.
Thus, the horizontal broken line gives the minimum Tg, that of a
linear MDI/POP polymer having a repeat unit of molar mass equal
to M_C^o, and the maximum value of Tg at $\alpha_c = 0.5$ was obtained by
extrapolation of $(1/M_C, Tg)$ data to $1/M_C^o$.
   The variation of Tg with α_c (or M_C) is a reflection of the
influence of junction-point density on the freedom of segmental
motion. The maximum range of Tg values shown, 301 to 312K,
possibly reflects the maximum influence for these MDI/POP triol
systems.

   Gel Point and Properties of Networks from Bulk Reaction Sys-
tems. The results in Figure 9 show clearly that the modulus of
(dry) networks formed at complete reaction depend strongly on the
amount of pre-gel intramolecular reaction that has occurred.
Even reactions in bulk, as indicated by the points at the lowest
values of $p_{r,c}$ for the various systems, yield networks with moduli
less than those predicted for the perfect networks for given
reactants.
   As is clear from the earlier discussions of pre-gel intra-
molecular reaction, such reaction in principle always occurs in
random polymerisations, although its amount may be reduced by
using reactants of higher molar mass, lower functionalities, and
stiffer chain structures. Thus, the use of end-linking reactions
to produce model networks (for example(35) and references quoted
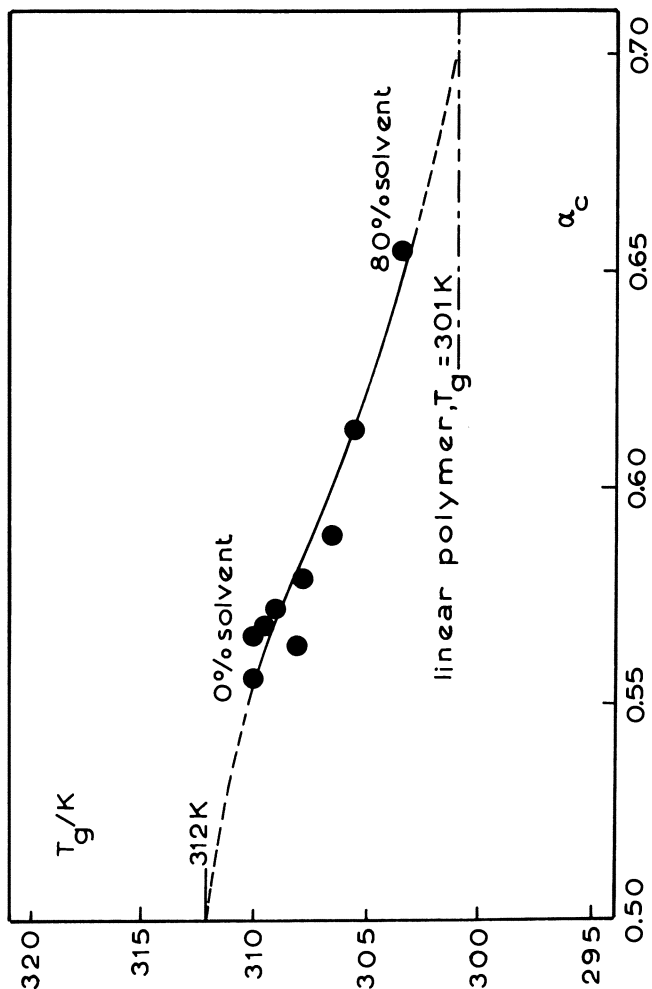
Figure 10. Tg versus α_c for dry, trifunctional polyurethane networks, ● (26). Reaction systems: MDI/LHT240 (system 3 of Figure 9), M_c° is 710 g/mol, v is 30, at various initial dilutions of reactants. – · – · is MDI/POP diol. $M_{repeat} = M_o^\circ$.

therein) does not in general lead to perfect networks. However, the results in Figure 9, in particular, show that the use of given reactants at various initial dilutions, linked with the determination of gel points and moduli, can give a measure of the network imperfections introduced by pre-gel intramolecular reaction.

The moduli and Tg's of the networks formed from the bulk reactions of the five systems of Figure 9 are shown in Table IV(29). The first five columns define the systems, the next two give the experimental values of G(at 298K) and Tg, and the last three give the values of $p_{r,c}$, M_c, and $G/G°$. The last quantity is the reduction in rubbery shear modulus on the basis of that expected for the perfect network(G°). $G/G°$ is in fact equal to $M_c°/M_c$.

The network from system 3 is distinct from the rest, being a glass at room temperature and also having a rubbery shear modulus near the value expected on the basis of G°. Possible reasons for this high value of $G/G°$ follow those discussed previously with reference to $M_c/M_c°$ and Figure 9. The more flexible chains of the aliphatic systems give lower values of Tg, resulting in elastomers at room temperature.

In general, the factor by which G is reduced depends on $M_c°$, f, chain stiffness, and the initial concentrations of reactive groups obtainable in bulk, in a manner which still needs to be resolved in detail. However, for bulk reaction mixtures, the moduli of networks with relatively flexible chain structures can be reduced by a factor of five below those expected for network formation in the absence of pre-gel intramolecular reaction.

Deviations from Gaussian Behaviour. It was generally found that the networks studied in compression(25,28,32) had small but significant deviations from Gaussian stress-strain behaviour. These have been discussed in detail for the polyester systems(32), where it was found that the deviations decreased as M_c increased, and for values of M_c greater than about 10^4 g mol^{-1} the deviations became negligible. They depend principally on M_c and not on whether a network was measured in the dry or swollen state. Thus, for the short chains between junction points in the present networks, the deviations were taken as reflecting the departures of the density distribution of end-to-end vectors from Gaussian form.

Table IV. Shear modulus and Tg of polyurethane networks prepared from bulk reactios (29). G(298K) - shear modulus at 298K, (a) from uniaxial compression, (b) from torsion pendulum measurements. G/G^o is the rubbery shear modulus relative to that expected for the perfect network well above Tg.

system	f	$(\alpha^o_c)^{\frac{1}{2}}$	ν	M^o_c/g mol^{-1}	G(298K)/Nm^{-2}	Tg/K	Pr,c	M_c/g mol^{-1}	G/G^o
1 HDI/LHT240	3	0.71	33	635	1.0×10^6 (a)	255	0.053	3024	0.21
2 HDI/LHT112	3	0.71	61	1168	0.8×10^6 (a)	228	0.055	3650	0.32
3 MDI/LHT240	3	0.71	30	705	3.0×10^9 (b)	311	0.034	881	0.80
4 HDI/OPPE-NH1	4	0.58	29	500	1.1×10^6 (b)	275	0.108	2273	0.22
5 HDI/OPPE-NH2	4	0.58	33	586	1.2×10^6 (a)	271	0.100	1953	0.30

The deviations from Gaussian stress-strain behaviour introduce uncertainties into the values of M_c/M_c^o discussed previously in this paper. However, such uncertainties have been shown to be of secondary importance compared with the ranges of M_c/M_c^o values found for networks from different reaction systems(25,32).

The observed deviations from Gaussian stress-strain behaviour in compression were in the same sense as those predicted by the Mooney-Rivlin equation, with modulus increasing as deformation ratio(Λ) decreases. The Mooney-Rivlin equation is usually applied to tensile data but can also be applied compression data(33). According to the Mooney-Rivlin equation

$$\sigma/(\Lambda-\Lambda^{-2}) = 2C_1 + 2C_2/\Lambda, \qquad (10)$$

where σ is the stress on the basis of undeformed cross-sectional area and C_1 and C_2 are constants, with C_1 associated with the shear modulus.

Figure 11 shows plots according to equation(10) of stress-strain data for triol-based polyester networks formed from the same reactants at three initial dilutions (0% solvent(bulk), 30% solvent and 65% solvent). Only the network from the most dilute reactions system has a strictly Gaussian stress-strain plot ($C_2 = 0$), and the deviations from Gaussian behaviour shown by the other networks are not of the Mooney-Rivlin type. As indicated previously, they are more sensibly interpreted in terms of departures of the distribution of end-to-end vectors from Gaussian form.

The deviations from Gaussian stress-strain behaviour for the tetrafunctional polyurethane networks of Figure 9 are qualitatively similar to these found for the trifunctional polyester networks(25), and the error bars on the data points for systems 4 and 5 in Figure 9 indicate the resulting uncertainties in M_c/M_c^o. It is clear that such uncetainties do not mask the increases in M_c/M_c^o with amount of pre-gel intramolecular reaction.

Conclusions

The factors which influence pre-gel intramolecular reaction in random polymerisations are shown to influence strongly the moduli of the networks formed at complete reaction. For the polyurethane and polyester networks studied, the moduli are always lower than those expected for no pre-gel intramolecular reaction, indicating the importance of such reaction in determining the number of elastically ineffective loops in the networks. In the limit of the ideal gel point, perfect networks are predicted to be formed. Perfect networks are not realised with bulk reaction systems. At a given extent of pre-gel intramolecular
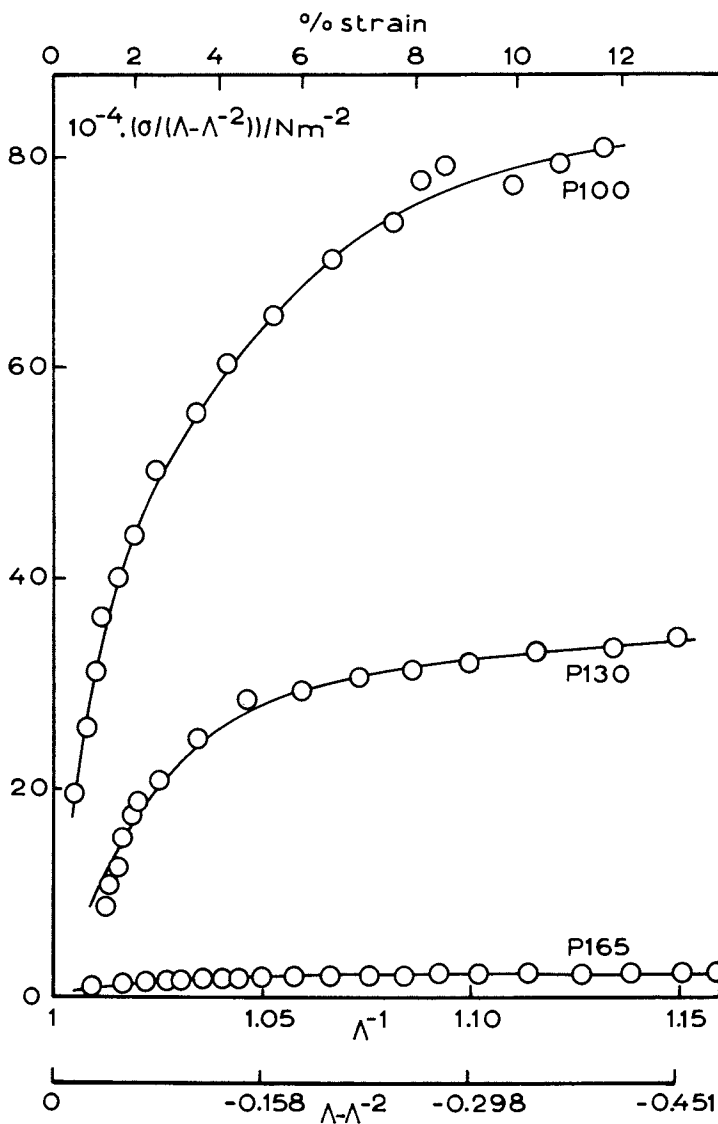
Figure 11. Mooney–Rivlin plot of stress–strain data (32) for three triol-based polyester networks prepared from sebacoyl chloride and LHT240 at various initial dilutions in diglyme as solvent. Conditions: P100 is 0% solvent; P130 is 30% solvent; P165 is 65% solvent.

reaction ($p_{r,c}$), the reductions in moduli below those expected
for the perfect networks are larger for trifunctional as compared
with tetrafunctional networks of similar chain structures, for
more flexible chains, and for reactants of lower molar mass.

Interesting deviations from Gaussian stress-strain behaviour
in compression have been observed which related to the M_c of the
networks formed, rather than their degrees of swelling during
compression measurements.

The reactants used to form the networks studied are generally
of lower molar mass than those used by other workers to form
perfect networks (e.g.(35)). However, the present results do
indicate that very little pre-gel intramolecular reaction can have
a marked effect on modulus. For example, for $p_{r,c}$ = 0.05, or α_c
= 0.58, with a trifunctional polyurethane-forming system of M_c^0
= 635g mol^{-1}, the modulus is reduced by a factor of five below
that calculated on the basis of the small-strain(affine) behaviour
of the perfect network. As a result, it is recommended that the
effective absence of pre-gel intramolecular reaction in end-
linking reactions to form 'perfect' networks be confirmed by
experiment rather than be assumed.

The use of the same reactants at different initial dilutions
to give dry networks of different moduli not only helps to define
a scale of network imperfections but also enables the range of
materials which can be prepared from given reactants to be use-
fully extended.

Literature Cited

1. Stanford, J.L.; Stepto, R.F.T. J.Chem.Soc.Faraday Trans.I 1975,
   71, 1292.
2. Stepto, R.F.T; Waywell, D.R. Makromol.Chem. 1972, 152, 247;
   263.
3. Stanford, J.L.; Stepto, R.F.T. Br.Polymer J. 1977, 9, 124.
4. Ahmad, Z. Ph.D. Thesis, University of Manchester, England, 1978.
5. Stepto, R.F.T. "Developments in Polymerisation-III'; Haward,
   R.N., Ed.; Applied Science Publishers Ltd.: London, in press;
   Chap. 3.
6.   Stepto, R.F.T. Faraday Disc.Chem.Soc. 1974, 57, 69.
7. Stanford, J.L.; Stepto, R.F.T. J.Chem.Soc.Faraday Trans. I
   1975, 71, 1292; Stanford, J.L., Stepto, R.F.T.; Waywell, D.R.
   J.Chem.Soc. Faraday Trans.I 1975, 71, 1308.
8. Kurata, M.; Iwama, M.; Kamada, K. "Polymer Handbook";
   Brandrup, J.; Immergut, E.H., Eds., Interscience Publishers:
   London, 1966; sect. IV-1.
9. Flory, P.J. "Statistical Mechanics of Chain Molecules";
   Intersciences Publishers: London, 1969; p.40.
10. Flory, P.J., "Principles of Polymer Chemistry"; Cornell
    University Press: Ithaca, New York, 1953; Chap. IX.
11. Gordon, M.; Temple, W.B. Makromol.Chem. 1972, 152, 277.
12. Gordon, M.; Temple, W.B. Makromol.Chem. 1972, 160, 263.
13. Temple, W.B. Makromol.Chem. 1972, 160, 277.
14. Stanford, J.L., Ph.D. Thesis, University of Manchester,
    England, 1972.
15. Cawse, J.L.; Stanford, J.L.; Stepto, R.F.T. Proc. 26th IUPAC
    Int.Symp. on Macromolecules, Mainz 1979, p.693.
16. Askitopoulos, V.; M.Sc. Thesis, University of Manchester,
    England, 1981.
17. Lloyd, A.C., M.Sc. Diss., University of Manchester, England,
    1981.
18. Stepto, R.F.T. Polymer 1979, 20, 1324.
19. Frisch, H.L. 128th Meeting Amer.Chem.Soc., Polymer Div.,
    Minneapolis, 1955.
20. Kilb, R.W. J.Physic.Chem. 1958, 62, 969.
21. Ahmad, Z.; Stepto, R.F.T. Colloid and Polymer Sci. 1980, 258
    663.
22. Smith, R.S.; Stepto, R.F.T. Makromol.Chem. 1974, 175, 2365.
23. Hopkins, W.; Peters, R.H.; Stepto, R.F.T. Polymer 1974, 15,
    315.
24. Hunt, N.G.K.; Stepto, R.F.T.; Still, R.H. Proc. 24th IUPAC
    Int.Symp. on Macromolecules, Dublin 1977, p.723.
25. Hunt, N.G.K.; Stepto, R.F.T.; Still, R.H. Proc. 26th IUPAC
    Int.Symp. on Macromolecules, Mainz, 1979, p.697.
26. Cawse, J.L. Ph.D. Thesis, University of Manchester, England,
    1979.
27. Yoji Hirasawa; Stepto, R.F.T.; Still, R.H. Proc. 28th IUPAC
    Int.Symp. on Macromolecules, Strasbourg, 1981, p.117.

28. Rose, S.V.; Stanford, J.L. unpublished work.
29. Stanford, J.L.; Stepto, R.F.T.; Still, R.H. in press;
    Presented in part at Div.Organic Coatings and Plastics Chem.,
    181st ACS National Meeting, Atlanta, 1981, p.164.
30. Fogiel, A.W. Macromolecules 1969, 2, 581.
31. Guise, G.B.; Zoch, C.G. J.Macromol.Sci.-Chem. 1976, A10, 1161;
    J.Polymer Sci. 1976, Symp. No. 55, 61.
32. Fasina, A.B.; Stepto, R.F.T. Makromol.Chem. 1981, 182, 2479.
33. Dusek, K.; Prins, W. Adv.Polymer Sci. 1969, 6, 1.
34. Flory, P.J. Polymer 1979, 20, 1317.
35. Mark, J.E. Pure and Appl.Chem. 1981, 53, 1495.

Structure and Elasticity of Loose Step Polyaddition Networks

KAREL DUŠEK and MICHAL ILAVSKÝ

Czechoslovak Academy of Sciences, Institute of Macromolecular Chemistry, 162 06 Prague 6, Czechoslovakia

For imperfect epoxy-amine or polyoxypropylene-urethane networks ($M_c = 10^3 - 10^5$), the front factor, A, in the rubber elasticity theories was always higher than the phantom value which may be due to a contribution by trapped entanglements. The crosslinking density of the networks was controlled by excess amine or hydroxyl groups, respectively, or by addition of monoepoxide. The reduced equilibrium moduli (equal to the concentration of elastically active network chains) of epoxy networks were the same in dry and swollen states and fitted equally well the theory with chemical contribution and $A \approx 1$ or the phantom network value of A and a trapped entanglement contribution due to the similar shape of both contributions. For polyurethane networks from polyoxypropylene triol (M=2700), $A \approx 2$ if only the chemical contribution was considered which could be explained by a trapped entanglement contribution.

Experimental examination of predictions of the new rubber elasticity theory (1,2) continues to be of great interest. However, numerous conflicting data as to the feasibility of reaching the phantom state behaviour and possible contribution coming from permanent (equilibrium) interactions between elastically active network chains (EANC)-usually called trapped entanglements-have accumulated in the literature (2-15). Experimental difficulties in reaching true equilibrium stress-strain isotherms may be a source of discrepancies, but the disagreement does not disappear even if there is no doubt about reaching the equilibrium state. A poor description of the network structure in terms of the concentration of EANC's, ν_e, may be, however, very serious. Perfect (and therefore, well-defined) networks, in which ν_e is given by the concentration of precursor elastomer chains, are sometimes preferred, but it is practically impossible to obtain a perfect structure due to (a) difficulty in reaching full conversion of functional

groups and (b) wastage of some bonds in closing elastically in-
active cycles (EIC) which always competes with the formation of
EANC´s. Possible small errors in the determination of the con-
centration of functional groups or molar ratios in alternating
type polyreactions may further contribute to a poor description
of the network structure. Although the resulting degree of imper-
fection may be small (e.g., a few percent in conversion or bonds
wasted in EIC) (16-19), a loss in ν_e in endlinked networks amount-
ing to 20-40% would not be surprising. A statement like that the
sol fraction was below 1%, which should have indicated the per-
fectness of the structure, does not mean much, because an increase
in the gel fraction from 99 to 100% usually means an increase in
ν_e by a factor of 1.3-1.4. It follows that "perfect" networks
do not have any perfect structure and, if the existing degree of
imperfectness is neglected, these networks are not well defined
any more.

     Well defined but imperfect networks widely differing in ν_e,
that are chemically inert and are prepared using non-stoichio-
metric alternating step polyaddition systems, offer another object
of study of relations between equilibrium elasticity and concen-
tration of EANC´s. Instead of using precursor chains of varying
length, the length and concentration of EANC´s is varied by an
excess of functional groups of one kind. In this way, dangling
chains are produced and the network chains are branched with many
side chains attached to them in contrast to the majority of smooth
unbranched chains in "perfect" networks.

     In this contribution, we report equilibrium modulus and sol
fraction measurements on diepoxide+monoepoxide-diamine networks
and polyoxypropylene triol-diisocyanate networks and a comparison
with calculated values. A practically zero (epoxides) or low
(polyurethanes) Mooney-Rivlin constant C_2 and a low and accounted
for wastage of bonds in elastically inactive cycles are the
advantages of the systems. Plots of reduced modulus against the
gel fraction have been used, because they have been found to mini-
mize the effect of EIC, incompleteness of the reaction, or possible
errors in analytical characteristics (16-20). A full account of
the work on epoxy and polyurethane networks including the statis-
tical derivation of various structural parameters will be publish-
ed separately elsewhere.

Experimental

     Epoxide networks were prepared from diglycidyl ether of
4,4´-dihydroxydiphenyl-2,2-propane (98.2% by gas chromatography),
phenyl glycidyl ether (99.3%) and recrystallized 4,4´-diaminodi-
phenylmethane. The crosslinking density was controlled by the
initial molar ratio $2[NH_2]/[epox] = r_A = 2.3-1.0$ and by the
fraction of epoxy groups in the monoepoxide, s. The reaction time
was 16 h at 65°C and 5 h at 130°C. The residual concentration of
epoxy groups was determined by IR spectrometry at 915 cm^{-1}.

Equilibrium stress-strain dependences were determined in extension
using a stress relaxation arrangement described earlier (21). Dry
non-extracted samples were measured at 150°C in nitrogen atmosphe-
re and extracted samples swollen in dimethylformamide were meas-
ured at 25°C. The equilibrium value of stress σ_e was reached
within 2-4 min except of a few dry samples with the lowest ν_e, for
which the equilibrium stress was determined using an extrapolation
procedure described earlier (21).

Polyurethane networks were prepared from polyoxypropylene
(POP) triols(Union Carbide Niax Polyols) after removal of water
by azeotropic distillation with benzene. For Niax LHT 240, the
number-average molecular weight determined by VPO was 710 and the
number-average functionality f_n, calculated from M_n and the con-
tent of OH groups, determined by using excess phenyl isocyanate
and titration of unreacted phenyl isocyanate with dibutylamine,
was 2.78; the content of residual water was 0.02 wt.-%. For the
Niax LG-56, M_n=2630, f_n=2.78, and the content of H_2O was 0.02wt.-%.
The triols were reacted with recrystallized 4,4´-diphenylmethane
diisocyanate in the presence of 0.002 wt.-% dibutyltin dilaurate
under exclusion of moisture at 80°C for 7 days. The molar ratio
r_{OH} = [OH]/ [NCO] varied between 1.0 and 1.8. For dry samples, the
stress-strain dependences were measured at 60°C in nitrogen atmo-
sphere. The relaxation was sufficiently fast and no extrapolation
to infinite time was necessary.

Calculation of structural parameters

The required structural parameters of the networks – the sol
fraction, w_s, the concentration of EANC´s in the gel, ν_{eg}, the
number-average functionality of elastically active crosslinks (21),
f_e, and the trapping factor (22,23), T_e, were calculated using
the theory of branching processes based on a tree-like model. For
epoxide networks, the substitution effect in the amine groups of
the diamine was taken into account. The calculation procedure was
described in ref. 20. For polyurethanes, the procedure derived for
a random ring-free diol-triol-diisocyanate reaction (17) can be
used in the calculation of w_s and ν_{eg}; the calculation of f_e and
T_{eg} follows from an analogy with epoxy networks. We do not give
explicit relations for the network parameters here, but only
summarize the principles on which the calculation is based.

The key parameter for the postgel stage is the extinction
probability. It is the probability that a bond issuing from a
given building unit has only a finite continuation, i.e. that the
respective subtree is finite. The other possibility for the issu-
ing bond is that it has a continuation to infinity (to the surface
of the sample). The sol fraction is composed of building units
issuing bonds with finite continuation only. The number of EANC´s
is derived from the number of elastically active crosslinks; an
elastically active crosslink is a junction issuing at least three
bonds with infinite continuation. Each junction issuing j bonds

with infinite continuation (j≥3) contributes j/2 to the number of
EANC´s. The value of f_e is the mean number of bonds with infinite
contribution averaged over elastically active crosslinks. The
Langley´s type trapping factor (23,24) is derived from the pro-
bability of a contact between two monomer units located in EANC´s.
The EANC´s are composed of units issuing just two bonds with in-
finite continuation. Units issuing more or less such bonds cannot
be part of an EANC, because they would themselves be elastically
active crosslinks or part of a dangling chain. The trapping factor
thus increases as the square of the fraction of units in EANC´s.

     Of interest are the critical exponents m in the proportion-
ality between network parameters $X = w_g$, ν_e, ν_{eg}, T_e, T_{eg}, f_e
(the subscript g indicates that the respective quantity is related
only to the gel) and the distance from the gel point measured as
a difference between the gel point (critical) ξ_c and the actual ξ
conversion $X \propto (\xi - \xi_c)^m$ for lim $(\xi - \xi_c) = 0$. For the tree-like
model, the following values of the critical exponents have been
found:

w_g	ν_e	ν_{eg}	f_e	T_e	T_{eg}
1	3	2	0	4	3

     In the foregoing considerations, formation of elastically
inactive cycles and their effect have not been considered. For
epoxy networks, the formation of EIC was very low due to the
stiffness of units and could not been detected experimentally:
the gel point conversion did not depend on dilution in the range
0-60% solvent; therefore, the wastage of bonds in EIC was neglect-
ed. For polyurethanes, the extent of cyclization was determined
from the dependence on dilution of the critical molar ratio
[OH] /[NCO] necessary for gelation (25) and this value was used
for the statistical calculation of the fraction of EIC and its
effect on ν_{eg} as described in (16). The calculation has shown
that the fraction of bonds wasted in EIC was 2-2.5% and 1.5-2% for
network from LHT-240 and LG-56 triols, respectively.

Results and Discussion

     According to the rubber elasticity theory (1,2), the equi-
librium shear modulus, G_e, is proportional to the concentration
of EANC´s and an additional contribution due to trapped entangle-
ments may also be considered:

$$G_e = G_{ec} + G_{ee} \qquad (1)$$

where for dry non-extracted networks

$$G_{ec} = ART\nu_e = ART\nu_{eg}w_g \; , \quad G_{ee} = RT\epsilon T_e = RT\epsilon T_{eg}w_g \qquad (2)$$

and for extracted swollen networks

$$G_{ec} = ART\nu_{eg}v_2^{1/3}w_g^{2/3} \quad , \quad G_{ee} = RT\mathcal{E}^{\check{}}v_2^{1/3}w_g^{2/3}T_{eg} \qquad (3)$$

Here, R is the gas constant, T is temperature in K, ν_e and ν_{eg} are concentrations of EANC's in the unit volume of the non-extracted sample and gel, respectively, T_e and T_{eg} are the corresponding values of the trapping factor, and v_2 is the volume fraction of the polymer; $\mathcal{E}$ and $\mathcal{E}^{\check{}}$ are proportionality constants.

According to the theory (1,2), for phantom imperfect (cf. al-so (17)) network the front factor A assumes the value

$$A_{ph} = (f_e - 2) /f_e \qquad (4)$$

for chemically tetrafunctional crosslink f_e increases from 3 to 4 and for trifunctional crosslinks it is 3 and independent of con-version.

The phantom network behaviour corresponding to volumeless chains which can freely interpenetrate one through the other and thus to unrestricted fluctuations of crosslinks should be approach-ed in swollen systems or at high strains (proportionality to the Mooney-Rivlin constant C_1). For suppressed fluctuations of cross-links, which then are displaced affinely with the strain, A for the small-strain modulus (equal to C_1+C_2) approaches unity. This situation should be characteristic of bulk systems. The constraints arising from interchain interactions important at low strains should be reflected in an increase of A above the phantom value and no extra G_{ee} contribution to the modulus is necessary. The upper limit of the predicted equilibrium modulus corresponds therefore, A = 1.

The G_{ee} contribution of the form given Eq.(2) represents the simplest form of permanent interchain interactions. The value of G_{ee} at T_{eg}=1 and w_g=1, i.e. the G_{ee} contribution of a perfect net-work, has been assumed equal to the plateau modulus of the corres-ponding linear polymer (10,15,23). This assumption has not always been confirmed and, therefore, for the purpose of this work we prefer to consider $\mathcal{E}$ of $\mathcal{E}^{\check{}}$ as proportionality constants.

The analyses of experimental data with respect to the value of A and G_{ee} contribution are usually carried out by rearranging Eqs. (1) and (2) into the form

$$G_e/T_e = ART(\nu_e/T_e) + RT\mathcal{E} \qquad (5)$$

The plot G_e/T_e vs. ν_e/T_e yields then A from the slope and from the intercept (Langley-Greassley plot). The applicability of this plot will be commented on below and it will be shown that this plot is not very suitable for endlinked networks with ν_e varying as a function of the conversion or molar ratio of com-ponents. The similarity between the shapes of ν_e and T_e and the resulting relative constancy of ν_e/T_e is the reason. The other disadvantage of analysis of experimental data using Eq.(1) or (5) based on the difference between the values G_e and ν_e is the sen-

sitivity of ν_e and T_e to composition, conversion, formation of
elastically inactive cycles, etc. This sensitivity is greatly re-
duced if one replots the data as G_e or ν_e against w_g (16-20). For
different initial compositions (cf. e.g. (20)), the log ν_{eg} vs.
log w_g plots are close and run in parallel, so that a small ver-
tical superposition can yield a single generalized curve. Although
this treatment does not allow the determination of A and $\mathcal{E}$ in one
step, in contrast to the Langley-Greassley plot, it is much safer
due to a considerable reduction of the effect of structural un-
certainty.

Epoxide Networks. The sol fraction (Figure 1) fits well the
calculated dependence for the final conversion of epoxide groups
determined by IR spectrometry, which may serve as evidence of the
applicability of the tree-like model. Only for the highest sol
fraction, the experimental points lie somewhat below the theor-
etical curve; difficulty involved in a full extraction of a rela-
tively high-molecular-weight and branched material may be the
reason. The calculated dependences of log ν_{eg} vs. low w_g obtained
by varying the molar ratio r_A or conversion run very close to each
other and are parallel. They have been superimposed by a small
vertical shift. This shift has been applied to the reduced moduli
$G_d = G_e/w_g$ and $G_d = G_e/v_2^{1/3} w_g^{2/3}$, respectively, according to Eqs. (2)
and (3) for dry and swollen networks in order to get the super-
imposed moduli G_d^s in Figure 2.

The results of stress-strain measurements can be summarized
as follows: (1) the reduced stress $G_e/(\Lambda - \Lambda^{-2})$ (Λ is the extension
ratio) is practically independent of strain so that the Mooney-
Rivlin constant C_2 is practically zero for dry as well as swollen
samples ($C_2/C_1 = 0 \pm 0.05$) ; (2) the values of G_d^s are practically the
same whether obtained on dry or swollen samples; (3) assuming
that $G_{ee} = 0$, the data are compatible with the chemical contribution
and $A \approx 1$; (4) the difference between the phantom network dependence
with the value of A given by Eq.(4) and the experimental moduli
fits well the theoretical dependence of G_{ee} in Eq.(2) or (3). The
proportionality constant $\mathcal{E}$ in G_{ee} for series of networks with
s equal to 0, 0.2, 0.33, and 0.5 was practically the same –
(8.2, 6.3, 8.8, and 8.5)x10^{-4} mol/cm^3 with the average value
7.95x10^{-4} mol/cm^3. Results (1) and (2) suggest that phantom
network behavior has been reached, but the result(3) is contrary
to that. Either the constraints do survive also in the swollen
and stressed states, or we have to consider an extra contribution
due to the incrossability of "phantom" chains. The latter expla-
nation is somewhat supported by the constancy of $\mathcal{E}$ in Eq.(2) for
a series of samples of different composition.

Polyurethane Networks. Again, for $r_{OH} \geqslant 1$ the sol fraction
fits well the theoretical curves, if the measured values of the
average functionality f_n of the polyoxypropylene (POP) triol , the
final conversion of isocyanate groups, and the formation of
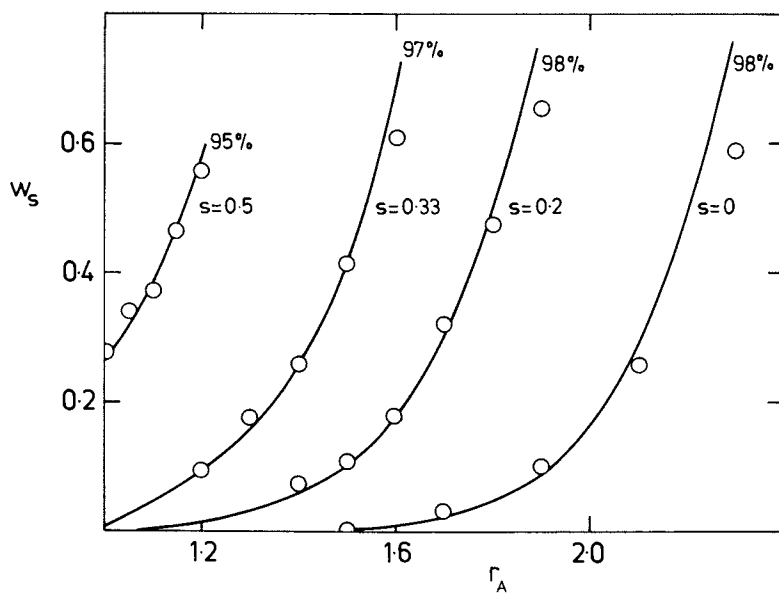
Figure 1.   Theoretical dependence of sol fraction w_s vs. molar ratio r_A is $2[NH_2]/$ [epox] for epoxyamine networks containing varying fraction of epoxy groups in monoepoxide s. Final conversion of epoxy groups in mol percent indicated.
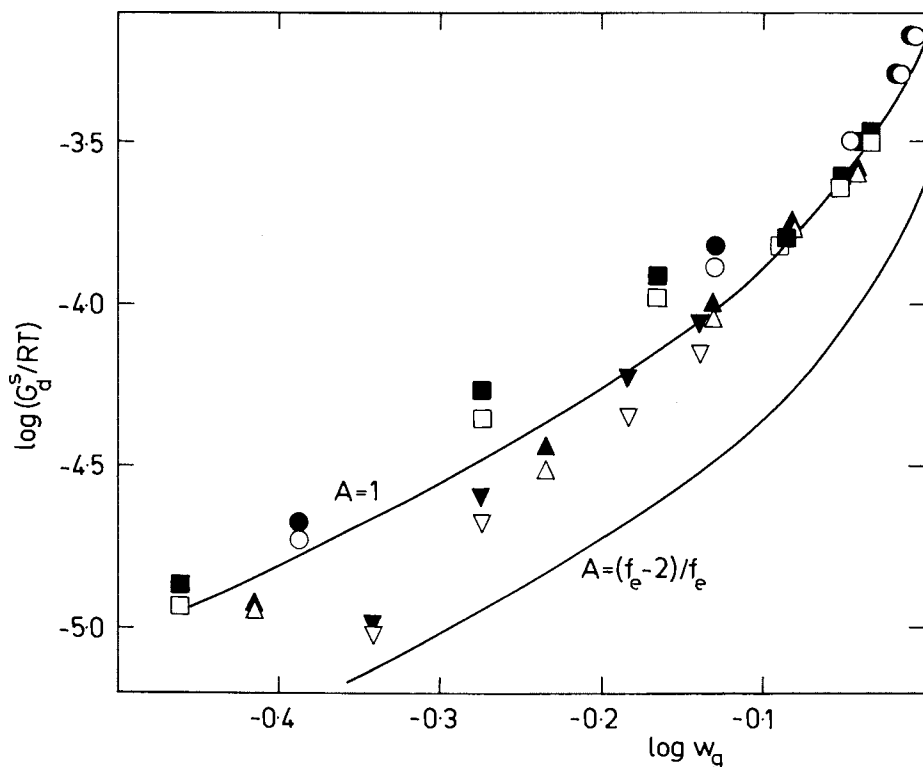
Figure 2.   Theoretical   curves   for   superimposed   reduced   moduli $G_d{}^s/RT(mol/cm^3)$ of epoxy–amine networks versus the gel fraction w_g. Fraction of epoxy groups in monoepoxide is ○, 0; □, 0.2; △, 0.33; ▽, 0.5. *Key:* ○, □, △, ▽, *dry networks;* ●, ■, ▲, ▼, *swollen networks; value of front factor A indicated.*

elastically inactive cycles are taken into account (the data are
shown in Fig.3). The results on elasticity measurements can be
summarized as follows: (1) There exists a weak Mooney-Rivlin de-
pendence characterized by the ratios $C_2/C_1 = 0.1 \pm 0.1$ for networks
from the smaller triol LHT 240 and $0.1 - 0.3 \pm 0.1$ for LG 56; (2).
If the trapped entanglement contribution is not considered, the
value A for the networks from the smaller triol decreases with
decreasing ν_e from 1 to about 0.5 (phantom network value of A is
1/3) (Figure 4a); such a decrease in A with decreasing crosslink-
ing density has already been observed for polyurethane networks
(17);(3) Networks from the larger triol, however, exhibit a much
larger modulus than would correspond to A=1, approximately by a
factor of 2 (Figure 4b); (4) The trapping factor T_{eg} and ν_{eg} have
again a similar shape. Therefore, for a network from LG-56 the
difference between the phantom network value and experimental
moduli can be well described by the trapped entanglement contri-
bution, but for the network from LHT-240 the fit is not so good
and a change in the A value is probable. The result (3) means that
the value of the equilibrium modulus considerably exceeds the
upper limit of the theory (i.e. A=1 corresponding to constraints
forcing the crosslink to move affinely with the macroscopic
strain), if a contribution from permanent interchain inter-
actions (trapped entanglements) is not allowed.

   Applicability of the Langley-Graessley Plot. According to
Eq. (5), the plot of G_e/T_e vs. ν_e/T_e extrapolated to $\nu_e/T_e=0$ gives
ξ as the intercept. It is sometimes assumed that $\nu_e/T_e \to 0$, if
$\nu_e \to 0$, i.e. if the system approaches the gel point. However, a
closer examination of ν_e/T_e shows that this ratio diverges if
$\nu_e \to 0$ and this divergence occurs because, as has been shown above,
$\nu_e \propto (\xi - \xi_c)^3$ and $T_e \propto (\xi - \xi_c)^4$. In other words, in the close
vicinity of the gel point ν_e is contributed by elastically active
crosslinks, which issue three infinite paths ($f_e=3$) irrespective
of the chemical functionality, whereas T_e is contributed by pairs
of units issuing two infinite paths each, that is four infinite
paths must issue from one point for an entanglement to be effec-
tive. Does the fact that one can never approach the situation when
$\nu_e/T_e \to 0$ and   in contrary, lim $(\nu_e/T_e) = \infty$ for $\nu_e \to 0$ invalid the
use of the Langley-Graessley plot?
   We will examine two ways for controlling ν_e characteristic of
step polyaddition networks: (1) by changing the reaction conver-
sion or, in alternating types of reaction, by taking excess of
functional groups of one type, and (2) in stoichiometric systems,
by varying the molecular weight of the components (e.g. of the
precursor chains). Figure 5 shows the calculated dependence of
ν_e/T_e on the sol fraction for the diepoxide+monoepoxide-diamine
networks. The curves representing either a conversion dependence
for the initial composition given by r_A and s, or a dependence on
the excess of amino groups r_{OH} at fixed s and conversion close to
100%, show that ν_e/T_e cannot fall below a limiting value - some
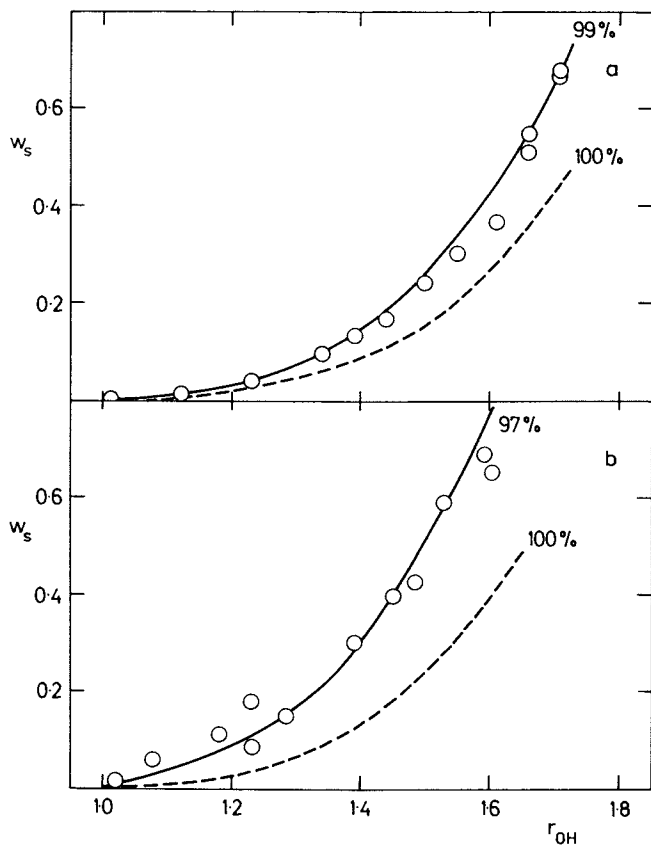
Figure 3. Sol fraction w_s vs. the molar ratio $r_{OH} = [OH]/[NCO]$ for polyurethane networks from polyoxypropylene triols. Key: ———, theoretical curve for indicated conversion of NCO groups in mole percent, taking into account formation of elastically inactive cycles (cf. (16)); – – –, theoretical curve for full conversion of NCO groups without formation of EIC; a, LHT–240; b, LG-56.
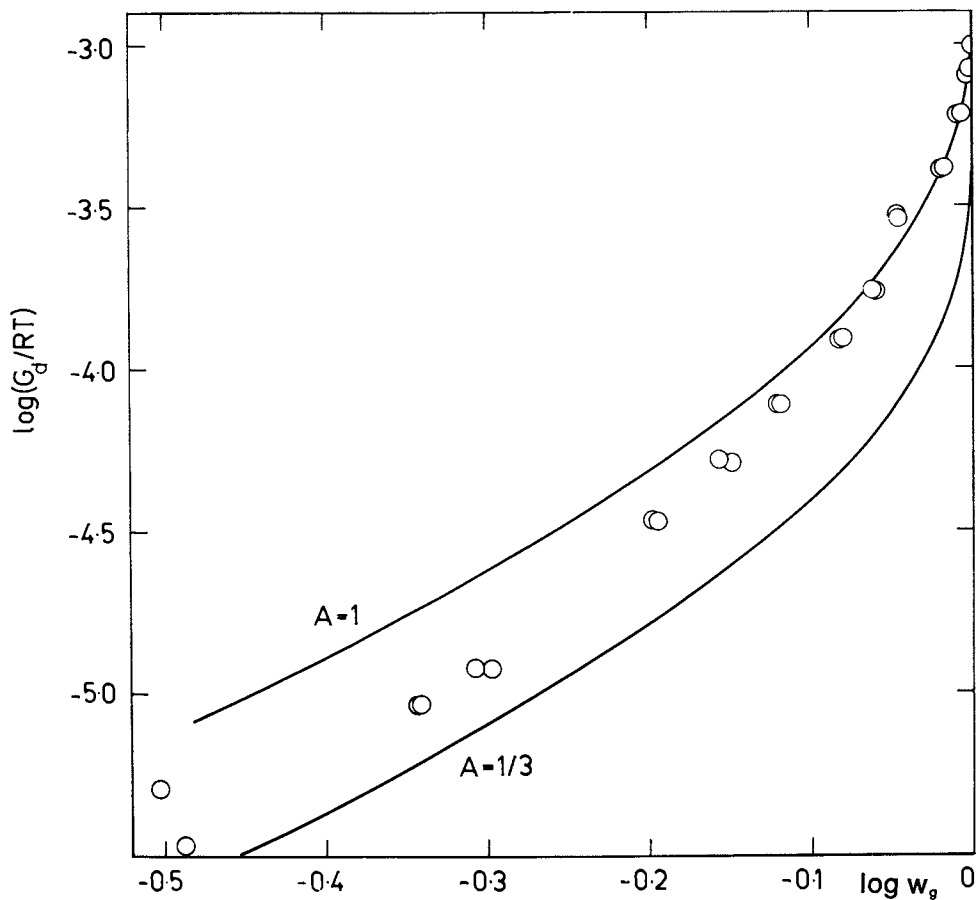
*Figure 4. Theoretical curves for reduced moduli G_d/RT (mol/cm³) of polyure-
thane networks from polyoxypropylene triols versus the gel fraction w_g. Value of
A indicated. Networks from LHT–240. Continued.*
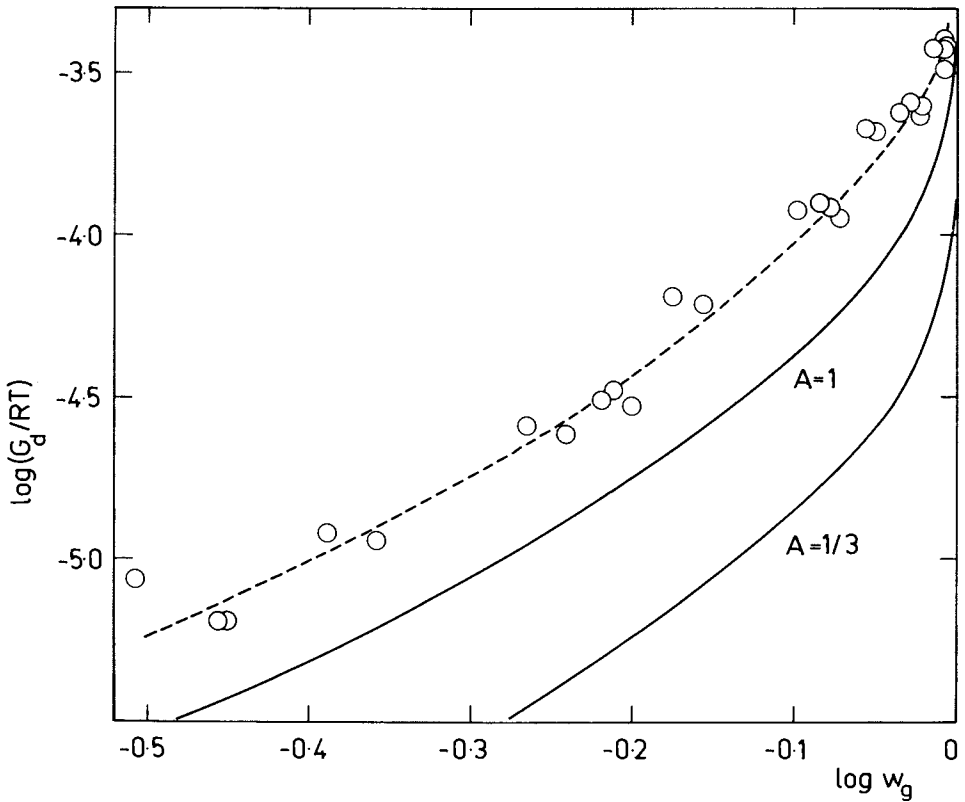
*Figure 4. Continued. Theoretical curves for reduced moduli G_d/RT (mol/cm³)
of polyurethane networks from polyoxypropylene triols versus the gel fraction w_g.
Value of A indicated. Networks from LG–56.*

dependences even pass through a minimum. In general, the variation
of ν_e/T_e in the significant range of $w_s{\sim}0{-}0.6$ is small; both the
slope and intercept of the Langley-Greasley plot would be greatly
affected if less accurate data at high sol fractions were taken
into account. Therefore, the Langley-Greassley plot is not suitab-
le for networks with crosslinking density controlled by the degree
of network imperfectness.

   A somewhat different situation arises for "perfect" networks,
in which the crosslinking density is controlled mainly by the
molecular weight of the elastomeric component and not by the
network imperfectness. The situation is schematically shown in
Figure 6: While the initial concentration of functional groups
in the system, c_0, falls approximately linearly with the inverse
of molecular weight of the elastomer component, a constant small
residual concentration of functional groups, c_r, is expected to
remain in the system after long but finite reaction times. Laws
of chemical kinetics predict c_r to be independent of M at least
for high M. For the network build-up, the reaction conversion
$\xi = 1 - c_r/c_0$ is decisive and this quantity falls sharply if c_0
approaches c_r. Therefore, a "perfect" network becomes very imper-
fect at high M due to incompleteness of the reaction. This fact is
the reason for the sharp upturn of ν_e/T_e as a function of $1/M$
shown in the right part of Figure 6. The value of ν_e/T_e does not
approach zero either, but there exists a relatively broad range of
ν_e/T_e values which can make the extrapolation of the Langley-
Greassley plot reliable.

Conclusions

   The sol fraction follows well the predictions of the tree-
like model and so does the shape of the dependence of the equilib-
rium modulus on the gel fraction irrespective of the value of the
front factor A and magnitude of the trapped entanglement con-
tribution. The equilibrium elasticity measurements show signifi-
cant departures from the predictions of the rubber elasticity
theory which assumes that the only effect of interchain inter-
actions constraints is reflected in the fluctuation freedom of
crosslinks. For epoxy networks, the departures can be seen in the
fact that A does not change with swelling and strain although it
is much higher than the phantom value. An additional contribution
due to permanent interchain interactions caused by incrossability
of chains (trapped entanglement contribution) seems likely and
the observed differences can be described adequately by the
approximation offered by Langley (23). The most convincing
argument in favor of such a contribution was obtained by analyzing
the data on polyurethane networks from the larger triol: the front
factor A would exceed the theoretical upper limit (A=1) by a fac-
tor of two, if an extra (trapped entanglement) contribution were
not taken into account. Such "excess" equilibrium moduli have
already been observed and have (7,8,10,11,12,14,15,24) or have not
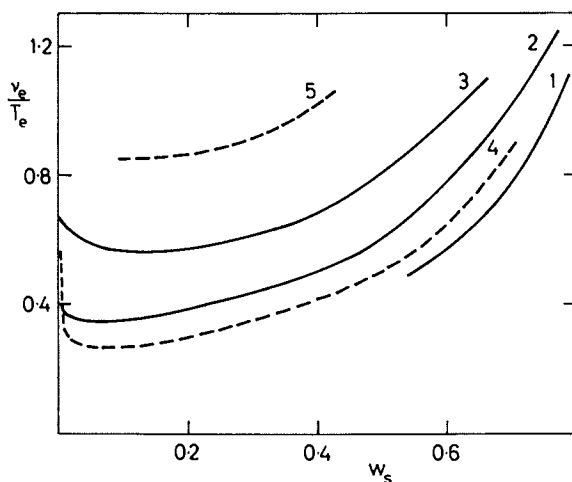
Figure 5.   Calculated dependence of the ratio v_e/T_e (mol/cm³) on sol fraction w_s for the epoxy–amine networks. Varying conversions for $s = 0$ and r_A for 1, 2, and 3 are 2.3, 1.9, and 1.5, respectively.   4 and 5 are 100% conversion and varying r, for $s = 0$ and 0.5, respectively.
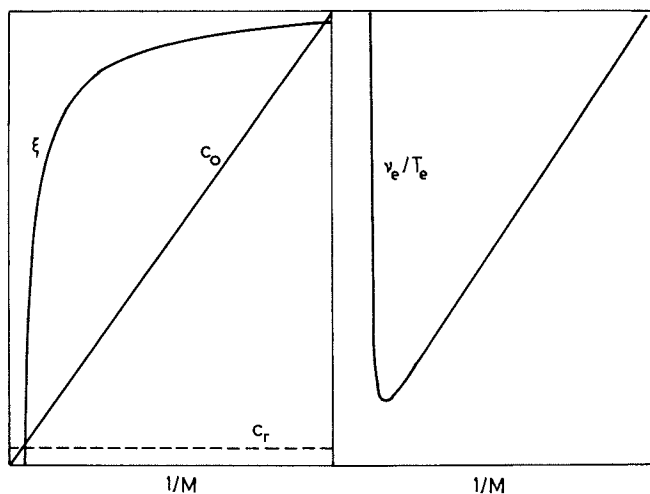
Figure 6.   Sketch of expected variation of the initial (c_0) and residual (c_r) concentration of functional groups, reaction conversion ξ, and the ratio v_e/T_e in end-linked networks as a function of molecular weight of elastomer component M. For discussion see text.

(26,27) been explained by the trapped entanglement contribution. However, identification of the proportionality constant ϵ with the plateau modulus of the corresponding linear chains may be too far reaching at least for step polyaddition and imperfect networks. The ability of network chains to become involved in trapped entanglements depends not only on the structure of the backbone but also on the number bulkiness of the side branches. The results given here indeed show that, at the same length of EANC's, the non-chemical contribution is the lower the more dangling chains the network chain bears.

Literature Cited

1. Flory, P. J. Proc. R. Soc. London 1976, A351, 351.
2. Flory, P. J. Polymer 1979, 20, 1317.
3. Erman, B.; Flory, P. J. J. Chem. Phys. 1978, 63, 4990.
4. Erman, B.; Wagner, W.; Flory, P. J. Macromolecules 1980, 13, 1554.
5. Mark, J. E. Makromol. Chem., Suppl. 2, 1979, 180, 87.
6. Llorente, M. A.; Mark, J. E. Macromolecules 1980, 13, 671.
7. Valles, E. M.; Macosko, C. W. Macromolecules 1979, 12, 673.
8. Gottlieb, M.; Macosko, C. W.; Benjamin, G. S.; Meyers, K. O.; Merrill, E. W. Macromolecules 1981, 14, 1039.
9. Oppermann, W.; Rehage, G. Proc. IUPAC Macro Mainz 1979, Vol.3 1360.
10. Dossin, L. M.; Pearson, D. S.; Graessley, W. W. Macromolecules 1979, 12, 123.
11. Allen, G.; Holmes, P. A.; Walsh, D. J. Faraday Disc. Chem. Soc. 1974, 57, 19.
12. Allen, G.; Egerton, P. L.; Walsh, D. J. Polymer 1976, 17, 65.
13. Stepto, R. F. T. Polymer 1979, 20, 1324.
14. Meyers, K. O.; Bye, M. L.; Merrill, E. W. Macromolecules 1980, 13, 1045.
15. Pearson, D. S.; Graessley, W. W. Macromolecules 1980, 13, 1001.
16. Dušek, K.; Vojta, V. Brit. Polym. J. 1977, 9, 164.
17. Dušek, K.; Hadhoud, M.; Ilavský, M. Brit. Polym. J. 1977, 9, 172.
18. Dušek, K. Makromol.Chem., Suppl. 2, 1979, 180, 35.
19. Dušek, K. Rubber Chem. Technol. in press.
20. Dušek, K.; Ilavský, M. Colloid Polym. Sci. 1980, 258, 605.
21. Ilavský, M.; Prins, W. Macromolecules 1970, 3, 415.
22. Dušek, K. Faraday Disc. Chem. Soc. 1974, 57, 191.
23. Langley, N. R. Macromolecules 1968, 1, 348.
24. Langley, N. R.; Polmanteer, K. E. J. Polym. Sci., Polym. Phys. Ed. 1974, 12, 1023.
25. Matějka, K.; Dušek, K. Polym. Bull. 1980, 3, 489.
26. Sung, P. H.; Mark, J. E. Polym. J. 1980, 12, 835.
27. Llorente, M. A.; Andrady, A. L.; Mark, J. E. J. Polym. Sci., Polym. Phys. Ed. 1980, 18, 2663.

Elastic Modulus, Network Structure, and Ultimate Tensile Properties of Single-Phase Polyurethane Elastomers

THOR L. SMITH

IBM Research Laboratory, San Jose, California 95193

The equilibrium shear modulus of two similar polyurethane elastomers is shown to depend on both the concentration of elastically active chains, ν_c, and topological interactions between such chains (trapped entanglements). The elastomers were carefully prepared in different ways from the same amounts of toluene-2,4-diisocyanate, a poly(propylene oxide) (PPO) triol, a dihydroxy-terminated PPO, and a monohydroxy PPO in small amount. Provided the network junctions do not fluctuate significantly, the modulus of both elastomers can be expressed as $\nu_c(1 + \nu_e/\nu_c)RT$, the average value of ν_e/ν_c being 0.61. The quantity ν_e equals $T_e G_e^{max}/RT$, where $T_e G_e^{max}$ is the contribution of the topological interactions to the modulus. Both ν_c and T_e were calculated from the sol fraction and the initial formulation. Discussed briefly is the dependence of the ultimate tensile properties on extension rate.

Studies have been made of the elastic (time-independent) properties of single-phase polyurethane elastomers, including those prepared from a diisocyanate, a triol, and a diol, such as dihydroxy-terminated poly(propylene oxide) (1,2), and also from dihydroxy-terminated polymers and a triisocyanate (3,4,5). In this paper, equilibrium stress-strain data for three polyurethane elastomers, carefully prepared and studied some years ago (6), are presented along with their shear moduli. For two of these elastomers, primarily, consideration is given to the contributions to the modulus of elastically active chains and topological interactions between such chains. Toward this end, the concentration of active chains, ν_c, is calculated from the sol fraction and the initial formulation which consisted of a diisocyanate, a triol, a dihydroxy-terminated polyether, and a small amount of monohydroxy polyether. As all active junctions are trifunctional, their concentration always

equals $(2/3)\nu_c$ and depends on the extend of the curing reaction and on the amount of the monohydroxy polyether.

Data are also presented that show the dependence of the tensile strength and ultimate elongation on extension rate and temperature. In the discussion, emphasis is placed on the behavior when the stress is sensibly in equilibrium with the strain prior to fracture.

Materials and Experimental Methods

Hydroxy-Terminated Poly(propylene oxide) (PPO). This material was nonacidified PPG-2025 (ONE grade) supplied by Union Carbide Chemicals Company, hereafter designated PPG. Although this material is largely dihydroxy-terminated PPO, it does contain some carbon-carbon double bonds. (The concentration of such bonds increases rapidly with the molecular weight of the PPG (7,8).) The double bonds are terminal groups, both allyl ether and cis-propenyl (9), and hence those molecules containing such groups are monohydroxy, or monofunctional when reacted with a diisocyanate.

After prolonged degassing of a large batch of PPG, analyses showed that its hydroxyl, unsaturation, and water contents were 0.97 meq/g, 0.033 meq/g, and 0.0035%, respectively. The hydroxyl content was determined by an acetylation method, carried out with acetic anhydride (10). The amounts of unsaturation and water were determined by the mecuric acetate and Karl Fischer methods (10), respectively. The obtained analytical results indicate that the number-average molecular weight of the dihydroxy material is 2062, provided its molecular weight is arbitrarily assumed to be twice that of the monohydroxy material, and that the mole fraction of the monohydroxy poly(propylene oxide) is 0.066. This value corresponds to a number-average functionality of 1.93 for the PPG.

Triols. One triol used was the propylene oxide adduct of 1,2,6-hexanetriol, designated LHT-240 and supplied by Union Carbide Chemicals Company. After degassing, its hydroxyl, unsaturation, and water contents were 4.31 meq/g, <0.01 meq/g, and 0.004%, respectively. Thus, the material was essentially trifunctional, and its number average molecular weight was 696. If the unsaturation was exactly 0.01 meq/g, then the number-average functionality was 2.99.

The other triol used was triisopropanolamine (TIPA).

Elastomers Prepared. The three elastomers discussed herein were prepared from PPG, toluene-2,4-diisocyanate (TDI), and either LHT-240 or TIPA. Elastomers prepared by a one-step procedure are designated LHT-240 and TIPA, indicative of the triol used. A third elastomer, designated Tri-NCO, was prepared by first reacting LHT-240 with all of the required TDI for two hours at 50°C to obtain a triisocyanate (or essentially

so) and thereafter adding the PPG. The concentration of triol in the elastomers was 1.00×10^{-4} mole/g, except possibly for that prepared with TIPA. This uncertainty results because an analysis of the used master batch of PPG and TIPA indicated its hydroxyl content to be 4% greater than expected from the recorded weights of the two components. Thus, the conclusions presented herein are based primarily on the properties of the elastomers prepared with LHT-240.

The elastomers crosslinked with LHT-240, including the Tri-NCO formulation, contained 0.03% dibutyltin dilaurate as a curing catalyst and were cured in closed molds (see below) for 8 hours at 100°C. Preliminary experiments showed that such a formulation after cure for either 4 or 8 hours at 100°C swelled the same amount in benzene and contained the same amount of extractable material, termed sol. The elastomer crosslinked with TIPA contained 0.02% ferric acetylacetonate as catalyst and was cured for 24 hours at 60°C. This formulation after cure for either 24 or 48 hours was found to swell the same amount in benzene.

Initially, a number of elastomers were prepared in which the isocyanate-to-hydroxyl (NCO/OH) molar ratio was varied from somewhat less to somewhat greater than one. The degree of swelling in benzene and the sol fraction were found to be minima when the NCO/OH ratio for the LHT-240 and TIPA elastomers was 1.02 and 1.00, respectively. (For the TIPA elastomer, the ratio was 1.00 only if the questionable hydroxyl content, mentioned above, is correct.) The existence of minima indicate that crosslinking by excess isocyanate through allophanate formation, or other side reactions, did not occur to a significant extent. In preparing the elastomers for detailed study, the NCO/OH ratios given above were used.

Preparative Procedures. Special precautions were taken to exclude moisture during the mixing, casting, and cure of the elastomers. For two of the elastomers, about 400 mL of an analyzed degassed master batch of PPG and triol was added to a 1-liter resin flask, which had been dried and sparged with dry high-purity nitrogen, equipped with a vacuum-tight mechanical stirrer. The mixture was degassed, and then the required amount of freshly distilled TDI was metered accurately into the mixture without exposure to air. After degassing again, the catalyst was added. This mixture was next cast, again without exposure to air, into two carefully dried Teflon-coated molds placed in a large vacuum chamber. The molds were circular and closed except for a funnel at the top which was filled with the curing formulation. After cure under the conditions already mentioned, cured sheets 12 inches in diameter and about 0.085-inch thick were obtained.

In preparing elastomers by the two-step procedure, the entire quantities of LHT-240 and TDI were mixed in the resin flask under high-purity nitrogen for 2 hours at 50°C. Even without catalyst, this period was sufficient to obtain complete reaction, or essentially so, because of the relatively high reactivity of the para isocyanate group in the TDI. The

mixture was cooled to room temperature, then the PPG was added and stirred for 15 minutes, and finally the catalyst was added. This mixture was vacuum cast in the manner mentioned above.

Stress-Strain Data. Tensile tests were made with an Instron tester at some seven crosshead speeds from 0.02 to 20 inches per minute at five or six temperatures from 30° to −46°C. The tests were made on rings cut with a special rotary cutter from the circular sheets of the elastomers. The dimensions of each ring were determined from the weights of the ring and the disc from its center, the thickness of the ring, accurately measured, and the density of the rubber. Typically, the outside and inside diameters were 1.45 and 1.25 inches, respectively, and the thickness was about 0.085 inch. The test procedure used is described elsewhere (11), and the cubic equation, eq 4 in ref. 12, was used to compute the average strain in a ring from the crosshead displacement.

Swelling and Sol Fraction. A small weighed specimen 0.085-inch thick was placed in benzene for four days. Thereafter, the swollen specimen was weighed, then dried in a vacuum oven, and finally weighed again. From the weights of the swollen and dried specimen and the densities of benzene and the unswollen specimen, the volume fraction of polymer in the swollen specimen, v_2, was calculated. (The densities of the elastomers prepared from LHT-240 and TIPA were 1.045 and 1.053 g/cm^3, respectively.) The sol fraction was calculated from the initial weight of the specimen and its "dry" weight after swelling. Values of v_2 and the percent sol are included in Table I.

Separate experiments showed that four days were sufficient to establish swelling equilibrium. Unfortunately, the sol possibly was not completely extracted because a swollen specimen was not placed in fresh benzene periodically and especially because four days may not have been sufficient for all of the sol to diffuse out of the relatively thick specimen.

To obtain accurate values of the sol, thin specimens (1 mm) in one study (13) were kept in the solvent for six weeks; in another study (14), thin specimens were extracted for more than 18 days in Soxhlet extractors. When the present experimental data were obtained (6), there was little interest in knowing the sol fraction accurately. However, as discussed subsequently, to compute the extent of the curing reactions and the concentration of elastically active network chains, the sol fraction must be known accurately.

Experimental Results

Stress-Strain Data. Figure 1 shows the tensile data obtained on the LHT-240 elastomer at 30°C and at seven crosshead speeds from 0.02 to 20 inches per minute. The nominal or engineering stress σ is plotted against

time on doubly logarithmic coordinates. The time equals $(\lambda-1)/\dot\lambda$ where λ is the extension ratio and $\dot\lambda(\equiv d\lambda/dt)$ is the extension rate. The lines, which have zero slope, connect values of the stress at strains from 7.5 to 200%. The scatter of points about each line is small and undoubtedly results because the test at each extension rate was made on a different specimen. At all extension rates except the highest, which corresponds to a crosshead speed of 20 inches per minute and gave the left-terminal point on each line, the specimen broke at a value of $(\lambda - 1)$ less than 2.0, i.e., 200%. The data on the other two elastomers at 30°C gave plots similar to those in Figure 1.

Values of stress and strain obtained from Figure 1 and from similar plots of data obtained on the other elastomers yield the plots of $\lambda\sigma$ vs. $(\lambda - 1)$ in Figure 2, where $\lambda\sigma$ is the true stress, i.e., the force per unit cross-sectional area of the deformed specimen. The data   at strains up to 1.0 (100% elongation) give straight lines whose slopes equal the equilibrium tensile moduli, E; values of E/3 are given in Table I.

In Figure 3, $\sigma/(\lambda-\lambda^{-2})$ is plotted against $1/\lambda$ to obtain the constants $2C_1$ and $2C_2$ in the Mooney-Rivlin equation. The intercepts at $1/\lambda = 0$ and the slopes of the lines give the values of $2C_1$ and $2C_2$, respectively, listed in Table I. If these plots actually represent data accurately as λ approaches unity, then $2(C_1 + C_2)$ would equal the shear modulus G which in turn equals E/3 where E is the Young's (tensile) modulus. An inspection of the data in Table I shows that $2(C_1 + C_2)/(E/3)$ is somewhat greater than one. This observation is in accord with the established fact that lines like those in Figure 3 overestimate the stress at small deformations, e.g., see ref. 15.

Table I. Properties of Elastomers

Designation	$\left(\dfrac{NCO}{OH}\right)^{(a)}$	$v_2^{(b)}$	% Sol[c]	$2C_1$ MPa	$2C_2$ MPa	E/3 MPa
LHT-240	1.02	0.178	4.1	0.217	0.151	0.340
Tri-NCO	1.02	0.182	2.8	0.212	0.196	0.367
TIPA	1.00	0.160	2.6	0.292	0.174	0.430

[a]Calculated from the quantities of ingredients and the determined hydroxyl concentrations.
[b]Volume fraction of network in specimen swollen with benzene at ambient temperature.
[c]Minimum values.
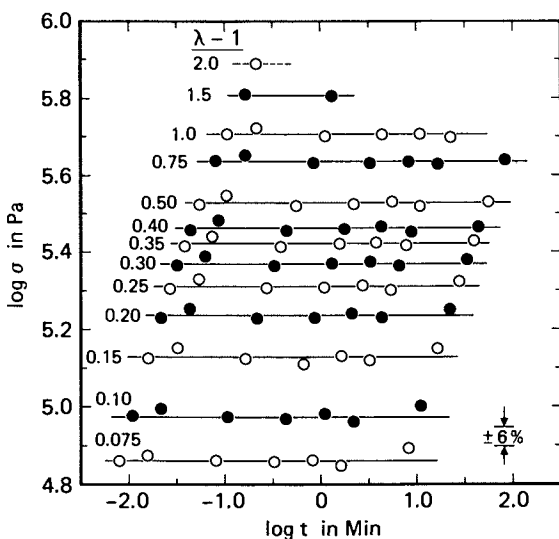
Figure 1. Stress–time data from stress–strain curves measured in simple tension at 30°C on the LHT–240 polyurethane elastomer at seven extension rates, $\dot{\lambda}$, from 9.4×10^{-3} to 9.4 min^{-1}. Key: ○,●, stress as a function of time; $(\lambda - 1)/\dot{\lambda}$, at the indicated values of strain, $(\lambda - 1)$.
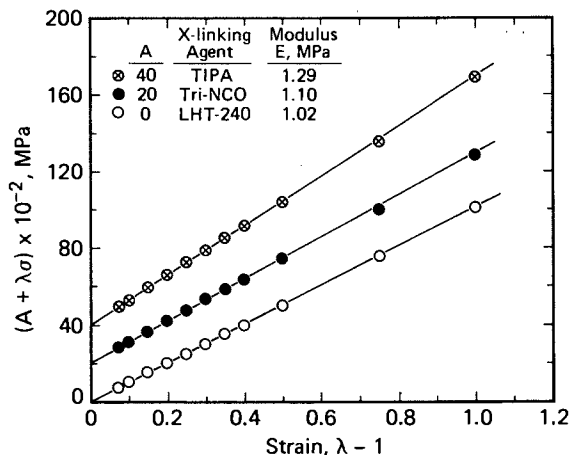
Figure 2. True stress plotted against strain. Data represent equilibrium behavior from Fig. 1 and similar plots of data on the other two polyurethane elastomers. Quantity A introduced for clarity.
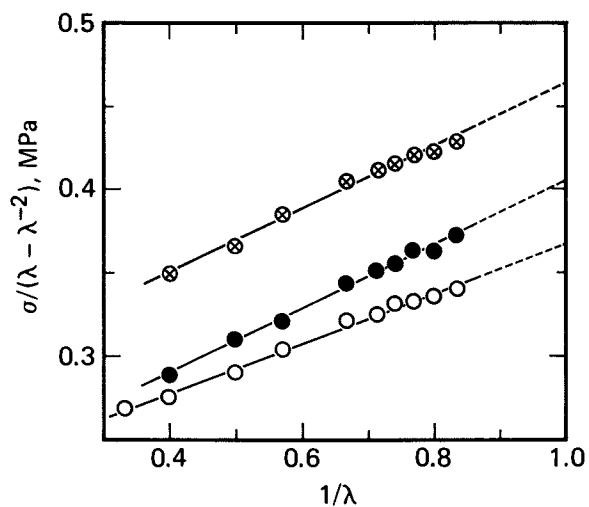
Figure 3.   Data from Figure 2 shown on plot of $\sigma/(\lambda - \lambda^{-2})$ versus $1/\lambda$, prepared to evaluate $2C_1$ and $2C_2$. Key to symbols given in Figure 2.

Evidence for Equilibrium. The lines in Figure 1, as well as those from data obtained on the other two elastomers, have a zero slope over three decades of time, an indication that the data represent elastic (time-independent) properties. Furthermore, the moduli of the elastomers at 5°C, evaluated as illustrated by Figures 1 and 2 and based on the dimensions of the specimens at 5°C, are less than those at 30°C. The ratio E_{30}/E_5 is 1.06 for the LHT-240 and Tri-NCO elastomers and 1.08 for the TIPA elastomer. These values are only slightly less than 303/278 (= 1.09) which is essentially the theoretical value for the ratio of elastic moduli at 30° and 5°C. Actually, the data at 5°C showed a slight amount of relaxation during three decades of times. But relaxation was complete at 30°C, as indicated by the above remarks.

Glass Temperature. The glass temperatures for a substantial number of polyurethane elastomers, similar to those discussed herein, were found (1) to increase linearly with the concentration of urethane moieties, [U]. For the present elastomers prepared using LHT-240 and TIPA, [U] should be 1.10 and 1.15 moles/kg, respectively. Their glass temperatures should be about −57°C, indicated by the previous data.

Discussion of Results

Background. Consider that pairwise interactions between active network chains (13), commonly termed trapped entanglements, do not significantly affect the stress in a specimen deformed in simple tension or compression. Then, according to recent theory (16,17), the shear modulus for a network in which all junctions are trifunctional is given by an equation which can be written in the form (13):

$$G_c = (1-2h/3)\nu_c RT = [\sigma/(\lambda-\lambda^{-2})] \lim_{\lambda \to 1} \tag{1}$$

where ν_c is the moles of elastically active chains per unit volume, RT is the usual product of the gas constant and the absolute temperature, and h is a parameter whose value is between zero and one. (When a junction is trifunctional, the three emanating chains must be active, otherwise the trifunctional moiety does not function as a network junction.)

When the network junctions are entirely immobilized by the surrounding chains, h equals zero. Then the junctions in a deformed specimen are displaced in proportion to the macroscopic strain, i.e., the deformation is affine. Alternatively, h equals unity when junction fluctuations are not impeded, the defining characteristic of a phantom network (16, 17). The parameter h was introduced (13) to allow empirically for different degrees of fluctuations. For undiluted networks at small deformations, h should usually be small, though not necessarily zero.

Data obtained by various investigators (13,14,18,19) indicate that trapped entanglements commonly contribute to the modulus. To represent the modulus, an equation has been used which, if all junctions are trifunctional, becomes:

$$G = (1-2h/3)\nu_c RT + T_e G_e^{max} \tag{2}$$

where G_e^{max} is the maximum possible contribution of entanglements to the modulus and T_e is the fraction that actually contribute. Now, unless $T_e G_e^{max}$ is essentially zero, h presumably can not be unity because if network chains are unable to suppress the fluctuations of junctions at all, then it seems unreasonable to expect that pairwise interactions between chains can contribute to the modulus.

Data have also been presented by other investigators (20,21,22 and references cited therein) who conclude that interchain interactions do not contribute to the modulus.

<u>Preliminary Considerations.</u> Table II gives the mole/kg of the components used in preparing the LHT-240 and Tri-NCO elastomers. The values are based on the assumption that the concentrations of hydroxyl and double-bond groups in the PPG are in fact those obtained from the analyses already discussed and that the NCO/OH ratio is 1.00 instead of 1.02, listed in Table I. In reality, this ratio may have been essentially unity because, as mentioned already, the degree of swelling in benzene and the sol fraction were found to be minima when the nominal ratio was 1.02. The results obtained from the calculations discussed subsequently, and summarized in Table III, do not differ significantly from those obtained if the NCO/OH ratio is equated to 1.02.

Table II. Components in LHT-240 and Tri-NCO Elastomers

Component	mole/kg	wt., g	a_i^*	w_i^{**}
LHT-240	0.100_5	69.9	0.271_6	0.0699
HO(PPO)OH	0.390_4	805.0	0.703_5	0.8050
HO(PPO)	0.027_6	28.5	0.024_9	0.0285
TDI	0.555_0	96.6	—	0.0966

[*] $a_i = f_i A_i / \Sigma f_i A_i$ where A_i is the moles of the ith hydroxy-terminated component and f_i is its functionality.
[**] w_i is the weight fraction of the ith component in the entire formulation.

Let us now assume momentarily that the elastomers are perfect, in the sense that all functional groups (originally present in equivalent amounts) have reacted in such a manner that no sol exists. Under such idealized conditions, each molecule of monohydroxy PPO will in effect produce one inactive junction. (Strictly speaking, i molecules of monohydroxy PPO can produce somewhat more than i inactive junctions.) Thus, the concentration of junctions in the network becomes about 0.073 mole/kg instead of 0.100 mole/kg (Table II). As each junction gives 3/2 chains, the modulus, after equating h to zero in eq 1, is given by

$$G = \rho(7.3 \times 10^{-5})(3/2)RT = 0.288 \text{ MPa} \qquad (3)$$

where the density ρ is 1.045 g/cm^3 and T equals 303 K. This value is substantially less than 0.340 and 0.367 MPa found for the LHT-240 and Tri-NCO elastomers (Table I). Thus, this simplified calculation indicates that entanglements contribute to the modulus.

Though unrealistic, the above calculations rest largely on the accuracy of the chemical analyses which show that the mole fraction of monohydroxy PPO in the PPG is 0.066. This value, which corresponds to a number-average functionality of 1.93, is similar to those found in previous studies of elastomers prepared from PPG, TDI, and other ingredients. The reported analytical data on separate batches of PPG-2025 used in two studies (1,23) give functionalities of 1.95 and 1.94. Furthermore, Sung and Mark (4), who recently studied elastomers prepared from several PPG's and a triisocyanate, report that the functionality of their PPG samples was "2.0 to within approximately ±4%", and thus the functionality could be as low as 1.92, though probably only for the two samples of highest molecular weight (8). The functionality of the samples was estimated from the determined hydroxyl content and the molecular weight obtained with a vapor pressure osmometer, probably a method of limited accuracy.

For present purposes, the exact value of the functionality need not be known because the concentration of active junctions depends strongly on the sol fraction.

Calculations. The presence of sol in a network indicates that the curing reaction was not complete or the ingredients were not present in stoichiometric amounts, either of which give elastically inactive chains, i.e., chains attached to the gel at one end only. (Also, the monohydroxy PPO in the present formulations will always give sol.)

Let P_{xi} be the probability that a chain originating in a trifunctional moiety terminates in the gel. For a trifunctional moiety to be an active junction, all three emanating chains must terminate in the gel, the probability of which is P_{xi}^3. Thus, the concentration of active junctions is [triol]P_{xi}^3 and the concentration of active chains is $(3/2)$[triol]P_{xi}^3, where [triol] denotes the mole/cm^3 of trifunctional moieties in the network.

According to the equations derived by Miller and Macosko (24), outlined in the Appendix, the probability that a short segment selected at random in the network is part of an elastically active chain is $(P_{xi}/p)^2$ where p is the final extent of the curing reaction. If an entanglement results from pairwise interactions between chains, as proposed (13), then T_e in eq 2 can be equated to $(P_{xi}/p)^4$, which is the probability that two interacting chains are active.

In studies of networks of polybutadiene (18) and an ethylene-propylene copolymer (13), h was found to be essentially zero, though for various poly(dimethylsiloxane) (PDMS) networks, h has been found (19) to be greater than zero. Nevertheless, without further justification, h will here be equated to zero. Equation 2 now becomes

$$G = (3/2)[\text{triol}]RTP_{xi}^3 + (P_{xi}/p)^4 G_e^{max} \qquad (4)$$

which is equivalent to

$$G = (\nu_c + \nu_e)RT \qquad (5)$$

where ν_e is a quantity, not precisely definable physically, that equals $T_e G_e^{max}/RT$. Stated otherwise, pairwise interactions between active chains increase the modulus by an amount that is equivalent to ν_e moles of chains per unit volume.

Equation A1 in the Appendix shows that P_{xi} is a function of p, and thereby the sol fraction (eq A2) depends solely on p and certain mole and weight fractions given by the a's and w's (Table II). From the determined minima values of the sol fraction (Table I), p and P_{xi} for the LHT-240 and the Tri-NCO elastomers were first evaluated by an iterative process, and then G_e^{max}, ν_c, and ν_e were obtained from eqs 4 and 5. These quantities are given in Table III. Those for the TIPA elastomer are not included because its composition is somewhat questionable, as mentioned earlier. However, if its initial ingredients were in fact 1.00×10^{-4} mole/g of TIPA, PPG, and a stiochiometric amount of TDI, the calculated values of G_e^{max}, $10^4\nu_c$, and $10^4\nu_e$ are 0.350 MPa, 0.966, and 0.741, respectively.

Table III. Calculated Quantities

Elastomer	p	P_{xi}	w_s	G_e^{max}, MPa	$10^4\nu_c$ mole/cm^3	$10^4\nu_e$ mole/cm^3
LHT-240	0.9859	0.8023	0.041	0.308	0.814	0.536
TRI-NCO	0.9907	0.8389	0.028	0.258	0.930	0.527

Comments on Calculated Data. In several studies ($\underline{13},\underline{18},\underline{19}$), G_e^{max} has been found to equal, or possibly be somewhat less than, the plateau modulus, G_N^o, of a high molecular weight polymer whose chemical composition is the same as that of the network chains. Although G_N^o for amorphous PPO has not been reported, it can be estimated from Z_c, the number of chain atoms per molecule above which the viscosity increases approximately with the 3.4 power of Z. This quantity has been reported ($\underline{25},\underline{26}$) to be about 400. As the chain atoms between entanglements is commonly about $Z_c/2$, it follows that the molecular weight between entanglement loci is about 3900, and thus G_N^o [$\simeq (\rho/M_e)RT$] is about 0.65 MPa at 30°C.

This estimated value of G_N^o is twofold or more larger than the computed values of G_e^{max} in Table III. This difference could result if the sol fractions (Table I) are actually less than the true values, for reasons mentioned earlier, and if h is greater than zero. For PDMS elastomers containing trifunctional junctions, h has been reported ($\underline{19}$) to be 0.95.

Other evidence suggests that the obtained values of G_e^{max} may be approximately correct. Allen et al. ($\underline{2}$) studied polyurethane elastomers prepared from 4,4'-diphenylmethane diisocyanate (MDI) and a series of mixtures of PPG and a PPO triol, the equivalent weight per hydroxyl group in each material being about 1000. Their plot of the shear modulus against the weight percent of triol in the polyol mixture extrapolates to 0.20 MPa at zero triol concentration which corresponds to linear chains formed from PPG and MDI. Though 0.20 MPa might at first sight be equated to G_N^o, this value is not likely to be correct for several reasons, including the fact that the extrapolation procedure underestimates G_N^o ($\underline{14}$). When a similar procedure was applied to data on PDMS networks containing trifunctional junctions ($\underline{19}$), the modulus obtained by extrapolation was about 30% less than G_N^o. Thus, if 0.20 MPa is arbitrarily increased by 30%, it becomes similar to the values obtained for G_e^{max}.

For networks prepared from MDI and a PPO triol whose molecular weight and functionality were 2630 and 2.89, respectively, Dusek and Ilavsky ($\underline{27}$) found the moduli to be about twofold greater than those calculated from the sol fraction when h and $T_e G_e^{max}$ in eq 2 are equated to zero. Thus, $\nu_c/(\nu_c + \nu_e)$ is about 0.50 whereas the data in Table III give 0.62, approximately.

Though somewhat invalid, the calculation given under Preliminary Considerations illustrates the sensitive of the modulus to the precise functionality of the PPG. However, if the mole fraction of monohydroxy PPO in the PPG is considered, for illustration, to be 0.040 instead of 0.066, the calculated values of G_e^{max}, $10^4\nu_c$, and $10^4\nu_e$ for the LHT-240 elastomer are 0.318 MPa, 0.789, and 0.551, respectively. These values differ only slightly from those in Table III. Such results because, both p and P_{xi} must become smaller with a decrease in the amount of monohydroxy PPO so that the calculated sol fraction will agree with that observed.

It is of interest to note that the concentration of active chains is highly sensitive to the extent of reaction. Such results because, as a first approximation, three inactive chains result from each isocyanate group that remains unreacted in the gel. Two molecules of monohydroxy PPO are required, again as a first approximation, to produce three inactive chains.

Ultimate Tensile Properties

The strength and extensibility of a noncrystallizable elastomer depend on its viscoelastic properties (28,29), even when the stress remains in equilibrium with the strain until macroscopic fracture occurs. In theory, such elastomers have a time- or rate-independent strength and ultimate elongation, but such threshold quantities apparently have not been measured, though rough estimates have been made (28,30).

Figure 4 shows stress-strain curves measured at an extension rate of 94% per minute on the TIPA elastomer at 30°, −30°, and −40°C. With a decrease in temperature from 30° to −40°C, the ultimate elongation increases from 170% to 600%. The modulus $E_{cr}(1)$, evaluated from a one-minute stress-strain isochrone, obtained from plots like shown in Figure 1, increases from 1.29 MPa at 30°C to only 1.95 MPa at −40°C. This small increase in the modulus and the large increase in the engineering stress and elongation at fracture results from viscoelastic processes.

Although the curve measured at 30°C represents equilibrium behavior, as discussed under Evidence for Equilibrium, the fracture point moves along the curve with a change in the extension rate, as illustrated in Figure 5. In this figure, the true stress-at-break is plotted against the strain-at-break for the three polyurethane elastomers. The lower curve, which represents data on the LHT-240 elastomer, shows that the elongation-at-break increases from 100% to 230% and the true stress-at-break increases six-fold with a 1000-fold increase in the extension rate. In moving from the top to the bottom of this curve, the time-to-break increases 400-fold.

Data obtained on the TIPA elastomer at various extension rates at six temperatures are shown in Figure 6 where the temperature-reduced true stress-at-break is plotted against the strain-at-break on doubly logarithmic coordinates. The fact that a single curve results suggests that an equivalence exists between an increase in extension rate and a decrease in temperature. Either of these changes effects an increase in the rate of energy dissipation. Energy dissipation clearly impedes the growth of a microcrack to a critical size at which catastrophic crack-propagation occurs (28,29). The tearing energy also increases by several orders of magnitude with an increase in the rate of energy dissipation (30).

When the tearing (fracture) energy is measured under conditions at which energy is not dissipated in viscous processes, its value is termed the threshold tearing energy, T_0 (30,31,32). If T_0 for the TIPA elastomer is the same as that for a hydrocarbon elastomer whose $2C_1$ equals that for the
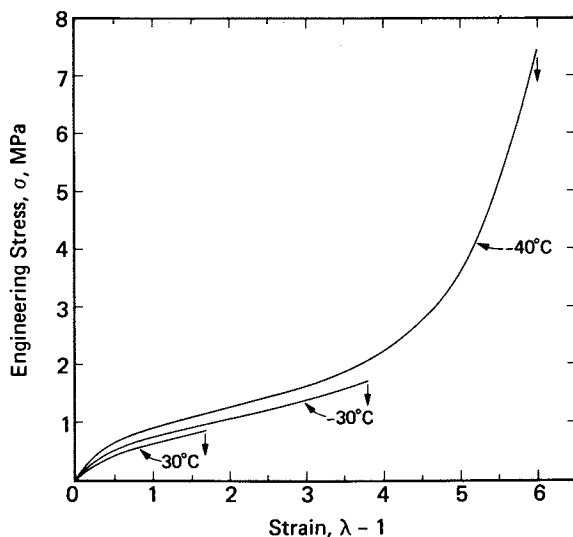
Figure 4. Stress–strain curves for the TIPA polyurethane elastomer measured at the indicated temperatures at an extension rate of 0.94 min^{-1}. Arrows indicate fracture.
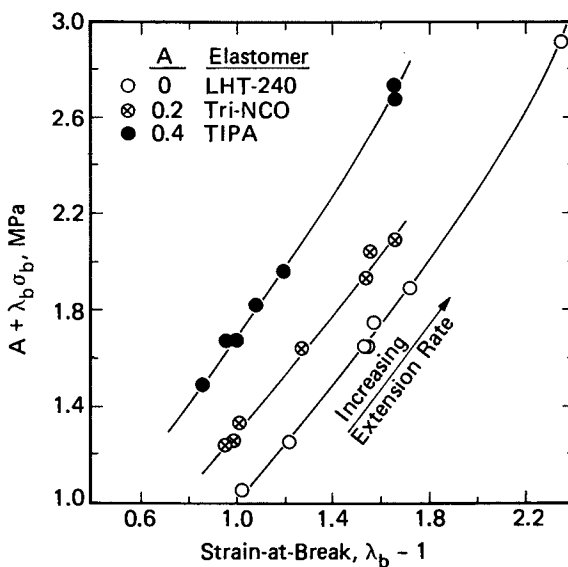
Figure 5. True stress-at-break plotted on doubly logarithmic coordinates against the strain-at-break. Conditions: 30°C; extension rates from 9.4 × 10^{-3} to 9.4 min^{-1}. Quantity A introduced for clarity.
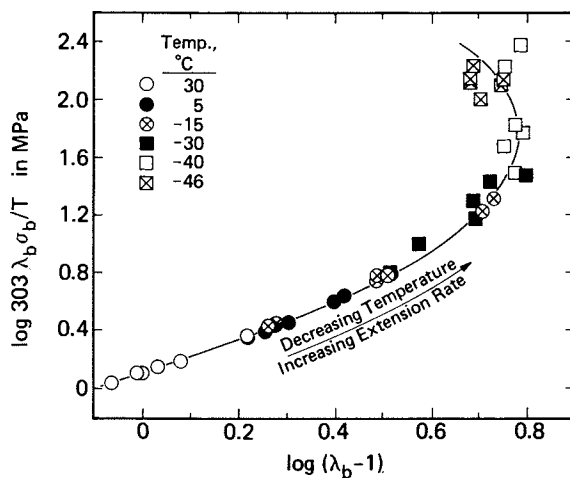
Figure 6.   Temperature reduced true stress-at-break plotted on doubly logarithmic coordinates against the strain-at-break. Ultimate elongation increases from 80 to 600% while decreasing in temperature and increasing in extension rate.

TIPA elastomer, then T_0 for the latter equals 80.7 J/m^2, obtained from $2C_1$ in Table I and the equations in ref. $\underline{32}$. A crude estimate can now be made of the minimum (threshold) values of $\lambda_b\sigma_b$ and $(\lambda_b - 1)$ by assuming they are given by ($\underline{28,30}$)

$$(\lambda_b\sigma_b)_0 = (ET_0/\pi c)^{1/2} \qquad (6)$$

and

$$(\lambda_b - 1)_0 = (\lambda_b\sigma_b)/E \qquad (7)$$

where E is again the equilibrium modulus and c is the size of an inherent flaw, which typically is 50 μm or thereabouts ($\underline{30,33}$). (The quantity c is considered to be the length of a crack that gives a stress concentration equal to that from the inherent flaw.) It now follows from eqs 6 and 7 that $(\lambda_b\sigma_b)_0$ and $(\lambda_b - 1)_0$ for the TIPA elastomer are about 0.81 MPa and 0.63, respectively. Figures 5 and 6 show that the smallest observed values (1.09 MPa and 0.86) are substantially larger than the estimated threshold quantities.

Summary and Conclusions

The results presented clearly show that topological interactions (trapped entanglements) contribute significantly to the (initial) shear modulus. Calculations based on the initial formulation and sol fractions show that the concentrations of elastically active chains, ν_c, in two similar polyurethane elastomers correspond to moduli ($\nu_c RT$) of 0.205 and 0.234 MPa, provided the fluctuations of junctions in the networks are suppressed completely. The observed moduli, G, are approximately 61% larger, the values being 0.340 and 0.367 MPa. For each elastomer, the difference $(G - \nu_c RT)$ is equated to $T_e G_e^{max}$, the contribution from topological interactions. Calculations of T_e, the probability that two interacting chains are both active, show that the average values of G_e^{max} and T_e are 0.28 MPa and 0.48. If fluctuations of the junctions are not suppressed completely, a likely possibility, then G_e^{max} becomes larger. Whether G_e^{max} is larger, in fact, cannot be determined because sufficient data are not available.

The conclusions reached are valid qualitatively if the amount of monohydroxy PPO is less than that obtained from the chemical analyses of the PPG. In fact, if no monohydroxy PPO were present, then the calculated values of $\nu_c RT$ and G_e^{max} for the LHT-240 elastomer become 0.13 MPa and 0.48 MPa, respectively. Such results because, to obtain the observed sol fraction (0.041), the extent of reaction must be 0.9728 instead of 0.9859 (Table III). Similarly, if the true values of the sol fraction are somewhat larger than those found, calculations then show that $\nu_c RT$ is less and G_e^{max} is larger than those reported in Table III.

The finding that ν_c is 0.814×10^{-4} mole/cm^3 for the LHT-240 elastomer indicates that $M_c/\rho_{ac} = 1.23 \times 10^4$ where M_c is here the molecular weight of the linear portion of the active chains and ρ_{ac} is the concentration (g/cm^3) of such chains. The concentration of the linear portion of the active chains is clearly less than the density of the elastomer because both sol and inactive chains are present.

The obtained values of $\nu_c RT$ differ from $2C_1$ by only 10% or less, whereas other investigators (13,18,34) have found that topological interactions contribute significantly to $2C_1$. To account for this different finding, additional data on polyurethane elastomers would be required.

Data are presented which illustrate that the tensile strength and elongation-at-break depend significantly on the extension rate even when the stress remains in equilibrium with the strain prior to fracture. A crude estimate was made of the threshold (lowest possible) values of the true stress-at-break and the elongation-at-break for the TIPA elastomer. The estimated quantities are about 26% less than those found at an extension rate of about 0.01 min^{-1} at 30°C.

Acknowledgements

Appendix

Miller and Macosko (24) have derived equations that enable p and P_{xi} in eq 4 to be calculated from the sol fraction. In the derivation, they assumed that all functional groups of a given type are equally reactive, that the groups react independent of one another, and that no small loops form. Although certain systems having groups of unequal reactivities have been considered (35), the effect of unequal reactivities gradually disappears as the reaction approaches completion, as shown by the treatment. Thus, unequal reactivities need not be considered here, even though the meta and para isocyanate groups in TDI have substantially different reactivities and some primary hydroxyl groups exist in LHT-240 and PPG, though the hydroxyls are largely secondary.

In the terminology of Miller and Macosko (24), the present formulations can be denoted by $A_3 + A_2 + A_1 + B_2$ where the A's are the tri-, di-, and monohydroxy materials and B_2 is TDI. The following equations are applicable only when the concentration of hydroxyl and isocyanate groups are equal, which is assumed to be true, as discussed in the text.

Equation 23 in ref. 24 gives

$$P_{xi} \equiv 1 - P(F_A^{out}) = [(2a_3 + a_2)p^2 - 1]/a_3 p^2 \qquad (A1)$$

where $a_i = f_i A_i / \Sigma f_i A_i$ in which A_i is the initial moles of component A_i (i = 1,2,3) whose functionality is f_i and p is the extent of reaction for the cured elastomer.

The probability that a randomly selected chain is elastically active can be equated, in the Miller-Macosko terminology, to either $[1 - P(F_B^{in})][1 - P(F_B^{out})]$ or $[1 - P(F_A^{out})][1 - P(F_A^{in})]$. By use of eq A1 and their eqs 17, 18, and 20, both of these expressions can be shown to equal $(P_{xi}/p)^2$. Thus, the probability, T_e, that two interacting chains are active is (P_{xi}/p).[4]

The sol fraction is given by

$$w_s = w_3 Q^3 + w_2 Q^2 + w_1 Q + w_B (1 - P_{xi}/p)^2 \qquad (A2)$$

where $Q \equiv (1 - P_{xi})$ and the w_i's are the weight fractions of the A_i's in the entire formulation, and similarly w_B is the weight fraction of TDI. The above expression is eq 39 in ref. 24 except that the factor $(1 - P_{xi}/p)$ is there denoted by $P(F_B^{out})$. These quantities can be shown to be equivalent.

Literature Cited

1. Smith, T. L.; Magnusson, A. B. J. Polym. Sci. 1960, 42, 391.
2. Allen, G.; Egerton, P. L.; Walsh, D. L. Polymer 1976, 17, 65.
3. Morton, M.; Rubio, D. C. Plastics and Rubber: Mat. Appl. 1978, 3, 139.
4. Sung, P.-H.; Mark, J. E. J. Polym. Sci., Polym. Phys. Ed. 1981, 19, 507.
5. Nelb, G. W.; Pedersen, S.; Taylor, C. R.; Ferry, J. D. J. Polym. Sci., Polym. Phys. Ed. 1980, 18, 645.
6. Dickie, R. A.; Smith, T. L. Technical Report AFML-TR-68-112, May 1968, prepared for the Air Force Materials Laboratory.
7. Simons, D. M.; Verbanc, J. J. J. Polym. Sci. 1960, 44, 303.
8. Havlik, A. J.; Moacanin, J.; Otterness, I. J. Polym. Sci. Part A, 1963, 1, 2213.
9. Dege, G. J.; Harris, R. L.; MacKenzie, J. S. J. Am. Chem. Soc. 1959, 81, 3374.
10. David, D. J.; Staley, H. B. "Analytical Chemistry of the Polyurethanes" (High Polymers, Vol. 16, Pt. III); Wiley-Interscience: New York, 1969; Chapt. V.
11. Smith, T. L. J. Appl. Phys. 1964, 35, 27.
12. Smith, T. L. J. Polym. Sci. Part C, 1967, 16, 841.
13. Pearson, D. S.; Graessley, W. W. Macromolecules 1980, 13, 1001.
14. Langley, N. R.; Polmanteer, N. R. J. Polymer Sci.; Polym. Phys. Ed. 1974, 12, 1023.
15. Erman, B.; Flory, P. J. J. Polym. Sci., Polym. Phys. Ed. 1978, 16, 1115.

16. Flory, P. J. Proc. Roy. Soc. (London) Ser. A 1976, 351, 351.
17. Flory, P. J. J. Chem. Phys. 1977, 66, 5720.
18. Dossin, L. M.; Graessley, W. W. Macromolecules 1979, 12, 123.
19. Gottlieb, M.; Macosko, C. W.; Benjamin, G. S.; Meyers, K. O.; Merrill, E. W. Macromolecules 1981, 14, 1039.
20. Llorente, M. A.; Mark, J. E. Macromolecules 1980, 13, 681.
21. Erman, B.; Wagner, W.; Flory, P. J. Macromolecules 1980, 13, 1554.
22. Mark, J. E. Rubber Chem. Technol. 1981, 54, 809.
23. Smith, T. L.; Magnusson, A. B., J. Appl. Polym. Sci. 1961, 5, 218.
24. Miller, D. R.; Macosko, C. W. Macromolecules 1976, 9, 206.
25. Havlik, A. J.; Moacanin, J. Research Summary No. 36-10, Vol. 1, p. 92, Jet Propulsion Laboratory, Pasadena, CA.
26. Fox, T. G.; Allen, V. R. J. Chem. Phys. 1964, 41, 344.
27. Dusek, K.; Ilavsky, M. Polym. Preprints 1981, 22(2), 167.
28. Smith, T. L. Polym. Eng. Sci. 1977, 17, 129.
29. Smith, T. L. in "Rheology", Eirich, F. R., Ed., Academic Press, 1969; Vol. 5, Chapter 4.
30. Gent, A. N. in "Science and Technol. of Rubber", Eirich, F. R., Ed., Academic Press, 1978; Chapter 10.
31. Ahagon, A.; Gent, A. N. J. Polym. Sci., Polym. Phys. Ed. 1975, 13, 1903.
32. Gent, A. N.; Tobias, R. H. Polym. Preprints 1981, 22(2), 163.
33. Lake, G. J.; Lindley, P. B. J. Appl. Polym. Sci. 1964, 8, 707.
34. Meyers, K. O.; Bye, M. L.; Merrill, E. W. Macromolecules 1980, 13, 1045.
35. Miller, D. R.; Macosko, C. W. Macromolecules 1978, 11, 656.

Recent Two-Network Results on the Effect of Chain Entangling in Cross-linked Elastomers

W. BATSBERG

Riso National Laboratory, Chemistry Department, DK-4000 Roskilde, Denmark

O. KRAMER

University of Copenhagen, Department of Chemistry, Universitetsparken 5, DK–2100 Copenhagen, Denmark

Chain entangling is found to dominate the elastic properties of highly cross-linked 1,2-polybutadiene at elastic equilibrium. Cross-linking of the linear polymer with 125 kGy of 10 MeV electrons in the strained state virtually separates the effects of chain entangling and chemical cross-links: $G_N \cong 0.75$ MPa and $G_X \cong 0.25$ MPa for the corresponding moduli, independent of type of strain during cross-linking. The two-network method and the required assumptions are examined in detail. A new stress-relaxation two-network method, requiring fewer assumptions, is also discussed. The latter method shows directly, without the need of a theory, that the equilibrium contribution of chain entangling is equal to the non-equilibrium stress-relaxation modulus prior to cross-linking in the strained state. The new method also directly confirms six of the eight assumptions required for the original two-network method.

The role of chain entangling in cross-linked elastomers is an old issue which has not yet been settled. The success of Flory's new rubber elasticity theory (1–5) in describing some of the departures from the simple Gaussian theory has acted as a strong catalyst for new work in this area.

Since the excellent work of Moore and Watson (6), who cross-linked natural rubber with t-butylperoxide, most workers have assumed that 'physical cross-links' contribute to the equilibrium elastic properties of cross-linked elastomers. This idea seems to be fully confirmed in work by Graessley and co-workers who used the Langley method on radiation cross-linked polybutadiene (7) and ethylene-propylene copolymer (8) to study trapped entanglements. Two-network results on 1,2-polybutadiene (9,10) also indicate that the equilibrium elastic contribution from chain entangling at high degrees of cross-linking is quantitatively equal to the pseudo-equilibrium rubber plateau modulus (11) of the uncross-linked polymer.

Ronca and Allegra (12) and Flory (1,2) assume explicitly in their new rubber elasticity theory that trapped entanglements make no contribution to the equilibrium elastic modulus. It is proposed that chain entangling merely serves to suppress junction fluctuations at small deformations, thereby making the network deform affinely at small deformations. This means that the limiting value of the front factor is one for complete suppression of junction fluctuations.

Experimental values of 4-6 for the apparent front factor (7,8) have been reported for networks produced by radiation cross-linking of long linear chains. Analyzing the data according to the Langley method, Graessley and co-workers (7,8) found very large contributions from trapped entanglements and front factors of one for the contribution from chemical cross-links. It seems to be clearly demonstrated that chain entangling plays a major role in elastomers such as polybutadiene, styrene-butadiene rubber, and ethylene-propylene copolymer which have high rubber plateau moduli (11).

Networks with tri- and tetra-functional cross-links produced by end-linking of short strands give moduli which are more in accord with the new theory if quantitative reaction can be assumed (3,13). However, the data on polydimethylsiloxane networks, may equally well be analyzed in terms of modulus contributions from chemical cross-links and chain entangling, both, if imperfect reaction is taken into account (14). Absence of a modulus contribution from chain entangling has therefore not been demonstrated by end-linked networks.

The two-network method (15) offers an alternative method for studying the effect of chain entangling in cross-linked elastomers. It is the only method which allows a virtual separation of the elastic effects of chain entangling and chemical cross-links: An uncross-linked elastomer is strained at a temperature of about T_g+8K in order to be in the rubber plateau region. Then the sample is quenched to below T_g and heavily cross-linked with high energy electrons. After heating and release, the sample retracts to a stress-free equilibrium state in which the elastic effects of chain entangling and chemical cross-links are equal and opposite in direction. It was found by Ferry and coworkers (16) that the modulus contribution from chemical cross-links is much smaller than the equilibrium contribution from chain entangling. And furthermore, the equilibrium contribution from chain entangling in a highly cross-linked network was found to be approximately equal to the non-equilibrium rubber plateau modulus (9,17).

In spite of these important results, the two-network method has had little impact on the discussion of the role of chain entangling in cross-linked elastomers. It was therefore decided to make a more detailed examination of the method and to try to develop a simpler method which would require fewer assumptions. The present paper is a discussion of recently published and unpublished work.

The paper is divided into three parts. The first part presents

some of the results of the two-network theory which forms the basis of the two-network method. The second part describes the two-network method and the necessary assumptions. Results for three different types of strain are presented. The third part is a discussion of a new stress-relaxation two-network method which requires fewer assumptions. It shows directly, without the need of a theory, that the equilibrium contribution from chain entangling is equal to the non-equilibrium stress-relaxation modulus immediately prior to cross-linking.

Part 1.   Two-Network Theory

The two-network theory for a composite network of Gaussian chains was originally developed by Berry, Scanlan, and Watson (18) and then further developed by Flory (19). The composite network is made by introducing chemical cross-links in the isotropic and subsequently in a strained state. The Helmholtz elastic free energy of a composite network of Gaussian chains with affine motion of the junction points is given by the following expression:

$$\Delta A_{el} = \tfrac{1}{2}\nu_1 RT(\lambda_x^2 + \lambda_y^2 + \lambda_z^2 - 3) + \tfrac{1}{2}\nu_2 RT(\lambda_{x;2}^2 + \lambda_{y;2}^2 + \lambda_{z;2}^2 - 3) \tag{1}$$

where ν_1 and ν_2 are the concentrations of elastically active network strands, R is the gas constant, and T is the absolute temperature. The extension ratios for the first network are to be measured relative to the isotropic state (λ_x, λ_y, λ_z) and for the second network relative to the strained state during cross-linking ($\lambda_{x;2}$, $\lambda_{y;2}$, $\lambda_{z;2}$). Although the composite network strands are physically part of both networks, the theory shows that the effects of the two networks are conveniently separated, mathematically. All elastic properties may be calculated from eq. 1.

After introduction of cross-links in the strained state, the composite network retracts, upon release, to a stress-free state-of-ease (19). The amount of retraction is determined by the degree of strain during cross-linking and by the ratio ν_1/ν_2. The elastic properties relative to the state-of-ease are isotropic for a Gaussian composite network (18,19,20).

Flory (19) has treated the interesting case of subsequent removal of the first stage cross-links without chain scission. Even after complete removal, i.e. $\nu_1 = 0$, there is still a certain memory of the structure of the first network since the composite network strands were physically part of both networks. According to Flory's theory, the resulting network may be treated as if a certain fraction, Φ, of the strands of the second network were effectively converted into strands of the first network, ν_{1e}.

$$\nu_{1e} = \Phi\nu_2 \tag{2}$$

$$\nu_{2e} = (1-\Phi)\nu_2 \tag{3}$$

Φ is given in Flory's paper as a function of ϕ_2 where

$$\phi_2 = \frac{\nu_2}{\nu_1 + \nu_2} \tag{4}$$

The result is important for the discussion in Part 3. Multiplication of the ν-values by RT gives the corresponding moduli. The effective modulus of the first network after removal of first network cross-links, G_{1e}, has been calculated for a first network modulus, G_1, of 0.75 MPa. In Figure 1, G_{1e} is plotted against the modulus of the second network before removal of the first network cross-links, G_2. It can be seen that the memory effect increases with increasing modulus or degree of cross-linking of the second network. G_x and $G_{2,max}$ are related to the experiment to be discussed in Part 3.

Part 2. Two-Network Method. Different Types of Strain.

Uncross-linked linear polymers of high molecular weight ex-hibit a pronounced rubber plateau for a certain range of time and temperature (11). In this region, the material behaves similarly to a cross-linked elastomer: The shear modulus is typically of the order of 1 MPa, the extensibility is several hundred percent with nearly complete recovery, and the isochronal stress-strain curve follows Mooney-Rivlin behavior (21). These properties are all non-equilibrium properties; given enough time the chains will disentan-gle, the modulus drops towards zero, and the recovery will be incomplete. However, the properties described above indicate that the highly entangled chains form a temporary network structure with rubberlike properties. The question is whether the introduc-tion of chemical cross-links will trap the entangled structure in such a way that it gives a large modulus contribution at elastic equilibrium or whether the effect relaxes to zero.

It was proposed by J.D. Ferry (15,22) that the temporary network of highly entangled chains could replace the first network of the two-network theory. The experiment is performed in the following manner: An uncross-linked amorphous polymer is strained at about T_g+8K. The central portion of the rubber plateau should be reached after a few minutes and the sample is quenched to a temperature well below T_g and irradiated with high energy electrons to a high degree of cross-linking. After heating and release, the sample retracts to the stress-free state-of-ease, see Figure 2.

Expressed in terms of moduli, the Helmholtz elastic free energy relation is given by eq. 5.

$$\Delta A_{el} = G_N(\lambda_x^2 + \lambda_y^2 + \lambda_z^2 - 3) + G_X(\lambda_{x;2}^2 + \lambda_{y;2}^2 + \lambda_{z;2}^2 - 3) \tag{5}$$

where G_N is the equilibrium modulus of the first network of entan-gled chains, and G_X is the equilibrium modulus of the second network due to chemical cross-links. From eq. 5, the stress-strain relations for different types of strain can be derived (10). Measurements of the stress-strain properties and the three lengths shown in Figure 2 allow calculation of G_N and G_X.
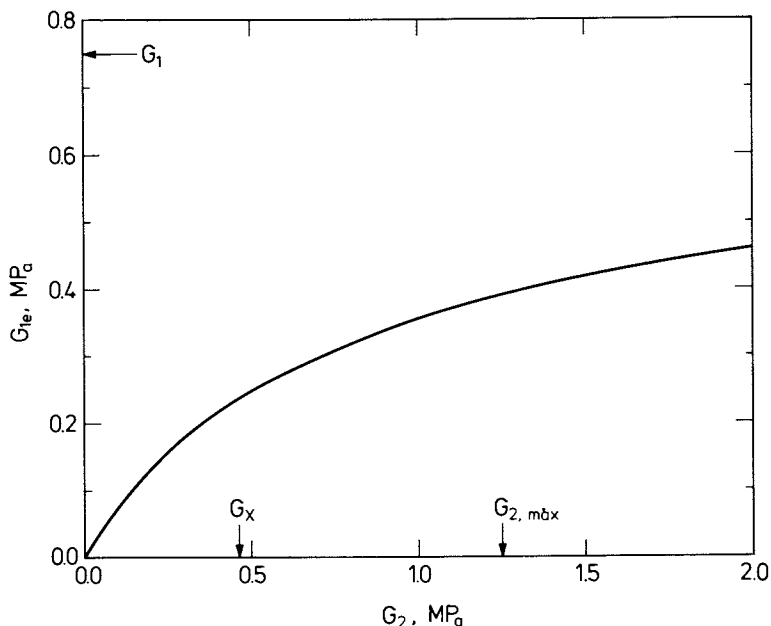
Figure 1.   Effective first network modulus, G_{1e}, after complete removal of first network cross-links plotted against second network modulus, G_2. Calculated from the composite network theory of Flory (19) for $G_1 = 0.75$ MPa.
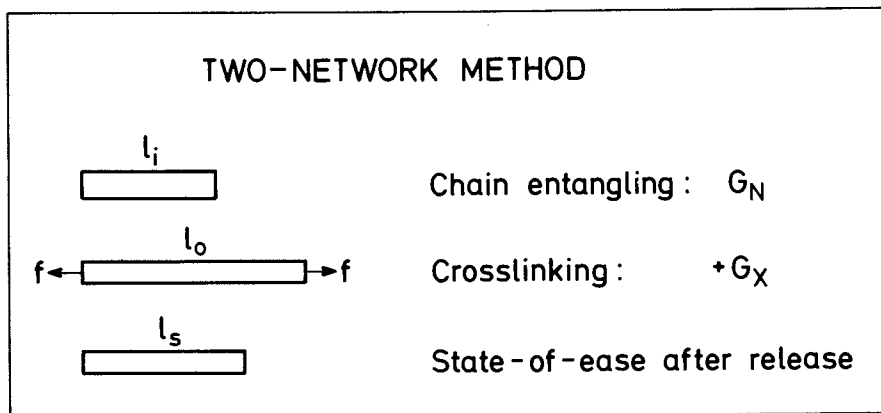
Figure 2.   The principle of the two-network method for cross-linking in a state of simple extension. First network with modulus G_N is entirely due to chain entangling. Second network with modulus G_X is formed by cross-linking in the strained state. Both G_N and G_X can be calculated from the two-network theory.

The results are shown in Figure 3 for 1,2-polybutadiene cross-linked in states of either simple extension, equibiaxial extension, or pure shear. The samples were allowed to relax for 30s at T_g+8K before quenching and irradiation with 10 MeV electrons at T_g-27K. It can be seen that the magnitude of the equilibrium modulus contribution from chain entangling is independent of type of strain. When extrapolated to zero strain, $G_N/G_X \cong 3$, which means that chain entangling contributes about 75% of the total modulus for these samples which are highly cross-linked (10). Furthermore, the equilibrium modulus contribution of chain entangling is found to be approximately equal to the pseudo-equilibrium plateau modulus, G_N^o, of a polybutadiene with a similar microstructure (11). Figure 3 shows that G_N decreases and G_X increases with increasing strain for simple extension. The stress-strain properties of the composite networks are clearly non-Gaussian for simple extension. For equi-biaxial extension and pure shear, the stress-strain properties are more nearly Gaussian (10).

The two-network method has several advantages, especially when the free energy is expressed in terms of moduli as shown in eq. 5. The following information need not be known:
1. Initial molecular weight and molecular weight distribution as long as the molecular weight is very high.
2. Functionality of the cross-links.
3. Value of the front factor.
4. Degree of cross-linking.
5. The relationship between degree of cross-linking and trapping of the entangled structure (the trapping is nearly complete in the present work).

Please note that the frequently used terms 'entanglements' and 'entanglement trapping' (7,8,11) in the present work are replaced by the less specific terms 'chain entangling' and 'trapping of the entangled structure'.

Unfortunately, the method is based on a fairly large number of assumptions. If we want to relate G_N to the pseudo-equilibrium rubber plateau modulus, G_N^o, and to the effect of chain entangling in ordinary networks produced by cross-linking in the unstrained state, the following assumptions are required:
A1. Crystallinity is negligible (23,24,25).
A2. Cross-links introduced at a certain strain contribute nothing to the stress at that particular strain.
A3. The end-to-end distance of the free strands is practically unchanged by the cross-linking process, i.e., the extent of chemical modification of the polymer chains produced by high energy radiation should be small.
A4. Chain scission is negligible.
A5. Chain disentangling prior to and after introduction of chemical cross-links in the strained state is negligible.
A6. The first network is practically at elastic equilibrium when the second network is being formed.
A7. The cross-linking process is fairly random (26).
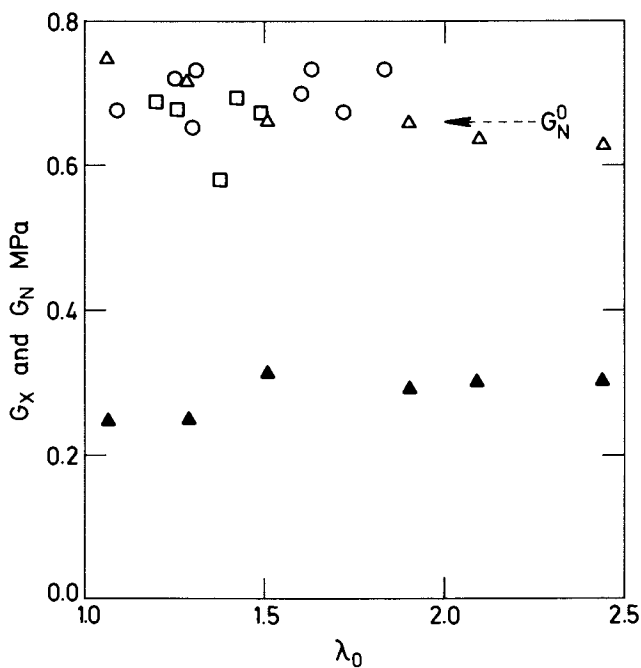
Figure 3. Modulus contributions from chemical cross-links (G_X, filled triangles) and from chain entangling (G_N, unfilled symbols) plotted against the extension ratio during cross-linking, λ_o, for 1,2-polybutadiene. Key: $\bigcirc$, G_N, equibiaxial extension; $\square$, G_N, pure shear; $\triangle$, G_N, simple extension; $G_N{}^\circ$, pseudo-equilibrium rubber plateau modulus for a polybutadiene with a similar microstructure. See Ref. 10.

A8. The Helmholtz elastic free energy relation of the composite network contains a separate term for each of the two networks as in eq. 5. However, the precise mathematical form of the strain dependence is not critical at small deformations.

Although all the assumptions seem to be reasonably fulfilled, a simpler method, which would require fewer assumptions, would obviously be desirable. A simpler method can be used if we just want to compare the equilibrium contribution from chain engangling in the cross-linked polymer to the stress-relaxation modulus of the uncross-linked polymer. The new method is described in Part 3.

Part 3. Stress-Relaxation Two-Network Method

The method (27) can best be explained with reference to Figure 2. After stretching to l_0, the force f is measured as a function of time. The strain is kept constant throughout the entire experiment. At a certain time, the sample is quenched to a temperature well below the glass-transition temperature, T_g, and cross-linked. Then the temperature is raised to the relaxation temperature, and the equilibrium force is determined. A direct comparison of the equilibrium force to the non-equilibrium stress-relaxation force can then be made. The experimental set-up is shown in Figure 4.

The results for a sample of 1,2-polybutadiene with a T_g of 263K (27) are shown in Figure 5. The upper curve shows the temperature, and the lower curve shows the logarithm of the stretching force plotted against the logarithm of time reduced (11) to the stress-relaxation temperature, T_g+8K. The sample is quenched to T_g-27K after 1000s, and chemical cross-links are introduced in the glassy state at a dose of 150kGy of 10 MeV electrons (the dose was erroneously given as 200 kGy in references 27 and 28). The spike observed on the force curve is due to thermal contraction of the sample and the connecting rods by cooling below T_g. As the rate of relaxation is practically zero in the glassy state, log t/a_T remains unchanged during the cross-linking process. After cross-linking, the rate of relaxation is observed to be extremely slow at T_g+8K. When the temperature is increased to T_g+68K, the rate of relaxation is increased approximately by a factor of 10^6. Ten minutes at T_g+68K means that log t/a_T is increased to about 9. The equilibrium force, f_{eq}, at T_g+8K is finally obtained by lowering the temperature to T_g+8K. The equilibrium force is found to be only 7% less than the non-equilibrium stress-relaxation force immediately prior to cross-linking. This difference is the mean of two experiments. A difference of only 4% has been observed in an experiment in which the stress-relaxation prior to cross-linking was extended to log t/a_T equal to 4.5.

Subsequent measurements of the strain (λ_s = 1.152) and the modulus (G_s = 1.29 MPa at 323K) in the state-of-ease together with the strain during cross-linking (λ_o = 1.49) allow calculation of G_N = 0.75 MPa and G_X = 0.49 MPa from the two-network theory (10).

The new method (27) has a number of advantages in comparison to the original two-network method (10). Sample dimensions and the
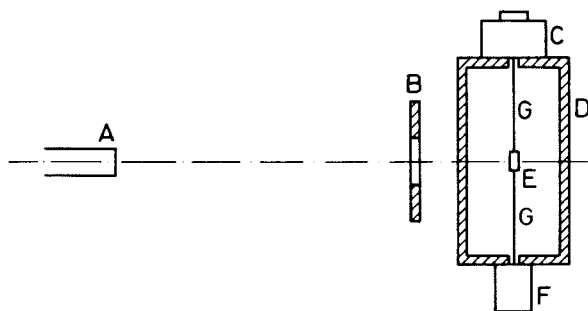
Figure 4. Experimental setup for stress–relaxation and cross-linking at constant simple extension. Key: A, electron accelerator; B, beam aperture; C, force transducer; D, thermostated box; E, sample; F, stretching device; G, connecting rods.
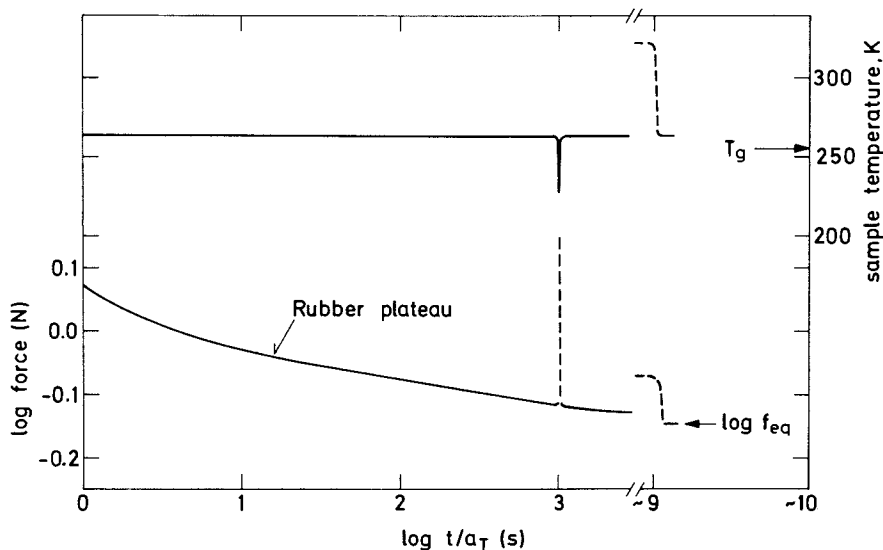
Figure 5. Logarithm of the retractive force at 49% strain (lower curve) and sample temperature (upper curve) plotted against logarithm of time reduced to 263 K. Cross-links are introduced at log t/a$_T$ is 3 in the glassy state where the spike on the force curve is due to thermal contraction upon cooling below the glass transition temperature. Equilibrium force at 263 K after cross-linking is f$_{eq}$. (Reproduced, with permission, from Ref. 27. Copyright 1981, Journal of Chemical Physics.)

degree of strain need not be known. Assumption 1 from Part 2 is
not required if we just want to make a comparison of the equilibrium
and non-equilibrium forces. It is still required if we want to find
the magnitude of the modulus contribution from chain entangling by
itself. This point will be discussed in detail below. The other
assumptions can quickly be disposed of. The experimental fact,
that the equilibrium and non-equilibrium forces are practically
equal, simplifies the analysis, and it shows directly that assump-
tions 2-6 of Part 2 are fulfilled, subject to the comments given
below. Assumptions 7 and 8 are unnecessary in the stress-relaxation
method since the sample is kept at constant length during the entire
experiment. The cross-links merely serve the purpose of trapping the
entangled structure.

Re A3. High energy radiation causes some cyclization of the pen-
        dant vinyl groups (29). This should cause a stiffening of
        the chain and thus an increase in $\langle r_0^2 \rangle$ of the free network
        strands. The modulus should then be decreased by the ratio
        $\langle r^2 \rangle / \langle r_0^2 \rangle$ (30). However, the effect is apparently too
        small to cause a significant decrease in the modulus.

Re A5. The experiment shows that no chain disentangling takes
        place after introduction of chemical cross-links in the
        strained state. Chain disentangling may take place prior
        to cross-linking if the relaxation period is long enough.

Re A6. It may seem surprising that the entangled network should
        be at virtual equilibrium when the second network is
        being formed. It probably means that there is short range
        equilibrium during most of the process of disentangling
        of linear chains, namely the reptation process (31). It
        is the latter process which is prevented by trapping of
        the entangled structure.

The stress-relaxation two-network experiment would have been dif-
ficult to analyze if the equilibrium force were much smaller than
the non-equilibrium force immediately prior to cross-linking. It
would then have been necessary to make a detailed discussion of
the possibility of complete disappearance of the first stage network
(19). The memory effect discussed in Part 1 could give rise to an
appreciable equilibrium force. However, Figure 1 shows that the
memory effect, expressed as the modulus G_{1e}, could never exceed
about 50% of G_1 for the degree of cross-linking produced in the
present experiment. The curve in Figure 1 is calculated for $G_1 =
G_N = 0.75$ MPa. Since the composite network modulus $G_s \geqslant G_1 + G_2$,
it follows that the maximum possible modulus of the second network
$G_{2,max} = 1.29$ MPa. This case is included for comparison only. G_x
is the modulus contribution from the second network calculated
from the two-network theory without taking disappearance of the
first network into consideration. It is concluded from Figure 1
that the memory effect cannot explain the experimentally observed
near equality of the non-equilibrium and equilibrium moduli shown
in Figure 5.

    The only question remaining, is the following: Is it possible

that the stress-relaxation modulus and the equilibrium modulus observed in Figure 5 could be partly due to crystallinity? The atactic 1,2-polybutadiene sample used in the experiment has a density of 885 kg m^{-3} and shows no sign of crystallinity by differential scanning calorimetry with a scanning rate of 40K per minute. It has been suggested by Flory (23) and by Mark and co-workers (24,25) that microcrystallites may still play a big role for the elastic properties. The stress-relaxation two-network experiment offers an ideal method for testing this hypothesis. Referring to Figure 2, only chain entangling and possibly crystallinity contribute to the retractive force at the length l_0. The equilibrium force should therefore be measured as a function of tempeature for constant extension ratio, λ_0, corrected for thermal expansion. Any melting of crystallites should give rise to an abrupt change in the force-temperature curve or in the slope of the curve. The results are shown in Figure 6. In the temperature range 263 to 373K the behavior is completely reversible, i.e., no melting has taken place. When the temperature is increased to 393K and slightly above, discoloration and degradation take place. The experiment is performed in a nitrogen atmosphere but consumption of the antioxidant in the cross-linking process has decreased the stability of the polymer. It is obvious from Figure 6 that no melting of crystallites takes place up to at least 383K. According to Obata and co-workers (32) any melting in atactic or nearly atactic 1,2-polybutadiene should take place below 340K. It is concluded that microcrystallinity plays no role in the present work.

Conclusions
     The two-network method has been carefully examined. All the previous two-network results were obtained in simple extension for which the Gaussian composite network theory was found to be inadequate. Results obtained on composite networks of 1,2-polybutadiene for three different types of strain, namely equibiaxial extension, pure shear, and simple extension, are discussed in the present paper. The Gaussian composite network elastic free energy relation is found to be adequate in equibiaxial extension and possibly pure shear. Extrapolation to zero strain gives the same result for all three types of strain: The contribution from chain entangling at elastic equilibrium is found to be approximately equal to the pseudo-equilibrium rubber plateau modulus and about three times larger than the contribution from chemical cross-links.
     A new stress-relaxation two-network method is used for a more direct measurement of the equilibrium elastic contribution of chain entangling in highly cross-linked 1,2-polybutadiene. The new method shows clearly, without the need of any theory, that the equilibrium contribution is equal to the non-equilibrium stress-relaxation modulus of the uncross-linked polymer immediately prior to cross-linking. The new method also directly confirms six of the eight assumptions required for the original two-network method.
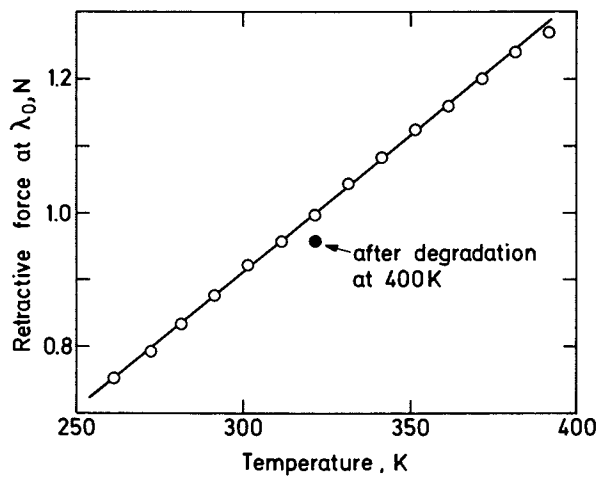
Figure 6.   Retractive force at constant strain, λ_0 corrected for thermal expansion, plotted against temperature. Behavior is completely reversible in range of 263 to 373 K. Serious degradation takes place above 393 K.

It is clearly shown that chain entangling plays a major role in networks of 1,2-polybutadiene produced by cross-linking of long linear chains. The two-network method should provide critical tests for new molecular theories of rubber elasticity which take chain entangling into account.

Literature Cited
1. Flory, P.J. Proc.R.Soc.London, Ser. A. 1976, 351, 351-378.
2. Flory, P.J. J.Chem.Phys. 1977, 66, 5720-5729.
3. Flory, P.J. Polymer 1979, 20, 1317-1320.
4. Flory, P.J. Macromolecules 1979, 12, 119-122.
5. Flory, P.J., paper in this book.
6. Moore, C.G.; Watson, W.F. J.Polym.Sci. 1956, 19, 237-254.
7. Dossin, L.M.; Graessley, W.W. Macromolecules 1979, 12, 123-130.
8. Pearson, D.S.; Graessley, W.W. Macromolecules 1980, 13, 1001-1009.
9. Carpenter, R.L.; Kramer, O.; Ferry, J.D. Macromolecules 1977, 10, 117-119.
10. Hvidt, S.; Kramer, O.; Batsberg, W.; Ferry, J.D. Macromolecules 1980, 13, 933-939.
11. Ferry, J.D. "Viscoelastic Properties of Polymers", 3rd ed.; Wiley: New York, N.Y., 1980.
12. Ronca, G.; Allegra, G. J.Chem.Phys. 1975, 63, 4990-4997.
13. Mark, J.E. Makromol.Chem.Suppl. 1979, 2, 87-97.
14. Gottlieb, M.; Macosko, C.W.; Benjamin, G.S.; Meyers, K.O.; Merrill, E.W. Macromolecules 1981, 14, 1039-1046.
15. Kramer, O.; Carpenter, R.L.; Ty, V.; Ferry, J.D. Macromolecules 1974, 7, 79-84.
16. Carpenter, R.L.; Kramer, O.; Ferry, J.D. J.Appl.Polym.Sci. 1978, 22, 335-342.
17. Kan, H.-C.; Ferry, J.D. Macromolecules 1979, 12, 494-498.
18. Berry, J.P.; Scanlan, J.; Watson, W.F. Trans.Faraday Soc. 1956, 52, 1137-1151.
19. Flory, P.J. Trans.Faraday Soc. 1960, 56, 722-743.
20. Lodge, A.S. Rheology Research Center Report, 61,University of Wisconsin, Madison, 1980.
21. Noordermeer, J.W.; Ferry, J.D. J.Polym.Sci., Polym.Phys.Ed. 1976, 14, 509-520.
22. Ferry, J.D. Prelim.Rept., ARPA Mater. Summer Conf. 1971, 1, 327.
23. Erman, B.; Wagner, W.; Flory, P.J. Macromolecules 1980, 13, 1554-1558.
24. Mark, J.E.; Llorente, M.A. Polymer J. 1981, 13, 543-553.

25. Llorente, M.A.; Mark, J.E. J.Polym.Sci., Polym.Phys.Ed. 1981,
    19, 1107-1120.
26. Falender, J.R.; Yeh, G.S.Y.; Mark, J.E. J.Chem.Phys. 1979, 70,
    5324-5325.
27. Batsberg, W.; Kramer, O. J.Chem.Phys. 1981, 74, 6507-6508.
28. Batsberg, W.; Kramer, O. Polymer Preprints 1981, 22(2),171-172.
29. von Raven, A.; Heusinger, H. J.Polym.Sci., Polym.Chem.Ed. 1974,
    12, 2255-2271.
30. Graessley, W.W. Adv.Polym.Sci. 1974, 16, 1-179.
31. de Gennes, P.G. J.Chem.Phys. 1971, 55, 572-579.
32. Obata, Y.; Tosaki, C.; Ikeyama, M. Polymer J. 1975, 7, 207-216.

Optical Studies of Rubbers

R. S. STEIN, R. J. FARRIS, S. KUMAR, and V. SONI

University of Massachusetts, Polymer Research Institute, Amherst, MA 01003

This paper deals with the application of
photoelastic, swelling, and light scattering
measurements to the study of crosslinked (model
networks as well as randomly crosslinked)
rubbers. Molecular weight between the crosslinks
is determined from equilibrium swelling measure-
ments. Deviations in the birefringence occur
from the Gaussian theory. Increase in the glass
transition temperature and in density is
observed with an increase in the crosslinking
density. Light scattering experiments are done
to study the inhomogeneities in the networks
which are of the order of the wavelength of
light. These experiments suggest the presence
of regions of varying degree of crosslinking in
the randomly crosslinked samples. Use of
neutron scattering is contemplated to study the
inhomogeneities which are of appreciably smaller
size than can be studied by light scattering.

There have been numerous studies to understand the
Gaussian statistical theory of rubber elasticity (or the
departures from it) (1-13). Deviations from Gaussian theory
occur for three reasons: (i) chains reach limiting extension
so that the Gaussian assumption inherent in both the
birefringence and the stress theories is no longer adequate,
(ii) when the Gaussian assumption no longer applies, the
assumption of affine transformation of crosslinking points (or
their mean positions) does not suffice, and (iii) for highly
extended chains, the assumption of entropic origin of stress
is inadequate. Enthalpic contributions ensue because of con-
formational changes, bond angle bending, and stretching.
Recent small angle neutron scattering experiments shed uncer-
tainty on the assumption of affine deformation (14-18). There

is significant work going on to understand the effect of junc-
tion fluctuations and that of chain entanglements on various
network properties (19-25). Deviations from ideal behavior
have conventionally been described by the empirical
Mooney-Rivlin equation. Since this equation is applicable
only to the restricted section of the stress-strain curve, an
alternative to the Mooney-Rivlin equation has recently been
proposed by Gee (28). The network collapse problem has been
worked on by Eichinger (29). The number of monomer units per
statistical segment could be determined either from stress-
birefringence (30) or from infrared dichroism (31).

   Inhomogeneities in a real network may occur either
because of a continuous distribution of molecular weight
between crosslinks or due to the regions of different average
molecular weights (as may be the case in randomly crosslinked
networks).

   A general treatment of the scattering of radiation by an
inhomogeneous material was developed by Debye and Bueche (32)
and visible light scattering was used to investigate the
inhomogeneities in the glass. Application of light scattering
to determine inhomogeneity in networks has been theoretically
demonstrated by Stein (33) and experimentally by Bueche (34).
This is based on the principle that the effect of heteroge-
neity on the local degree of swelling results in enhanced
light scattering arising from resulting refractive index fluc-
tuations in the swollen state (33). Wun and Prins (35) have
also given a separate theoretical treatment and experimental
results to assess the non-random crosslinking in polymers
using light scattering. However, light scattering will deter-
mine the inhomogeneities of the order of wavelength of light.
Inhomogeneities of smaller order in magnitude may be deter-
mined using x-ray or neutron scattering. X-ray scattering may
not be very useful because of the small difference in electron
density of most diluents from that of the polymer.

   The present study was undertaken to understand and
possibly answer some of the above questions. Some of the pre-
liminary results of this study are presented in this paper.

Experimental

   Two types of networks were prepared (i) randomly
crosslinked polybutadiene, and (ii) model urethane networks,
(a) polybutadiene based, and (b) poly(ε-caprolactone) based.
The randomly crosslinked networks were prepared from polybuta-
diene (Duragen® 1203 obtained from General Tire and Rubber
Co.) crosslinked with di-cumyl peroxide. Specifications of
the as obtained polybutadiene are given in Table I.
Polybutadiene was purified by dissolving in benzene and preci-
pitating in methanol. Precipitated polybutadiene was
redissolved in benzene. Seven different weights of dicumyl

TABLE I

Sample	DCP wt. %	v_{2m}*	$(1-v_{2c})$**	ρ	M_c	N†	T_g(°K)	$a(v_{2m})^{1/3}$ (Å)††	
BUT-21	2	0.165	0.047	0.91	7900	146	166.7	-	Polybutadiene (Duragen® 1203)
BUT-22	4	0.196	0.035	0.91	5350	99	167.7	2500	(i) cis 92%
BUT-23	7.7	0.222	0.088	0.91	4000	74	167.5	6500	(ii) Trans 4%
BUT-24	11	0.23	0.080	0.91	3700	68	169.5	5100	(iii) Vinyl 4%
BUT-25	15.3	0.25	0.094	0.91	3000	55	170.0	4900	$M_n = 149000$
BUT-26	20.3	0.376	0.145	0.93	1100	20	173.0	4500	$M_w = 401000$
BUT-27	30.0	0.446	0.136	0.95	650	12	179.5	4700	

*Volume fraction of polymer at equilibrium swelling in C_6H_6.

**Fraction of the extracted material (extraction in C_6H_6).

†Average number of monomer units between crosslinks.

††Inhomogeneity length in unswollen sample as determined by light scattering.

peroxide (hereafter referred to as DCP) were dissolved in ben-
zene and these solutions were mixed in seven solutions of
polybutadiene in such a way that the concentration of DCP in
polybutadiene was 2%, 4%, 7.7%, 11%, 15.3%:, 20.3%, and 30% by
weight. One percent (by weight of polybutadiene) antioxidant
[2,2'-methylene bis(6-tert-butyl-p-cresol)] was added in each
solution. Films were cast from these solutions in Teflon
lined molds, and later cured at 140°C under a pressure of 2000
lbs./sq. inch for 40 min. These networks are hereafter
referred to as But 21, But 22, But 23, But 24, But 25, But 26,
and But 27.
    Model networks were prepared using hydroxyl terminated
polymer and isocyanates. (a) Bifunctional hydroxyl terminated
polybutadiene (Butarez, from Phillips Petroleum) was
crosslinkined with tris (p-isocyanatophenyl)-thiophosphate
(Desmodur RF, from Mobay Chemical Co.). This crosslinked
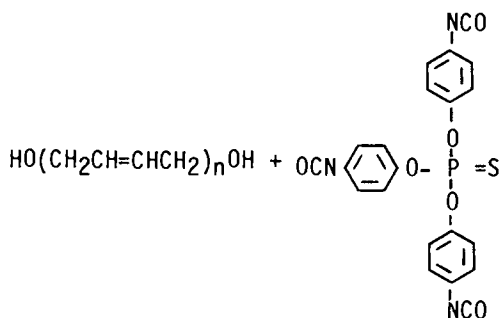
network is hereafter referred to as B2. (b) Trifunctional
poly(ε-caprolactone) (PCP-0310, from Union Carbide) was cross-
linked with hexamethylene diisocyanate.

$$\varepsilon = [(CH_2)_5 \overset{\overset{O}{\|}}{C}-O]_n$$

$$HO - \varepsilon - CH_2 - \underset{\underset{\varepsilon}{\underset{|}{CH_2}}}{\overset{\overset{CH_3}{|}}{C}} - CH_2 - \varepsilon - OH \;+\; OCN(CH_2)_6NCO$$

$$OH$$
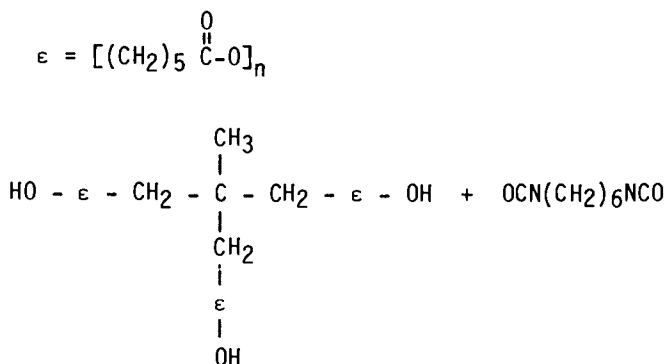
This network is hereafter referred to as PCP2. In both cases

(a) and (b), the hydroxyl terminated polymer was degassed in vacuum for about 2 hours at 50°C. Stoichiometric ratio of the corresponding isocyanate was added and reactants mixed under vacuum for about 15 minutes. During this time, temperature rose to about 75°C. The reaction mixture was then poured into Teflon lined molds and cured at 100°C for 24 hours.

All these networks, B2, PCP2, and But 21-27, were stirred in benzene for 5 days and the uncrosslinked polymer extracted.

Equilibrium swelling measurements have been done on B2 and on But 21-27 in benzene. No swelling data is reported for the PCP2 system for the reasons stated later in this paper. For the measurement of the stress-optical coefficient, birefringence was measured on a special set up on the Instron (36). This set up uses the principle of transmission of light through crossed polaroids (polaroids make 45° angles to the stretching axis) and the transmitted light intensity was recorded using a photomultiplier tube. For the calculation of true birefringence, thickness of the sample at extension ratio λ was taken to be $t/\sqrt{\lambda}$, where t is the thickness of the unstretched sample.

The glass transition temperature was measured on a Perkin-Elmer DSC-II at a heating rate of 20°C/minute on But21-27 samples. Light scattering studies have also been done on these samples at equilibrium swelling using a one dimensional optical multichannel analyzer (37). In a second experiment, light scattering was measured on a sample which has polybutadiene, dicumyl peroxide, and benzene in the same weight fractions as the crosslinked sample at equilibrium swelling.

Theory

The swelling of a network is described by the Flory-Rehner theory (38) which gives

$$M_C = \frac{\rho \overline{V}_1 (v_{2m} - 2v_{2m}^{1/3})}{2[\ln(1 - v_{2m}) + v_{2m} + \chi v_{2m}^2]} \tag{1}$$

where M_C is the molecular weight between crosslinks, v_{2m} is the volume fraction of rubber in the swollen network, ρ is the density of the dry rubber, $\overline{V}_1$ is the partial molar volume of the solvent, and χ is the solvent-solute interaction parameter. Equation (1) is applicable if chains deform affinely. Since the assumption of affine deformation may not be true (14-18), the most reliable interpretation of the swelling results utilizes the recent theory of Flory (39). In this the extent to which the deformation is non-affine depends on the looseness with which the crosslinks are embedded in the

network structure. From this theory the molecular weight
between crosslinks is given by the following relationship
($\underline{13},\underline{39}$)

$$M_c = \frac{-F_3 \, \rho \cdot V_1 v_{2c}{}^{2/3} \cdot v_{2m}{}^{1/3}}{\ln(1 - v_{2m}) + v_{2m} + X_1 v_{2m}{}^2} \tag{2}$$

where F_3 is a factor characterizing the extent to which the
deformation in swelling approaches the affine limit and v_{2c} is
the volume fraction of polymer incorporated in the network
structure.

   Calculation of χ. The heat of mixing per unit volume is
given by ($\underline{40}$)

$$\Delta H_m = v_1 v_2 (\delta_1 - \delta_2)^2 \tag{3}$$

where v_1 and v_2 are volume fractions of the diluent and
polymer, respectively. δ_1 and δ_2 are solubility parameters
of the diluent and the polymer respectively. Heat of mixing
per unit volume is given by ($\underline{41}$)

$$\Delta H_m = kT X_H n_1 v_2 \tag{4}$$

where k is the Boltzman constant, T the absolute temperature,
X_H is the enthalpic contribution to the interaction parameter
between diluent and polymer [interaction parameter (χ) =
entropic contribution (χ_s) + enthalpic contribution (X_H)], and
n_1 is the partial number of moles of diluent in one molar
volume of the mixture. Under the assumption that at low con-
centration of the polymer, the partial molar volume $\overline{V}_1$ is
approximated to the molar volume V_1, eqns. (3) and (4) gives

$$X_H = \frac{(\delta_1 - \delta_2)^2 V_1}{RT} \tag{5}$$

Solubility parameter values for the diluents were taken from
the literature ($\underline{42}$) and for polymers these values were calcu-
lated using Small's method ($\underline{43}$), according to which

$$\delta = \frac{\sum F}{V}$$

where $\sum F$ is the summation of molar attraction constants over all groups, and is defined as $\sum F = (EV)^{1/2}$, where E is the molar cohesive energy. Using the values of F given by Small, the value of χ_H calculated for the polybutadiene-benzene system is 0.199.

There is an enthalpic as well as entropic contribution to the interaction parameter. It was thought (44) that probably the major contribution is enthalpic. However, empirical values between 0.1 - 0.2 (44) and between 0.2 - 0.3 (43) were quoted for entropic contribution to the interaction parameter by Huggins and Small, respectively. Flory (45) has shown for a number of polymer-solvent systems that entropic contribution to the interaction parameter is very significant and sometimes much larger than enthalpic contribution. For the polybutadiene-benzene system, Rowland and Labun (46) have given an experimental value of $\chi = 0.387$. Using $\chi_H = 0.199$ for this system as previously calculated, we obtain $\chi_S = 0.188$. Though χ_H was calculated for the PCP2-benzene system, χ could not be obtained in the absence of χ_S for this system and hence M_C was not calculated from the swelling data on PCP2.

The above values are applicable only in the limiting case of infinite dilution. The interaction parameter varies with the volume fraction of polymer network as has been demonstrated for the PDMS-benzene system by Flory (47) and PDMS-methyl ethyl ketone, PDMS-methyl isobutyl ketone, PDMS-ethyl-n-butyl ketone, and PDMS-diisobutyl ketone by Shiomi et al. (48). Theoretically calculated and experimentally observed values of χ as a function of volume fraction of polymer are given for PDMS in alkanes, aromatic hydrocarbons, and dimethylsiloxane oligomers by Gottlieb and Herskowitz (49). In the case of PDMS-alkanes, χ was practically independent of the volume fraction of polymer.

Birefringence. The birefringence of a crosslinked Gaussian rubber subjected to an affine deformation is described by the theories of Kuhn and Grün (1) and Treloar (2). These predict a stress-optical coefficient given by

$$C = \frac{2\pi(\bar{n}^2 + 2)^2}{45k\,T\bar{n}}\,(b_1 - b_2)_s \qquad (6)$$

where $\bar{n}$ is the average refractive index of the rubber, k is the Boltzman constant, T is the absolute temperature and $(b_1 - b_2)_s$ is the difference between the principal polarizabilities of the statistical segment. $(b_1 - b_2)_s$ may be related to bond polarizabilities, molecular geometry, and conformational energies using the rotational isomer theory of Flory (50). The theory predicts that C should be independent of

degree of crosslinking and inversely proportional to T. This
prediction has been borne out by early experiments of Treloar
(51), Saunders (52), and more recent work by Fukuda et al.
(3). However, it is found that deviations occur at high
degrees of crosslinking and at limiting extension. These
deviations may occur because at limiting extensions the
chain's deformation may not be Gaussian, and the assumption of
affine transformation of crosslinking points may not be
correct as discussed earlier. Kuhn and Grün (1), Treloar (7),
and Treloar and Riding (8) have given non-Gaussian theories
for stress as well as for birefringence. Under the assumption
that (i) all the chains in the network have n links, (ii)
chain vector lengths in the unstrained state are equal to the
root mean square vector length of the free chain, (iii) defor-
mation is affine, and (iv) deformation takes place with change
of volume, Treloar has given the following non-Gaussian
equation for optical anisotropy

$$\frac{(\beta_1 - \beta_2)}{Nn(b_1 - b_2)_s} = \frac{1}{5n} (\lambda^2 - 1/\lambda) + \frac{1}{150n^2} (6\lambda^4 + 2\lambda - 8/\lambda^2)$$

$$+ \frac{1}{350n^3} (10\lambda^6 + 6\lambda^3 - 16/\lambda^3) \qquad (7)$$

where N is the number of chains per unit volume, n is the
number of statistical segments in a chain, β_1 and β_2 are the
principal polarizabilities per unit volume, and λ is the
extension ratio. In addition, temperature dependence (53) of
$(b_1 - b_2)_s$ and distortional birefringence (54) may also be
responsible for departures from eqn. (6). These effects
become more important as the temperature is lowered toward Tg
and dominate as Tg is reached. This has been demonstrated by
Stein et al. (55) in studies of the temperature coefficient of
C for lactoprene rubbers.

        Light Scattering. A perfectly homogeneous medium will
not scatter and that scattering results from fluctuations from
uniformity. The fluctuation in polarizability is defined by

$$n(\underline{r}) = \alpha(\underline{r}) - \overline{\alpha}$$

(For x-ray scattering, the fluctuation in electron density
rather than in polarizability is used.)
        The intensity of scattering of light by a swollen network
is related to two factors. One of these is the mean square
fluctuation in refractive index $\langle \Delta n^2 \rangle$ which is proportional to
the mean squared fluctuation in M_c, $\langle \Delta M_c^2 \rangle$ with a propor-
tionality constant determined by the difference in refractive
index between the rubber and the diluent. The second is the

size of the region of inhomogeneity which may be related to
the correlation function of these fluctuations

$$\gamma(r) = \frac{\langle \Delta n_i \cdot \Delta n_j \rangle_r}{\langle \Delta n^2 \rangle} = \frac{\langle \Delta M_i \cdot \Delta M_j \rangle_r}{\langle \Delta M_c^2 \rangle} \tag{8}$$

where Δn_i and ΔM_i refer to the difference between the refractive index and the molecular weight between crosslinks respectively, and $\langle \, \rangle_r$ refers to an average over pairs separated by distance r. $\gamma(r)$ may be obtained from a Fourier inversion of the variation of scattered intensity $I(q)$ with scattering vector q or else may be approximated by an exponential function as proposed by Debye and Bueche (32)

$$\gamma(r) = \exp(-r/a) \tag{9}$$

where a is a correlation distance which serves as a measure of the average size of the region of crosslink heterogeneity.
     Scattering powers are conventionally represented in terms of the Rayleigh factor defined as

$$R = \frac{I_s}{I_0} \frac{r^2}{V_s}$$

where I_s is the scattered intensity, r is the sample to the detector distance, I_0 is the incident intensity, and V_s is the scattering volume. The Rayleigh factor for exponential expression of eqn. (9) can be written as

$$R_{V_V} = \frac{\omega^4 \sin^2 \psi}{c^4} \cdot \frac{8\pi a^3 \overline{\eta^2}}{(1 + q^2 a^2)^2} \tag{10}$$

where q is the scattering vector given by $(4\pi/\gamma) \sin \theta/2$, and θ is the scattering angle and γ is the wavelength of the radiation. From this eqn. a plot of $R^{-1/2}$ vs q^2 should give a straight line of slope/intercept equal to a^2. The stretching of an inhomogeneously crosslinked network leads to inhomogeneity in the local strain characterized by $\langle \Delta \epsilon^2 \rangle$, and also in the local fluctuations in the orientation. Since the local birefringence is related to local strain via Kuhn and Grün type theory (1), fluctuations in local refractive index anisotropy $\delta = n_\parallel - n_\perp$ will result which will be associated with enhanced depolarized light scattering of the sort discernible by an extension of the theory of Stein and Wilson (56).
     Wun and Prins (32) have used a Gaussian form for the correlation function, and then defined a non-random index in terms of a correlation volume rather than in terms of correlation length.

Results and Discussion

The data on DCP crosslinked polybutadiene is given in
Table I. The characteristics of the uncrosslinked polybuta-
diene are also given in Table I. The values given in various
columns of Table I are weight percent of dicumyl peroxide in
polybutadiene, volume fraction of polymer at equilibrium
swelling (v_{2m}), fraction of the extracted material ($1-v_{2c}$),
density of the crosslinked samples, molecular weight between
crosslinks (M_c), average number of monomer units between
crosslinks (N), glass transition temperature (Tg), and inhomo-
geneity length [$a(v_{2m})^{1/3}$). M_c values for these randomly
crosslinked samples were calculated using eqn. (1) and $\chi=0.387$
(41). These molecular weights (M_c) between crosslinks are
plotted in Figure 1 as a concentration of DCP. A GPC test on
the extracted material did not show a peak in the molecular
weight range of the uncrosslinked polybutadiene. This was
expected however, because the extracted polymer would be the
degraded one. For the calculation of M_c for this system, eqn.
(2) was not employed, due to uncertainty in v_{2c}. Because in
the extracted material, the reaction byproduct may also be

$$\text{C}_6\text{H}_5 - \overset{\overset{\displaystyle CH_3}{|}}{\underset{\underset{\displaystyle CH_3}{|}}{C}} - OH$$
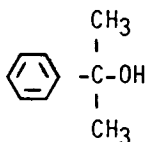
present (a major part of it is likely to evaporate). However,
since the degree of nonaffine deformation is likely to be
greater in higher crosslinked samples, the actual M_c may be
lower than the one reported in Table I. It has been reported
that the density of the crosslinked rubber is higher than the
density of the stoichiometric ratio of the reactants (24, 27).
The density estimates for But 21-27 networks were made by
measuring their reduction in weight in methanol. These den-
sity values are also given in Table I, and the density
increases at higher degrees of crosslinking. It was these
density values which were used in the calculation of M_c.
Glass transition temperature is plotted with increasing degree
of crosslinking in Figure 2. There is a significant increase
in glass transition with increasing degree of crosslinking.
      The data on isocyanate crosslinked polybutadiene (B2) is
given in Table II, and for this the molecular weight (M_c) was
calculated using eqn. (2) ($M_c=10,100F_3$). The expected value
of M_c as obtained from GPC on uncrosslinked polymer should be
somewhere in the range of Mn (5100) to Mw (7400). Comparison
of GPC and swelling data yields that F_3 is in the range of
0.51-0.73, which in turn determines the extent up to which the
chains deform non-affinely.
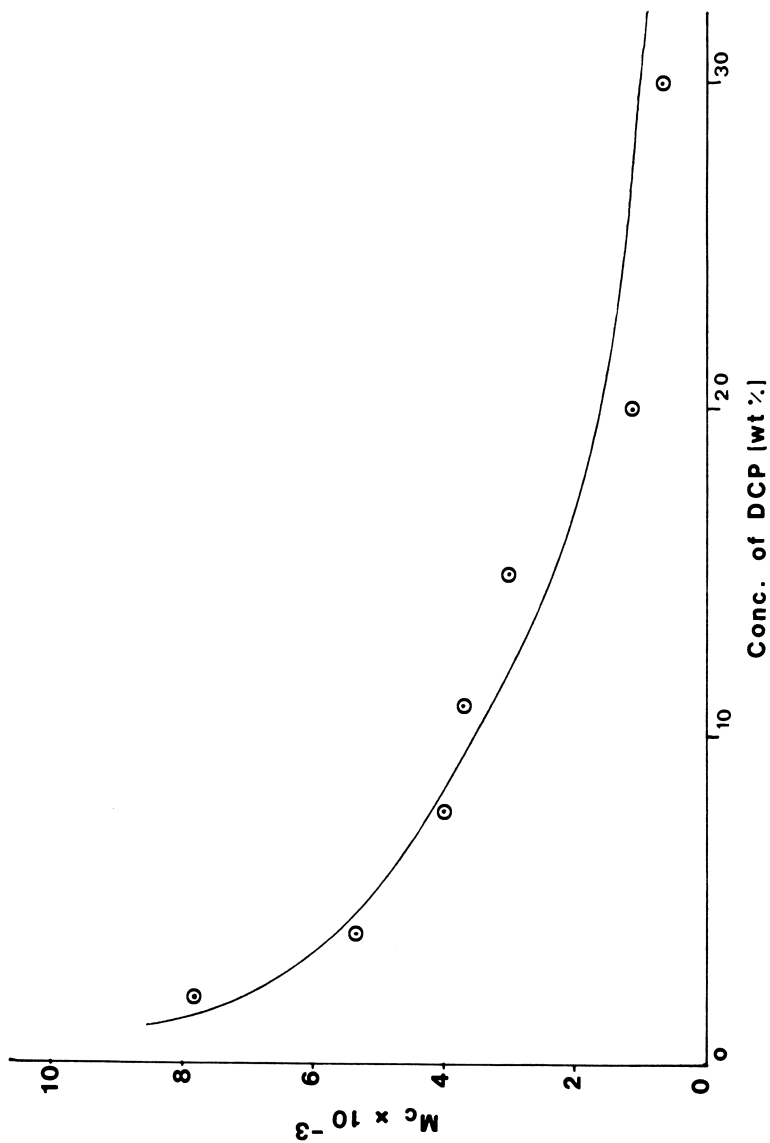
Figure 1.   Molecular weight between cross-links obtained from swelling data as a function of DCP concentration.
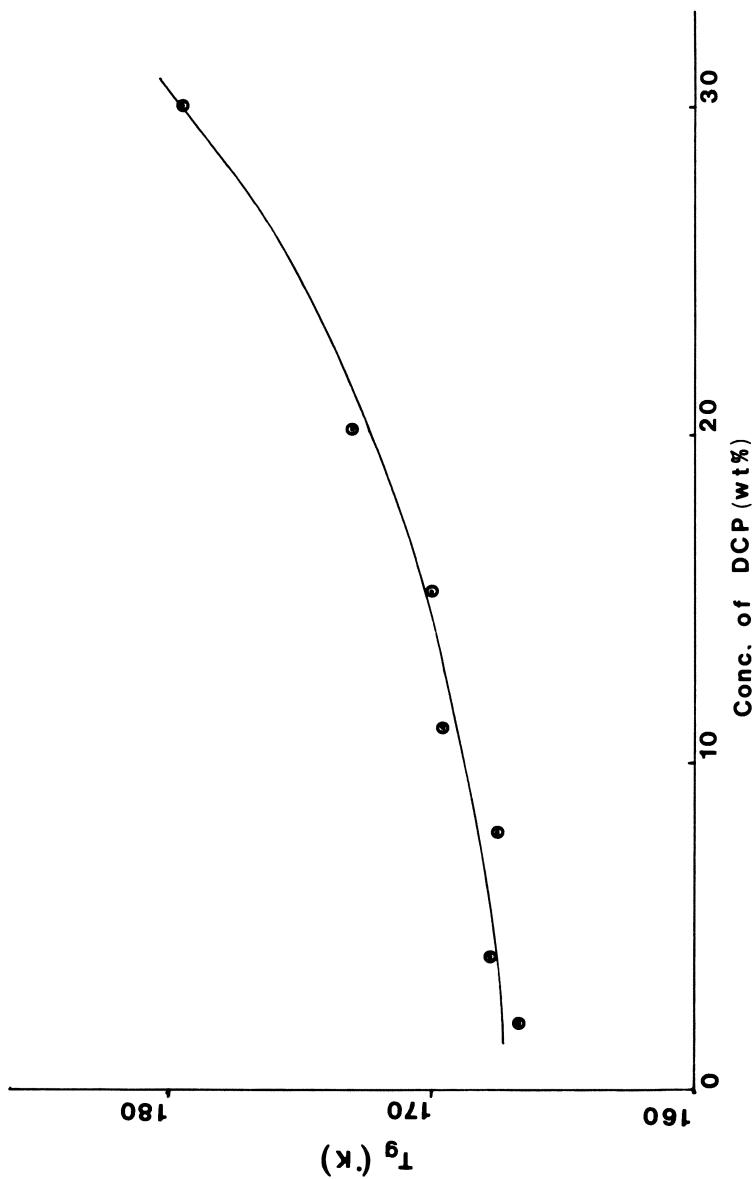
Figure 2.　Glass transition temperature from DSC in cross-linked polybutadiene as a function of DCP concentration.

TABLE II*

Butarez	Crosslinked Polybutadiene (B2)			
Trans 38%	diluent	v_{2m}	v_{2c}	M_c
Cis 35%	benzene	0.154	0.92	10100F$_3$
Vinyl 27%				
Specific Gravity 0.91				
GPC { Mn=5100 Mw=7400				

*See text for details.

Birefringence of isocyanate crosslinked polybutadiene (B2) and for HMDI crosslinked poly(ε-caprolactone) (PCP2) is plotted as a function of stress in Figures 3 and 4 respectively at room temperature. Now in the framework of eqn. (6) such a plot should be linear. In the case of the B2 system (Figure 3) we observe significant deviations from linearity while in the case of the PCP2 deviation from linearity is insignificant. However, in both cases birefringence has a downward turn, that is to say that the stress optical coefficient is decreasing with increasing tensile deformation. Ilavsky et al. (57) have also observed a decrease in the stress optical coefficent at higher extension ratios. The molecular weight of the uncrosslinked poly(ε-caprolactone) (triol) was 900. The effective molecular weight between junctions will be equal to 2/3 of the molecular weight of the polymer plus the molecular weight of hexamethylene diisocyanate (at low molecular weights of polymer, the molecular weight of HMDI cannot be neglected). Therefore, an effective M_c for the PCP2 system is approximated as 800. The extensibility of these samples was very low [λ (at break) = 1.40], and this may be the manifestation of the low molecular weight between crosslinks or the overall inhomogeneity in the network.

For the B2 system (Figure 3), the deviations from linearity are significant and well beyond the limits of experimental error (Δn is accurate within $\pm 0.4 \times 10^{-4}$). Birefringence for this system is also plotted as a function of $\lambda^2 - 1/\lambda$ in Figure 5. This figure also shows a downward turn of birefringence. Though the M_c value for this network is about 5000, the extensibility was still poor [λ (at break) = 1.75]. The deviation from linearity can occur because of two reasons: (i) strain induced crsytallization, and (ii) non-Gaussian deformation of molecular chains. To consider the effect of strain induced crystallization, birefringence of a semicrystalline polymer can be written as (neglecting the effect of form birefringence)

$$\Delta n = X \Delta n_c^\circ f_c + (1 - X) \Delta n_a^\circ f_a \qquad (11)$$

where Δn_c° and Δn_a° are intrinsic birefringences of crystalline and amorphous regions respectively, f_c and f_a are their orientation factors, and X is the volume fraction of crystallites. It has been calculated (58) that the intrinsic birefringence values for the crystallites of polybutadiene are cis $\Delta n_c^\circ = 0.286$, trans $\Delta n_c^\circ = 0.183$, and syndiotactic-1,2 PBD $\Delta n_c^\circ = 0.0054$. In another study (59), the birefringence of the amorphous regions of polybutadiene (60% trans, 30% cis, and 10% vinyl) in the case of limiting orientation was estimated to be 0.0296. Strain induced crystallites will also have very high orientation. Therefore, in the event of strain induced
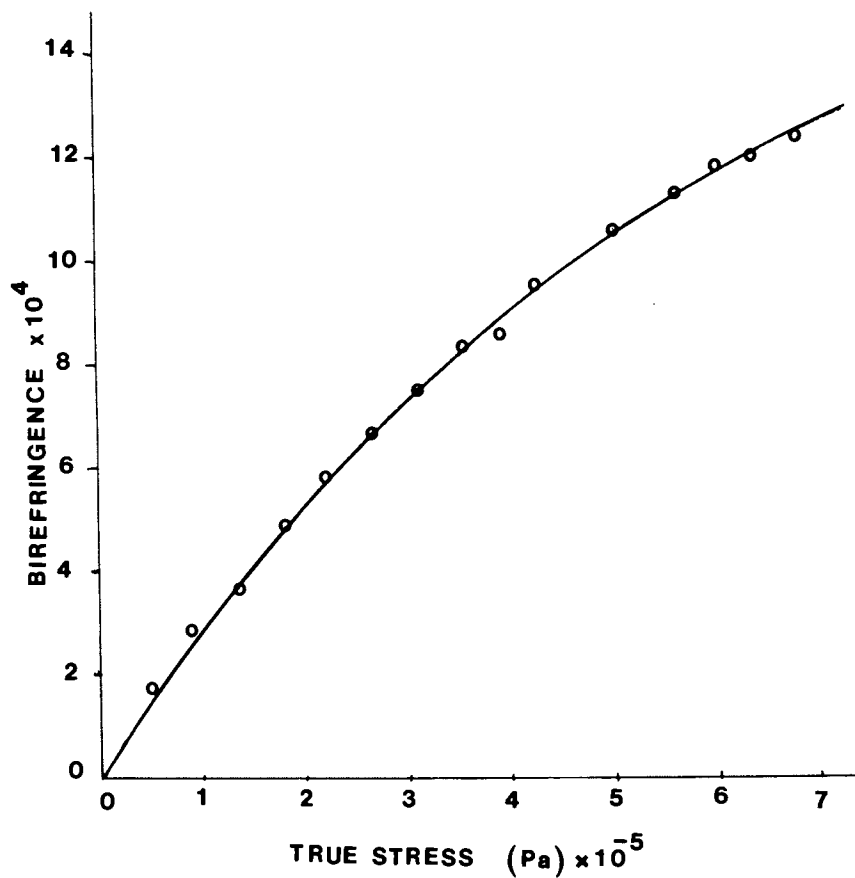
Figure 3. *Birefringence of triisocyanate cross-linked polybutadiene (B2) vs. stress (at room temperature).*
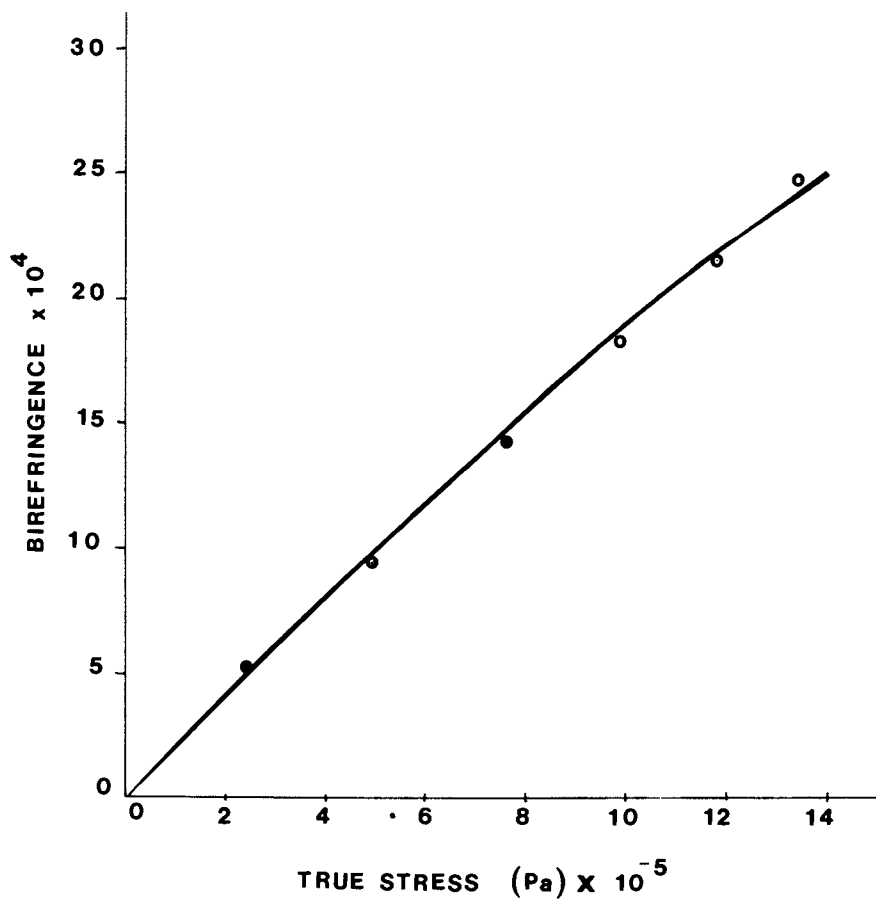
Figure 4.   Birefringence of HMDI cross-linked polycaprolactone (PCP2) as a function of stress (at room temperature).
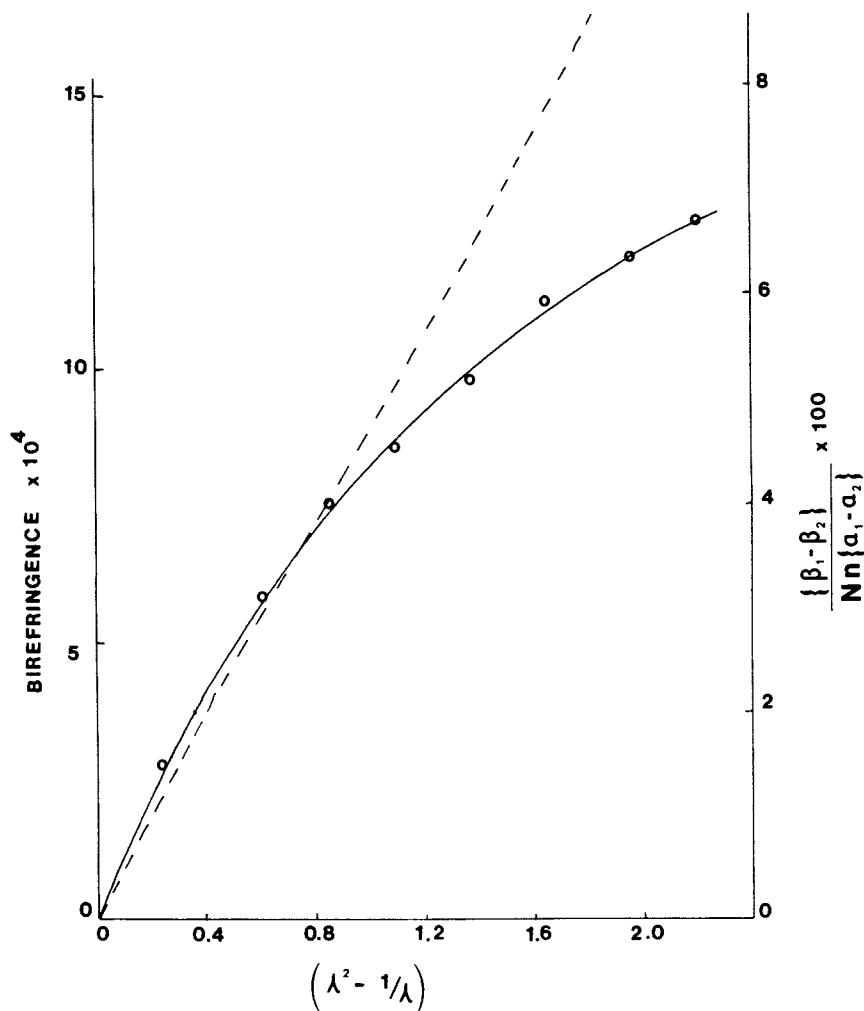
Figure 5.   Birefringence vs. ($\lambda^2 - 1/\lambda$) for B2 system. Optical anisotropy (Eq. 7) for non-Gaussian theory. Key: – – –, n = 5.

crystallization ($f_c>f_a$) and ($\Delta n_c°>\Delta n_a°$), the birefringence
curve in Figure 5 is expected to take an upward turn rather
than a downward turn. This suggests the predominance of a
different phenomenon over strain induced crystallization (if
not the complete absence of it).

Attempts were made to explain the data of Figure 5 in
terms of non-gaussian eqn. (7). Optical anisotropy calculated
from eqn. (7) for n=5 is plotted as a function of ($\lambda^2 - 1/\lambda$)
in Figure 5. In this curve the departures from linearity are
not very significant (however this is not unexpected, because
deviations from gaussian theory occur at high strains). From
Figure 5 it is evident that the non-gaussian theory repre-
sented by eqn. (7) does not explain the experimental results.
Doherty et al. (4) (Figure 2 of reference 4) have observed
similar results on styrene butadiene rubber, with the dif-
ference that in their case the deviation occurs at much larger
extensions and at low temperatures (M_c values for their
samples are not known). Attempts were also made to explain
the results of Figure 5 in terms of a four-chain model (7)
(non-gaussian, non-affine deformation). In the limits of
small strains, the optical anisotropy results of this model
(n=5) almost superposes the results of eqn. (7) (n=5). For
the four chain non-gaussian model if the optical anisotropy is
plotted as a function of stress (Figure 10.3, reference 2),
this curve gives a downward curvature, and this curvature
increases with decreasing n. Though it seems possible to fit
our birefringence-stress data in Figure 3 using small values of
n (less than 5) in terms of four chain model, but that cannot
explain the birefringence-strain results of Figure 5.

To explain the difference between the experimental
results and theory, Doherty et al. (4) have given an empirical
and a theoretical hypothesis. The theoretical hypothesis
concerns the question of the meaning to be attached to the
concept of the "equivalent random link" in the statistical
theory of the randomly-jointed chain. According to Doherty et
al., the assumption that the optical properties of the chain
are describable by a randomly jointed model, using the same
value of n, as for the description of stress has no strictly
logical foundation.

In the derivation of eqn. (7) it was assumed that n
(number of equivalent random links) is the same for all chains.
For our samples (B2 system, Mw/Mn=1.45), this assumption is
definitely not correct. Therefore, it is desirable to obtain
birefringence results on networks prepared from monodisperse
polymer (in that n is constant), before the validity of n
itself is questioned.

Figures 6 and 7 give the data of Fukuda et al. (3) and
that of Saunders (52). The variation of stress optical coef-
ficient of the high cis and high trans, 1,4-polybutadiene is
plotted against M_c in Figure 6, where it is compared with
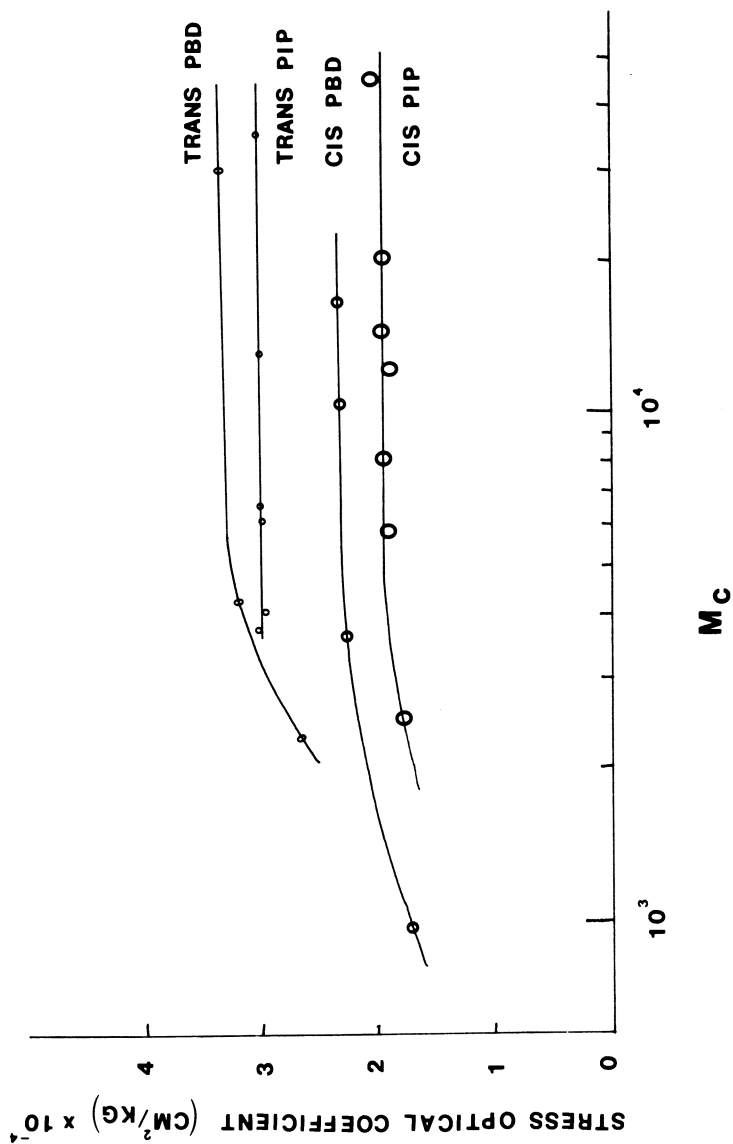
Figure 6. *PIP after Saunders, 1956. Stress optical coefficient as a function of molecular weight between cross-links (3, 52). PBD is polybutadiene. PIP is polyisoprene.*
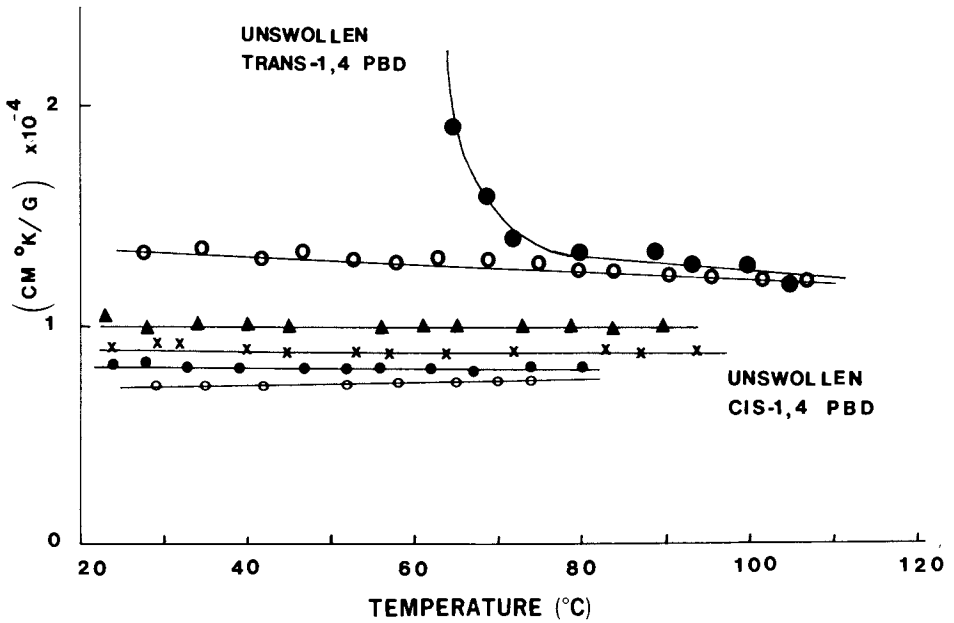
Figure 7.   Stress optical coefficient $\times$ temperature as a function of temperature (3). PBD is polybutadiene. Key: $\bigcirc$, p-xylene; $\blacktriangle$, toluene; $\bullet$, benzene; $\ominus$, CCl$_4$; all of swollen trans–1,4 PBD.

values by Saunders (52) for cis- and trans-1,4 polyisoprene.
It is noted that SOC is independent of M_C above values of
M_C of about 5000 (even more). At lower values of M_C network
chains are sufficiently short that non-gaussian contributions
must be considered.

Figure 7 shows the data on PBD in the swollen and in the
unswollen state. From this it is evident that the product of
stress optical coeffient and temperature is almost constant
with temperature in the swollen state, while in the unswollen
state it exhibits considerable deviation from birefringence
theory (eqn. 6) due to crystallization. Therefore, it is best
to compare experiments and theory in the swollen state.
Gumbrell et al. (60) use the following empirical relationship
for the stress in the swollen state.

$$\frac{\sigma v_2^{1/3}}{2(\lambda - 1/\lambda^2)} = C_1 + C_2/\lambda \tag{12}$$

where σ is the stress referred to the unstrained unswollen
area, λ is the extension ratio referred to the unstrained
swollen dimensions, and v_2 is the volume fraction of rubber in
the swollen state. C_1 and C_2 are independent of the swelling
liquid, but C_2 decreases with increased degree of swelling and
$C_2=0$ at $v_{2m}=0.25$. This is another advantage of doing experi-
ments at high degrees of swelling, so that stress can be
interpreted by a simpler relationship, when $C_2=0$.

Typical light scattering data at equilibrium swelling
(But 22, But 24, But 27) are given in Figure 8, where the
Rayleigh factor is plotted as a function of square of the
scattering vector. Several light scattering tests were run on
uncrosslinked PBD and DCP and antioxidant dissolved in
benzene. These components were taken in the ratio as they
were originally present in But 21-27 samples at equilibrium
swelling. The variation in the scattered intensity with these
different ratios was not very significant. A representative
scattering pattern of this uncrosslinked system is also given
in Figure 8. Scattered intensity increases with increasing
degree of crosslinking, and the intensity of the uncrosslinked
system is very small. Inverse square root of the difference
of the two Rayleigh factors (crosslinked-uncrosslinked) is
plotted in Figure 9 as a function of square of the scattering
vector, and this is a straight line as predicted by the theory
(eqn. 10). Correlation distance 'a' was calculated from
Figure 9 and is given as (slope/intercept)$^{1/2}$. Now since the
light scattering studies were done at equilibrium swelling,
the correlation distance in the unswollen state is defined by
$a(v_{2m})^{1/3}$. These correlation distances are reported in Table
I for But 22-But 27 samples, and are plotted in Figure 10 as a
function of the concentration of DCP. $\overline{\eta^2}$ is proportional to
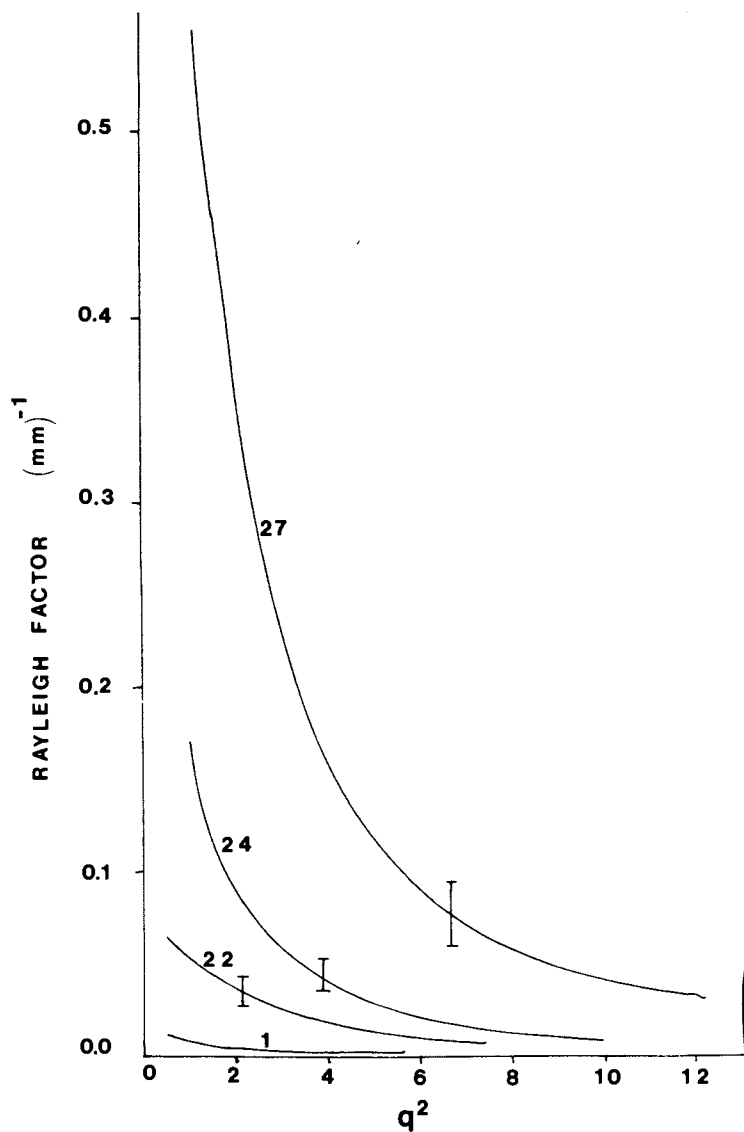
Figure 8.   Rayleigh factor as a function of the square of the scattering vector for But 27, But 24, But 22, and 1. Key: q, units of scattering vector, $(\mu m)^{-1}$.

But 2 7
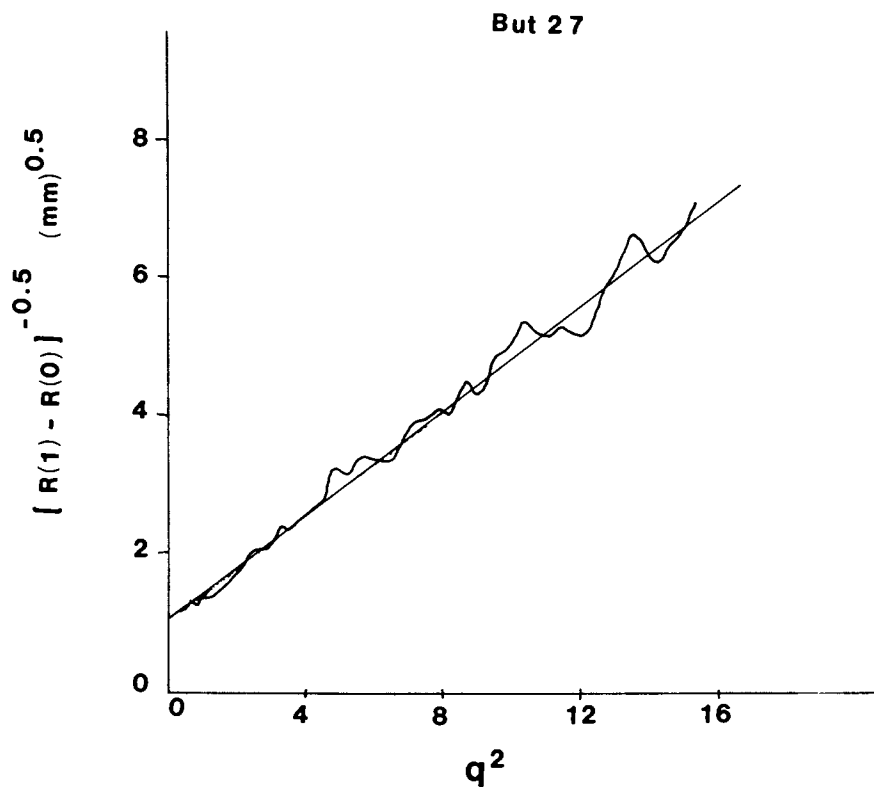
Figure 9. *Inverse square root of the difference of the Rayleigh factors of cross-linked [R(1)] and uncross-linked [R(0)] samples as a function of square of the scattering vector.*
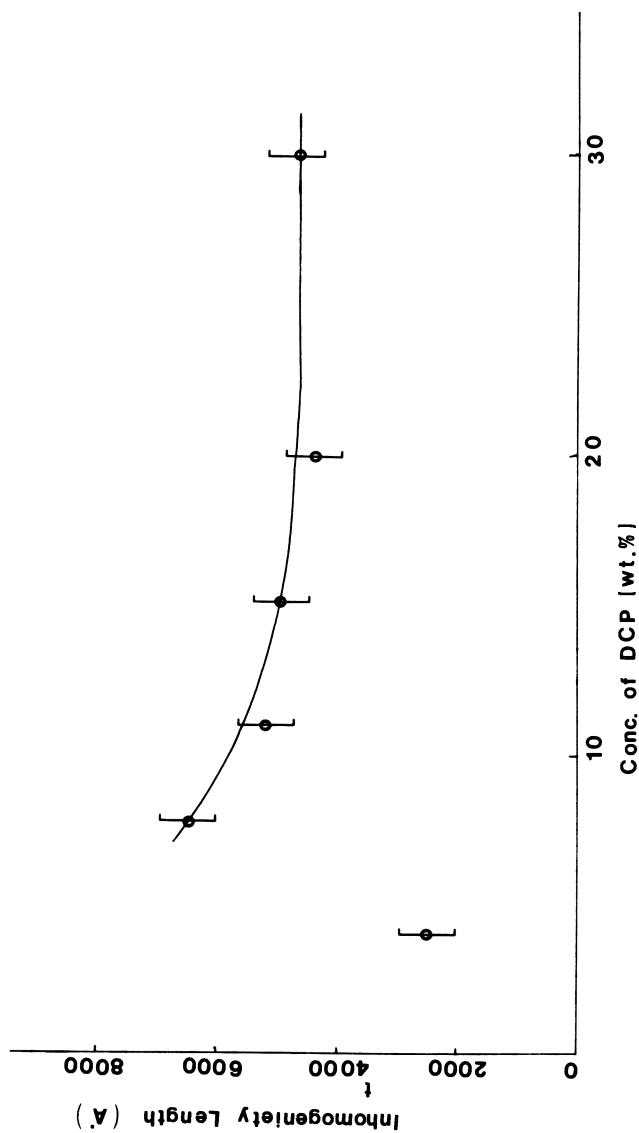
Figure 10.   Inhomogeneity length as a function of concentration of DCP.

$\langle \Delta M_c^2 \rangle$, therefore from eqn.   (10)

$$\Delta M_c = \sqrt{\langle \Delta M_c^2 \rangle} = \left(K \frac{R_{V_v}(1 + q^2 a^2)^2}{a^3} \right)^{1/2} \tag{13}$$

Where K is a constant obtainable from eqn. 10. Therefore,
from the values of a obtained in swollen state (since R_{V_v} is
measured in swollen state), the relative magnitudes of
ΔM_c were calculated using the above relationship (averaged
over several q values). The variation of ΔM_c (in arbitrary
units) as a function of M_c is plotted in Figure 11.
     The correlation function yields a measure of the size of
the regions of inhomogeneity (Figure 10). This size for our
samples is of the order of 5000 Å. Considering But 27, for
which M_c=650, the average junction to junction distance in
this sample would be of the order of 50 Å. Inhomogeneities of
the order of 5000 Å in magnitude could not arise because of
the molecular weight distribution. Large dissymmetries are
also observed by Bueche (34) in polymeric methacrylate and
styrene gels. A possible cause for such a large inhomogeneity
may be the presence of regions of varying degree of cross-
linking at the microscopic level. Such a situation is
explained in Figure 12, where we have several regions, each of
molecular weight between crosslinks equal to M_c and size a_i.
The average of these sizes will be measured from light scat-
tering as correlation function 'a'.
     In Figure 11, ΔM_c is shown as a function of M_c. At
high degrees of crosslinking ΔM_c is small and increases as
M_c is increased. However, if one looks at the dependence of
$(\Delta M_c/M_c)$ on M_c, it is found to increase as M_c is reduced.
Using $(\Delta M_c/M_c)$ as a measure of the inhomogeneity of a net-
work, we find that these networks become more inhomogeneous
as the degree of crosslinking is increased. Such an
increase in network structure inhomogeneity could possibly
account for the low elongations at break of the highly
crosslinked samples.

Acknowledgment
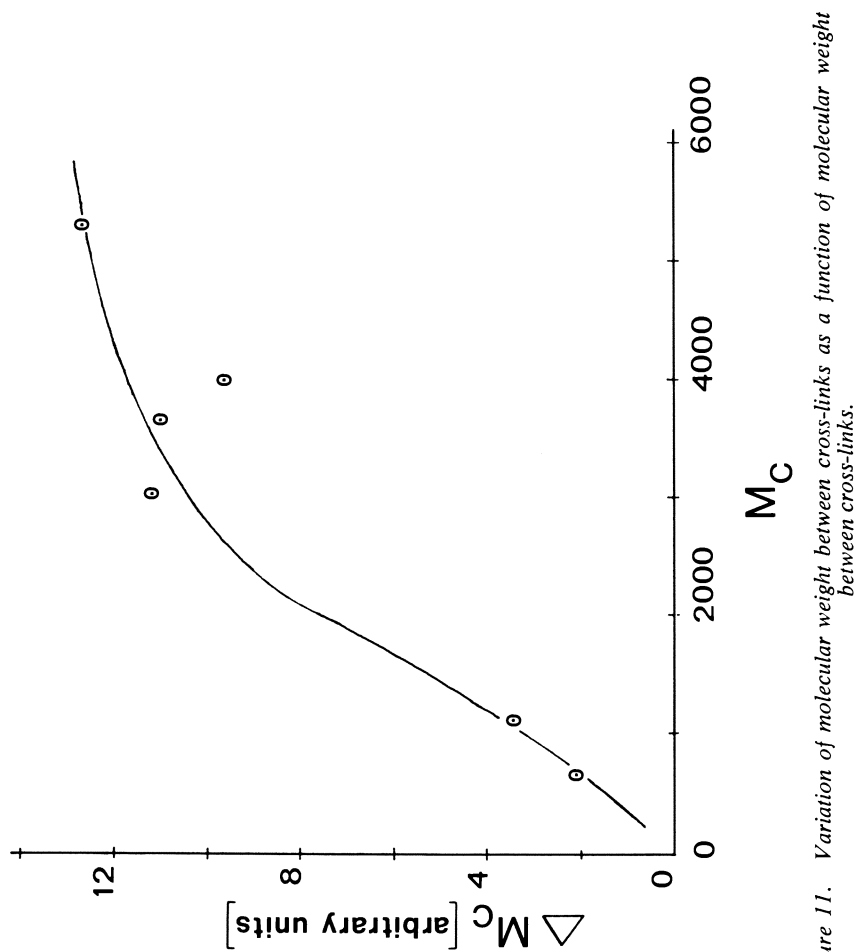
Figure 11.   Variation of molecular weight between cross-links as a function of molecular weight between cross-links.

1

a_1

2

a_2
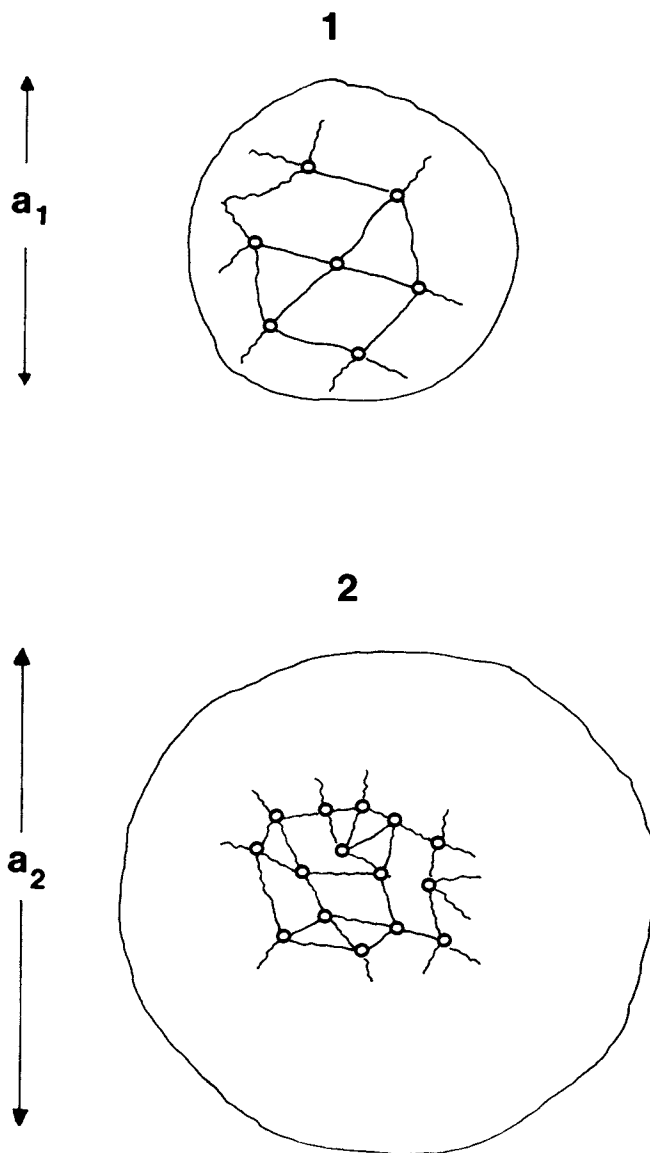
Figure 12.   Inhomogeneity model.

Literature Cited

1. Kuhn, W.; Grün. F. Kolloid Z. 1942, 101, 248.
2. Treloar, L.R.G. "The Physics of Rubber Elasticity", 3rd. ed., Clarendon, Oxford, 1975.
3. Fukuda, M; Wilkes, G.L.; Stein, R.S. J. Polym. Sci. 1971, A2(9), 1417.
4. Doherty, W.O.S.; Lee, K.L.; Treloar, L.R.G. Brit. Polym. J. 1980, 12(1), 19.
5. James, H.M.; Guth, E. J. Chem. Phys. 1943, 11, 455.
6. Mark, J.E.; Kato, M; Ko, J.H. J. Polym. Sci.(Polym. Symp.) 1976, No. 54, 217.
7. Treloar, L.R.G. Trans. Faraday Soc. 1954, 50, 881.
8. Treloar, L.R.G.; Riding, G. Proc. Roy. Soc. 1979, A369, 261 and 281.
9. Sung, P.H.; Mark, J.E. Polym. J. 1980, 12(11), 835.
10. Llorente, M.A.; Andrady, A.L.; Mark, J.E. J. Polym. Sci. 1981, A2(19), 621.
11. Andrady, A.L.; Llorente, M.A.; Mark, J.E. J. Chem. Phys. 1980, 72, 2282.
12. Andrady, A.L.; Llorente, M.A.; Mark, J.E. J. Chem. Phys. 1980, 73(3), 1439.
13. Mark, J.E.; Llorente, M.A. Polym. J. 1981, 13(6), 543.
14. Nierlich, M.; Williams, C.; Boue, F.; Cotton, J.P.; Daoud, M.; Farnoux, M.; Jannink, G.; Picot, C. J. Appl. Cryst. 1978, 11, 504.
15. Picot, C.; Duplessix, R.; Decker, D.; Benoit, H.; Boue, F.; Cotton, J.P.; Daoud, M.; Farnoux, B.; Jannink, G.; Nierlich, M.; deVries, A.J.; Pincus, P. Macromolecules 1977, 10, 436.
16. Benoit, H.; Decker, D.; Duplessix, R.; Picot, C.; Rempp, P.; Cotton, J.P.; Farnoux, B.; Jannink, G.; Ober, R. J. Polym. Sci., Polym. Phys. Ed. 1976, 14, 2119.
17. Hinkley, J.A.; Han, C.C.; Mozer, B.; Yu, H. Macromolecules 1978, 11, 836.
18. Clough, S.B.; Maconnachie, A; Allen, G. Macromolecules 1980, 13, 774.
19. Graessley, W.W. Macromolecules 1975, 8(2), 186.
20. Ronca, G; Allegra, G. J. Chem. Phys. 1975, 63(11), 4990.
21. Dossin, L.M.; Graessley, W.W. Macromolecules 1979, 12(1), 123.
22. Marrucci, G. Macromolecules 1981, 14, 434.
23. Flory, P.J. J. Chem. Phys. 1977, 66(12), 5720.
24. Meyers, K.O.; Bye, M.L.; Merrill, E.W. Macromolecules 1980, 13, 1045.
25. Llorente, M.A.; Mark, J.E. Macromolecules 1980, 13, 681.
26. Mooney, M. J. Appl. Phys. 1940, 11, 582.
27. Rivlin, R.S. Pilos. Trans. 1948, A241, 379.
28. Gee, G. Macromolecules 1980, 13, 705.
29. Eichinger, B.E. Macromolecules 1981, 14, 1071.

30. Stein, R.S.; Tobolsky, A.V. J. Polym. Sci. 1953, 11, 285.
31. Stein, R.S. J. Polym. Sci. 1958, 28, 83.
32. Debye, P; Bueche, A.M. J. Appl. Phys. 1949, 20, 518.
33. Stein, R.S. J. Polym. Sci., Polym. Lett. Ed. 1969, 7, 657.
34. Bueche, F. J. Colloid and Interf. Sci. 1970, 33, 61.
35. Wun, K.L.; Prins, W. J. Polym. Sci., Polym. Phys. Ed.
    1974, 12, 533.
36. Parpart, M.K., Ph.D. Dissertation, Polymer Science &
    Engineering, University of Massachusetts, Amherst, 1979.
37. Wasiak, A.; Peiffer, D.; Stein, R.S. J. Polym. Sci.,
    Polym. Lett. Ed. 1976, 14, 381.
38. Flory, P.J.; Rehner, J., Jr. J. Chem. Phys. 1943, 11,
    521.
39. Flory, P.J. Macromolecules 1979, 12, 119.
40. Hilderbrand, J.H.; Scott, R.L. "The Solubility of
    Non-Electrolytes", Rheinhold, New York, 1959 (3rd ed.).
41. Flory, P.J. "Principles of Polymer Chemistry", Cornell
    University Press, Ithaca, New York, 1953.
42. "Polymer Handbook", J. Brandrup and E.H. Immergut, ed.,
    John Wiley, 1975 (2nd ed.).
43. Small, P.A. J. Appl. Chem. 1953, 3, 71.
44. Huggins, M.L.; Annals of the New York Academy of Sciences
    (ed. W.G. Valentine) Vol. XLIV, 431, 1943.
45. Flory, P.J. Discuss. Faraday Soc. 1970, No. 49, 7.
46. Rowland, T.J.; Labun, L.C. Macromolecules 1978, 11(3),
47. Flory, P.J.; Tatara, Y.I. J. Polym. Sci., Polym. Phys.
    Ed. 1975, 13, 683.
48. Shiomi, T.; Izumi, Z.; Hamada, F.; Nakajima, A.
    Macromolecules 1980, 13, 1149.
49. Gottlieb M.; Herskowitz, M. Macromolecules 1981, 14, 1468.
50. Flory, P.J. "Statistical Mechanics of Chain Molecules",
    Interscience, New York, 1969.
51. Treloar, L.R.G. Trans. Faraday Soc. 1947, 43, 277.
52. Saunders, D.W. Trans. Faraday, Soc. 1956, 52, 1414 and
    1425.
53. Volungis, R.J.; Stein, R.S. J. Chem. Phys. 1955, 23, 1179.
54. Anderson, D.P., Ph.D. Dissertation, Polymer Science &
    Engineering, University of Massachusetts, Amherst, 1981.
55. Stein, R.S.; Krimm, S.; Tobolosky, A.V. Textile Res. J.
    1949, 19, 8.
56. Stein, R.S.; Wilson, P.R. J. Appl. Phys. 1962, 33, 1914.
57. Ilavsky, M.; Hrouz, J.; Dusek, K. J. Macromol. Sci.-Phys.
    1981, B19(2), 227.
58. Hashiyama, M., Ph. D. Thesis, University of Massachusetts,
    Amherst, 1976.
59. Kumar, S.; Stein, R.S., to be published.
60. Gumbrell; Mullins; Rivlin, R.S. Trans. Faraday Soc. 1953,
    49, 1495.

Some Comments on Thermoplastic Elastomers

ROBERT E. COHEN

Massachusetts Institute of Technology, Department of Chemical Engineering, Cambridge, MA 02139

A brief review is given of the important quali-
tative features of thermoplastic elastomers. Parti-
cular emphasis is given to the molecular structure,
bulk morphology and interfacial character of these
materials. Both equilibrium and nonequilibrium
structures are discussed

A large proportion of the papers in this symposium on "Elas-
tomers and Rubbery Elasticity" have been based on research on
materials which may be called "conventional elastomers", which
are part of the larger category of materials known as thermosets.
In a conventional elastomer the long flexible macromolecules are
chemically linked together to form a single interconnected macro-
molecular network. Many of the advantageous properties of these
materials can be related to the details of the structure of the
covalent network, as discussed in detail in other papers in this
volume. For completeness, it is worthwhile to include a brief
review of another category of materials known as "thermoplastic
elastomers". This relatively new class of materials (commercially
available since around 1960), was developed in response to certain
disadvantages inherent in the thermoset character of conventional
elastomers. In particular, thermoplastic elastomers exhibit
thermal- or solvent-induced reversibility in their network struc-
tures. This allows recycling of off-grade or scrap materials
after processing. Furthermore many of the high-rate processing
operations developed for engineering thermoplastics are readily
adaptable for use with thermoplastic elastomers. The paragraphs
which follow will provide a very brief review of this broad
class of materials; emphasis will be given to the strong relation-
ship between molecular structure, bulk morphology and the rubbery
mechanical properties of these materials. For more complete de-
tails, the reader is referred to the excellent reviews which have
already appeard on this topic (1-7).

Structure and Properties

To explain the unique properties of thermoplastic elastomers, it is necessary to appreciate the fact that these materials generally exhibit phase-separated morphologies in the bulk state. The long flexible chains of the rubbery network are held together at multifunctional junctions which act as physical, rather than chemical, linkages. In one major catagory of thermoplastic elastomers, these physical linkages are discrete domains (e.g. spheres of ca. 20 nm diameter) of a rigid glassy polymer embedded in a rubbery matrix. Because many flexible rubbery chains originate in a given domain and terminate in neighboring domains, a continuous network structure is obtained. At temperatures above the softening point (in the present example, the glass transition temperature, T_g) of the domains, the material can be made to flow like a thermoplastic polymer melt; it is important to note, however, that the two-phase domain structure may persist in the melt state giving rise to very complicated rheological behavior (8). After the melt processing is complete, the material is cooled below the domain T_g, the fixed network structure is re-established, and elastomeric behavior is observed. Thus, the upper limit of temperature for utilizing a given thermoplastic elastomer as a rubbery component is dictated by the softening temperature of the dispersed domains. The lower bound on utilization temperature is, as in conventional elastomers, governed by the value of T_g (or the crystallization temperature, T_m) of the continuous rubbery phase of the material.

Variations of the glassy/rubbery structure described above are also found in commercial thermoplastic elastomers. In addition to dispersed glassy domains, multifunctional linkages can be formed by regions of crystallinity, ionic attraction or strong hydrogen bonding. In many cases the characteristic dimensions of the domains are smaller than the wavelength of visible light so that, even though a phase-separated morphology exists, optical transparency is observed. The fact that these domains are, however, much larger than the typical tetrafunctional chemical linkage of a conventional elastomer means that some account must be made of the filler effect imparted by the domains. Often this filler effect has a favorable, reinforcing influence on the large-strain mechanical history. Another aspect of the submicron domain size characteristic of thermoplastic elastomers is the fact that for a given volume fraction of rigid phase, the surface-to-volume ratio is relatively large (9,10) compared to that of a corresponding polymer blend in which very much larger (tens or hundreds of microns) domains are found; furthermore the nature of the connectivity of chains across the interfaces in thermoplastic elastomers has a covalent bond character whereas relatively weak forces act across the interfaces in conventional blends. Thus in thermoplastic elastomers knowledge and control of the details of the interfacial structure are likely to be especially important in the understanding of physical properties (11,12).

The microphase-separated morphologies which give rise to the characteristic behavior of thermoplastic elastomers is often a result of a structure at the molecular level which is of a block copolymer nature (2). Considerable progress has been made in the field of thermodynamics in predicting the complete details of the microphase morphology (domain size, shape, spatial arrangement) from knowledge of the block copolymer molecular structure and composition (13-15). Some theoretical work has also been done on the nature of the interfaces in block copolymer thermoplastic elastomers (16-17). Although careful experimental work has shown that the predictive capabilities of thermodynamic theories are quite good (18), this is only true for samples which have been carefully prepared so as to achieve, as nearly as possible, an equilibrium structure in the phase separated morphologies. In actual practice, kinetic effects will strongly influence the morphology, and therefore the properties, of a processed thermoplastic elastomer article; strong thermal history effects have been found (e.g. changes in properties on annealing (19) or isothermal ageing (20)) and remarkably strong processing history effects are seen in solvent casting operations (nature of the solvent (21), or rate of solvent evaporation (22)). Nonequilibrium structures in the interfacial regions of thermoplastic elastomers can also be envisioned with a corresponding possibility for influencing properties. On the one hand, these strong nonequilibrium effects add greatly to the difficulty of establishing structure/property relationships for thermoplastic elastomers at the same level as has been achieved for conventional elastomers. On the other hand, however, nonequilibrium effects may be used to advantage in achieving various levels of performance for a single thermoplastic elastomer composition.

Methods of Synthesis

The methods of synthesis of thermoplastic elastomers vary widely as may be expected from the wide variety of molecular structures which can be used to provide the desired morphologies and properties (1). One particularly versatile synthetic method is homogeneous anionic polymerization (23,24) which can be used to obtain an essentially unlimited variety of block copolymers. Using this technique it is possible to control the essential details of the chain structure, including tacticity, microstructure, molecular weight and its distribution, in each block sequence of the copolymer. Condensation polymerizations involving monomers and prepolymers, heterogeneous (Ziegler-type) catalytic polymerization, end-or graft-linking of functionalized polymers, and mechano-chemistry can also be used to provide compositions which exhibit the properties of thermoplastic elastomers.

With such a variety of powerful synthetic methods available it appears certain that new and improved types of thermoplastic

elastomers will be developed in the future and that further under-
standing of the relationships between the molecular structure of
these materials and their properties will be obtained. At the
present time the anionically polymerized styrene-diene block co-
polymers and their hydrogenated analogs hold the largest share of
the thermoplastic elastomer market (1). Segmented polyurethane
block copolymers account for another large fraction of the current
market for these materials.

Summary

     Reversible network structure is the single most important
characteristic of a thermoplastic elastomer. This novel property
generally arises from the presence of a phase-separated morphology
in the bulk material which in turn is dictated by the molecular
structure, often of a block copolymer nature. A wide variety of
synthetic methods can, in principle, produce endless varieties
of thermoplastic elastomers; this fact coupled with the advanta-
geous processing characteristics of these materials suggest that
the use of thermoplastic elastomers will continue to grow in the
1980's.

Acknowledgements

Literature Cited

1.   Dreyfus, P.; Fetters, L.J.; Hansen, D.R. Rubber   Chemistry
       and Technology 1980, 53(3), 728.
2.   Noshay, A; McGrath, J. "Block Copolymers: Overview and
       Critical Survey"; Academic Press, NY, 1977.
3.   Manson, J.A.; Sperling, L.H. "Polymer Blends and Composites";
       Plenum Press, NY 1976.
4.   Holden, G.; Moacanin, J.; Tschoegl, N.W., eds. "Block Copoly-
       mers"; J. Polymer Science, 1969, C-26.
5.   Sperling, L.H., ed. "Recent Advances in Polymer Blends, Grafts
       and Blocks"; Plenum Press, NY 1974.
6.   Allport, D.G.; Janes, W.H., eds. "Block Copolymers"; Wiley,
       NY, 1973.
7.   Aggarwal, S.L. ed. "Block Copolymers"; Plenum Press, NY, 1970.
8.   Gouinlock, E.; Porter, R. Polymer Eng. Sci. 1977, 17, 535.
9.   Meier. D.J. Polymer Preprints 1970, 11, 400.
10. Meier, D.J. Polymer Preprints 1974, 15, 171.
11. Chen, Y.D.M.; Cohen, R.E. J. Appl. Polymer Sci. 1977, 21,
       629.
12. Leary, D.F.; Williams, M.C. J. Polymer Sci., Phys. 1973,
       11, 345.

13. Meier, D.J. J. Polymer Sci. 1969, C-26, 81.
14. Helfand, E.; Wasserman, Z. Macromolecules 1978, 11, 960.
15. Leibler, L. Macromolecules 1980, 13, 1602.
16. Helfand, E. Macromolecules 1975, 8, 552.
17. Meier, D.J. Prepr. Polym. Colloq. Soc. Polym. Sci. Japan 1977, 83.
18. Hashimoto, T.; Shibayama, M.; Kawai, H. Macromolecules 1980, 13, 1237.
19. Cohen, R.S.; Tschoegl, N.W. Intern. J. Polymeric Mater 1972, 2, 49.
20. Tant, M.R.; Wilkes, G.L. Polymer Eng. Sci. 1981, 21, 325.
21. Beamish, A.; Goldberg, R.A.; Hourston, D.J. Polymer 1977, 18, 49.
22. Bates, F.S.; Cohen, R.E. J. Polymer Sci, Phys. 1980, 18, 2143.
23. Fetters, L.J. J. Polymer Sci. 1977, C-26, 1.
24. Szwarc, M. "Carbanions, Living Polymers, and Electron Transfer Processes"; Interscience, NY, 1968.

Homogeneous and Heterogeneous Rubbery–Rubbery Diblock Copolymers and Polymer Blends: A Unified View

ROBERT E. COHEN

Massachusetts Institute of Technology, Department of Chemical Engineering, Cambridge, MA 02139

The present paper describes a unified framework in which to view the results of previous experimental studies on rubbery/rubbery diblock copolymers and blends. This framework takes the form of a three dimensional plot which specifies three quantities for each blend: (i) the overall composition (weight fraction) of the AB mixture (ii) the percentage (weight basis) of diblock copolymer in the blend and (iii) the number average molecular weight of the blend. Existing thermodynamic theories of phase separation in homopolymer blends and in block copolymers were used to define certain limiting boundaries of the three dimensional diagram, and some ad hoc assumptions were made to extend these ideas to intermediate regions of the plot. Solubility parameters were used to provide estimates of the AB interaction parameters required for the thermodynamic theories. Quantitative comparison with a large array of experimental data indicates that such a framework is a meaningful way to consolidate the results of experiments and to anticipate the behavior of untested blends.

For the past several years, experimental work in this laboratory (1-7) has led to the accumulation of a large body of data on various elastomer blends and corresponding rubbery/rubbery diblock copolymers. Certain binary mixtures of one rubbery homopolymer with a diblock copolymer have been studied, as well as ternary mixtures consisting of two homopolymers and the corresponding diblock copolymer. Using a variety of techniques, including thermal analysis, transmission electron microscopy and dynamic mechanical testing, we have been able to establish the morphological nature (whether homogeneous or heterogeneous) of each of these compositions. What has emerged to date is a qualitative understanding

of the following: (i) Certain rubbery/rubbery diblock copolymers
are homogeneous materials even though the corresponding binary
blends of homopolymers are heterogeneous. (ii) Variations in
block molecular weights and copolymer composition may result in
a change from a heterogeneous to a homogeneous morphology in a
given AB system. (iii) Diblock copolymers act as emulsifying
agents in ternary blends, regulating the size and shape of the
dispersed phase of the heterogeneous morphology. (iv) Diblock
copolymers, in certain cases, may also act as homogenizing agents,
transforming an otherwise incompatible system into a compatible
one.

What has been missing in all of this previous work is a uni-
fied framework (7,8) in which to view all of the results obtained
to date and from which the phase behavior of new materials (co-
polymers and blends) might be predicted. The purpose of the pre-
sent paper is to provide such a unified view for the particular
case of the multicomponent rubbery systems described above. Be-
cause we have restricted our studies to rubbery materials which
at room temperature are well above their glass transition tempera-
tures, we can expect relatively little influences of the non-
equilibrium effects which greatly complicate the interpretation
of multicomponent systems containing one or more glassy components
(9-11). Thus from the outset we can hope to find a unifying
framework in the regime of equilibrium thermodynamics, a field in
which considerable progress has been made in describing the mor-
phological behavior of polymer blends (12-14) and block copolymers
(15-18). Similarly since our data have been obtained on macro-
molecules with essentially non-polar hydrocarbon structures, it
seems reasonable as a first attempt to estimate the AB interaction
parameters required for the above-mentioned thermodynamic theories
using readily available solubility parameters (19,20) and Van-Laar
type interactions (21).

Materials

Table 1 lists some of the homopolymers and diblock copolymers
which have been employed in our experimental investigations (1-8).
Particular emphasis has been placed on blends containing 1,4
polybutadiene (1,4B). In one case, 1,4B was blended with various
amounts of 1,2 polybutadiene (1,2B) and the corresponding 1,2B/1,4B
diblock copolymer. A second major set of samples was constructed
from various combinations of 1,4B and cis 1,4 polyisoprene (1,4I)
and 1,4I/1,4B diblock copolymers. A large number of ternary
blends were studied, the preponderence of which contained either
25%, 50% or 75% (by weight) of a selected diblock copolymer, the
remainder of the blend being comprised of one or both of the cor-
responding homopolymers. Homopolymer blends (0% diblock) and
the pure copolymers (100% diblock) were also studied in detail.

TABLE 1   Homopolymers and Diblock Copolymers

Sample Code	Weight Fraction of:			$\overline{M}n$ of block:[f]		
	1,4I	1,2B	1,4B	1,4I	1,2B	1,4B
30K 1,2B[a]	0	1.00	0	0	28900	0
90K 1,2B[a]	0	1.00	0	0	85000	0
100K 1,4B[b]	0	0	1.00	0	0	97000
45K 1,4B[b]	0	0	1.00	0	0	43000
30/50	0	0.38[e]	0.62	0	32000	52000
30/100	0	0.23[e]	0.77	0	31000	102000
30/150	0	0.17[e]	0.83	0	28000	137000
30/200	0	0.13[e]	0.87	0	26000	176000
120K 1,4B[c]	0	0	1.00	0	0	120000
133K 1,4I[d]	1.00	0	0	133000	0	0
Diblock 3	0.56	0	0.44	140000	0	110000
Diblock 4	0.39	0	0.61	103000	0	161000
Diblock 8	0.71	0	0.29	192000	0	78000

(a)   Microstructure is greater than 98% 1,2 addition (22,23)

(b)   36% cis 1,4: 51% trans 1,4; 13% 1,2 addition

(c)   45% cis 1,4; 45% trans 1,4; 10% 1,2 addition

(d)   Greater than 90% cis 1,4 addition

(e)   Weight fraction of the block 1,2 polybutadiene. This number does not include the contribution of the 13% 1,2 addition in the 1,4 polybutadiene block

(f)   Microstructures of the 1,2B and 1,4B blocks of copolymers 30/50, 30/100, 30/150 and 30/200 are essentially identical to those of the corresponding homopolymers: 30K 1,2B; 90K 1,2B; 100K 1,4B; 45K 1,4B. Similarly Diblocks 3,4 and 8 are matched in microstructure to homopolymers 120K 1,4B and 133K 1,4I.

Results and Discussion

Surveying the various theories for microphase separation in block copolymers (14-18) reveals a general qualitative prediction that the critical molecular weight [M_{crit}] for the appearance of a heterogeneous structure is higher for a diblock copolymer than for the case of the corresponding homopolymer blend. In other words, it is expected from these thermodynamic theories that in principle, there is a regime of molecular weight in which a certain diblock copolymer sample is homogeneous but would spon-

taneously form a heterogeneous morphology if all of the diblock molecules were suddenly cut at the junction between the dissimilar blocks. Leibler's theory (18) makes the specific prediction that $M_{crit}^{diblock}$ should exceed M_{crit}^{blend} by a factor of 5.25.

The existence, on a qualitative basis, of the above-mentioned region (homogeneous diblocks and heterogeneous blends) adds measurably to the understanding of much of our earlier data on rubbery/ rubbery systems. We have recently extended this explanation to a more quantitative level by calculating (7) values of M_{crit} for various AB pairs. The AB interaction parameter for each pair, required for the calculation of $M_{crit}^{diblock}$ or M_{crit}^{blend}, was estimated (7) using solubility parameters (19,20) and the previously published interaction parameter for the system polystyrene/polyisoprene (24). Results of these calculations, shown in Table 2, reveal that for the two rubbery/rubbery systems under consideration here (1,2B/1,4B and 1,4I/1,4B) the "standard" regime of polymer molecular weights, say 50,000 - 250,000, falls directly in the region of homogeneous diblocks and heterogeneous blends. Furthermore, it is clear from Table 2 that for all but the most closely similar polymers ($\delta_A \sim \delta_B$), the values of M_{crit} are so low that both heterogeneous diblocks and blends will be expected at essentially all molecular weights of practical significance. All of this discussion, of course, is predicated on the assumption mentioned in the introduction that the selected polymers are of a type that AB interactions are well-described by simple solubility parameter considerations. For other types of polymers a more complicated formalism will be required.

Using the results of Table 2 and data from the previously described experimental work, we have constructed (7) a "phase diagram" describing the overall picture for rubbery/rubbery diblock copolymers and the corresponding binary blends of homopolymers (Figure 1). The upper curve in Figure 1, based on calculations using Helfand's Fortran program (15,16), describes the boundary between homogeneous and heterogeneous diblock copolymers; the use of dimensionless molecular weight for the ordinate and weight fraction for the abcissa makes it possible to compare results obtained for various diblock copolymers (7). The lower curve in Figure 1, representing the boundary between homogeneous and heterogeneous homopolymer blends, is the locus of points describing the spinodal curve calculated from the Flory-Huggins theory (14); for binary blends of this type, the value of M on the abcissa signifies the number average molecular weight of the overall sample, thus allowing for the case in which $M_A \neq M_B$. An examination of the various data points in Figure 1 indicates that the previous experimental findings are reasonably well described by this approach. For example, the four diblocks of 1,2B/1,4B (solid squares in Figure 1) closely follow the boundary for block copolymers; the point for sample 30/50 lies just inside the
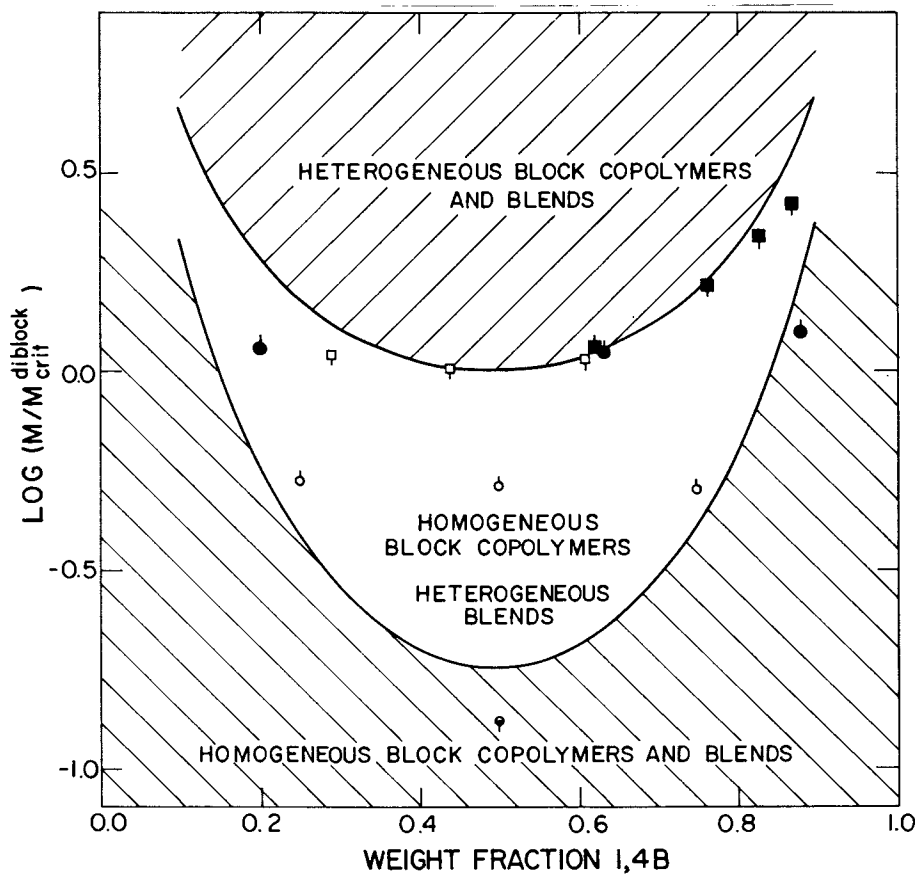
Figure 1. *Phase diagram showing the three distinct regions discussed in the text. Key: □, diblock copolymers; ○, homopolymer blends; pip up, heterogeneous; pip down, homogeneous; solid points, 1,2B/1,4B; open points, 1,4I/1,4B; half-open point, 1,4I/1,2B with the abscissa representing the weight fraction of 1,2B.*

heterogeneous region while the other three samples fall somewhat
below the curve, in the homogeneous region, as expected from pre-
vious results ($\underline{7}$). Similarly, the diblocks of 1,4I/1,4B lie just
within the homogeneous region. All of the homopolymer blends
(1,4I + 1,4B and 1,2B + 1,4B) were found to be heterogeneous in
our earlier work and all but one of the data points for these
samples lie within the region of heterogeneous blends. Finally a
single data point for a blend of 1,2B and 1,4I has been included
in Figure 1; because of the very large value of M_{crit}^{blend} for this
combination (Table 2) this point falls inside the region of homo-
geneous blends, and this is in agreement with experimental obser-
vations for this system ($\underline{2},\underline{7},\underline{8}$).
     With the discussion above in mind, it is now possible to
provide a similar semiquantitative framework in which to view the
results obtained on ternary systems (homopolymer A, homopolymer B,
diblock AB) and on binary blends of one homopolymer and a diblock
copolymer. Of particular importance is the need for an explana-
tion of the fact that the diblock copolymer may serve either as
an emulsifying agent ($\underline{9},\underline{25}$) or as a homogenizing agent ($\underline{1},\underline{4}$) in
ternary blends.
     The three dimensional representation of Figure 2 is useful
for clarifying the experimental observations on ternary blends.
The curve in the plane at the right side of this figure is the
boundary between homogeneous and heterogeneous diblocks (i.e.
the uppercurve of Figure 1); this right hand plane represents AB
compositions composed entirely of AB diblock copolymer. The plane
at the extreme left of the three dimensional diagram represents
AB homopolymer blends, and the curve lying in this plane is the
Flory-Huggins spinodal separating regions of homogeneous and
heterogeneous behavior (lower curve of Figure 1). The shape and
location of curves on intermediate planes (the plane of AB compo-
sitions containing 50% diblock copolymer is shown in Figure 2) is
open to speculation; there is need for theoretical work to provide
guidance in this regard. As a first and arbitrary approximation,
a linear combination of the two extreme curves has been chosen to
represent the behavior of our rubbery/rubbery blends. The curve
in the central plane of Figure 2 shows the result of this approach.
All ternary compositions above the curve are expected to be
heterogeneous and here the diblock copolymer will function as an
emulsifying agent. Below the curve, the block copolymer serves
as a homogenizing agent. "Positive deviations" from the assumed
linearity (i.e. a concave downward locus of critical points) would
result if the selected block copolymer had strong tendencies to
act as a homogenizing agent; "negative deviations" would be ob-
served for block copolymers with strong emulsifying tendencies.
     A quantitative test of these ideas is shown in Figure 3.
Here the solid curve representing the boundary between homogene-
ous and heterogeneous blends is located at a position halfway
between the two curves of Figure 1. The various data points shown

TABLE 2   Quantitative Considerations
of Selected Polymer Pairs

(a) Solubility parameter, δ $(cal/cm^3)^{1/2}$

Polymer	Range of δ in literature (19,20)	Value selected for determination of α (19,20)
Polystyrene (PS)	8.6 - 9.7	9.12
1,4 Polybutadiene	8.35-8.60	8.38
1,2 Polybutadiene	8.10	8.10
cis 1,4 Polyisoprene	7.9 - 8.35	8.22

(b) Interaction parameter, α (m^{-3})

Polymer Pair, AB	$10^3 T^{-1} (\delta_A - \delta_B)^{2\,(\ddagger)}$	α	$M_{crit}^{diblock\,(\#)}$	$M_{crit}^{blend\,(@)}$
PS/1,4B	1.5	1111[*]	14,300	2,700
1,2B/1,4B	0.26	193	76,800	13,800
1,4I/1,4B	0.081	60.0	247,000	42,000
1,4I/1,2B	0.048	16.3	930,000	76,200

‡ For the polystyrene-containing pair, the glass transition temperature of PS(T = 373K) was used; for all other pairs T=298K.

* This value of α is used by Helfand (15) for PS/1,4B and is based on the experiments of Rounds (24). All other values of α were obtained by scaling to this PS/1,4B value.

Obtained using Helfand's program to search for the molecular weight at which the free energy of mixing, ΔG, equals zero for the case of a diblock copolymer in which $M = M_A + M_B$ and at a weight fraction of 0.5.

@ Obtained by searching for the molecular weight at which $\delta^2 \Delta G / \delta V_A^2 = 0$ (spinodal) using the Flory-Huggins expression (14,7) for a 50:50 AB polymer blend. Here M is the number average molecular weight for the two component system, which allows for the possibility that the two monodisperse homopolymers in the blend may not be of identical molecular weight.
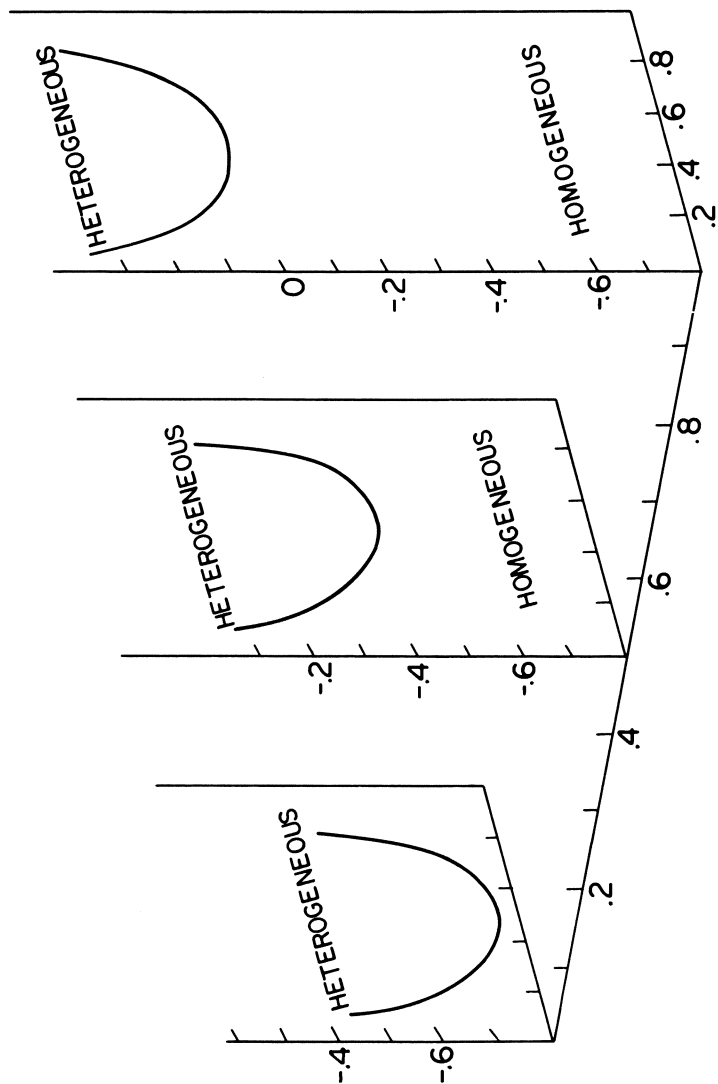
Figure 2.   Schematic three-dimensional plot showing various planes of AB polymer/polymer composition. From left to right: homopolymer blends; blends containing 50 weight percent diblock copolymer; diblock copolymers.
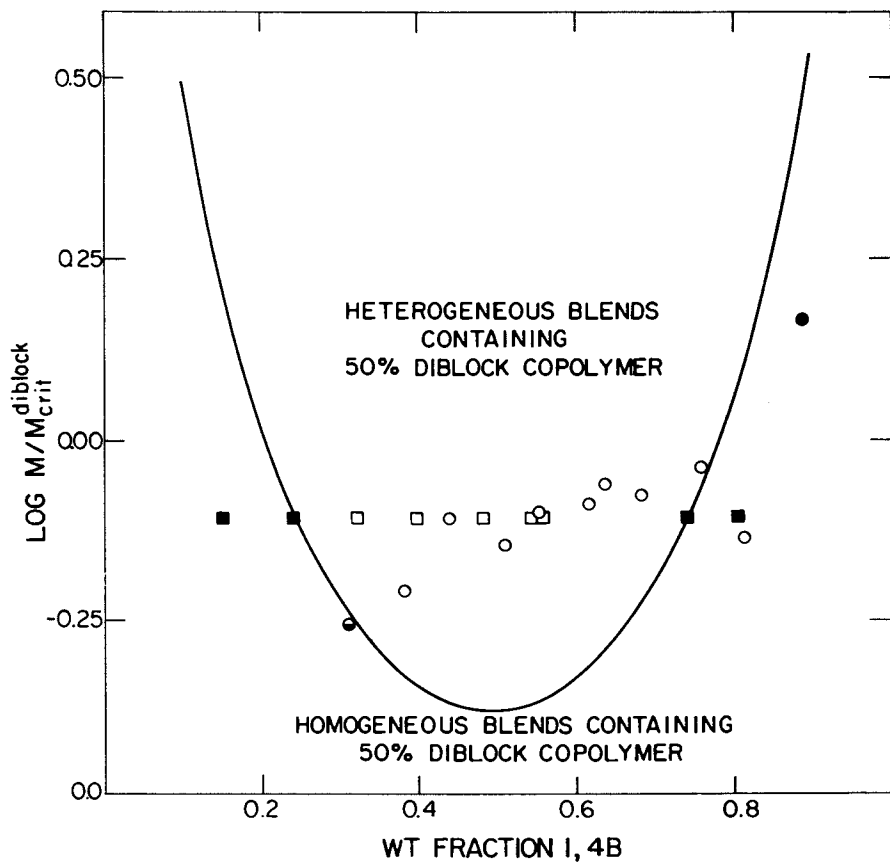
Figure 3. Detail of the plane at 50 weight percent diblock content in Fig. 2 including various data points from previous studies (1, 4, 26). Key: □, 1,4I/1,4B; ○, 1,2B/1,4B; solid points, homogeneous materials; open points, heterogeneous materials; half solid point, a blend for which contradictory results were obtained in various experimental modes (26).

are taken from our earlier studies on 1,4I/1,4B (1-4) and from
ongoing work on 1,2B/1,4B (26). In every case the blend contains
50 wt % of a diblock copolymer, the remainder of the composition
being comprised of one or both of the corresponding homopolymers.
Inspection of Figure 3 reveals immediately that shifting the lo-
cation of the boundary to an intermediate position is clearly the
correct approach; all of the homogeneous blends lie on or out-
side the curve as required, and essentially all of the heterogene-
ous blends are located inside the curve. There is no doubt that
neither the boundary for pure diblocks (upper curve in Figure 1)
nor the one for homopolymer blends (lower curve in Figure 1)
would adequately fit the data points of Figure 3. Similar good
fits were obtained for the arrays of data at 25% and 75% diblock
(1,4,26) using the appropriate linear combinations of the two
limiting curves.

    More experimental work is needed to define the various
boundaries more precisely, and theoretical work is needed to
justify or refute some of the ad hoc assumptions made here.
Nevertheless, the ideas presented here do provide a semiquantita-
tive, unified explanation for a large set of experimental observa-
tions. A three dimensional representation such as Figure 3 is
also useful for predicting in advance whether or not a given
binary or ternary composition will be homogeneous or heterogeneous
and for anticipating how much of a given homogeneous diblock co-
polymer will be required to homogenize an incompatible polymer
blend.

Conclusions

    Existing thermodynamic theories can be used to describe
the morphological behavior of rubbery/rubbery compositions com-
prised of diblock copolymers and one or both of the corresponding
homopolymers. The required interaction parameter for the theories
can be estimated from solubility parameter data if only nonpolar
hydrocarbon rubbers are considered. A three dimensional plot,
which simultaneously describes (i) the overall composition of a
given blend, (ii) the proportion of the blend which is comprised
of block copolymer molecules and (iii) the number average molecu-
lar weight of the blend, provides a clear picture of the role
of diblock copolymers in these systems. More experimental work
is needed to define precisely the shape and location of the
contours of this three dimensional plot, and guidance is required
from theory regarding the correct form of the plot for various
types of polymer systems.

Acknowledgements

Literature Cited

1. Cohen, R.E.; Ramos, A.R. Macromolecules,1979, 12, 131.
2. Cohen, R.E.; Ramos, A.R. Advances in Chemistry Series, 1979, 176, 237.
3. Cohen, R.E.; Ramos, A.R. J. Macromol Sci., Phys.,1980, B17(4), 625.
4. Ramos, A.R.; Cohen, R.E. Polymer Eng. Sci., 1977, 17, 699.
5. Ramos, A.R.; Bates, F.S.; Cohen, R.E. J. Polymer Sci., Phys., 1978, 16, 753.
6. Cohen, R.E.; Torradas, J.M.; Wilfong, D.E.; Halasa, A.F. Polymer Preprints, 1980, 21(2), 216.
7. Cohen, R.E.; Wilfong, D.E. Macromolecules, submitted.
8. Cohen, R.E. Polymer Preprints, 1981, 22(2), 173.
9. Kawai, H.; Soen, T.; Inoue, T.; Ono, T.; Uchida, T. "Progress in Polymer Sci., Japan", Vol. 4, Imahori, K.; Iwakura, Y., Eds., Halsted Press, NY, 1972.
10. Beamish, A.; Goldberg, R.A.; Hourston, D.J. Polymer, 1977, 18, 49.
11. Kovacs, A.J.; Aklonis, J.J.; Hutchinson, J.M.; Ramos, A.R. J. Polymer Sci., Phys., 1979, 17, 1097.
12. Olabisi, O.; Robeson, L.E.; Shaw, M.T. "Polymer-Polymer Misci-bility", Academic Press, NY, 1979.
13. "Polymer Blends"; Paul, D.R.; Newman, S.; Eds., Academic Press, NY, 1978.
14. Krause, S. J. Macromol Sci. Rev. Macromol Chem., 1979 C7(2), 251.
15. Helfand, E.; Wasserman, Z.R. "Developments in Block Copoly-mers", Goodman, I.; Ed., Applied Sciences Publishers, Ltd., in press.
16. Helfand, E.; Wasserman, Z.R.; Macromolecules, 1978, 11, 960.
17. Meier, D.J.; J. Polymer Sci., 1969, C26, 81.
18. Leibler, L. Macromolecules, 1980, 13, 1602.
19. "Polymer Handbook", Brandrup, J.; Immergut, E.H., Eds., 2nd Edition, NY, 1975.
20. Ahmad, H.; Yaseen, M.; Polymer Eng. Sci., 1979, 19, 858.
21. Reid, R.C.; Prausnitz, J.M.; Sherwood, T.K. "Properties of Gases and Liquids", 3rd ed.; McGraw Hill, NY 1977, p. 326.
22. Halasa, A.F.; Rubber Chem. Tech., 1981, 54, 627.
23. Halasa, A.F.; Schulz, D.N.; Tate, D.P.; Mocel, V.D.; Adv. Organometallic Chem.,1980, 16, 55.
24. Rounds, N.A., Ph.D. Thesis, University of Akron, 1970.
25. Reiss, G.; Jolivet, Y. Adv. Chem. Series, 1975, 142, 243.
26. Torradas, J.M.; Cohen, R.E.; to be published.

Fundamental Aspects of the Chemical Applications of Cross-linked Polymers

DAVID LIVE and STEPHEN B. H. KENT[1]

The Rockefeller University, New York, NY 10021

High resolution NMR spectroscopy has been used to study in detail the properties of swollen copoly-(styrene-1%divinylbenzene) with an emphasis on factors relating to its use as a support in novel solid-phase methods for chemical synthesis. 1% cross-linked and linear polystyrene in chloroform and dimethylformamide have been compared. We have been able to demonstrate a high degree of mobility in chain segments at frequencies $\geq 10^8$/s uniformly throughout the resin comparable with linear polystyrene. This implies good solvation of the chain segments even though the polymer beads are macroscopically insoluble. Pendant chains show an even greater degree of freedom, and their effects on the properties of the system have been investigated. The environment in the swollen 1% cross-linked bead is substantially like a solution of linear polymer with no evidence for a fundamental resin-caused physical limitation to the solid-phase synthesis method.

The novel concept of synthesizing a molecule while attached to a swollen cross-linked resin bead was introduced and demonstrated by R. B. Merrifield with the solid-phase peptide synthesis method about 20 years ago (1,2). The procedure involves the covalent attachment of an amino-acid residue to the polymer bead followed by the addition of subsequent amino-acid units in a stepwise manner under conditions that do not disrupt the attachment to the support. At the completion of the assembly of the peptide, the product is cleaved from the resin and recovered. The macroscopically insoluble support provides convenient containment of the desired product so that isolation and purification from soluble co-products in the synthesis can be achieved by simple

[1] Current address: Molecular Genetics, Incorporated, Minnetonka, Minnesota 55343.

washing and filtration procedures. The speed and simplicity of
the manipulations are an important advantage compared to conven-
tional solution synthesis methods. This allows for the stand-
ardization of reaction conditions in the solid-phase method.
Recently it has been realized that there are also intrinsic
chemical advantages which derive from the solvation effects im-
parted to the pendant molecule by the supporting polymer (3).
This has the potential for extending the range of environments in
which a particular chemical transformation can take place which
has important implications for the general usefulness of the
solid-phase method.

     Although a variety of supports have been employed for solid-
phase syntheses in general and the peptide version in particular
(4), cross-linked polymer beads produced by suspension co-
polymerization have been by far the most widely and successfully
employed. In particular co-poly(styrene-divinylbenzene), the
support originally used (2), is the most popular, typically   1%
cross-linked. Among its advantages are favorably physical and
chemical properties and availability. From time to time, however,
questions have been raised about limitations on the use of this
methodology purportedly arising from inadequacies in the physical
properties of this support. Generally the hypotheses have been
based on rationalization of chemical difficulties and have not
been substantiated by direct physical investigations (5, 6).

     It is our goal to investigate the physical properties of the
swollen, cross-linked resin-pendant molecule system to develop a
fundamental understanding of the behavior of components in the
system and their interplay. This has been accomplished by exam-
ining the molecular structure and dynamics of the polymer and
pendant chain at a molecular level using high-resolution NMR
spectroscopy. The study has been carried out in the context of
the solid-phase peptide synthesis method because it offers a means
of correlating chemical to physical effects, practical applicabil-
ity of the results to a widely used technique, and proven chemical
procedures for manipulating the system. The relevance of the
results is not limited to improving the use of these supports in
chemistry, but also to provide a better understanding of the
phenomena of rubber elasticity.

Approach

     Although high-resolution NMR has been widely used in stud-
ying polymers (7, 8, 9), there are only scattered reports of its
application to cross-linked material (10, 11, 12, 13, 14, 15).
This is probably because the swollen cross-linked polymer gives
the appearance of an insoluble phase, and from this it might be
concluded that the rapid molecular tumbling and internal rotations
associated with a dissolved species, and required to observe a

high resolution spectrum, would be absent. The necessity for
rapid motions in this experiment arises from the need to average
out the effects of local magnetic fields from other nuclei in the
sample on the one being observed. If this condition is not met,
the lines in the spectrum can increase in width by several orders
of magnitude and much more elaborate procedures are required to
extract the desired data. Even though the NMR spectroscopist
might be put off by the appearance of the sample, there is ev-
idence that some of the criteria might be met from the fact that
the cross-linked resin swells in certain solvents. This implies
an intimate interaction of solvent and chain segment akin to dis-
solution (16). The possibility of using high-resolution NMR to
study the system of interest here, cross-linked polystyrene, has
been recognized by several investigators, and has been used as an
analytical method and to examine physical properties (11, 12, 14,
15). The use of electron spin resonance has also been reported to
address some of the questions under study here (17). Although
ESR has the substantial advantage of being readily observable in a
variety of physical states of the sample, its observation in these
systems requires   the   introduction of a spin label or spin
probe whose ability to monitor the complex motions of the native
polymer is not always clear. NMR, on the other hand, uses the
indigenous nuclei to monitor a variety of interactions within the
sample. We have employed both ^{1}H and ^{13}C NMR to examine some of
the basic aspects of the material that are relevant to solid-phase
synthesis.

The Proton NMR has the advantage of relative experimental ease
due mainly to its intrinsic high sensitivity, though the relaxa-
tion properties of the proton resonances are generally more
difficult to interpret in terms of dynamics than are those from
protonated carbon nuclei. The widths of the proton resonances
can conveniently be used as a qualitative measure of some of the
motional properties.

The ^{13}C NMR sensitivity can sometimes be a problem, but for
the kind of samples studied here the effective concentration of
monomer units is several molar which does not place excessive
demands on present Fourier transform NMR spectrometers. In addi-
tion to the sensitivity of the chemical shift to structure (9),
the relaxation of protonated carbons is dominated by dipole-dipole
interaction with the attached proton (9). The dependence of the
relaxation parameters T_{1}, or spin-lattice, and T_{2}, or spin-spin,
on isotropic motional correlation time for a C-H unit is shown
schematically in Figure 1. The T_{1} can be determined by standard
pulse techniques (9), while the linewidth at half-height is often
related to the T_{2}. Another parameter which is related to the
correlation time is the nuclear Overhauser enhancement factor, η.
The value of this factor for ^{13}C coupled to protons, varies from
about 2 at short correlation times to 0.1 at long correlation

times (9). A problem ·that can complicate a quantitative inter-
pretation of the data in terms of molecular fluctuations arises
from the anisotropy of the molecular motion which is neither
known in detail nor simply characterized mathematically. The
problem of dealing with this situation has been recently reviewed
(9). The functional dependence remains basically the same,
however, and the values derived from the isotropic case can be
used as a semi-quantitative estimate.

Materials and Methods

3000 and 17,500 MW polystyrene (PS) were from Polysciences.
Copoly(styrene-1%divinylbenzene) (S-DVB) was in the form of Bio-
Beads SX-1, 200-400 mesh from Bio-Rad Laboratories. Peptide
samples were prepared using standard methods (4). The 4(oxymethyl)
phenylacetamidomethyl (PAM) (4) linkage to the resin was used.
        NMR spectra were obtained in continuous wave mode on a Varian
T-60, and in the pulsed Fourier transform mode on a Varian HR-220
with Nicolet TT-100 Fourier transform accessory, a Nicolet NT-300
wide bore system, and a Bruker WM-500. ^{13}C T_1 data were obtained
at 25 °C using the inversion recovery method (9). Integrated peak
intensities were analyzed to give relaxation times using the T13IR
data reduction routine in the Nicolet software package (18).
Little difference was noted when peak heights were used. The
error in the T_1 data is less than $\pm$ 10%. Nuclear Overhauser
enhancement factors (η) were obtained by measuring the integrated
intensity of peaks in a difference spectrum from one with enhance-
ment minus one with no enhancement and dividing that value by the
integral from the one with no enhancement; i.e. $\eta = (I_{nOe} - I_{no\ nOe})/$
$(I_{no\ nOe})$. Accuracy should be 10% or better. Linewidths were
measured at half heights, and chemical shifts are relative to TMS.

Results

Proton NMR. An example of the ^1H NMR spectrum of $CDCl_3$
swollen 1% cross-linked PS is in Figure 2. There are four resolv-
able regions of the spectrum: meta and para protons at 7.04 ppm,
the ortho protons at 6.52 ppm, the methine proton at 1.82 ppm, and
the methylene protons at 1.41 ppm. These assignments have been
previously reported (19). The widths of these envelopes are due
to a combination of effects: to coupling between nuclei (not
resolved here), to the chemical shift range for each of the
protons from the distribution of conformations in the polymer, and
to the intrinsic linewidth of each component related to molecular
motion. Since the calculated width contribution from couplings,
based on simulations with published values (19) are somewhat less
than we observe, and the widths are proportional to magnetic field
over the range of 1.4 T to 11.7 T (60-500 MHz), it can be conclud-
ed that the major factor is the chemical shift dispersion due to
the atactic nature of the polymer and incomplete averaging of
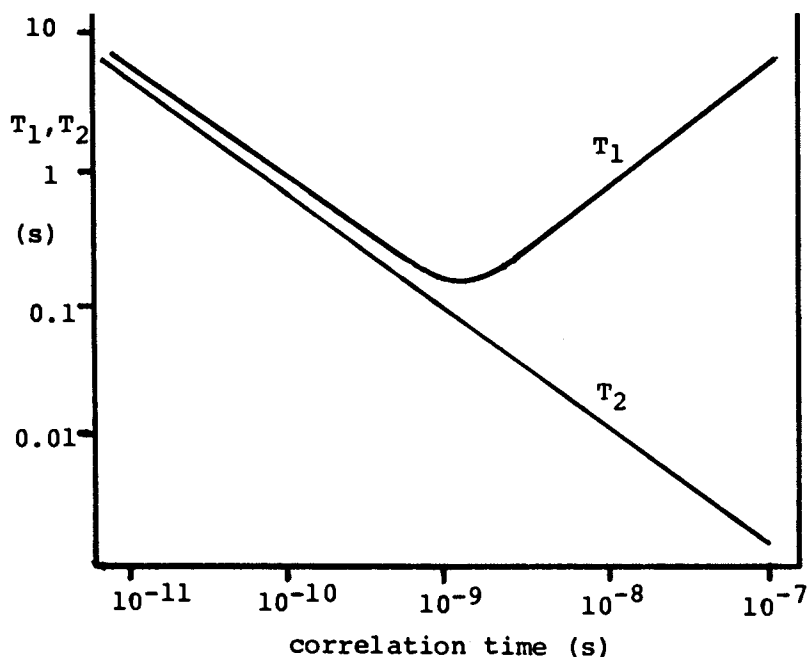
Figure 1. Schematic representation of dependence of the T_1 and T_2 relaxation times on isotropic correlation time (τ_c) of motion for a C-H fragment assuming dipole–dipole relaxation and 7 T magnetic field.
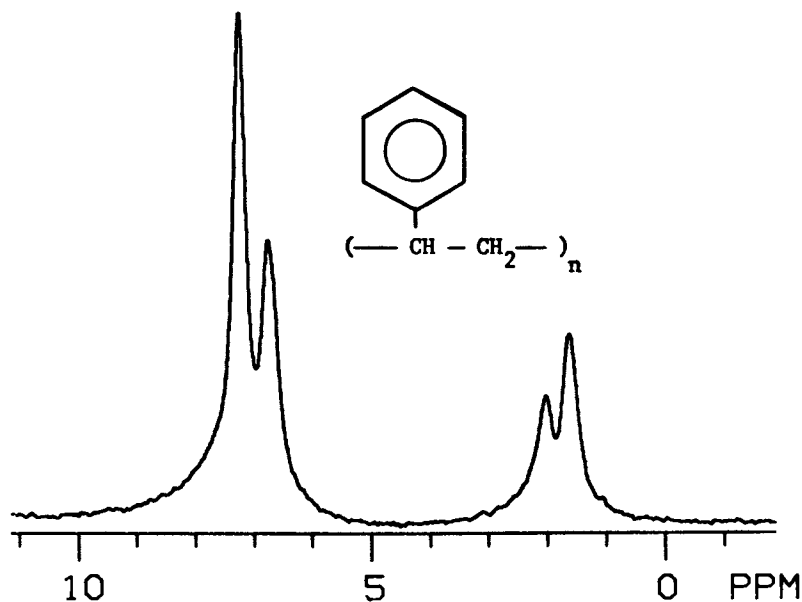
Figure 2. A 300-MHz ^1H NMR spectrum of 1% cross-linked polystyrene (Biobeads SX–1) in CDCl$_3$. Shifts relative to TMS.

rotational conformers. The observed linewidths in Table I are
then upper limits on the intrinsic linewidths of the component
resonances.

Table I
Proton Multiplet Widths in Hz at 220 MHz[a]

Solvent	Chloroform		Dimethylformamide	
Sample	Aromatic protons	Aliphatic protons	Aromatic protons	Aliphatic protons
PS (3000 MW)	40	50		
PS (17500 MW)	40	50	40	75
Bio-Beads SX-1	50	60	125	150
Bio-Beads SX-1-(LAGV)x1[b]	200	175	200	175
Bio-Beads SX-1-(LAGV)x5[b]	250	200		

[a]Average widths at half height of the two resolvable envelopes
in each region.
[b]Peptide resin with the designated number of units of(leucyl-
alanylglycylvalyloxymethylphenylacetyl) attached. Peptide
loading was 0.2 mmole/g PS (1 phenyl in 50 substituted).

    The linewidth is of interest here since it can be used as a
qualitative if not quantitative measure of the rate and amplitude
of molecular motion. The widths of these envelopes for linear PS,
1% cross-linked PS and 1% cross linked PS with peptide attached
are given in Table I. The data for the respective spectral com-
ponents of linear and 1% cross-linked PS in chloroform are not
substantially different. These results suggest two conclusions.
First that the motions involved in the relaxation of linear and
cross-linked material are comparable, and second, that the dis-
tribution of conformers is probably similar. It has been previous-
ly observed (8) that local segmental motion is the dominant mo-
tion for relaxation in these systems. With the peptide-resin in
chloroform there is substantial broadening of both the aromatic
and aliphatic resonances. This indicates an increase in lower
frequency motions and/or a reduction in the rate of conformation-
al averaging (for example phenyl group reorientation). These
could be caused by the pendant chains entangling the PS chain
segments or by branch points acting to load down the chain seg-
ments so they cannot move as freely as before. We prefer the lat-
ter explanation since the phenomenon is not strongly dependent on
on the length and amount of peptide present. Our preliminary data

indicate that behavior in methylene chloride is similar to that
in chloroform. Another solvent which is used widely in solid-
phase synthesis is DMF, a poorer solvent for polystyrene. The
breadth of the aliphatic resonances in linear PS is greater here
than for the aromatics. This would suggest less freedom of motion
in the backbone of the polymer and would be consistent with a more
ordered structure as expected in a poorer solvent. The widths
for the cross-linked sample in DMF are substantially greater than
for the linear material in DMF or the cross-linked resin in chlo-
roform. Physically the beads swell half as much in DMF than in
chloroform or methylene chloride (3) resulting in a concentration
within the bead of 40% w/v PS. At this concentration interference
of neighboring chains may play an important role. This concentra-
tion was greater than that used for the linear material or, in
fact, achievable with it. With a tetrapeptide unit attached, the
widths in chloroform and DMF are quite similar which is likely
related to the fact that the swellings of such peptide resin beads
in the two solvents are comparable (3).

An estimate of the rate of the dominant motion in the relaxa-
tion can be made using the isotropic motional model (9). This
gives an upper limit of about 10^{-8}s for the correlation time. It
should be pointed out that a variation of less than an order of
magnitude would be required to explain all the variation in widths
Integrals of the cross-linked resin sample relative to a reference
indicate that all of the protons are being observed. That means
there are not any significant regions where the motion is highly
restricted in the bead.

In a recent study on the proton spectrum of 2% cross-linked
PS in CCl_4, a solvent of comparable quality to chloroform, the
lines were found to be much broader than reported here (11). The
lines could be narrowed by rapidly spinning the sample at the
magic angle (54.7°) relative to the magnetic field. This indi-
cates that dipolar interactions are the primary mechanism of
broadening in their case, which suggests a reduction in frequency
of motion of two orders of magnitude or more relative to that
observed in this study. The trend of the results for 1% and 2%
of cross-linked material argues in favor of using the former for
synthesis.

^{13}C NMR of linear cross-linked PS. The proton decoupled ^{13}C
NMR spectra of linear and 1% cross-linked PS at 75 MHz in chloro-
form are illustrated in Figure 3. These spectra are similar to
those for linear and cross-linked chloromethylated PS previously
reported at lower field (14), although we have been able to re-
solve more structure in the aliphatic and aromatic regions here.
The quarternary and methylene carbon resonances at about 146 ppm
and between 40 and 50 ppm respectively, are the most strongly
affected by stereochemistry (20). The ortho and meta resonances
at 128.4 ppm show partially resolved structure in the linear PS,
as does the para carbon at 126.1 ppm. The methine resonance at
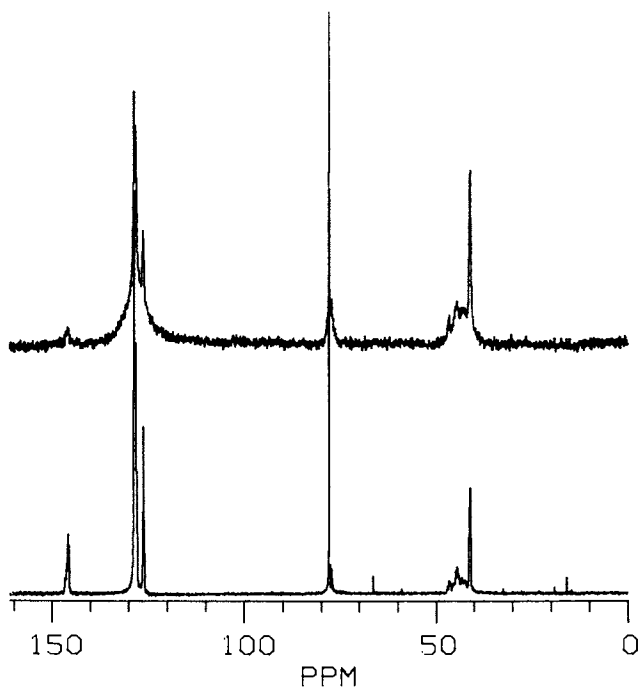
Figure 3. Protein decoupled ^{13}C NMR spectrum at 75 MHz of 17,500 MW poly-styrene at 20% w/v in $CDCl_3/CHCl_3$ (lower trace). One percent cross-linked poly-styrene (Biobeads SX-1) in the same solvent (upper trace).

40.9 ppm appears as an overlapping doublet. The spectra of these samples in DMF are of similar appearance. Several parameters from the ^{13}C spectra which we can use to elucidate molecular dynamics are given in Table II. The widths of the ortho, meta

Table II

^{13}C Linewidth (Hz), Nuclear Overhauser Enhancement Factor (η), and T_1 (s), for Linear PS and 1% Cross-Linked PS in Chloroform and Dimethylformamide.[a]

17,500 MW PS	LW	η	T_1
ortho,[b] meta	45.0 (61.8)	0.77 (0.56)	0.23 (0.20)
Para	20.1 (18.6)	0.78 (0.58)	0.22 (0.21)
methylene		0.86 (0.65)	0.12 (0.12)
methine	33.0 (35.0)	0.90 (0.49)	0.21 (0.22)
1% cross-linked PS			
ortho,[b] meta	54.6 (66.5)	0.73 (0.55)[c]	0.21 (0.23)[c]
methylene		0.68 (0.58)	0.11 (0.14)
methine	32.0 (34.0)	0.88 (0.55)	0.20 (0.23)

[a] Values for dimethylformamide in parentheses following those for chloroform. Measured at 75 MHz.

[b] Full width of combined ortho and meta resonances.

[c] Includes contribution from para carbon.

para and methine carbons show little effect of solvent. The width of the para carbon cannot be measured accurately in the cross-linked sample because of its position on the side of the combination ortho and meta peaks that have almost completely coalesced. The overall width of the ortho-meta combination peak here can be accounted for with only a slight broadening relative to linear PS. The width of this combination peak varies proportionally with field between 7.0 and 11.7 T indicating chemical shift dispersion as the main mechanism for broadening. The methine resonance, which also shows a field dependence, does not change significantly on cross-linking. Using these data as upper limits, as for the

protons, the same limiting value for the correlation time of
10^{-8}s is obtained.

T$_1$ values (Table II) for linear PS in chloroform and DMF are
about the same, and fall within the region of the minimum T$_1$
values (Figure 1) where this parameter is least sensitive to cor-
relation time. The η value, which is at its most sensitive in
the region, is greater for the chloroform solution. From the com-
bination of these results we can conclude that the correlation
time(s) effective in chloroform are shorter, indicating more rapid
molecular motion. Factors contributing to the difference may be
the concentration of the samples (the DMF was 30% w/v PS to em-
ulate the concentration in the swollen bead as opposed to 20% for
the chloroform), and the poorer nature of DMF as a solvent for PS.

In the cross-linked resin samples the T$_1$'s are again not
solvent dependent and the η's remain greater for the sample in
chloroform. The values for the T$_1$ and parameters again indicate
a lower limit of less than 10^{-8}s for the correlation time.

Integrations of the spectra of linear and cross linked
material accumulated without nuclear Overhauser enhancement give
ratios of intensities that are consistent with the chemical struc-
ture. If a significant number of carbon nuclei were affected by
dipolar broadening this would probably not be the case since
different classes of carbons would likely be affected to different
levels. These ^{13}C NMR results show no gross differences between
linear and 1% cross-linked material and are consistent with sub-
stantial freedom of motion within the bead. The results we have
observed reflect at least qualitatively the changes expected with
magnetic field when they are compared to data on linear and cross-
linked material previously reported (14, 21).

Peptide-resin. The behavior of a pendant chain is more
effectively examined by ^{13}C NMR than by ^{1}H NMR because of the
relatively greater chemical shift dispersion and narrower res-
onances of the former (9). In addition, ^{13}C specific labelling
can be used to identify a site of interest. As an example of a
peptide-resin we have investigated H$_2$N isoleucylalanylglutamyl-
(γ-0-benzyl)-PAM-resin with 20% [13]C uniformly enriched isoleucine
incorporated. The resin was derivatized to a level of 1.8 meq/g
of PS, resulting in about one pendant chain for 5 or 6 styrene
units. This is substantially above the normal levels of 0.3 to
0.5 meq/g commonly used in solid-phase peptide synthesis, which
should exacerbate any potential problems. Synthetic target mol-
ecules are usually significantly longer than the three residues in
this model, but in light of the peptide-resin results from ^{1}H NMR
discussed earlier, this case should be of general relevance.

A proton decoupled ^{13}C NMR spectrum of the resin-peptide
sample swollen in methylene chloride is shown in Figure 4. The
spectrum obtained in DMF is quite similar. The strong line at
175 ppm is from the Ile carbonyl, and the six intense resonances
between 60 and 10 ppm are due, in order of increasing field to the
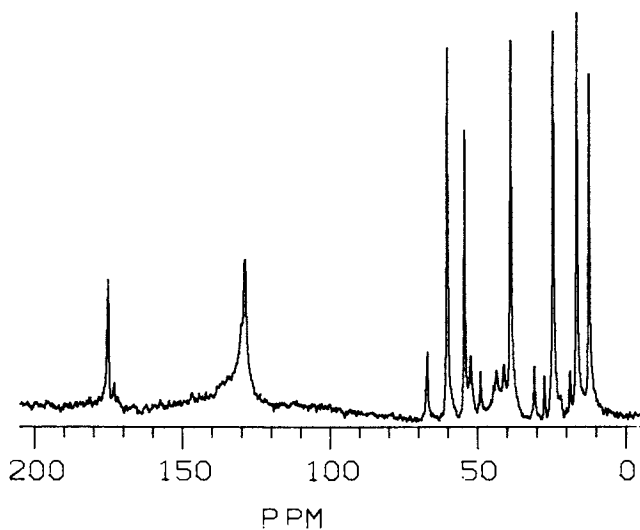
Figure 4. *Proton decoupled ^{13}C NMR spectrum at 75 MHz of $H_2NIleAlaGlu(O-Bzl)-(PAM)-(s-DVB)$ in CH_2Cl_2/CD_2Cl_2. Shifts relative to TMS.*

C^α, the solvent, the C^β, the C^{γ^1}, the C^{γ^2}, and the C^δ respect-
ively. Weaker lines deriving from other portions of the peptide
are also visible in this region. The peak immediately downfield
of the C^β resonance is from the methine of the PS. The aromatic
region around 129 ppm is made up of resonances from PS phenyl
carbons and the aromatic carbons of the PAM group and the benzyl
group. Some of the latter ones are probably responsible for the
sharp component of the peak. In relaxation studies it was clearly
observed that there was a sharp central component that relaxed
more slowly than the rest. These non-styrene carbons should ac-
count for about 20% of the intensity in the region and they will
tend to bias the width measurement, T_1, and Overhauser enhancement
values since the peak in that region was considered a single unit.

Table III

^{13}C Linewidth (Hz), Nuclear Overhauser Enhancement Factor (η) and
T_1 (s) of H_2N-IleAlaGlu(γ-O-Bzl)-PAM-(S-DVB) in Chloroform and
Dimethylformamide.[a]

		$\underline{LW}$	$\underline{\eta}$	$\underline{T_1}$
Aromatic[b]		125.9 (87.4)	0.82 (0.98)	0.37 (0.67)
Ile	C^α	29.6 (25.2)	1.32 (1.32)	0.46 (0.42)
	C^β	28.6 (23.1)	1.21 (1.38)	0.38 (0.45)
	C^{γ^1}	29.4 (28.0)	1.44 (1.46)	0.33 (0.34)
	C^{γ^2}	24.3 (23.6)	1.70 (1.34)	0.57 (0.67)
	C^δ	24.9 (24.4)	1.67 (1.62)	0.64 (0.86)

[a]Dimethylformamide value follows the chloroform value in
parentheses. Measured at 75 MHz.

[b] Includes contirgutions from all aromatic carbons.

[c] Labeling of isoleucyl reisidue is $-\overset{O}{\overset{\|}{C}}'-\overset{N}{\overset{|}{C}}^\alpha-\overset{C^{\gamma^2}}{\overset{|}{C}}^\beta-C^{\gamma^1}-C^\delta$

     The widths of resonances arising from the Ile residue (Table
III) are fairly uniform, and do not show much solvent dependence.
Those numbers probably reflect a significant contribution from
the field inhomogeneity in this heterogeneous sample since the
normally sharp (less than 1 Hz) solvent line is 20 Hz wide.

The aromatic region provides the only PS related line that is readily measurable, although it can only provide an approximation for the reasons mentioned above. The width of this combination is somewhat greater than found in the resin above, which is consistent with the proton results.

The values of T_1 and η of the Ile carbons point clearly to an increase of mobility over that for chain segments in the cross-linked samples. In general a linear chain attached to a polymer shows greater mobility (22) from the additional degrees of rotational freedom about its bonds . It is of great interest from the chemical point of view that these T_1 values are comparable with those for small free peptides in solution (23). The use of the approximation of isotropic motion improves as the mobility becomes greater, and using this, a correlation time on the order of 10^{-10}s is estimated for the Ile moiety. Even allowing for unavoidable bias, the results for the aromatic protons are suggestive of an increase of motional freedom for the resin.

The similarity of results for peptide resins in both solvents fits nicely with the estimate that this resin sample with about 50 weight % peptide should have similar swelling characteristics in the two solvents (3). In these samples we have measured the integrals of the aromatic region relative to an unenriched peptide peak, and the results are consistent with the observation of all the carbon nuclei, and hence the results are typical of all portions of the cross-linked matrix.

Conclusions

The aim of this work has been to develop an understanding of the environment at a molecular level within the cross-linked PS resin matrix and to determine if there were any fundamental physical limitations to the use of such supports in chemical synthesis. The physical evidence has shown that to a good approximation the properties of chain segments in swollen copoly(styrene-1%divinylbenzene) closely reflect those of linear PS molecules in solution under conditions typical of those used in solid-phase synthesis. The dynamics of both chain segments and free molecules are characterized by rapid fluctuations of substantial magnitude at frequencies of 10^8/s or greater arising from segmental motions in the chain. The high degree of mobility in the cross-linked material indicates that for the samples examined PS chain segments are well solvated. From the intensities of the NMR signals, our data show that these characteristics are present uniformly throughout the matrix. This is the contrast with an analysis of results reported by others (14) on a cross-linked, 25% chloromethylated resin.

From the chemical point of view, the rapid fluctuations mean that diffusion of solvents and reagents should be rapid, all sites on the resin readily accessible,and pendant chains easily accommodated throughout the matrix. The uniformity of physical

properties should rule out any dispersion in reactivity from site to site on the resin. The pendant chains appear to have even greater rotational freedom than the PS chain segments, approaching that typical of such a free molecule in solution. From the data presented here there is no evidence for a fundamental resin-caused physical limitation on the application of the solid phase method. These results indicate that older notions of pore-like cavities in a semi-rigid matrix were incorrect (24); on the contrary the interior of the resin bead can be visualized as a solution of intermingled polymer and pendant chains.

An additional point illustrated in this paper is the usefulness of high resolution NMR techniques in examining elastomer gels. This provides a relatively simple approach to dynamic and conformational information at a basic molecular level. The interpretation of the data in terms of a complete picture of molecular motion may be complicated by the nature of the distribution of motional modes, but by sampling at a variety of frequencies of different nuclei and at different magnetic fields it should be possible to develop a more accurate picture than we have been able to present here.

Acknowledgements

Literature Cited

1. Merrifield, R. B. Fed. Am. Soc. Exp. Biol. 1962, 21, 412.
2. Merrifield, R. B. J. Am. Chem. Soc. 1963, 85, 2149.
3. Sarin, V. K.; Kent, S. B. H.; Merrifield, R. B. J. Am. Chem. Soc. 1980, 102, 5463.
4. Barany, G.; Merrifield, R. B. "The Peptides"; Gross, E.; Meienhofer, J., Eds.; Academic Press: New York, 1980; Vol II, Chap. 1.
5. Sheppard, R. C. "Peptides 1971"; Nesvadba, H., Ed.; North-Holland: Amsterdam, 1973; p. 111.
6. Stahl, G. L.; Walter, R.; Smith, C. W. J. Am. Chem. Soc. 1979, 101, 5383.
7. Bovey, F. A. "High Resolution NMR of Macromolecules"; Academic Press: New York, 1972.
8. Schaefer, J. "Topics in Carbon-13 NMR Spectroscopy"; Levy, G. C., Ed., J. Wiley: New York, 1974; Vol. I, Chap. 4.
9. Heatley, F. "Progress in NMR Spectroscopy"; Emsley, J. W.; Feeney, J.; Sutcliffe, L. H., Eds., Pergamon Press: Oxford, 1979, Vol. 13, p. 47.

10. Liu, K.-J.; Burlant, W. J. Polymer Sci, Pt. A-1 1967, 5, 1407.
11. Doskocilova, D.; Schneider, B.; Jakes, J. J. Mag. Res. 1978, 29, 79.
12. Manatt, S. L.; Horowitz, D.; Horowitz, R.; Pinnell, R. P. Anal. Chem. 1980, 52, 1532.
13. Doskocilova, D.; Schneider, B.; Jakes, J. Polymer 1980, 21, 1185.
14. Ford, W. T.; Balakrishnan, T. Macromolecules 1981, 14, 284.
15. Ford, W. T.; Yacoub, S. A.; J. Org. Chem. 1981, 46, 819.
16. Flory, P. J. "Principles of Polymer Chemistry"; Cornell University Press: Ithaca, N.Y. 1953.
17. Regen, S. L. J. Am. Chem. Soc. 1975, 97, 3108.
18. "NTCFT-1180 Manual"; Nicolet Magnetics, Mountain View, Calif. 1980.
19. Bovey, F. A.; Hood III, F. P.; Anderson, E. W.; Snyder, L. C. J. Chem. Phys. 1965, 42, 3900.
20. Inoue, Y.; Nishioka, A.; Chujo, R. Die Macromolecular Chemie 1972, 156, 207.
21. Schaefer, J.; Natusch, D. F. S. Macromolecules 1973, 5, 416.
22. Levy, G. C.; Rinaldi, P. L.; Dechter, J. J.; Axelson, P. E.; Mandelkern, L. "Polymer Characterization by ESR and NMR", Woodward, A. E.; Bovey, F. A., Eds. ACS Symposium Series No. 142, American Chemical Society: Washington, D.C., 1980, p. 119.
23. Deslauries, R. Smith, I. C. P. "Topics in Carbon-13 NMR Spectroscopy"; Levy, G. C., Ed., J. Wiley and Sons; New York, 1976; Vol. II, Chap. 2.
24. Heitz, W. Adv. Polymer Sci. 1977, 23, 1.

Approximative Methods for the Evaluation of Equilibrium Moduli of Relaxing Rubber Networks

BOUDEWIJN J. R. SCHOLTENS and HENK C. BOOIJ

DSM, Central Laboratories, Geleen, Netherlands

An examination was made of several methods for eva-
luating the equilibrium moduli of strongly relaxing
rubbers, in this case peroxide-cured EPDM networks,
from oscillatory measurements in torsion. A
somewhat modified time-temperature superposition
method could be used to extend the experimental
frequency range at the lower side. Further extension
by time-crosslink density superposition appeared
to be impossible. Because no frequency-independent
modulus was found, five formulas for separating the
storage moduli into their relaxational and their
equilibrium components were tested. Of these curve-
fitting equations, the one based on the generalized
Maxwell model proved to be the most successful. This
approach is applicable only after evaluation of the
relaxation spectrum over a very broad time interval,
which could be accomplished very accurately with an
iterative method. That the other four analytical
curve-fitting equations offer only limited possi-
bilities could best be demonstrated by comparing
their corresponding relaxation spectra.

From a theoretical point of view, the equilibrium modulus
very probably gives the best characterization of a cured rubber.
This is due to the relationship between this macroscopic quantity
and the molecular structure of the network. Therefore, the deter-
mination of the equilibrium modulus has been the subject of many
investigations (e.g. 1-9). For just a few specific rubbers, the
determination of the equilibrium modulus is relatively easy. The
best example is provided by polydimethylsiloxane vulcanizates,
which exhibit practically no prolonged relaxations (8, 9).
However, the networks of most synthetic rubbers, including
natural rubber, usually show very persistent relaxations which
impede a close approach to the equilibrium condition (1-8).

Consequently, one is forced either to extrapolate from the measured time-dependent moduli in one way or another, or to estimate their time-independent component.

All usual methods to estimate equilibrium properties are based on an empirical extrapolation in the terminal region. Some approaches extend this terminal region by considering either the temperature (10, 1), or the network concentration (11, 4), or even the crosslink density (6, 3, 4), as a reducing variable. Another very popular procedure is to fit the time-dependent modulus by an analytical relationship in which the equilibrium modulus is one of the adjustable parameters (1-5). It should be pointed out here that, in very many studies, these approaches were tested with or applied to rubbers with a relatively low entanglement plateau modulus, so that the intensities of the relaxations in the terminal region were only small. Moreover, usually only one transient quantity was measured, which was a very smooth function of time due to these low relaxation intensities. Therefore, we found it useful to test these approaches more critically with rubber networks which exhibit strong relaxations. For this purpose we employed terpolymers of ethylene, propylene and a diene monomer, EPDM, which possess an extremely high entanglement modulus, about three times as high as natural rubber and even five times as high as polydimethyl-siloxane. This is probably bound up with the high flexibility, low molar volume and small chain thickness (12) of EPDM. Oscillation measurements were performed, because these provide at least two viscoelastic characteristics with quite different frequency dependences; one of these is insensitive to the actual dimensions of the sample (viz. the loss angle). This facilitates a critical testing of any empirical superposition or extrapolation method and, in addition, these data are indispensible for our new approach, the spectrum method.

Experimental

Three EPDM samples were chosen, two containing 5-ethylidene-2-norbornene as the diene monomer, viz. samples D and K with 1.0 and 2.5 mol % respectively, and one, viz. sample N, comprising 1.0 mol % 1,4-hexadiene. Sample D contained 58 mol % ethylene, K and N both 65, and their M_n was 65 kg/mol. Measurements with a Perkin Elmer DSC-2 confirmed that the K and N samples were amorphous at T > 283 K, whereas sample D was amorphous at T > 240 K.

The samples were cured with 0.2, 0.4, 0.8 and 1.6 wt.% dicumyl peroxide. In this way, we obtained twelve different networks with great variations in relaxation intensities. Dynamic mechanical measurements were performed in torsion in the linear region (deformations smaller than 5 %) with a mechanical spectrometer, using the parallel-plate geometry. The frequency ranged from 0.01 to 15 Hz and the temperature was usually between 300 and 435 K.

At the highest temperature we performed stress relaxation
measurements to extend the experimental frequency range. From
these relaxation experiments, the corresponding oscillatory data
were calculated with the well-known approximate relationships of
Schwarzl (13). More details on the preparation of the networks
and on the measurements were published previously (14).

Approximative methods to estimate the equilibrium modulus

The following approaches were used to estimate, from the
measured storage moduli $G'(\omega)$, the frequency independent
equilibrium part, $G'(o)$:
  1. time-temperature superposition of the oscillation isotherms
     to form $G'(\omega a_T)$ master curves;
  2. curve-fitting of the resulting $G'(\omega a_T)$ master curves with
     various functions, in which $G'(o)$ is one of the adjustable
     parameters;
  3. time-crosslink density superposition of a set of $G'(\omega a_T)$
     master curves of one network family with differences in
     crosslink density only.

Results and Discussion

Time-temperature superposition. Because of the relatively
strong relaxations in the frequency range at room temperature
(300 K), oscillation measurements were also performed at 345, 390
and 435 K; in addition the D networks were measured at 265 K.
For all networks we were able to superimpose the oscillation
isotherms to form one very smooth master curve. In Figure 1 the
storage and loss modulus master curves at the reference tem-
perature T_o = 300 K are presented for the complete D family.
Within one family, the horizontal shift factor a_T could be taken
independent of the degree of crosslinking. Table I summarizes the
log a_T values for the three families. The vertical shift factors
b_T were derived from the shifting of the $G''(\omega a_T)$ curves, and are
given in Table II for the four D networks. For the other families
very similar values were found. The $G'(\omega a_T)$ curves needed an
additional correction due to differences in vertical shift factor
between the equilibrium and relaxational components of $G'(\omega a_T)$.
The details of this superposition scheme were discussed in (14).
Figure 1 clearly demonstrates that a frequency-independent value
of $G'(\omega a_T)$ is not observed for any of the D networks within the
experimental frequency range of more than eight decades; this
held also true for the other networks.

Curve-fitting of the storage modulus master curve. All
individual $G'(\omega a_T)$ master curves were smoothed out and digitized
equidistantly (d log(ωa_T) = 0.2). The data so obtained were
analyzed with the following curve-fitting equations:
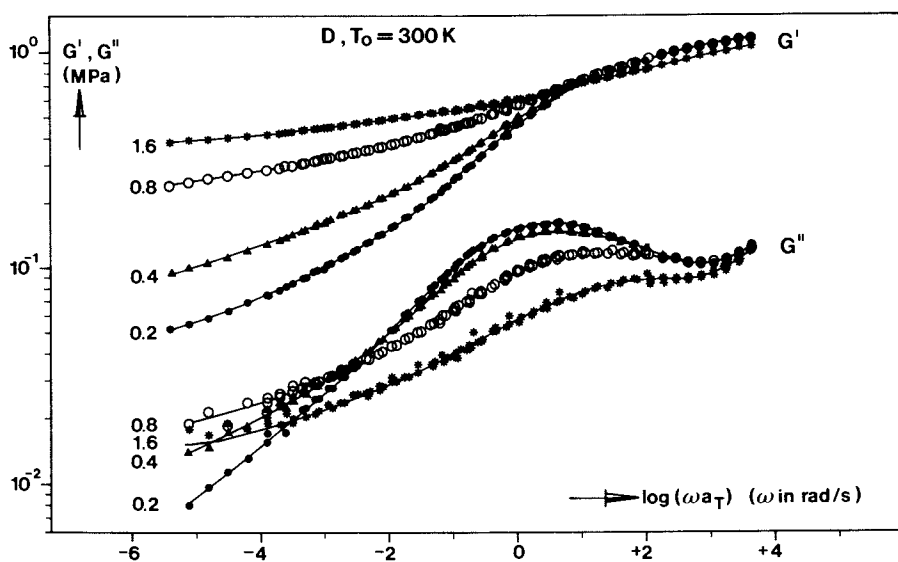
Figure 1.   *Time–temperature superimposed master curves of storage and loss moduli as functions of reduced frequency. The four networks belong to the D family. Numbers indicate wt. % dicumyl peroxide.*

Table I: The values of the horizontal shifts log a_T for the net-work families K, D and N with respect to the reference temperature T_o = 300 K.

network code	log a_T			
	265 K	345 K	390 K	435 K
K	–	-1.51	-2.38	-3.06
D	+1.65	-1.36	-2.15	-2.70
N	–	-1.27	-2.06	-2.61

Table II: The values of the vertical shift factors b_T for the four D networks with respect to T_o = 300 K.

network code	b_T			
	265 K	345 K	390 K	435 K
D 0.2	1.11	0.97	0.98	0.96
D 0.4	1.11	0.95	0.93	0.91
D 0.8	1.17	0.90	0.85	0.84
D 1.6	1.16	0.91	0.86	0.86

$$G'(\omega) = G'(o) + G'(o) \ (\omega\tau_o)^m \tag{1}$$

$$G'(\omega) = G'(o) + \Delta G \ (\omega\tau_o)^\alpha/(1 + (\omega\tau_o)^\alpha) \tag{2}$$

$$G'(\omega) = G'(o) + \Delta G \ (\omega\tau_o)^\beta/(1 + \omega\tau_o)^\beta \tag{3}$$

$$G'(\omega) = G'(o) + \Delta G \ (\omega\tau_o)^{\alpha\beta}/(1 + (\omega\tau_o)^\alpha)^\beta \tag{4}$$

The adjustable parameters, $G'(o)$, τ_o, m, ΔG, α and β were deter-
mined by a least-squares analysis. In physical terms $G'(o)$ is the
equilibrium modulus, ΔG represents the increment to the entangle-
ment plateau modulus, τ_o is a characteristic time, related, for
the last three equations, to the frequency in the point of
inflection, and the exponents m, α and β relate to the slope at
the characteristic frequency.

Relation [1] is the frequency-dependent analogue of a for-
mula proposed by Chasset and Thirion (2, 3) which has since been
applied very frequently to relaxation measurements on cured rub-
bers. The next three equations are inspired by similar relations
in dielectrics (they are not derived from these): Equation [2] by
the Cole-Cole and Equation [3] by the Davidson-Cole relation (15,
16). Both are special cases of the most general Equation [4]
which contains five parameters (17).

This most general Equation [4] was always very difficult to
work with, because it had many relative least-squares minima.
However, in the lowest minimum, which was usually hard to find,
the values of its parameters always degenerated to those of
Equation [3], with $\alpha \approx 1$ and the values of α and β showing strong
coupling. For this reason we shall further neglect the results of
this equation and concentrate on the other three.

We found that none of the empirical equations could cover
all G' master curves within the experimental accuracy (about 1 %)
over the frequency range of eight decades. Omission of part of
the high frequency data resulted in a considerable improvement,
as demonstrated in Table III. For five representative samples,
this table presents the results of the three curve-fitting
equations. The second column indicates the frequency range, since
the lower limit was always -5.5. Relatively the best results were
usually obtained with Equation [3], which could cover the widest
frequency interval with the lowest standard deviation. Equation
[1] must always fail for a curve with an inflection point, which
all our curves had. Therefore it can only be applied in a very
limited frequency range. Below this inflection point the results
of Equations [1] and [3] are comparable for soft rubbers, but
differ alarmingly for harder rubbers (see e.g. N 1.6 and K 1.6).
With Equation [2] the largest systematic deviations always showed
up at the low frequency side, where the experimental curvature
was always weaker than described by this equation. Apparently,
this relation contains too few long relaxation times, which makes
it inappropriate for extrapolation purposes. At the high fre-

Table III: Comparison of the results for five representative samples obtained with Equations [1]-[3] and [5]; $G'(o)$ in MPa and the standard deviation s in %.

sample code	upper limit of log(ωa_T)	Equation [1] $G'(o)$	s	Equation [2] $G'(o)$	s	Equation [3] $G'(o)$	s	Equation [5] $G'(o)$
D 0.2	2.3	.036	10.1	.046	3.0	.039	2.2	.035 ± .005
	1.3	.038	4.6	.046	3.1	.041	1.7	
	0.3	.040	1.6	.046	3.5	.041	1.8	
D 0.8	2.3	.18	1.6	.23	2.0	.20	0.8	.19 ± .015
	1.3	.19	0.8	.22	1.6	.20	1.0	
	0.3	.19	0.7	.22	1.7	.19	0.8	
K 0.8	2.3	.36	1.3	.45	1.6	.42	0.5	.38 ± .02
	1.3	.36	1.0	.44	0.9	.41	0.3	
	0.3	.35	0.7	.43	0.5	.40	0.3	
N 1.6	2.3	.34	2.1	.50	1.0	.47	0.2	.48 ± .02
	1.3	.34	1.6	.49	0.5	.47	0.2	
	0.3	.33	1.2	.49	0.2	.47	0.2	
K 1.6	2.3	.38	2.5	.64	1.6	.64	1.1	.63 ± .03
	1.3	.37	1.2	.62	0.7	.61	0.5	
	0.3	.37	0.5	.60	0.3	.57	0.2	

quency side, however, it is superior. Because Equation [3] always had its largest deviations at that high frequency side, far away from G'(o), and the value of G'(o) was usually not much dependent on the width of the frequency interval, we must conclude, in view also of the other arguments given above, that our results are clearly in favour of the use of this Equation [3], not the far more widely applied Equation [1].

The spectrum method. Since we are dealing with linear viscoelastic measurements, the following equation might provide a very general approach for an estimate of G'(o):

$$G'(\omega) = G'(o) + \int_{-\infty}^{+\infty} H(\tau) \, (\omega\tau)^2/(1 + (\omega\tau)^2) \, d\ln\tau \qquad [5]$$

This equation, based on the generalized Maxwell model (e.g. 1, p. 68), indicates that G'(o) can be determined from the difference between the measured modulus and its relaxational part. A prerequisite, however, is that the relaxation spectrum $H(\tau)$ should be known over the entire relaxation time range from zero to infinity, which is impossible in practice. Nevertheless, the equation can still be used, because this time interval can generally be taken less wide, as will be demonstrated below.

From each G" (and/or G') master curve, a corresponding part of a provisional spectrum can be estimated by means of one of the well-known approximative methods (e.g. 1, chapter 4). Only in the middle of its frequency interval is good agreement observed between the original G" master curve and the one recalculated from this provisional spectrum as:

$$G''(\omega) = \int_{\ln \omega_{min}}^{\ln \omega_{max}} H(\tau) \, \omega\tau/(1 + (\omega\tau)^2) \, d\ln\tau \qquad [6]$$

where ω_{min} and ω_{max} represent the lower and upper limits of the reduced frequency interval. On approaching these ends of the interval, increasing differences are found between G" measured and G" recalculated.

The next step is, therefore, to extrapolate this provisional spectrum at both ends. At the short time side, the extension usually covers three decades of time, any farther extrapolation not resulting in a further improvement because the kernels in both Equations [5] and [6] approach zero. The extrapolation to longer times always consists of the two possible extremes: a linear extension, and a sharply deflecting one with ultimate slope of −1. Theoretical arguments for such a sharp increase in the slope of $H(\tau)$ at long times were given in a molecular theory (20).

Both extended spectra are now optimized by trial and error corrections of $H(\tau)$ in such a way that, over the entire reduced frequency interval, $G''(\omega)$ calculated by means of [6] approximates $G''(\omega)$ measured, and $G'(\omega)$ measured minus $G'(\omega)$ calculated by means of [5] approximates a constant value. Of course, Equations [5] and [6] are now used with the extended integration limits. With some routine, this procedure yields two optimized spectra after about eight iterative adjustments of the entire extended spectra.

In Figure 2, these two extreme spectra are shown for the typical network D 0.4. Over a very wide interval, the two spectra coincide exactly, namely from the short time limit to approximately $-\log \omega_{min} + 1.5$, as indicated by the bold part of the curves. The long time extensions are in fact the extremes of a whole fan of extrapolations which all describe the measurements equally well. The only difference between these spectra is the increasing value needed for the adjustable constant $G'(o)$ in [5] with increasing negative slope of $H(\tau)$. Figure 3 illustrates the close agreement between the experimental data, the symbols, and the G' and G'' master curve recalculated from any of the spectra of Figure 2 with $G'(o)$ as the only adjustable constant. Apparently, the correspondence is excellent. So we are unable to discriminate with our experimental data between any of the extensions within the two extremes. The value of $G'(o)$ must therefore fall within the limiting values obtained with these extreme spectra. The spectra with the short- and long-dash extrapolations require the values of 0.065 and 0.046 MPa, respectively, for $G'(o)$ in [5], so that $G'(o) = 0.056 \pm 0.009$ MPa. The limits are relatively wide for these low values of $G'(o)$, but they come closer together for higher values (as indicated in the last column of Table III). In Figure 2 we should note the very long relaxation times required to approach equilibrium. For all EPDM networks these times were of the same order of magnitude, so that this seems a phenomenon specific for EPDM.

Although our spectrum method is admittedly time-consuming because of its iterative character, it is more powerful, versatile and reliable than the usual curve-fitting approaches: all G' and G'' data are used to estimate $G'(o)$, ultimate limits are obtained for $G'(o)$, and it is absolutely necessary that the G' and G'' master curves be internally consistent. The method is applicable over the entire experimental frequency range. This is illustrated in Figure 4, which shows the difference between G' measured and its relaxational part as a function of reduced frequency for six representative samples. This difference indeed proves to be frequency-independent. The last column in Table III compares the results of the spectrum method with those of the three empirical curve-fitting equations. The results of the best analytical function [3] usually fall within the limits obtained with [5], whereas Equation [1] clearly fails alarmingly for hard rubbers with less strong relaxations.
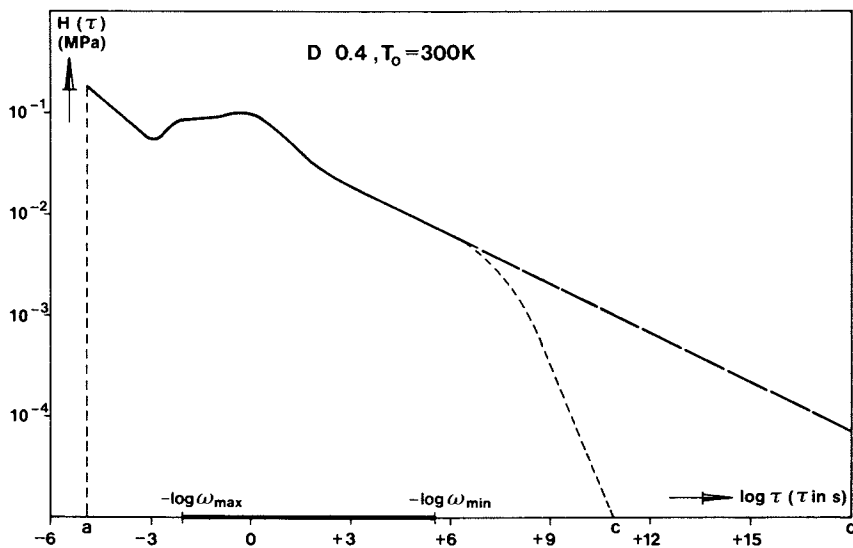
Figure 2.   Two optimized extreme spectra for network D 0.4. Bold axis indicates reduced frequency interval.
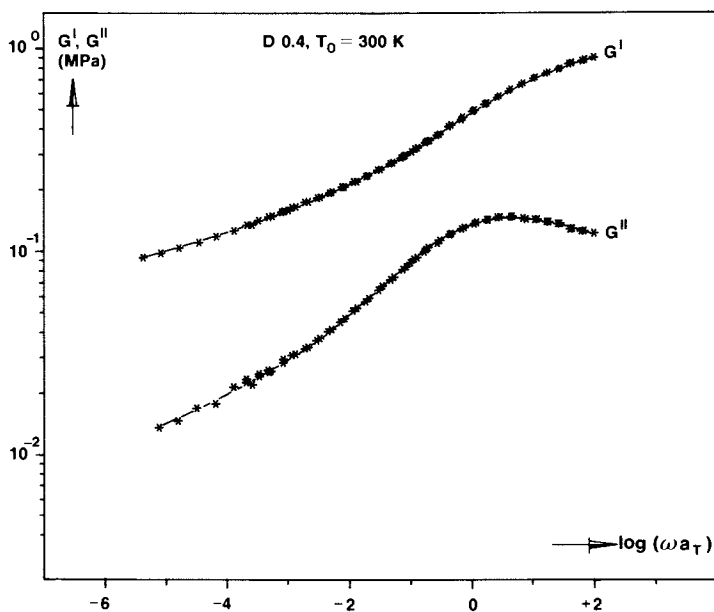
Figure 3.   Comparison of experimental data of network D 0.4 and calculated master curves, using any of the curves of Fig. 2 and Eqs. 5 and 6 with appropriate adjustable constant and integration limits.

Comparison of the relaxation spectra with those relating to the empirical functions [1]-[4] provided us with more insight into the inherent shortcomings of these functions. The analytical expressions for these spectra were derived from the Equations [1]-[4] by a substitution method involving complex algebra (1, 17, 18, 19). For Equations [1] and [4], these formulas read:

$$H(\tau) = (2/\pi) \; G'(o) \; (\tau/\tau_o)^{-m} \; \sin \; (m\pi/2) \qquad [1A]$$

$$H(\tau) = \frac{(2/\pi) \; \Delta G \; \sin \; (\alpha\beta\pi/2 - \phi)}{[1 + (\tau/\tau_o)^{2\alpha} + 2 \; (\tau/\tau_o)^{\alpha} \; \cos \; (\alpha\pi/2)]^{\beta/2}} \qquad [4A]$$

$$\text{with } \phi = \beta \; \text{arc} \; \tan \; [\frac{\sin \; (\alpha\pi/2)}{(\tau/\tau_o)^{\alpha} + \cos \; (\alpha\pi/2)}] \qquad [4B]$$

with $o < \phi < \alpha\beta/2$ and $o < \alpha\beta < 1$.

The spectra for Equations [2] and [3] are obtained from [4A] and [4B] by inserting $\beta = 1$ and $\alpha = 1$, respectively. For $\tau \gg \tau_o$ all spectra are straight lines with a slope equal to minus the exponent of ω in Equations [1]-[4]. Their differences show mainly around and below τ_o. Figures 5 and 6 compare, for two representative networks, the optimum spectra, represented by the symbols, with the analytical functions. Figure 5 compares the results of Equations [1] and [3], and Figure 6 collates those of [2] and [4]. The curves in long dashes are based on the parameters which cover all eight decades, whereas the short-dash curves relate to the parameters describing only the lowest five decades of frequency. Note first of all the difference in slope at long times for these two networks with differences in crosslink density only. Secondly, Figure 5 shows why Equation [1] must always fail over too wide a frequency interval because of the non-linear character of the spectrum at short times. Figure 6 shows why Equation [2] can give a good description of $G'(\omega)$ at high, but not at low frequencies: at short times the curvature is all right, but at long times the spectrum is usually too steep. Finally, the spectra of [3] and [4] are usually closest to the symbols, with the largest deviations at the short-time side. In addition, these fall better within the two extreme extrapolations of the spectrum.

Time-crosslink density superposition. Work of Plazek (6) and Chasset and Thirion (3, 4) on cured rubbers suggests that there is one universal relaxation function in the terminal region, independent of the crosslink density. Their results indicate that the molar mass between crosslinks might be considered as a reducing variable. However, these findings were obtained from compliance measurements on natural rubber vulcanizates,
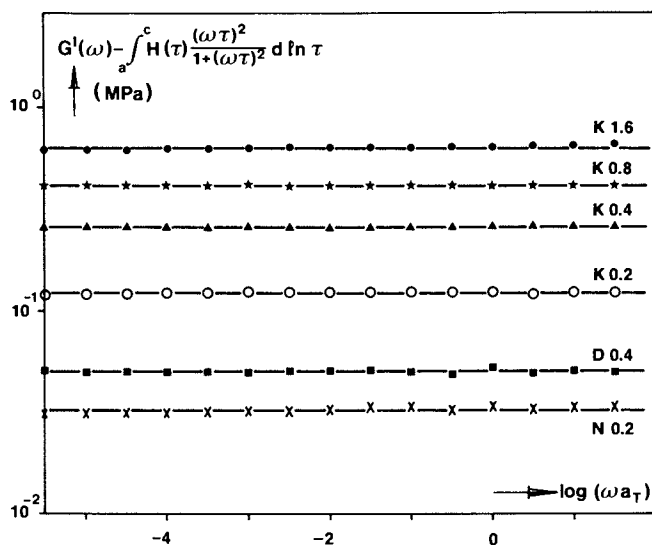
Figure 4.   Plot of the difference between experimental $G'(\omega a_T)$ and its relaxational contribution versus the reduced frequency for six representative networks.
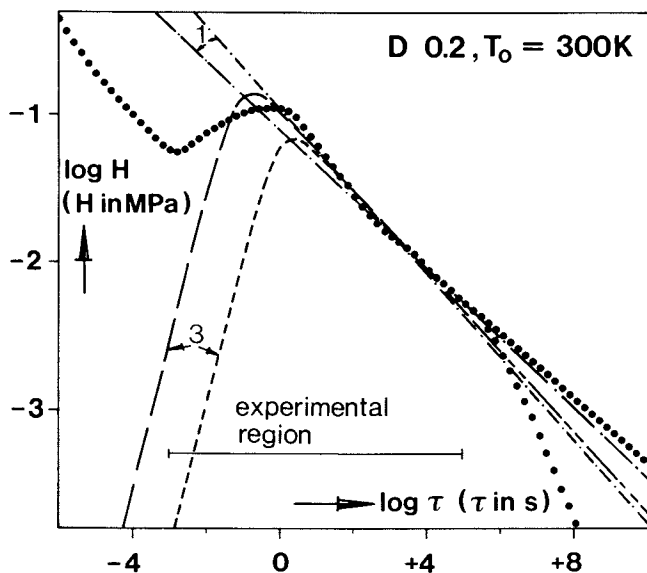
Figure 5.   Comparison of relaxation spectra of D 0.2 obtained by different methods. Symbols assessed by the spectrum method (1). Curves drawn from the analytical expressions relating to Eq. 1 and Eq. 3, respectively (2). Key: ————, — · — ·, parameters for $-5.5 < \log \omega a_T < 2.3$; — — —, — · — ·, parameters for $-5.5 < \log \omega a_T < -0.7$. The two sets of points at long times are two possible extreme extrapolations.
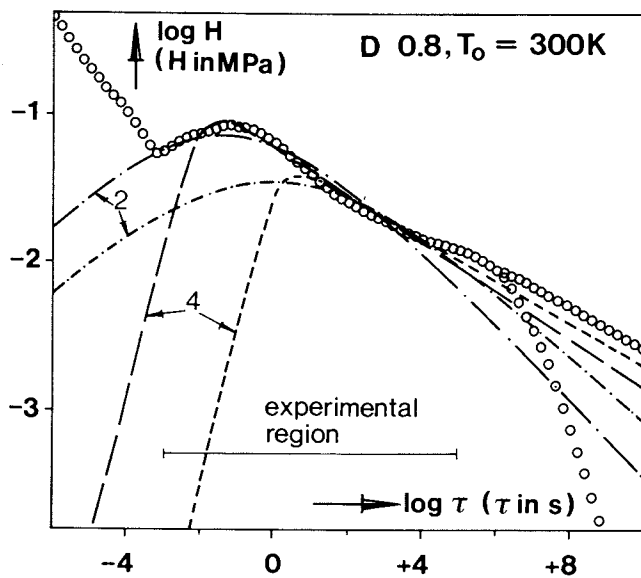
Figure 6. Comparison of relaxation spectra of D 0.8 obtained by the different methods used in Fig. 5 but for Eqs. 2 and 4.

which approach has been commented on above. Actually, this method of time-crosslink density superposition implies that the relaxation spectra of all networks of one family have the same shape in the terminal region and thus are superimposable there.

All our attempts to extend the frequency range of the time-temperature superimposed master curves to lower values by time-crosslink density superposition failed completely. We were not able to superimpose any two sets of G' and G" master curves over several decades of frequency. Because of the very strong relaxations of EPDM, and because we had G' and G" data at our disposal, we could check this point very profoundly. The reason for this can be made clear very easily by comparing the corresponding relaxation spectra. We observed that, in the terminal region, the slopes of these spectra decreased systematically with an increase in degree of crosslinking, as is exemplified in Figure 7 for all networks of the D family. As has been shown the exponents in the four analytical curve-fitting equations represent the negative slope of the relaxation spectrum at long times. All four equations showed the same trend: with an increase in crosslink density the value of this exponent decreased. This is exemplified in Fig. 8, in which the best fitting values of the exponent β of Equation [3] for all twelve networks are plotted versus the extrapolated equilibrium modulus. Apparently, time-crosslink density superposition is not applicable to our networks, which is in sharp contrast with (3, 4, 6). We suspect this finding to have more general validity.

Conclusions

- The terminal region of EPDM networks can be extended by time-temperature superposition.
- At all degrees of crosslinking the relaxation times are very much prolonged.
- The spectrum method appears to be the most reliable method to estimate G'(o) and to describe G'(ω) and G"(ω). The spectrum required can be evaluated very accurately by an approach of iterative adjustments.
- The most satisfactory empirical relationship proves to be Equation [3], not the far more widely used Equation [1].
- Time-crosslink density superposition is inapplicable to our data.

Acknowledgments
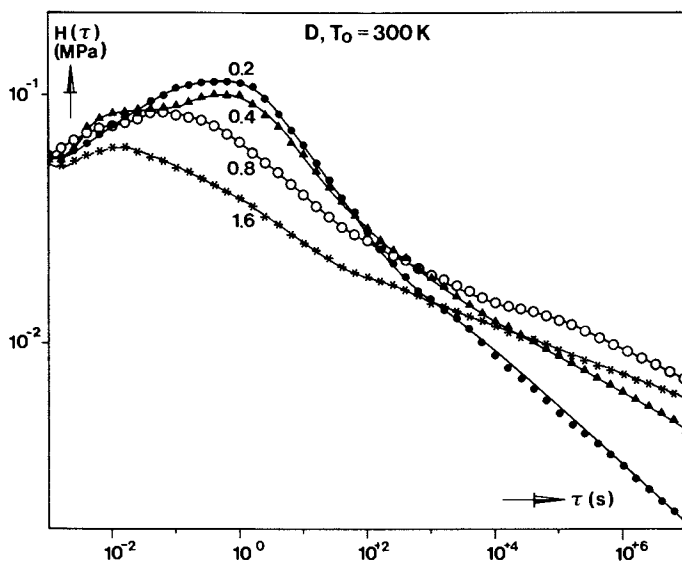
Figure 7.   Relaxation spectra of the four samples of Fig.1.
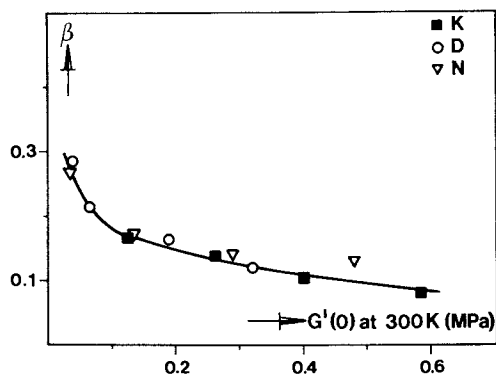
Figure 8.   Value of the exponent of Eq. 3 as a function of the degree of cross-linking for all 12 networks.

Literature Cited

1. Ferry, J.D. 'Viscoelastic Properties of Polymers'; 2nd ed.; J. Wiley and Sons: New York, 1970.
2. Chasset, R.; Thirion, P. Proc. Int. Conf. on Physics of Non-Crystalline Solids; J.A. Prins, ed.; North Holland Publ. Comp.: Amsterdam, 1965; p. 345.
3. Chasset, R.; Thirion, P. J. Rubber Res. Inst. Malaya 1969, 22, 331.
4. Thirion, P.; Chasset, R. Pure Appl. Chem. 1970, 23, 183.
5. Dickie, R.A.; Ferry, J.D. J. Phys. Chem. 1966, 70, 2594.
6. Plazek, D.J. J. Polym. Sci. Part A-2 1966, 4, 745.
7. Sperling, L.H.; Tobolsky, A.V. J. Polym. Sci. Part A-2 1968, 6, 259.
8. Oppermann, W. Ph.D Thesis; T.U. Clausthal, 1979.
9. Valles, E.M. Ph. D. Thesis; Univ. Minnesota, 1978; Univ. Microfilms Int. no. 7906386.
10. Williams, M.L.; Landel, R.F.; Ferry, J.D. J. Am. Chem. Soc. 1955, 77, 3701.
11. Ferry, J.D. J. Am. Chem. Soc. 1950, 72, 3746.
12. Graessley, W.W. Polym. Prepr. 1981, 22, 152.
13. Schwarzl, F.R. Rheol. Acta 1971, 10, 165.
14. Scholtens, B.J.R.; Booij, H.C. Polym. Bull. 1980, 3, 465.
15. Cole, K.S.; Cole, R.H. J. Chem. Phys. 1941, 9, 341.
16. Davidson, D.W.; Cole, R.H. J. Chem. Phys. 1950, 18, 1417.
17. Havriliak, S.; Negami, S. J. Polym. Sci., Part C 1966, 14, 99.
18. Smith, T.L. J. Polym. Sci., Part C 1971, 35, 39.
19. Scholtens, B.J.R.; Booij, H.C. Polym. Prepr. 1981, 22, No. 2, 176.
20. Chompff, A.J.; Duiser, J.A. J. Chem. Phys. 1966, 45, 1505.

Characterization of Elastomers for Use in Circulatory Assist Devices

CARL R. McMILLIN

Monsanto Research Corporation, Dayton Laboratory, Dayton, OH 45418

The introduction of newer and better elastomers for use in the rubber diaphragm of circulatory assist devices is currently hampered by a lack of short-term fatigue tests to evaluate candidate materials. Monsanto Research Corporation (MRC) has been evaluating a variety of accelerated fatigue tests that could be used to test candidate elastomers. Although blood is generally considered to be a very corrosive environment, our tests indicate that it actually extends the fatigue life of elastomers compared to air or water environments. A combination of fatigue tests using both cut-initiated and uncut test specimens appears to provide the most information to predict the long-term fatigue characteristics of elastomers for use in circulatory assist devices.

The development of cardiac assist devices and other instrumentation and components which come in contact with the cardiovascular system requires materials which will perform in a physiological environment. One particularly difficult application is the diaphragm for blood pumps, which requires an elastomer to undergo cyclic deformation and/or flexing while in contact with blood.

Currently, few data are available on the fatigue properties of elastomers cycled at body temperature and in contact with blood. Artificial heart device applications are particularly demanding of elastomers since even a three-year implantation of a heart will involve in excess of 10^8 cycles.

Evaluation of the fatigue properties of elastomers suitable for cardiovascular application is currently a long, and therefore, costly proposition. This is especially true if the fatigue tests are to be conducted in contact with blood.

The objectives of this research are to develop short-term
in vitro fatigue test methodologies that will predict long-term
in vivo performance of elastomers used in cardiac assistance and
related devices and to evaluate the fatigue life of candidate
materials for potential use in these applications.

Materials Characterization

Many studies, particularly in the life sciences area, are not
reproducible because small quantities of unique materials were
used in the research. A commitment was made when the present pro-
gram began to characterize fully the elastomers utilized in the
development of accelerated fatigue tests. At the start of the
program, a limited number of candidate materials was selected to
be obtained in quantity, characterized, and used for all of the
developmental testing.

The materials selected for evaluation included three mate-
rials currently being used in these applications: Biomer
(Thoratec Laboratories Corporation, Emeryville, CA), representa-
tive of segmented ether-type polyurethanes; Avcothane-51 (Avco
Everett Research Laboratory, Inc., Everett, MA), a block copolymer
of 10% silicone rubber and 90% polyurethane; and Hexsyn (Goodyear
Tire and Rubber Company, Akron, OH), a sulfur vulcanized hydro-
carbon rubber that is essentially a polyhexene. Also selected,
because of their easy availability, were Pellethane (Upjohn Com-
pany, North Haven, CT), an ether-type of polyurethane capable of
being extruded in sheet form, and a butyl rubber formulation,
compounded and molded at the National Bureau of Standards. The
material thickness varied, but the sheets were generally about
1 mm thick.

The quantity of these materials needed for all of the in-
tended fatigue testing research (by three contractors) was esti-
mated to be about 10 m^2 each. Since this is about two orders of
magnitude greater than the amount of these specialized materials
generally manufactured at any one time, a substantial manufactur-
ing effort was required prior to any fatigue testing. All of
these materials were extensively characterized (physical/
mechanical/and biological properties) prior to the initiation of
the fatigue tests. These tests have included tensile strength,
elastic modulus, and elongation at several temperatures, differen-
tial scanning calorimetry, thermal gravimetric analysis in dif-
ferent atmospheres, surface tension, permeability to fluids,
molecular weight, cytotoxicity, mutagenicity, thermal mechanical
analysis, rheovibron testing, oxygen aging, Fourier transform
infrared analysis of surface and interior absorbed protein, tear
strength and tear energy before and after long term exposure to
blood, and many other properties and characteristics.

The majority of the characterization for Hexsyn and Pelle-
thane were conducted at MRC while Biomer was characterized at the
University of Washington in St. Louis by Dr. J. Kardos and Avco-
thane and butyl were characterized at the National Bureau of
Standards by Dr. R. Penn. A few of the characteristics of the

Pellethane and Hexsyn are summarized here. The Pellethane 2363-80A tested by MRC is commercially available. Our samples had a tensile strength of 7,830 psi and an elongation of 380% at 37°C.

Hexsyn is a trade name of Goodyear Tire and Rubber Company, Akron, OH, for a family of materials synthesized by the copolymerization of a C_4 to C_{10} α-olefin with a mixture of 4-methyl- and 5-methyl-1,4-hexadiene (1, 2). The "standard" Hexsyn in use has been produced by Goodyear by polymerizing a mixture of 95% 1-hexene and 5% methyl hexadiene with the 4-methyl and 5-methyl in a 2:3 ratio using a Ziegler-Natta hetrogeneous catalyst. The gum rubber has a molecular weight of Mw = 781,000 by light scattering. The gum rubber is then vulcanized using a traditional accelerated, high crosslink efficiency carbon black filled mixture. The resulting rubber has a tensile strength of 1,740 psi and elongation of 285% at 37°C. The glass transition temperature has been found to be -52°C by differential scanning calorimetry.

Fatigue Tests
In the literature it is easy to observe that different types of fatigue tests rank materials in different orders. Thus, to predict a material's behavior for specific long-term end-use application, it is important to select the correct fatigue test.

Most early artificial hearts and left ventricular assist devices consisted of a hemispherical diaphragm alternately inflated and deflated by compressed air. The controls generally consisted of the amounts of pressure and vacuum applied to the device. In this case, the elastomeric diaphragm was exposed to an alternating pressure or stress and would deform (or strain) accordingly. For this situation, the most predictive type of fatigue test would be a constant stress test that applied an alternating stress or load on the test specimens. That is, in each cycle a load of 2 kg, for example, would be applied to each test specimen. Creep tests tend to rank the candidate materials in the same order as constant stress fatigue tests.

More recently, the National Institutes of Health have been emphasizing hearts and assist devices capable of mechanical or electrical operation. Most of these devices have a pusher plate that moves back and forth to displace the diaphragm a fixed (but adjustable) distance, generally independent of the pressure of each stroke. The fatigue test which most closely mimics this condition will deform the test specimens to a fixed deformation or strain in each cycle. This is the type of fatigue test machine that MRC has constructed for this program.

All of the uniaxial fatigue data reported to date have been generated using a fatigue testing machine built by MRC that is based on the principal of a wobble plate. The machine has positions for 30 specimens and is capable of operation at controlled

temperatures using a wide variety of testing media. The tester provides a sinusoidal strain to the specimens and has a variable speed, although all data presented here were tested at 120 cycles per minute.

Standard fatigue tests normally require extended periods of time to complete regardless of the type of stress/strain used. Accelerated fatigue tests change some conditions of the test in the hope of reaching the same end point in less time. Potential means of accelerating the tests include changing factors such as the temperature, frequency, chemical environment, levels of stress or strain, or the addition of stress concentrators.

If the strain or stress is to be changed, one possible method of accelerating the fatigue test involves increasing the strain (or stress) in either discrete steps or in a progressive manner (3, 4). This type of fatigue test has now been used for testing steel, polystyrene, poly(methyl methacrylate), nylon, and reinforced plastic (5). Although some deviations have been noted (4, 6), this type of test has the advantages of speed, elimination of long-term run-outs, and reduction of scatter of the data near the endurance limit. One potential problem with all methods that use a higher than end-use strain or stress is the possibility that the failure mechanism changes at higher strains, which may lead to erroneous predictions. However, all accelerated fatigue tests suffer from this potential difficulty; conditions for all of them vary from real life.

An increasing strain was used to accelerate the test for all of the uniaxial fatigue data generated at MRC to date. Five inch ASTM "dog bone" tensile specimens were used. The strain was generally increased 5% each day. In addition to using normal test specimens, some of these tests were conducted after a 1 mm razor blade cut was placed in the side of the fatigue test specimen. These specimens were tested under conditions where the strain was increased 1.5% each day. The type of test conducted can be seen in Table I where the maximum cyclic strain is increasing from 1.7% on day 1 to 35% on day 20. These data were plotted as cumulative probability to failure versus percent strain at failure, as shown in Figure 1. Regression lines are then fit to the data. The strain at 50% probability of failure has been used for all comparisons of data.

Uniaxial Fatigue Test Results

Increasing temperature decreases the modulus of elasticity of elastomers at the same time that accelerated chemical effects occur. In our constant strain fatigue tests it has been found that the effect on the modulus (lower stress at the same strain) is significantly more important than chemical degradation effects, as shown in Figure 2. Thus, failure occurred much more rapidly at 4°C than at 37°C or 60°C. This may be one manner in which fatigue

TABLE I. CHRONOLOGICAL FATIGUE LIFE FOR AVCOTHANE-51,
          MRC LOTS 141265 AND 1412690 CUT-INITIATED
          SPECIMENS, CYCLED AT 120 CPM IN DISTILLED
          WATER AT 37°C

Testing day	Percent cyclic strain	Specimens failed	Accumulated cycles
1	0-1.7		
2	0-3.5		
3	0-5.2		
4	0-7.0		
5	0-8.5		
6	0-10.0		
7	0-11.5		
8	0-13.0		
9	0-15.0		
10	0-17.0		
11	0-19.0		
12	0-21.0		
13	0-22.8		
14	0-24.6	*	2,332,800
15	0-26.3		
16	0-28.0	*	2,678,400
17	0-29.8	*	2,851,200
18	0-31.5	*	3,024,000
19	0-33.3		
20	0-35.0	*	3,369,600
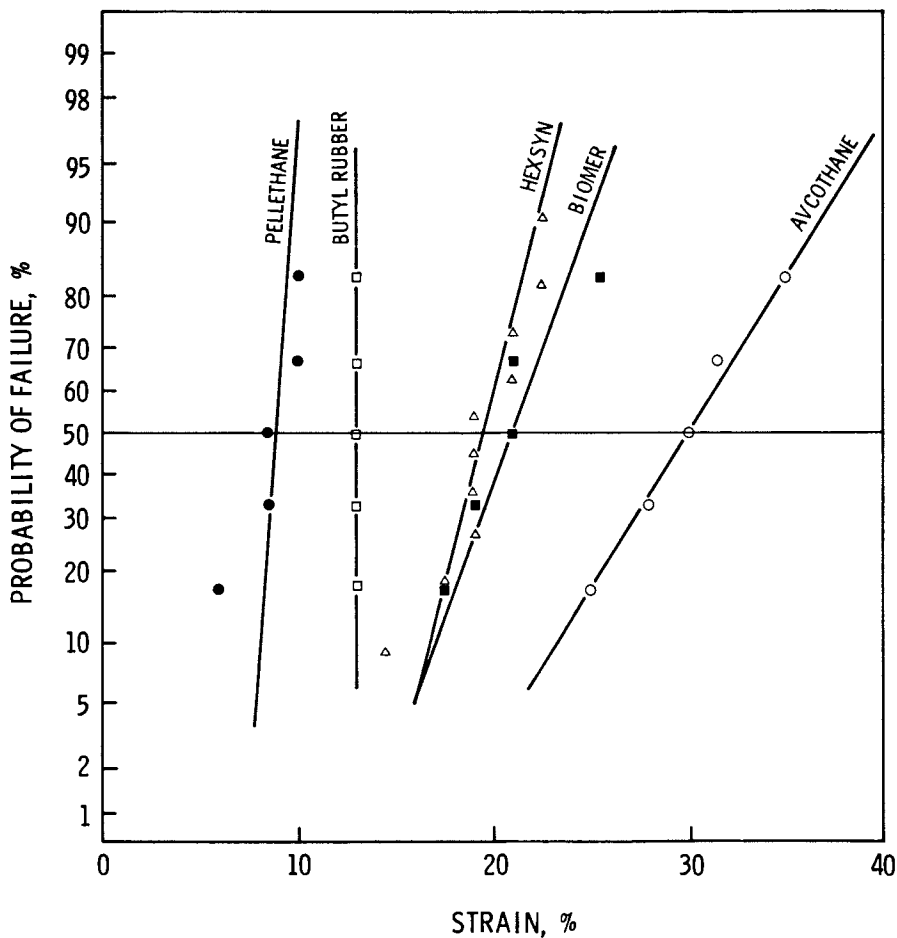
Figure 1.   Cumulative distribution function for a step-increasing strain fatigue test cycled at 120 cpm in distilled water at 37°C using cut-initiated specimens.
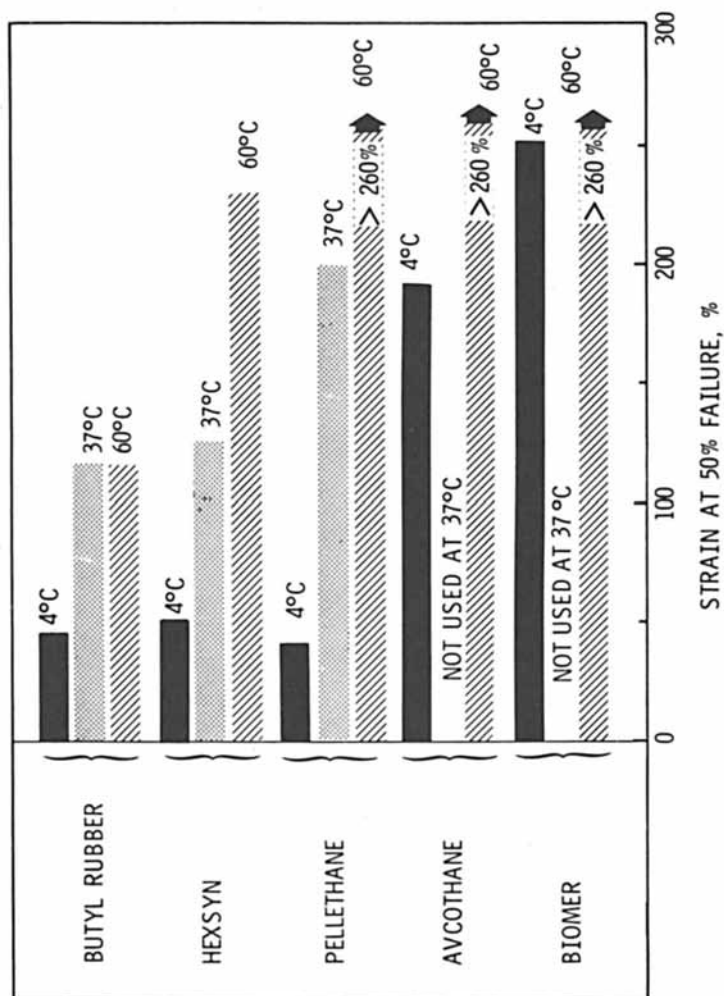
Figure 2.   Strain at 50 percent failure for uncut specimens tested in saline solution.

tests can be accelerated. Extreme care must be taken, however, to assure that the tests remain valid, even at 4°C, since the glass transition temperature [Tg] of the candidate materials are different. Extrapolating data taken close to the Tg of one material to end-use conditions may not be the equivalent of reduced temperature testing of other materials with much lower glass transition temperatures.

Another set of fatigue tests evaluated the effect of oxygen on accelerated fatigue tests. These tests found no apparent effect of oxygen on the fatigue life of the uncut test specimens, as shown in Figure 3. On the other hand, fatigue tests using test specimens with a 1-mm cut in the side showed a substantial decrease in fatigue life in the presence of oxygen, as shown in Figure 4. The dependence on oxygen for the cut-initiated tests is believed by MRC to be significant. The period of testing was approximately three to six weeks in both tests. One hypothesis we are investigating is that unless accelerated fatigue tests demonstrate an oxygen dependence, they are probably representative of the wrong portion of the fatigue life curve and may not properly predict long-term results. Further research on the significance of oxygen dependence on the validity of predictive accelerated fatigue tests will be conducted by MRC.

Environmental effects also need to be considered when developing fatigue testing methodology. The human body presents an unbelievably corrosive environment for foreign materials. The best stainless steels, cobalt alloys, and even platinum undergo pitting, cracking, and failure when used in vivo. It is little wonder that the physical properties of polymers are generally degraded after in vivo implantation.

MRC has evaluated the effect of fatigue testing of candidate cardiovascular materials in human blood versus fatigue testing in air and saline - all at 37°C (Figures 5 and 6). Whole human blood was chosen as one of the mediums for testing at 37°C, in spite of the difficulties associated with this testing.

We used outdated human CPD (citrate-phosphate-dextrose) blood from the Dayton Community Blood Center. At 21 days, CPD blood still retains 78% survival of the red blood cells and would fairly well simulate in vivo physiological conditions. During these tests, many enzymes and proteins may denature and/or precipitate. Even after suffering that trauma, the resulting fluid is more suitable for material testing than other pseudo-physiological fluids, since it still contains most of the salts, lipids, hormones, oligomers, nucleotides, saccharides, etc., found in whole blood in vivo.

We have found that blood used in our fatigue tester needs to be changed about once a week. We routinely add penicillin, streptomycin, and mycostatin to the blood to prevent bacterial and
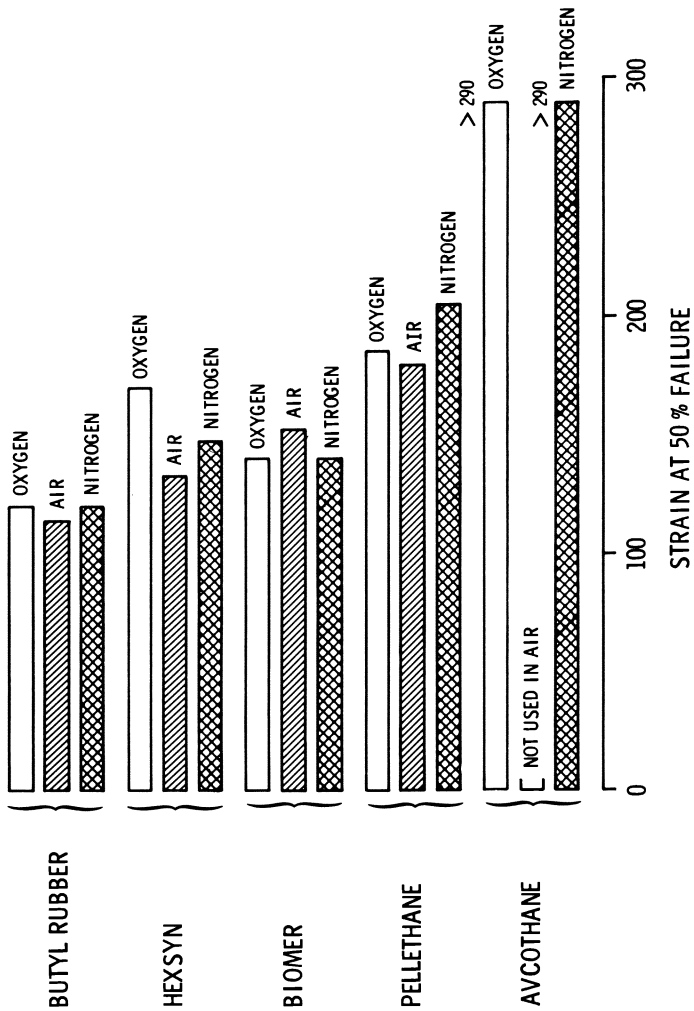
Figure 3.   Oxygen influences upon uncut specimens from step-increasing strain fatigue tests cycled at 120 cpm and at 37°C.
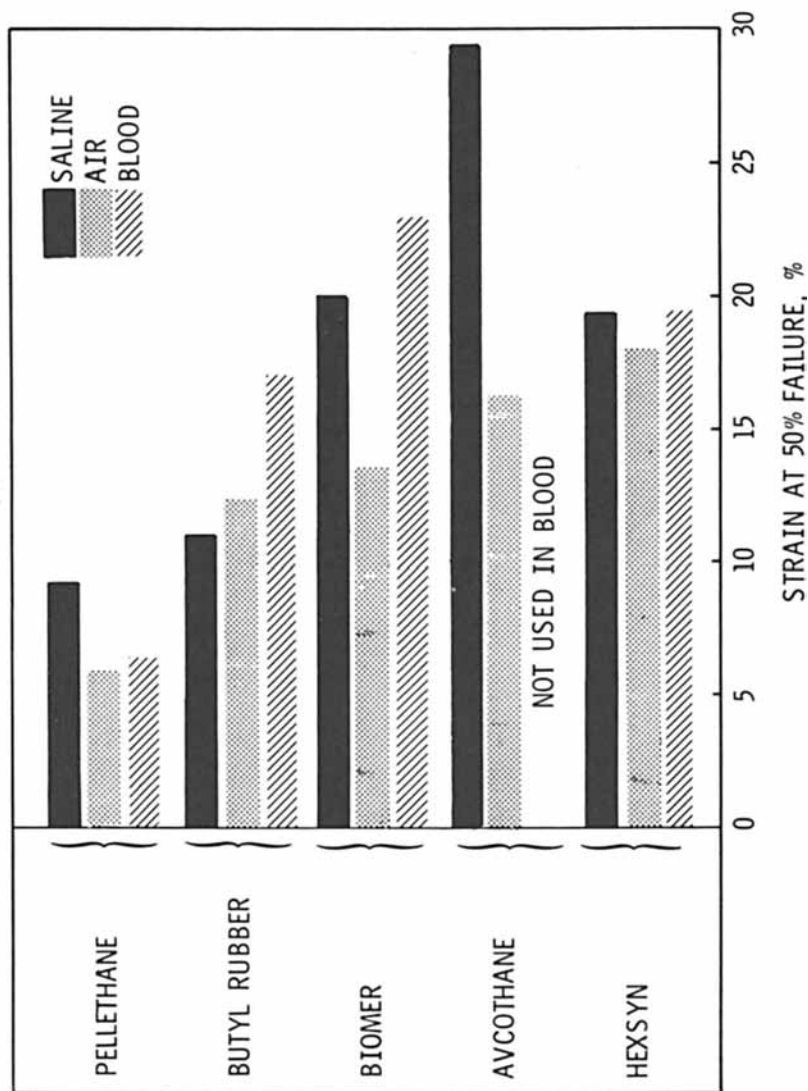
Figure 4. Oxygen influences upon cut-initiated specimens from step-increasing strain fatigue tests cycled at 120 cpm and at 37°C.
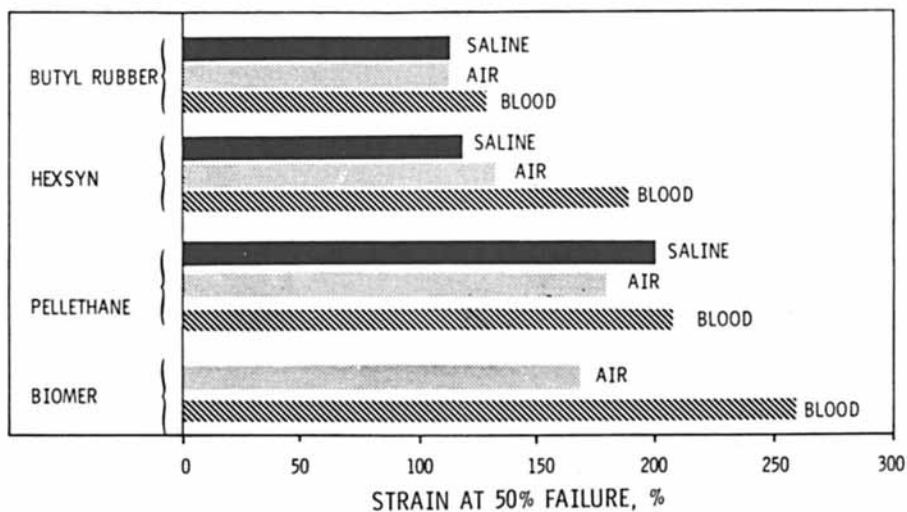
Figure 5.   *Strain at 50 percent failure in fatigue tests conducted at 37°C on uncut specimens.*
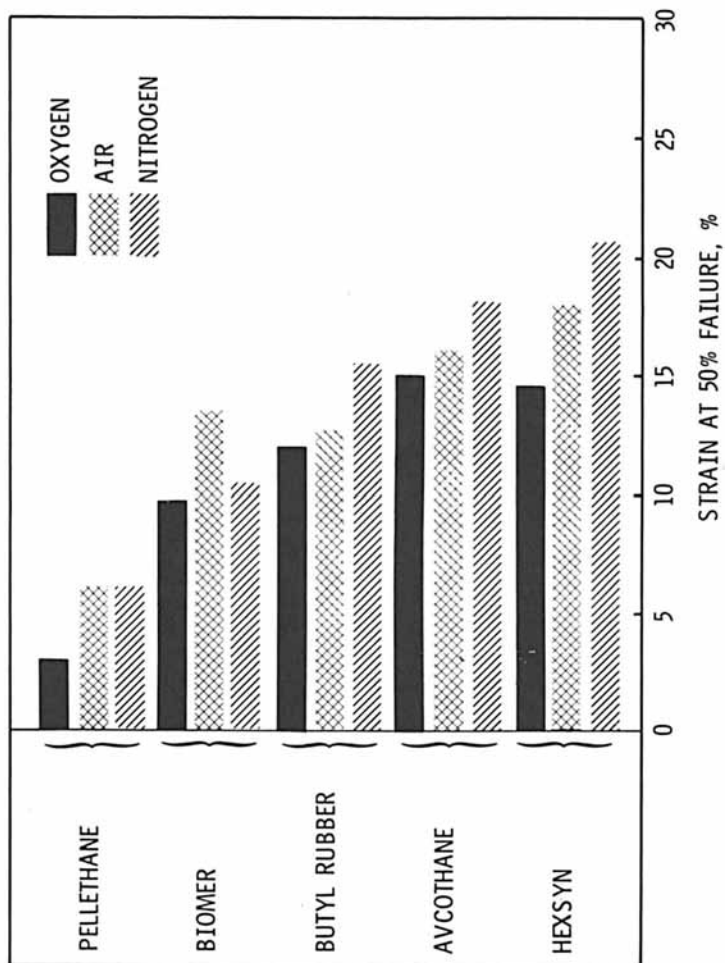
Figure 6.   Strain at 50% failure in fatigue tests conducted at 37°C on cut-initiated specimens.

mold growth.   Also, heparin and/or ethylenediaminetetraacetate
(EDTA) (a calcium chelator) are added to prevent blood clotting.
In spite of these precautions, the viscosity of the blood begins
to increase and microbiological growth begins to occur after about
one week.   The instrument is therefore drained, cleaned with a
mild soapy solution, and refilled on a weekly basis.

Results from our fatigue tests have shown that, in the one-
to two-month accelerated fatigue tests, blood is a less severe
environment than saline or air.   This may be due to adsorption of
the blood components into the microcracks, resulting in reduced
stress concentrations.   More work is anticipated to study the
effect of blood on the fatigue life of elastomers.

All of the above results were generated by tests in which the
cyclic strain was started low and gradually increased until all of
the specimens broke.   Longer term fatigue tests at different, dis-
crete, strain levels are also planned for the future.

Ranking of the Candidate Cardiovascular Materials

Results from our accelerated fatigue tests and static
mechanical/physiological tests have confirmed our assumption that
a durability ranking of the selected materials with respect to
their usefulness in cardiovascular devices is decidely influenced
by the type of testing methodology selected.   Table II is a com-
parison of five candidate materials' relative rankings using five
test methodologies.   The asterisk denotes the material with the
longest durability or highest resistance to the particular test
method indicated.   All five materials tested were each found to be
superior in one of the five tests cited in Table II.   Thus, all
five materials being tested could be argued to be the superior
elastomer currently being tested.   This illustrates the difficulty
of ranking candidate materials.

Care must be taken to assure that the correct types of tests
are used to rank materials for specific applications.   For
example, most recently designed circulatory assist devices utilize
a pusher plate mechanism in which the pusher plate is displaced a
predetermined distance.   This type of device would best be modeled
by a constant strain fatigue test.   Materials which creep and have
a high permanent set tend to fail more rapidly on a constant
stress fatigue test but last a longer time in constant strain
fatigue tests.   The bending and compression of finger joint pros-
theses or the rolling of the side material in pusher plate cir-
culatory assist devices may not be well modeled by either of the
above tests.

TABLE II.   FATIGUE RANKING IS INFLUENCED BY
THE TEST SELECTED

Elastomer	Cut growth air at 37°C	Uncut blood at 37°C strain at 50% failure	Uncut N$_2$ at 37°C	Uncut air at 37°C	Cut growth fixed strain cycle 1 hr. failure strain
Hexsyn	18*	190	150	125	30
Biomer	12	260*	140	150	25
Avcothane	16	-	>290*	-	-
Pellethane	6	210	205	175*	12
Butyl	12	140	110	115	>45*

*The material with the longest durability or highest resistance
to the particular test method indicated. All numbers
represent percent strain at 50% failure.

Conclusions

After extensively characterizing and fatigue testing the five candidate materials, we have some opinions on their usefulness in cardiovascular applications:

Biomer - This material performs well under a variety of experimental conditions and should be considered for use in most cardiovascular applications. Particular advantages are the low permanent set, high resistance to creep, and generally good fatigue resistance. Disadvantages include a relatively high permeability to fluids, a necessity to be film cast in multiple layers as the only method of fabrication, and an uncertainty as to the effect of thickness on performance (better fatigue results were obtained with the thinner films).

Hexsyn - Performance varies from adequate to very good in a variety of fatigue tests, and Hexsyn should be considered for use in most cardiovascular applications. Particular advantages include low permeability to fluids, high resistance to cut growth in fatigue, the ability to be compression molded (good for high volume application), relatively low cost of the raw materials, and ready in medical grade material. Disadvantages include an intermediate amount of permanent set, lower resistance to creep, lower modulus of elasticity (which may be an advantage in some applications), and low tear strength (although Hexsyn has a high resistance to cut growth in fatigue).

Avcothane - This material performs exceptionally well in most constant strain fatigue tests and should be considered for use in most cardiovascular applications. A particular advantage is its fatigue test performance under a variety of conditions. Disadvantages include a very high permeability to fluids, a very high permanent set, a very low resistance to creep, a high cost of materials, and a necessity to be film cast in multiple layers under rigid controls available only at the material suppliers' facilities.

Pellethane - This material performed satisfactorily in some of the fatigue tests and should be considered for some cardiovascular applications, particularly in noncritical locations. Advantages of this inexpensive, commercially available thermoplastic include its ability to be formed into parts by a wide variety of methods such as extrusion, blow molding, injection molding, or film casting. In fatigue situations without stress concentrators, Pellethane's performance was similar to that of Biomer. From our tests, if a thick part were required, Pellethane should be considered. Disadvantages include a rapid decrease in fatigue resistance in the presence of cuts or other stress concentrators. Its permeability to fluids is similar to Biomer's, but it has a slightly higher permanent set and lower resistance to creep. Although Pellethane is probably the most inexpensive material tested, it is not available in a specific, closely controlled, medical grade.

Butyl rubber - This material generally had the least endur-
ance in fatigue tests, but it may be adequate for some cardiovas-
cular applications. Advantages include less sensitivity to stress
concentrators than Pellethane, a very low permeability to fluids,
a moderate creep resistance and widespread availability at low
cost. Disadvantages include a relatively low fatigue resistance
compared to the elastomers specifically designed for these appli-
cations. The rubber tested was not designed for medical applica-
tions and had standard rubber additives and modifiers that were
cytotoxic unless the material was extracted after manufacture.
Further testing of these and a wide variety of other mate-
rials is continuing at MRC.

Literature Cited
1.   Lal, J.; Sandstrom, P. H. U.S. Patent 3,794,696, Febru-
      ary 26, 1974, assigned to Goodyear Tire and Rubber Company.
2.   Lal, J.; Sandstrom, P. H. U.S. Patent 3,991,262, November 9,
      1976, assigned to Goodyear Tire and Rubber Company.
3.   Lazar, L. S. ASTM Bulletin, 67-72, February 1957.
4.   Weibull, W. "Fatigue Testing and Analysis of Results;"
      Pergammon Press: New York, New York, 1961.
5.   Thorkildsen, R. L. In "Engineering Design for Plastics;"
      E. Baer, Ed., Reinhold Publishing Corporation: New York, New
      York, 1964.
6.   Prevorsek, D. C.; Brooks, M. L.   J. Appl. Poly. Sci. 1967,
      11, 925-927.

INDEX

549